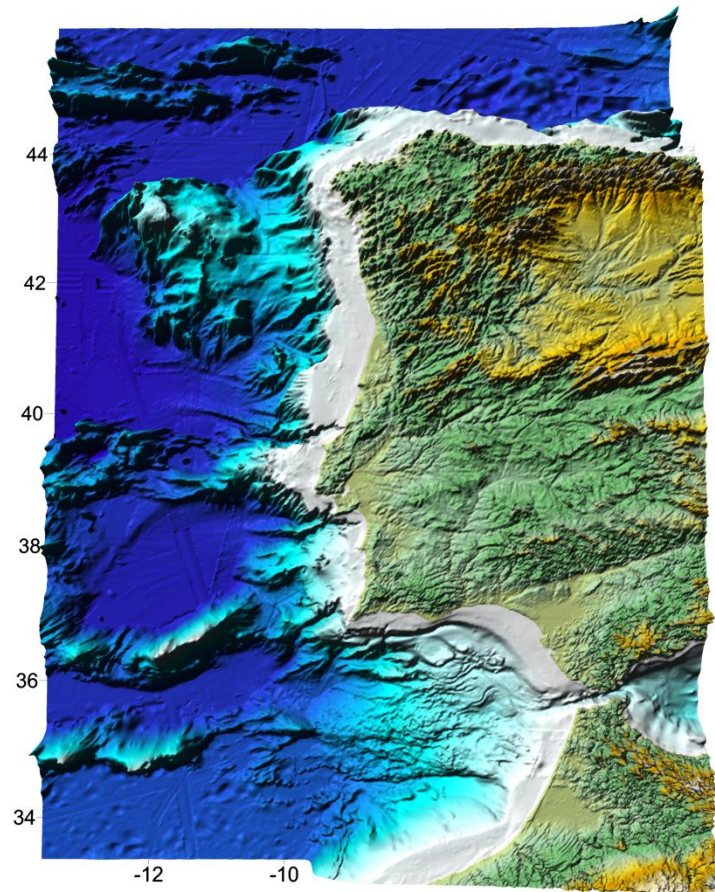


**UNIVERSIDADE DE LISBOA**

**INSTITUTO SUPERIOR TÉCNICO**



# **Coupling watersheds, estuaries and regional seas through numerical modelling for Western Iberia**

**FRANCISCO JAVIER CAMPUZANO GUILLEN**

**Supervisor: Doctor Ramiro Joaquim de Jesus Neves**

**Co-Supervisor: Doctor Maria Manuela Fraga Juliano**

**Thesis approved in public session to obtain the PhD Degree in  
Environmental Engineering**

**Jury final classification: Pass with Distinction**

**2018**

**UNIVERSIDADE DE LISBOA**

**INSTITUTO SUPERIOR TÉCNICO**

# **Coupling watersheds, estuaries and regional seas through numerical modelling for Western Iberia**

**FRANCISCO JAVIER CAMPUZANO GUILLEN**

**Supervisor:** Doctor Ramiro Joaquim de Jesus Neves

**Co-Supervisor:** Doctor Maria Manuela Fraga Juliano

**Thesis approved in public session to obtain the PhD Degree in  
Environmental Engineering**

**Jury final classification:** Pass with Distinction

## **Jury**

**Chairperson:** Doctor José Manuel de Saldanha Gonçalves Matos, Instituto Superior Técnico, Universidade de Lisboa.

## **Members of the Committee:**

Doctor Ramiro Joaquim de Jesus Neves, Instituto Superior Técnico, Universidade de Lisboa;

Doctor António Manuel dos Santos Pascoal, Instituto Superior Técnico, Universidade de Lisboa;

Doctor Aires José Pinto dos Santos, Instituto Superior Técnico, Universidade de Lisboa;

Doctor Manuel Ruiz Villareal, Instituto Espanhol de Oceanografía, A Corunha, Espanha;

Doctor Paulo Nogueira Brás de Oliveira, Instituto Português do Mar e da Atmosfera, Lisboa.

**2018**

To my wife Nana and my son Pablo  
that made this thesis possible,  
without them perhaps I would have finished it earlier  
but it definitely wouldn't have been the same.

# **Title: Coupling watersheds, estuaries and regional seas through numerical modelling for Western Iberia**

## **Abstract**

In order to determine the inland waters contribution to the open ocean in terms of volume and composition, an original methodology to integrate the water cycle components including the watershed, estuarine and ocean phases through a system of models was set up. The interfaces that the run-off water found in their way to the sea were reproduced through numerical models for the first time for the continental Portuguese territory using the different components of the MOHID Water Modelling System (<http://www.mohid.com>).

To reproduce the water continuum from the precipitation areas to its evacuation in the open ocean, a system of coupled models with different time and space resolutions allowed including the different spatial and temporal scales. At the watershed level, the MOHID Land provided operationally the water flow and properties, including nutrients, for the main river catchments for the Iberian Western area with a 2 km horizontal resolution and for the whole Iberian Peninsula with 10 km horizontal resolution to characterize the transnational watersheds. Downstream, several operational hydrodynamic and biological estuarine applications use the previous results to provide fresh water input flows for those rivers where data is non-existent. The estuarine models would reproduce the inner dynamics of the estuary and its connection to the coastal waters. Fluxes from the latter model, which are intermittent due to the tidal signal, were then imposed in the Portuguese Coast Operational Modelling System (PCOMS), a fully baroclinic 3D hydrodynamic and ecological regional model that covers the Iberian Atlantic region and that also provides boundary conditions to the estuarine applications. The estuarine and the PCOMS models are operated by the MOHID Water model. The model integration and synchronisation of the different models is achieved through the ART tool, a software for model simulations automation.

This set of operational models when combined is able, through this methodology, to fill gaps in information and to obtain better results when compared with the use of river climatology. The employed methodology is generic and was applied to several estuaries in the Portuguese coast to achieve more precise coastal circulation forecasts and to study their influence in the generation of salinity and temperature fronts which are relevant to fisheries management in the coastal zone among other uses.

**Key-words:** MOHID model, freshwater inputs, numerical modelling, estuaries, Western Iberia

# **Título: Integração de bacias hidrográficas, estuários e oceano regional a traves de modelação numérica para Ibéria ocidental**

**Nome:** Francisco Javier Campuzano Guillen

**Doutoramento em:** Engenharia do Ambiente

**Orientador:** Doctor Ramiro Joaquim de Jesus Neves

**Co- Orientador:** Doctor Maria Manuela Fraga Juliano

## **Resumo**

Para determinar a contribuição das águas interiores no oceano aberto em termos de caudal e composição, desenhou-se uma metodologia original para integrar as componentes do ciclo da água incluindo a fase da bacia hidrográfica, estuário e oceano. As interfaces encontradas, no seu caminho para o mar aberto, pelas águas que escoam foram reproduzidas pela primeira vez para o território continental português usando as diferentes componentes do sistema de modelo numérico MOHID (<http://www.mohid.com>).

Para reproduzir o contínuo da água, desde as áreas de precipitação até a sua descarga no mar aberto, foi desenhado um sistema de modelos numéricos tendo em conta as diferentes escalas espaciais e temporais. A nível de bacias hidrográficas, o modelo MOHID Land forneceu de forma operacional o caudal e as diferentes propriedades da água, incluindo nutrientes, para os principais rios da vertente ocidental ibérica com uma resolução horizontal de 2 km e para a Península Ibérica completa com uma resolução horizontal de 10 km para caracterizar as bacias transnacionais. A jusante, vários modelos operacionais de estuário incorporam estas entradas nos seus cálculos hidrodinâmicos e biológicos, preenchendo desta forma as lacunas na rede de monitorização hidrográfica. Dos modelos estuarinos, são obtidos os fluxos de água e propriedades da água tendo em conta a sua modulação pelo efeito da maré. Finalmente, estes fluxos são incluídos no Sistema de Modelação Operacional da Costa Portuguesa (PCOMS) e vários estuários na costa portuguesa. O modelo PCOMS é um modelo regional hidrodinâmico e ecológico 3D totalmente baroclínico que cobre o frente ibérico Atlântico e que fornece condições de fronteira para os modelos estuarinos. Os modelos de estuário e o PCOMS são simulados com o modelo MOHID Water. A integração e sincronização das diferentes componentes são realizadas pela ferramenta ART, uma aplicação informática para automatização de modelos.

Este conjunto de modelos uma vez combinado é capaz de preencher as lacunas na informação e melhorar os resultados de modelagem em comparação com a utilização de climatologias para os diferentes rios. A metodologia descrita é genérica e tem sido

aplicada a vários estuários na costa portuguesa para obter uma circulação costeira mais precisa e para estudar a sua influência na geração de frentes de temperatura e salinidade que são relevantes, entre outras aplicações, para a gestão da pesca na área costeira.

**Palavras-chave:** modelo MOHID, entradas de água doce, modelação numérica, estuários, Ibéria ocidental

# Acknowledgements

---

First of all, the author would like to acknowledge Prof. Ramiro Neves and Prof. Manuela Juliano, his supervisor and co-supervisor respectively. I want to thank Prof. Neves for providing me the opportunity to join his team for the last thirteen years and for encouraging me to complete this PhD. I have learned a lot with our discussions both about modelling and life. I will also like to thank Prof. Juliano for her collaboration in every project I've involved in the last few years and I'm sure that this thesis would not be the same without our long skype conversations and screen sharing. Even if the distance between our locations is large, I've felt a very close support.

I would like also to thank my family and friends that has patiently excused me for being absorbed in this research for the last few years. I would like to specially thank my wife Nana that has been truly supportive taking care of our home and our son Pablo, especially during the last writing period. I would also like to thank to my mother and brothers that have been very interested in how this work was progressing and have understood the importance that it had for me and gave me strengths for completing it.

I would like also thank to my present and past colleagues in MARETEC the support that I have received during the preparation of this thesis. I would like give some special thanks to Rodrigo Fernandes that sit next to me when both our PhD adventures started and have been completed with very similar timing. The discussions with him were the base of the development of the MARETEC operational framework resulting in the ART software which is briefly described in this thesis. I would like also to give special thanks to David Brito that believed in the usefulness of the needed developments in MOHID Land so this numerical framework could be implemented. I would also like to thank Paulo Leitão, Luis Fernandes and Guillaume Riflet for the professional and personal welcome and support I received since I joined the MARETEC research group. The author would like to acknowledge also the contributions of Hilda de Pablo, João Sobrinho, Guilherme Franz and Isabella Ascione Kenov for some of the estuarine applications and for their advice in some key moments of this research. The author would like also to thank to Ligia Pinto for helping maintaining the PCOMS system operational and for developing some tools to downloading and converting the CMEMS data into ready-to-use formats. Other current and past colleagues from MARETEC contributed to this research with tools, know-how sharing or suggestions to the completion of this thesis: i.e. Eduardo Jauch, Frank Braunschweig, Madalena Malhadas, Marcos Mateus, Susana Nunes, Carla Garcia, Sofia Saraiva and Angela Canas.

The author would like also to acknowledge also the IST meteorological group (<http://meteo.tecnico.ulisboa.pt/>) for providing the meteorological data used in this thesis, specially to Rosa Trancoso and Jorge Palma for the implementation and maintenance of the meteorological operational model MM5.

The author would like to thank to Maria Manuel Angélico and Paulo Oliveira from Portuguese Institute for Sea and Atmosphere, I.P. (IPMA IP) for providing access to the data collected during the PELAGOS11 and PELAGOS15 cruises.

The author acknowledges the ERDF funds of the Competitiveness Factors Operational Programme (COMPETE), and national funds from the Foundation for Science and Technology (FCT) (project UID/EEA/50009/2013) that funded the open access publication of Chapter VI.

The author would like to thank to the institutions that are contributing to this research by uploading their observations to data sharing initiatives such as EMODnet, CMEMS, SNIRH, etc.

During this research, the author participated and was funded by several international research projects such as:

- EMOSEM project, a two-year project (2013-2014) funded by the French National Research Agency (ANR) and the Belgian Science Policy (BELSPO) in the frame of EU FP7 ERA-NET Seas-era.
- Turnkey project - Transforming Underutilised Renewable Natural Resource into Key Energy Yields (2014-2016). Atlantic area Interreg project (Contract Number 2013-1/279) <http://www.turnkeyproject.eu/>
- EnergyMare project - Cooperation for the use of renewable energies in the Atlantic arc (2012-2015). Atlantic area Interreg project (Contract Number 2011-1/157). <http://www.energymare.eu/>
- EASYCO project - Collaborative European Atlantic Water Quality Forecasting System (2009 – 2012) project, financed by the Atlantic Area Transnational Programme of the European Commission (EC), priority 2, through the European Regional Development Fund (ERDF), (Contract Number 2008-1/002). <http://easyco.maretec.org/>
- ECOMANAGE - Integrated Ecological Coastal Zone Management System (2004-2007) Sixth Framework Programme (FP6) of the European Commission (Contract Number INCO-CT-2004-003715). [http://cordis.europa.eu/result/rcn/47746\\_en.html](http://cordis.europa.eu/result/rcn/47746_en.html)

# List of acronyms

---

ART – Automatic Running Tool

Chl  $\alpha$  – Chlorophyll  $\alpha$

CMEMS – Copernicus Marine Environment Monitoring Service

EA – East Atlantic index

EO – Earth Observation

FES2004 – Finite Element Solution, global tidal model version 2004

FES2012 – Finite Element Solution, global tidal model version 2012

IP – Iberian Peninsula

IPC – Iberian Poleward Current

IP MOHID Land – Iberian Peninsula MOHID Land application with 10 km horizontal resolution

MIP Index – Meridional Iberian Peninsula Index

MM5 – Meteorological Model 5

MSFD – EU Marine Strategy Framework Directive (Directive 2008/56/EC)

NAO – North Atlantic Oscillation

NPZD – Nutrient-Phytoplankton-Zooplankton-Detritus model

OPeNDAP – Open-source Project for a Network Data Access Protocol

PCOMS – Portuguese Coast Operational Modelling System

ROFI – Region of Fresh water Influence

SCM – Subsurface Chlorophyll Maximum

SLP – Sea Level Pressure

SSS – Sea Surface Salinity

SST – Sea Surface Temperature

TASK-2000 – Tidal Analysis Software Kit 2000

TDS - THREDDS Data Server

UWWTP – Urban Waste Water Treatment Plant

WI – Western Iberia

WI MOHID Land – West Iberia MOHID land application with 2 km horizontal resolution

WIBP – Western Iberia Buoyant Plume

WICP – Western Iberia Central Plume

WFD – EU Water Framework Directive (Directive 2000/60/EC)

WOA09 – World Ocean Atlas 2009

# Table of Contents

Abstract .....	iv
Resumo.....	v
Acknowledgements.....	vii
List of acronyms .....	ix
<b>Introduction</b>	
I.1 Introduction.....	I
I.2 Objectives.....	II
I.3 Thesis structure and rationale .....	II
I.4 Related publications, communications and awards .....	IV
I.4.1. Publications .....	IV
I.4.2. Communications in international conferences.....	IV
<b>Chapter I - The Portuguese Coast Operational Modelling Framework</b>	
1.1 Introduction .....	1
1.2 Modelling domains.....	2
1.1.1. Bathymetry.....	2
1.3 The PCOMS hydrodynamic configuration .....	2
1.4 Boundary Conditions.....	4
1.4.1. Tidal forcing.....	4
1.4.2. Atmospheric boundary conditions.....	4
1.4.3. Open ocean general circulation .....	5
1.4.4. Nutrient and oxygen initial and open boundary conditions .....	7
1.5 Operationalisation.....	8
1.5.1. The ART Software .....	8
1.5.2. The PCOMS operationalisation .....	9
1.6 Downstream services .....	10
1.6.1. Offline downscaling for coastal/estuarine applications.....	10
1.6.2. Forecast services based on PCOMS results .....	10
1.7 Conclusions .....	12
1.8 Future work.....	12
1.9 References.....	12

## Chapter II - Atmospheric variability in the Western Iberian region evaluated through numerical modelling and observations.

2.1.	Introduction .....	15
2.2.	Material and Methods.....	17
2.2.1.	Data Sources and Analysis.....	17
2.2.2.	Numerical Model and modelling domains .....	18
2.3.	Data analysis and validation.....	18
2.3.1.	Atmospheric Pressure .....	18
2.3.2.	Air Temperature .....	21
2.3.3.	Wind Intensity and direction.....	26
2.4.	Western Iberia weather climatology maps.....	33
2.4.1.	Atmospheric Pressure .....	33
2.4.2.	Air Temperature .....	36
2.4.3.	Wind intensity and direction.....	39
2.5.	Discussion.....	47
2.6.	Conclusions .....	48
2.7.	Acknowledgements.....	48
2.8.	References.....	49

## Chapter III - Evaluation of tides in 2D barotropic and 3D baroclinic numerical model applications for Western Iberia.

3.1	Introduction .....	51
3.2	Material and Methods.....	52
3.2.1.	Data Sources and Analysis.....	52
3.2.2.	Harmonic components error and previous studies .....	56
3.3	Numerical Model and modelling domains.....	57
3.4	Tidal Forcing .....	57
3.5	Tidal forcing configuration .....	58
3.6	Tidal constituents analysis and validation.....	59
3.7	Water levels and residuals analysis.....	67
3.8	Water levels spatial analysis .....	69
3.9	Conclusions .....	72
3.10	References.....	73

## Chapter IV - Evaluation of surface temperature, salinity and baroclinic circulation in Western Iberia by means of numerical modelling and remote sensing.

4.1.	Introduction .....	75
4.2.	Material and Methods.....	75
4.2.1.	Modelling results evaluation with <i>in situ</i> data .....	75
4.2.1.1.	Surface current velocities.....	76
4.2.1.2.	Surface Water temperature .....	83
4.2.1.3.	Surface Salinity .....	88
4.2.2.	Modelling results evaluation with remote sensing products.....	90
4.2.2.1.	Sea Surface Temperature (SST) .....	90
4.2.2.2.	Sea surface salinity (SSS) .....	94
4.3.	Western Iberia surface circulation climatology maps.....	97
4.3.1.	Surface currents .....	97
4.3.2.	Sea Surface Temperature.....	101
4.3.3.	Sea Surface Salinity .....	104
4.4.	Discussion and Conclusion .....	107
4.5.	References.....	109

## Chapter V - Coupling watersheds, estuaries and regional ocean through numerical modelling for Western Iberia: a novel methodology.

5.1	Introduction .....	111
5.2	Study Area .....	112
5.3	Materials and Methods.....	114
5.3.1.	Numerical models .....	114
5.3.2.	Coupling the Estuary-Ocean Interface .....	116
5.3.3.	Operational Modelling .....	118
5.4	Results and Discussion .....	118
5.4.1.	Watershed Modelling.....	118
5.4.2.	Estuarine Modelling .....	119
5.4.3.	Ocean Modelling .....	120
5.5	Conclusions .....	122
5.6	References.....	124

## Chapter VI - Coupling watersheds, estuaries and regional oceanography through numerical modelling in the Western Iberia: Thermohaline flux variability at the ocean-estuary interface.

6.1.	Introduction .....	127
6.2.	Study Area .....	128
6.3.	Material and methods.....	128
6.3.1.	Monitoring networks.....	128
6.3.2.	Numerical models .....	130
6.4.	Results and Discussion .....	132
6.5.	Conclusions .....	139
6.6.	References.....	139

## Chapter VII - Coupling of watersheds, estuaries and regional seas through numerical modelling for Western Iberia: Regional ocean sea surface salinity and temperature patterns

7.1.	Introduction .....	143
7.2.	Material and Methods.....	145
7.2.1.	Numerical modelling .....	145
7.2.2.	<i>In situ</i> observations .....	149
7.2.2.1.	IPMA Cruises .....	149
7.2.2.2.	Multiparametric buoys.....	150
7.3.	Results .....	150
7.3.1.	Model validation .....	150
7.3.1.1.	IPMA Cruises .....	150
7.3.1.2.	Multiparametric buoys.....	154
7.3.2.	Sea Surface Salinity climatology.....	156
7.3.3.	Case study: April 2013 extreme event .....	161
7.4.	Discussion.....	164
7.5.	Conclusions .....	167
7.6.	References.....	169

## Chapter VIII - Evaluation of Upwelling transport in Western Iberia through ocean circulation and meteorological numerical models.

8.1.	Introduction .....	173
8.2.	Study area and numerical model .....	174
8.3.	Data and Methods.....	174
8.3.1.	Ekman Transport Calculation .....	174
8.3.2.	Ekman Pumping.....	175

8.3.3.	Hydrodynamic model vertical transport .....	176
8.4.	Results .....	176
8.4.1.	Upwelling Index from meteorological numerical model .....	176
8.4.2.	Upwelling pumping from meteorological numerical model .....	183
8.4.3.	Vertical transport from ocean numerical model.....	189
8.4.4.	Upwelling from remote sensing and modelled SST .....	190
8.5.	Discussion.....	193
8.6.	Conclusions .....	199
8.7.	References.....	200

## Chapter IX - Comparative analysis of modelled surface and vertically integrated Chl *a* in Western Iberia waters.

9.1.	Introduction .....	205
9.2.	Study area .....	205
9.3.	Methods .....	205
9.3.1.	Numerical model and configurations.....	205
9.3.2.	Satellite products .....	206
9.4.	Validation .....	206
9.5.	Chl <i>a</i> Climatology.....	210
9.6.	Discussion and conclusions .....	216
9.7.	References.....	217

## Chapter X - Discussion, final remarks and future work

10.1.	Introduction .....	219
10.2.	Discussion.....	219
10.2.1.	Upwelling versus river nutrient discharge .....	219
10.2.2.	Influence of nutrients from land source in coastal waters .....	221
10.3.	Final remarks.....	222
10.4.	Future work.....	224
10.5.	References.....	225

## Appendix I - Additional tidal components maps

## Appendix II - Water quality module parameters

## Annex I - Thesis related publications

## Annex II - Awarded poster

# Introduction

## I.1 Introduction

Traditionally the water continuum connecting the ocean and the land areas has been studied from a fragmented perspective considering watersheds, estuaries, including their area of influence, and the open ocean as disconnected areas. Despite recent efforts to analyse the water continuum from a more holistic point of view, only few studies were made covering all the existing interfaces. This thesis aims to contribute to change this paradigm by analysing from an integrated point of view the response in the near ocean to changes in atmospheric and watershed conditions in western Iberia (Figure I.1).

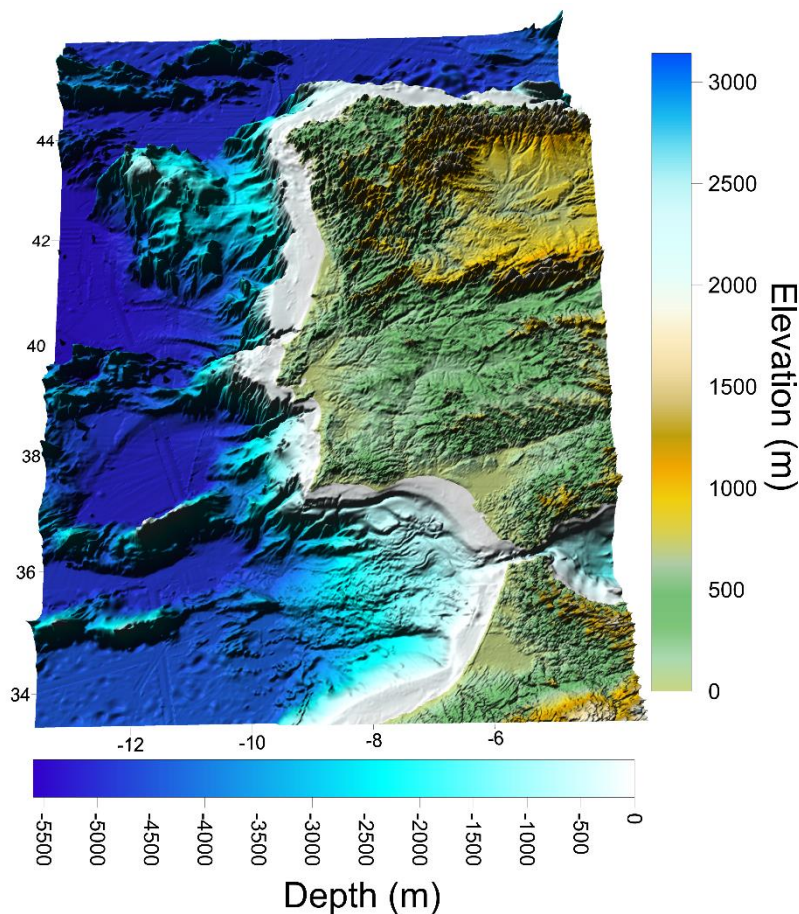


Figure I.1 Topography (source: Global 30 Arc-Second Elevation, GTOPO30) and bathymetry (derived from the EMODnet Hydrography portal, <http://www.emodnet-hydrography.eu>) for the Western Iberia.

The growing capacities of numerical models and tools allow to simulate, with sufficient detail, the temporal and spatial scales of each area of interest from the rain areas to its evacuation in the open ocean. The research presented in this thesis was performed with the aim of improving the forecasting performance of oceanographic operational services by improving the implementation of land-ocean boundary conditions. The methods developed in this research were built on existing numerical models and applications that were developed in the framework of previous projects and services. During this work, these applications were evaluated, corrected, updated and completed in order to accommodate them, without large modifications, for the desired objective.

The main output of this research consists in the development and implementation of a novel methodology to improve land-boundary conditions and thus the performance of regional ocean models. The proposed methodology was demonstrated in the Western Iberia region which is the main area of research of the MARETEC research group and allowed the author to capitalise previous efforts in numerical model implementations.

The selected study area is a good representative of the necessity of a land-ocean integrated view. Located in the westernmost limit of continental Europe, the Iberian Peninsula (IP) is regarded as the northern limit of one of the four main eastern boundary upwelling systems, the Canary Current Ecosystem (CCE). This coastal area is subjected to upwelling conditions during large periods of the year due to the predominant northern winds related to the North Atlantic Oscillation (NAO) generating southern surface coastal currents that counteract with the permanent poleward current that runs over the slope. Exposed to the open ocean atmospheric conditions, most of the Atlantic storm fronts cross this area in their way to the European continent. The rain water discharged over the IP drains two thirds of the territory to the Atlantic Ocean carrying nutrients and sediments to the coastal area. Both the rain and the upwelling patterns present spatial variability along the western coast of the IP that will be subject of this thesis.

## I.2 Objectives

In this work, the author explored individually each component of the system atmosphere, watersheds, estuaries and surface regional ocean waters with the following five objectives:

1. To gather a set of observed data to evaluate the performance of the Portuguese Coast Operational Modelling System (PCOMS). A comprehensive list of available coastal and ocean stations from several sources was collected, analysed and cleaned from outliers and suspicious observations for the 2010-2015 period. This period and modelling results will also serve as a benchmark for future PCOMS versions;
2. To describe and compare with observations each component that integrate the water cycle modelling system in order to demonstrate that the employed numerical models applications are reliable;
3. To enunciate and demonstrate a numerical modelling methodology to integrate the different components of the water cycle from the rainwater draining areas to the regional ocean waters passing through the estuarine areas;
4. To generate a preliminary climatology of the main analysed air and water properties able to characterise the processes governing the study area and to evaluate its annual and interannual variability;
5. To study two of the main processes governing the near ocean thermohaline fields in Western Iberia such as the upwelling transport and the Western Iberia Buoyant Plume (WIBP).

## I.3 Thesis structure and rationale

The initial rationale of this thesis was to publish most of contents, or at least the most originals, in international publications. This challenge was partly accomplished and several publications were produced to date. However due to the time limitation, some of the thesis chapters will be adapted for publication and submitted in the near future. This rationale conditions the conception of the thesis and each chapter was conceived in the sense that it could be published independently. For this reason, each chapter has its own description of the methods used, focusing on each chapter particularities, and includes its own bibliography. A short description of the chapters included in this thesis can be found below:

Chapter I describes the PCOMS numerical model current configuration and its boundary conditions, the operationalisation tools and philosophy, the improvements from previous versions and the provided downstream services

Chapter II evaluated the performance of the meteorological model used, the validation of the main variables affecting the ocean surface with *in situ* ocean and coastal observations and a description of its annual and interannual evolution in the studied period (2010-2015). Additionally, a new atmospheric index based in the meridional difference of atmospheric pressure in the Iberian Peninsula was defined.

In Chapter III a comprehensive analysis of the tidal data available for the Western Iberia region was gathered and the performance of the PCOMS regional ocean model when forced with the most recent versions of the FES (Finite Element Solution) global tide model (FES2012) both in barotropic (2D) and baroclinic (3D) mode was evaluated.

Chapter IV evaluated the PCOMS surface circulation, salinity and temperature for the Western Iberia region during the period 2010-2015. Modelled results were described and evaluated using a comprehensive list of *in situ* monitoring stations and SST and SSS remote sensing products.

Chapter V describes an original methodology for integrating the water cycle from the rain water to the open ocean by numerical models using an offline coupling technique. The different components of the water continuum, including watersheds, estuaries and ocean, for Western Iberia were reproduced using numerical components of the MOHID Water Modelling System (<http://www.mohid.com>).

In Chapter VI the main eight Portuguese estuaries were modelled using the MOHID Water numerical model for the period 2010-2015. Water fluxes and associated properties were computed numerically at each estuarine mouth. These results served to estimate precisely tidal prisms, tidal flows and to describe the annual evolution of water temperature and salinity at the estuarine mouths.

In Chapter VII the impact of the estuarine and river fluxes, described in previous chapters, were implemented as land-ocean boundary conditions in a regional ocean model covering the Western Iberia region. The performance of the methodology was evaluated with the aid of data from *in situ* cruises and observations and served to study the seasonal and interannual evolution of the sea surface salinity including the Western Iberia Buoyant Plume (WIBP) patterns and its interaction with the described Western Iberia Central Plume (WICP).

Chapter VIII evaluated the upwelling conditions for the Western Iberia region using as indexes the offshore and coastal Ekman transport, Ekman pumping, offshore and coastal sea surface temperature difference and vertical velocity from a 3D ocean circulation model. The methods, limitations and results for upwelling estimation methods were described and intercompared.

Chapter IX described the parameterisation of the biogeochemical module coupled the PCOMS. Modelling results were evaluated by comparing phytoplankton results with remote sensing products. Vertically integrated and surface patterns were compared and their monthly, seasonal and interannual evolution was described by generating a preliminary Chl *a* climatology for western Iberian waters.

In Chapter X some issues raised during this thesis preparation and that were not included in previous chapters are briefly presented. In addition, a summary of the main conclusions from this research along with the description of the future developments and evolution of the research here presented.

The thesis also includes two appendices and two annexes described below:

Appendix I includes the tidal harmonic components maps for western Iberian waters not included in Chapter III.

Appendix II includes the parameters of the biogeochemical model coupled to the PCOMS and presented in Chapter IX.

Annex I includes the currently published or accepted publications generated during this research that should be completed with future publication of some of this thesis contents.

Annex II includes the poster awarded as best student poster in the ECSA54 international conference (more details in section I.4).

## I.4 Related publications, communications and awards

During the preparation of this thesis, the author shared the main findings and outcomes with the scientific community by publications in international journals and book chapters and through oral and poster communications in national and international conferences. In this section, the main related publications and communications are listed.

### I.4.1 Publications

Some parts of the methodology developed and implemented in this thesis were described in a series of publications including a general description of the methodology (Campuzano *et al.*, 2016), the watershed component (Brito *et al.*, 2015) and the estuarine fluxes variability (Campuzano *et al.*, accepted). The published versions of these documents are annexed to the thesis (Annex I). Despite the author of this thesis is not the first author of Brito *et al.* (2015), he is the corresponding author of that publication and participated in the design and validation of the numerical model applications described in that article and their operationalisation. For these reasons and for the sake of completeness, the article describing the watershed component of the developed method was included in this thesis only as an annex and not as a thesis chapter. The series of publications is expected to be completed with a final publication describing the influence of this implementation in the West Iberia regional ocean, described in Chapter VIII.

- **Campuzano F**, Brito D, Juliano M, Fernandes R, de Pablo H, Neves R. Coupling watersheds, estuaries and regional ocean through numerical modelling for Western Iberia: a novel methodology. *Ocean Dynamics*. 2016; 66(12): 1745–1756. DOI: [10.1007/s10236-016-1005-4](https://doi.org/10.1007/s10236-016-1005-4).
- **Campuzano FJ**, Juliano M, Sobrinho J, de Pablo H, Brito D, Fernandes R, Neves R (2018). Coupling Watersheds, Estuaries and Regional Oceanography through Numerical Modelling in the Western Iberia: Thermohaline Flux Variability at the Ocean-Estuary Interface. In: *Estuary. W. Froneman (Ed), InTech, Rijeka, Croatia*. DOI: [10.5772/intechopen.72162](https://doi.org/10.5772/intechopen.72162).
- Brito D, **Campuzano FJ**, Sobrinho J, Fernandes R, Neves R. Integrating operational watershed and coastal models for the Iberian Coast: Watershed model implementation – A first approach. *Estuarine, Coastal and Shelf Science*. 2015; 167, Part A: 138-146. DOI: [10.1016/j.ecss.2015.10.022](https://doi.org/10.1016/j.ecss.2015.10.022).

### I.4.2 Communications in international conferences

#### I.4.2.1 Oral Communications

- **Campuzano FJ**, Brito D, Juliano M, De Pablo H, Sobrinho J, Fernandes R, Neves R. Coupling of watersheds, estuaries and regional seas through numerical modelling for Western Iberia: river discharge influence in the near open ocean. 10<sup>th</sup> HyMeX Workshop, 4-7 July 2017, Barcelona, Spain. A PDF version of the presentation is available [here](#).
- **Campuzano FJ**, Brito D, Juliano M, Fernandes R, Neves R. Coupling of watersheds, estuaries and regional seas through numerical modelling for Western Iberia. 7<sup>th</sup> Eurolag: European Coastal Lagoons Symposium, 1-4 March 2016, Murcia, Spain.

- **Campuzano FJ**, Ascione-Kenov I, Brito D, Juliano M, De Pablo H, Sobrinho J, Fernandes R, Neves R. Coupling of watersheds, estuaries and regional seas through numerical modelling for Western Iberia: Estuarine fluxes influence in the near open ocean. ECSA 56 Symposium, 4-7 September 2016, Bremen, Germany.
- **Campuzano F**, Brito D, Juliano M, Sobrinho J, Fernandes R, Pinto L, Neves R. Integração espacial e temporal por métodos numéricos dos processos associados às bacias hidrográficas, estuários e oceano regional para a costa ocidental da Península Ibérica. VIII Congresso sobre Planeamento e Gestão das Zonas Costeiras dos Países de Expressão Portuguesa. 14-16 October 2015, Aveiro, Portugal. Artigo 114. An extended abstract of the communication is available [here](#) (In Portuguese).
- **Campuzano FJ**, Kenov I, Brito D, Juliano M, Fernandes R, Pinto L, Neves R. Numerical evaluation of the river nutrients influence for the Western Iberian coastal region. 3.as Jornadas de Engenharia Hidrográfica, 24-26 June 2014, Lisbon, Portugal. Extended abstracts: 263-266. An extended abstract of the communication is available [here](#).
- **Campuzano F**, Brito D, Juliano M, Fernandes R, Neves R. Effect of the river discharge implementation in an operational model for the West Iberia coastal area. European Geosciences Union (EGU), General Assembly 2014, Vienna (Austria), 27 April-02 May 2014. The abstract of this communication is available [here](#).
- **Campuzano FJ**, Fernandes R, Leitão PC, Viegas C, de Pablo H, Neves R. Implementing local operational models based on an offline downscaling technique: The Tagus estuary case. 2.as Jornadas de Engenharia Hidrográfica, 20-22 June 2012, Lisbon, Portugal. Extended abstracts: 105-108. An extended abstract of the communication is available [here](#).

#### I.4.2.2 Posters

- **Campuzano FJ**, Brito D, Juliano M, Fernandes R, Neves R. Coupling of watersheds, estuaries and regional seas through numerical modelling for Western Iberia: a novel methodology. Copernicus Marine Week, 25-29 September 2017, Brussels, Belgium.
- **Campuzano FJ**, Kenov I, Brito D, Juliano M, Fernandes R, Pinto L, Neves R. Numerical estimation of the nutrients origin and fate for the Western Iberia coastal region. Encontro de Ciência 2016 4-6 June 2016, Lisbon, Portugal. A PDF version of the poster is available [here](#).
- **Campuzano FJ**, Kenov I, Brito D, Juliano M, Fernandes R, Pinto L, Neves R. Effect of the river discharge implementation in an operational model for the West Iberia coastal area. 7<sup>th</sup> EuroGOOS conference, 28-30 October 2014, Lisbon, Portugal. An extended abstract of the communication is available [here](#).
- **Campuzano FJ**, Kenov I, Brito D, Juliano M, Fernandes R, Pinto L, Neves R. Numerical estimation of the nutrients origin and fate for the Western Iberia coastal region. ECSA54 conference, 12-16 May 2014, Sesimbra, Portugal. Winner of the best student conference poster.

#### I.4.2.3 Awards

Award for Best Student Presentation – Poster: **Campuzano FJ**, Kenov I, Brito D, Juliano M, Fernandes R, Pinto L, Neves R. Numerical estimation of the nutrients origin and fate for the Western Iberia coastal region. ECSA 54 Symposium, 12-16 May 2014, Sesimbra, Portugal. Diploma and Poster are found in the Annex II.

#### I.4.2.4 Video Communications

- Campuzano F. Modelación numérica de procesos ecológicos e hidrodinámicos en áreas costeras y oceánicas <https://www.youtube.com/watch?v=AG06GflziCQ>. Universidad de Las Palmas de Gran Canaria, Tercer Ciclo de Ciencia compartida, n. 42. 28 May 2014, Tafira, Gran Canaria, Spain (In Spanish).
- Campuzano F. CMEMS and Nutrient Budgets assessment/Primary Production in Coastal Zones <https://www.youtube.com/watch?v=FCS1ksvurSA>. Copernicus Marine Service Regional User and Training Workshop dedicated to the IBI Area (Atlantic European South West Shelf Ocean). 10-11 December 2015, Lisbon, Portugal.

# Chapter I - The Portuguese Coast Operational Modelling Framework

## 1.1 Introduction

The Portuguese Coast Operational Modelling System (hereafter referred as PCOMS) is the operational modelling system that covers the Western Iberia regional ocean being designed to provide an operational solution for the Portuguese continental coast. This system is providing operational hydrodynamics and ecology forecasts for the Western Iberia regional ocean since 2009 and 2012 respectively, being probably the first operational model of its kind covering western Iberia. The PCOMS system has been broadly described in previous publications (Mateus *et al.*, 2012; Pinto *et al.*, 2012; Riflet *et al.*, 2007 & 2008). This chapter aims to describe the current configuration and its boundary conditions, the operationalisation tools and philosophy, the improvements from previous versions and the provided downstream services.

The initial setup, including horizontal resolution, vertical discretisation and modelling domains' limits and the atmospheric and hydrodynamic boundary conditions were defined by Paulo Leitão, Guillaume Riflet and Luís Fernandes at the MARETEC research centre (<http://maretec.org/>) from the Instituto Superior Técnico (<https://tecnico.ulisboa.pt/pt/>) part of the Universidade de Lisboa (<https://www.ulisboa.pt/>). Since 2011, Francisco Campuzano has been the main responsible of its operation, maintenance and update until its current version. In these last years, the PCOMS has improved its performance mainly due to update of the bathymetry information and to corrections in the boundary conditions relaxation definition. Additionally, the MOHID Water Quality module, basically consisting in a Nutrient-Phytoplankton-Zooplankton-Detritus (NPZD) model, was coupled to the PCOMS.

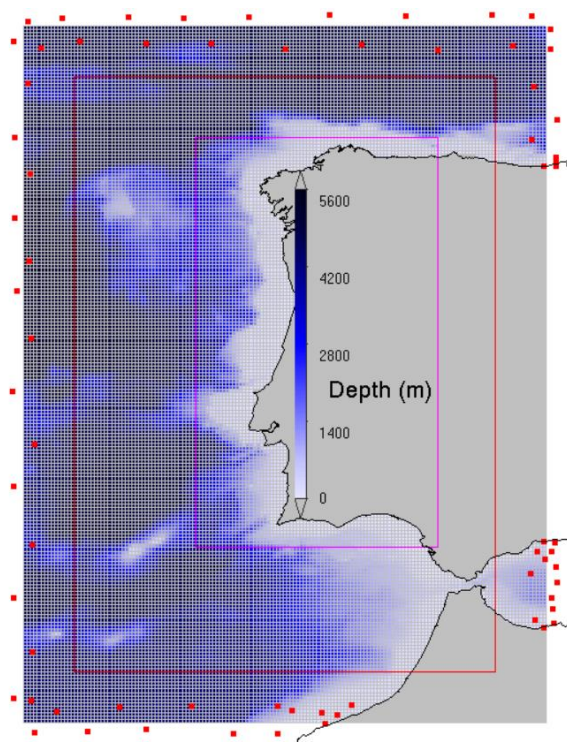


Figure 1 PCOMS regional ocean operational system domains, grids and current bathymetry. The red rectangle indicates the outer limit of the Portugal domain. The purple rectangle indicates the high frequency output window used for coastal downscaling. Red dots indicate the FES2004 virtual tidal gauges location.

## 1.2 Modelling domains

The PCOMS system is composed of two nested domains: WestIberia (2D) and Portugal (3D) covering the Iberian Atlantic coast and its contiguous ocean. The WestIberia domain covers the area limited the following range of latitudes (33.48 °N, 45.90 °N) and longitudes (4.20 °W, 13.50 °W) resulting in a grid of 207 x 155 cells with maximum depths around 5600 m. The Portugal domain covers the area comprised by the latitudes (34.38 °N, 45.00 °N) and the longitudes (5.10 °W, 12.60 °W) resulting in a grid of 177 x 125 cells and maximum depths around 5300 m. Both domains use a constant horizontal spatial resolution of 0.06°, resulting in cells approximately 6.7 km tall and 5.2 km wide. The Portugal domain is located centred in the West Iberia domain leaving 15 cells of difference in every direction (Figure 1). Vertically, the Portugal domain use a hybrid discretisation consisting of a sigma domain with 7 layers from the surface until 8.68 m depth, with variable thickness decreasing up to 1 m at the surface, on top of a Cartesian domain with 43 layers with thickness increasing towards the bottom (Table I). The vertical distribution of the Cartesian domain is inspired in vertical discretisation used by the Mercator-Océan PSY2V4 model solution that serves as initial and boundary conditions (Drillet *et al.*, 2005; hereafter referred as MERCATOR).

**Table I. Width (W) of the vertical layers (L) used by the Portugal domain of the PCOMS system. The top seven layers correspond to subdivisions of a single sigma layer (S) followed by 43 pure Cartesian layers (C).**

L	W (m)	L	W (m)						
<b>1 S</b>	0.95	<b>11 C</b>	2.46	<b>21 C</b>	13.08	<b>31 C</b>	79.89	<b>41 C</b>	295.83
<b>2 S</b>	1.13	<b>12 C</b>	2.91	<b>22 C</b>	15.87	<b>32 C</b>	94.41	<b>42 C</b>	320.69
<b>3 S</b>	1.13	<b>13 C</b>	3.29	<b>23 C</b>	18.93	<b>33 C</b>	110.55	<b>43 C</b>	344.04
<b>4 S</b>	1.22	<b>14 C</b>	3.94	<b>24 C</b>	22.95	<b>34 C</b>	128.98	<b>44 C</b>	366.20
<b>5 S</b>	1.30	<b>15 C</b>	4.52	<b>25 C</b>	27.42	<b>35 C</b>	149.03	<b>45 C</b>	386.22
<b>6 S</b>	1.48	<b>16 C</b>	5.46	<b>26 C</b>	33.13	<b>36 C</b>	171.17	<b>46 C</b>	404.68
<b>7 S</b>	1.48	<b>17 C</b>	6.36	<b>27 C</b>	39.57	<b>37 C</b>	194.54	<b>47 C</b>	420.80
<b>8 C</b>	1.78	<b>18 C</b>	7.70	<b>28 C</b>	47.56	<b>38 C</b>	219.38	<b>48 C</b>	435.34
<b>9 C</b>	1.89	<b>19 C</b>	9.08	<b>29 C</b>	56.61	<b>39 C</b>	244.68	<b>49 C</b>	447.64
<b>10 C</b>	2.23	<b>20 C</b>	11.01	<b>30 C</b>	67.56	<b>40 C</b>	270.54	<b>50 C</b>	458.63

### 1.1.1. Bathymetry

In the current version, WestIberia and Portugal domain grids are populated with bathymetric information derived from the EMODnet Hydrography portal (<http://www.emodnet-hydrography.eu>) as available in January 2012. That modification allowed improving the model performance by correcting areas with poor interpolation. That modification had a strong impact in the continental shelf where abnormal structures were corrected (Figure 2).

## 1.3 The PCOMS hydrodynamic configuration

The PCOMS model application is a 3D full baroclinic hydrodynamic and ecological regional ocean application covering the Iberian Atlantic coast and its adjacent ocean that downscales the Mercator-Océan PSY2V4 (Releases 1-4) North Atlantic solution (Drillet *et al.*, 2005). Its performance relies strongly on its core: the MOHID Water model, part of the MOHID Water Modelling System (<http://www.mohid.com>; Neves, 2013).

The MOHID Water Modelling System is open source (<https://github.com/Mohid-Water-Modelling-System>) allowing that its code is continuously improved and updated by the MOHID community. The MOHID Water model is capable of simulating a wide range of processes, i.e. hydrodynamics,

transport, water quality, oil spills, in surface water bodies (oceans, coastal areas, estuaries and reservoirs).

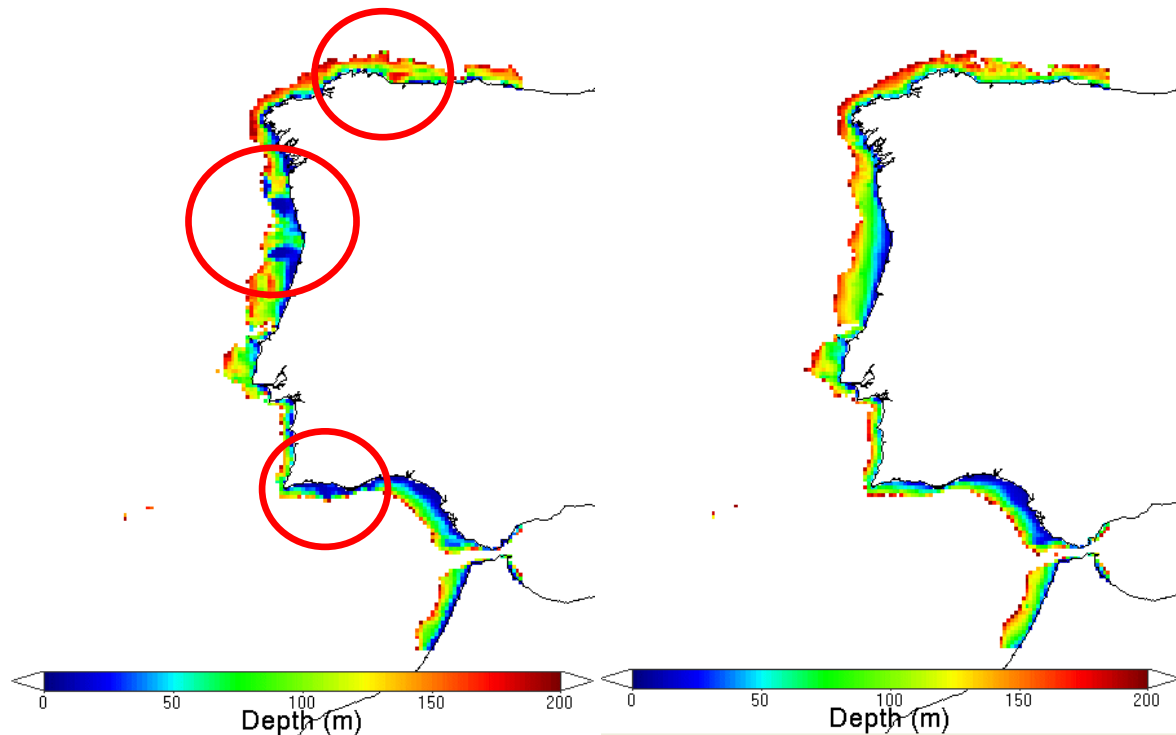


Figure 2 PCOMS bathymetry for the upper 200 m in the PCOMS original version (left) and the current version (right). Red circles indicate abnormal structures and largely modified areas by the new version.

Recently, the PCOMS benefited of the implementation of a parallelisation method following a domain decomposition approach in MOHID (Chambel-Leitão, 2014). By incorporating the Message Passing Interface (MPI) protocol, that allows high performance computing (HPC), the modelling domain is split and distributed between the cores in the computer microprocessors. By taking advantage of this development, the PCOMS system is currently running in a PC computer using six cores (one core for the Westlberia domain and five cores for the Portugal domain) and has reduced its computational running time to 50 minutes per day approximately.

The Westlberia domain (2-dimensional) is forced on its open boundary only by astronomic tides while the Portugal domain (3-dimensional) receives the water levels from the Westlberia domain and correct them at the open boundary using the MERCATOR daily water level and the inverted barometer approximation using the mean sea level pressure provided by the MM5 meteorological model (described in the next section). Water levels are also corrected in each cell of the Portugal domain by the atmospheric pressure and the winds convergence/divergence effect.

The horizontal turbulent viscosity is set to a value of  $55 \text{ m}^2\text{s}^{-1}$  for the entire domain, this value increases exponentially in the last 10 cells next to the open boundary up to  $60000 \text{ m}^2\text{s}^{-1}$ . For the vertical turbulent viscosity, the PCOMS model uses the GOTM (General Ocean Turbulence Model) model (<http://www.gotm.net>; Burchard *et al.*, 1999) coupled in the MOHID model (Ruiz-Villareal *et al.*, 2005). The module contains one-dimensional water column turbulence models library including a k- $\epsilon$  model as the Mellor-Yamada second order turbulent closure model (Mellor and Yamada, 1982) used in this application.

The Westlberia domain uses Blumberg-Kantha barotropic boundary radiation conditions (Blumberg & Kantha, 1985) for the water levels on the open boundary. The application also uses a biharmonic filter (Kantha & Clayton, 2000) that is added in the horizontal turbulent viscous flux and filters high frequency oscillations in a numerical model of advection-diffusion of a property. This term is

commonly used to dissipate the short wavelength waves without interfering with the large scale processes (Leitão, 2003). The biharmonic coefficient (B) used for the Portugal and WestIberia domain were  $5.5 \cdot 10^9 \text{ m}^4 \text{ s}^{-1}$  and  $1 \cdot 10^{10} \text{ m}^4 \text{ s}^{-1}$  respectively. The order of magnitude of that coefficient was based in the following equation:

$$B = \frac{U}{16} \cdot \delta_x^3$$

where U is a typical maximum velocity ( $0.1 \text{ ms}^{-1}$ ) and  $\delta_x$  is the horizontal cell resolution in meters.

The PCOMS application is also considering the Coriolis term and the tide potential for 12 harmonic components ( $M_2, S_2, K_2, N_2, K_1, O_1, P_1, Q_1, S_{sa}, M_m, M_f, M_3$ ) as described by Lefèvre (2000).

## 1.4 Boundary Conditions

The PCOMS results also relies on the quality of its ocean and atmospheric boundary and initial conditions. At the open boundaries, the system receives the following type of conditions: hydrodynamic, including tides and regional ocean circulation, meteorological and ecological boundary conditions. In this section, a brief description of the sources and parameters used by the PCOMS application is provided.

### 1.4.1. Tidal forcing

In the current version of the PCOMS system, tides were forced along the open ocean boundary of the WestIberia domain using the tidal harmonics components provided by the FES2012 version of the FES (Finite Element Solution) global tidal model (Carrère *et al.*, 2013). Previous versions of PCOMS were forced with the FES2004 version (Lyard *et al.*, 2006).

The implementation of those global models in the open boundary consists in *virtual tidal gauges* obtained from global tide solution along the ocean open boundary. In the case of FES2004 implementation, those stations were located at several positions (Figure 1) and the MOHID Water performed the interpolation between stations to provide the tidal conditions at each open boundary cell. In the current version of the PCOMS, FES2012 tidal conditions are directly calculated at each open boundary cell due to higher data density. Along to the provided tidal components the MOHID Water was able to include new harmonics through the admittance technique. In Chapter III, tidal components forcing, results and applications is provided in greater detail.

### 1.4.2. Atmospheric boundary conditions

The PCOMS system is forced at the atmospheric boundary by hourly results obtained from a MM5 model application (Meteorological Model 5; Grell *et al.*, 1994) based in two nested grids with a horizontal resolution of 27 km and 9 km respectively (Figure 3) implemented by the IST meteorological group (<http://meteo.tecnico.ulisboa.pt/>; Trancoso, 2012). The 27 km domain covers the Northern part of Morocco and most of the Iberian Peninsula while the 9 km domain is slightly larger than mainland Portugal. The Portugal domain is not completely covered by the 9 km domain and uses information from the 27 km domain to complete the atmospheric forcing. The information from both MM5 domains is interpolated to the PCOMS Portugal domain grid.

Once interpolated, the PCOMS atmosphere module uses the following MM5 fields: air temperature, atmospheric pressure, relative humidity, solar radiation and wind velocity X and Y components. Additionally the downward long wave radiation field is used by the interface water air module.

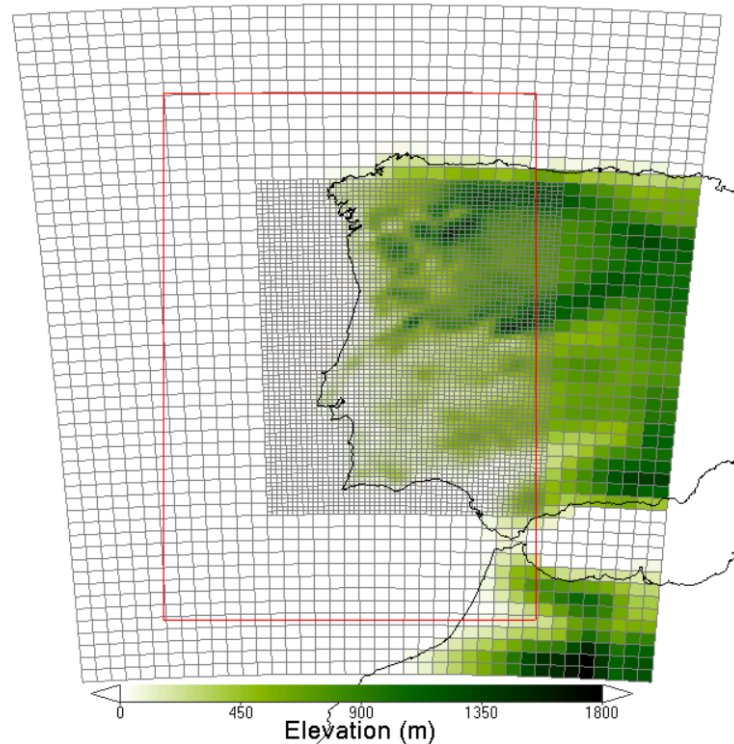


**Figure 3 Topography and nested grids (27 km and 9 km) used by the meteorological model MM5 for the Portuguese mainland application. The red box indicates the limits of the PCOMS 3D domain.**

### 1.4.3. Open ocean general circulation

The PCOMS system downscales the Mercator-Océan PSY2V4 North Atlantic solution (Drillet *et al.*, 2005; hereafter referred as MERCATOR) for the West Iberian Atlantic coast and its contiguous ocean. Since 2009, the MARETEC centre receives on a weekly basis the general circulation solution for the following 2 weeks and the analysis for the previous 2 weeks in a daily format, 28 days in total. The solution received from MERCATOR consist on the 3D hydrodynamic circulation properties for a region limited by the following range of latitudes (29.89 °N, 47.84 °N) and longitudes (3.35 °W, 14.37 °W) of 275 x 124 cells with a horizontal size of 0.08° approximately and 50 Cartesian vertical layers (Figure 4).

The PCOMS system use the available properties of the MERCATOR solution to initialize the velocity, water level and temperature and salinity fields. Additionally, those fields are used as open boundary conditions (OBCs) being included by nudging so boundary values do not diverge from the general circulation values imposed at the boundary. This is a common practice in ocean regional models especially for long-term integration (Chen *et al.*, 2013).

Currently, the PCOMS incorporates in the Portugal domain OBCs the following MERCATOR properties: U and V velocity components, water level, salinity and temperature. Previous PCOMS version implemented in 2009 disregarded the water level producing inconsistencies in the boundary that affected to the PCOMS results near the open boundary. Figure 5 illustrates the surface velocities field obtained by incorporating and excluding the water level.

The nudging technique is implemented in the model by a sponge consisting on the last 10 boundary cells where the radiation coefficients increase exponentially from  $1 \cdot 10^5$  seconds, around one day, in the outer cell to the inner cell with  $1 \cdot 10^9$  seconds. Those values implies that the PCOMS system inside the sponge is running free in relation to the general MERCATOR solution.

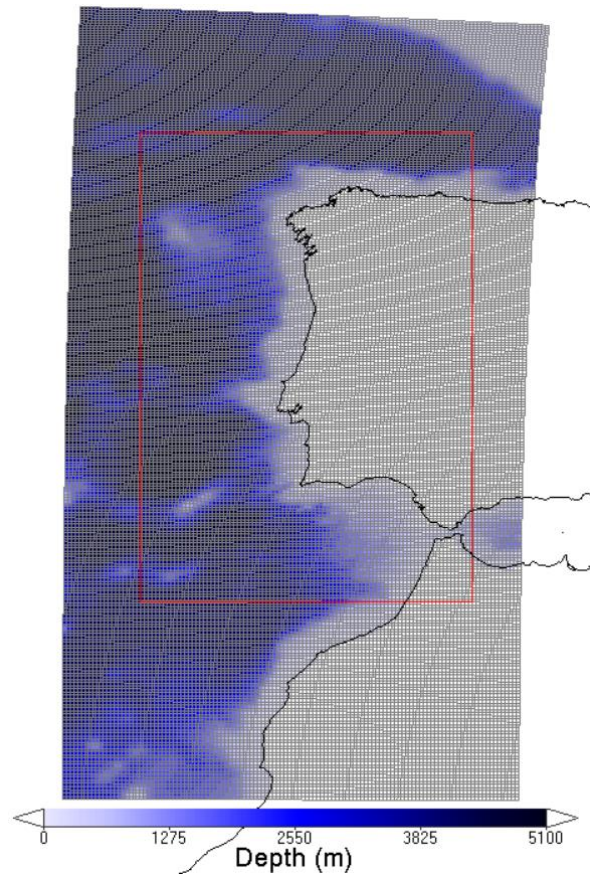


Figure 4 Bathymetry and grid of the Mercator-Océan PSY2V4 solution received weekly by the MARETEC group. The red rectangle indicates the limits of the PCOMS Portugal domain.

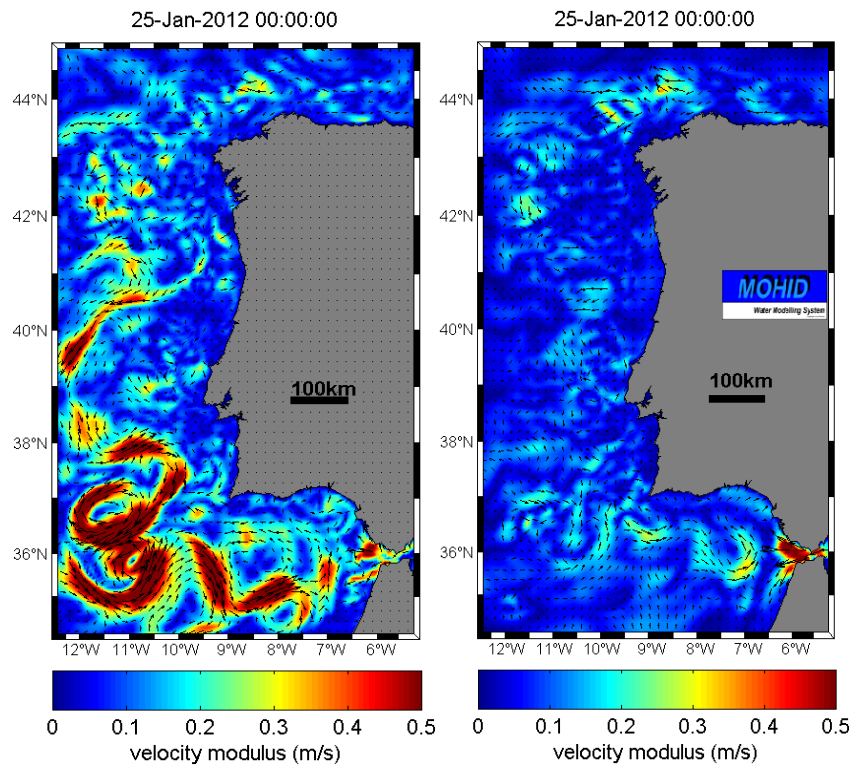


Figure 5 PCOMS surface velocity modulus for the same instant excluding (left) and including (right) the MERCATOR water levels in the open boundary condition.

#### 1.4.4. Nutrient and oxygen initial and open boundary conditions

Since 2012, the PCOMS is running coupled with a water quality module, named MOHID WaterQuality. This module includes inorganic and organic forms of nitrogen and phosphorus on its dissolved and particulate forms as the source of nutrients. Oxygen, nutrient, phytoplankton and zooplankton concentrations are modified based in the phytoplankton growth, respiration and predation by zooplankton limited by the availability of light and nutrients. In the current application the phytoplankton growth has not been limited by temperature considering the maximum optimum interval for phytoplankton growth between 10 and 25 °C.

The Portugal domain was initialised and imposed at its open boundary, in a similar fashion than the MERCATOR properties, by monthly climatological 3D fields of oxygen, nitrate and phosphate from the World Ocean Atlas 2009 (WOA09; Garcia *et al.*, 2010a and 2010b). WOA09 provides concentration profiles for 32 depths with distances between values increasing with depth starting with 10 m intervals at the surface and 500 m intervals from 2000 m depth onwards. Monthly values are only available for the top 500 meters and 1500 m for oxygen and nutrient concentrations respectively; those values were completed until the seabed using the annual average profile. In previous versions of the PCOMS, the model was forced with a monthly vertical profile extracted at the latitude 38.5 °N and longitude 12.5 °W (Figure 6). In the most recent PCOMS version, and in order to include the spatial gradients, the Portugal domain was initialised and forced on its boundary by a 3D climatology with the original horizontal resolution of the WOA09 (1° grid) (Figure 7).

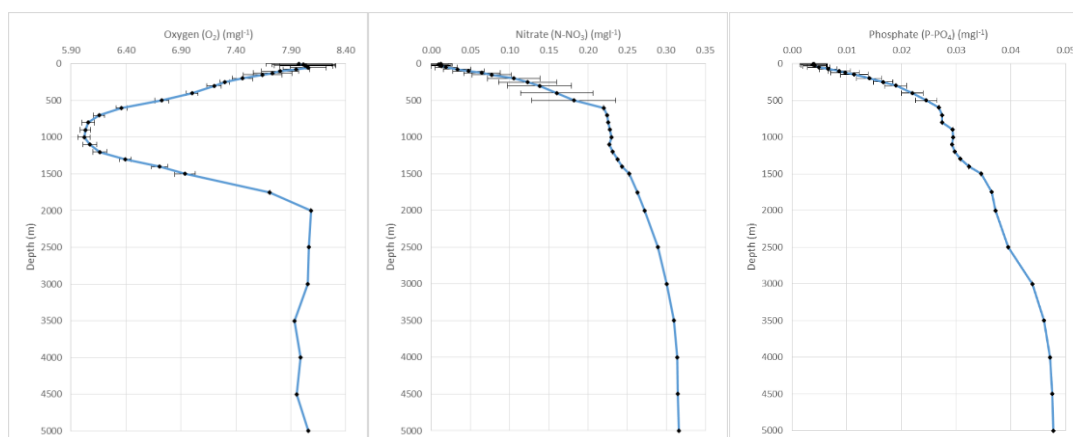


Figure 6 WOA09 oxygen (left), nitrate (centre) and phosphate (right) vertical profile at latitude 38.5 °N and longitude 12.5 °W used to force the PCOMS initial and boundary conditions. Error bars indicate the standard deviation associated to the monthly value.

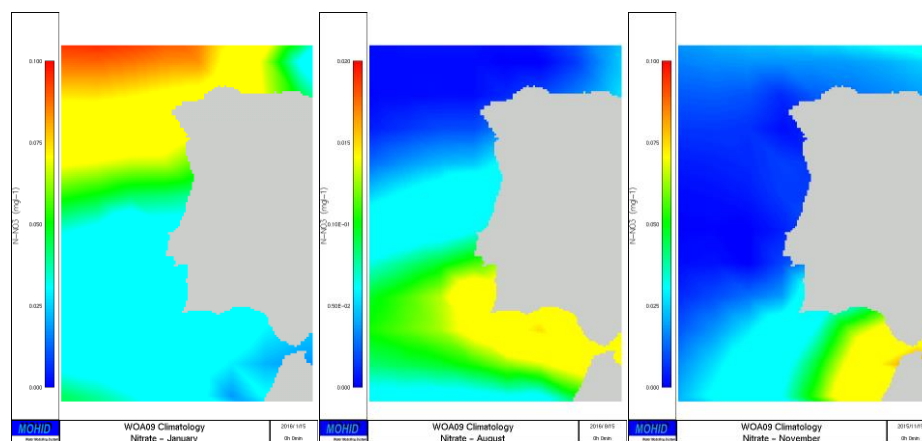


Figure 7 WOA09 N-NO<sub>3</sub> concentration for January (left), August (centre) and November (right) used to force the PCOMS initial and boundary conditions. Please note that the August scale is five times smaller than for January and November.

## 1.5 Operationalisation

The term “operational models” can be easily replaced by the term “automatic model applications”. In this section, a brief description of the rationale and software developed for the operationalisation of model applications, i.e. the PCOMS system, is provided.

### 1.5.1. The ART Software

In order to provide operational results the open boundary conditions and the numerical models need to be integrated and synchronised. The ART software (Automatic Running Tool), a software for the automation of model simulations developed at IST that is currently used to control many operational applications (Ascione Kenov *et al.*, 2014; Brito *et al.*, 2015; Campuzano *et al.*, 2012, 2013, 2014, 2016; Pinto *et al.*, 2012). The ART tool is a standalone application, independent, compiled, and able to run in any Windows operative system without any pre-requisite. Developed in .NET framework, which is oriented and deployed by a group of different end-users, allowing them to configure and customize the automatic run of a different group of numerical models, including MOHID Water, MOHID Land, WaveWatch III and WRF. The end-user is able to automatize these different models using a configuration file, with different keywords.

This tool can be seen as the “heart” of an operational framework, controlling the execution of other auxiliary standalone applications or even scripts (e.g. conversion of file formats, interpolation and specific downloading procedures), adapting automatically the configuration files and launching those applications (Figure 8). The ART tool pre-processes the boundary conditions from the different sources needed to run the model as the atmospheric models results (i.e. MM5), the global circulation model results (i.e. MERCATOR), run-off monitoring stations, etc. Right after, during the simulation phase, the ART software executes the MOHID Water or Land model using the preconfigured files and the defined model settings (OpenMP, MPI, number of processors, etc.). Finally, the operational tool finally stores, graphs and distributes 3-hour 3D model results via OPeNDAP (Open-source Project for a Network Data Access Protocol) in a THREDDS Data Server (TDS) ([http://opendap.mohid.com:8080/thredds/catalog/IST\\_MOHID\\_BIO\\_DATA/PORTUGAL\\_0.06DEG\\_50\\_L\\_3H/](http://opendap.mohid.com:8080/thredds/catalog/IST_MOHID_BIO_DATA/PORTUGAL_0.06DEG_50_L_3H/)), ftp, smartphone and webpages (i.e. <http://forecast.maretec.org/>) during the post-processor operations. Later in this thesis, when a particular application is described, the components used by the ART software will be described.

The ART tool allows the communication between different numerical models in a cascade scheme through a “trigger” technique. Downstream models have their ART software permanently detecting changes in a file that indicate that the immediate upstream model have finished running and the needed boundary conditions are stored and ready to be accessed. In that sense, ART is not an online coupling tool. It allows the management of models in an offline coupling and reduces the computational time, as different models can run in separate machines.

Other features of this tool is the possibility to define a second source of ocean and atmospheric boundary conditions in case that the first source of information fails. The ART tool informs the operator by email after the completion of a pre-processing, simulation and post-processing cycle and also in case that any operation has gone wrong attaching the log files to the email. The system also alerts the operator of the storage capacity when is below a user-defined percentage.

This software allows to automatize real time nowcast/forecast solutions, hindcast scenarios, or mixed solutions (hindcast + nowcast + forecast) also due to its simplicity allow that an operational model can be easily moved to another machine and to easily include new tools to the framework. In order to include new tools the only requirement is that the tool to be incorporated is controlled by an ASCII file where the start and end date are written with the following format:

```
START      : yyyy mm dd hh mm ss
END        : yyyy mm dd hh mm ss
```

Once the model has finished its simulation, the tools stores and backup the results in three folders for each model domain: Restart, Results\_HDF and Results\_TimeSeries. The restart folder collects the final instant files needed for continuous simulations, the Results\_HDF and the Results\_TimeSeries folders store the modelling results in HDF format, including the model window results, and MOHID TimeSeries respectively. Those folders will be accessed by the ART post processing for validation and distribution procedures and by the ART simulation process when needing of upstream boundary conditions and restart conditions for continuous simulation.

The ART tool was designed to split the simulation time into single calendar days. This approach presents several benefits. A) Storage space: the stored results consists on daily folders that are overwritten every time that a forecast is performed for that day and only preserving the latest simulation for each day as it's considered to have the most reliable external forcing (general ocean circulation, river discharge, atmospheric forcing, etc). B) Reduce downscale delivery time: Results including downscaling windows are made available as soon as the simulation of the day is finished so off-line nested models are able to copy their window of results and start simulating the same day while the parent model is continuously running the following days reducing the computing time of the overall operational system. C) Results distribution: Once a day is simulated, the results are also provided to different services as plots generation, OPeNDAP distribution, time series distribution etc. making them available as soon as they are produced.

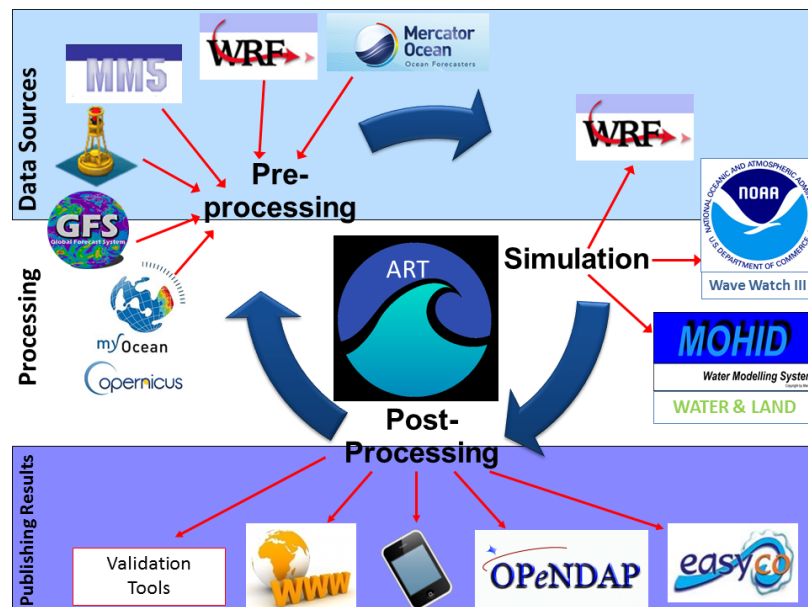


Figure 8. General scheme of the Automatic Running Tool (ART) where it can be distinguished the pre-processing, simulation and post-processing cycle of operations including some of the elements used for the MOHID Land and MOHID Water applications used in this work.

### 1.5.2. The PCOMS operationalisation

Since 2011, this PCOMS model application has been continuously in operation and running on a daily basis. Currently, the PCOMS operational model is running in two dedicated computers. The forecast application runs on a daily basis simulating the previous day, in order to use the best atmospheric forecast available, followed by 5-day forecast. On a weekly basis, when the MERCATOR solution is received, the model simulates the previous fortnight period with the best solution provided by MERCATOR. The PCOMS is not reinitialized during this procedure and is running continuously since the initialisation date in September 2009. When significant changes are incorporated into the PCOMS for a new version the system is re-run from the initialisation date.

## 1.6 Downstream services

The readiness, reliability and availability of the model results allow to develop downstream services based on the PCOMS results. Model results can be directly accessed internally by the MARETEC group and externally through the OPeNDAP TDS. In this section, some examples of services depending on the PCOMS model are described.

### 1.6.1. Offline downscaling for coastal/estuarine applications

Typical downscaling techniques, consists on running simultaneously nested models. In those cases, the running time is defined by the most downstream model which usually has the smallest time step and is the slowest model. In order to surpass this difficulty, a delayed mode (offline) technique has been designed to provide boundary conditions to the local models at the open ocean boundaries. The Window Downscaling Technique consists in saving a 3D window of model results from the PCOMS model application (Figure 1) with a high temporal resolution, 900 seconds, able to represent the main processes coming from the open ocean (i.e. the tide signal) that serve as boundary conditions to other coastal and estuarine models with higher horizontal resolution. Afterwards, in delayed mode the local model is implemented as a nested model of the window of results. The described technique allows the local model to run independently, saving running time and reducing redundancy, while improving results. This technique also does not increase the running time of the upstream models and allow running several downstream models at the same time. The window downscaling technique is implemented in several estuaries in the Portuguese coast, including the Tagus estuary, which is also able to provide boundary conditions to even more refined local models (i.e. Campuzano *et al.*, 2012).

### 1.6.2. Forecast services based on PCOMS results

The 3-hour 3D PCOMS results provided by the OPeNDAP TDS are freely available and serve to perform model result analysis (i.e. Oliveira *et al.*, 2016), to simulate transport processes including spills of inert material, hydrocarbons or the displacement of Harmful Algae Blooms as in the bi-directional tool developed during the EASYCO project (2008-1/002) and the real-time dynamic risk tool and MOHID Desktop spill simulator developed during the ARCOPOL project (2008-1/061). Also the PCOMS results are currently used to provide guidance to the European Maritime Safety Agency (EMSA) related with oil spills in continental Portugal as part of the EMSA-MARETEC agreement (CleanSeaNet). Other forecast services as the web platform developed by Action Modulers (i.e. <http://forecast.actionmodulers.com>; Figure 9) integrates the PCOMS results.

In order to easy the access to the forecast products for the general public, the PCOMS data is provided in the form of maps and time series in webpages located at <http://forecast.maretec.org>:

- Maps (<http://forecast.maretec.org/maps/>): Hourly results are automatically graphed for the main hydrodynamic and biogeochemical properties at the surface layer, generating images as shown in Figure 5. Graphs are created, updated and published automatically in the ART postprocessor phase.
- Time Series (<http://forecast.maretec.org/stations/>): hourly time series results at selected locations are extracted from modelling results and made available for analysis and forecast purposes (Figure 10). This webpage has validation purposes as allow the comparison with in situ observations obtained from the *In Situ* Thematic Assemble Centre (INS-TAC) from the Copernicus Marine Environment Monitoring Service (<http://marine.copernicus.eu/>).
- THREDDS Data Server (TDS):  
[http://opendap.mohid.com:8080/thredds/catalog/IST\\_MOHID\\_BIO\\_DATA/PORTUGAL\\_0.06\\_DEG\\_50L\\_3H/](http://opendap.mohid.com:8080/thredds/catalog/IST_MOHID_BIO_DATA/PORTUGAL_0.06_DEG_50L_3H/)

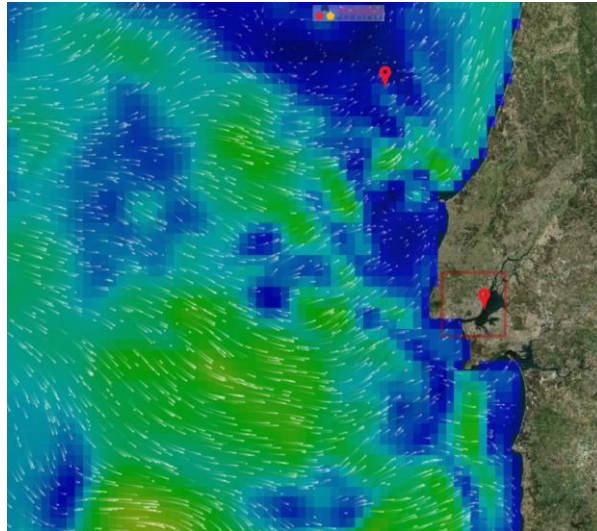


Figure 9. Snapshot of PCOMS current velocity and direction displayed in Action Modulers Forecast Service (<http://forecast.actionmodulers.com>).

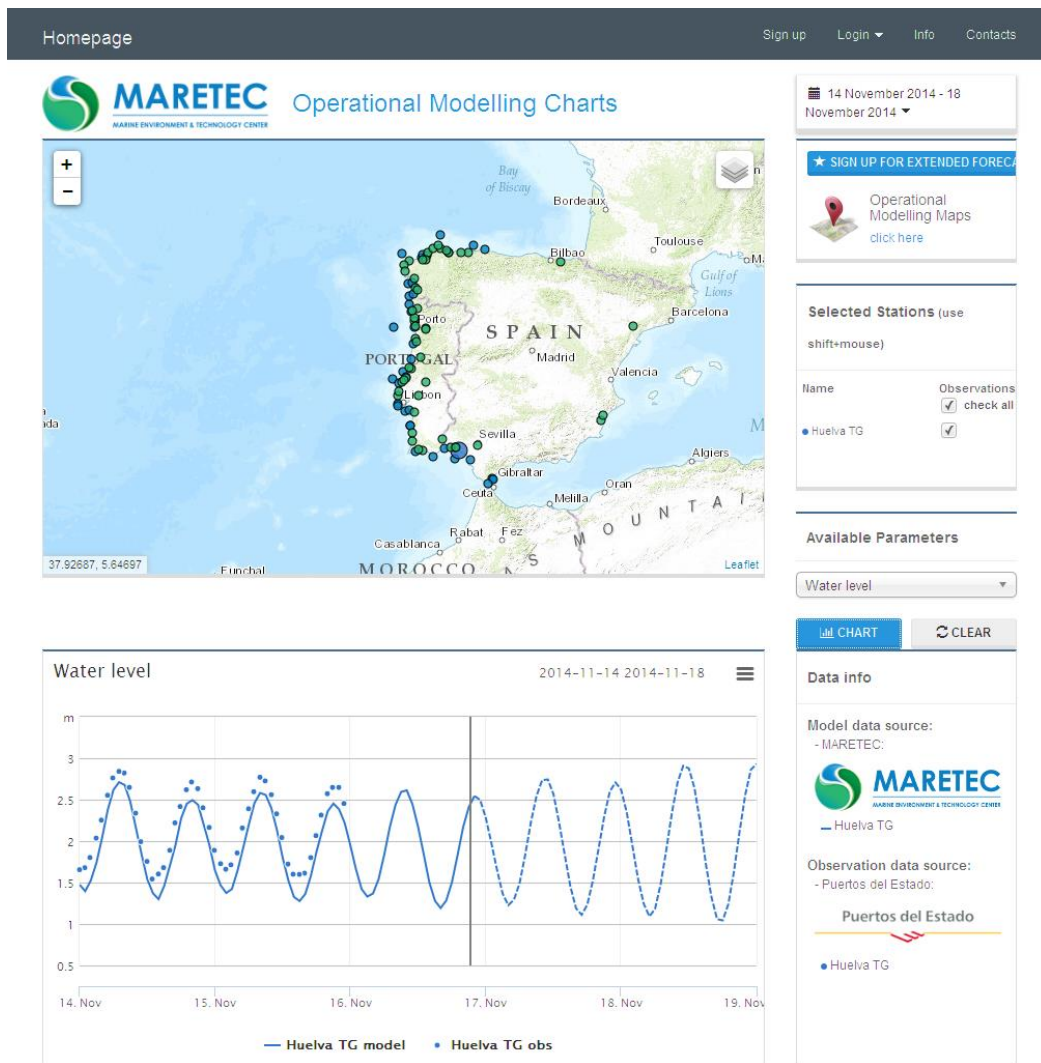


Figure 10. Screen caption of the time series distribution webpage at <http://forecast.maretec.org/stations/>. The webpage shows a map with stations that when selected shows the previous four days (solid line) and two-day forecast (dashed line). In this case, it is represented the water level at Huelva (SW Spain) and tidal gauge data (dots) observed by Puertos del Estado.

## 1.7 Conclusions

Regional models make the bridge between global circulation models and local coastal and estuarine models that are in fact the most important in terms of socio-economics. At the global scale free surface fluxes are the only relevant forcing, while at the local scale tide is often the most important forcing. Downscaling of global circulation models to force local models needs for consequence an intermediate regional model forced at the open boundary by results of a global circulation model and by a global tidal model.

The implementation of this set of models is a scientific issue of socio-economic importance allowing the development of the blue economy. Regional models must be maintained and should produce reliable results for local models and for maintaining the associated services and generate products that benefit the society as some of the described in next chapters.

## 1.8 Future work

The future evolution of the PCOMS model application will go in two directions: the integration into larger MOHID modelling systems and the improvement of the model resolution by nesting the PCOMS into the Lusitania model application (Campuzano *et al.*, 2013). That solution will allow that the PCOMS move into a finer horizontal resolution and will improve the boundary conditions at the Mediterranean Sea as the Lusitania domain include the western Mediterranean and is able to better resolve the pressure gradient that control the water exchanges with the Atlantic Ocean.

## 1.9 References

Ascione Kenov I, Campuzano F, Franz G, Fernandes R, Viegas C, Sobrinho J, de Pablo H, Amaral A, Pinto L, Mateus M, Neves R. (2014). Advances in Modeling of Water Quality in Estuaries, In: Remote Sensing and Modeling, C.W. Finkl & C. Makowski (Eds.). Springer International Publishing, pp. 237-276. DOI: [10.1007/978-3-319-06326-3\\_10](https://doi.org/10.1007/978-3-319-06326-3_10)

Blumberg AF, Kantha LH. Open boundary condition for circulation models. *Journal of Hydraulic Engineering*. 1985; 111(2): 237-55.

Brito D, Campuzano FJ, Sobrinho J, Fernandes R, Neves R. (2015). Integrating operational watershed and coastal models for the Iberian Coast: Watershed model implementation – A first approach. *Estuarine, Coastal and Shelf Science*, 167, Part A: 138-146. DOI: [10.1016/j.ecss.2015.10.022](https://doi.org/10.1016/j.ecss.2015.10.022)

Burchard H, Bolding K, Villarreal M. GOTM, a general ocean turbulence model: Theory, implementation and test cases, Rep. EUR 18745, 103 pp., Eur. Comm., 1999.

Campuzano F, Brito D, Juliano M, Fernandes R, de Pablo H, Neves R. Coupling watersheds, estuaries and regional ocean through numerical modelling for Western Iberia: a novel methodology. *Ocean Dynamics*. 2016; 66(12): 1745–1756. DOI: [10.1007/s10236-016-1005-4](https://doi.org/10.1007/s10236-016-1005-4)

Campuzano FJ, Fernandes R, Leitão PC, Viegas C, de Pablo H, Neves R. Implementing local operational models based on an offline downscaling technique: The Tagus estuary case. 2.as Jornadas de Engenharia Hidrográfica, 20-22 June 2012, Lisbon, Portugal. Extended abstracts: 105-108.

Campuzano FJ, Juliano M, Fernandes R, Pinto L, Neves R. Downscaling from the deep ocean to the estuarine intertidal areas: an operational framework for the Portuguese exclusive economic zone. 6th SCACR – International Short Course/Conference on Applied Coastal Research, 4-7 June 2013, Lisbon, Portugal.

Campuzano FJ, Kenov I, Brito D, Juliano M, Fernandes R, Pinto L, Neves R. Numerical evaluation of the river nutrients influence for the Western Iberian coastal region. 3.as Jornadas de Engenharia Hidrográfica, 24-26 June 2014, Lisbon, Portugal. Extended abstracts: 263-266.

Carrère L, Lyard F, Cancet M, Guillot A, Roblou L. FES2012: A new global tidal model taking advantage of nearly 20 years of altimetry. Proceedings of 20 Years of Altimetry meeting. Venice, Italy, 24-29 September 2013.

Chambel-Leitão P. MOHID parallelization following a domain decomposition approach. Technical Report, 33 pp, 2014. Available at: [Mohid MPI DomainDecomposition.pdf](#)

Drillet Y, Bourdalle-Badi R, Siefrid L, Le Provost C. Meddies in the Mercator North Atlantic and Mediterranean Sea eddy-resolving model. Journal of Geophysical Research. 2005; 110(C3): C03016. DOI: [10.1029/2003JC002170](#).

Garcia HE, Locarnini RA, Boyer TP, Antonov JI, Baranova OK, Zweng MM, Johnson DR (2010a). World Ocean Atlas 2009, Volume 3: Dissolved Oxygen, Apparent Oxygen Utilization, and Oxygen Saturation. S. Levitus, Ed. NOAA Atlas NESDIS 70, U.S. Government Printing Office, Washington, D.C., 344 pp.

Garcia HE, Locarnini RA, Boyer TP, Antonov JI, Zweng MM, Baranova OK, Johnson DR (2010b). World Ocean Atlas 2009, Volume 4: Nutrients (phosphate, nitrate, silicate). S. Levitus, Ed. NOAA Atlas NESDIS 71, U.S. Government Printing Office, Washington, D.C., 398 pp.

Kantha LH, Clayson CA (2000). Numerical Models of Oceans and Oceanic Processes. International Geophysics Series. Volume 66. Academic Press.

Leitão P C (2003). Integração de escalas e de processos na modelação no ambiente marinho. PhD thesis. Technical University of Lisbon, Portugal.

Lefèvre F (2000). Modélisation des marées océaniques à l'échelle globale : assimilation de données in situ et altimétriques. PhD thesis. Université Toulouse III - Paul Sabatier, France.

Lyard F, Lefevre F, Letellier T, Francis O (2006). Modelling the global ocean tides: modern insights from FES2004, Ocean Dynamics, 56: 394-415.

Mateus M, Riflet G, Chambel P, Fernandes L, Fernandes R, Juliano M, Campuzano F, de Pablo H, Neves R (2012). An operational model for the West Iberian coast: products and services, Ocean Science, 8: 713-732.

Mellor GL, Yamada T. Development of a turbulence closure model for geophysical fluid problems, Reviews of Geophysics. 1982; 20(4): 851–875. DOI: [10.1029/RG020i004p00851](#).

Neves R (2013). The MOHID concept. In: Ocean modelling for coastal management - Case studies with MOHID. M. Mateus & R. Neves (eds.), IST Press, Lisbon, Portugal, pp. 1-11.

Oliveira PB, Santos M, Moita T, Amorim A. Circulação costeira no barlavento Algarvio no verão e outono de 2015. 4.as Jornadas de Engenharia Hidrográfica, 21-23 June 2016, Lisbon, Portugal. Extended abstracts: 199-202.

Pinto L, Campuzano FJ, Fernandes R, Fernandes L, Neves R. An operational model for the Portuguese coast. 2.as Jornadas de Engenharia Hidrográfica, 20-22 June 2012, Lisbon, Portugal. Extended abstracts: 85-88.

Riflet G, Juliano M, Fernandes L, Leitão PC, Neves R. Operational ocean forecasting of the portuguese waters. Mercator-Ocean Quarterly Newsletter. 2008; 30: 20-32.

Riflet G, Leitão PC, Fernandes R, Neves RJJ. A simple pre-operational model for the portuguese coast. In: CMNE/XXVIII CILAMCE, 13-15 June 2007, Porto, Portugal

Ruiz-Villareal M, Bolding K, Burchard H, Demirov E (2005). Coupling of the GOTM turbulence module to some three-dimensional ocean models, In: Marine Turbulence: Theories, Observations, and

Models. Results of the CARTUM Project, H.Z. Baumert, J.H. Simpson & J. Sundermann (eds.), Cambridge University Press. pp 225-237.

Trancoso AR (2012). Operational modelling as a tool in wind power forecast and meteorological warnings. PhD Thesis, Instituto Superior Técnico, Universidade Técnica de Lisboa, 146p.

# Chapter II - Atmospheric variability in the Western Iberian region evaluated through numerical modelling and observations.

---

## Abstract

In this chapter, the performance of the MM5 meteorological model application for Western Iberia is evaluated using *in situ* data collected by multiparametric ocean buoys and coastal stations equipped with meteorological sensors for the period 2010-2015. As a result, the ability and the uncertainty to reproduce by numerical models the main meteorological variables that affects the ocean in this ocean region are quantified.

MM5 results were used to generate a preliminary climatology for the Western Iberia ocean region. Also a new atmospheric index based in the meridional difference of atmospheric pressure in the Iberian Peninsula was defined. This chapter provides support to the evaluation of other ocean processes analysed in this thesis such as tides, upwelling processes and regional circulation patterns.

## 2.1. Introduction

Meteorological variables such as wind intensity and direction, air temperature and atmospheric pressure influence coastal and regional hydrodynamics by modifying water level, sea surface temperature, coastal circulation, upwelling intensity and front generation. In recent years, meteorological models have emerged as a powerful tool for simulating and forecasting the atmospheric processes and their temporal evolution and spatial distribution. As a key component of the regional ocean operational models, the inherent error in meteorological variables is consequently transferred to the ocean variables forecasts. So far most of this kind of applications has been validated inland where most of the atmospheric sensors are located.

The Western Iberia region is located in the easternmost limit of the North Atlantic atmospheric system. The North Atlantic air circulation is dominated by the North Atlantic Oscillation (NAO) which consists in the atmospheric pressure difference between the Icelandic low- and the Azores high-pressure centres (Ottersen *et al.*, 2001; Hurrell and Dickson, 2005). The NAO variation is a major driving force of the climatic systems of the northern hemisphere linked to the temporal physical and ecological patterns, the buoyancy driven ocean circulation and coastal currents (Ottersen *et al.*, 2001).

A high or positive index is characterised by an intense Icelandic Low and a strong Azores High while the negative phase the sea level pressure (SLP) gradient reduces. As air flows counter clockwise around low pressure systems and clockwise around high pressure systems in the northern hemisphere, westerly winds occurs throughout the year in middle latitudes (Figure 1). The wind intensities are related to the pressure gradient and thus westerly winds are strongest during winter when the Icelandic low-pressure centre predominates. In the subtropical Atlantic north-easterly winds, also known as trade winds, are relatively steady but strongest during summer favouring the upwelling transport along the eastern Atlantic coasts when the Azores high-pressure cover almost all the North Atlantic.

In terms of air temperature, western Iberia climate can be classified in the temperate type group according to the Köppen climate classification with air temperatures for the hottest month higher

than 10°C and temperature of the coldest month lower than 18°C (Peel *et al.*, 2007). Within this group, most of western Iberia would be classified as temperate Mediterranean climate (Csb), including the western coast of Portugal and Galicia except the valleys of the Tagus and Sado that are classified as warm Mediterranean Climate (Csa), along with the southern coast and Portugal and the Gulf of Cádiz area. Only a minor part in the Western Galicia coast is classified as temperate Oceanic climate (Cfb).

To illustrate the mean atmospheric conditions for the Western Iberian region in the context of the North Atlantic system, mean values for sea level pressure, air temperature and wind intensity and direction were computed for the first decade of the XXI century from the NCEP FNL Operational Model Global Tropospheric Analyses (Figure 1; NCEP/NWS/NOAA/U.S. Department of Commerce, 2000).

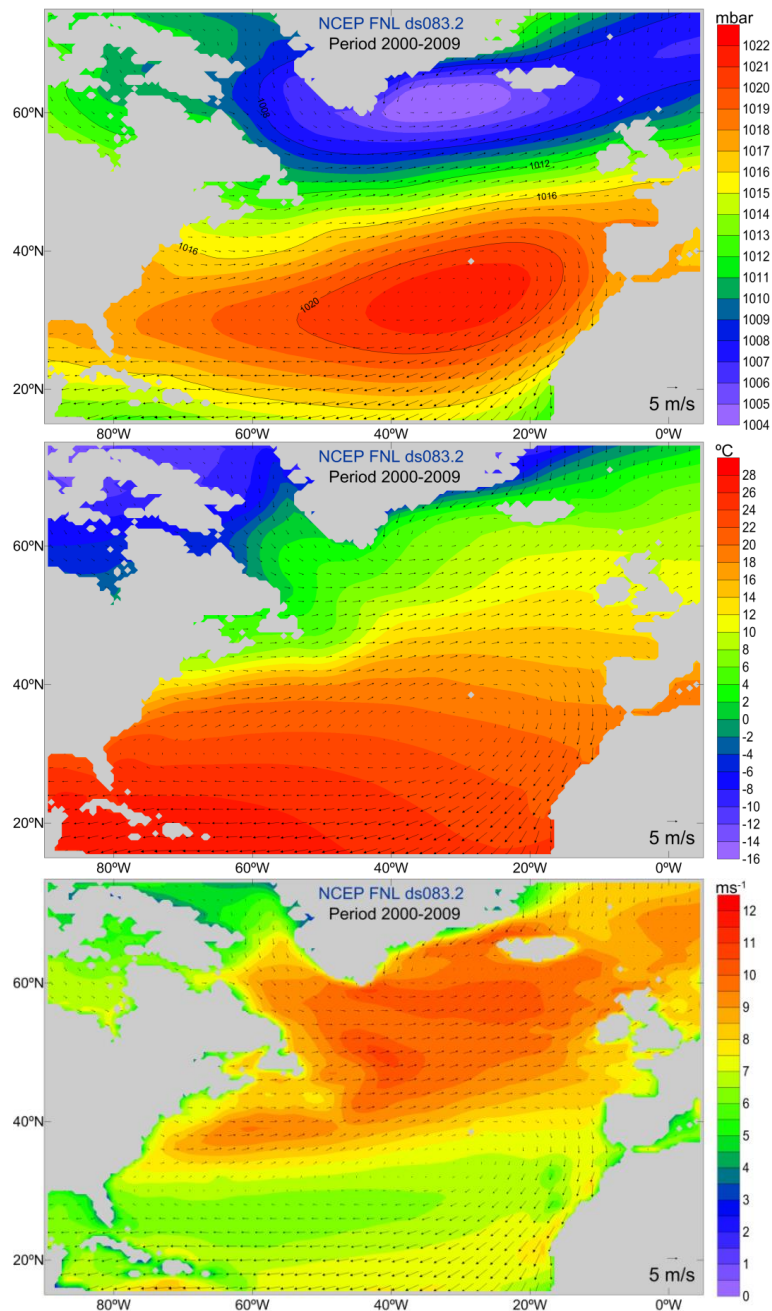
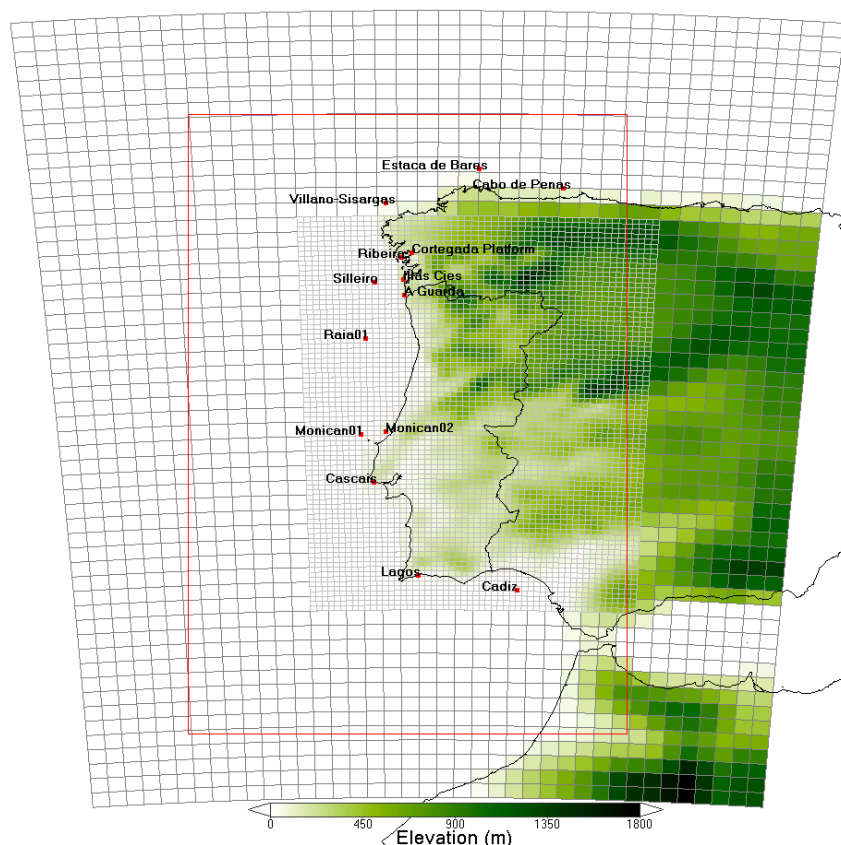


Figure 1 Mean values for sea level pressure (top), air temperature (middle) and wind speed at 10 m in  $\text{ms}^{-1}$  (bottom) in the North Atlantic Ocean for the period 2000-2009 from the NCEP FNL Operational Model Global Tropospheric Analyses. Black arrows indicate the wind direction and intensity.

## 2.2. Material and Methods

### 2.2.1. Data Sources and Analysis

Along the Western Iberia coast, several buoys and platforms equipped with meteorological sensors are maintained by Portuguese and Spanish institutions (Table I; Figure 2). The collected observations include meteorological variables such as air temperature, atmospheric pressure, wind intensity and wind direction.



**Figure 2** MM5 modelling domains (27 km and 9 km) and location of the monitoring stations used in this chapter. The red box indicates the limits of the PCOMS 3D domain and the colour scale represents the terrain elevation.

In recent times, public access through online services to operational monitoring platforms in European waters, and more particularly along the Iberian Peninsula (IP), has been granted through several initiatives being probably the more important the Copernicus Marine Environment Monitoring Service (CMEMS; <http://marine.copernicus.eu/>), through its *In Situ* Thematic Assembly Centre (INS-TAC). That service grants access to observations collected by the Puertos del Estado (Spain), Xunta Galicia/MeteoGalicia/IM (Spain) and Instituto Hidrográfico (Portugal). Additionally, two other Portuguese meteorological stations, Cascais and Lagos, maintained by the Instituto Geográfico and providing information online ([www.igeo.pt/](http://www.igeo.pt/)) completed the analysed dataset.

In total, meteorological variables for 14 stations were collected, processed and their outliers were removed for the 2010-2015 period (Table I). This set of stations represents adequately the western Iberia climate variability with a distribution covering the entire coastline and including both ocean and coastal stations. Ocean stations are more representative of the open ocean climate while coastal locations illustrate the land influence in the seafront meteorological variables.

Table I. Ocean and coastal buoys equipped with meteorological sensors used in this study indicating their location, available data period and meteorological variables observed: Air Temperature (AT), Atmospheric Pressure (AP) and Wind. The superscript next to the station name indicates the institution responsible for the tidal gauge: <sup>1</sup> stations maintained by Puertos del Estado (Spain), <sup>2</sup> stations maintained by Xunta Galicia/MeteoGalicia/IM (Spain), <sup>3</sup> stations maintained by Instituto Hidrográfico (Portugal) and <sup>4</sup> stations maintained by Instituto Geográfico (Portugal). Stations are listed from North to South and coastal stations are indicated with \*.

Monitoring Station	Lat.	Long.	Data Period	AT	AP	Wind
Estaca de Bares <sup>1</sup>	44.06 °N	7.62 °W	01/01/2010 - 31/12/2015	✓	✓	✓
Cabo de Peñas <sup>1</sup>	43.73 °N	6.19 °W	01/01/2010 - 31/12/2015	✓	✓	✓
Villano-Sisargas <sup>1</sup>	43.49 °N	9.21 °W	01/01/2010 - 31/12/2015	✓	✗	✓
Cortegada Platform <sup>2,*</sup>	42.63 °N	8.78 °W	01/01/2010 - 31/12/2015	✓	✗	✓
Ribeira <sup>2,*</sup>	42.55 °N	8.95 °W	01/01/2012 - 31/12/2015	✓	✗	✓
Illas Cíes <sup>2,*</sup>	42.17 °N	8.91 °W	01/01/2010 - 31/12/2015	✓	✗	✓
Silleiro <sup>1</sup>	42.12 °N	9.40 °W	01/01/2010 - 31/12/2015	✓	✗	✓
A Guarda <sup>2,*</sup>	41.90 °N	8.90 °W	06/06/2011 - 31/12/2015	✓	✗	✓
Raia01 <sup>3</sup>	41.16 °N	9.56 °W	12/06/2010 - 31/12/2015	✓	✗	✓
Monican02 <sup>3,*</sup>	39.56 °N	9.21 °W	12/06/2010 - 31/12/2015	✓	✓	✓
Monican01 <sup>3</sup>	39.51 °N	9.64 °W	14/03/2010 - 31/12/2015	✓	✓	✓
Cascais <sup>4,*</sup>	38.69 °N	9.42 °W	01/01/2010 - 31/12/2015	✓	✓	✗
Lagos <sup>4,*</sup>	37.10 °N	8.67 °W	01/01/2010 - 31/12/2015	✓	✓	✗
Cádiz <sup>1</sup>	36.84 °N	6.98 °W	01/01/2010 - 31/12/2015	✓	✓	✓

### 2.2.2. Numerical Model and modelling domains

The MM5 model (Meteorological Model 5; Grell *et al.*, 1994) was implemented for Western Iberia by the IST meteorological group (<http://meteo.tecnico.ulisboa.pt>; Trancoso, 2012) and their results are currently forcing the PCOMS modelling system. The application consists in two nested domains with horizontal resolution of 9 and 27 km (Figure 2). The outer domain covers the area limited the following range of latitudes (33.12°N, 46.78°N) and longitudes (1.39°W, 15.61°W) with a grid of 39x54 cells that includes the Western Iberia region and its contiguous ocean. Nested to the previous domain, a finer domain provide results with higher spatial resolution to mainland Portugal and its near ocean. This domain covers the area comprised by the latitudes (36.45°N, 43.26°N) and the longitudes (4.54°W, 10.74°W).

For the each monitoring station and variable, hourly model results for the period 2010-2015 were extracted from the model best forecasts in the corresponding model domain cell. Most of the analysed stations fall within the 9 km domain except for the three northernmost stations (Estaca de Bares, Cabo de Peñas and Villano-Sisargas) that are located in the 27 km domain (Figure 2).

## 2.3. Data analysis and validation

### 2.3.1. Atmospheric Pressure

Seven oceanic buoys provide atmospheric pressure data in Western Iberia: Estaca de Bares and Cabo de Peñas in the North of the IP; Monican02, Monican01 and Cascais in the centre of Portugal; and

Lagos and Cádiz in Southern Iberia. Table II lists the mean, minimum and maximum values for each station. In order to avoid the influence of possible remaining outliers, the 5<sup>th</sup> percentile ( $P_{05}$ ) and 95<sup>th</sup> percentile ( $P_{95}$ ) were considered as the minimum and maximum data respectively.

**Table II. Mean observed and modelled SLP expressed in mb and coefficient of determination ( $R^2$ ) for modelled and observed datasets. The 5<sup>th</sup> percentile ( $P_{05}$ ) and 95<sup>th</sup> percentile ( $P_{95}$ ) for both datasets are included within brackets. Coastal buoys are indicated with \*.**

Station Name	Mean Observed Atmospheric Pressure in mb ( $P_{05} - P_{95}$ )	Mean Modelled Atmospheric Pressure in mb ( $P_{05} - P_{95}$ )	$R^2$	N (Valid %)
Estaca de Bares	1019.28 (1005.00 – 1033.00)	1019.17 (1005.40 – 1032.38)	0.99	32 304 (61.87 %)
Cabo de Peñas	1018.45 (1003.00 – 1032.00)	1018.30 (1003.45 – 1031.33)	0.98	47 882 (91.71 %)
Monican02	1019.31 (1007.32 – 1031.74)	1019.34 (1007.78 – 1031.63)	0.99	24 773 (51.25 %)
Monican01	1019.09 (1007.34 – 1031.34)	1018.72 (1006.84 – 1031.05)	0.98	22 228 (44.02 %)
Cascais*	1021.16 (1009.67 – 1033.00)	1018.32 (1006.90 – 1030.02)	0.98	44 280 (84.81 %)
Lagos*	1018.99 (1009.00 – 1030.00)	1017.83 (1008.08 – 1028.62)	0.98	45 360 (86.88 %)
Cádiz	1017.14 (1008.00 – 1028.00)	1017.29 (1008.38 – 1027.95)	0.97	45 425 (87.01 %)

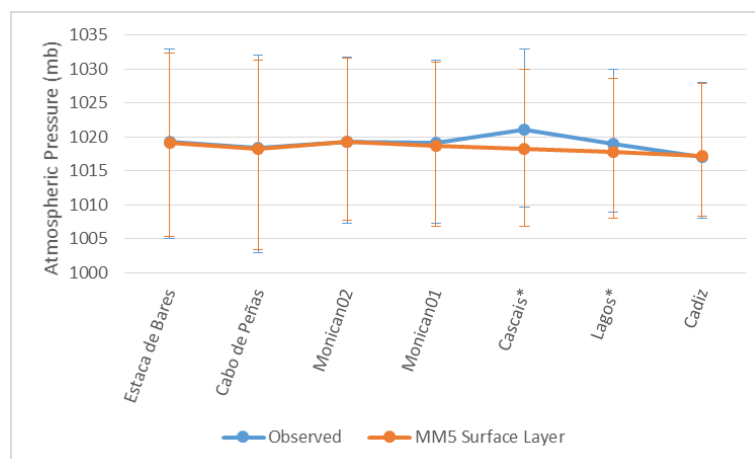


**Figure 3 Mean observed (blue) and modelled (orange) sea level pressure in the Western Iberia region for the period 2010-2015. Monitoring stations are ordered from North to South (left to right). Bars indicate maximum ( $P_{95}$ ) and minimum value ( $P_{05}$ ). Coastal buoys are indicated with \*.**

Mean SLP from MM5 model results and observations present a high level of agreement with coefficient of determination ( $R^2$ ) higher than 0.97 for each of the stations. Observed and modelled atmospheric pressure draw a latitudinal gradient decreasing southwards with the only exception of the Cascais station (Figure 3). The SLP range, regarded as the difference between maximum and minimum value, also reduces from southwards from around 29 to 20 mb. Atmospheric pressures observed at Cascais station present a permanent difference of 3 mb with the average, maximum and minimum modelled values (Table II, Figure 4). That difference could be due to sensor calibration in the monitoring station or due to the model resolution that is not adequate to represent the observed values in this station located in a sheltered coastal bay. MM5 model results are able to represent extreme atmospheric low and high pressure values as those observed during the low pressure events in January 2013 and November 2014 with SLP values under 980 mb and high pressure events in February 2012 and January 2015 with values over 1040 mb (Figure 4).



**Figure 4** Observed (grey) and modelled (orange) sea level pressure in the Western Iberia region for the period 2010-2015. Monitoring stations are ordered from North to South (left to right and top to bottom).

MM5 monthly averaged atmospheric pressure show the typical weather cycle in the Iberian Peninsula: during summer periods, atmospheric pressure increases as the Azores High approach the Iberian Peninsula by the North. During this period, Estaca de Bares and Cabo de Peñas stations registered higher pressures than southern stations generating a gradient that enhances upwelling-favourable wind conditions (positive differences) (Figure 5). During winter the situation is inverted and northern stations present lower atmospheric pressure than in the southern part of IP generating enabling southern winds circulation and favouring downwelling wind conditions (negative differences). Following this simplistic approach, upwelling events in the western Iberian coast will take place mainly during the summer period. Nonetheless, upwelling conditions were also registered during winter months (DJF) such in February 2012 and December 2014 (Figure 5). The atmospheric pressure difference between the northernmost station (Estaca de Bares) and the southernmost

station (Cádiz) were considered to quantify the meridional SLP gradient in Western Iberia. This SLP difference will be referred hereafter as the Meridional Iberian Peninsula Index (MIP Index).

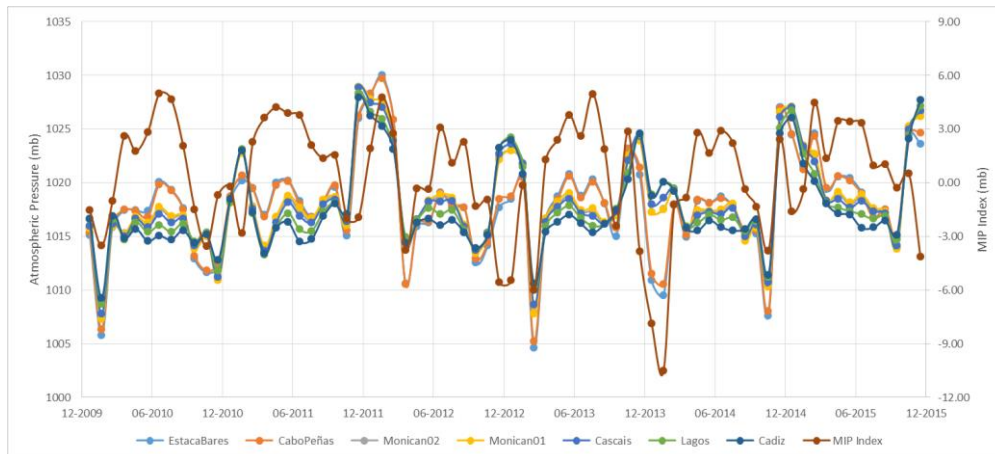


Figure 5 MM5 monthly averaged atmospheric pressure for the Western Iberia stations and MIP index.

The SLP gradient in the IP (MIP index) describes a clear annual pattern when the interannual monthly average is derived for the entire period (Table III, Figure 6). During the summer period (JJA), positive differences reach a maximum generating wind from high pressure areas (North) to low pressure areas (South) while during the winter period (NDJ) the opposite situation takes place with winds blowing from the south although in a lesser degree. Both patterns start to manifest in the previous month and extent to the first month of the following season. Maximum positive and negative differences are obtained in July and January respectively. On the other hand, March, April and October present on average SLP latitudinal gradients lower than 1 mb.

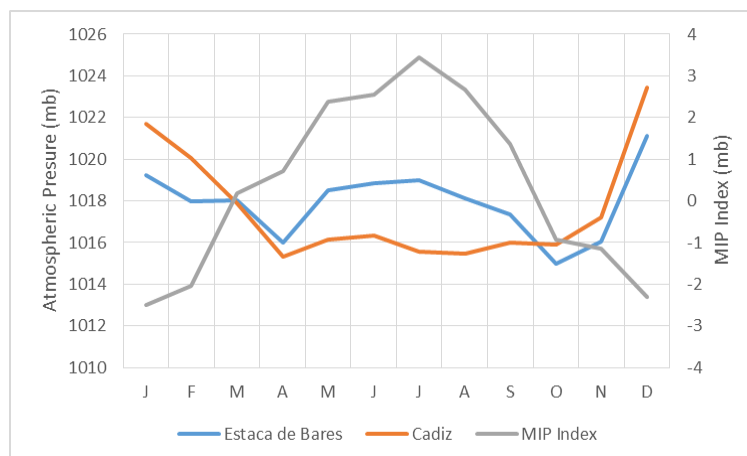


Figure 6 MM5 monthly SLP climatology for the Western Iberia for the most distant stations (Estaca de Bares and Cádiz) and Meridional Iberian Peninsula Index (MIP Index).

### 2.3.2. Air Temperature

In western Iberia, mean air temperature increases southwards with total difference between the two most distant stations around 3°C (Table IV, Figure 7). MM5 model results are able to reproduce the observed air temperature values with a coefficient of determination higher than 0.75 for all the stations (Table IV, Figure 8). In general, air temperature range ( $P_{95}$  minus  $P_{05}$ ) is larger in coastal stations with values from 10°C up to 16°C (Figure 7). Mean values from observed data could be biased due to data collection problems that for some stations could be higher than half of the total observing period (i.e. Monican01 and Raia01) because observing failures tend to concentrate during the winter season associated to rough sea periods (Figure 8).

Table III. Mean modelled monthly and seasonal SLP for the most distant stations (Estaca de Bares and Cádiz) and the Meridional Iberian Peninsula Index (MIP)

Month	Estaca de Bares	Cádiz	MIP Index
January	1019.22	1021.71	-2.49
February	1017.98	1020.04	-2.05
March	1018.03	1017.86	0.17
April	1016.00	1015.30	0.70
May	1018.51	1016.13	2.38
June	1018.86	1016.32	2.54
July	1019.01	1015.58	3.44
August	1018.10	1015.44	2.66
September	1017.37	1016.00	1.36
October	1014.96	1015.88	-0.92
November	1016.03	1017.19	-1.16
December	1021.13	1023.43	-2.30
Spring	1017.52	1016.43	1.09
Summer	1018.66	1015.77	2.88
Autumn	1016.11	1016.35	-0.25
Winter	1019.49	1021.77	-2.29

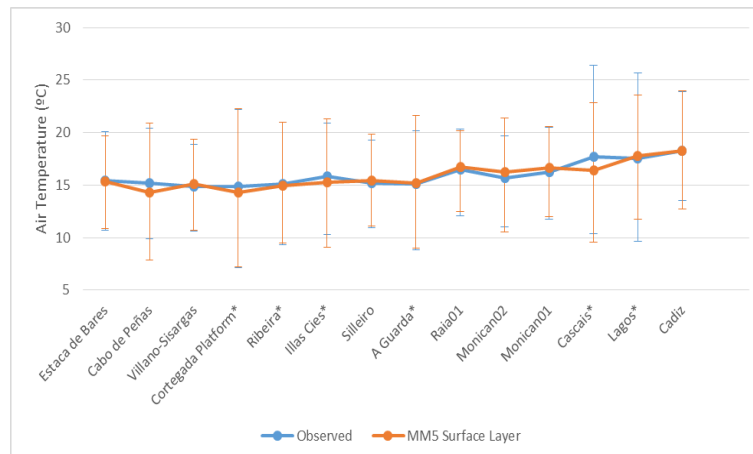


Figure 7 Mean observed (blue) and modelled (orange) air temperature in the Western Iberia region for the period 2010-2015. Monitoring stations are ordered from North to South (left to right). Bars indicate maximum ( $P_{95}$ ) and minimum value ( $P_{05}$ ). Coastal buoys are indicated with \*.

Differences between observed and modelled air temperatures are larger in coastal buoys that are affected in a higher degree by land heating and cooling processes. In fact, maximum air temperatures for coastal stations, such as Cascais and Lagos, are underestimated (more than 1 °C difference) by the modelling results (Figure 8). Also in A Guarda buoy, maximum temperature is overestimated and minimum temperature is underestimated for Illas Cíes station (more than 1°C difference). In the case of Cabo de Peñas station, model results present slightly lower mean and minimum values than observed probably to the location of this station in the 27 km model domain where the modelling cell is under the influence of the land (Figure 2). In conclusion, it can be stated that MM5 model application represents successfully, for the scope of the work, the ocean and coastal air temperature patterns for the Western Iberia region as average deviation from maximum and minimum values are below 1°C difference.

Table IV. Mean,  $P_{05}$  and  $P_{95}$  for observed and simulated air temperature and coefficient of determination ( $R^2$ ) for each monitoring station ordered from North to South. The number of available data is also indicated as well as the percentage of valid observations for the period 2010-2015. Coastal buoys are indicated with \*.

Station Name	Mean Observed Air Temperature in °C ( $P_{05} - P_{95}$ )	Mean Modelled Air Temperature in °C ( $P_{05} - P_{95}$ )	$R^2$	N (Valid %)
Estaca de Bares	15.44 (10.70 – 20.09)	15.38 (10.88 – 19.71)	0.95	32 304 (61.75 %)
Cabo de Peñas	15.17 (9.90 – 20.40)	14.33 (7.86 – 20.90)	0.83	44 543 (85.32 %)
Villano-Sisargas	14.87 (10.60 – 18.90)	15.10 (10.70 – 19.34)	0.92	47 073 (90.16 %)
Cortegada Platform *	14.85 (7.17 – 22.23)	14.31 (7.22 – 22.30)	0.88	46 965 (89.96 %)
Ribeira *	15.12 (9.34 – 20.96)	14.96 (9.51 – 20.96)	0.88	29 919 (85.47 %)
Illas Cíes *	15.81 (10.32 – 20.86)	15.30 (9.09 – 21.32)	0.81	37 338 (71.52 %)
Silleiro	15.16 (10.90 - 19.30)	15.45 (11.09 - 19.84)	0.90	46 254 (88.59 %)
A Guarda *	15.10 (8.85 - 20.16)	15.20 (8.97 - 21.61)	0.76	28 759 (77.24 %)
Raia01	16.46 (12.04 - 20.36)	16.72 (12.47 - 20.19)	0.89	21 095 (43.64 %)
Monican02	15.67 (11.02 - 19.69)	16.21 (10.52 - 21.36)	0.78	24 749 (51.20 %)
Monican01	16.27 (11.77 - 20.47)	16.67 (11.97 - 20.61)	0.91	21 628 (42.83 %)
Cascais *	17.66 (10.33 - 26.42)	16.44 (9.56 - 22.86)	0.81	43 142 (82.63 %)
Lagos *	17.53 (9.65 - 25.67)	17.76 (11.78 - 23.56)	0.87	45 352 (86.87 %)
Cádiz	18.30 (13.50 - 23.90)	18.23 (12.71 - 23.98)	0.92	46 413 (88.90 %)

MM5 monthly averaged air temperature shows the typical boreal weather cycle with maximum values observed during summer period (JJA) and minimum values during winter months (DJF) with small interannual variation (Figure 9). The meridional thermal gradient is maintained during the entire analysed period. The temperature series also shows how abrupt changes in atmospheric pressure (Figure 5) are associated with air temperature variations such as the event registered in February-March 2012.

MM5 interannual monthly averages show that minimum air temperature are reached in February while maximum values are observed during August (Figure 10). Differences between most distant stations can reach up to nearly 5°C in May while in December that difference reduces to only 2°C.

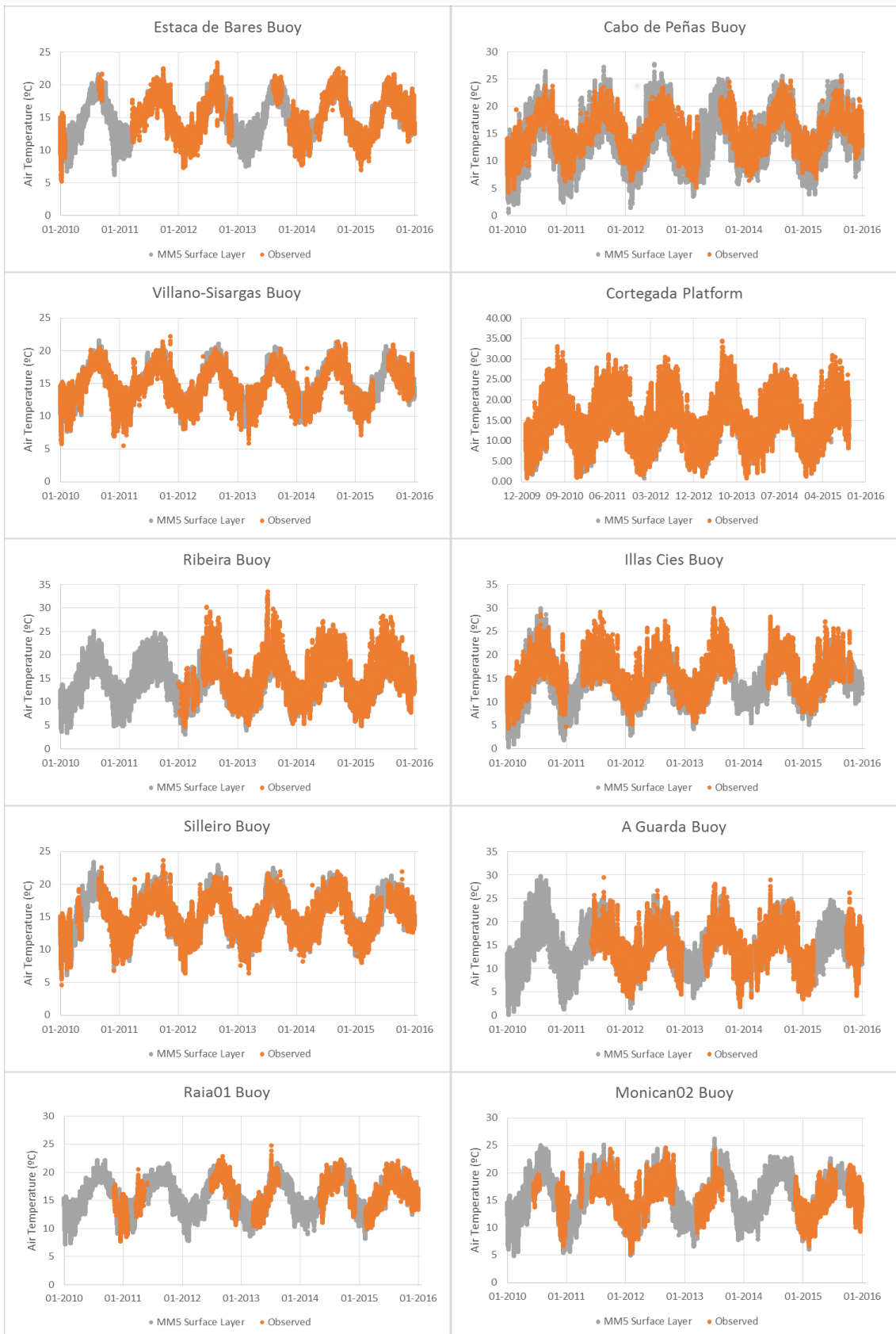


Figure 8 Observed (grey) and modelled (orange) air temperature in the Western Iberia region for the period 2010-2015. Monitoring stations are ordered from North to South (left to right and top to bottom).

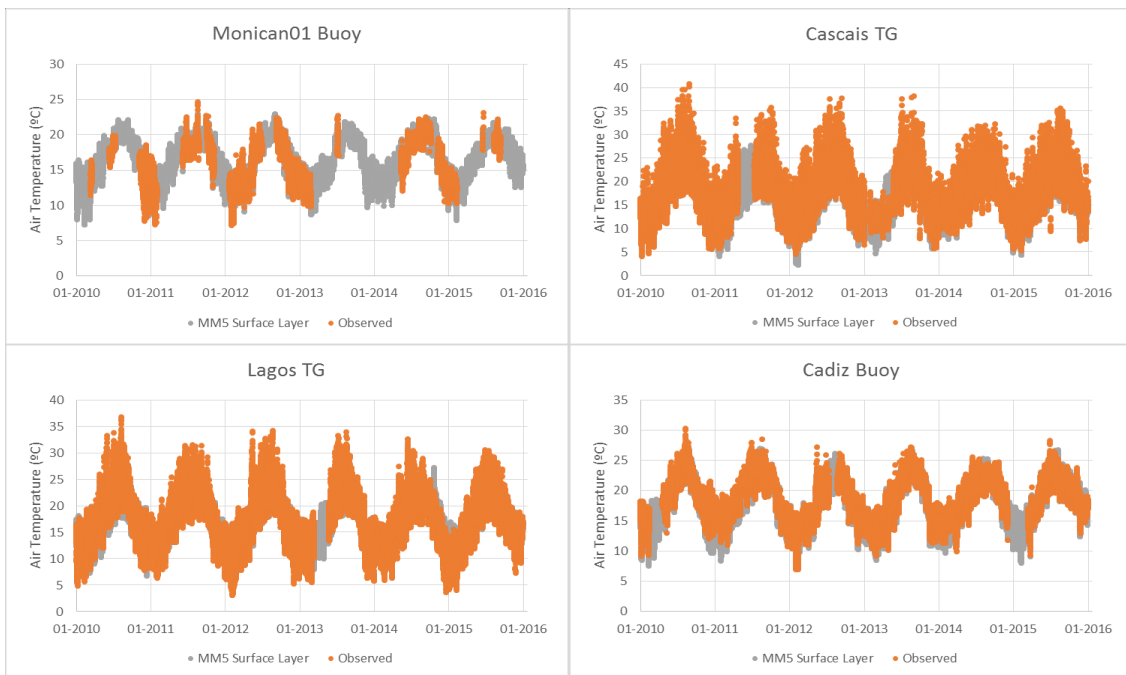


Figure 8 Cont. Observed (grey) and modelled (orange) air temperature in the Western Iberia region for the period 2010-2015. Monitoring stations are ordered from North to South (left to right and top to bottom).

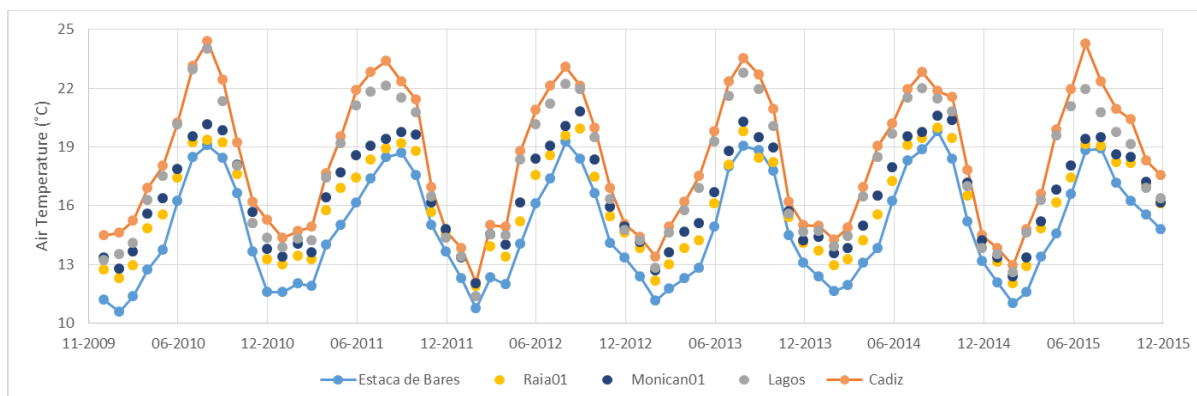


Figure 9 MM5 monthly averaged air temperature for several stations in the Western Iberia region including the northernmost (Estaca de Bares, blue line) and southernmost (Cádiz, orange line) stations.

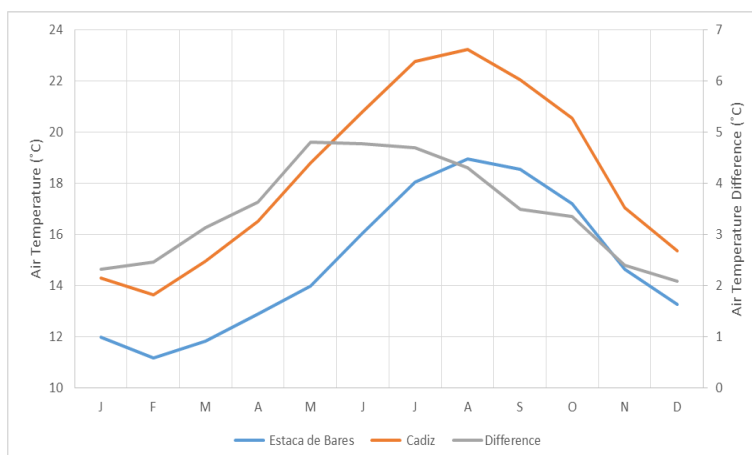


Figure 10 MM5 monthly climatology air temperature for the Western Iberia and difference between the most distant stations (Estaca de Bares and Cádiz).

### 2.3.3. Wind Intensity and direction

Wind intensity and direction govern the hydrodynamic and ecological processes in the IP Atlantic coasts. Western Iberia coastal orientation can be simply regarded as three sides of a rectangle where northern and southern coast have an East-West orientation while the western coast faces the Atlantic with a north-south orientation. Due to this coastal configuration, wind direction favouring upwelling/downwelling conditions is different for each coastal section. Zonal winds condition the upwelling conditions as eastern winds favour upwelling conditions while western winds support downwelling conditions in the Northern section and vice versa for the southern coast. In the western coast are the meridional winds that play the leading role as northern winds enhance upwelling conditions while southern winds favour downwelling conditions.

The velocity range will be used in this section as an indicator of maximum wind speeds as the 5<sup>th</sup> percentile ( $P_{05}$ ) could be regarded as the maximum velocity in the negative sense of the axis (East and South for the U and V wind components respectively) and the 95<sup>th</sup> percentile ( $P_{95}$ ) in the positive sense of the axis (West and North for the U and V wind components respectively). Maximum modulus ( $\bar{U}$ ) is thus calculated as  $(U_{range}^2 + V_{range}^2)^{1/2}$ .

From the results, two clear gradients can be observed (Table V, Figure 11): a meridional gradient and an off-shore in-shore gradient. Maximum wind speed is observed in Villano-Sisargas station with values around  $25 \text{ ms}^{-1}$  while Cortegada Platform, the most inshore station, presents values under  $19 \text{ ms}^{-1}$  and Cádiz buoy, the southernmost station, registered also values around  $20 \text{ ms}^{-1}$  (Figure 12). Observed values in A Guarda station are higher than expected according to that rationale probably due to some local features.

Observed data presented in Table V can be biased due to the quality and quantity data. Some stations have managed to stay operational during long periods of the studied period reaching high percentages of available data, up to 90% (i.e. Cabo de Peñas). In the other hand, Portuguese stations have registered satisfactorily winds between 36% and 52% of the total analysed period and data failures tend to concentrate during the winter season (Figure 13).

The alongshore component is the prevailing wind direction (indicated in bold in Table V) in the monitoring stations. Villano-Sisargas station due to its location in the North-western part of the study domain present similar intensities in both directions. While Estaca de Bares, Cabo de Peñas in the North and Cádiz in the south have the zonal direction as their main axis of variation, western monitoring stations have the meridional direction as their main vector of variation.

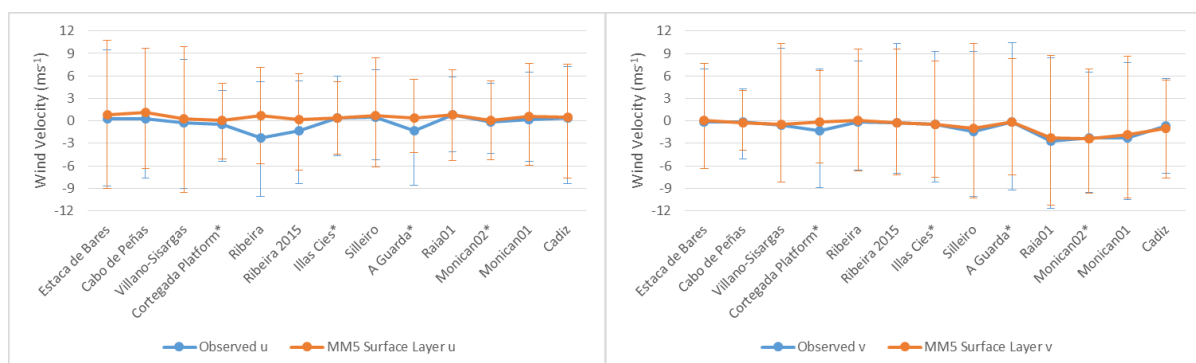


**Figure 11 Mean observed (blue) and modelled (orange) wind velocity for zonal wind, u-component, (top) and the meridional wind, v-component, (bottom) in the Western Iberia region for the period 2010-2015. Monitoring stations are ordered from North to South (left to right). Bars indicate maximum ( $P_{95}$ ) and minimum value ( $P_{05}$ ). Coastal buoys are indicated with \*.**

Table V. Mean observed and modelled wind velocity and coefficient of determination ( $R^2$ ) between both datasets for each wind component (U and V). The wind component (Comp.) with larger range of values is marked in bold. The 05<sup>th</sup> percentile ( $P_{05}$ ) and 95<sup>th</sup> percentile ( $P_{95}$ ) for observed and modelled wind velocity are included within brackets. The number of available data is also indicated as well as the percentage of valid observations for the period 2010-2015. Buoys are listed from North to South and those located close to the coastal area are indicated with an \*. The Ribeira buoy has two set of values: one for the entire analysed period and other only considering the year 2015.

Station Name	Comp.	Mean Observed Wind ( $P_{05} - P_{95}$ )	Mean Modelled Wind ( $P_{05} - P_{95}$ )	$R^2$	Obsv. $\bar{U}_{range}$	MM5 $\bar{U}_{range}$	N (Valid %)
Estaca de Bares	<b>U</b>	0.26 (-8.73 – 9.52)	0.86 (-9.05 – 10.76)	0.87	22.58	24.28	31 325 (60.00 %)
	V	-0.15 (-6.39 – 6.90)	0.03 (-6.36 – 7.68)	0.70			
Cabo de Peñas	<b>U</b>	0.33 (-7.69 – 9.70)	1.16 (-6.37 – 9.74)	0.80	19.73	17.95	47 010 (90.04 %)
	V	-0.15 (-5.03 – 4.29)	-0.24 (-3.89 – 4.05)	0.43			
Villano-Sisargas	U	-0.26 (-9.07 – 8.18)	0.31 (-9.61 – 9.91)	0.83	24.81	26.90	44 338 (84.92 %)
	V	-0.54 (-8.12 – 9.71)	-0.50 (-8.14 – 10.37)	0.77			
Cortegada Platform*	U	-0.52 (-5.41 – 4.10)	0.03 (-5.11 – 4.98)	0.20	18.56	15.96	39 949 (76.52 %)
	<b>V</b>	-1.31 (-8.96 – 6.98)	-0.13 (-5.59 – 6.77)	0.47			
Ribeira	U	-2.31 (-10.08 – 5.23)	0.66 (-5.71 – 7.19)	0.09	21.13	20.75	25 704 (73.43 %)
	V	-0.13 (-6.59 – 7.97)	0.06 (-6.66 – 9.61)	0.50			
Ribeira 2015	U	-1.33 (-8.43 – 5.37)	0.21 (-6.55 – 6.33)	0.73	22.15	21.18	8 712 (24.89 %)
	<b>V</b>	-0.25 (-6.98 – 10.35)	-0.22 (-7.23 – 9.58)	0.70			
Illas Cíes*	U	0.35 (-4.63 – 6.00)	0.38 (-4.48 – 5.26)	0.47	20.43	18.35	32 592 (62.43 %)
	<b>V</b>	-0.45 (-8.12 – 9.33)	-0.50 (-7.56 – 7.99)	0.63			
Silleiro	U	0.54 (-5.22 – 6.87)	0.74 (-6.20 – 8.46)	0.74	22.75	25.34	42 106 (80.65 %)
	<b>V</b>	-1.42 (-10.04 – 9.23)	-0.94 (-10.29 – 10.37)	0.86			
A Guarda*	U	-1.35 (-8.59 – 5.56)	0.39 (-4.22 – 5.53)	0.54	24.26	18.28	26 487 (66.53 %)
	<b>V</b>	-0.11 (-9.28 – 10.43)	-0.18 (-7.16 – 8.31)	0.74			
Raia01	U	0.86 (-4.09 – 5.84)	0.86 (-5.28 – 6.86)	0.63	22.42	23.34	24 261 (50.19 %)
	<b>V</b>	-2.64 (-11.67 – 8.42)	-2.30 (-11.21 – 8.72)	0.88			
Monican02*	U	-0.15 (-4.37 – 4.98)	0.08 (-5.18 – 5.33)	0.65	18.64	19.63	24 778 (51.26 %)
	<b>V</b>	-2.24 (-9.57 – 6.56)	-2.37 (-9.63 – 6.94)	0.80			
Monican01	U	0.22 (-5.38 – 6.53)	0.57 (-5.92 – 7.65)	0.78	23.33	21.88	18 263 (36.17 %)
	<b>V</b>	-2.23 (-10.55 – 7.81)	-1.80 (-10.29 – 8.69)	0.87			
Cádiz	<b>U</b>	0.42 (-8.36 – 7.23)	0.49 (-7.69 – 7.57)	0.78	20.10	20.08	46 146 (88.39 %)
	V	-0.69 (-6.98 – 5.71)	-0.97 (-7.63 – 5.42)	0.69			

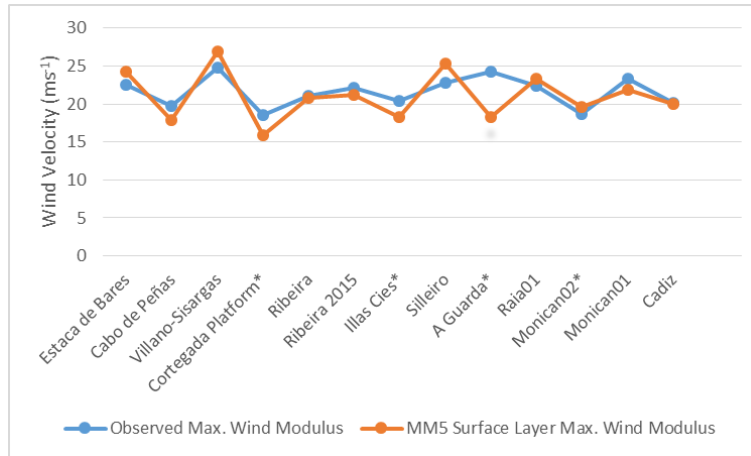


**Figure 12** Mean observed (blue) and modelled (orange) maximum wind velocity for each station in the Western Iberia region for the period 2010-2015. Monitoring stations are ordered from North to South (left to right). Coastal buoys are indicated with \*.

When dealing with observed data, its reliability is an important subject as sometimes it is not trivial to separate the invalid from the valid values, especially when the suspicious data is located within the possible range of values. In order to illustrate this challenge, the Ribeira buoy was used as example. This buoy mean value, ranges and coefficient of determination have been calculated for the entire dataset and for the year 2015 (Table V). When considering only the year 2015, the coefficient of determination between modelling results and observed values improves dramatically and allow determining the dominant wind direction. The common zero hypotheses indicating that observed values are free of error and that models should approximate to them as much as possible is questioned here. Though this is a dramatic example, some of the observed data should be also regarded as valid with some caution as it is acknowledged the great challenge of maintaining instrumentation calibrated in off-shore buoys during long periods. Modelling results play here an important role in identifying miscalibrated monitoring sensors and aiding to complete the datasets.

MM5 modelling results are able to represent quite accurately the alongshore wind components with coefficients of determination up to 0.88 (Table V). On the contrary, model performance with cross-shore winds is lower. On average the capacity to simulate cross-shore wind intensities decreases more than 15% when compared with the alongshore component. Coefficients of determination are also lower in coastal stations when compared with off-shore stations due to the model resolution and to the influence of local factors such as topography.

Since one of the main objectives of this thesis is related to the evaluation of the upwelling processes, which are controlled by alongshore winds, it can be assumed that the model is fitted for this purpose and represents satisfactory the wind intensity and direction (Figure 13).

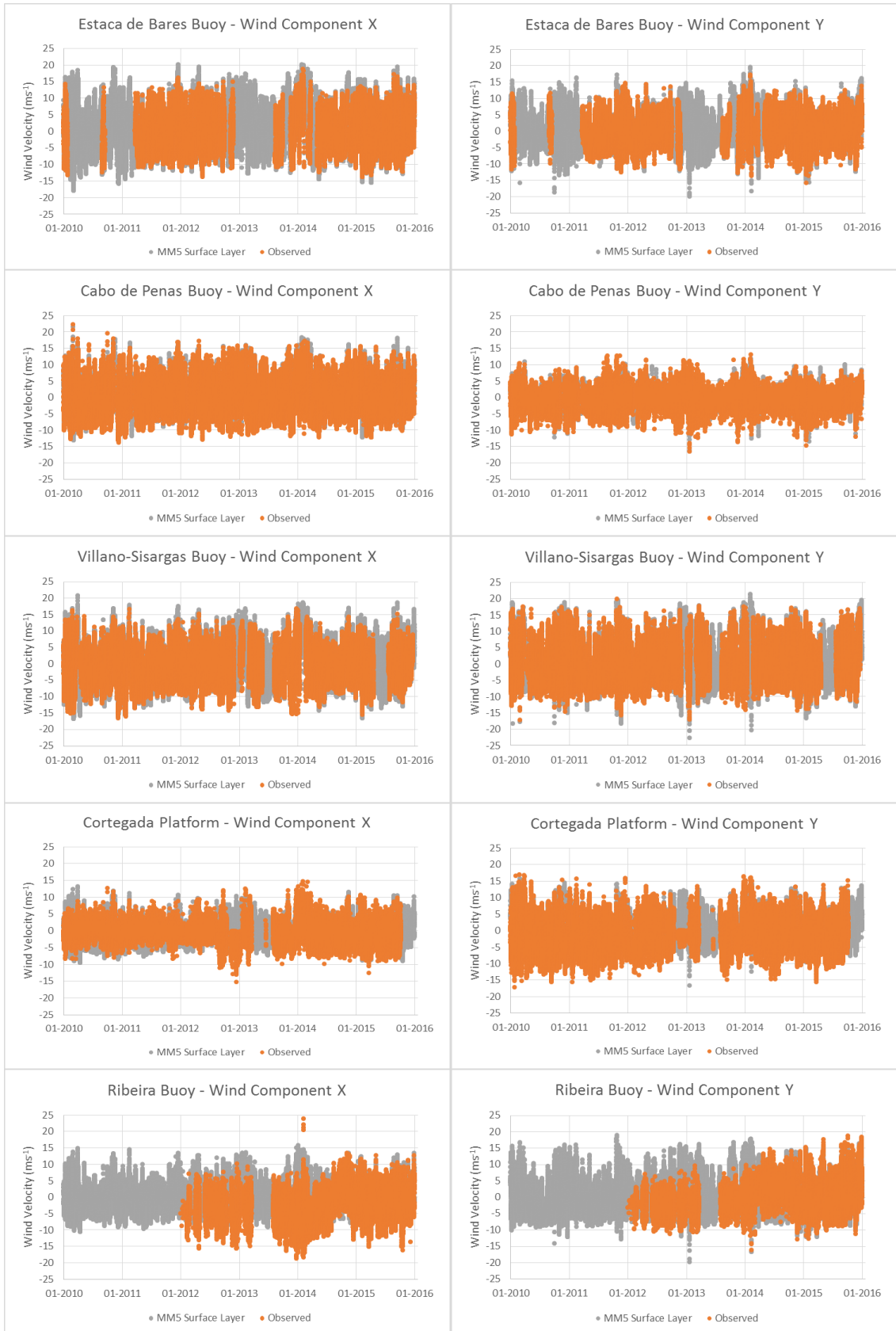


Figure 13 Observed (grey) and modelled (orange) wind component X (left) and Y (right) for the period 2010-2015 by the Western Iberia monitoring stations. Stations are ordered from North to South.

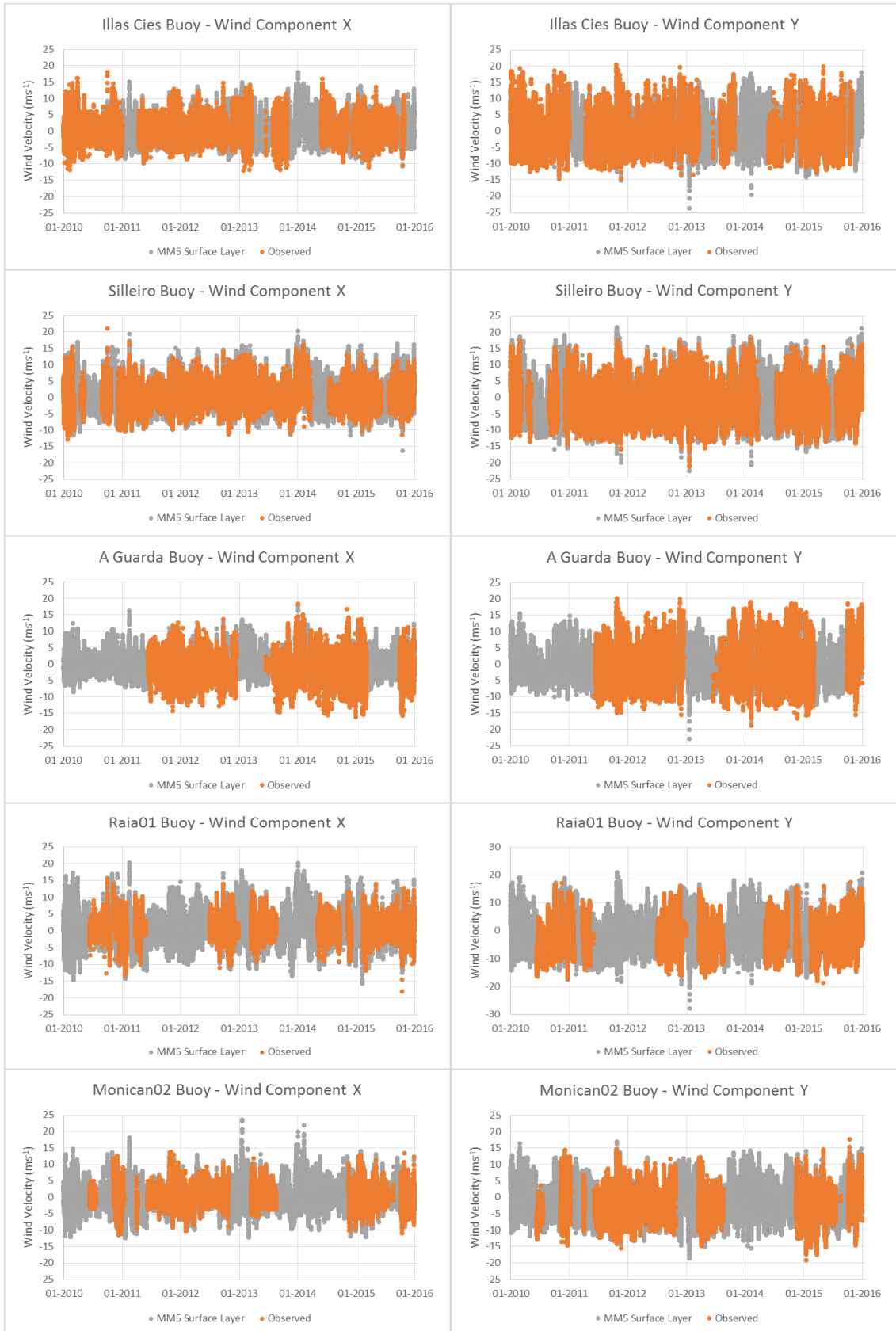
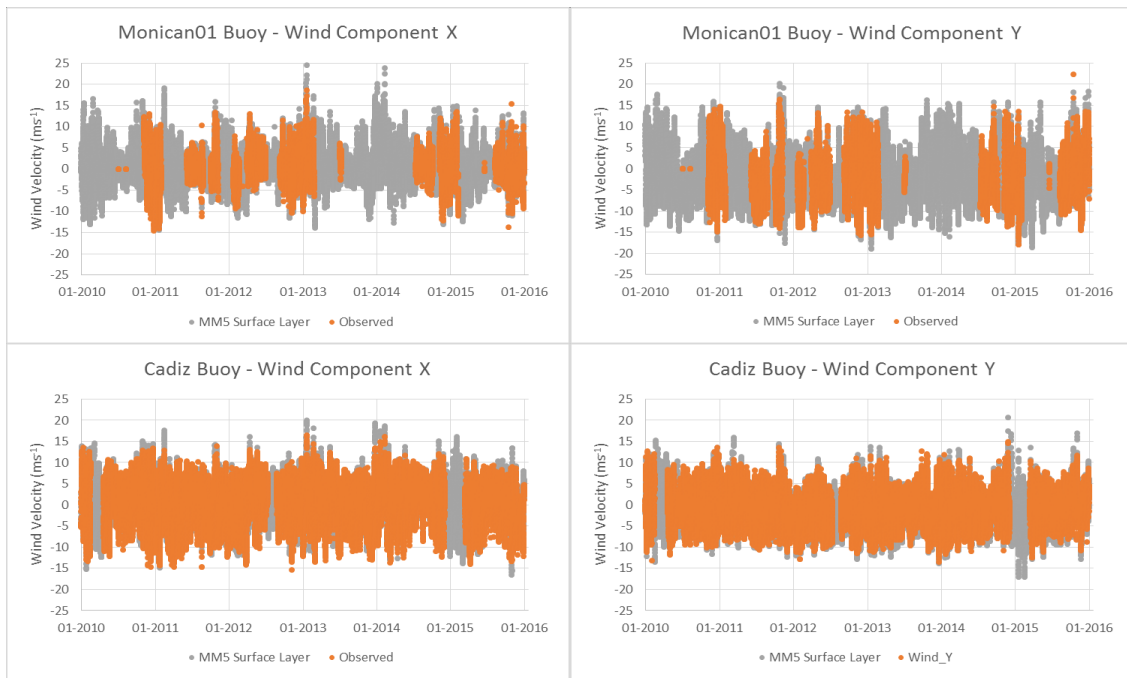


Figure 13 Cont. Observed (grey) and modelled (orange) wind component X (left) and Y (right) for the period 2010-2015 by the Western Iberia monitoring stations. Stations are ordered from North to South.



**Figure 13 Cont. Observed (grey) and modelled (orange) wind component X (left) and Y (right) for the period 2010-2015 by the Western Iberia monitoring stations. Stations are ordered from North to South.**

Monitoring stations were grouped according to the dominant wind component, the one with greater variability, to evaluate the temporal evolution of the MM5 results during the study period. Estaca de Bares, Cabo de Peñas and Cádiz were associated to the zonal wind component and the rest of stations to the meridional wind component (Figure 14). Western winds (positive X values) dominate the northern and southern coast and maximum values take place during winter. Eastern winds were observed around the summer period nevertheless they can also be observed in winter periods such as in February 2012. Northern winds (negative Y values) dominate the western coast during most of the year facilitating upwelling conditions being their maximum values observed during summer. Southern winds, associated to downwelling-favouring conditions, were mainly observed during the winter periods. Nevertheless, during some winter periods, such as in the early months of 2012 and 2015, northern winds could also be observed.

When performed the interannual monthly average on wind intensities, the existence of a meridional gradient in the western coast was distinguished (Figure 15). Northern winds that favour upwelling in the western coast intensify southwards reaching its maximum in the month of July and only during some winter months the wind clearly turns polewards. Eastern winds in the North and western winds in the South, related to upwelling-favourable winds, take place simultaneously during the summer period while downwelling conditions prevail during the winter period. Meridional winds can reach larger intensities when compared with the observed magnitudes in the zonal wind component. Their relation to the upwelling and downwelling processes and their quantification of the process will be described in greater detail in Chapter VIII.

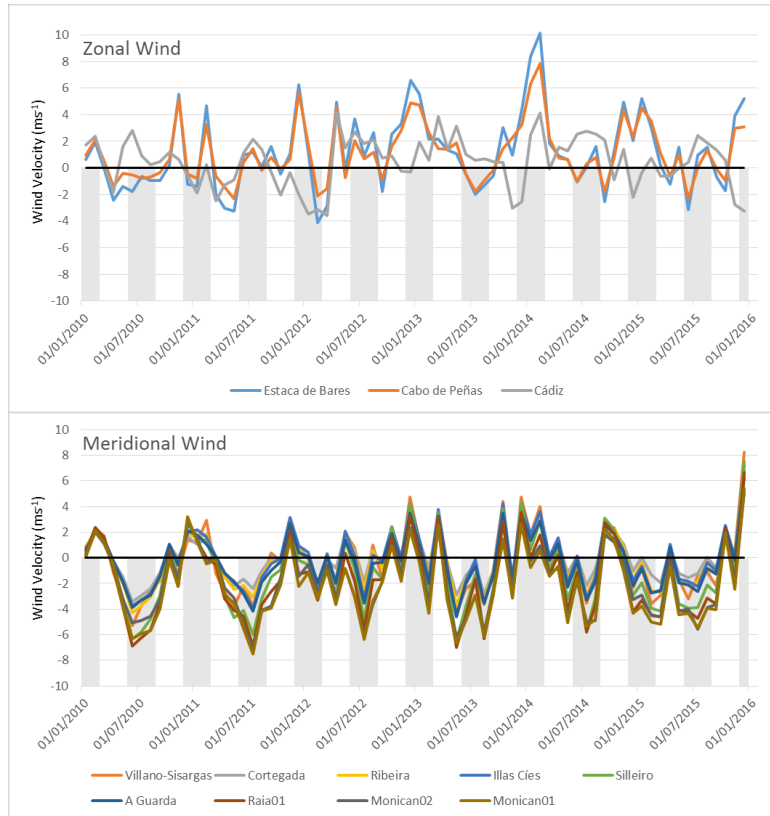


Figure 14 MM5 monthly wind intensity for the zonal wind (top) and meridional wind (bottom) for the Western Iberia region. For clarity, stations have been represented only in one figure according to their main wind component.

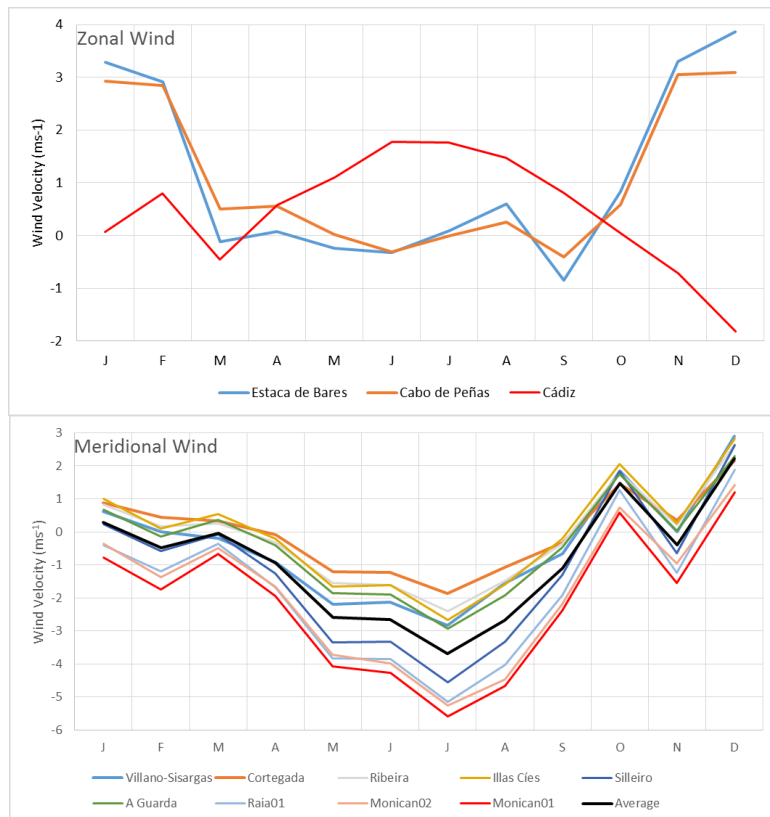


Figure 15 Mean MM5 monthly wind intensity for the zonal wind (top) and meridional wind (bottom) for the period 2010-2015. For clarity, stations have been represented only in one figure according to their main wind component.

## 2.4. Western Iberia weather climatology maps

Once that the model application for the Western Iberia region were compared and validated with monitoring stations data, model results were used to draw the synoptic view of the most relevant variables from the monthly, seasonal, annual and interannual perspective that could be regarded as a preliminary climatology for the Western Iberia regional ocean. This is one of the many advantages of numerical models that allow to complete the observed information in time and space.

This section summarises the western Iberia climate simulated by the atmospheric model at 10 m height. For each of the three climate elements, atmospheric pressure, air temperature and wind intensity, the following maps are provided: monthly, seasonal, annual and full period. Seasons were defined to include the full months with the following criteria: winter (December, January and February), spring (March, April and May), summer (June, July and August) and autumn (September, October and November).

### 2.4.1. Atmospheric Pressure

On average and during the study period, lower pressures were located in the south-eastern area of the IP while high pressures are located in the open Atlantic Ocean side though the total gradient is limited to a few milibars. The origin of the low pressure spreading from Northern Africa could be related to generation of a thermal low-pressure cell that develops over the heated land and that generates a gradient with the higher pressure existing over the cooler ocean (Bakun, 2010).

Figure 16 depicts the mean interannual atmospheric pressure for the entire study period. Though the SLP distribution changes for each analysed year (Figure 17), some horizontal distribution patterns are common. A zonal increasing gradient between the IP and the open Atlantic Ocean and a decreasing gradient between the IP and the African coast is observed every year. That SLP distribution describe the dominant pattern responsible of the wind blowing almost parallel to the IP.

During spring-summer (Figure 18), mainly March to September (Figure 19), the dominant pattern consist on NE-SW isobars that would generate northern winds responsible the summer upwelling in western IP coast. The gradient maximum is observed during July and in the southern part of the IP. The situation is inverted during winter with an atmospheric pressure spatial distribution that allow the generation of downwelling conditions in the northern half of the IP and mainly during the month of December, as will be confirmed in the wind graphs below.

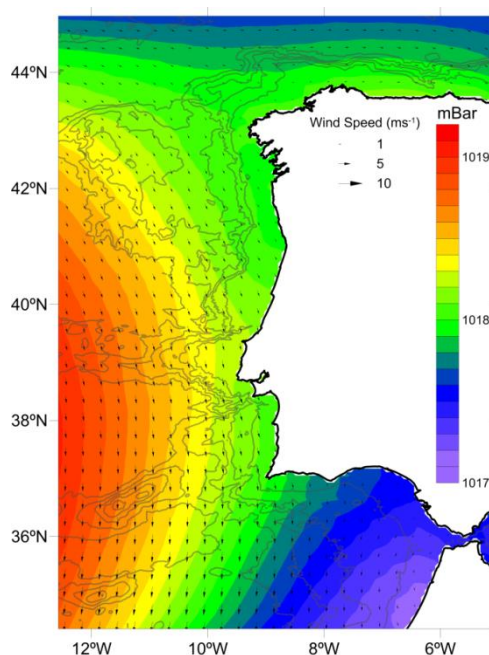


Figure 16 Mean atmospheric sea level pressure for the 2010-2015 period.

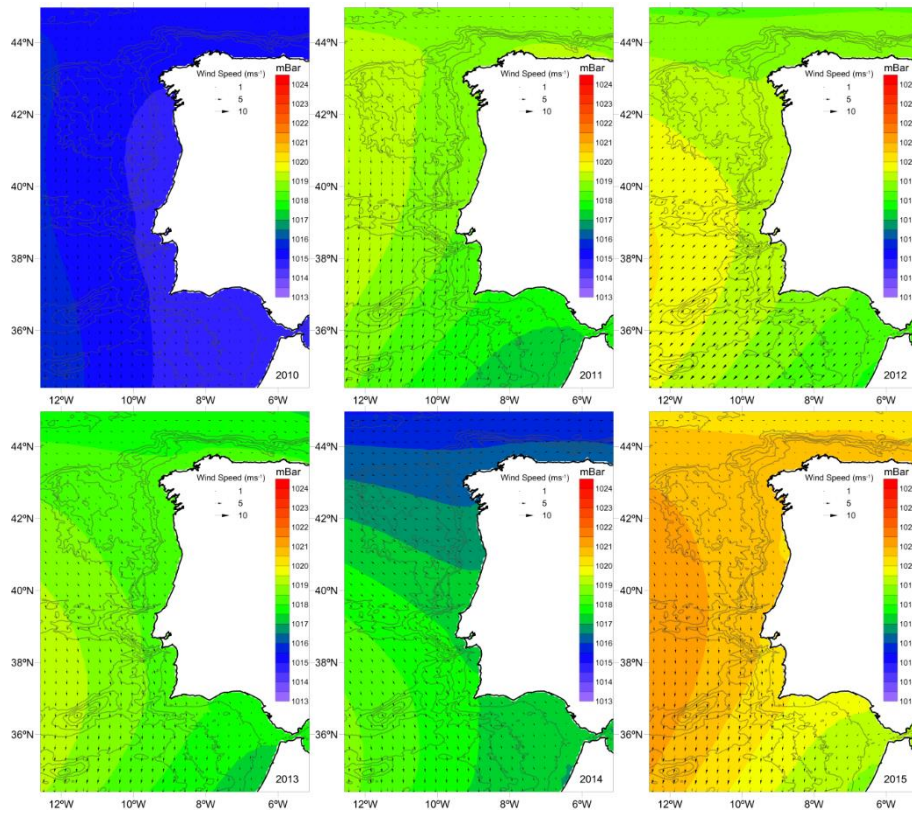


Figure 17 Mean annual atmospheric sea level pressure for each year of the studied period. Isobaths are represented every 1000 m starting at 500 m.

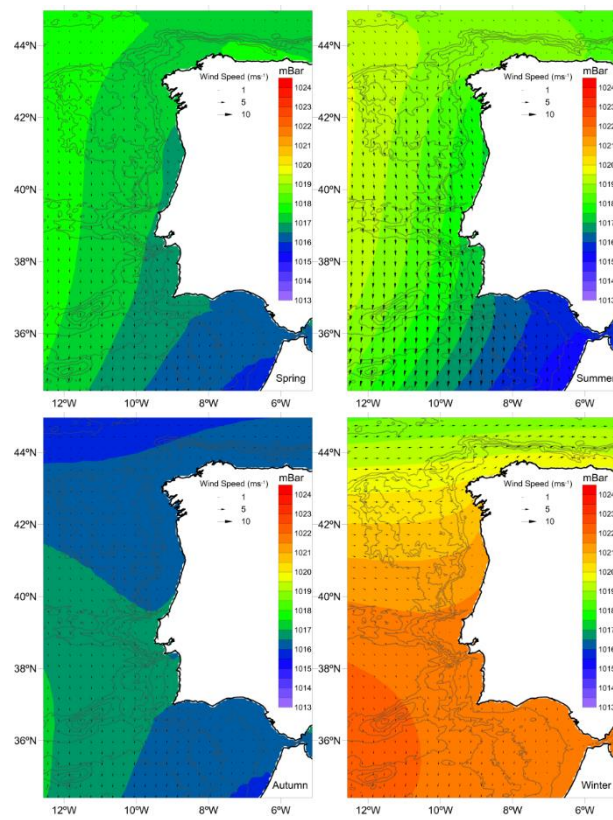


Figure 18 Seasonal atmospheric sea level pressure for the entire analysed period. Isobaths are represented every 1000 m starting at 500 m.

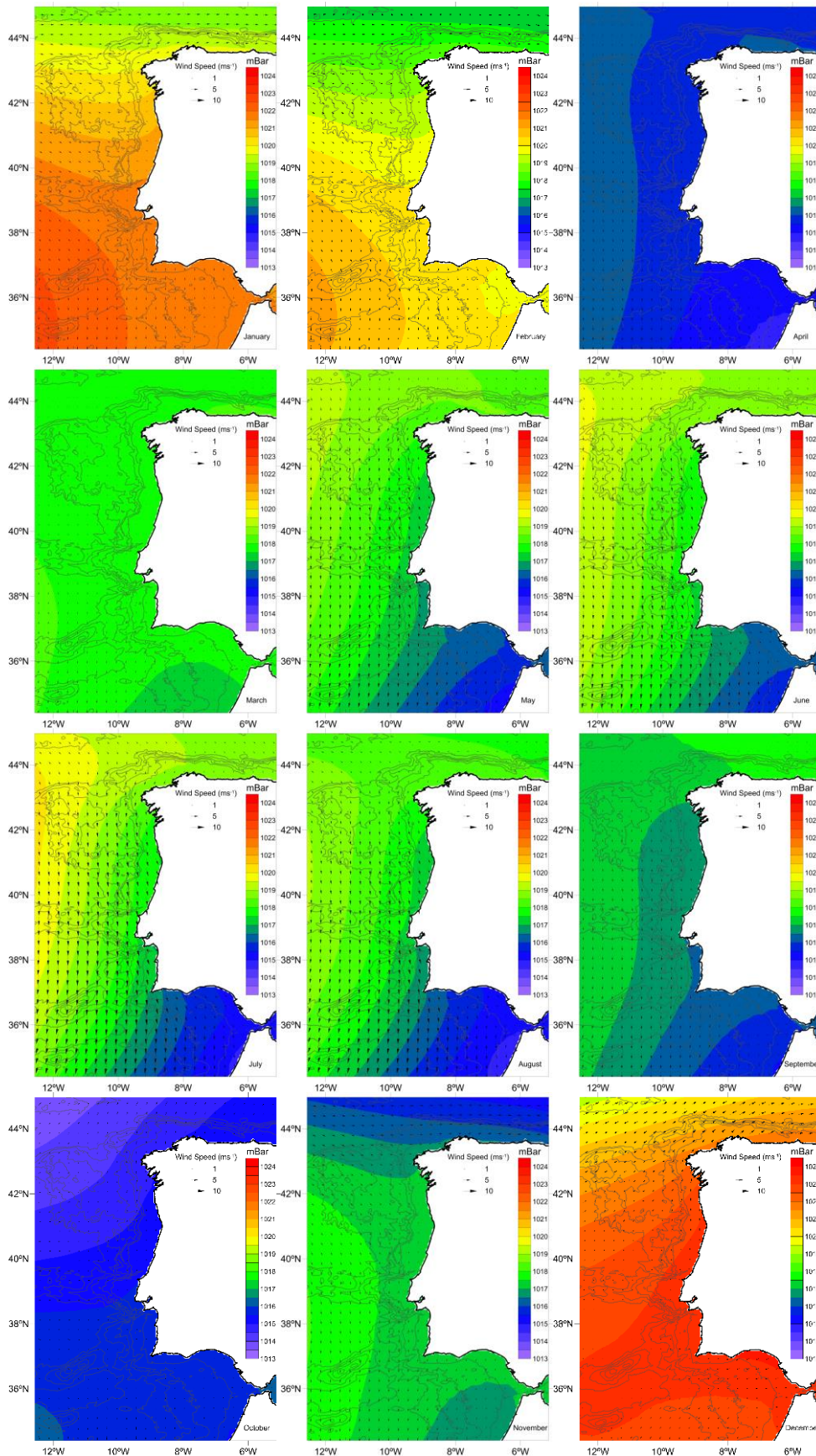


Figure 19 Monthly atmospheric sea level pressure for the entire analysed period. Isobaths are represented every 1000 m starting at 500 m.

### 2.4.2. Air Temperature

Mean air temperature values for the entire study period in Western Iberia decrease northwards and landwards (Figure 20). While maximum values ( $\approx 20^{\circ}\text{C}$ ) are located near the African coast at the southernmost limit of the domain, minimum air temperatures ( $\approx 13^{\circ}\text{C}$ ) are observed in the northern coastal area. Mean air temperature gradient is softer than the observed inland the IP where the annual mean values are comprised between  $10^{\circ}\text{C}$  and values above  $22^{\circ}\text{C}$  (AEMET and IM, 2011). From  $43^{\circ}\text{N}$ , coastal areas present colder air temperatures than in the surrounding western Iberia regional ocean.

On average, years 2012 and 2013 were colder (about  $0.5^{\circ}\text{C}$ ) for the entire region showing some inter-annual variability (Figure 21). Inter-annual variability is larger in coastal areas north to  $41^{\circ}\text{N}$ . Maximum air temperatures, as usual in the northern hemisphere, are registered during the summer period (Figure 22) and in particular during the month of August (Figure 23) with values near  $26^{\circ}\text{C}$ . During the summer period and its warmest month, minimum air temperature values were around  $17^{\circ}\text{C}$  and  $18^{\circ}\text{C}$  respectively. On the other hand, February was the coldest month reaching minimum temperatures around  $8^{\circ}\text{C}$  and maximum values are under  $16^{\circ}\text{C}$  (Figure 23). While for the entire winter period, air temperatures were comprised between  $9$  and  $17^{\circ}\text{C}$  (Figure 22). In between these two seasons, the autumn season was warmer than the spring period as September and October presented maximum values over  $20^{\circ}\text{C}$ .

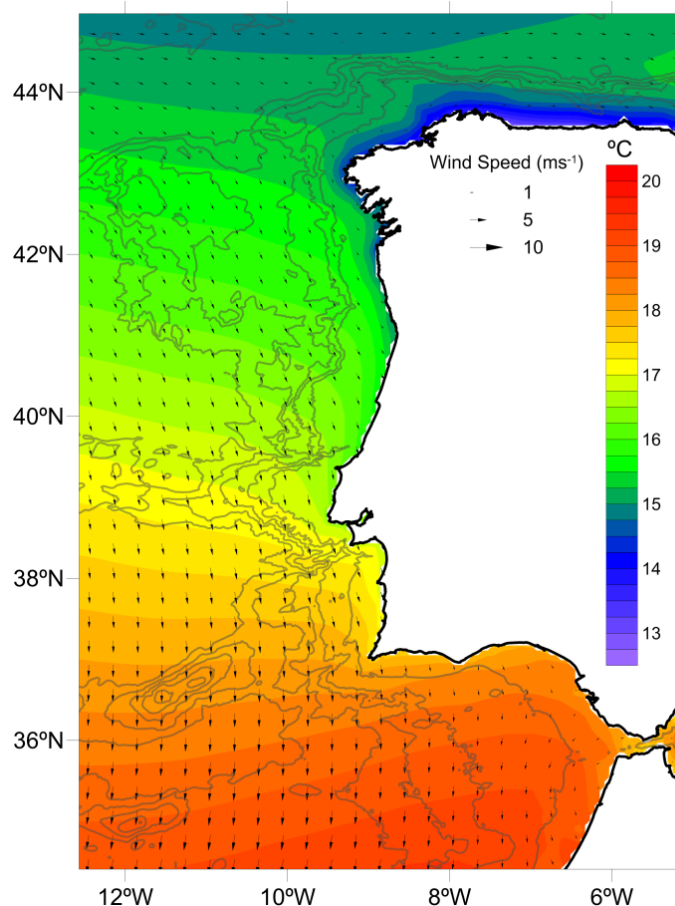


Figure 20 Mean air temperature at 10 m for the 2010-2015 period.

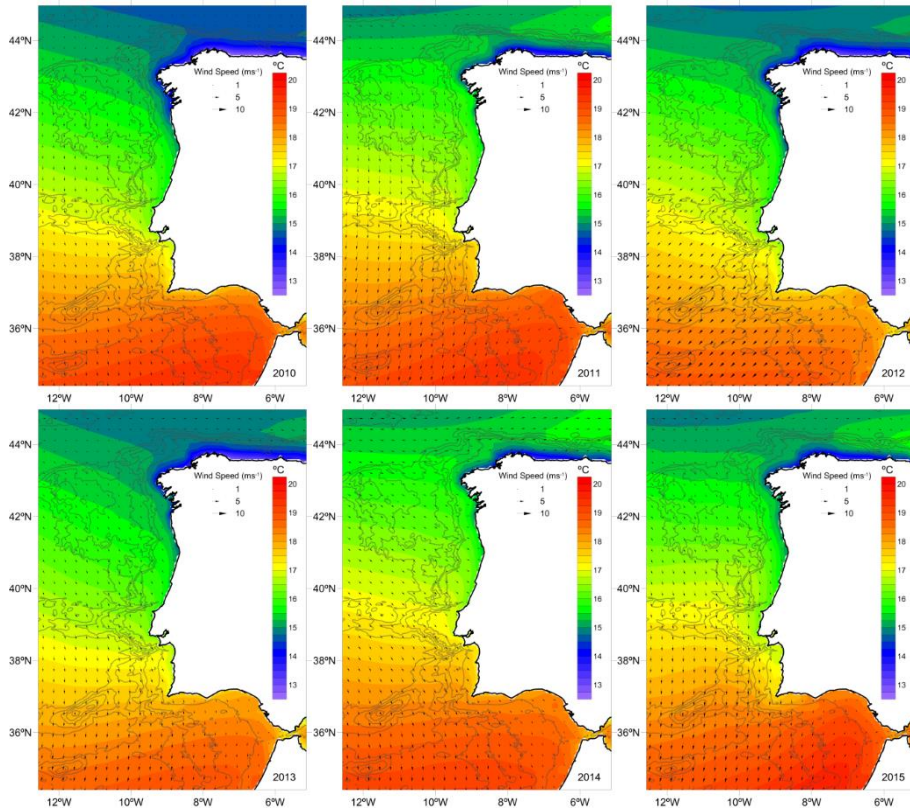


Figure 21 Mean annual air temperature at 10 m for each year of the studied period. Isobaths are represented every 1000 m starting at 500 m.

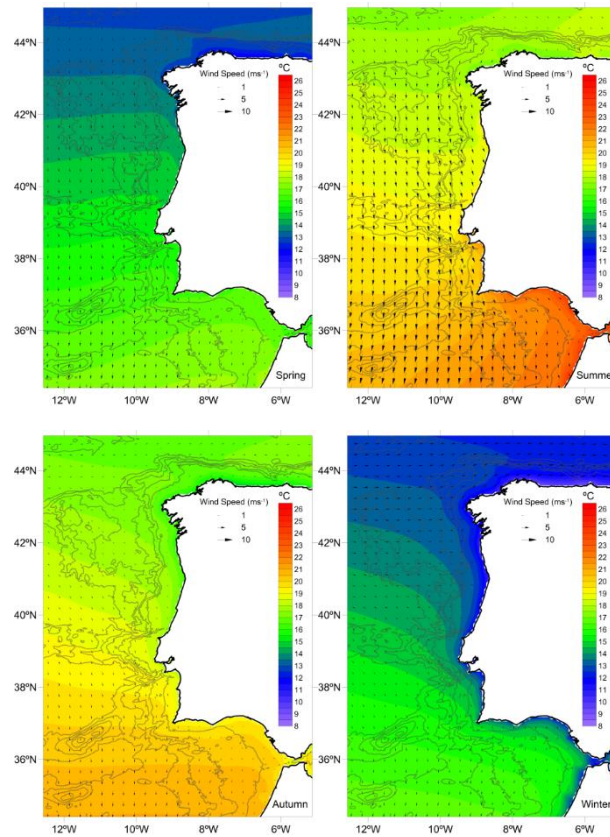


Figure 22 Seasonal air temperature at 10m for the 2010-2015 period. Isobaths are represented every 1000 m starting at 500 m.

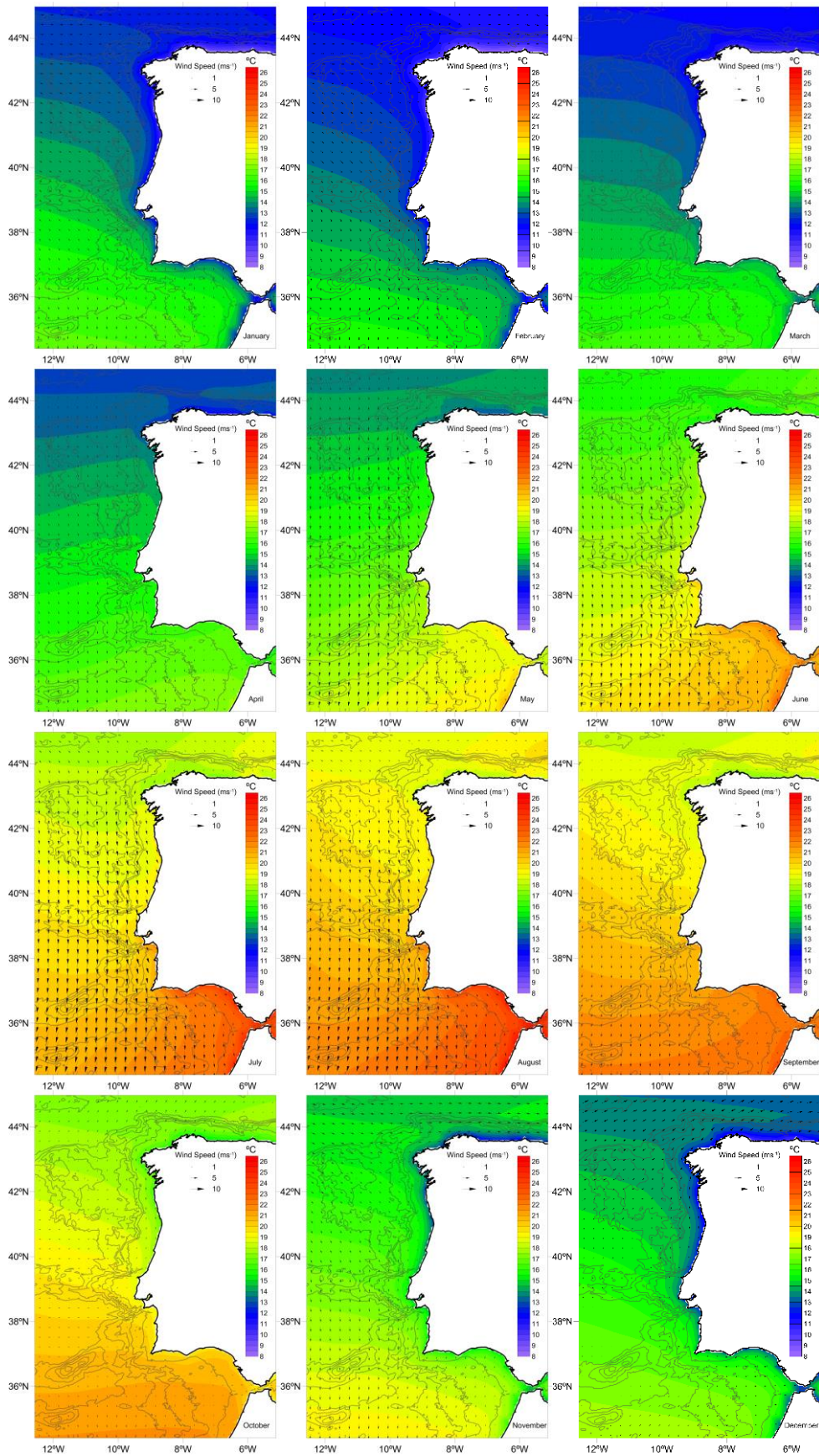


Figure 23 Monthly air temperature at 10 m for the 2010-2015 period. Isobaths are represented every 1000 m starting at 500 m. Every fifth vector is plotted.

### 2.4.3. Wind intensity and direction

Mean wind modulus horizontal distribution in the western Iberia ocean region decreases from the NW of the IP with maximum velocities near  $8 \text{ ms}^{-1}$ , landwards and southwards. Typical mean velocities in most of the coastal areas are under  $6 \text{ ms}^{-1}$  (Figure 24). Wind blowing into the IP diverges in the NW area with and wind direction is southwards in the western (Atlantic coast) and southern (Gulf of Cádiz) coasts while in the northern coast (Cantabrian Sea) the mean direction is eastward.

Discriminating by wind components, the U component or zonal wind is dominated by eastward winds from the ocean with the exception of the Gibraltar Strait area and the southern boundary limit while the V component or meridional wind is almost controlled by northern winds that increase southwards (Figure 25). The meridional wind intensities are larger than the zonal wind reaching values near the coast around  $3 \text{ ms}^{-1}$  although its maximum is reached in the southwest limit of the domain in the open ocean. This cross-shore wind velocity gradient is responsible of generating the wind stress curl that influences the formation and development of upwelling filaments as will be discusses later in the upwelling chapter (Chapter VIII). The meridional wind component has a key role in controlling the upwelling/downwelling regime in the western coast while the zonal component will be important in the northern and southern sector of the Iberian Peninsula.

In each year of the studied period (Figure 26), the wind modulus distribution present similar patterns and intensities than the mean interannual wind distribution (Figure 24). The years 2011 and 2012 were slightly weaker than the inter-annual average and eastward wind in the northern area of the IP was not as defined as in the other years.

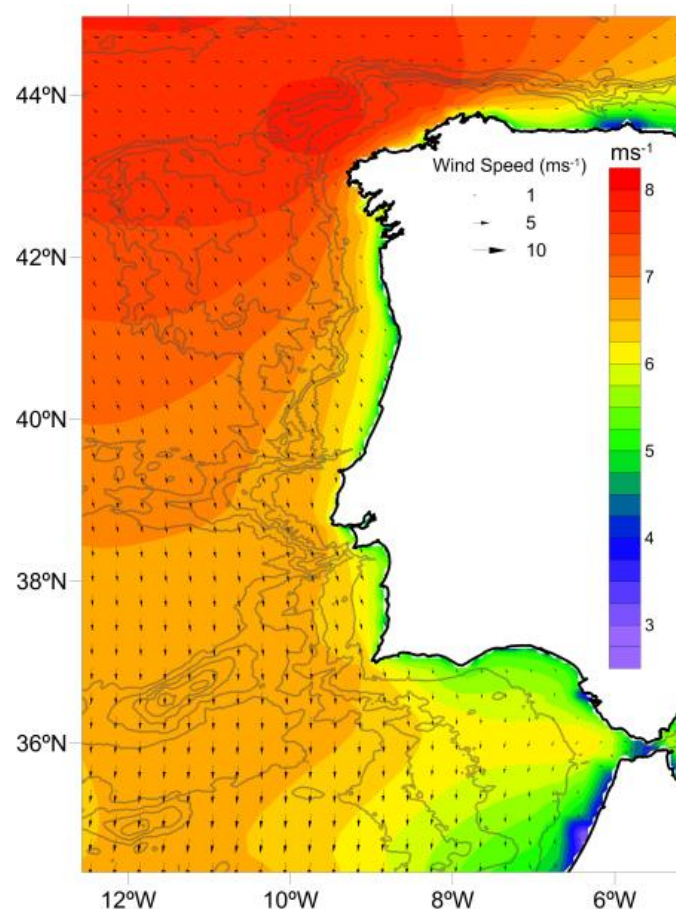


Figure 24 Annual mean wind modulus at 10 m for the 2010-2015 period. Vectors represent the mean direction and only every fifth vector is plotted.

Eastward winds in the Cantabrian Sea reach their maximum intensities during the winter season (Figure 27). In contrast, during summer this eastward transport is reduced and near the coast it turns westwards while northern winds dominate the Atlantic and Gulf of Cádiz areas. Summer wind maximum velocity is around  $7 \text{ ms}^{-1}$  while during the winter period was  $9 \text{ ms}^{-1}$  and though the mean wind intensity is lower during the summer period, the wind direction is more constant as indicated by the arrow size. The dominant eastward wind in the Cantabrian Sea is clear from November to February and the southwards wind is clearly recognisable from May to August (Figure 28).

The zonal wind distribution (Figure 29), although with a clear predomination of western winds, present a large inter-annual variability when compared with the meridional wind (Figure 31), as the northern wind is more regular through the years. The western character of the zonal wind is stronger during autumn and winter dominating most of the studied area. During spring and summer, it can be observed eastern winds around the NW coast of the IP while in the southern coast winds blow eastwards (Figure 30). Those zonal winds are responsible of the upwelling in both coasts and coincide with the northern winds that favour also upwelling processes in the western coasts (Figure 32). As a consequence, during spring and summer months, March to September, most of the western coast is under upwelling conditions enhancing the coastal primary production (Figure 33 and Figure 34). On the other hand, during December, and in minor scale November, northern and southern zonal winds enhance the downwelling circulation. Also in the western coast, between October and January, meridional winds favour downwelling being this process more intense in the northern half of the coast.

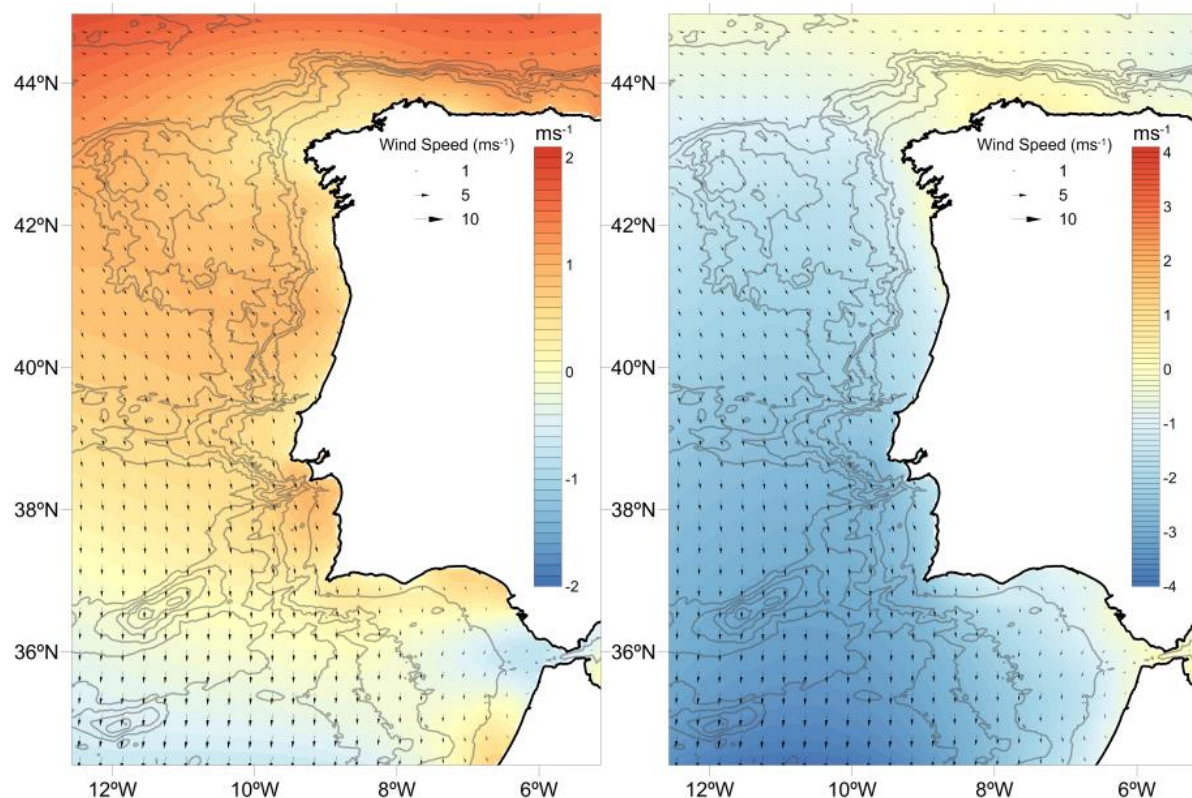


Figure 25 Annual mean wind intensity for the zonal (left) and meridional component (right) at 10 m for the 2010-2015 period. Vectors represent the mean direction and only every fifth vector is plotted.

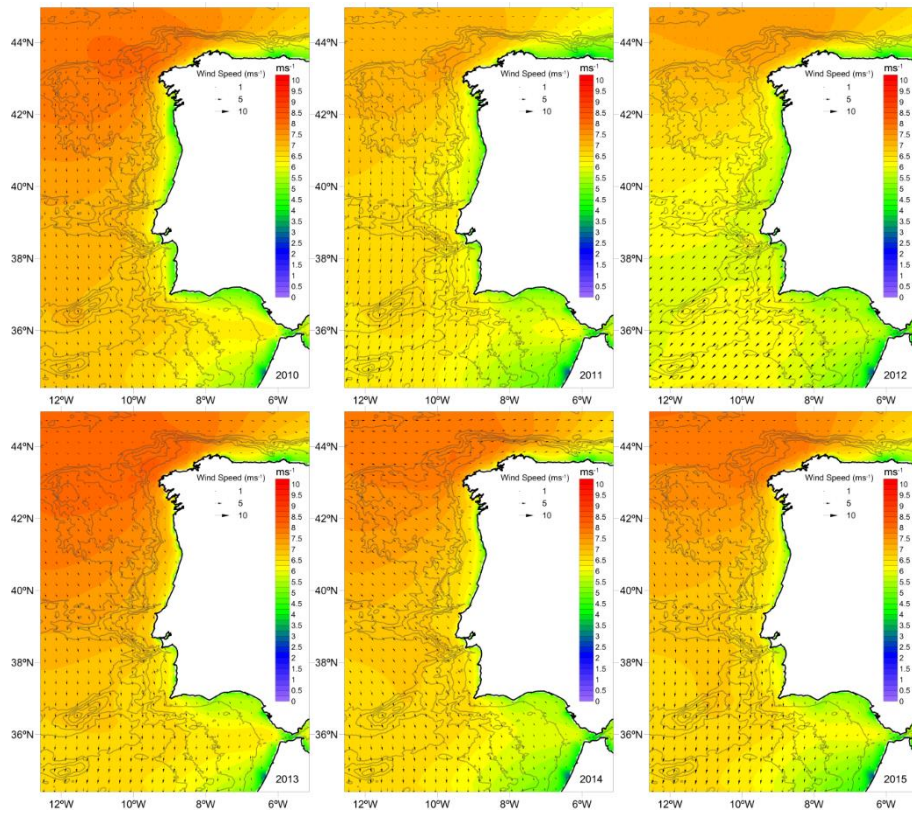


Figure 26 Mean wind intensity at 10 m for each year of the studied period. Isobaths are represented every 1000 m starting at 500 m. Vectors represent the mean direction and only every fifth vector is plotted.

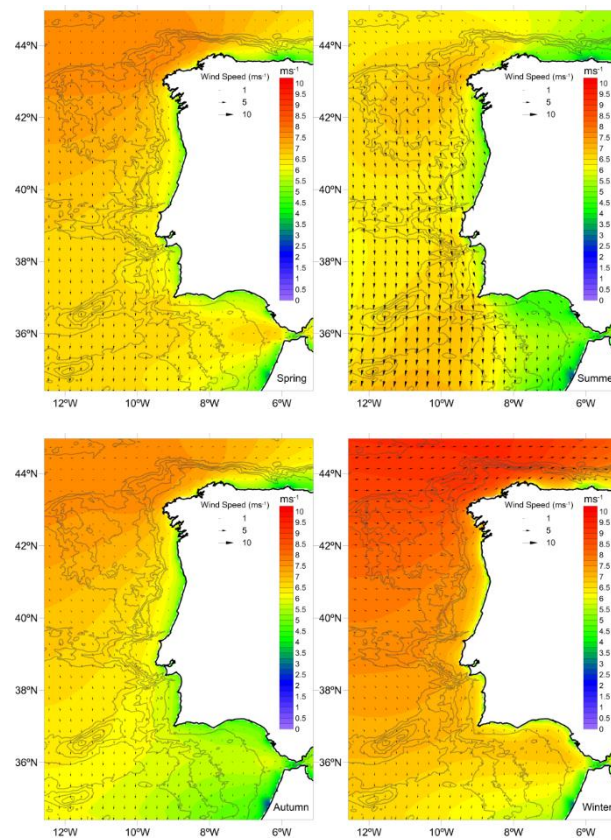


Figure 27 Seasonal mean wind intensity at 10 m for the 2010-2015 period. Isobaths are represented every 1000 m starting at 500 m. Vectors represent the mean direction and only every fifth vector is plotted.

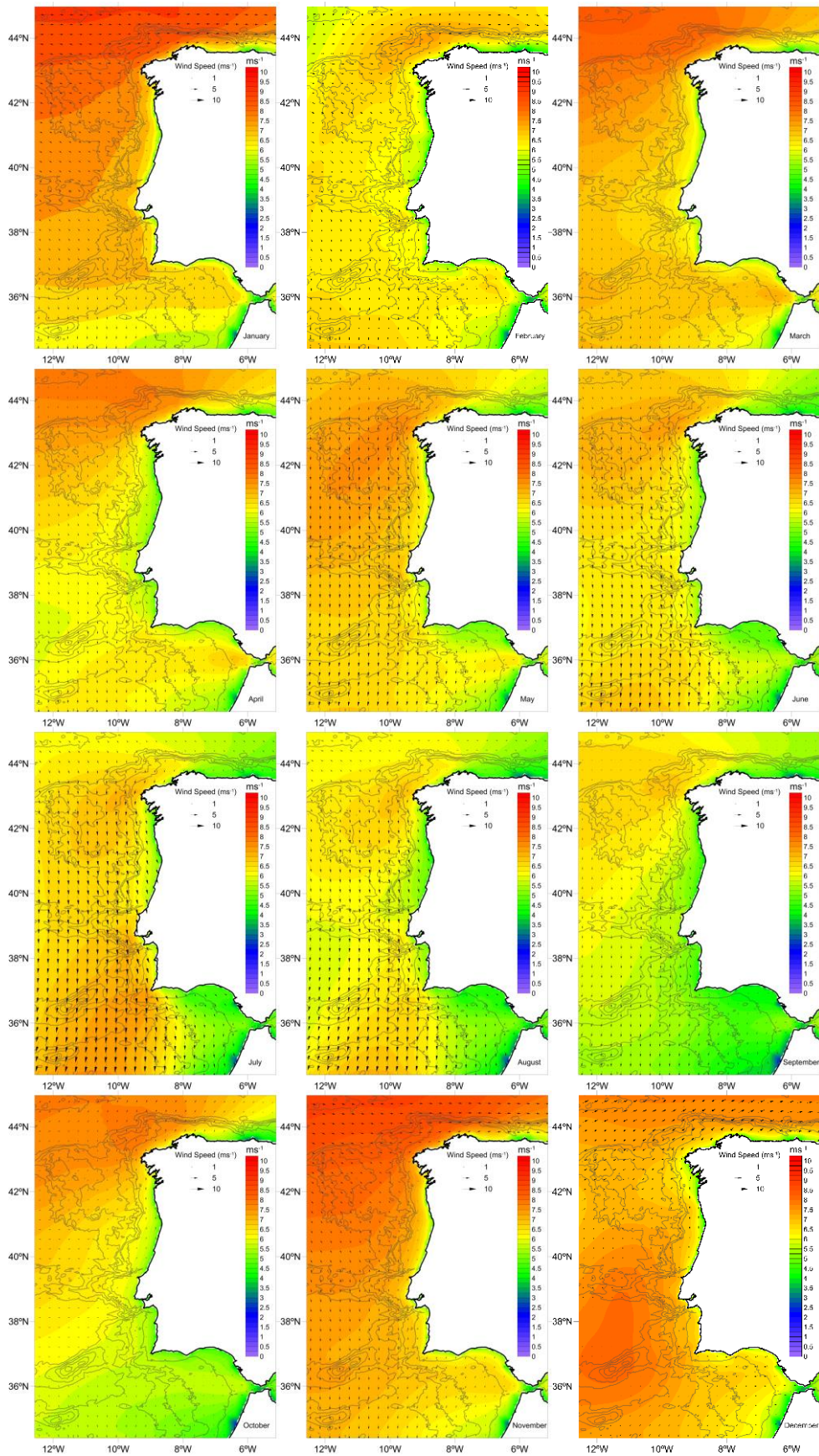


Figure 28 Monthly mean wind intensity at 10 m for the 2010-2015 period. Isobaths are represented every 1000 m starting at 500 m. Vectors represent the mean direction and only every fifth vector is plotted.

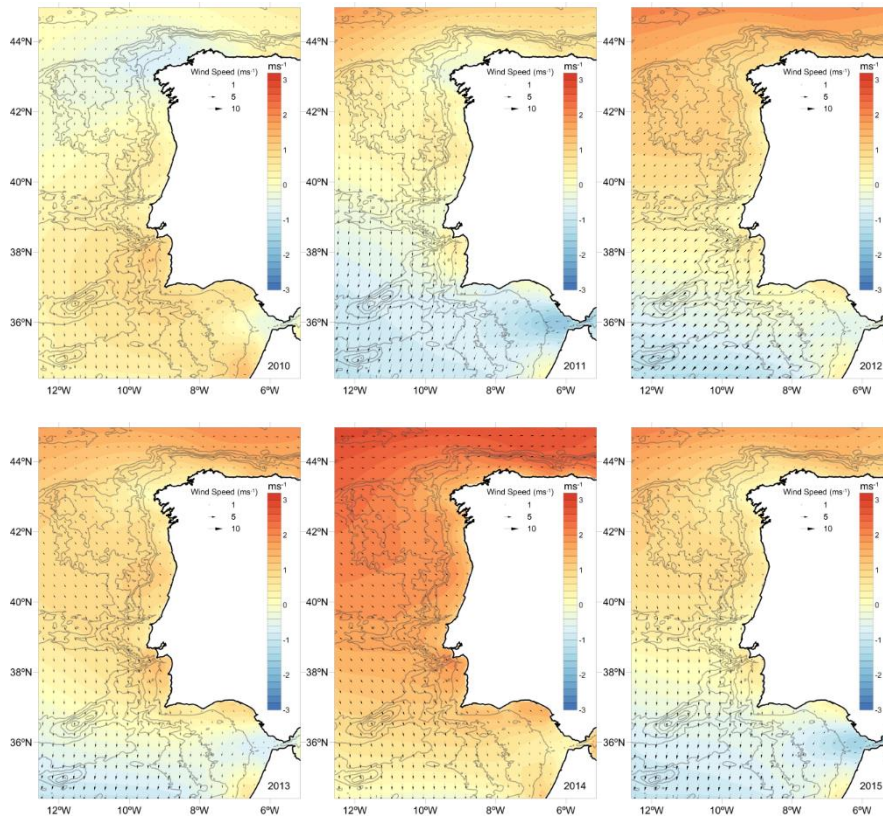


Figure 29 Mean annual zonal wind velocity at 10 m for each analysed year. Isobaths are represented every 1000 m starting at 500 m. Vectors represent the mean direction and only every fifth vector is plotted.

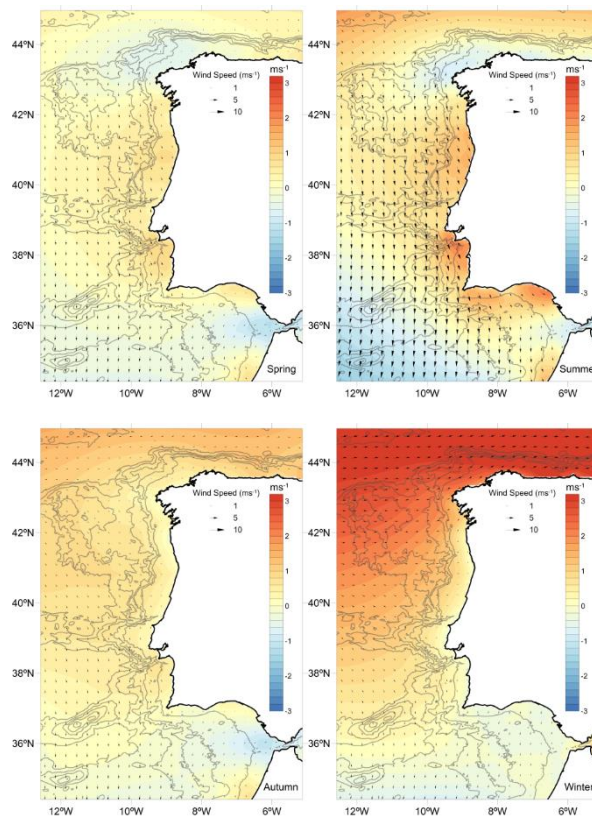


Figure 30 Seasonal mean zonal wind velocity at 10 m for the 2010-2015 period. Isobaths are represented every 1000 m starting at 500 m. Vectors represent the mean direction and only every fifth vector is plotted.

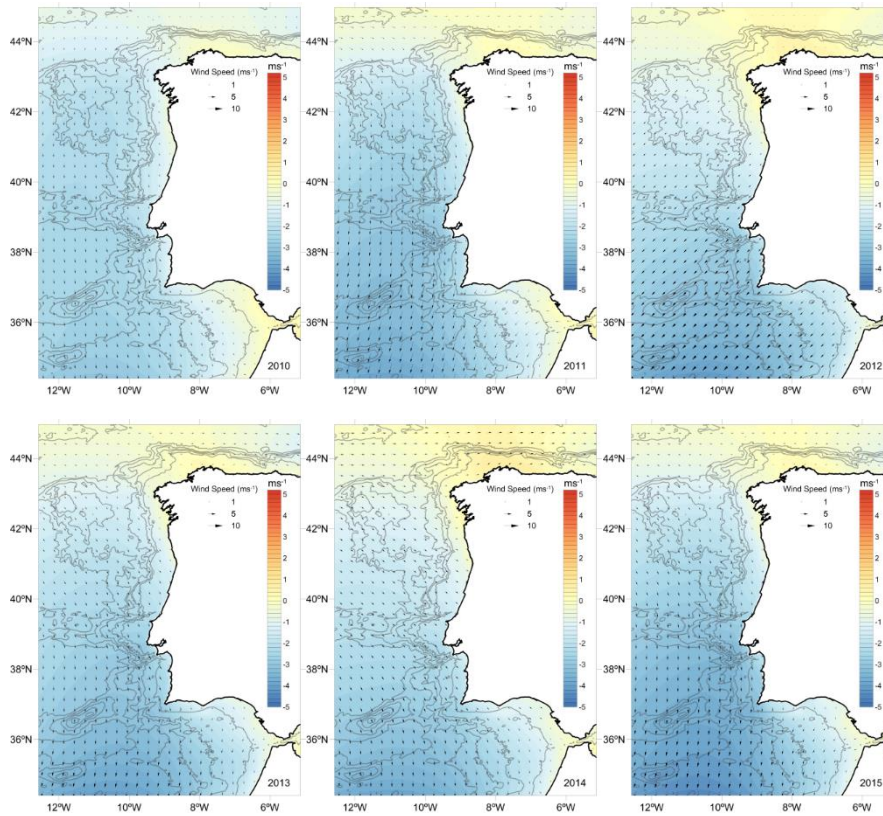


Figure 31 Mean meridional wind velocity at 10 m for each analysed year. Isobaths are represented every 1000 m starting at 500 m. Vectors represent the mean direction and only every fifth vector is plotted.

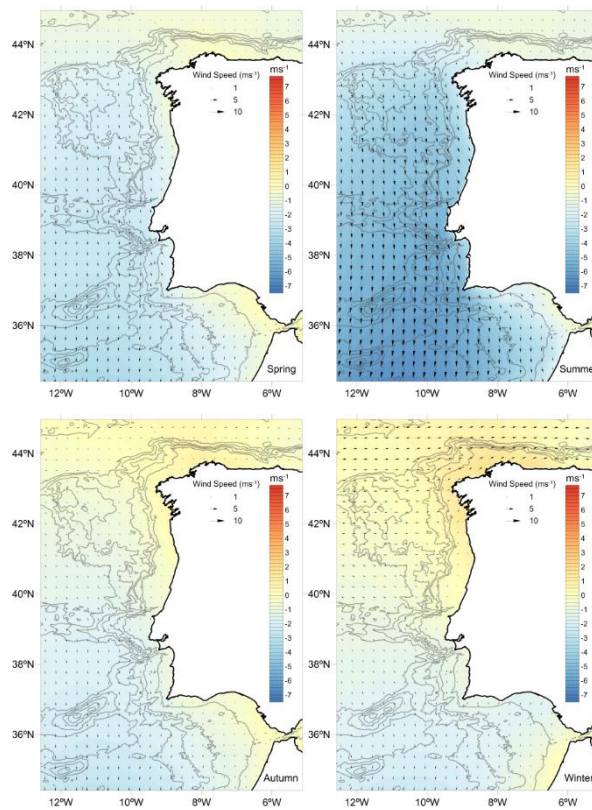


Figure 32 Seasonal mean meridional wind velocity at 10 m for the 2010-2015 period. Isobaths are represented every 1000 m starting at 500 m. Vectors represent the mean direction and only every fifth vector is plotted.

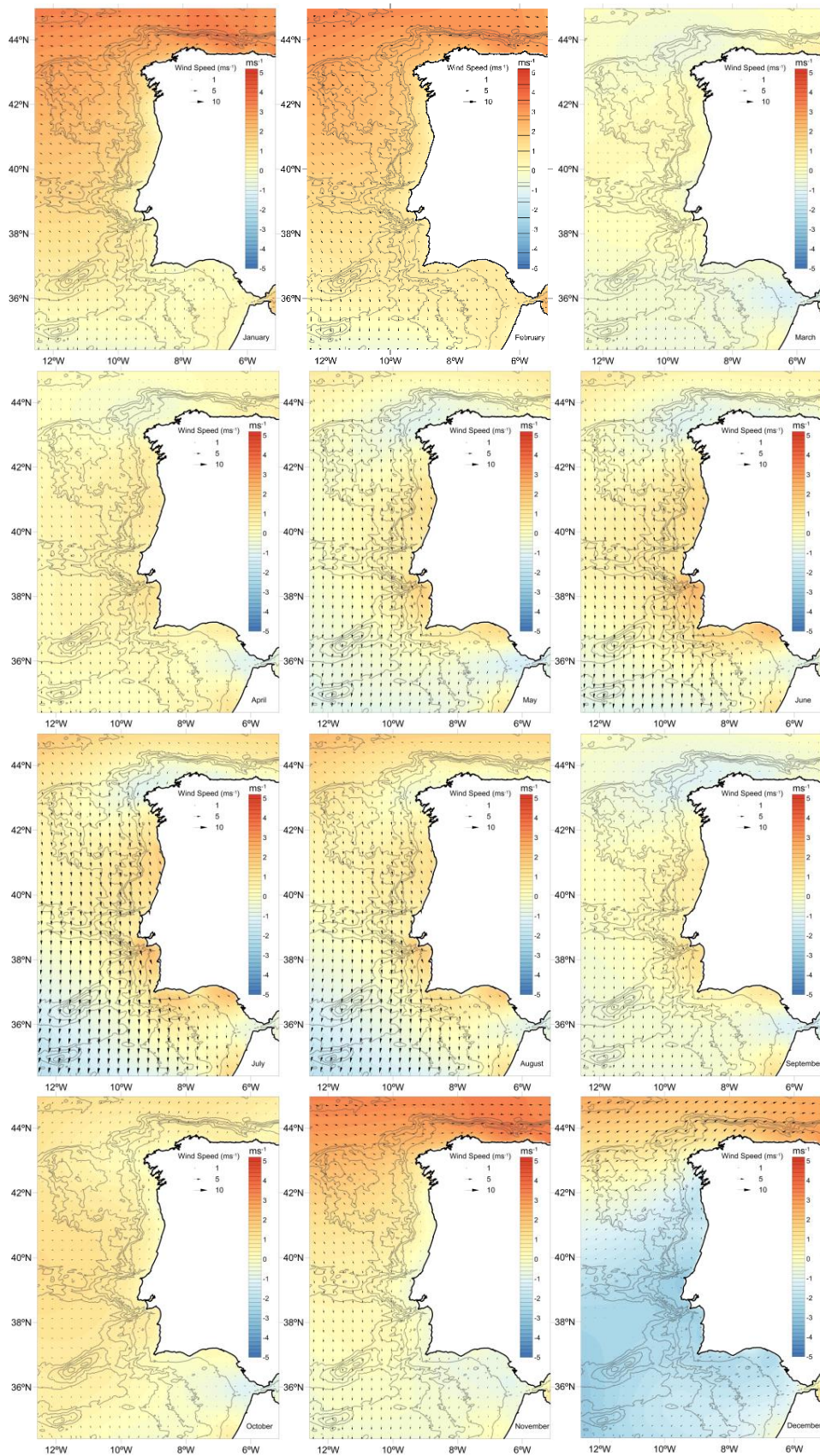


Figure 33 Monthly mean zonal wind velocity at 10 m for the 2010-2015 period. Isobaths are represented every 1000 m starting at 500 m. Vectors represent the mean direction and only every fifth vector is plotted.

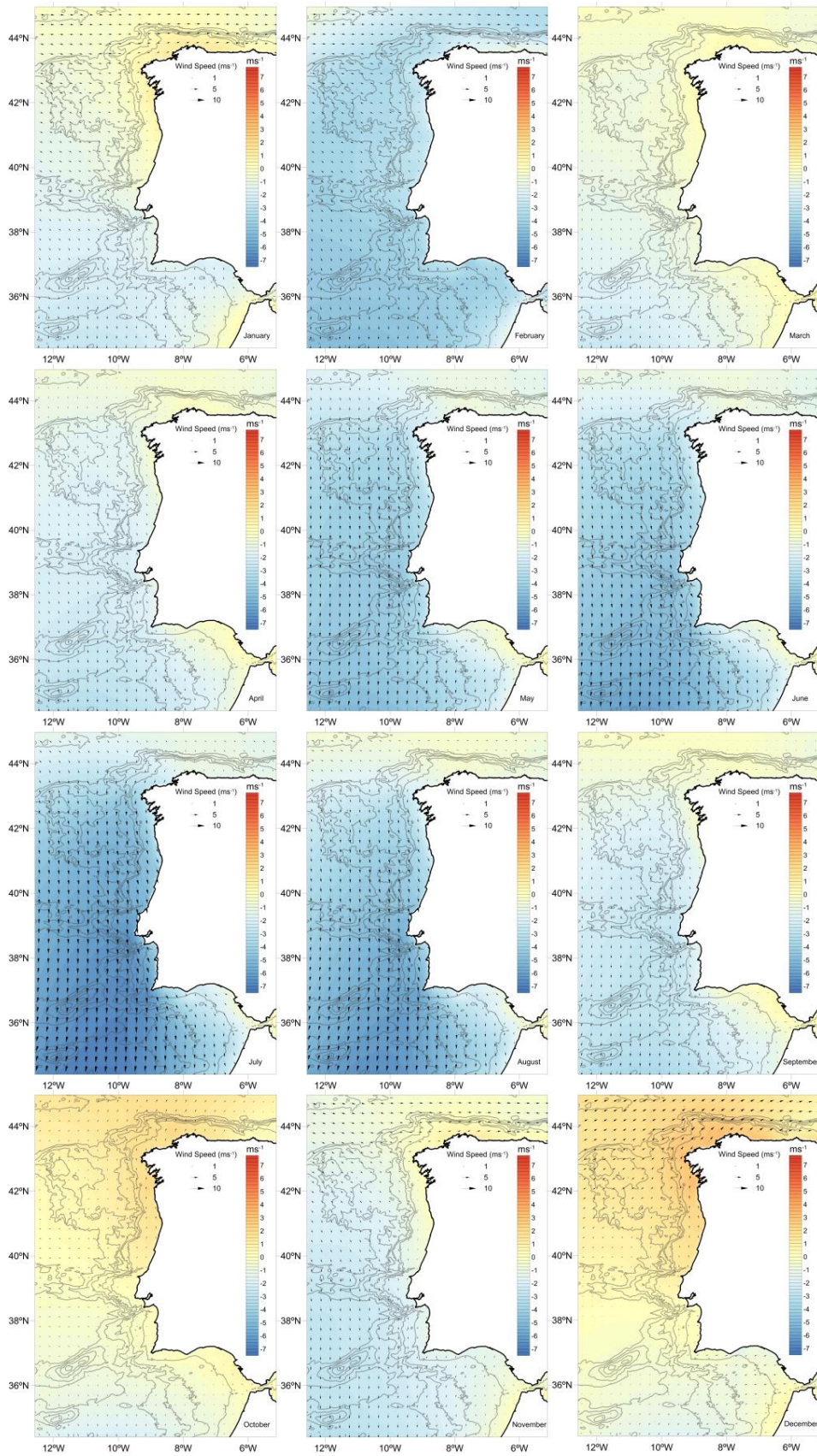


Figure 34 Monthly mean meridional wind velocity at 10 m for the 2010-2015 period. Isobaths are represented every 1000 m starting at 500 m. Vectors represent the mean direction and only every fifth vector is plotted.

## 2.5. Discussion

Atmospheric processes are the key forcing for many ocean hydrodynamic and ecological processes. Atmospheric sea level pressure distribution is connected to the wind intensity and direction patterns and the spreading of the atmospheric temperature that exerts an influence in the WI regional ocean circulation. The link between the different atmospheric variables exerts a strong influence in the intensity and direction of the surface circulation, favour vertical transport in both senses and is responsible of the formation of deep waters. These processes condition the water properties including temperature, pH and nutrient concentrations in which the ocean life is based on. Due to the location of the IP in the eastern boundary of the North Atlantic, the atmospheric processes are linked to larger scales systems. For this reason, the relation of our model results were compared to the performance of classic atmospheric modes in the North Atlantic: the NAO and the EA.

The NAO index estimates the pressure difference between the Icelandic Low (Reykjavík station) and the Azores High (Lisbon or Ponta Delgada stations) and positive/negative phases are associated to the frequency, intensity and track of storms. Negative phases of NAO (NAO-) has been related to the enhancement of surface wind speed and precipitation in the IP (Jerez *et al.*, 2013; Trigo *et al.*, 2002)

EA is also a North-South dipole that is displaced south-eastward to NAO linking with subtropical modulations and its positive phase is associated with above-average surface temperatures and meridional rain gradients in Europe. Monthly values of the NAO and EA indexes for the analysed period were obtained from the National Oceanic and Atmospheric Administration/Climate Prediction Center (NOAA/CPC; [www.cpc.ncep.noaa.gov](http://www.cpc.ncep.noaa.gov); Figure 35).

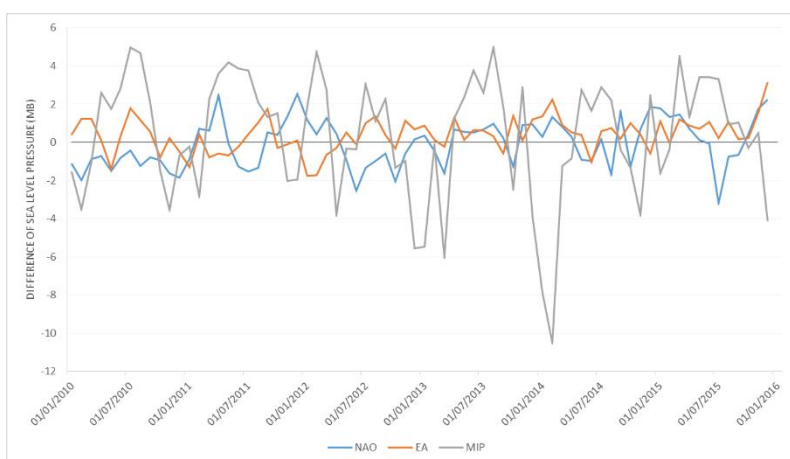


**Figure 35 Monthly NAO, EA and MIP indexes for the period 2010-2015. NAO and EA indexes were obtained from the National Oceanic and Atmospheric Administration/Climate Prediction Center (NOAA/CPC; <http://www.cpc.ncep.noaa.gov/>) and MIP index values were calculated from MM5 model results.**

In this chapter, an atmospheric pressure index for the Iberian Peninsula (MIP – Meridional Iberian Peninsula Index) was developed by calculating the meridional air pressure gradient in the IP using Estaca de Bares and Cádiz stations, located in the Cantabrian Sea and the Gulf of Cádiz respectively, to study its relation in the generation of upwelling-favourable winds in the WI coasts. The MIP index was defined using a north–south dipole and following the rational used for defining the North Atlantic Oscillation (NAO) and East Atlantic (EA) indexes (<http://www.cpc.ncep.noaa.gov/>). Monthly averaged MIP values are able to explain, for the analysed period, between the 45% and 67% of the meridional wind variability and between 17% and 73% of the zonal wind for all the wind analysed stations with the exception of the Cádiz station where correlation is almost non-existent (Table VI). The correlation with the meridional wind is more stable than with the zonal wind probably due to local coastal effects.

From the upwelling point of view, the EA pattern has shown a larger relation with the meridional wind component responsible of the upwelling events at the western coast of the IP, although the influence of the NAO pattern was also detected but limited to a minor extent (deCastro *et al.*, 2008a; deCastro *et al.*, 2008b). The NAO index showed positive correlation with the number of upwelling filaments in summer (Sánchez *et al.*, 2007). When comparing the two classic indexes with the MIP, EA index present an instantaneous coefficient of determination of -0.28 while in order to obtain some correlation with the NAO values it was necessary a 2-month time lag ( $R^2$  of 0.22).

**Table VI. Coefficient of determination ( $R^2$ ) between the monthly Meridional Iberian Peninsula Index (MPI index) and the datasets for the zonal and meridional wind components. Buoys are listed from North to South and those located close to the coastal area are indicated with an \*.**

Station Name	$R^2$ MIP-Zonal Wind	$R^2$ MIP-Meridional Wind
Estaca de Bares	0.60	0.54
Cabo de Peñas	0.57	0.67
Villano-Sisargas	0.73	0.56
Cortegada Platform *	0.71	0.67
Ribeira *	0.68	0.60
Illas Cies *	0.40	0.55
Silleiro	0.62	0.54
A Guarda *	0.29	0.54
Raia01	0.53	0.50
Monican02	0.17	0.47
Monican01	0.40	0.45
Cádiz	0.05	0.03

## 2.6. Conclusions

Even with the above described limitations, numerical meteorological models are a key component of the ocean modelling systems and contribute significantly to reproduce adequately the ocean processes by including the atmospheric temporal and spatial variability.

The Iberian Peninsula due to its location as the interface between the Atlantic Ocean and the European Continent is exposed to the open ocean meteorological dynamics but also to local meteorological patterns such as the diversion of winds in NW of the IP and the influence of the north African Low. For that reason though is subjected to global meteorological patterns such as NAO and EA, local indexes could aid to explain better the meteorological variables distribution in the near ocean.

The analysis of meteorological processes and numerical models in the open ocean should be encouraged to reduce the uncertainties. In addition, integration of meteorological models and the MOHID model should also be pursued further.

## 2.7. Acknowledgements

The author would like to thank in this chapter the IST meteorological group, nowadays part of MARETEC, and in particular to its current operator Jorge Palma for the maintenance and delivery of the MM5 model results during the last few years.

## 2.8. References

- AEMET, IM, 2011. Atlas climático ibérico/Iberian climate atlas. Agencia Estatal de Meteorología, Ministerio de Medio Ambiente y Rural y Marino, Madrid. Instituto de Meteorologia de Portugal, 80 pp. Available for download [here](#).
- Bakun A, Field DB, Redondo-Rodriguez A, Weeks SJ. Greenhouse gas, upwelling-favorable winds, and the future of coastal ocean upwelling ecosystems. *Global Change Biology*. 2010; 16: 1213–1228. DOI: [10.1111/j.1365-2486.2009.02094.x](https://doi.org/10.1111/j.1365-2486.2009.02094.x).
- Cropper TE, Hanna E, Bigg GR. Spatial and temporal seasonal trends in coastal upwelling off Northwest Africa, 1981–2012. *Deep Sea Research Part I: Oceanographic Research Papers*. 2014; 86: 94-111.
- deCastro M, Gomez-Gesteira M, Alvarez I, Cabanas JM, Prego R. Characterization of fall–winter upwelling recurrence along the Galician western coast (NW Spain) from 2000 to 2005: dependence on atmospheric forcing. *Journal of Marine Systems*. 2008a; 72: 145-148.
- deCastro M, Gomez-Gesteira M, Lorenzo MN, Alvarez I, Crespo AJC. Influence on atmospheric modes on coastal upwelling along the western coast of the Iberian Peninsula, 1985 to 2005. *Climate Research* 2008b; 36: 169-179.
- Grell GA, Dudhia J, Stauffer D, 1994. A description of the fifth-generation Penn State/NCAR Mesoscale Model (MM5). NCAR Technical Note NCAR/TN-398+STR.
- Hurrell JW, Dickson RR, 2005. Climate Variability over the North Atlantic. In: N. C. Stenseth, G. Ottersen, J. W. Hurrell & A. Belgrano (eds.). *Marine Ecosystems and Climate Variation: The North Atlantic: A Comparative Perspective*. Oxford University Press, 15-31. DOI: [10.1093/acprof:oso/9780198507499.003.0002](https://doi.org/10.1093/acprof:oso/9780198507499.003.0002).
- Jerez S, Trigo RM, Vicente-Serrano SM, Pozo-Vazquez D, Lorente-Plazas R, Lorenzo-Lacruz J, Santos-Alamillos F, Montavez JP. The Impact of the North Atlantic Oscillation on Renewable Energy Resources in Southwestern Europe. *Journal of Applied Meteorology and Climatology*. 2013; 52: 2204-2225
- NCEP/NWS/NOAA/U.S. Department of Commerce, 2000. NCEP FNL Operational Model Global Tropospheric Analyses, continuing from July 1999, <http://dx.doi.org/10.5065/D6M043C6>, Research Data Archive at the National Center for Atmospheric Research, Computational and Information Systems Laboratory, Boulder, Colorado, USA. <https://rda.ucar.edu/datasets/ds083.2/>; accessed 11 Feb. 2015.
- Ottersen G, Planque B, Belgrano A, Post E, Reid PC, Stenseth NC. Ecological effects of the North Atlantic Oscillation. *Oecologia*. 2001; 128(1): 1-14.
- Peel MC, Finlayson BL, McMahon TA. Updated world map of the Köppen-Geiger climate classification, *Hydrology and Earth System Sciences*. 2007; 11: 1633-1644.
- Sánchez RF, Relvas P, Delgado M. Coupled ocean wind and sea surface temperature patterns off the western Iberian Peninsula. *Journal of Marine Systems*. 2007; 68(1): 103-127. DOI: [10.1016/j.jmarsys.2006.11.003](https://doi.org/10.1016/j.jmarsys.2006.11.003).
- Trancoso AR, 2012. Operational Modelling as a Tool in Wind Power Forecasts and Meteorological Warnings”, PhD in Environmental Engineering, Instituto Superior Técnico, Lisbon Technical University.
- Trigo RM, Osborn TJ, Corte-Real JM. The North Atlantic Oscillation influence on Europe: Climate impacts and associated physical mechanisms. *Climate Research*. 2002; 20(1): 9-17.



# Chapter III – Evaluation of tides in 2D barotropic and 3D baroclinic numerical model applications for Western Iberia.

---

## Abstract

The observed sea level in any coastal area is the resultant of the interaction of the astronomical tides with the local bathymetry and the influence of other forces such as wind and barometric pressure changes, known as meteorological tides. Despite the importance of atmospheric tides to reproduce the observed water levels and to improve their forecasts, they have been generally neglected compared to the astronomical tides. The continuous improvement of global tide models based on altimetry data has allowed to increase the accuracy of numerical models to forecast water levels in coastal areas.

In this chapter the author completed a comprehensive analysis of the tidal data available for the Western Iberia region and evaluated the performance of the PCOMS regional ocean model when forced with a recent versions of the FES (Finite Element Solution) global tide model (FES2012) both in barotropic (2D) and baroclinic (3D) mode. The 3D baroclinic mode includes the atmospheric influence using meteorological numerical models.

The modelling results show that the PCOMS regional ocean models represents satisfactorily the tides of the Western Iberia region and demonstrate the advantages of 3D baroclinic applications including the meteorological processes compared to the 2D barotropic model applications and to water level reconstruction by tidal harmonic analysis.

## 3.1 Introduction

The Western Iberia coast is exposed to the open ocean dynamics and to the atmospheric climate events, including fronts and low pressure systems, that enters the European continent mainly from the Atlantic Ocean. Generally, these atmospheric systems have a north-south orientation and influence the observed water levels along the entire coast.

When these energetic low pressure systems coincide with high tides, especially with spring tides, the observed water levels increase and maximum differences, i.e. in the order of a meter, between astronomical and observed water level are registered. Commonly, these events are associated with the generation of waves with large heights and adverse conditions coincide resulting in catastrophic events (Taborda and Dias, 1992). On the other hand, low tides combined with extreme high pressures could influence navigation routes increasing the risk of running aground.

The barotropic tides of the Western Iberia region have been studied previously using numerical models by several authors whether using 2D (Sauvaget *et al.*, 2000; Fortunato *et al.*, 2002; Quaresma and Pichon, 2013) or 3D model applications (Fanjul *et al.*, 1997; Marta-Almeida and Dubert, 2006). Those studies analysed the tides evolution in the study region disregarding the baroclinic and meteorological effects in water levels. This is the first study of its kind where tides in this region are evaluated by means of a three-dimensional baroclinic model. A 3D model would be more appropriate to capture the flow details and improve the simulated water levels (Fortunato *et al.*, 2002).

This work is related to the improvement and validation of the Portuguese Coast Operational Modelling System (hereafter referred as PCOMS; Mateus *et al.* 2012), the regional ocean

operational model application that provides boundary conditions to several coastal and estuarine applications (Campuzano *et al.* 2012).

The main objectives of this work are the validation of the modelling results of the 3D operational model currently running for the Western Iberia coast, the analysis of the tidal observations along the Western Iberia coast thus providing a comprehensive set of harmonic components and model simulation and the evaluation of the contribution to the displacement from the astronomical tides due to baroclinic and atmospheric effects.

## 3.2 Material and Methods

### 3.2.1. Data Sources and Analysis

In recent times, public access to coastal tidal gauge records in Europe, and more particularly along the Iberian Peninsula, has been granted through several initiatives being probably the more important the Copernicus Marine Environment Monitoring Service (CMEMS; <http://marine.copernicus.eu/>), through its *In Situ* Thematic Assemble Centre (INS-TAC), that provides access, among others, to long time series from the Puertos del Estado (Spain) tidal network and has recently added some tidal gauges managed by the Instituto Hidrográfico (Portugal). In addition, two Portuguese long-record stations, Cascais and Lagos, maintained by the Instituto Geográfico ([www.igeo.pt/](http://www.igeo.pt/)) were collected and analysed. Finally, the Ceuta tidal station located in Northern Africa and maintained by the Spanish Institute of Oceanography was obtained through the University of Hawaii Sea Level Center (<http://uhslc.soest.hawaii.edu>).

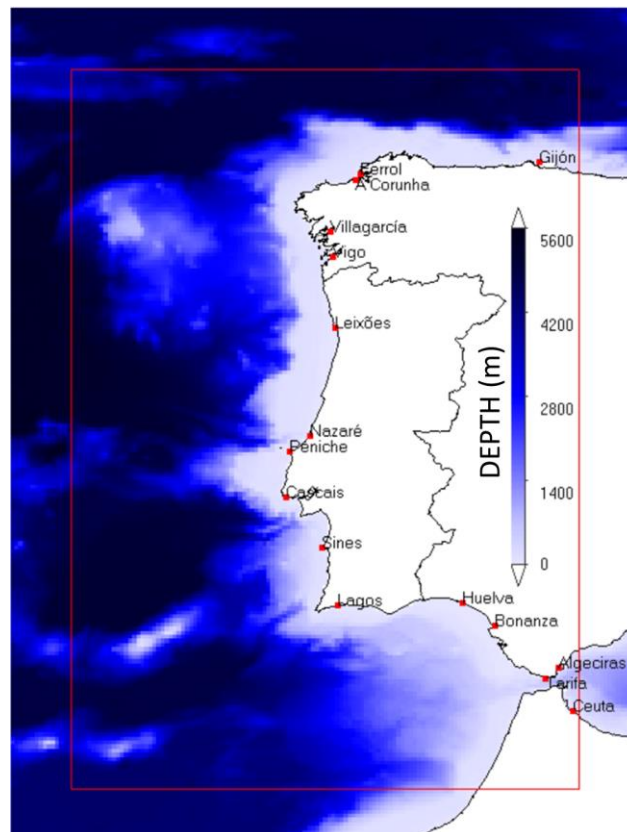


**Figure 1** Bathymetry of the PCOMS modelling domains. The entire domain corresponds to the 2D West Iberia domain while the red box represent the 3D Portugal domain limits. The location of the tidal gauge stations analysed in this chapter are marked with red squares along its name.

Tidal records from those stations (Table I, Figure 1), with a minimum length of a year and maximum of 6 years, were analysed using the PSMSL/POL Tidal Analysis Software Kit 2000 (TASK-2000 Package; Bell *et al.*, 1999). Included in the TASK-2000 Package and developed at

the Proudman Oceanographic Laboratory, the TIRA software allowed through tidal harmonic analysis, based on least squares procedures (Murray, 1964), to obtain 62 tidal components for each tidal gauge. The obtained tidal constituents are able to reproduce the water levels and represent their main source of variability explaining a minimum of 98 % for all the Atlantic tidal gauges (Table I Figure 1). The capacity of the harmonic components in explaining the water levels decreases in the Mediterranean stations down to 91 %.

**Table I. List of tidal gauges, location, analysed period and coefficient of determination ( $R^2$ ) between the observed water levels (OBS) and the water levels reconstructed using the harmonic components obtained from the tidal analysis (TA). The superscript next to the station name indicates the institution responsible for the tidal gauge: <sup>1</sup> stations maintained by Puertos del Estado (Spain) <sup>2</sup> stations maintained by Instituto Hidrográfico (Portugal), <sup>3</sup> stations maintained by Instituto Geográfico (Portugal) and <sup>4</sup> station maintained by Instituto Español de Oceanografía (Spain). Stations are listed from North to South.**

Tidal Gauge	Latitude	Longitude	Data Period	OBS -TA $R^2$
Gijón <sup>1</sup>	43.62 °N	5.69 °W	01/01/2011 - 31/12/2015	0.988 (N = 43375)
Ferrol <sup>1</sup>	43.46 °N	8.33 °W	01/01/2011 - 31/12/2015	0.986 (N = 42543)
A Corunha <sup>1</sup>	43.36 °N	8.39 °W	01/01/2011 - 31/12/2015	0.987 (N = 43769)
Vilagarcía <sup>1</sup>	42.60 °N	8.77 °W	01/01/2011 - 31/12/2015	0.981 (N = 43348)
Vigo <sup>1</sup>	42.24 °N	8.73 °W	01/01/2011 - 31/12/2015	0.982 (N = 43505)
Leixões <sup>2</sup>	41.18 °N	8.70 °W	20/09/2014 - 30/09/2015	0.986 (N = 7535)
Nazaré <sup>2</sup>	39.59 °N	9.07 °W	20/09/2014 - 30/09/2015	0.989 (N = 8215)
Peniche <sup>2</sup>	39.35 °N	9.37 °W	01/10/2014 - 30/09/2015	0.991 (N = 7825)
Cascais <sup>3</sup>	38.69 °N	9.42 °W	01/01/2010 - 30/09/2015	0.984 (N = 43133)
Sines <sup>2</sup>	37.95 °N	8.89 °W	20/09/2014 - 30/09/2015	0.993 (N = 8161)
Lagos <sup>3</sup>	37.10 °N	8.67 °W	01/01/2012 - 30/09/2015	0.990 (N = 27162)
Huelva <sup>1</sup>	37.13 °N	6.83 °W	01/01/2011 - 31/12/2015	0.989 (N = 43588)
Bonanza <sup>1</sup>	36.80 °N	6.34 °W	01/01/2011 - 31/12/2015	0.983 (N = 42928)
Algeciras <sup>1</sup>	36.18 °N	5.40 °W	01/01/2011 - 31/12/2015	0.923 (N = 42722)
Tarifa <sup>1</sup>	36.01 °N	5.60 °W	01/01/2011 - 31/12/2015	0.955 (N = 43099)
Ceuta <sup>4</sup>	35.90 °N	5.32 °W	01/01/2011 - 31/05/2015	0.917 (N = 38140)

It is important to include some remarks about the location of some of the tidal gauges stations. Algeciras, Tarifa and Ceuta tidal gauges are located in the Mediterranean Sea close to the limits of the PCOMS modelling domains. The PCOMS numerical application was originally designed to provide accurate forecasts for the Western Iberia region and not to reproduce accurately the hydrodynamics near the Mediterranean Sea. Those four stations were included in the current analysis to make it as comprehensive as possible and to include information that would be useful to compare with past and future studies in the study area. Additionally, the Bonanza tidal gauge is located in the inner area of the Guadalquivir estuary and thus its levels are influenced by the more complex estuarine dynamics that cannot be solved by a regional ocean model application. In the spite of completeness, data analysis for this station and for the modelling results at its closest water point will be presented in this chapter.

In this work, from the obtained 62 tidal components, the analysis focused in the analysis of the main semidiurnal ( $M_2$ ,  $S_2$ ,  $N_2$ ,  $K_2$ ), diurnal ( $O_1$ ,  $K_1$ ,  $P_1$ ,  $Q_1$ ), radiational ( $S_a$ ,  $S_{sa}$ ) and overtimes ( $M_4$ ) tidal components in Western Iberia. Amplitude and phase for those components are listed in Table II and Table I Table III respectively. The amplitude is led, in every station, by three semidiurnal components ( $M_2$ ,  $S_2$ ,  $N_2$ ). In the Atlantic area, those three stations are followed by a fourth semidiurnal component  $K_2$  while on the Mediterranean side (Algeciras, Tarifa and Ceuta) the  $K_2$  component decreases sharply, being overpassed by other diurnal and radiational

tides. In the North, the semidiurnal components are followed in amplitude by the diurnal components ( $O_1$ ,  $K_1$ ) however the radiational components overpass them as they increase their importance from Leixões southwards.

**Table II. Amplitude in meters of the main tidal components for the analysed stations in the Western Iberia region. The table includes the main semidiurnal constituents ( $M_2$ ,  $S_2$ ,  $N_2$ ,  $K_2$ ), the main diurnal constituents ( $O_1$ ,  $K_1$ ,  $Q_1$ ,  $P_1$ ), the main long tide constituents ( $Sa$ ,  $Ssa$ ), the main overtide component ( $M_4$ ) and the Formzahl coefficient ( $F$ ) for each station.**

Tidal Gauge	$M_2$	$S_2$	$N_2$	$K_2$	$O_1$	$K_1$	$Q_1$	$P_1$	$Sa$	$Ssa$	$M_4$	$F$
Gijón	1.286	0.448	0.271	0.125	0.067	0.067	0.022	0.020	0.053	0.034	0.021	0.077
Ferrol	1.186	0.414	0.252	0.115	0.065	0.073	0.022	0.023	0.048	0.039	0.012	0.086
A Corunha	1.185	0.413	0.252	0.115	0.065	0.074	0.022	0.023	0.050	0.043	0.012	0.087
Vilagarcía	1.138	0.397	0.242	0.110	0.064	0.075	0.021	0.024	0.049	0.047	0.008	0.090
Vigo	1.099	0.384	0.234	0.106	0.064	0.073	0.021	0.023	0.046	0.050	0.008	0.092
Leixões	1.050	0.366	0.225	0.103	0.065	0.071	0.022	0.021	0.095	0.086	0.008	0.095
Nazaré	0.998	0.351	0.215	0.099	0.061	0.070	0.022	0.021	0.083	0.073	0.009	0.097
Peniche	1.032	0.360	0.221	0.100	0.065	0.078	0.022	0.024	0.091	0.077	0.009	0.102
Cascais	0.992	0.350	0.213	0.097	0.060	0.070	0.018	0.022	0.046	0.043	0.010	0.097
Sines	0.988	0.350	0.212	0.098	0.063	0.072	0.022	0.022	0.071	0.066	0.012	0.100
Lagos	1.001	0.359	0.214	0.099	0.061	0.069	0.019	0.023	0.067	0.055	0.015	0.096
Huelva	1.042	0.374	0.222	0.104	0.058	0.065	0.019	0.022	0.067	0.053	0.029	0.087
Bonanza	0.893	0.306	0.184	0.086	0.061	0.062	0.018	0.022	0.049	0.052	0.050	0.102
Algeciras	0.325	0.117	0.066	0.033	0.009	0.023	0.004	0.008	0.065	0.038	0.019	0.073
Tarifa	0.419	0.156	0.088	0.044	0.005	0.025	0.005	0.008	0.050	0.042	0.038	0.053
Ceuta	0.302	0.114	0.062	0.034	0.020	0.037	0.002	0.011	0.056	0.036	0.026	0.138

**Table III. Phase in degrees of the main tidal components for the analysed stations in the Western Iberia region including the main semidiurnal constituents ( $M_2$ ,  $S_2$ ,  $N_2$ ,  $K_2$ ), the main diurnal constituents ( $O_1$ ,  $K_1$ ,  $Q_1$ ,  $P_1$ ), the main long tide constituents ( $Sa$ ,  $Ssa$ ) and the main overtide component ( $M_4$ ) for each station.**

Tidal Gauge	$M_2$	$S_2$	$N_2$	$K_2$	$O_1$	$K_1$	$Q_1$	$P_1$	$Sa$	$Ssa$	$M_4$
Gijón	91.23	123.47	71.80	121.09	324.10	71.04	271.78	60.59	212.62	68.70	318.58
Ferrol	86.80	117.69	67.83	115.59	325.55	72.13	270.08	62.78	216.38	67.87	298.08
A Corunha	86.35	117.17	67.45	114.67	325.21	71.80	270.21	61.15	208.26	67.19	289.03
Vilagarcía	79.20	109.03	60.65	106.69	321.50	63.79	265.46	54.99	223.41	64.51	241.00
Vigo	77.47	106.91	59.02	104.47	320.61	62.93	264.50	54.93	209.48	61.49	228.64
Leixões	74.61	103.19	56.69	102.86	319.07	60.24	269.70	47.73	185.52	83.70	216.77
Nazaré	69.66	97.28	51.86	95.90	317.59	60.29	270.88	45.24	184.12	83.51	190.92
Peniche	69.95	97.47	51.61	96.07	316.04	55.86	267.15	45.36	184.26	83.03	185.41
Cascais	64.61	91.26	47.39	88.20	314.47	54.41	256.62	43.23	203.61	65.41	184.60
Sines	62.92	89.65	45.62	87.80	313.90	54.87	269.45	45.66	177.24	90.79	167.04
Lagos	57.91	83.68	41.58	80.69	310.74	48.61	257.66	38.95	180.00	75.56	163.13
Huelva	57.11	83.56	41.05	80.83	311.02	47.52	258.72	39.43	157.65	61.80	168.17
Bonanza	63.72	90.50	48.20	88.48	323.45	59.91	269.83	51.51	157.95	49.40	86.47
Algeciras	48.98	76.91	34.00	77.32	162.69	129.69	196.27	132.71	177.05	63.94	177.05
Tarifa	41.72	69.22	26.95	67.23	126.60	129.03	218.22	131.75	170.44	62.93	118.10
Ceuta	48.78	76.95	35.30	66.65	102.45	141.71	192.25	140.78	173.44	67.00	160.47

The Formzahl coefficient ( $F$ ) provides a quantification of the degree of influence of the semidiurnal and diurnal components. It's calculated by dividing the sum of the two main

diurnal tidal components ( $K_1$  and  $O_1$ ) by the sum of the two main semidiurnal components ( $M_2$  and  $S_2$ ). According to the F ratio, tides can be considered diurnal ( $F > 3$ ), semidiurnal ( $F < 0.25$ ) or mixed ( $0.25 < F < 3$ ). Tides in Western Iberia present a clear semidiurnal character along the entire coast; however in central Portugal diurnal components have larger impact (Table II).

Among the semidiurnal components, the  $M_2$  tidal component presents the largest amplitude followed by the  $S_2$ ,  $N_2$  and  $K_2$  components. The semidiurnal components (Table II, Figure 2) decrease steadily from North to South except for some amplification taking place in the Gulf of Cadis (i.e. Lagos and Huelva stations). All the values drop drastically as Strait of Gibraltar is approached (i.e. Algeciras, Tarifa and Ceuta stations).

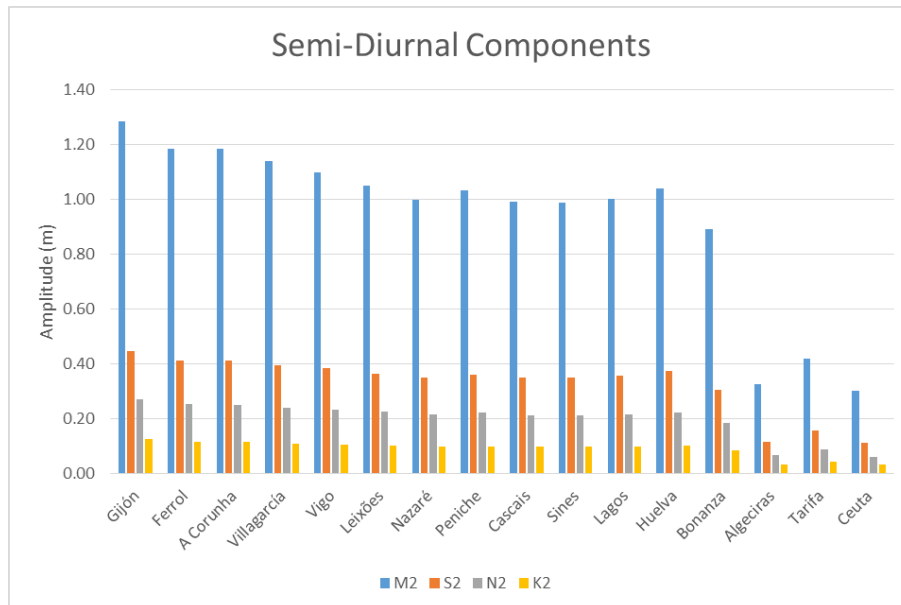


**Figure 2** Amplitude, in meters, for the main semidiurnal tidal components in the analysed stations of the Western Iberia region. Stations are ordered from North (left) to South (right).

Main diurnal components evolve along the West Iberia coast in a different fashion than the semidiurnal components only with the exception of the  $O_1$  component that decreases southwards as the semidiurnal components (Table II, Figure 3). The  $K_1$  component has its maximum amplitude in the Peniche tidal gauge in the central part of Portugal while the  $P_1$  and  $Q_1$  components present stable values all along the coast until reaching the Strait of Gibraltar where all the diurnal components decrease in magnitude.

Long-period components, also known as radiational tides due to their relationship with the solar radiation cycles and generated by periodic meteorological forcing, such as the solar semiannual ( $S_{sa}$ ) and annual ( $S_a$ ) constituents have been identified also relevant in this coastal area (Quaresma and Pichon, 2015). With amplitudes of the same order of magnitude than the diurnal components, maximum values for those components were also observed in central Portugal between Leixões and Peniche where the  $S_a$  constituent is larger than the  $K_1$  constituent (Table II, Figure 4).

The so-called compound tides, overtides or shallow water constituents (i.e.  $M_4$ ,  $MS_4$  and  $MN_4$ ) are generated by nonlinear interactions of primary constituents with the seabed and are largely dependent on the bathymetry, the shape of the shelf, and the regional tidal regime (Andersen, 1999). Their contribution is important in the Gulf of Cadiz and the vicinity of the Strait of Gibraltar with amplitudes similar to the  $K_1$  component (Table II, Figure 4).  $M_4$  maximum value was found in the Bonanza station that can be explained due to its location inside the Guadalquivir estuary.

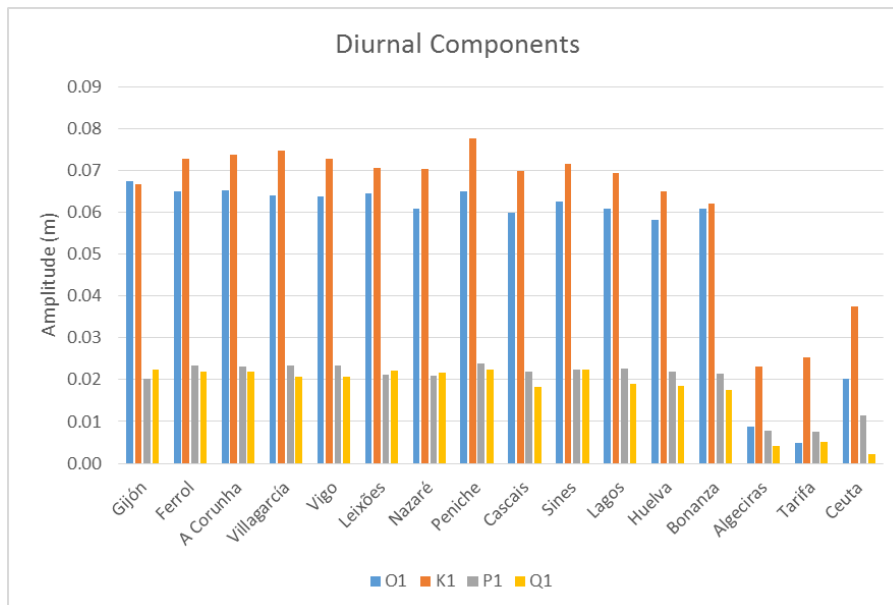


Figure 3 Amplitude, in meters, for the main diurnal tidal components in the analysed stations of the Western Iberia region. Stations are ordered from North (left) to South (right).

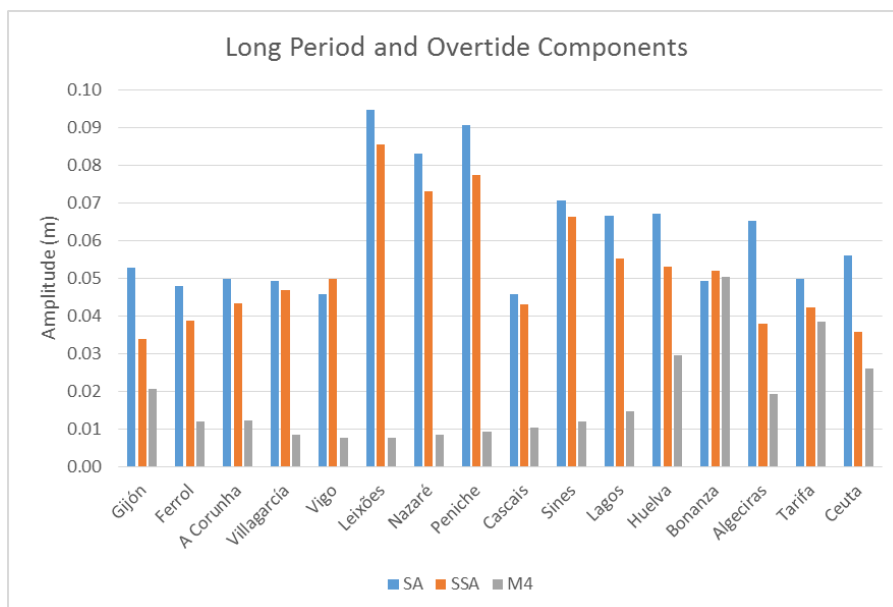


Figure 4 Amplitude, in meters, for the main long period tidal and overtide components in the analysed stations of the Western Iberia region. Stations are ordered from North (left) to South (right).

### 3.2.2. Harmonic components error and previous studies

The amplitudes and phases obtained during this study are similar to previous studies (Fanjul *et al.*, 1997; Fortunato *et al.*, 2002; Quaresma and Pichon, 2013). However, values between different studies can present for some tidal components differences up to 10% in amplitude and phase. These differences could probably be related with the methods and periods used for each study. Fortunato *et al.* (2002) found, using the same method of analysis, an inter-annual variability up to 4% and 1% for amplitudes and phases respectively.

To evaluate the variability associated to the tidal records analysis method and period, values provided for the main tidal components ( $M_2$ ,  $N_2$ ,  $S_2$ ,  $K_2$ ,  $Q_1$ ,  $O_1$ ,  $P_1$  and  $K_1$ ) and common tidal gauges (Gijón, A Corunha, Leixões, Peniche, Cascais, Sines, Lagos and Huelva) in Fanjul *et al.* (1997), Fortunato *et al.* (2002) and Quaresma and Pichon (2013) were compared with the ones obtained in the present study. Average values for amplitude and phase for each station were calculated and those values were compared with the amplitude and phase provided in each study. Note that to calculate the phase percentages it was considered that a phase difference

of 180° would represent 100% error. Diurnal components showed the maximum variability between studies reaching 10% for the amplitude and 3.5% for the phase. On the other hand, semidiurnal components presented maximum differences around 2.4% both for amplitude and phase. On average, there is an error around 1.25% and 0.40% associated to the amplitude and phase calculation respectively. The analysis performed in the current work has an error of amplitude and phase estimation with the same order of magnitude than the previous figures.

### 3.3 Numerical Model and modelling domains

In order to evaluate the tides evolution in western Iberia, a numerical application covering the study area was ran using the MOHID Water which is part of the MOHID Modelling System (<http://www.mohid.com>; Neves, 2013). The MOHID Water Modelling System is an open source modular finite volumes modelling system written in ANSI FORTRAN 95 using an object oriented programming philosophy integrating several numerical programs and supported by graphical user interfaces that manage all the pre- and post-processing. The MOHID Water model is a 3D integrated model, capable of simulating a wide range of processes (e.g. hydrodynamics, transport, water quality, oil spills) in surface water bodies (oceans, coastal areas, estuaries and reservoirs). This system is being developed since 1985 mainly by the MARETEC research group at the Instituto Superior Técnico (IST) part of the Universidade de Lisboa.

The regional ocean operational model application for the Western Iberia, PCOMS, is composed of two nested domains: the West Iberia (2D) and the Portugal (3D) domains covering the Iberian Atlantic coast and its contiguous ocean (Figure 1). Both domains present a constant horizontal resolution of 0.06° ( $\approx$  6 km) populated with bathymetric information derived from the EMODnet Hydrography portal (<http://www.emodnet-hydrography.eu>; as available in January 2012). The West Iberia domain covers the area limited the following range of latitudes (33.48 °N, 45.90 °N) and longitudes (4.20 °W, 13.50 °W) resulting in a grid of 207X155 cells with maximum depths around 5600 m. The Portugal domain covers the area comprised by the latitudes (34.38 °N, 45.00 °N) and the longitudes (5.10 °W, 12.60 °W) resulting in a grid of 177X125 cells and maximum depths around 5300 m. Tides are forced, along the ocean boundary of the West Iberia (2D) model domain and provide boundary conditions to the Portugal domain. The Portugal Domain is located centred in the West Iberia domain, leaving 15 cells of difference in every direction, and downscales the Mercator-Océan PSY2V4 North Atlantic solution (Drillet *et al.*, 2005).

The Portugal modelling domain is a full 3D baroclinic hydrodynamic and ecological model application operated by the MOHID Water model. Its vertical discretisation consists on a mixed vertical geometry composed of a sigma domain with 7 layers from the surface until 8.68 m depth, with variable thickness decreasing up to 1 m at the surface, on top of a Cartesian domain of 43 layers with thickness increasing towards the bottom. As atmospheric boundary conditions, this domain uses MM5 modelling results (Grell *et al.*, 1994) with 9 km horizontal resolution provided by the IST meteorological group (<http://meteo.tecnico.ulisboa.pt/>).

### 3.4 Tidal Forcing

Tides in the PCOMS are forced along the open boundary of the WestIberia domain that also provides to the nested Portugal modelling domain. For this study, the PCOMS simulated the year 2011 using as tidal conditions a version of the FES (Finite Element Solution) global tidal model: the FES2012 model (Carrère *et al.*, 2012).

FES2012 takes advantage of longer altimeter time series, improved modelling and data assimilation techniques and a more accurate ocean bathymetry than the previous version the FES2004 model (Lyard *et al.*, 2006). The new global finite element grid,  $\sim$ 1.5 million nodes, led to a twice more accurate 'free' solution than the FES2004 version with  $\sim$ 1 million nodes and the gridded resolution of the distributed package is now 1/16° instead of 1/8°. Finally, FES2012

solution shows strong improvement compared to FES2004, particularly in coastal and shelf regions and due to the incorporation of several non-linear hydrodynamic waves (i.e.  $M_4$ ,  $M_6$ ,  $M_8$ ,  $MN_4$  ...) however no tidal gauge has been assimilated. Despite the increase in nodes and horizontal resolution, slight degradation was detected in some deep ocean regions and some tidal gauge (Carrère *et al.*, 2012). For this reason, this study aims to evaluate the performance of this solution in the Western Iberia coast.

The MOHID Water tidal module allows the implementation of 30 out of the 32 tidal constituents of the FES2012, all but MTM and  $N_4$ . The imposed FES2012 harmonic constituents were:  $2N_2$ ,  $E_2$ ,  $J_1$ ,  $K_1$ ,  $K_2$ ,  $L_2$ ,  $LDA_2$ ,  $M_2$ ,  $M_3$ ,  $M_4$ ,  $M_6$ ,  $M_8$ ,  $M_f$ ,  $MKS_2$ ,  $Mm$ ,  $MN_4$ ,  $MS_4$ ,  $MSF$ ,  $MU_2$ ,  $N_2$ ,  $NU_2$ ,  $O_1$ ,  $P_1$ ,  $Q_1$ ,  $R_2$ ,  $S_1$ ,  $S_2$ ,  $S_4$ ,  $Ssa$ ,  $T_2$ . For the FES2004 simulations the following tidal components were used:  $M_2$ ,  $S_2$ ,  $K_1$ ,  $K_2$ ,  $N_2$ ,  $2N_2$ ,  $O_1$ ,  $Q_1$ ,  $P_1$ ,  $M_4$ ,  $MF$ ,  $MM$ ,  $MSqm$ .

To evaluate the performance of the tides modelling in Western Iberia, the observed data and their harmonic analysis were compared with 2D and 3D modelling results from the WestIberia and Portugal modelling domains respectively for the year 2011. This approach allows evaluating the effect of the atmospheric and 3D baroclinic processes in the water levels.

### 3.5 Tidal forcing configuration

The FES2012 tidal components were provided directly to each cell located in the open boundary. The MOHID model also calculate the tidal potential for 12 harmonic components ( $M_2$ ,  $S_2$ ,  $K_2$ ,  $N_2$ ,  $K_1$ ,  $O_1$ ,  $P_1$ ,  $Q_1$ ,  $S_{sa}$ ,  $M_m$ ,  $M_f$ ,  $M_3$ ) as described in Lefèvre (2000).

Regarding the PCOMS model parameterisation, both domains use a constant horizontal turbulent viscosity  $20 \text{ m}^2\text{s}^{-1}$ . A biharmonic filter was added in the boundary condition. The biharmonic filter (Equation 1) consists on an extra term that is added in the horizontal turbulent viscous flux,  $J$ , that filters high frequency oscillations in a numerical model of advection-diffusion of a property  $C$  (i.e. oscillations with a wave-length equal to one or two widths of the horizontal resolution):

$$J = -K \cdot \nabla C + \nabla_h (\kappa_4 \nabla_h^2 C) \quad \text{Equation 1}$$

where  $K$  is the Laplacian diffusion tensor,  $\kappa_4$  is the horizontal coefficient for biharmonic mixing, that for the Portugal and WestIberia domain were set as  $5.5 \cdot 10^9 \text{ m}^4\text{s}^{-1}$  and  $1 \cdot 10^{10} \text{ m}^4\text{s}^{-1}$  respectively, and  $\nabla_h$  is the horizontal isopycnic part of the  $\nabla$  differential operator (Delhez and Deleersnijder, 2007).

The 3D Portugal numerical domain use the inverse barometer correction added at the boundary conditions to correct the tidal signal and the water level in every cell of the model according to the inverse relationship between the atmospheric pressure and water levels, known as the local inverse barometer (LIB) equation (Equation 2) (Wunsch and Stammer, 1997):

$$\Delta \zeta = -\Delta P_A (\rho g)^{-1} \quad \text{Equation 2}$$

Where  $\Delta \zeta$  and  $\Delta P_A$  correspond to sea-level and air pressure changes respectively and  $\rho$  is water density and  $g$  is the acceleration due to gravity. In the MOHID numerical model the water density is regarded as the surface density and in practical terms 1 mb decrease of atmospheric pressure results in a 1.01 cm increase in water level. Moreover, wind forcing was added to the 3D Portugal domain that could influence water levels. Instantaneous atmospheric pressure and wind intensity and direction values were obtained from the MM5 model application implemented by the IST meteorological group (<http://meteo.tecnico.ulisboa.pt/>; Trancoso, 2012).

### 3.6 Tidal constituents analysis and validation

In order to evaluate the performance of the numerical modelling application for reproducing the water levels along the western Iberian coast, a harmonic analysis, following the same methodology used with the observed data, was performed for time series extracted at the nearest water cell from each tidal gauge station location.

The same 62 tidal components were obtained for each location that can be compared with the values previously obtained for the observed tidal gauge data and with the original values from the FES2012 global tide model at the same locations. For practical reasons comparisons of harmonic components were limited to the main semidiurnal components ( $M_2$ ,  $S_2$ ,  $N_2$  and  $K_2$ ), the main diurnal components ( $O_1$ ,  $K_1$ ,  $Q_1$  and  $P_1$ ), the main overtide component ( $M_4$ ) and the greater radiational component ( $Ssa$ ). Though identified in previous sections as an important component, the  $Sa$  radiational component was excluded from this analysis as it's not included in the FES2012 model dataset.

The harmonic components obtained from the observed tidal gauge served to reconstruct the astronomic water levels for the stations where the available data did not include the analysed period, the year 2011 (Table I). The MARIE software, also included in the TASK-2000 Package, served to generate hourly time series for those locations (i.e. Leixões, Nazaré, Sines and Lagos).

Figure 5 and Figure 6 show the tidal amplitude and phase, respectively, for each of the analysed tidal components at each tidal gauge location ordered from North to South (Left to Right in the figures) obtained from observations, from the global tide model FES2012, from the MOHID model for the WestIberia 2D domain forced with FES2012 (PCOMS\_2D scenario) and finally from the surface layer of the MOHID model Portugal 3D domain forced with FES2012 (PCOMS\_3D scenario). Note that although Tarifa is positioned southern to Algeciras, its location is in the oceanic side of the Strait of Gibraltar compared with Algeciras that is located in the Mediterranean side (Figure 1).

The tidal amplitude for the main semidiurnal constituents decreases steadily in the North South direction and reduces dramatically when entering the Mediterranean waters. The diurnal components reproduced the same pattern as the semidiurnal components until the Strait of Gibraltar. However, after entering the Mediterranean waters, the diurnal constituents evolve differently due to the presence of amphidromic points in this area (See Appendix I). The overtide component  $M_4$  indicates the shallow water effect in the tidal signal. To resolve satisfactory the shallow water constituents in the southern stations a higher resolution model able to reproduce the bathymetry effect in the water levels will be required.

While the previous constituents can be termed as gravitational tides, the movement due to regular meteorological forces named as meteorological tides or more usually radiational tides because their period is linked to the solar day. As those seasonal changes in water levels due to the climate variations are regular thus they are regarded as tidal (Howarth and Pugh, 1983).



Figure 5 Amplitude of the harmonic constituents ( $M_2$ ,  $S_2$ ,  $N_2$ ,  $K_2$ ,  $O_1$ ,  $K_1$ ,  $Q_1$ ,  $P_1$ ,  $M_4$ ,  $S_{sa}$ ) for the tidal gauges in Western Iberia ordered from North to South (left to right in the graphs). The amplitudes correspond for the Observed values (orange line), FES2012 (light blue line), MOHID WestIberia domain 2D forced with FES2012 (dark blue line) and MOHID Portugal domain 3D forced with FES2012 (green line).



Figure 6 Phase of the harmonic constituents ( $M_2$ ,  $S_2$ ,  $N_2$ ,  $K_2$ ,  $O_1$ ,  $K_1$ ,  $Q_1$ ,  $P_1$ ,  $M_4$ ,  $S_{sa}$ ) for the tidal gauges in Western Iberia ordered from North to South (left to right in the graphs). The amplitudes correspond for the Observed values (orange line), FES2012 (light blue line), MOHID WestIberia domain 2D forced with FES2012 (dark blue line) and MOHID Portugal domain 3D forced with FES2012 (green line).

Table IV. Amplitude for the main semidiurnal harmonics obtained by harmonic analysis of the observed data, their correspondent value in FES2012 global tidal models for those locations and calculated with modelling results of PCOMS\_2D and PCOMS\_3D scenarios. Percentage of error respect the observed harmonic amplitude within brackets.

STATION	HARMONIC	OBSERVED	FES2012	PCOMS_2D	PCOMS_3D
Gijón	M <sub>2</sub>	1.286	1.269 (-1.29)	1.335 (3.80)	1.319 (2.57)
	S <sub>2</sub>	0.448	0.448 (-0.08)	0.46 (2.68)	0.457 (1.90)
	N <sub>2</sub>	0.271	0.271 (0.04)	0.28 (3.06)	0.276 (1.81)
	K <sub>2</sub>	0.125	0.124 (-1.02)	0.128 (2.64)	0.128 (1.92)
Ferrol	M <sub>2</sub>	1.186	1.17 (-1.32)	1.22 (2.88)	1.205 (1.63)
	S <sub>2</sub>	0.414	0.414 (0.06)	0.419 (1.21)	0.416 (0.46)
	N <sub>2</sub>	0.252	0.249 (-1.12)	0.255 (0.99)	0.252 (-0.20)
	K <sub>2</sub>	0.115	0.116 (0.93)	0.12 (4.00)	0.119 (3.22)
A Corunha	M <sub>2</sub>	1.185	1.168 (-1.50)	1.22 (2.92)	1.205 (1.65)
	S <sub>2</sub>	0.413	0.412 (-0.17)	0.419 (1.45)	0.416 (0.73)
	N <sub>2</sub>	0.252	0.249 (-1.39)	0.255 (1.07)	0.252 (-0.16)
	K <sub>2</sub>	0.115	0.115 (0.48)	0.119 (3.92)	0.119 (3.39)
Villagarcía	M <sub>2</sub>	1.138	1.092 (-4.12)	1.13 (-0.78)	1.137 (-0.17)
	S <sub>2</sub>	0.397	0.386 (-2.56)	0.39 (-1.64)	0.39 (-1.59)
	N <sub>2</sub>	0.242	0.231 (-4.48)	0.238 (-1.37)	0.24 (-0.87)
	K <sub>2</sub>	0.110	0.108 (-1.65)	0.11 (0.18)	0.11 (0.00)
Vigo	M <sub>2</sub>	1.099	1.078 (-1.88)	1.129 (2.79)	1.134 (3.25)
	S <sub>2</sub>	0.384	0.379 (-1.22)	0.39 (1.75)	0.393 (2.35)
	N <sub>2</sub>	0.234	0.228 (-2.74)	0.239 (1.84)	0.239 (1.96)
	K <sub>2</sub>	0.106	0.106 (-0.33)	0.11 (3.76)	0.111 (4.23)
Leixões	M <sub>2</sub>	1.050	1.036 (-1.31)	1.098 (4.55)	1.084 (3.27)
	S <sub>2</sub>	0.366	0.364 (-0.37)	0.38 (4.08)	0.375 (2.54)
	N <sub>2</sub>	0.225	0.222 (-1.25)	0.233 (3.65)	0.231 (2.76)
	K <sub>2</sub>	0.103	0.101 (-1.31)	0.107 (4.09)	0.105 (2.34)
Nazaré	M <sub>2</sub>	0.998	0.998 (-0.02)	1.058 (5.99)	1.047 (4.95)
	S <sub>2</sub>	0.351	0.353 (0.55)	0.368 (4.84)	0.366 (4.33)
	N <sub>2</sub>	0.215	0.216 (0.53)	0.225 (4.74)	0.223 (3.81)
	K <sub>2</sub>	0.099	0.098 (-1.45)	0.103 (3.63)	0.102 (3.12)
Peniche	M <sub>2</sub>	1.032	1.005 (-2.70)	1.067 (3.31)	1.075 (4.15)
	S <sub>2</sub>	0.360	0.356 (-0.94)	0.372 (3.50)	0.373 (3.67)
	N <sub>2</sub>	0.221	0.217 (-1.88)	0.227 (2.53)	0.23 (3.66)
	K <sub>2</sub>	0.100	0.099 (-1.19)	0.104 (3.70)	0.104 (3.90)
Cascais	M <sub>2</sub>	0.992	0.982 (-0.97)	1.025 (3.29)	1.033 (4.11)
	S <sub>2</sub>	0.350	0.353 (0.73)	0.361 (3.17)	0.364 (3.91)
	N <sub>2</sub>	0.213	0.212 (-0.30)	0.219 (2.63)	0.22 (3.33)
	K <sub>2</sub>	0.097	0.098 (0.65)	0.1 (3.09)	0.1 (3.30)
Sines	M <sub>2</sub>	0.988	0.987 (-0.10)	0.993 (0.50)	1.035 (4.73)
	S <sub>2</sub>	0.350	0.356 (1.69)	0.352 (0.57)	0.365 (4.23)
	N <sub>2</sub>	0.212	0.216 (1.88)	0.213 (0.28)	0.221 (4.25)
	K <sub>2</sub>	0.098	0.098 (-0.08)	0.097 (-1.22)	0.101 (2.34)
Lagos	M <sub>2</sub>	1.001	0.999 (-0.25)	1.022 (2.02)	1.039 (3.73)
	S <sub>2</sub>	0.359	0.364 (1.44)	0.365 (1.76)	0.371 (3.46)
	N <sub>2</sub>	0.214	0.219 (2.19)	0.218 (1.68)	0.221 (3.22)
	K <sub>2</sub>	0.099	0.1 (1.45)	0.1 (1.52)	0.101 (2.63)
Huelva	M <sub>2</sub>	1.042	1.02 (-2.06)	1.058 (1.54)	1.082 (3.90)
	S <sub>2</sub>	0.374	0.377 (0.91)	0.379 (1.31)	0.388 (3.69)
	N <sub>2</sub>	0.222	0.227 (2.10)	0.226 (1.53)	0.23 (3.69)
	K <sub>2</sub>	0.104	0.104 (-0.08)	0.104 (0.29)	0.106 (2.31)
Bonanza	M <sub>2</sub>	0.893	1.021 (14.40)	1.066 (19.42)	1.092 (22.26)
	S <sub>2</sub>	0.306	0.378 (23.53)	0.382 (24.67)	0.392 (27.81)
	N <sub>2</sub>	0.184	0.227 (22.91)	0.227 (23.21)	0.232 (25.87)
	K <sub>2</sub>	0.086	0.104 (21.86)	0.105 (22.81)	0.107 (25.03)
Algeciras	M <sub>2</sub>	0.325	0.483 (48.80)	0.306 (-5.76)	0.33 (1.51)
	S <sub>2</sub>	0.117	0.18 (53.21)	0.116 (-1.53)	0.124 (5.20)
	N <sub>2</sub>	0.066	0.104 (58.02)	0.064 (-3.48)	0.069 (4.09)
	K <sub>2</sub>	0.033	0.051 (53.70)	0.032 (-3.93)	0.033 (0.91)
Tarifa	M <sub>2</sub>	0.419	0.314 (-25.02)	0.486 (16.05)	0.507 (21.14)
	S <sub>2</sub>	0.156	0.118 (-24.31)	0.178 (13.87)	0.186 (18.86)
	N <sub>2</sub>	0.088	0.067 (-24.44)	0.102 (15.72)	0.107 (20.81)
	K <sub>2</sub>	0.044	0.034 (-22.16)	0.049 (10.48)	0.051 (15.26)
Ceuta	M <sub>2</sub>	0.302	0.241 (-20.02)	0.311 (3.15)	0.261 (-13.59)
	S <sub>2</sub>	0.114	0.092 (-18.78)	0.116 (2.46)	0.099 (-12.59)
	N <sub>2</sub>	0.062	0.051 (-18.74)	0.065 (4.33)	0.054 (-13.62)
	K <sub>2</sub>	0.034	0.026 (-23.08)	0.032 (-3.58)	0.027 (-20.60)

Table V. Phase for the main semidiurnal harmonics obtained by harmonic analysis of the observed data, their correspondent value in FES2012 global tidal models for those locations and calculated with modelling results of PCOMS\_2D and PCOMS\_3D scenarios. Percentage of error respect the observed harmonic phase within brackets (considering 180° as 100% of error).

STATION	HARMONIC	OBSERVED	FES2012	PCOMS_2D	PCOMS_3D
Gijón	M <sub>2</sub>	91.23	91.29 (0.03)	93.86 (1.46)	94.42 (1.77)
	S <sub>2</sub>	123.47	122.54 (0.51)	124.41 (0.52)	125.01 (0.86)
	N <sub>2</sub>	71.80	71.73 (0.04)	74.16 (1.31)	74.79 (1.66)
	K <sub>2</sub>	121.09	120.15 (0.52)	122.77 (0.94)	123.53 (1.36)
Ferrol	M <sub>2</sub>	86.80	86.58 (0.12)	87.95 (0.64)	88.16 (0.76)
	S <sub>2</sub>	117.69	116.36 (0.74)	118.05 (0.20)	118.49 (0.44)
	N <sub>2</sub>	67.83	66.75 (0.60)	69 (0.65)	69.41 (0.88)
	K <sub>2</sub>	115.59	113.71 (1.04)	115.88 (0.16)	116.33 (0.41)
A Corunha	M <sub>2</sub>	86.35	86.75 (0.22)	87.82 (0.82)	88.03 (0.93)
	S <sub>2</sub>	117.17	116.52 (0.36)	117.92 (0.42)	118.35 (0.66)
	N <sub>2</sub>	67.45	66.83 (0.34)	68.9 (0.80)	69.27 (1.02)
	K <sub>2</sub>	114.67	114.1 (0.32)	115.74 (0.59)	116.08 (0.78)
Vilagarcía	M <sub>2</sub>	79.20	78.36 (0.47)	79.87 (0.37)	80.41 (0.67)
	S <sub>2</sub>	109.03	107.03 (1.11)	109.24 (0.12)	110.29 (0.70)
	N <sub>2</sub>	60.65	59.23 (0.79)	61.84 (0.66)	62.16 (0.84)
	K <sub>2</sub>	106.69	104.36 (1.29)	105.48 (0.67)	106.32 (0.20)
Vigo	M <sub>2</sub>	77.47	76.92 (0.31)	78.76 (0.72)	79.13 (0.92)
	S <sub>2</sub>	106.91	105.6 (0.72)	108.04 (0.63)	108.96 (1.14)
	N <sub>2</sub>	59.02	58 (0.57)	60.8 (0.99)	61.16 (1.19)
	K <sub>2</sub>	104.47	102.8 (0.93)	104.16 (0.17)	105.05 (0.32)
Leixões	M <sub>2</sub>	74.61	74.37 (0.14)	75.79 (0.66)	76.94 (1.29)
	S <sub>2</sub>	103.19	102.82 (0.20)	104.61 (0.79)	105.91 (1.52)
	N <sub>2</sub>	56.69	55.17 (0.84)	58.09 (0.78)	59.2 (1.39)
	K <sub>2</sub>	102.86	100.71 (1.19)	100.57 (1.27)	101.7 (0.65)
Nazaré	M <sub>2</sub>	69.66	69.48 (0.10)	70.84 (0.66)	71.27 (0.90)
	S <sub>2</sub>	97.28	96.79 (0.27)	98.94 (0.92)	99.65 (1.32)
	N <sub>2</sub>	51.86	51.12 (0.41)	53.59 (0.96)	54.14 (1.27)
	K <sub>2</sub>	95.90	94.28 (0.90)	94.83 (0.60)	95.44 (0.26)
Peniche	M <sub>2</sub>	69.95	69.47 (0.26)	70.51 (0.31)	71.81 (1.03)
	S <sub>2</sub>	97.47	96.77 (0.39)	98.51 (0.58)	100.02 (1.42)
	N <sub>2</sub>	51.61	51.13 (0.27)	53.33 (0.95)	54.51 (1.61)
	K <sub>2</sub>	96.07	94.05 (1.13)	94.42 (0.92)	95.34 (0.41)
Cascais	M <sub>2</sub>	64.61	63.65 (0.53)	64.7 (0.05)	65.42 (0.45)
	S <sub>2</sub>	91.26	90.12 (0.63)	91.96 (0.39)	93.4 (1.19)
	N <sub>2</sub>	47.39	46.13 (0.70)	48.08 (0.39)	48.77 (0.77)
	K <sub>2</sub>	88.20	87.49 (0.39)	87.69 (0.28)	88.91 (0.39)
Sines	M <sub>2</sub>	62.92	62.05 (0.48)	61.27 (0.92)	64.19 (0.71)
	S <sub>2</sub>	89.65	88.56 (0.61)	87.79 (1.03)	92.02 (1.32)
	N <sub>2</sub>	45.62	45.23 (0.22)	45.09 (0.29)	47.68 (1.14)
	K <sub>2</sub>	87.80	85.99 (1.01)	83.76 (2.25)	87.3 (0.28)
Lagos	M <sub>2</sub>	57.91	57.42 (0.27)	58.55 (0.36)	59.21 (0.72)
	S <sub>2</sub>	83.68	83.49 (0.11)	85.11 (0.79)	86.67 (1.66)
	N <sub>2</sub>	41.58	41.36 (0.12)	42.61 (0.58)	43.19 (0.90)
	K <sub>2</sub>	80.69	81.48 (0.44)	80.9 (0.12)	81.86 (0.65)
Huelva	M <sub>2</sub>	57.11	55.42 (0.94)	56.85 (0.15)	57.7 (0.32)
	S <sub>2</sub>	83.56	81.41 (1.20)	83.45 (0.06)	85.24 (0.93)
	N <sub>2</sub>	41.05	39.66 (0.77)	40.99 (0.03)	41.77 (0.40)
	K <sub>2</sub>	80.83	79.61 (0.68)	79.23 (0.89)	80.53 (0.17)
Bonanza	M <sub>2</sub>	63.72	53.89 (5.46)	55.49 (4.57)	56.49 (4.01)
	S <sub>2</sub>	90.50	80.03 (5.82)	82.11 (4.66)	84.08 (3.57)
	N <sub>2</sub>	48.20	37.85 (5.75)	39.69 (4.72)	40.61 (4.21)
	K <sub>2</sub>	88.48	78.13 (5.75)	77.84 (5.91)	79.47 (5.00)
Algeciras	M <sub>2</sub>	41.72	53.99 (6.82)	52.18 (5.81)	45.29 (1.98)
	S <sub>2</sub>	69.22	78.24 (5.01)	76.51 (4.05)	72.73 (1.95)
	N <sub>2</sub>	26.95	36.88 (5.52)	36.21 (5.14)	28.99 (1.13)
	K <sub>2</sub>	67.23	79.47 (6.80)	75.02 (4.33)	68.98 (0.97)
Tarifa	M <sub>2</sub>	48.98	51.88 (1.61)	53.94 (2.75)	52.84 (2.14)
	S <sub>2</sub>	76.91	77.19 (0.16)	79.33 (1.35)	80.59 (2.05)
	N <sub>2</sub>	34.00	35.71 (0.95)	38.49 (2.49)	37.64 (2.02)
	K <sub>2</sub>	77.32	76.53 (0.44)	76.68 (0.36)	76.36 (0.53)
Ceuta	M <sub>2</sub>	48.78	63.2 (8.02)	61.78 (7.23)	52.82 (2.25)
	S <sub>2</sub>	76.95	85.1 (4.53)	84.93 (4.43)	78.11 (0.65)
	N <sub>2</sub>	35.30	48.76 (7.48)	46.16 (6.03)	37.17 (1.04)
	K <sub>2</sub>	66.65	84.82 (10.09)	83.21 (9.20)	74.7 (4.47)

Table VI. Amplitude for the main diurnal harmonics obtained by harmonic analysis of the observed data, their correspondent value in FES2012 global tidal models for those locations and calculated with modelling results of PCOMS\_2D and PCOMS\_3D scenarios. Percentage of error respect the observed harmonic amplitude within brackets.

STATION	HARMONIC	OBSERVED	FES2012	PCOMS_2D	PCOMS_3D
Gijón	K <sub>1</sub>	0.067	0.072 (7.23)	0.074 (10.93)	0.078 (16.92)
	O <sub>1</sub>	0.067	0.069 (2.14)	0.074 (9.79)	0.061 (-10.24)
	P <sub>1</sub>	0.020	0.024 (17.74)	0.021 (5.97)	0.023 (12.94)
	Q <sub>1</sub>	0.022	0.020 (-11.80)	0.022 (-2.69)	0.021 (-6.28)
Ferrol	K <sub>1</sub>	0.073	0.080 (9.99)	0.066 (-9.08)	0.067 (-7.70)
	O <sub>1</sub>	0.065	0.065 (0.04)	0.067 (3.23)	0.067 (3.23)
	P <sub>1</sub>	0.023	0.026 (11.28)	0.020 (-14.10)	0.020 (-12.82)
	Q <sub>1</sub>	0.022	0.020 (-10.90)	0.022 (1.82)	0.023 (2.73)
A Corunha	K <sub>1</sub>	0.074	0.080 (7.89)	0.066 (-11.11)	0.067 (-8.94)
	O <sub>1</sub>	0.065	0.064 (-2.02)	0.067 (2.30)	0.067 (3.22)
	P <sub>1</sub>	0.023	0.026 (12.17)	0.020 (-13.36)	0.021 (-11.64)
	Q <sub>1</sub>	0.022	0.019 (-11.81)	0.022 (0.91)	0.023 (3.20)
Vilagarcía	K <sub>1</sub>	0.075	0.079 (5.40)	0.071 (-4.56)	0.067 (-10.32)
	O <sub>1</sub>	0.064	0.061 (-4.69)	0.067 (4.99)	0.067 (4.52)
	P <sub>1</sub>	0.024	0.026 (8.89)	0.022 (-5.96)	0.022 (-7.66)
	Q <sub>1</sub>	0.021	0.019 (-7.24)	0.023 (9.22)	0.021 (0.97)
Vigo	K <sub>1</sub>	0.073	0.079 (8.53)	0.071 (-2.47)	0.067 (-7.69)
	O <sub>1</sub>	0.064	0.062 (-3.37)	0.069 (8.48)	0.067 (4.40)
	P <sub>1</sub>	0.023	0.026 (10.45)	0.022 (-4.70)	0.022 (-6.41)
	Q <sub>1</sub>	0.021	0.018 (-10.78)	0.022 (4.35)	0.021 (0.48)
Leixões	K <sub>1</sub>	0.071	0.070 (-0.97)	0.070 (-0.28)	0.068 (-4.11)
	O <sub>1</sub>	0.065	0.058 (-9.85)	0.066 (1.71)	0.063 (-2.17)
	P <sub>1</sub>	0.021	0.023 (10.51)	0.023 (6.13)	0.021 (0.94)
	Q <sub>1</sub>	0.022	0.018 (-18.49)	0.022 (-1.81)	0.020 (-7.69)
Nazaré	K <sub>1</sub>	0.070	0.074 (5.43)	0.070 (-1.14)	0.067 (-5.54)
	O <sub>1</sub>	0.061	0.057 (-5.79)	0.060 (-1.31)	0.063 (2.79)
	P <sub>1</sub>	0.021	0.024 (16.89)	0.023 (8.13)	0.022 (3.35)
	Q <sub>1</sub>	0.022	0.017 (-19.71)	0.020 (-7.87)	0.020 (-8.80)
Peniche	K <sub>1</sub>	0.078	0.078 (0.89)	0.069 (-10.70)	0.075 (-2.96)
	O <sub>1</sub>	0.065	0.058 (-10.13)	0.072 (10.15)	0.065 (0.62)
	P <sub>1</sub>	0.024	0.026 (10.13)	0.023 (-5.46)	0.026 (7.98)
	Q <sub>1</sub>	0.022	0.018 (-20.22)	0.020 (-12.11)	0.019 (-13.00)
Cascais	K <sub>1</sub>	0.070	0.074 (6.13)	0.070 (-0.14)	0.072 (2.58)
	O <sub>1</sub>	0.060	0.057 (-4.06)	0.062 (3.67)	0.060 (0.33)
	P <sub>1</sub>	0.022	0.024 (12.18)	0.023 (3.21)	0.024 (7.80)
	Q <sub>1</sub>	0.018	0.017 (-5.03)	0.020 (8.79)	0.018 (-0.55)
Sines	K <sub>1</sub>	0.072	0.075 (5.25)	0.071 (-0.42)	0.071 (-0.56)
	O <sub>1</sub>	0.063	0.057 (-9.13)	0.058 (-7.67)	0.062 (-1.76)
	P <sub>1</sub>	0.022	0.025 (10.08)	0.024 (5.83)	0.024 (8.97)
	Q <sub>1</sub>	0.022	0.017 (-22.13)	0.018 (-20.63)	0.019 (-13.90)
Lagos	K <sub>1</sub>	0.069	0.072 (3.56)	0.074 (7.20)	0.078 (11.67)
	O <sub>1</sub>	0.061	0.056 (-8.30)	0.060 (-2.13)	0.060 (-1.15)
	P <sub>1</sub>	0.023	0.024 (4.26)	0.025 (11.06)	0.027 (19.91)
	Q <sub>1</sub>	0.019	0.017 (-12.60)	0.018 (-6.81)	0.018 (-7.33)
Huelva	K <sub>1</sub>	0.065	0.068 (3.79)	0.072 (10.29)	0.075 (15.51)
	O <sub>1</sub>	0.058	0.058 (0.65)	0.061 (5.34)	0.060 (3.10)
	P <sub>1</sub>	0.022	0.022 (0.96)	0.024 (9.59)	0.027 (24.66)
	Q <sub>1</sub>	0.019	0.017 (-8.12)	0.018 (-0.54)	0.018 (-0.54)
Bonanza	K <sub>1</sub>	0.062	0.067 (7.46)	0.072 (15.65)	0.078 (25.00)
	O <sub>1</sub>	0.061	0.061 (-0.18)	0.063 (2.80)	0.066 (8.39)
	P <sub>1</sub>	0.022	0.022 (1.91)	0.024 (11.63)	0.027 (25.12)
	Q <sub>1</sub>	0.018	0.017 (-0.69)	0.019 (6.25)	0.020 (11.93)
Algeciras	K <sub>1</sub>	0.023	0.008 (-64.75)	0.018 (-21.98)	0.004 (-81.90)
	O <sub>1</sub>	0.009	0.016 (75.99)	0.020 (128.09)	0.024 (169.66)
	P <sub>1</sub>	0.008	0.002 (-68.91)	0.007 (-11.39)	0.003 (-60.76)
	Q <sub>1</sub>	0.004	0.006 (52.85)	0.003 (-29.27)	0.008 (82.93)
Tarifa	K <sub>1</sub>	0.025	0.022 (-15.03)	0.011 (-56.69)	0.017 (-31.50)
	O <sub>1</sub>	0.005	0.024 (390.20)	0.008 (68.75)	0.013 (162.50)
	P <sub>1</sub>	0.008	0.008 (4.13)	0.005 (-36.00)	0.008 (9.33)
	Q <sub>1</sub>	0.005	0.003 (-40.81)	0.007 (33.33)	0.008 (50.98)
Ceuta	K <sub>1</sub>	0.037	0.032 (-13.81)	0.026 (-31.82)	0.014 (-62.30)
	O <sub>1</sub>	0.020	0.026 (29.27)	0.019 (-5.47)	0.020 (0.50)
	P <sub>1</sub>	0.011	0.012 (2.77)	0.010 (-15.79)	0.007 (-38.60)
	Q <sub>1</sub>	0.002	0.001 (-52.63)	0.002 (0.00)	0.006 (185.71)

Table VII. Phase for the main diurnal harmonics obtained by harmonic analysis of the observed data, their correspondent value in FES2004 and FES2012 global tidal models for those locations and calculated with modelling results of FES2004\_2D, PCOMS\_2D and PCOMS\_3D scenarios. Percentage of error respect the observed harmonic phase within brackets (considering 180° as 100% of error).

STATION	HARMONIC	OBSERVED	FES2012	PCOMS_2D	PCOMS_3D
Gijón	K <sub>1</sub>	71.04	74.25 (3.21)	68.82 (2.22)	67.55 (3.49)
	O <sub>1</sub>	324.10	320.23 (2.15)	326.02 (1.07)	327.59 (1.94)
	P <sub>1</sub>	60.59	77.45 (9.36)	69.43 (4.91)	61.64 (0.58)
	Q <sub>1</sub>	271.78	270.66 (0.62)	279.34 (4.20)	286.28 (8.06)
Ferrol	K <sub>1</sub>	72.13	70.21 (1.92)	61.91 (10.22)	67.08 (5.05)
	O <sub>1</sub>	325.55	324.98 (0.31)	323.00 (1.41)	329.52 (2.21)
	P <sub>1</sub>	62.78	70.54 (4.31)	68.70 (3.29)	69.93 (3.97)
	Q <sub>1</sub>	270.08	269.86 (0.13)	269.57 (0.29)	277.69 (4.23)
A Corunha	K <sub>1</sub>	71.80	70.31 (1.48)	62.32 (9.47)	67.07 (4.73)
	O <sub>1</sub>	325.21	325.34 (0.07)	322.89 (1.29)	329.48 (2.37)
	P <sub>1</sub>	61.15	71.00 (5.47)	69.05 (4.39)	69.82 (4.82)
	Q <sub>1</sub>	270.21	270.30 (0.05)	269.88 (0.18)	277.41 (4.00)
Vilagarcía	K <sub>1</sub>	63.79	65.89 (2.10)	65.81 (2.01)	68.05 (4.25)
	O <sub>1</sub>	321.50	324.57 (1.71)	321.99 (0.27)	320.96 (0.30)
	P <sub>1</sub>	54.99	68.74 (7.64)	67.89 (7.17)	72.54 (9.75)
	Q <sub>1</sub>	265.46	265.70 (0.13)	263.26 (1.22)	263.13 (1.29)
Vigo	K <sub>1</sub>	62.93	65.32 (2.39)	64.95 (2.02)	67.99 (5.06)
	O <sub>1</sub>	320.61	323.43 (1.57)	318.99 (0.90)	320.04 (0.32)
	P <sub>1</sub>	54.93	67.98 (7.25)	67.49 (6.98)	72.96 (10.02)
	Q <sub>1</sub>	264.50	264.62 (0.07)	260.49 (2.22)	262.52 (1.10)
Leixões	K <sub>1</sub>	60.24	65.98 (5.74)	63.42 (3.19)	65.93 (5.69)
	O <sub>1</sub>	319.07	323.82 (2.64)	322.32 (1.81)	319.00 (0.04)
	P <sub>1</sub>	47.73	71.22 (13.05)	65.27 (9.74)	70.62 (12.72)
	Q <sub>1</sub>	269.70	265.24 (2.47)	263.00 (3.72)	262.01 (4.27)
Nazaré	K <sub>1</sub>	60.29	63.72 (3.44)	63.61 (3.32)	68.59 (8.31)
	O <sub>1</sub>	317.59	319.17 (0.87)	318.22 (0.35)	317.04 (0.31)
	P <sub>1</sub>	45.24	66.66 (11.90)	65.31 (11.15)	73.76 (15.84)
	Q <sub>1</sub>	270.88	262.96 (4.40)	262.31 (4.76)	259.58 (6.28)
Peniche	K <sub>1</sub>	55.86	66.12 (10.26)	69.77 (13.91)	68.79 (12.93)
	O <sub>1</sub>	316.04	318.86 (1.57)	310.96 (2.82)	313.08 (1.65)
	P <sub>1</sub>	45.36	68.22 (12.70)	76.18 (17.12)	73.32 (15.53)
	Q <sub>1</sub>	267.15	261.35 (3.22)	249.65 (9.73)	251.84 (8.51)
Cascais	K <sub>1</sub>	54.41	62.85 (8.44)	62.10 (7.70)	63.59 (9.19)
	O <sub>1</sub>	314.47	315.73 (0.70)	315.97 (0.83)	313.20 (0.71)
	P <sub>1</sub>	43.23	65.14 (12.17)	62.67 (10.80)	65.54 (12.39)
	Q <sub>1</sub>	256.62	258.23 (0.90)	254.91 (0.95)	256.26 (0.20)
Sines	K <sub>1</sub>	54.87	60.25 (5.39)	60.97 (6.11)	65.65 (10.78)
	O <sub>1</sub>	313.90	313.91 (0.01)	311.29 (1.45)	312.68 (0.68)
	P <sub>1</sub>	45.66	60.48 (8.24)	61.93 (9.04)	68.31 (12.59)
	Q <sub>1</sub>	269.45	257.34 (6.73)	254.14 (8.51)	253.60 (8.81)
Lagos	K <sub>1</sub>	48.61	55.61 (6.99)	58.57 (9.95)	59.14 (10.53)
	O <sub>1</sub>	310.74	310.13 (0.34)	308.19 (1.42)	308.86 (1.04)
	P <sub>1</sub>	38.95	55.28 (9.08)	59.49 (11.41)	58.38 (10.80)
	Q <sub>1</sub>	257.66	252.94 (2.62)	252.39 (2.93)	251.86 (3.22)
Huelva	K <sub>1</sub>	47.52	52.56 (5.03)	54.57 (7.05)	56.20 (8.68)
	O <sub>1</sub>	311.02	306.57 (2.47)	304.85 (3.42)	306.48 (2.52)
	P <sub>1</sub>	39.43	51.48 (6.69)	55.73 (9.05)	57.00 (9.76)
	Q <sub>1</sub>	258.72	249.98 (4.85)	251.30 (4.12)	250.63 (4.49)
Bonanza	K <sub>1</sub>	59.91	51.00 (8.91)	53.15 (6.76)	56.13 (3.78)
	O <sub>1</sub>	323.45	304.38 (10.59)	303.57 (11.04)	307.35 (8.94)
	P <sub>1</sub>	51.51	49.71 (1.00)	54.19 (1.49)	58.09 (3.65)
	Q <sub>1</sub>	269.83	247.97 (12.15)	250.80 (10.57)	252.65 (9.55)
Algeciras	K <sub>1</sub>	129.69	182.10 (53.07)	177.98 (48.95)	214.30 (85.27)
	O <sub>1</sub>	162.69	147.77 (11.76)	140.93 (7.96)	199.55 (40.53)
	P <sub>1</sub>	132.71	184.26 (29.18)	179.29 (26.41)	157.65 (14.39)
	Q <sub>1</sub>	196.27	191.66 (14.76)	198.80 (10.79)	195.29 (12.74)
Tarifa	K <sub>1</sub>	129.03	149.82 (20.13)	99.91 (29.78)	86.45 (43.24)
	O <sub>1</sub>	126.60	196.12 (18.57)	208.75 (25.59)	252.11 (49.68)
	P <sub>1</sub>	131.75	152.45 (10.97)	124.35 (4.65)	103.66 (16.14)
	Q <sub>1</sub>	218.22	216.75 (11.38)	226.44 (16.76)	227.89 (17.57)
Ceuta	K <sub>1</sub>	141.71	170.85 (29.14)	159.18 (17.47)	186.50 (44.79)
	O <sub>1</sub>	102.45	108.26 (3.23)	109.25 (3.78)	178.96 (42.51)
	P <sub>1</sub>	140.78	169.46 (15.93)	162.99 (12.34)	165.81 (13.90)
	Q <sub>1</sub>	192.25	279.74 (48.61)	250.24 (32.22)	193.47 (0.68)

Table VIII. Amplitude for the  $M_4$  and  $Ssa$  harmonics obtained by harmonic analysis of the observed data, their correspondent value in FES2012 global tidal models for those locations and calculated with modelling results of PCOMS\_2D and PCOMS\_3D scenarios. Percentage of error respect the observed harmonic amplitude within brackets.

STATION	HARMONIC	OBSERVED	FES2012	PCOMS_2D	PCOMS_3D
Gijón	$M_4$	0.021	0.019 (-6.87)	0.017 (-18.45)	0.017 (-18.93)
	$Ssa$	0.034	0.004 (-89.55)	0.003 (-89.97)	0.032 (-4.42)
Ferrol	$M_4$	0.012	0.013 (5.14)	0.012 (-3.36)	0.012 (-3.36)
	$Ssa$	0.039	0.003 (-91.04)	0.003 (-91.75)	0.043 (10.57)
A Corunha	$M_4$	0.012	0.013 (3.45)	0.011 (-6.56)	0.012 (-5.74)
	$Ssa$	0.043	0.003 (-91.97)	0.003 (-92.84)	0.044 (0.69)
Villagarcía	$M_4$	0.008	0.010 (22.26)	0.009 (4.76)	0.009 (5.95)
	$Ssa$	0.047	0.003 (-93.04)	0.003 (-93.58)	0.058 (24.41)
Vigo	$M_4$	0.008	0.010 (25.48)	0.009 (15.58)	0.009 (15.58)
	$Ssa$	0.050	0.003 (-93.65)	0.003 (-94.37)	0.061 (22.94)
Leixões	$M_4$	0.008	0.010 (34.38)	0.009 (18.42)	0.009 (15.79)
	$Ssa$	0.086	0.003 (-96.60)	0.003 (-96.96)	0.053 (-38.01)
Nazaré	$M_4$	0.009	0.010 (13.26)	0.009 (10.59)	0.009 (9.41)
	$Ssa$	0.073	0.003 (-96.38)	0.002 (-96.84)	0.060 (-17.83)
Peniche	$M_4$	0.009	0.010 (4.60)	0.009 (2.20)	0.009 (3.30)
	$Ssa$	0.077	0.003 (-96.63)	0.003 (-96.77)	0.065 (-15.65)
Cascais	$M_4$	0.010	0.011 (7.39)	0.011 (5.88)	0.011 (4.90)
	$Ssa$	0.043	0.002 (-94.23)	0.002 (-94.65)	0.064 (47.91)
Sines	$M_4$	0.012	0.012 (0.00)	0.012 (-3.36)	0.011 (-7.56)
	$Ssa$	0.066	0.002 (-96.32)	0.002 (-96.68)	0.061 (-7.70)
Lagos	$M_4$	0.015	0.015 (4.63)	0.014 (-2.04)	0.014 (-2.04)
	$Ssa$	0.055	0.002 (-95.66)	0.002 (-96.02)	0.054 (-2.17)
Huelva	$M_4$	0.029	0.020 (-31.60)	0.019 (-37.07)	0.019 (-36.73)
	$Ssa$	0.053	0.002 (-95.44)	0.002 (-95.67)	0.051 (-3.39)
Bonanza	$M_4$	0.050	0.021 (-58.51)	0.019 (-62.15)	0.019 (-62.35)
	$Ssa$	0.052	0.002 (-95.34)	0.002 (-95.57)	0.046 (-11.37)
Algeciras	$M_4$	0.019	0.013 (-34.36)	0.012 (-38.22)	0.011 (-41.36)
	$Ssa$	0.038	0.002 (-95.84)	0.002 (-94.44)	0.025 (-34.92)
Tarifa	$M_4$	0.038	0.013 (-66.17)	0.020 (-48.44)	0.015 (-60.42)
	$Ssa$	0.042	0.002 (-95.04)	0.002 (-94.80)	0.031 (-27.42)
Ceuta	$M_4$	0.026	0.011 (-59.28)	0.013 (-49.23)	0.009 (-64.62)
	$Ssa$	0.036	0.002 (-93.40)	0.002 (-93.54)	0.028 (-22.47)

Table IX. Phase for the  $M_4$  and  $Ssa$  harmonics obtained by harmonic analysis of the observed data, their correspondent value in FES2012 global tidal models for those locations and calculated with modelling results of PCOMS\_2D and PCOMS\_3D scenarios. Percentage of error respect the observed harmonic phase within brackets (considering  $180^\circ$  as 100% of error).

STATION	HARMONIC	OBSERVED	FES2012	PCOMS_2D	PCOMS_3D
Gijón	$M_4$	318.577	306.09 (6.94)	309.62 (4.97)	309.13 (5.25)
	$Ssa$	68.703	129.28 (94.83)	137.46 (38.20)	79.49 (5.99)
Ferrol	$M_4$	298.084	279.02 (10.59)	279.15 (10.52)	278.79 (10.72)
	$Ssa$	67.866	129.57 (93.62)	135.89 (37.79)	72.03 (2.32)
A Corunha	$M_4$	289.028	275.39 (7.57)	278.28 (5.97)	278.00 (6.13)
	$Ssa$	67.189	129.90 (88.40)	134.33 (37.30)	72.10 (2.73)
Villagarcía	$M_4$	241.004	241.28 (0.15)	237.67 (1.86)	235.64 (2.98)
	$Ssa$	64.511	127.09 (63.29)	133.11 (38.11)	73.99 (5.27)
Vigo	$M_4$	228.639	232.36 (2.07)	234.67 (3.35)	236.11 (4.15)
	$Ssa$	61.491	125.49 (57.31)	129.45 (37.76)	73.20 (6.51)
Leixões	$M_4$	216.765	214.99 (0.99)	220.65 (2.16)	220.18 (1.90)
	$Ssa$	83.702	119.21 (54.20)	122.14 (21.36)	72.56 (6.19)
Nazaré	$M_4$	190.920	193.60 (1.49)	201.10 (5.65)	200.85 (5.51)
	$Ssa$	83.506	108.13 (45.99)	110.56 (15.03)	67.87 (8.69)
Peniche	$M_4$	185.408	192.83 (4.12)	198.55 (7.30)	198.10 (7.05)
	$Ssa$	83.028	106.99 (43.56)	106.69 (13.15)	67.13 (8.83)
Cascais	$M_4$	184.598	175.26 (5.19)	182.69 (1.06)	182.89 (0.95)
	$Ssa$	65.413	102.24 (45.76)	99.93 (19.18)	64.31 (0.61)
Sines	$M_4$	167.038	171.91 (2.71)	171.96 (2.73)	179.00 (6.65)
	$Ssa$	90.789	95.45 (39.77)	90.18 (0.34)	60.22 (16.98)
Lagos	$M_4$	163.130	162.31 (0.46)	169.18 (3.36)	169.45 (3.51)
	$Ssa$	75.562	88.75 (41.32)	84.99 (5.24)	53.46 (12.28)
Huelva	$M_4$	168.173	161.66 (3.62)	168.98 (0.45)	170.55 (1.32)
	$Ssa$	61.799	93.07 (41.72)	88.60 (14.89)	50.69 (6.17)
Bonanza	$M_4$	86.466	162.33 (42.15)	169.30 (46.02)	170.47 (46.67)
	$Ssa$	49.398	91.54 (2.82)	85.32 (19.96)	49.17 (0.13)
Algeciras	$M_4$	118.098	177.72 (33.12)	162.59 (24.72)	175.32 (31.79)
	$Ssa$	62.934	70.08 (26.68)	68.15 (2.90)	26.55 (20.22)
Tarifa	$M_4$	162.900	158.92 (2.21)	139.38 (13.07)	123.41 (21.94)
	$Ssa$	63.943	87.96 (41.63)	73.29 (5.19)	45.48 (10.26)
Ceuta	$M_4$	160.474	168.44 (4.42)	158.10 (1.32)	179.05 (10.32)
	$Ssa$	66.996	63.93 (53.63)	72.15 (2.86)	47.95 (10.58)

The seasonal cycle observed in a single tide gauge record for these components can differ considerably from year to year (Pugh and Woodworth, 2014). In our study case, the semi-annual astronomical tidal contribution (Ssa) which is a long period radiational tidal component is present in the Western Iberian coast with amplitudes with the same order of magnitude of the diurnal components (Table II, Figure 4). The observed amplitudes (Figure 5) show an increase of the importance in the central part of the study area, with moderate values (3–6 cm) which are typical of mid-latitudes in the North Atlantic. That harmonic component is only detected in the 3D modelling results that included the atmospheric influence and seems to reproduce satisfactorily the spatial evolution in terms of amplitude and phase (Figure 5 and Figure 6).

The tidal amplitude and phases obtained through harmonic analysis for the observed data and the model simulations is listed in the following tables for the semidiurnal components (Table IV and Table V), the diurnal components (Table VI and Table VII) and for the main shallow water ( $M_4$ ) and radiational constituents (Ssa) (Table VIII and Table IX). The error of amplitude and phase in percentage between the modelling solutions and the observed value was estimated in each table, within brackets. In the case of the phase the maximum error was considered a difference of  $180^\circ$  that would represent opposite phases.

To summarise the amplitude and phase errors, the complex error, ( $H_c$ ; Chanut *et al.*, 2008) was calculated for the observed and modelled harmonics. Each group of tidal constituents was compared with the observed components by using the Equation 3:

$$H_c = \left[ (h_2 \cos(\varphi_2) - h_1 \cos(\varphi_1))^2 + (h_2 \sin(\varphi_2) - h_1 \sin(\varphi_1))^2 \right]^{\frac{1}{2}} \quad \text{Equation 3}$$

where  $h_1$  and  $\varphi_1$  correspond to the observed amplitude and phase respectively and  $h_2$  and  $\varphi_2$  correspond to the amplitude and phase from each model implementation. Table X presents the averaged complex error for the ten analysed harmonic constituents for all the tidal gauge stations including and excluding the Mediterranean and estuarine tidal gauges (Bonanza, Algeciras, Tarifa and Ceuta). From this analysis it can be concluded that the MOHID model reproduce successfully the tidal propagation from the boundary as the total error is of the same scale than the forcing solution original error. Mediterranean and inner estuary stations contribute approximately to a third of the total error. The 3D model reduces the error around 10% when compared to the 2D modelling results.

**Table X. Mean complex error between modelling and observed values for the ten selected harmonic components. The mean error was calculated for all the analysed stations (left) and excluding the Mediterranean tidal gauges (Bonanza, Algeciras, Tarifa and Ceuta).**

Model	Hc (m)	Hc (m) excluding Med Stations
FES2012	0.0177	0.0116
PCOMS_2D	0.0194	0.0142
PCOMS_3D	0.0177	0.0125

### 3.7 Water levels and residuals analysis

As the main objective of the numerical model is to reproduce accurately the observed water levels, the time series obtained from the 2D and 3D PCOMS domains were compared with the raw observed water levels. Observed water levels include the contributions from meteorological and astronomical tides. For that reason, as expected, a clear improvement in the simulation of water levels can be observed in the PCOMS\_3D scenario that include atmospheric pressure and wind corrections. Table XI lists the coefficient of determination between the 2D and 3D modelling scenarios with the registered water levels. This list is limited to the stations that have available observations during the year 2011. The capacity to

represent the observed water levels increase around 2.5 % with the 3D model when compared with the compared with the 2D model. Regardless the modelling scenario, the coefficient of determination obtained with the model is elevated with values over 0.98 in the Atlantic Area. Those values slightly decrease in the Mediterranean stations.

**Table XI. Coefficient of determination between modelling and observed values for the PCOMS\_2D and PCOMS\_3D modelling scenarios. The analysis was restricted to the tidal gauges stations with observed data available for the year 2011.**

Tidal Gauge	N	Coefficient of Determination ( $R^2$ )	
		PCOMS_2D	PCOMS_3D
Gijón	8760	0.986	0.995
Ferrol	8694	0.983	0.996
A Corunha	8760	0.985	0.996
Vilagarcía	8353	0.981	0.996
Vigo	8664	0.981	0.995
Cascais	6716	0.983	0.993
Huelva	8735	0.985	0.995
Bonanza	8581	0.952	0.970
Algeciras	8468	0.897	0.948
Tarifa	8343	0.895	0.932
Ceuta	8524	0.845	0.926
<b>Average</b>	-	<b>0.952</b>	<b>0.977</b>

The residual water levels are the results of subtracting the astronomical water levels to the raw observed or modelled water levels. They represent the water level deviation from the astronomic tides and are associated to the meteorological tides and to the local effects. Maximum and minimum values correspond to extreme water levels associated to high and low pressure systems.

Table XII summarises the maximum and minimum residual values observed and modelled with the PCOMS\_3D. The latter is the only modelling scenario reproducing and including the meteorological tide effects. Maximum positive deviations tend to be larger than negative deviations as low pressure systems, associated to storms, can reach lower values. This effect can increase the water levels in around 50 cm reaching local values over 70 cm in Ferrol. The model reproduce approximately the maximum and minimum trends in the Western Iberia. However the modelled results do not reach the maximum values as those are very local observed values while the model cells with larger horizontal resolution that do not allow to reproduce fully the gradients and reduce the results variability. Vigo, Cascais, Huelva and Bonanza are using 9 km horizontal resolution MM5 results while Gijon, Ferrol, A Corunha, Algeciras, Tarifa and Ceuta stations are using 27 km horizontal resolution for the meteorological forcing. To reduce the outliers and punctual maximum values, it was decided to analyse the percentile 5 and 95 as representative of the maximum and minimum water levels deviation of those stations. Maximum residuals are slightly larger than minimum residuals and can contribute to deviations up to 20 cm of the astronomical tides. Local effects due to the location of the tidal gauges, being located in the surroundings of estuaries and capes that modify the atmosphere and water levels, can also contribute to these deviations. The correlation between the observed and modelled residuals is especially high in the northern part of the study area and decrease in the Mediterranean stations. The location of Cascais tidal gauge in the Gulf of Lisbon, a sheltered area with wind gradients, can be the cause of the reduced performance of the residuals coefficient of determination. For this area in particular, finer atmospheric and ocean models should be needed to reproduce accurately the water levels.

By using numerical models, accurate water levels can be predicted as the deviations due to the meteorological tide can be included and aiding to implement risk reduction measures those results would be more precise than the obtained by simple water levels generation from the harmonic components.

**Table XII. Maximum and minimum residuals (m) for the observed water levels when subtracted the water levels obtained by the observations harmonic analysis and the water levels for each modelling scenarios PCOMS\_2D and PCOMS\_3D. The analysis was restricted to the tidal gauges stations with observed data available for the year 2011.**

Tidal Gauge	Observations				PCOMS_3D				Coefficient of Determination ( $R^2$ )
	Min	P <sub>05</sub>	P <sub>95</sub>	Max	Min	P <sub>05</sub>	P <sub>95</sub>	Max	
Gijón	-0.31	-0.17	0.18	0.47	-0.23	-0.14	0.18	0.40	0.84
Ferrol	-0.30	-0.17	0.19	0.73	-0.27	-0.15	0.19	0.45	0.88
A Corunha	-0.28	-0.16	0.18	0.46	-0.27	-0.15	0.19	0.45	0.85
Vilagarcía	-0.31	-0.17	0.20	0.54	-0.27	-0.16	0.19	0.45	0.81
Vigo	-0.29	-0.16	0.20	0.53	-0.27	-0.16	0.19	0.45	0.81
Cascais	-0.40	-0.14	0.18	0.46	-0.17	-0.11	0.16	0.32	0.61
Huelva	-0.20	-0.11	0.20	0.40	-0.17	-0.11	0.15	0.35	0.73
Bonanza	-0.25	-0.12	0.21	0.45	-0.18	-0.11	0.16	0.34	0.64
Algeciras	-0.25	-0.11	0.18	0.46	-0.17	-0.11	0.13	0.34	0.62
Tarifa	-0.21	-0.08	0.18	0.49	-0.16	-0.10	0.14	0.35	0.62
Ceuta	-0.27	-0.11	0.16	0.38	-0.17	-0.10	0.13	0.33	0.66

### 3.8 Water levels spatial analysis

A major advantage of modelling results, in comparison with observed records, is the capacity of analysing results and producing products for the entire study area and not only for a few selected stations.

In order to obtain the tidal amplitude and phase for the Western Iberia region, the T\_Tide Harmonic Analysis Toolbox (Pawlowicz *et al.*; 2002), based on the classic FORTRAN tidal analysis packages written by Mike Foreman (<http://www.dfo-mpo.gc.ca/science/data-donnees/tidal-marees/index-eng.html>), was applied to the PCOMS\_2D and PCOMS\_3D modelling results for the year 2011 obtaining the amplitude and phase of 59 components. Figure 7, Figure 8 and Figure 9 show the propagation of the main diurnal ( $M_2$ ), semidiurnal ( $K_1$ ) and overtide ( $M_4$ ) components along the 2D and 3D domains. The phase contours propagates northward along the coast according to Kelvin wave dynamics. And in the case of semidiurnal components they remain approximately perpendicular to the coast. In Figure 7 and Figure 9 can be observed how the 2D modelling maps present a more smooth contours for the phase and amplitude than the obtained 3D surface layer, however as described before they present a larger error. The same effect has been described for the  $M_2$  baroclinic tidal component in Monterey Bay Region (i.e. Carter, 2010). This effect is negligible in the coastal area as the amplitude horizontal distribution is almost the same. Semidiurnal and diurnal components suffer an amplification of their amplitude in the Gulf of Cadiz in the 3D implementation (Appendix I). Figure 10 shows the distribution of the amplitude of the main radiational component in the 3D model application and the original values of the FES2012 model. In this figure, note the different colour scales, it can be seen how this component increase its value when approaching the coastal area. Thus being an important component in the Western Iberian coast. The rest of maps for the tidal constituents analysed in this document and the original solution from the FES2012 model can be found in Appendix I.

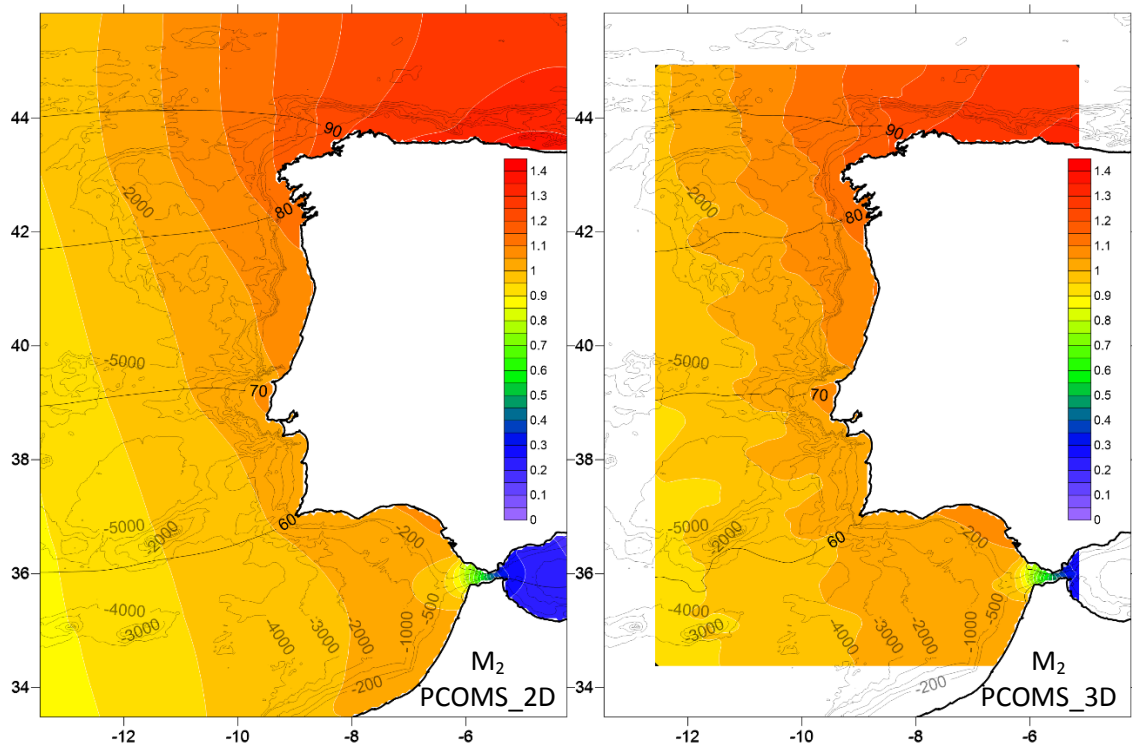


Figure 7  $M_2$  harmonic component map for the PCOMS 2D Westlberia domain (left) and the PCOMS 3D Portugal domain (right) forced with FES2012 model. Co-amplitude (m) and co-phase (degrees UT) are represented by the colour scale and by dark isolines respectively. Isobaths for 200 m, 500 m, 1000 m, 2000 m, 3000 m, 4000 m and 5000 m depths were added to ease interpretation.

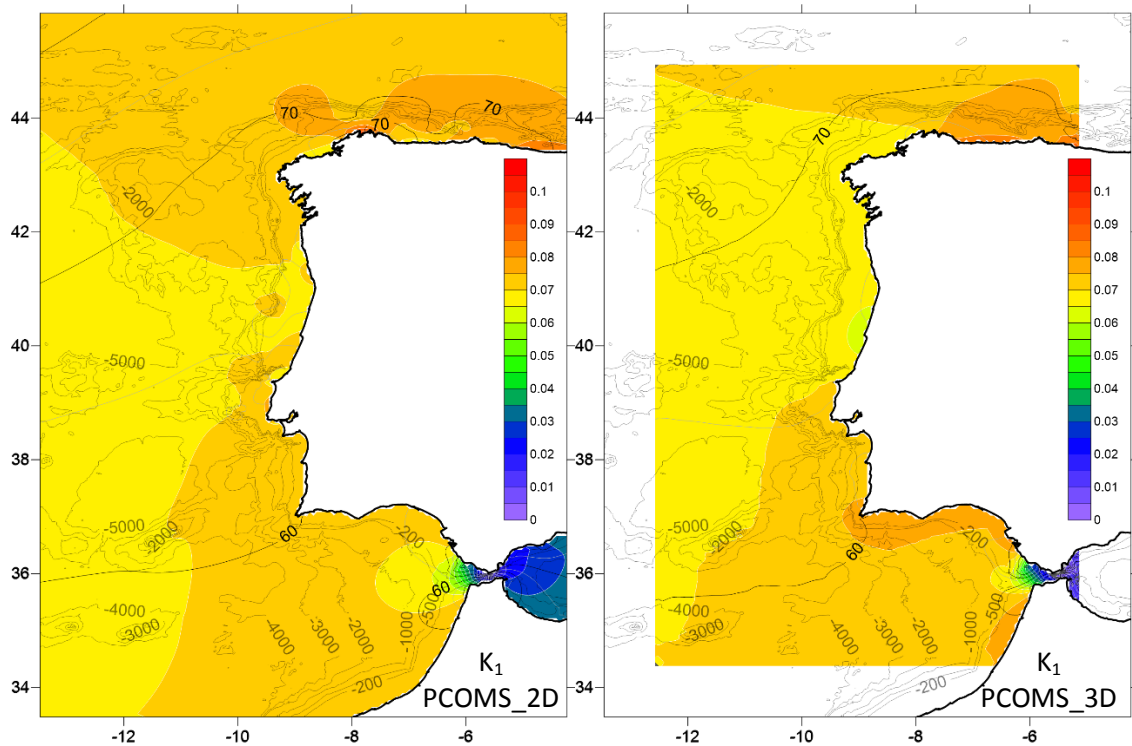


Figure 8  $K_1$  harmonic component map for the PCOMS 2D Westlberia domain (left) and the PCOMS 3D Portugal domain (right) forced with FES2012 model. Co-amplitude (m) and co-phase (degrees UT) are represented by the colour scale and by dark isolines respectively. Isobaths for 200 m, 500 m, 1000 m, 2000 m, 3000 m, 4000 m and 5000 m depths were added to ease interpretation.

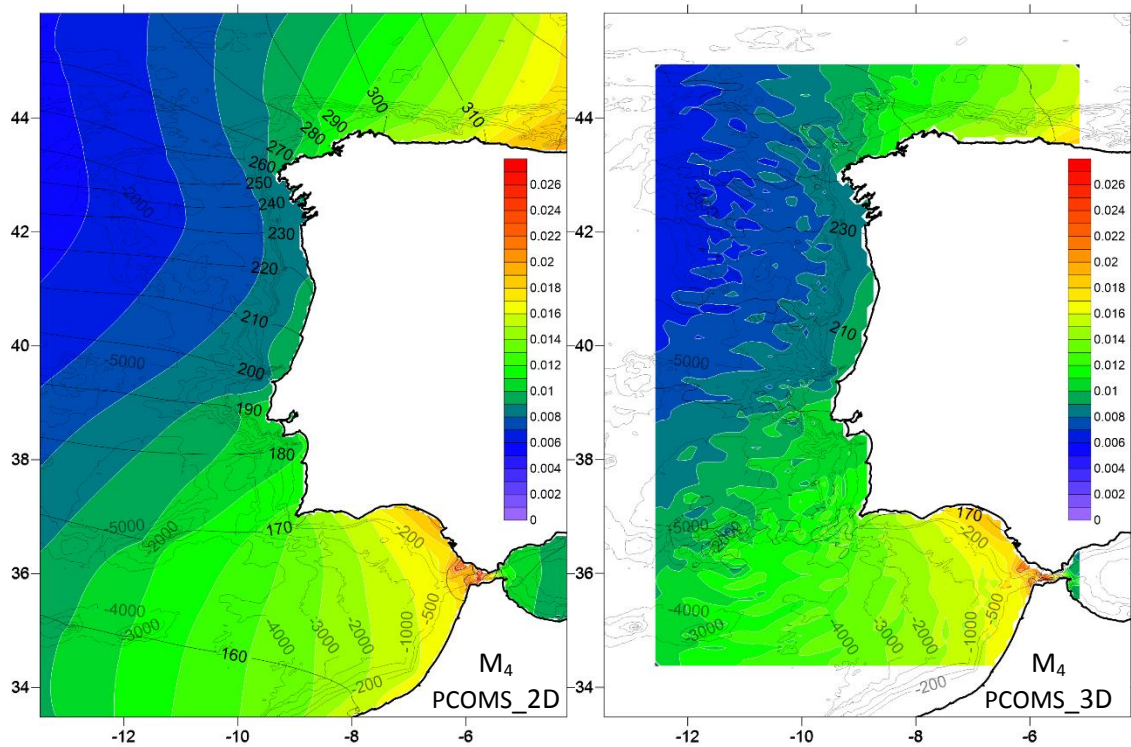


Figure 9 M<sub>4</sub> harmonic component map for the PCOMS 2D Westlberia domain (left) and the PCOMS 3D Portugal domain (right) forced with FES2012 model. Co-amplitude (m) and co-phase (degrees UT) are represented by the colour scale and by dark isolines respectively. Isobaths for 200 m, 500 m, 1000 m, 2000 m, 3000 m, 4000 m and 5000 m depths were added to ease interpretation.

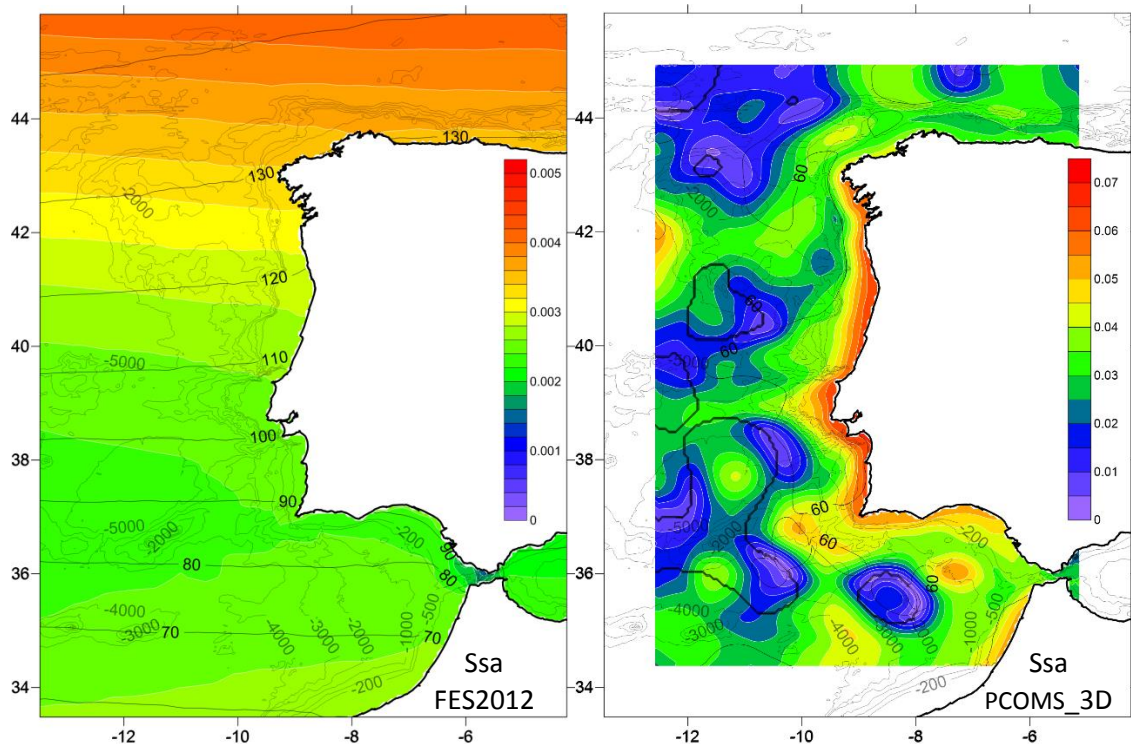


Figure 10 Ssa harmonic component map for the PCOMS model (left) and PCOMS Portugal domain 3D forced with the FES2012 model (right). Co-amplitude (m) and co-phase (degrees UT) are represented by the colour scale and by dark isolines respectively. Isobaths for 200 m, 500 m, 1000 m, 2000 m, 3000 m, 4000 m and 5000 m depths were added to ease interpretation. Note the different colour scales used in each figure.

The modelling tools also allow us to understand the evolution of the tidal range along the analysed area. This information is very relevant for marine renewable energy site characterisation (Campuzano *et al.*, 2015). Using the PCOMS\_2D modelling scenario, the average tidal range during spring and neap tides was obtained for the Western Iberia region. Mean tidal range for Portugal during Spring tides is comprised between 2.9 and 3.2 m in the southern and northern limits respectively while during Neap tides their range reduce to the interval between 1.4 and 1.6 m (Figure 11). The tidal range values drop rapidly when entering the Mediterranean Sea with values around 0.6 and 0.3 m for the Spring and Neap tides in the domain limits. From the northern limit of Portugal, the tidal amplitude continue increasing reaching in the Northwest area Spring and Neap tidal ranges around 4 and 1.9 m respectively.

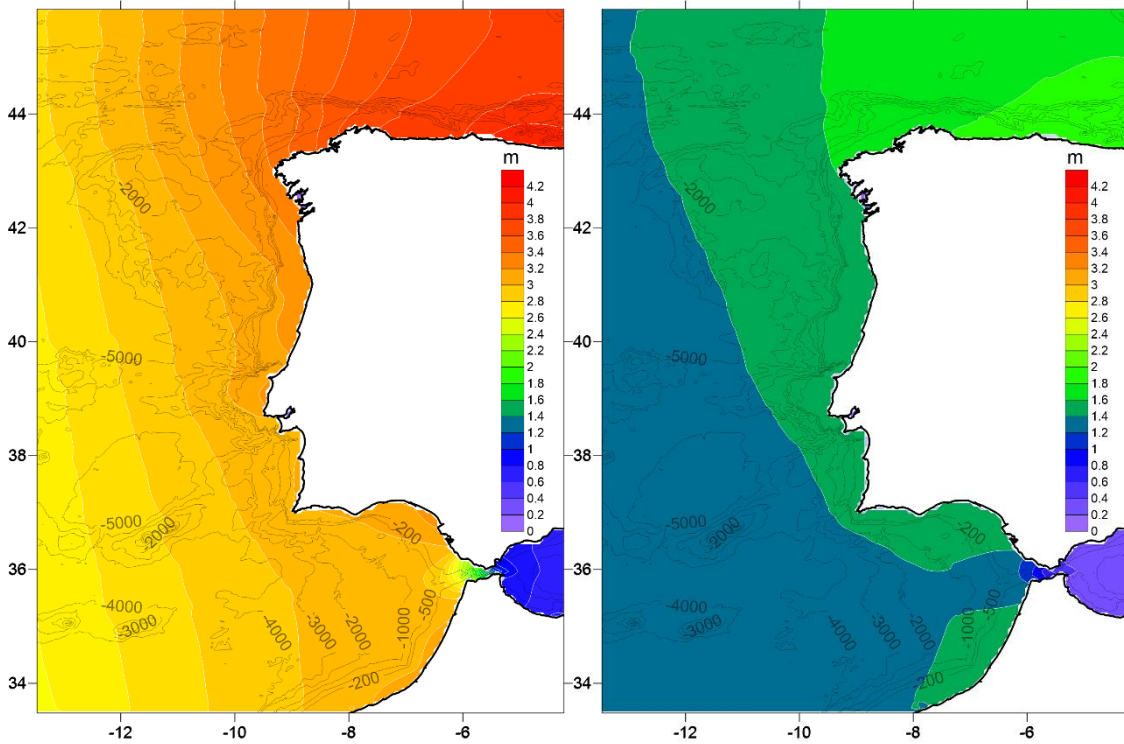


Figure 11 Mean Spring tidal range (left) and mean Neap tidal range (right) obtained with the PCOMS\_2D. Isobaths for 200 m, 500 m, 1000 m, 2000 m, 3000 m, 4000 m and 5000 m were added to ease interpretation.

### 3.9 Conclusions

The continuous improvement in global tide models benefit the implementation and development of regional ocean models. As such the Portuguese Coast Operational Modelling System (PCOMS) on its current version is able to reproduce accurately the tides in barotropic and baroclinic applications when using the FES2012 global tide solution in rough horizontal resolutions for regional scale model applications. Although the PCOMS numerical application was originally designed to provide accurate forecast for the Western Iberia region, the model performance obtained for the Strait of Gibraltar area are quite satisfactory.

Harmonic analyses performed on observed and modelled water levels, using the POL/PSMSL Tidal Analysis Software Kit 2000 (TASK-2000), served to obtain their tidal components and to study the tide evolution, propagation and evaluate the correct model performance.

The semidiurnal and diurnal barotropic tide distribution is similar to the maps presented in previous studies (i.e.  $M_2$ ,  $N_2$ ,  $S_2$ ,  $K_2$ ,  $K_1$ ,  $O_1$ ,  $P_1$  and  $Q_1$  in Sauvaget *et al.*, 2000;  $M_2$  and  $K_1$  in Quaresma and Pichon, 2013) and improves the coastal solution when compared with the FES2012 original solution. This improvement can be observed, for example, in the

amplification of the diurnal components between Cape Raso and Cape Carvoeiro observed those previous studies that is not detectable in the FES2012 model solution (Appendix I) and where no tidal gauges are installed.

3D baroclinic tidal maps illustrate the modification of the tidal contours due to the density gradients and meteorological effects. When including the meteorological forcing in the simulations, the modelled water levels allow to represent the radiational components in a more realistic way (i.e. Ssa). Those improvements increase the capacity of the model to simulate the observed water levels and to produce accurate forecasts with residuals from the same order of magnitude than the observed ones.

The improvement of regional ocean model tides is critical to improve the forecasting of extreme events and risk management and also for marine renewable energies applications. In fact, they are the pillar on top of which services and products are developed to aid in the coastal management. For this reason, this chapter has been exhaustive on the analysis of data and modelling results with the objective of aid managers and future research.

### 3.10 References

Andersen OB. Shallow water tides in the northwest European shelf region from TOPEX/POSEIDON altimetry, *Journal of Geophysical Research*. 1999; 104(C4): 7729–7741. DOI: [10.1029/1998JC900112](https://doi.org/10.1029/1998JC900112).

Bell C, Vassie JM, Woodworth PL. POL/PSMSL Tidal Analysis Software Kit 2000 (TASK-2000). Technical Report, Permanent Service for Mean Sea Level, CCMS Proudman Oceanographic Laboratory. 1999; 20pp

Campuzano FJ, Fernandes R, Leitão PC, Viegas C, de Pablo H, Neves R. Implementing local operational models based on an offline downscaling technique: The Tagus estuary case. 2.as Jornadas de Engenharia Hidrográfica, 20-22 June 2012, Lisbon, Portugal. Extended abstracts: 105-108.

Campuzano FJ, Juliano M, Fernandes R, Neves R. (2015) Marine Renewable Energy Resources - Atlas for Continental Portugal. Report for the EnergyMare Project (Atlantic area Interreg project Contract Number: 2011-1/157).

Carrère L, Lyard F, Cancet M, Guillot A, Roblou L. FES2012: A new global tidal model taking advantage of nearly 20 years of altimetry, *Proceedings of meeting "20 Years of Altimetry"*, Venice 2012.

Carter GS. Barotropic and Baroclinic  $M_2$  Tides in the Monterey Bay Region. *Journal of Physical Oceanography*. 2010; 40: 1766-1783. DOI: [10.1175/2010JPO4274.1](https://doi.org/10.1175/2010JPO4274.1).

Chanut J, Le Galloudec O, Léger F. Towards North East Atlantic Regional modelling at  $1/12^\circ$  and  $1/36^\circ$  at Mercator Ocean. *Mercator Ocean Quarterly Newsletter*. 2008; 30: 4-12.

Delhez E, Deleersnijder E. Overshootings and spurious oscillations caused by biharmonic mixing. *Ocean Modelling*. 2007, 17(3), 183-198.

Drillet Y, Bourdalle-Badi R, Siefrid L, Le Provost C. Meddies in the Mercator North Atlantic and Mediterranean Sea eddy-resolving model. *Journal of Geophysical Research*. 2005; 110(C3): C03016.

Fanjul EA, Gómez BP, Sánchez-Arevalo IR. A description of the tides in the Eastern North Atlantic. *Progress in Oceanography*. 1997; 40: 217-244.

Foreman MGG. Manual for Tidal Heights Analysis and Prediction, Pacific Marine Science Report 78-6. Institute of Ocean Sciences. 1978; 57pp.

- Fortunato AB, Pinto L, Oliveira A, Ferreira JS. Tidally generated shelf waves off the western Iberian coast. *Continental Shelf Research*. 2002; 22: 1935–1950.
- Grell GA, Dudhia J, Stauffer D. (1994). A description of the fifth-generation Penn State/NCAR Mesoscale Model (MM5). NCAR Technical Note NCAR/TN-398+STR.
- Howarth MJ, Pugh DT, 1983. Observations of tides over the continental shelf of North-West Europe. In: *Physical Oceanography of Coastal and Shelf Seas*. Ed. B. Johns, pp. Elsevier Oceanography Series, Volume 35, pp 135-188. DOI: [10.1016/S0422-9894\(08\)70502-6](https://doi.org/10.1016/S0422-9894(08)70502-6).
- Lefèvre F. Modélisation des marées océaniques à l'échelle globale: assimilation de données in situ et altimétriques. PhD Thesis. Université Paul Sabatier (Toulouse III, France), 2000.
- Lyard F, Lefevre F, Letellier T, Francis O. Modelling the global ocean tides: modern insights from FES2004. *Ocean Dynamics*. 2006; 56: 394 – 415.
- Marta-Almeida M, Dubert J. The structure of tides in the Western Iberian region. *Continental Shelf Research*. 2006; 26: 385-400.
- Mateus M, Riflet G, Chambel P, Fernandes L, Fernandes R, Juliano M, Campuzano F, de Pablo H, Neves R. An operational model for the West Iberian coast: products and services. *Ocean Science*. 2012; 8: 713-732.
- Murray MT. A general method for the analysis of hourly heights of the tide. *International Hydrographic Review*. 1964; 41(2): 91-101.
- Neves R, 2013. The MOHID concept. In: *Ocean modelling for coastal management - Case studies with MOHID*. M. Mateus & R. Neves (Eds.), IST Press. pp. 1-11.
- Pawlowicz R, Beardsley B, Lentz S. Classical tidal harmonic analysis including error estimates in MATLAB using T\_TIDE. *Computers and Geosciences*. 2002; 28: 929-937.
- Pugh D, Woodworth P. *Sea-Level Science*. 1st ed. Cambridge: Cambridge University Press, 2014.
- Quaresma LS, Pichon A. Modelling the barotropic tide along the West-Iberian margin. *Journal of Marine Systems*. 2013; 109-110; S3-S25.
- Sauvaget P, David E, Guedes Soares C. Modelling tidal currents on the coast of Portugal. *Coastal Engineering*. 2000; 40: 393-409.
- Trancoso AR (2012). Operational modelling as a tool in wind power forecast and meteorological warnings. PhD Thesis, Instituto Superior Técnico, Universidade Técnica de Lisboa, 146p.
- Wunsch C, Stammer D. Atmospheric loading and the oceanic “inverted barometer” effect. *Reviews of Geophysics*. 1997; 35, 1.

# Chapter IV - Evaluation of surface temperature, salinity and baroclinic circulation in Western Iberia by means of numerical modelling and remote sensing.

---

## Abstract

In this chapter surface circulation, salinity and temperature obtained by the PCOMS numerical model application for the Western Iberia region during the period 2010-2015 were described and evaluated using a comprehensive list of *in situ* monitoring stations and remote sensing Sea Surface Temperature (SST) and Sea Surface Salinity (SSS) products.

## 4.1. Introduction

The Western Iberian ocean region falls at the northern extreme of the Canary Upwelling Ecosystem (CUE), one of the four main Eastern Boundary Upwelling Systems (EBUSs), along with the Benguela ecosystem, the California current and the Humboldt Current (Fréon *et al.*, 2006; Mason *et al.*, 2006). Surface thermohaline circulation is influenced by seasonal upwelling/downwelling favourable conditions along with the generation of the Iberian Poleward Current (IPC) and the contribution of river inputs from the land-ocean boundary.

Sea surface temperature is a commonly used indicator of upwelling events and the difference between the coastal and offshore values are used as an index of this process. Though water temperature is a non-conservative indicator, its use for this purpose is common due to the difficulty to observe the other variables of the thermohaline circulation that originate those gradients i.e. currents and salinity. While surface temperature are easily obtained by multiple Earth Observation (EO) systems and temperature sensors are quite reliable during long term monitoring, remote sensing currents are giving their first steps and *in situ* observations require higher maintenance and EO salinity products are under development and salinity sensors are less reliable and common in multiparametric ocean buoys. For these reasons, numerical modelling is a crucial tool that allow to study those processes continuously and processes that generate fronts.

## 4.2. Material and Methods

In this chapter, surface modelling results from a PCOMS version without fresh water inputs from rivers nor evaporation/precipitation processes were compared with *in situ* monitoring stations and EO sea surface temperature (SST) and salinity (SSS).

### 4.2.1. Modelling results evaluation with *in situ* data

In recent times, public access to ocean and coastal buoys along the Iberian Peninsula has been granted through several international initiatives such as *In Situ* Thematic Assemble Centre (INS-TAC) of the Copernicus Marine Environment Monitoring Service (CMEMS; <http://marine.copernicus.eu/>). Through this service providers including from Puertos del Estado (Spain), Xunta Galicia/MeteoGalicia/IM (Spain) and Instituto Hidrográfico (Portugal) allow access to the operational observations and historical records of their buoys networks. In this study two Portuguese stations with long records, Cascais and Lagos, and maintained by the Instituto Geográfico ([www.igeo.pt/](http://www.igeo.pt/)) were also collected and analysed (Table I, Figure 1). In total, twenty-two ocean and coastal stations collected and made available water surface temperature during the period 2010-2015. From these

stations, five and nine stations monitored currents and salinity respectively (Table I), unfortunately none of them was located in Portuguese waters.

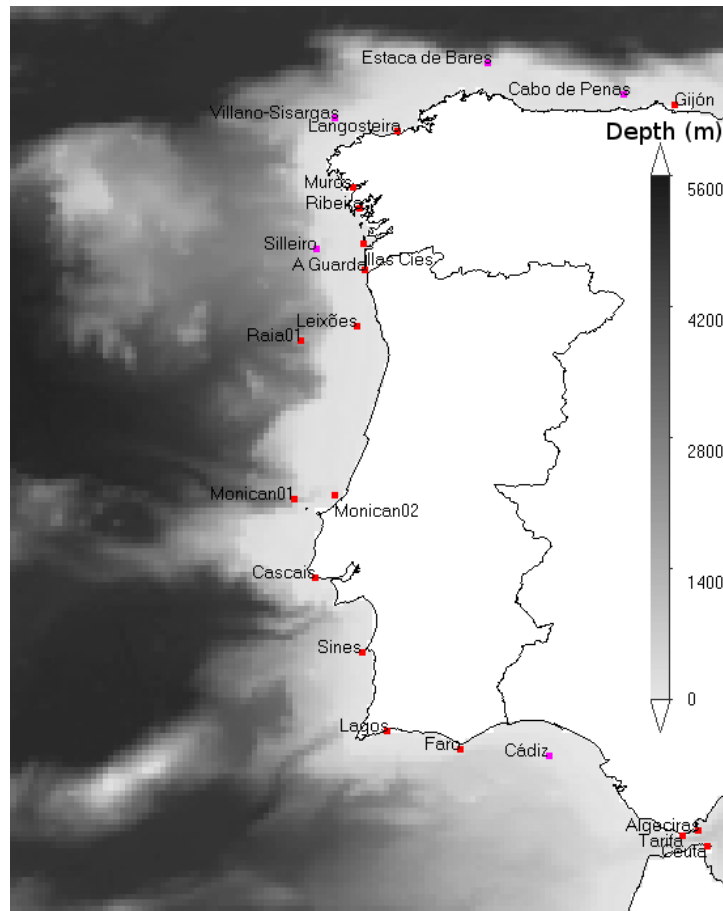


**Figure 1** Location of the multiparametric monitoring buoys around Western Iberia. Purple markers indicate the coastal buoys measuring both surface temperature and currents while red markers indicate station with only surface temperature data available.

#### 4.2.1.1. Surface current velocities

Five ocean buoys monitored and provided continuous currents observations on the continental shelf of Western Iberia (Figure 1). These observations were located only in Spanish waters and were obtained through the Copernicus Marine Environment Monitoring Service (CMEMS; <http://marine.copernicus.eu/>). To compare and validate numerical model results and observed currents in open ocean is a complex task. While common bay and estuarine currents have their flow direction restricted, denominated as reversing currents, open ocean currents are rotary. During ebb and flood conditions, reversing currents flow mainly in two opposite directions while rotary currents change their direction continuously along the tidal cycle without defining clear flood or ebb directions (NOAA Technical Memorandum 21, 1999).

Offshore the continental shelf, large scale ocean circulation currents and atmospheric processes of various magnitudes and time scales contribute to the observed current making complicated to determine whether the observed current correspond to permanent feature representative of the area. An additional factor to bear in mind is that offshore buoys stay sometimes deployed for long periods without calibration and data validation. Unlike other sensors where odd values can be easily identified, the range of values make difficult the identification of dubious values. The latter issue is especially important in an area subject to extreme events such as the open waters of the Atlantic Iberian shelf. Modelling results can contribute to identify suspicious observations.

Efforts were made to extract the tidal contribution of the current signal and to evaluate its weight for each monitoring station (Table I and Figure 1). Once outliers were removed, velocity U and V components from each observed record were analysed using the PSMSL/POL Tidal Analysis Software Kit 2000 (TASK-2000 Package) (Bell *et al.*, 1999) for the period 2010-2015. The TIRA software, developed at the Proudman Oceanographic Laboratory (Murray, 1964), allowed through tidal harmonic analysis based on least squares procedures to obtain 62 tidal components plus the reference level for each current velocity direction.

**Table I. List of multiparametric buoys used in this study indicating their location and the available data period. In the table is also indicated those that have current and salinity data available are indicated. The superscript next to the station name indicates the institution responsible for the monitoring station: <sup>1</sup> stations maintained by Puertos del Estado (Spain) <sup>2</sup> stations maintained by Xunta Galicia/MeteoGalicia/IM (Spain), <sup>3</sup> stations maintained by Instituto Hidrográfico (Portugal) and <sup>4</sup> stations maintained by Instituto Geográfico (Portugal). Coastal stations are indicated with \*. Please note that some stations have less than 1 year of data available for the analysed period.**

Station Name	Latitude	Longitude	Data Period	Currents	Salinity
Estaca de Bares <sup>1</sup>	44.06 °N	7.62 °W	01/01/2010 - 31/12/2015	✓	✓
Cabo de Peñas <sup>1</sup>	43.73 °N	6.19 °W	01/01/2010 - 31/12/2015	✓	✓
Gijón <sup>1,*</sup>	43.61 °N	5.66 °W	01/01/2011 - 31/12/2015	✗	✗
Villano-Sisargas <sup>1</sup>	43.49 °N	9.21 °W	01/01/2010 - 31/12/2015	✓	✓
Langosteira <sup>1,*</sup>	43.35 °N	8.56 °W	01/02/2015 - 31/12/2015	✗	✗
Muros <sup>1,*</sup>	42.76 °N	9.02 °W	06/10/2015 - 31/12/2015	✗	✓
Ribeira <sup>2,*</sup>	42.55 °N	8.95 °W	01/01/2012 - 31/12/2015	✗	✓
Illas Cíes <sup>2,*</sup>	42.17 °N	8.91 °W	01/01/2010 - 31/12/2015	✗	✓
Silleiro <sup>1</sup>	42.12 °N	9.40 °W	01/01/2010 - 31/12/2015	✓	✓
A Guarda <sup>2,*</sup>	41.90 °N	8.90 °W	14/06/2011 - 31/12/2015	✗	✓
Leixões <sup>3,*</sup>	41.31 °N	8.98 °W	01/01/2010 - 31/12/2015	✗	✗
Raia01 <sup>3</sup>	41.16 °N	9.56 °W	12/06/2010 - 31/12/2015	✗	✗
Monican02 <sup>3</sup>	39.56 °N	9.21 °W	12/06/2010 - 31/12/2015	✗	✗
Monican01 <sup>3</sup>	39.51 °N	9.64 °W	14/03/2010 - 31/12/2015	✗	✗
Cascais <sup>4,*</sup>	38.69 °N	9.42 °W	01/01/2010 - 31/12/2015	✗	✗
Sines <sup>3,*</sup>	37.92 °N	8.93 °W	01/01/2010 - 31/12/2015	✗	✗
Lagos <sup>4,*</sup>	37.10 °N	8.67 °W	03/02/2014 - 31/12/2015	✗	✗
Faro <sup>3,*</sup>	36.90 °N	7.90 °W	01/01/2010 - 31/12/2015	✗	✗
Cádiz <sup>1</sup>	36.84 °N	6.98 °W	01/01/2010 - 31/12/2015	✓	✓
Algeciras <sup>1,*</sup>	36.07 °N	5.42 °W	02/01/2011 - 31/12/2015	✗	✗
Tarifa <sup>1,*</sup>	36.00 °N	5.58 °W	01/01/2011 - 31/12/2015	✗	✗
Ceuta <sup>1,*</sup>	35.90 °N	5.33 °W	19/02/2014 - 31/12/2015	✗	✗

The application of the harmonic analysis to currents observations is a more complex procedure compared to its application in water level analysis. In this case, the least squares method can lead to more unstable results when applied for different years and the tidal current amplitude could appear associated to harmonic constituents with close frequencies to major constituents. To illustrate the latter effect, Table II and Table III list the reference level and the main radiational, diurnal and semidiurnal component for the velocity component U and V respectively. Along with them two minor tidal components ( $S_1$  and  $MKS_2$ ), according to the results obtained in Chapter III, were

included in the tables. Current amplitudes associated to  $S_1$  are in most of the stations larger than any of the other diurnal components. The  $S_1$  frequency is located between the  $P_1$  and  $K_1$  frequencies that are considered relevant tidal components in this study area. However, their relevance is not reflected in their contribution to the current velocity and can be concluded that an amplitude transfer between these components. In some stations, the  $M_2$  tidal constituent, which is the main tidal constituent in Western Iberia regional ocean, is not the leading contributor to the current velocity while the  $MKS_2$  constituent, an usually irrelevant component with similar frequency, present large values when compared with other tidal constituents. Another example of the harmonic analysis difficulty to capture tidal currents in open ocean is that in Villano-Sisargas modelled zonal velocity the  $MKS_2$  constituent amplitude is even larger than  $M_2$  amplitude. Reference levels ( $Z_0$ ) indicate a net northern and westward circulation in the analysed stations.

**Table II. Observed (Obs.) and modelled (Mod.) harmonic velocity in  $\text{cms}^{-1}$  for the reference level ( $Z_0$ ) and the radiational (Sa, Ssa), diurnal ( $Q_1$ ,  $O_1$ ,  $P_1$ ,  $S_1$ ,  $K_1$ ) and semidiurnal ( $N_2$ ,  $M_2$ ,  $MKS_2$ ,  $S_2$ ,  $K_2$ ) tidal components obtained by harmonic analysis of the zonal velocity (U component). Components are ordered according to the frequency. The total harmonic velocity using from all the harmonic frequencies, except the reference level and the radiational components is shown.**

Tidal Comp.	Frequency ( $^\circ/\text{hour}$ )	Cádiz		Cabo de Peñas		Estaca de Bares		Silleiro		Villano-Sisargas	
		Obs.	Mod.	Obs.	Mod.	Obs.	Mod.	Obs.	Mod.	Obs.	Mod.
$Z_0$	0.000	4.57	1.32	0.07	2.57	4.16	0.59	1.71	0.00	2.58	3.41
Sa	0.041	4.53	2.72	7.41	9.98	4.26	8.10	3.33	3.45	6.03	10.27
Ssa	0.082	0.46	0.87	3.27	4.36	2.51	3.59	0.91	1.24	1.86	4.48
$Q_1$	13.399	0.37	0.41	0.11	0.35	0.11	0.34	0.23	0.05	0.19	0.29
$O_1$	13.943	0.69	0.79	0.08	1.11	0.14	0.79	0.13	0.21	0.09	0.68
$P_1$	14.959	1.52	2.05	0.42	0.61	0.25	0.96	0.92	1.40	0.32	0.51
$S_1$	15.000	3.84	4.17	1.12	1.85	0.69	1.36	2.27	2.92	0.76	1.61
$K_1$	15.041	2.68	2.84	0.39	1.03	0.13	2.03	1.13	1.48	0.72	0.81
$N_2$	28.440	0.41	1.00	0.42	0.77	1.11	0.92	0.49	0.81	1.32	0.31
$M_2$	28.984	2.39	4.78	2.67	3.07	4.38	4.12	2.28	2.45	5.71	1.13
$MKS_2$	29.066	0.89	0.54	0.61	0.56	1.46	0.41	1.58	1.43	0.82	1.78
$S_2$	30.000	1.46	0.91	0.45	1.13	0.93	1.09	0.36	0.47	1.25	1.67
$K_2$	30.082	0.23	0.36	0.15	0.14	0.33	0.37	0.38	0.31	0.34	0.50
<b>Total (60 Comp.)</b>		25.91	29.20	14.85	19.88	23.74	19.66	19.74	19.95	31.05	20.59

The radiational components such as the solar semiannual (Ssa) and annual (Sa) appear to have a great importance in the harmonic analysis and in some stations lead the contribution to the tidal currents. These components are related with the solar radiation cycles and with periodic meteorological forcing. Since they may include the climatological circulation patterns which are the subject of this study, the signal from those stations were kept with the residuals.

Tidal currents obtained with the harmonic analysis served to define a typical order of magnitude of the periodic surface current for this area since they are not the main source of currents variability. The sum of all the tidal components velocity, excluding the radiational components, shows that tidally induced currents are between 0.13 and 0.33  $\text{ms}^{-1}$  in the analysed stations (Table II and Table III).

In order to describe the seasonal currents affecting the western Iberia waters, the current velocity records were detided by subtracting their harmonic signal and obtaining the residual currents. The radiational components and their contribution were maintained in the residuals records in order to evaluate the currents seasonal evolution. The spreading of current intensities between the different frequencies did not affect the residuals analysis as all the 61 constituents, including the reference level, were removed from the current signal.

In order to ease comparisons between modelling and observed currents, the mean daily current were calculated for each component of the detided current residuals. Table IV summarises the maximum and minimum velocities for the offshore buoys observations and for the modelling results.

**Table III. Observed (Obs.) and modelled (Mod.) harmonic velocity in  $\text{cms}^{-1}$  for the reference level ( $Z_0$ ) and the radiational ( $S_a, S_{sa}$ ), diurnal ( $Q_1, O_1, P_1, S_1, K_1$ ) and semidiurnal ( $N_2, M_2, MKS_2, S_2, K_2$ ) tidal components obtained by harmonic analysis of the meridional velocity (V component). Components are ordered according to the frequency. The total harmonic velocity using from all the harmonic frequencies, except the reference level and the radiational components is shown.**

Tidal Comp.	Frequency ( $^{\circ}$ /hour)	Cádiz		Cabo de Peñas		Estaca de Bares		Silleiro		Villano-Sisargas	
		Obs.	Mod.	Obs.	Mod.	Obs.	Mod.	Obs.	Mod.	Obs.	Mod.
<b>Z<sub>0</sub></b>	0.000	7.12	1.30	0.38	0.67	0.33	0.57	0.94	5.96	3.49	3.23
<b>S<sub>a</sub></b>	0.041	5.25	1.99	0.90	3.12	2.37	0.78	3.82	9.88	2.26	5.66
<b>S<sub>sa</sub></b>	0.082	1.43	1.49	0.83	0.46	1.24	0.46	1.33	4.71	0.59	3.03
<b>Q<sub>1</sub></b>	13.399	0.28	0.29	0.02	0.15	0.04	0.10	0.09	0.16	0.11	0.08
<b>O<sub>1</sub></b>	13.943	0.06	0.61	0.10	0.43	0.15	0.36	0.03	0.70	0.18	0.20
<b>P<sub>1</sub></b>	14.959	1.38	2.14	0.39	0.70	0.20	0.75	0.73	1.55	0.35	0.49
<b>S<sub>1</sub></b>	15.000	4.01	3.70	1.03	1.66	0.58	1.03	2.12	3.46	0.65	1.11
<b>K<sub>1</sub></b>	15.041	2.62	2.45	0.63	0.65	0.29	0.95	0.85	1.62	0.33	0.57
<b>N<sub>2</sub></b>	28.440	0.30	1.32	0.31	0.68	1.32	1.40	0.43	0.94	0.99	1.17
<b>M<sub>2</sub></b>	28.984	1.87	6.13	2.18	2.62	5.53	6.50	2.16	6.78	8.18	4.89
<b>MKS<sub>2</sub></b>	29.066	0.78	0.51	0.52	0.42	2.03	0.33	1.30	1.22	0.81	1.73
<b>S<sub>2</sub></b>	30.000	0.48	1.86	0.70	1.07	1.31	1.49	1.75	2.13	0.99	1.30
<b>K<sub>2</sub></b>	30.082	0.13	0.47	0.16	0.18	0.68	0.44	0.86	0.85	0.68	0.38
<b>Total (60 Comp.)</b>		22.90	30.19	13.50	13.94	23.90	20.64	20.99	26.86	32.53	22.35

In order to compare with the observations and to describe the western Iberia currents two values are given for the modelling results: one calculated for the entire analysed period and another for the dates when observations were available.

The dominant current direction, thus presenting a larger range of values, is the zonal component for the three northernmost stations located northern to Cape Finisterre while the meridional component clearly dominates in the Silleiro station located in the open Atlantic Ocean and it's slightly larger than the zonal component in the Gulf of Cádiz. The dominant direction coincides with the prevailing wind direction (Chapter II) in the case of Estaca de Bares, Cabo de Peñas and Silleiro stations however Villano-Sisargas did not show any prevailing wind direction and in Cádiz the mean direction was the zonal component. Modelling results tend to overestimate the maximum and minimum current values except for the Cádiz buoy. The source of this difference could be due to the observation method that collect data a few meters below the surface. The coefficient of determination ( $R^2$ ) between the modelled and observed residuals are similar to the correspondent coefficients found between the raw observations and the modelled results (not shown) as the residuals could be regarded as the main source of variability for all the stations.  $R^2$  reach values between 0.30 and 0.47 in the dominant current direction which can be considered satisfactory taking into consideration the constraints for the comparison and validation described above and the limitations of the meteorological models described in Chapter II.

The studied buoys present a similar performance for the U-component above 0.35, except for the Cádiz buoy. The Cádiz buoy is located in a complex circulation area, the Gulf of Cádiz, where the Strait of Gibraltar dynamics exerts a large influence that are disregarded in this model due to the model domain limits and as consequence none of the directions present high  $R^2$  values. A possible solution to improve the performance in this area consists in nesting the PCOMS in the Lusitania model application (Campuzano *et al.*, 2013) which domain includes the western Mediterranean

waters. In any case, the range of values and some of the patterns existing in the observations are recognisable in the modelling results at the Cádiz buoy location (Figure 2).

Regarding the current V component, the  $R^2$  performance is poorer due to the vicinity of the land in this direction for most of the buoys. This effect is similar to the observed in the wind V component. In Silleiro buoy, where the wind propagation in the V axis is less interfered by the land proximity the  $R^2$  presents its highest value. In this same station, the U component present a high correlation as the main direction of propagation is landwards. For this reasons, the Silleiro station could be considered as the most representative station of open ocean conditions in the Iberian Peninsula Atlantic front.

The monitoring buoys were able to collect currents information during most of the study period with percentages of valid data over 80% except for Estaca de Bares that only managed to register the observations during halve of the study period. Unfortunately, no current data for this period was available for any station located in the Portuguese coast.

**Table IV. Maximum ( $P_{95}$ ) and minimum ( $P_{05}$ ) mean daily current velocity for observations and modelling results and coefficient of determination ( $R^2$ ) between both datasets for each component (U and V). The modelling results are shown for the same dates where observations were available and for the entire period. The current component with larger range of velocities is marked in bold. The number of available data is also indicated as well as the percentage of valid observations for the period 2010-2015. Buoys are listed from North to South.**

Station Name	Water Velocity Component	Observed Velocity		Surface Modelled Velocity		Entire period Surface Modelled Velocity		$R^2$	N (Valid %)
		$P_{05}$	$P_{95}$	$P_{05}$	$P_{95}$	$P_{05}$	$P_{95}$		
Estaca de Bares	<b>U</b>	-16.39	16.63	-23.61	21.94	-21.36	25.81	0.36	1176 (53.63 %)
	V	-9.44	10.94	-8.50	9.36	-9.03	8.87	0.13	
Cabo de Peñas	<b>U</b>	-20.24	21.01	-29.35	30.25	-29.34	30.96	0.42	1906 (86.95 %)
	V	-9.67	10.53	-6.92	7.18	-7.68	6.97	0.03	
Villano-Sisargas	<b>U</b>	-17.24	17.29	-24.73	26.38	-24.88	26.33	0.47	1819 (82.98 %)
	V	-11.91	12.57	-14.63	18.41	-14.46	18.14	0.14	
Silleiro	U	-13.78	12.12	-14.32	14.00	-14.54	13.88	0.43	1866 (85.12 %)
	<b>V</b>	-13.07	14.58	-19.71	24.18	-19.30	23.44	0.30	
Cádiz	U	-13.06	14.50	-11.90	11.38	-12.01	12.73	0.01	1900 (86.67 %)
	<b>V</b>	-15.61	13.82	-12.48	14.05	-13.07	14.11	0.11	

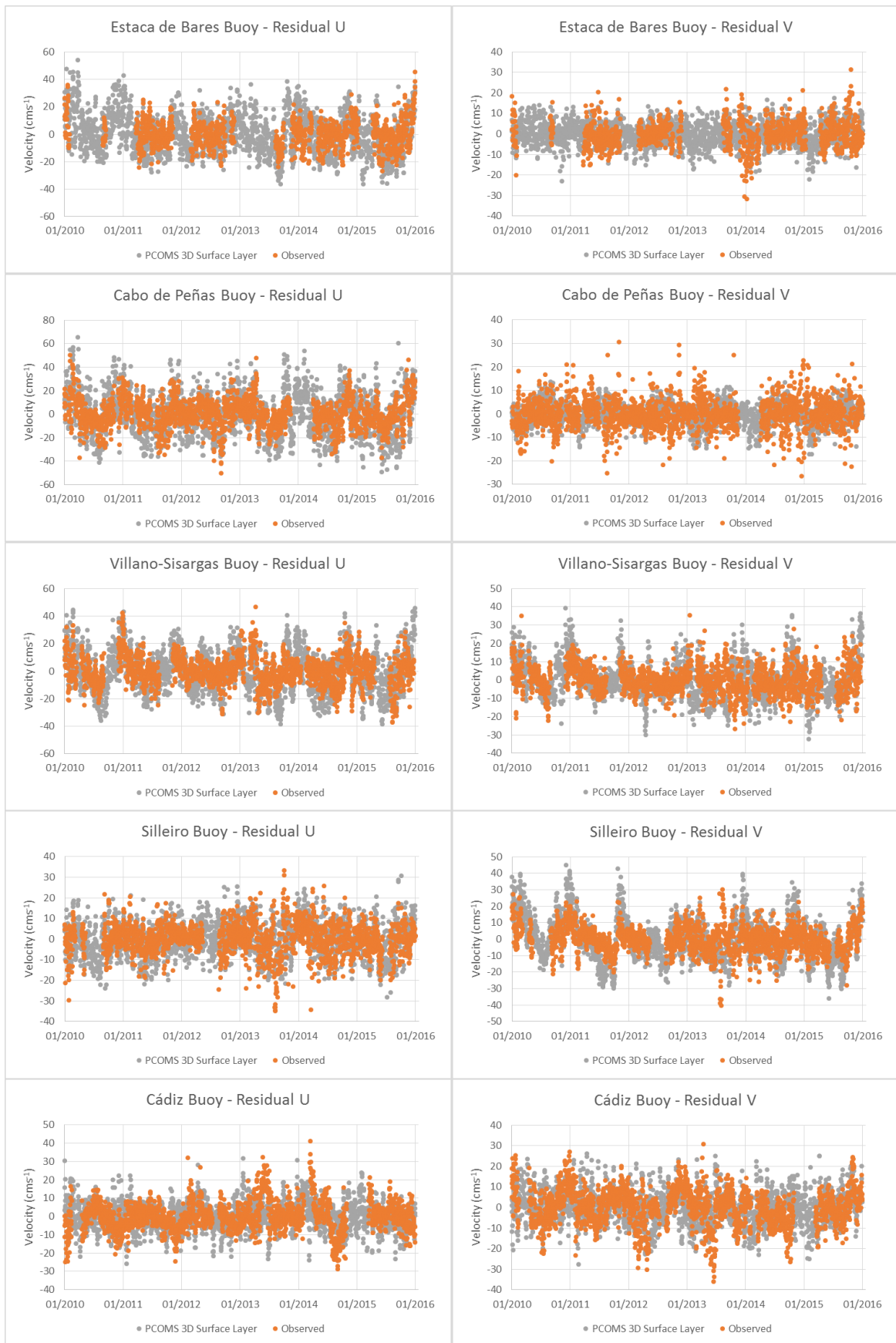


**Figure 2** Observed and modelled daily averaged residual currents for the U (left) and V (right) velocity components at each of the current monitoring buoys in Western Iberia for the period 2010-2015.

Due to its location (Figure 1), Silleiro buoy is the most representative of the Portuguese western coast and the signature of the upwelling processes in the Western Iberia coast could be detected in the seasonal and monthly observed and modelled values (Table V). Along the year, surface currents in Silleiro showed a clear pattern with currents flowing southwards and offshore during summer indicating the presence of upwelling events while during winter the currents turn poleward and landwards indicating downwelling processes. The upwelling and downwelling processes are more intense during the months of August and December respectively. Interannual variations can be also be identified being the total balance for the years 2012, 2013 and 2015 of upwelling-dominated years while 2011 and 2014 were almost neutral and 2010 a downwelling-dominated year. However, when analysing the monthly average (Figure 3), during the year 2011 it can be observed the most intense upwelling event of the record as indicated by the meridional currents and winds (Figure 14 from Chapter II). It should be noted that observed Silleiro buoy records missed to describe some of this patterns as many data gaps were located during the summer months (Figure 2, Table V). Current intensity differences between observed and modelled values could be related to the depth where data were collected, ADCP systems do not measure above the top five meters while the model results average current intensities in the top 2-3 meters.

**Table V. Monthly, seasonal and annual average intensities for the observed and modelled U and V current components in cm for the Silleiro station. Positive values indicates eastward and northward currents for U and V components respectively. A column indicates the amount of observed data valid for each time period.**

Time Period	Observed U	Observed V	Modelled U	Modelled V	% Observed data
January	1.36	2.29	2.44	6.80	<b>98.68</b>
February	2.35	-0.05	2.48	1.99	<b>99.70</b>
March	1.41	0.79	1.48	2.29	<b>84.66</b>
April	-0.06	-0.93	1.27	1.96	<b>89.77</b>
May	-3.83	-3.22	-3.39	-3.29	<b>75.83</b>
June	-2.49	-3.41	-3.71	-7.70	<b>53.13</b>
July	-3.33	-3.06	-4.78	-10.91	<b>54.44</b>
August	-4.72	-2.31	-2.27	-12.37	<b>68.50</b>
September	-0.66	-4.49	0.38	-6.26	<b>99.72</b>
October	2.04	1.71	1.79	8.04	<b>98.03</b>
November	0.94	2.31	0.73	7.56	<b>87.96</b>
December	2.53	6.31	3.79	11.93	<b>96.48</b>
Spring	-0.71	-1.04	-0.23	0.30	<b>83.35</b>
Summer	-3.63	-2.87	-3.59	-10.36	<b>58.75</b>
Autumn	0.77	-0.25	0.97	3.16	<b>95.27</b>
Winter	2.07	2.90	2.91	7.06	<b>98.24</b>
2010	-0.22	5.05	-1.99	9.05	<b>58.14</b>
2011	0.43	0.00	-0.98	-0.27	<b>97.92</b>
2012	1.13	-0.03	2.19	-3.39	<b>70.98</b>
2013	-1.03	-0.85	-0.19	-2.24	<b>92.32</b>
2014	0.40	-0.74	1.94	0.28	<b>98.69</b>
2015	-0.63	-1.65	-0.98	-3.42	<b>84.78</b>

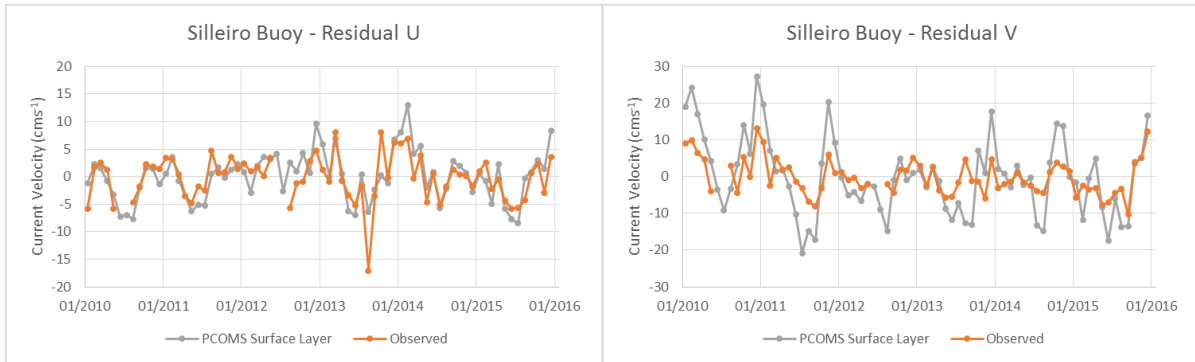
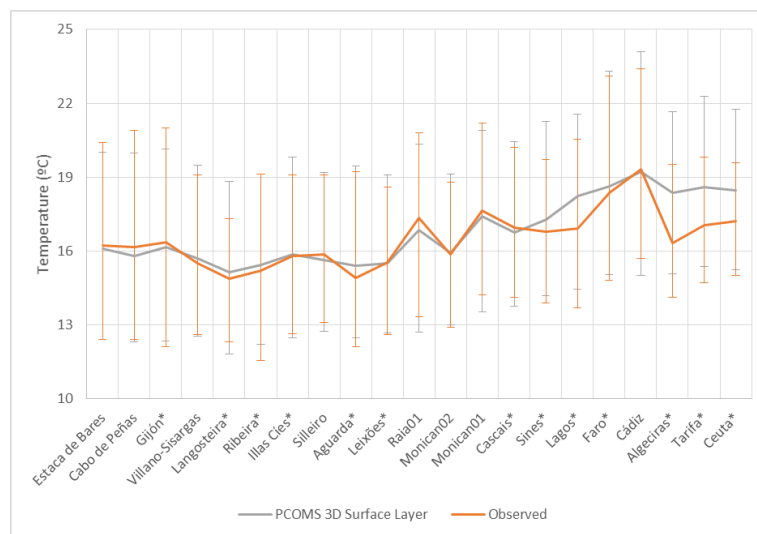


**Figure 3** Observed and modelled monthly averaged residual currents for the U (left) and V (right) velocity components at Silleiro buoys in Western Iberia for the period 2010-2015.

#### 4.2.1.2. Surface Water temperature

Surface water temperature is commonly used as an indicator of water circulation. Despite being a non-conservative property, due to the heat fluxes exchange with the atmosphere, this property distribution can aid in model hydrodynamics interpretation. Surface water temperature is easily observed using remote sensing technology that provide daily information covering the entire ocean with high horizontal resolutions. Temperature is a property commonly measured by all the ocean buoys allowing to use a larger network of buoys when compared with surface currents. In total twenty-two buoys along the western Iberian coast observe operationally surface temperature. In order to classify the water temperature from the analysed stations, the mean averaged value and the 5<sup>th</sup> and 95<sup>th</sup> percentile ( $P_{05}$  and  $P_{95}$  respectively) were obtained for each station (Table I, Figure 4). Coastal and ocean buoys were distinguished to analyse their different patterns. Data gaps represent more than 55% of the total data for all the Portuguese stations and are able influence the station analysis. When examining water temperature, a relevant issue to bear in mind is that observations are also subjected to measurement errors and sensor decalibration.

Model results show a high level of agreement between the observed and modelled data with coefficient of determination ( $R^2$ ) above 0.85 for all the ocean stations. In general, the level of agreement reduce in coastal stations where local hydrodynamics produce larger temperature ranges (i.e. Gijón buoy) including the estuarine influence (i.e. Illas Cíes) or high frequency variabilities (i.e. Tarifa buoy).



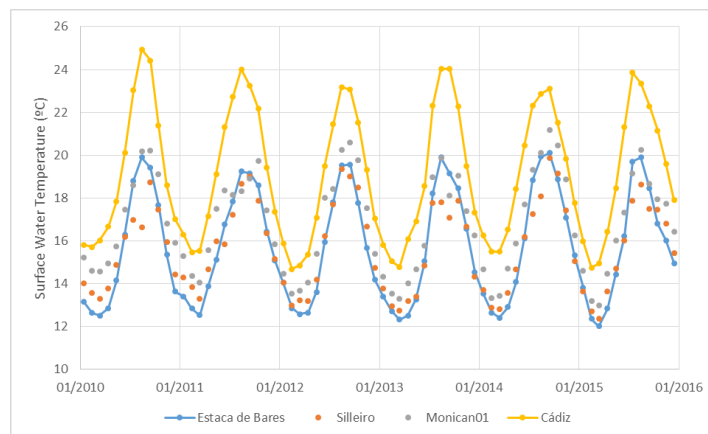
**Figure 4** Mean observed and modelled temperature for the period 2010-2015. Error bars indicate their correspondent 5<sup>th</sup> ( $P_{05}$ ) and 95<sup>th</sup> ( $P_{95}$ ) percentile. Stations are ordered from North to South (left to right) and coastal stations are indicated with \*.

Table VI. List of multiparametric buoys, mean observed and modelled temperature and coefficient of determination ( $R^2$ ) between both datasets. The 5<sup>th</sup> ( $P_{05}$ ) and 95<sup>th</sup> ( $P_{95}$ ) percentile for observed and modelled temperature are indicated. Muros buoy has been included for completeness though the observed period is only of 3 months. Lagos temperature range and percentages were calculated for the period shown in Figure 6 as previous records were unreliable. Coastal stations are indicated with \*.

Station Name	Mean Observed Temperature ( $P_{05} - P_{95}$ )	Mean Modelled Temperature ( $P_{05} - P_{95}$ )	$R^2$	N (Valid %)
Estaca de Bares	16.21 (12.40 - 20.40)	16.08 (12.39 - 20.02)	0.97	31 915 (60.75 %)
Cabo de Peñas	16.17 (12.40 - 20.90)	15.81 (12.29 - 19.98)	0.96	48 576 (92.60 %)
Gijón *	16.36 (12.10 - 21.00)	16.17 (12.32 - 20.13)	0.93	26 998 (61.60 %)
Villano-Sisargas	15.50 (12.60 - 19.10)	15.70 (12.53 - 19.47)	0.87	48 868 (89.21 %)
Langosteira *	14.86 (12.30 - 17.30)	15.13 (11.82 - 18.83)	0.79	6 746 (84.16 %)
Muros *	15.51 (13.79 - 16.89)	15.86 (14.51 - 17.00)	0.76	2 079 (100.00 %)
Ribeira *	15.19 (11.56 - 19.13)	15.45 (12.19 - 19.13)	0.81	25 154 (71.74 %)
Illas Cíes *	15.79 (12.62 - 19.08)	15.86 (12.48 - 19.80)	0.77	22 299 (42.44 %)
Silleiro	15.85 (13.10 - 19.10)	15.62 (12.74 - 19.19)	0.89	45 472 (86.55 %)
A Guarda *	14.90 (12.10 - 19.21)	15.40 (12.48 - 19.45)	0.84	24 796 (62.18 %)
Leixões *	15.53 (12.60 - 18.60)	15.51 (12.67 - 19.09)	0.75	29 036 (55.21 %)
Raia01	17.33 (13.33 - 20.78)	16.83 (12.72 - 20.33)	0.90	18 072 (37.12 %)
Monican02	15.86 (12.91 - 18.78)	15.92 (12.98 - 19.12)	0.86	20 884 (42.90 %)
Monican01	17.65 (14.22 - 21.18)	17.42 (13.52 - 20.88)	0.90	13 262 (26.11 %)
Cascais *	16.96 (14.10 - 20.20)	16.76 (13.77 - 20.44)	0.60	43 502 (82.80 %)
Sines *	16.77 (13.90 - 19.70)	17.26 (14.17 - 21.25)	0.76	30 950 (58.85 %)
Lagos *	16.92 (13.70 - 20.53)	18.22 (14.44 - 21.56)	0.71	16 715 (85.10 %)
Faro *	18.37 (14.80 - 23.10)	18.64 (15.03 - 23.30)	0.88	30 365 (57.74 %)
Cádiz	19.30 (15.70 - 23.40)	19.23 (15.00 - 24.08)	0.94	46 164 (84.84 %)
Algeciras *	16.32 (14.10 - 19.50)	18.36 (15.09 - 21.66)	0.36	16 227 (35.57 %)
Tarifa *	17.06 (14.70 - 19.80)	18.58 (15.37 - 22.28)	0.72	40 816 (93.13 %)
Ceuta *	17.21 (15.00 - 19.57)	18.47 (15.25 - 21.74)	0.74	15 547 (95.19 %)

Mean temperatures in the Western Iberia are relatively uniform in the North and West coast of the study area increasing in the Gulf of Cádiz under the influence of warmer Mediterranean waters. Mean offshore values increase southwards from around 15.5°C to 19.5°C. Coastal buoys in the West coast (i.e. Ribeira, A Guarda, Monican02) present lower values in their 5<sup>th</sup> percentile when compared with ocean buoys from the same area (i.e. Villano-Sisargas, Raia01, Monican01) due to the influence of upwelled waters.

PCOMS monthly averaged surface water temperature follow the expected temperature cycle where maximum values are observed during the late summer (JAS) and minimum values during late winter months (JFM) with small interannual variation (Figure 5). In contrast with the air temperature pattern, the meridional thermal gradient is broken during the summer period and the northernmost station, Estaca de Bares, present higher water temperature than stations located southwards, such as Silleiro buoy, due to the influence of upwelled waters in the western Iberian coast. For that reason, climatological maximum temperature for the Silleiro buoy occurs during September while for the other three stations analysed in Figure 5 the month with warmest surface waters is August. Figure 6 represents the observed and modelled SST for each of the analysed monitoring stations.



**Figure 5** MMS monthly averaged water temperature for several stations in the Western Iberia region including the northernmost (Estaca de Bares, blue line) and southernmost (Cádiz, orange line) stations.

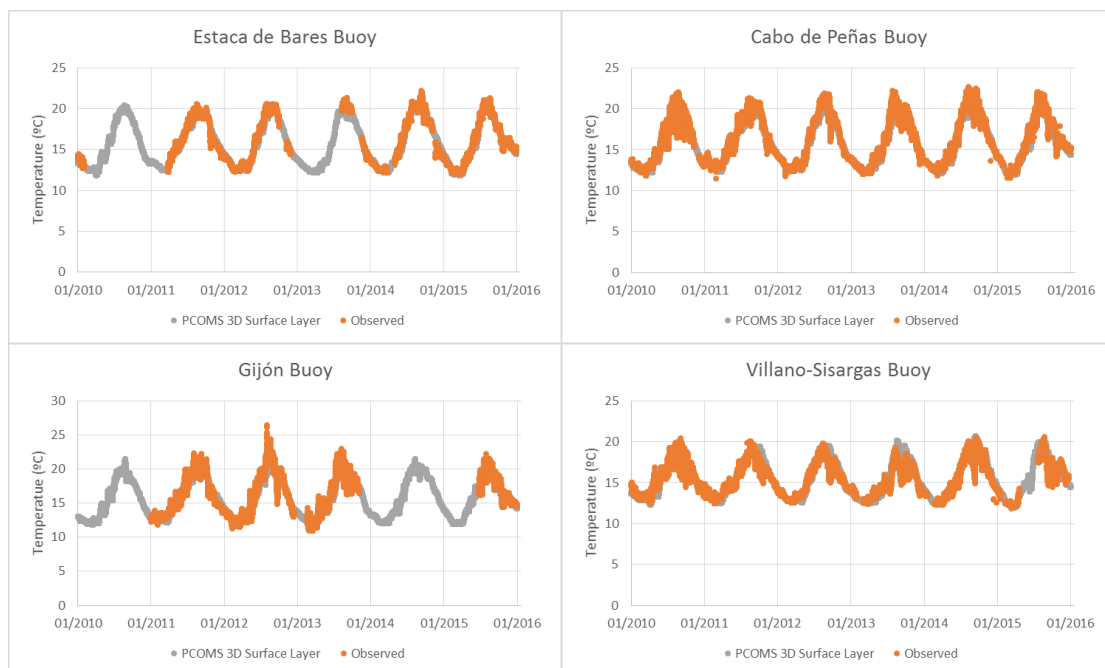


**Figure 6.** Mean observed (orange dots) and modelled (grey dots) surface water temperature for the Western Iberia coastal buoys for the period 2010-2015. Stations are ordered according to its latitude from top (North) to bottom (South).

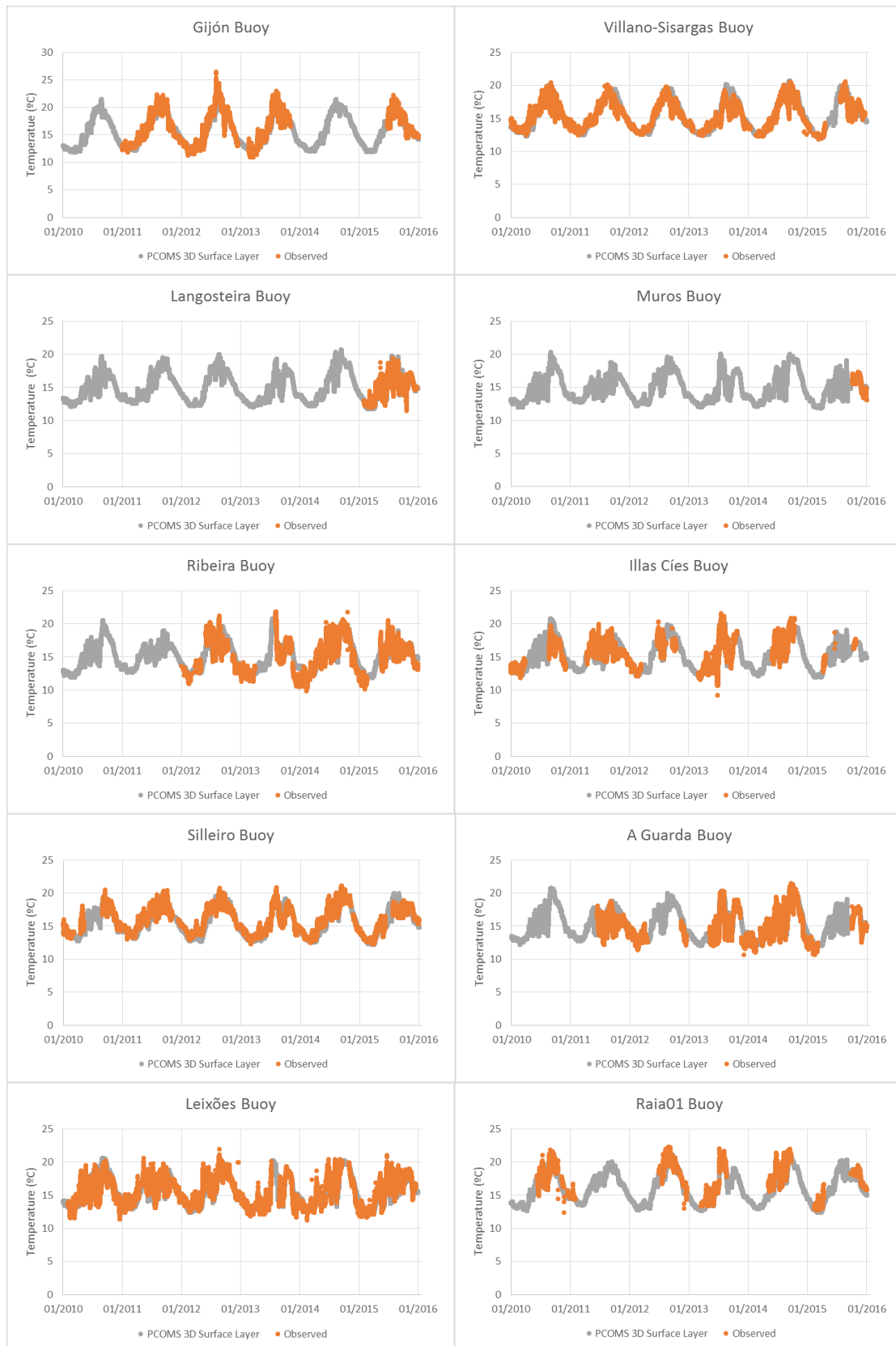


**Figure 6 Cont. Mean observed (orange dots) and modelled (grey dots) surface water temperature for the Western Iberia coastal buoys for the period 2010-2015. Stations are ordered according to its latitude from top (North) to bottom (South).**



**Figure 6 Cont. Mean observed (orange dots) and modelled (grey dots) surface water temperature for the Western Iberia coastal buoys for the period 2010-2015. Stations are ordered according to its latitude from top (North) to bottom (South).**

#### 4.2.1.3. Surface Salinity

Since the main source of salinity variability comes from fresh water discharges in coastal areas and the model application analysed in this chapter does not include these inputs and neither consider the precipitation and evaporation processes, the main aim of this section aims to illustrate the general distribution of salinity in the western Iberia waters due to thermohaline circulation and to evaluate the available data sources.

Five out of the nine stations with salinity sensors are located offshore where fresh water from land sources rarely exert any influence (Table VII). Observations in ocean buoys, once cleared from obvious outliers are shown in Figure 7. Silleiro buoy observations present a loss of calibration between 2011 and 2013. Observations during that period described a similar pattern to the modelling results with a permanent offset that was corrected after that period. In coastal areas, the task to distinguish between valid and ambiguous data is even harder. A model including fresh water discharges and higher spatial resolution would be helpful to identify valid data from incorrect observations. In fact, salinity valid data percentage is lower when compared with temperature observations.

From the data, two salinity gradients can be distinguished from the observed data, a coastal-ocean gradient due to the entry of fresh water inputs and a meridional gradient due to the thermohaline circulation and linked to the evaporation processes (Figure 8). While ocean buoys register narrow salinity intervals below 1 unit of salinity, coastal stations observed larger intervals of salinities from 10 to 15 units of salinity due to the presence of fresh water sources. Modelled salinity results were never below 35 units of salinity due to the described limitations. The meridional gradient, considering only the ocean buoys, increases in average between 0.60 and 0.80 units of salinity according to the modelled and observed values respectively (Figure 8). Even if model results follow the general trend in the offshore stations, coefficient of determination are low due to the absence of some sources of salinity variability and the presence of ambiguous data in the time series. In this section, the main objective was to illustrate the technical difficulties for long-term salinity validation (i.e. wrong observations, lack of reliable data and uncertainties from land boundary conditions) and to describe the general value distribution rather than obtaining good comparisons.

**Table VII. Mean observed and modelled salinity and coefficient of determination ( $R^2$ ). The 5th ( $P_{05}$ ) percentile and 95<sup>th</sup> ( $P_{95}$ ) for observed and modelled salinity are indicated within brackets. Muros buoy has been included for completeness though the observed period is only of 3 months. Coastal stations are indicated with \*.**

Station Name	Mean Observed Salinity ( $P_{05} - P_{95}$ )	Mean Modelled Salinity ( $P_{05} - P_{95}$ )	$R^2$	N (Valid %)
Estaca de Bares	35.63 (35.42 - 35.82)	35.62 (35.47 - 35.71)	0.44	24 269 (46.19 %)
Cabo de Peñas	35.48 (35.01 - 35.81)	35.61 (35.42 - 35.71)	0.28	32 091 (61.08 %)
Villano-Sisargas	35.69 (35.45 - 35.93)	35.67 (35.55 - 35.77)	0.20	30 752 (58.53 %)
Muros *	33.35 (29.22 - 35.34)	35.61 (35.55 - 35.67)	0.02	2 079 (100.00 %)
Ribeira *	28.94 (19.31 - 34.66)	35.69 (35.58 - 35.79)	0.04	25 154 (71.74 %)
Illas Cíes *	32.66 (25.87 - 35.87)	35.74 (35.62 - 35.89)	0.00	21 066 (40.10 %)
Silleiro	35.77 (35.34 - 36.09)	35.72 (35.57 - 35.89)	0.07	41 570 (79.12 %)
A Guarda *	30.95 (23.81 - 35.52)	35.71 (35.61 - 35.82)	0.15	24 796 (62.18 %)
Cádiz	36.43 (36.15 - 36.66)	36.22 (36.05 - 36.34)	0.07	39 355 (74.91 %)

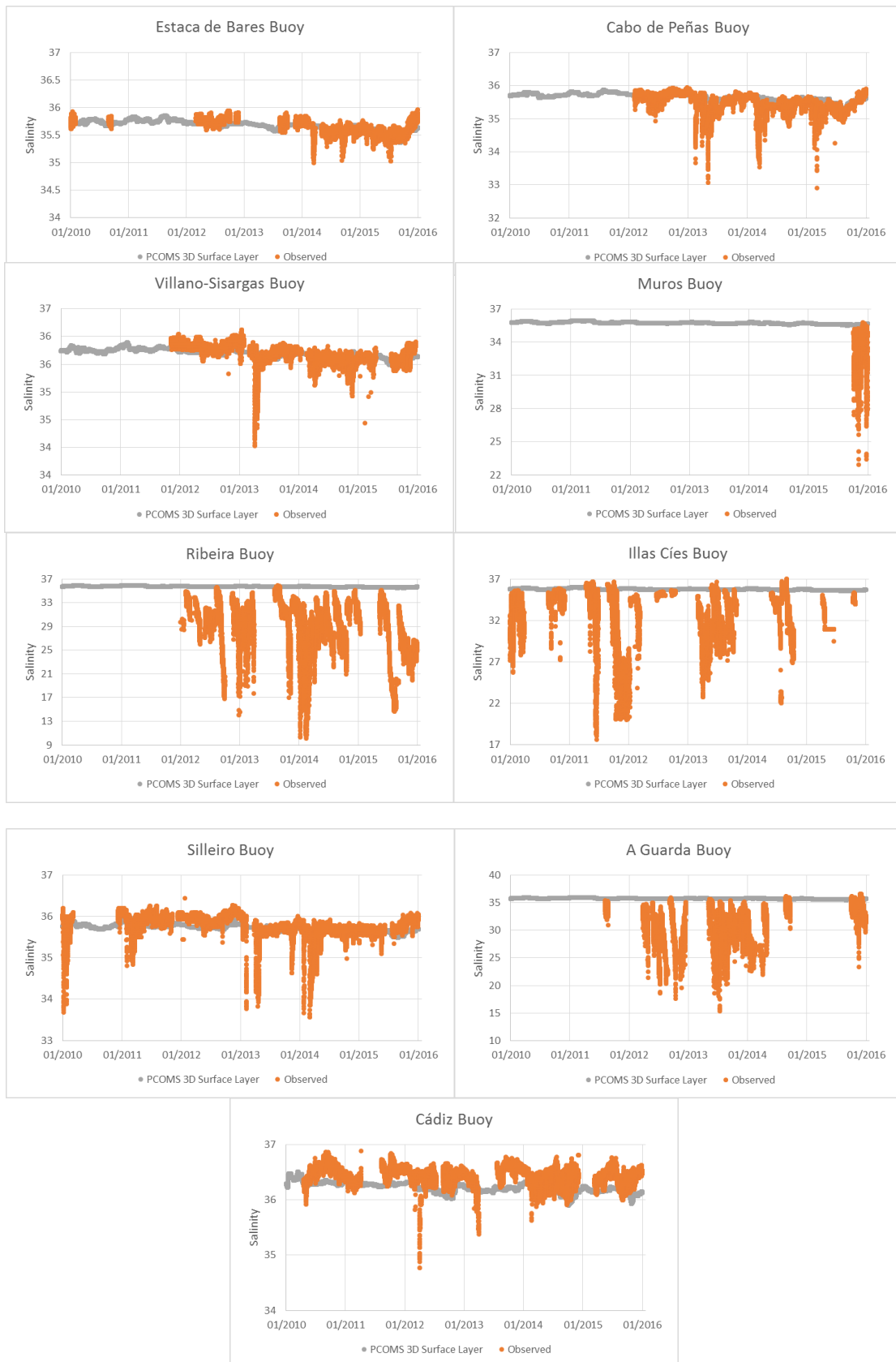


**Figure 7 Mean observed (orange dots) and modelled (grey dots) salinity in the Western Iberia ocean and coastal buoys for the period 2010-2015. Stations are ordered according to its latitude from top (North) to bottom (South).**

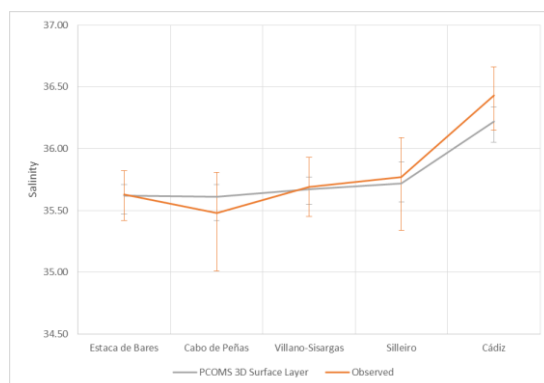


**Figure 8** Mean observed and modelled salinity for the ocean buoys during the period 2010-2015. Error bars indicate their correspondent 5<sup>th</sup> (P<sub>05</sub>) and 95<sup>th</sup> (P<sub>95</sub>) percentile. Stations are ordered from North to South (left to right).

#### 4.2.2. Modelling results evaluation with remote sensing products

In this section, temperature and salinity modelling results at the surface layer were compared with state-of-the-art products for sea surface temperature (SST) and salinity (SSS) for the period 2010-2015 and 2011-2015 respectively, since the chosen SSS product is only available from mid-2010. In a similar fashion to the validation methodology used in Lorente *et al.* (2016), daily SST and SSS products were compared with PCOMS modelling results and the Mercator-Océan PSY2V4 model solution that served as reference solution (Drillet *et al.*, 2005; hereafter referred as MERCATOR), since it provides initial and boundary conditions to the PCOMS model application. The MERCATOR operational system produces daily fields for the following variables: U and V velocity components, water level, salinity and temperature. Each weekly release include a week forecast and two weeks hindcast (analysis). The MERCATOR analysis solution, two-week delay with respect to its release date, was used for comparison. Mean value, coefficient of determination, bias and root mean square error (RMSE) for SST and for SSS were obtained. It is relevant to remind that the PCOMS model is only relaxing the MERCATOR properties at the open boundary strip while MERCATOR fields have assimilated daily AVHRR-AMSR SST along with altimetry Sea Level Anomalies and T-S profiles from ARGO floats (Lellouche *et al.*, 2013). The PCOMS model application simulated continuously the entire analysed period without reinitialising their properties.

##### 4.2.2.1. Sea Surface Temperature (SST)

The remote sensing product chosen to evaluate the sea surface temperature (SST) of the PCOMS and MERCATOR modelling results is the Multi-scale Ultra-high Resolution (MUR). The current version (Version 4.1, <http://dx.doi.org/10.5067/GHGMR-4FJ04>, accessed in Sept. 2017) provides daily SST estimates on a global 0.01°×0.01° grid and features the 1-km resolution MODIS retrievals, which are fused with AVHRR GAC, microwave, and *in situ* SST data by applying internal correction for relative biases among the data sets (Chin *et al.*, 2017).

SST average for the entire study period shows good correspondence between the EO product and both modelling results patterns (Figure 9). Mean spatially averaged temperature value for the full period is similar in both modelling products (Table VIII) and similar to the mean value obtained from MUR (17.50°C). On average, a clear meridional temperature gradient can be observed in the Western Iberia waters going from around 20°C in the southern sector to around 14°C in the Northwest area. It's in the northern sector where the three solutions slightly differ on average. Another clear gradient can be distinguish between the coastal areas of western Iberia, mainly west from 8°W, with the surrounding waters due to the upwelling processes. The limits and intensity of these gradients is slightly different between the three compared solutions.

Modelling results demonstrate that the temperature field does not degrade significantly with time and thus the heat transfers calculated within the PCOMS modelling domain are satisfactory. Daily

spatially-averaged sea surface temperature from PCOMS and MERCATOR modelling results reproduce accurately the values obtained by MUR during the period 2010-2015 (Figure 10). Spatially averaged maximum temperatures were observed by the end of summer in September-October while minimum values were obtained during the early spring months March-April. Those values do not match the timing for maximum and minimum air surface temperature which are August and February respectively. This lag between air and water peak temperatures might be related to the upwelling/downwelling influence in water temperature on top of the continental shelf.

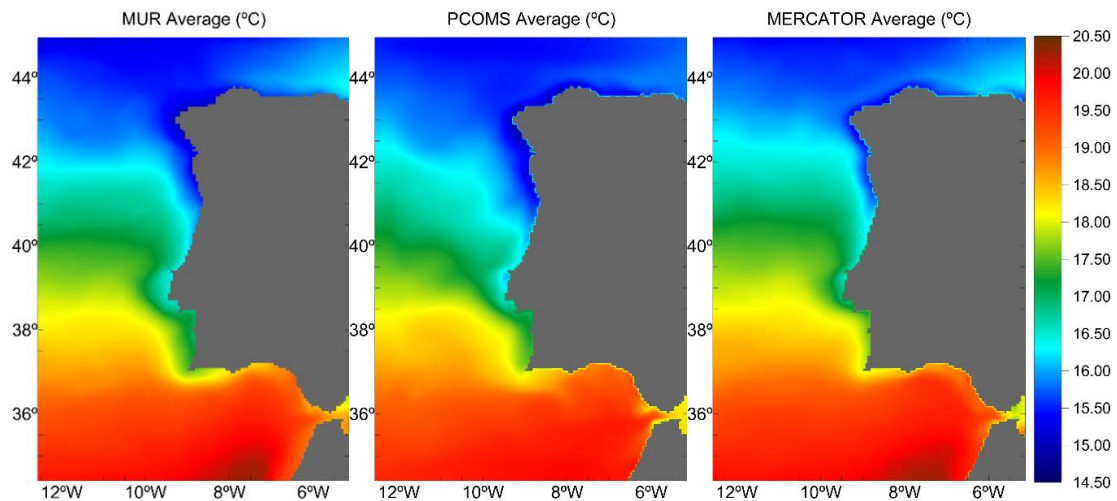


**Figure 9 Mean sea surface temperature from MUR (left), PCOMS (centre) and MERCATOR (right) in the western Iberia region for the period 2010-2015.**

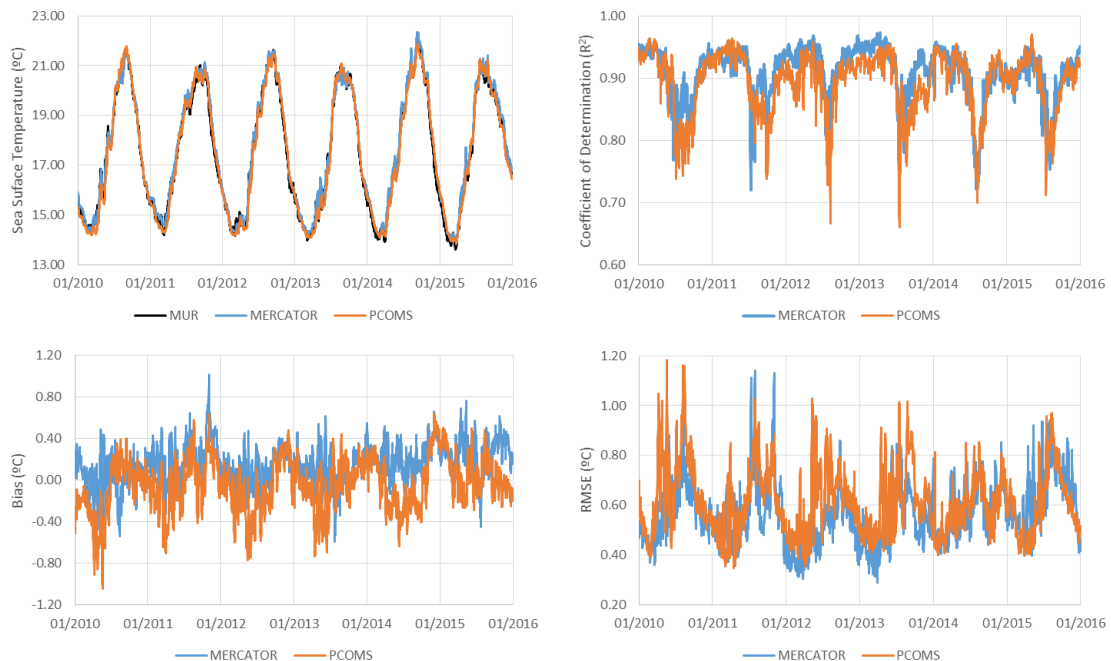


**Figure 10 Daily mean sea surface temperature from PCOMS, MERCATOR and the remote sensing product MUR spatially averaged over the study-domain for the period 2010-2015 (top left). Temporal evolution of the daily metrics for the PCOMS and MERCATOR when compared with the MUR SST spatially averaged over the study-domain: correlation coefficient (top right), bias (bottom left) and RMSE (bottom right).**

In general, daily coefficients of determination ( $R^2$ ) were satisfactory for both modelling set of results with values over 0.60 for the entire analysed period and over 0.90 during most of the time (Figure 10). On average, mean daily  $R^2$  values were 0.89 and 0.91 for PCOMS and MERCATOR respectively.

Mean daily bias was  $-0.04^{\circ}\text{C}$  and  $0.15^{\circ}\text{C}$  for PCOMS and MERCATOR respectively and mean daily RMSE was  $0.61^{\circ}\text{C}$  and  $0.56^{\circ}\text{C}$  for the same products.

A seasonal pattern can be distinguished in the daily integrated statistics (Figure 10),  $R^2$  values drop during the summer periods on both modelling products and the highest RMSE values tend to concentrate also during the same season though that pattern was not that explicit. Daily spatially averaged bias describe an annual cycle and is more balanced for PCOMS than for MERCATOR. In order to analyse with more detail this period, the same statistical analysis was performed only considering the summer months (JJA) for the entire period (Figure 11, Table VIII).

**Table VIII. Mean sea surface temperature spatially averaged over the study-domain of PCOMS and MERCATOR and the main statistics when compared with the MUR SST during the entire period 2010-2015 and when only considering the summer months (JJA).**

Statistic	PCOMS	MERCATOR	PCOMS (JJA)	MERCATOR (JJA)
Mean ( $^{\circ}\text{C}$ )	17.45	17.65	19.52	19.67
$R^2$	0.89	0.91	0.85	0.87
Bias ( $^{\circ}\text{C}$ )	-0.04	0.15	0.71	0.64
RMSE ( $^{\circ}\text{C}$ )	0.61	0.56	1.65	1.71

The temperature range in Western Iberian waters grows during the summer period since the minimum temperature decreases  $1^{\circ}\text{C}$  and maximum values increase in  $4^{\circ}\text{C}$  (Figure 11) due to the presence of upwelled waters in the coastal area and to the higher solar radiation respectively. Coldest waters were mainly located in the north-western region of Iberia while the warmest waters were observed in the Gulf of Cádiz area. This pattern was observed in all the SST sources: MUR, PCOMS and MERCATOR (Figure 11). However, the extension and intensity of the upwelled water is slightly different in each SST solution. Table VIII shows that the metrics obtained by comparing the modelling products with the MUR SST were worse when considering only the summer months than when the entire dataset was used.

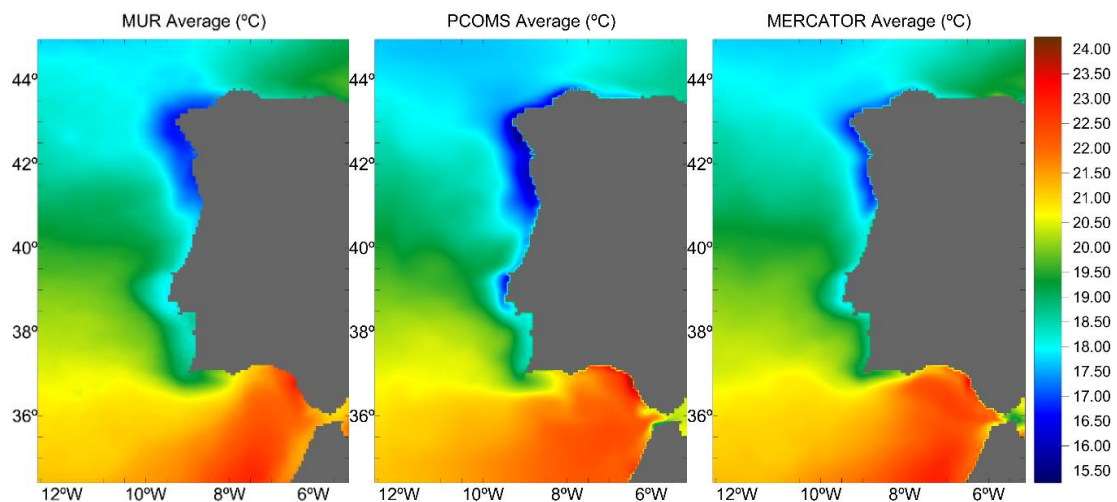


**Figure 11 Mean sea surface temperature from MUR (left), PCOMS (centre) and MERCATOR (right) in the western Iberia region for the summer months (JJA) of the period 2010-2015.**

In order to evaluate which areas were performing better on each modelling solutions, the same statistics were obtained for each cell of the modelling results (Figure 12). When analysed spatially, the main differences between the EO SST and the modelling products were concentrated in the coastal area with minor differences between PCOMS and MERCATOR patterns. MERCATOR present slightly higher  $R^2$  values than PCOMS and tends to overestimate water temperature along the entire western Iberia coast. The PCOMS underestimate slightly the temperature in the west coast and overestimate in the southern coast. RMSE is higher in some areas of the PCOMS northern than  $40^{\circ}\text{N}$  when compared with MERCATOR.

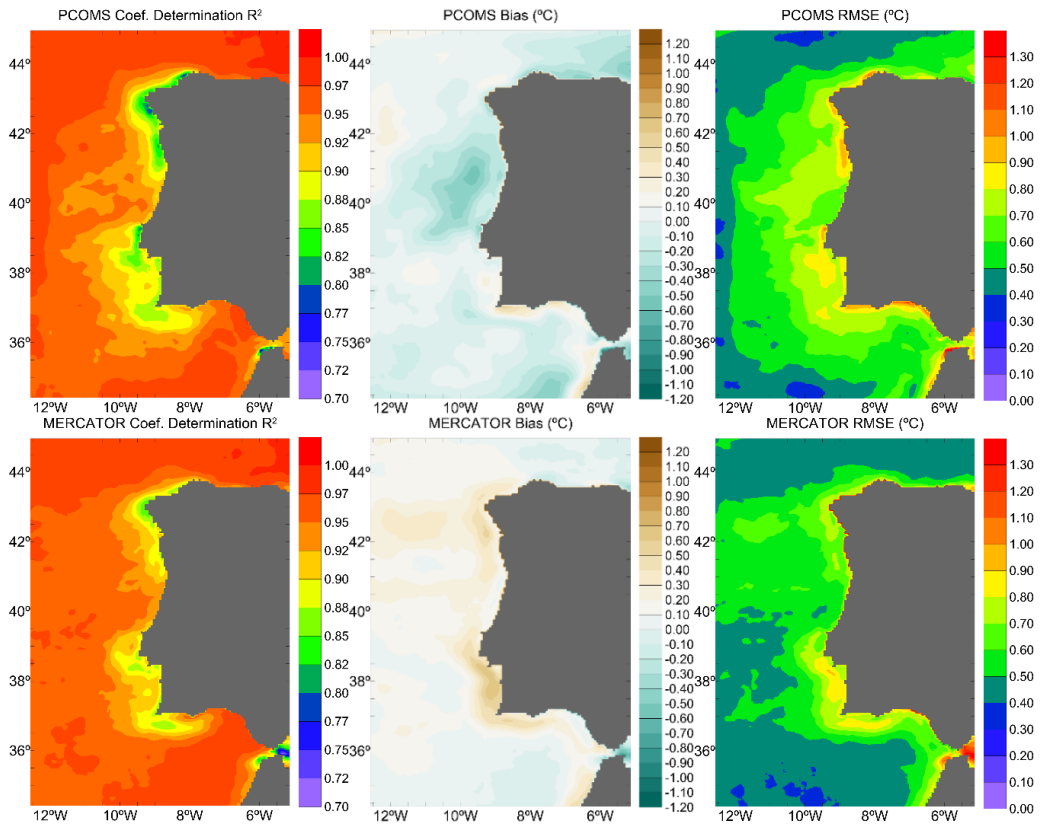


Figure 12 Coefficient of determination (left), bias (centre) and RMSE (right) maps obtained by comparing sea surface temperature from PCOMS (top) and MERCATOR (bottom) with MUR SST for the period 2010-2015.

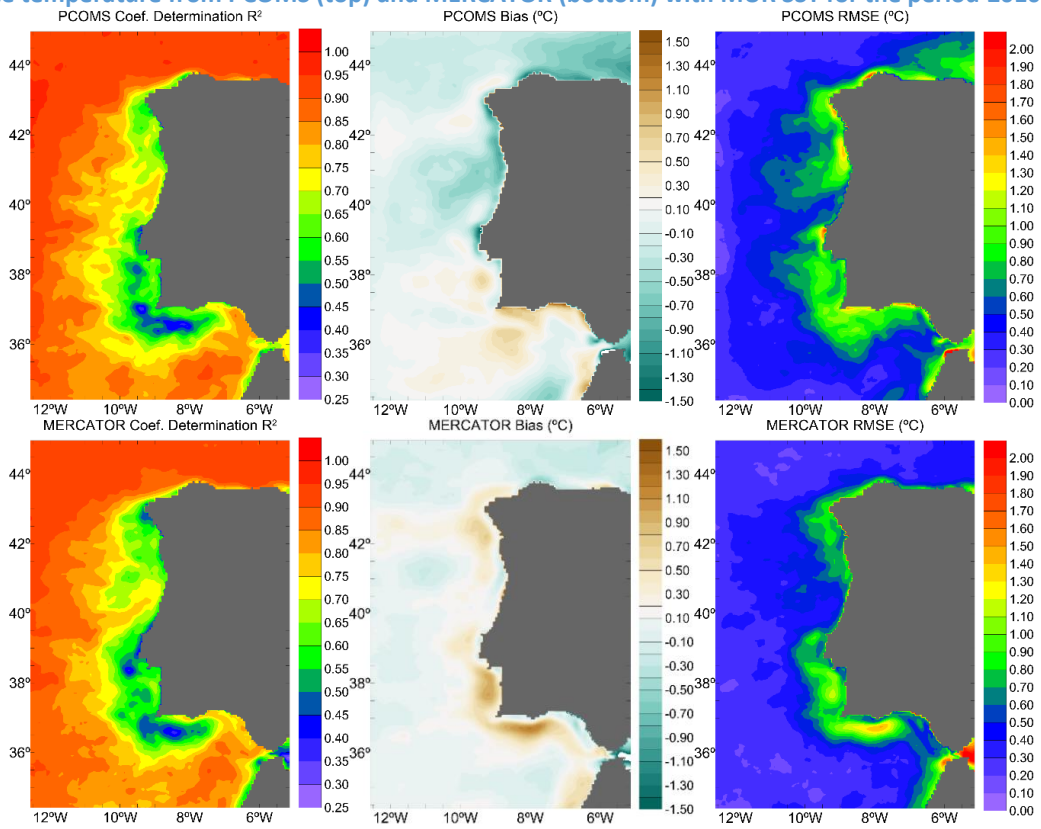


Figure 13 Coefficient of determination (left), bias (centre) and RMSE (right) maps obtained by comparing sea surface temperature from PCOMS (top) and MERCATOR (bottom) with MUR SST for the summer months (JJA) of the period 2010-2015.

The same statistical analysis was performed for the summer months and the outputs confirm what the daily statistics results. The coefficient of determination is lower, for both MERCATOR and PCOMS modelling results, in all the coastal area and in particular in the south-western region with values under 0.5 for large regions (Figure 13). Bias and RMSE maps confirm this result.

Some of the differences between the modelling results and the MUR SST could be due to the nature of the comparison itself. While remote sensing SST observe the top layer of the water, SST is referred as the skin temperature of the ocean surface water, modelling results show its upper layer that represents the average value for the first meters. During winter, due to vertical mixing, surface waters are more homogeneous that during summer period when stratification intensifies. The latter effect could explain the worsening of the statistical indexes during the summer months. In addition, during the summer period, as was described in Chapter II, wind blows generally from North and meteorological models tend to be less precise when wind blows from land as would be the case for southern Portugal region. This effect can partly explain the spatial differences in the south west region. Nevertheless, these conclusions should be further analysed to verify the origin of the difference and to try to minimise it in future versions of PCOMS. A difference between PCOMS and MERCATOR SST was the ability to represent, by the latter, the offshore temperature pattern around 40°N both in Figure 9 and Figure 11. This capacity could be related with the thermohaline circulation and for thus the SSS analysed in the next subsection should be taken into consideration.

#### 4.2.2.2. Sea Surface Salinity (SSS)

More than 7 years after its launch, ESA (European Space Agency)'s Soil Moisture and Ocean Salinity (SMOS) mission continues providing global observations of two key variables on the knowledge of the water cycle: the soil moisture and the ocean salinity. A recently developed algorithm (Olmedo *et al.*, 2017) for SSS retrieval has demonstrated to mitigate the biases that systematically appeared close to the coast. This recent development, in particular, thanks a new methodology described in Isern-Fontanet *et al.* (2016), allowed to detect the Algerian eddies in the Mediterranean Sea where previous SMOS products failed. The daily L4 maps at 0.05°×0.05° grid obtained by means of a fusion technique (Olmedo *et al.*, 2016) which uses Sea Surface Temperature from OSTIA to improve the spatial and temporal resolution of the maps are used for comparison with the PCOMS salinity fields and are hereafter referred as SMOS-BEC. Though this product is a remarkable improvement from other SMOS products, a key issue in the development of SMOS processor is the definition of filtering criteria that if settled too restrictively can remove salinity gradients. In the current version of the L4 product, the western Iberia river plumes cannot be detected and the use of this product served for a general description of the salinity fields in Western Iberian waters.

The PCOMS version used for comparison in this section excludes fresh water/estuarine inputs and precipitation/evaporation processes. MERCATOR fresh water input consist on a monthly runoff climatology that is built with data on coastal runoffs and 100 major rivers (Lellouche *et al.*, 2013) and thus is the only product compared in this section with coastal salinity gradients (Figure 14).

In order to ease comparisons, Figure 15 shows the mean value for the SMOS-BEC, PCOMS and MERCATOR SSS fields for the period 2011-2015 with a common colour range. The salinity field decrease polewards with a meridional salinity gradient of around 1.2 salinity units in the offshore waters of western Iberia.

MERCATOR salinity field presents similar patterns than SMOS-BEC in almost the entire modelling domain with the exception of the north-eastern boundary. Since the PCOMS model receives its boundary conditions from MERCATOR, the excess of salinity on that boundary influences the northern half of the PCOMS results and had an effect on the thermohaline circulation that modify the meridional gradient around the 40°N. The PCOMS version analysed in this chapter was unable to modify the salinity balance significantly within the modelling domain as no land/atmosphere input/output was included and for this reason correct boundary conditions are essential.

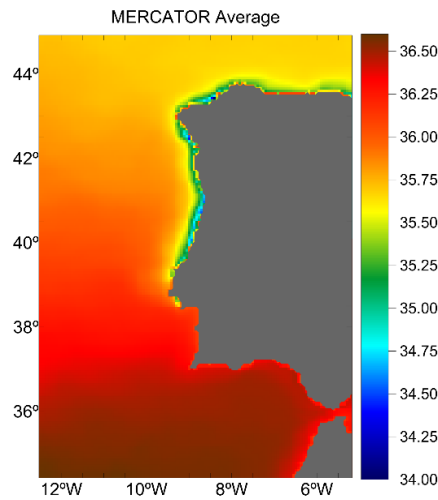


Figure 14 Mean sea surface salinity from MERCATOR in the western Iberia region for the period 2011-2015.

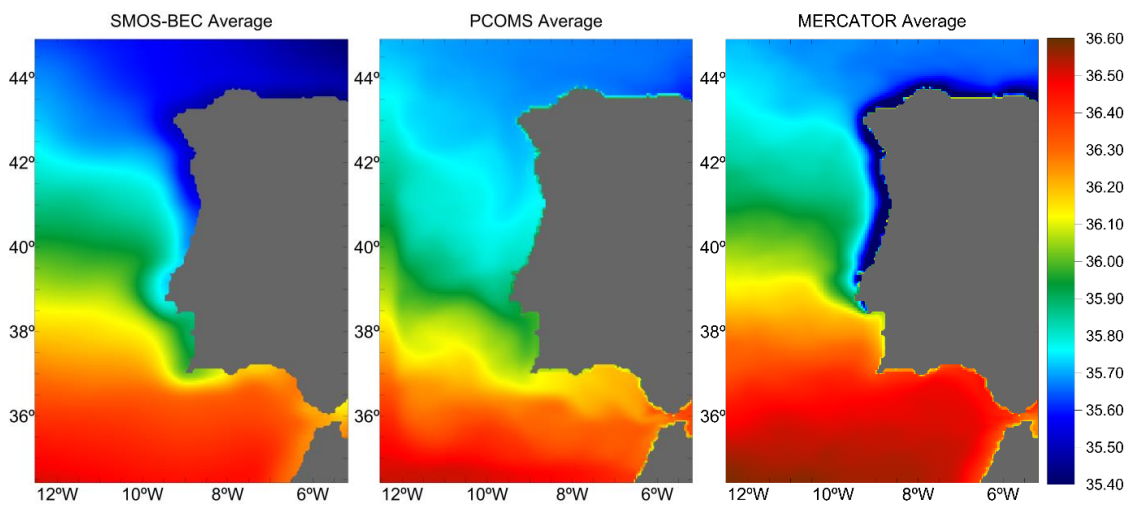


Figure 15 Mean sea surface salinity from SMOS-BEC (left), PCOMS (centre) and MERCATOR (right) in the western Iberia region for the period 2011-2015.

Mean daily salinity values describe an annual cycle where maximum values are observed during the summer period and minimum values are generally observed by the end of the winter season (Figure 16). On average, mean salinity values for western Iberia waters observed by the three components of the analysis SMOS-BEC, PCOMS and MERCATOR present similar mean values 35.98, 35.99 and 36.07 respectively (Table IX). In the other hand, it can be seen how the daily average value for MERCATOR and PCOMS model results does not match the mean daily value of the EO SSS product as well as with the EO SST product (Figure 16). This weakness translates into low daily  $R^2$  and high bias and RMSE values compared to the SSS full range of variability in this ocean region. The MERCATOR  $R^2$  cycle is related to the fresh water discharges imposed in the land boundary during the winter period while in the PCOMS is more related to the propagation of open boundary conditions errors. The daily  $R^2$  indicates if the variability of the property evolves in a similar manner in two samples, for that reason modelling domains that represent in a similar way the meridional variability obtain a relatively high  $R^2$ . However when the  $R^2$  is calculated for every cell to evaluate the time evolution of the property along the study period (Figure 17), the  $R^2$  drop drastically in both models and only in some areas of the southern limit of the domain the  $R^2$  were over 0.30. In this same figure, Bias and RMSE for the MERCATOR product was higher due to the fresh water inputs in the coastal waters.

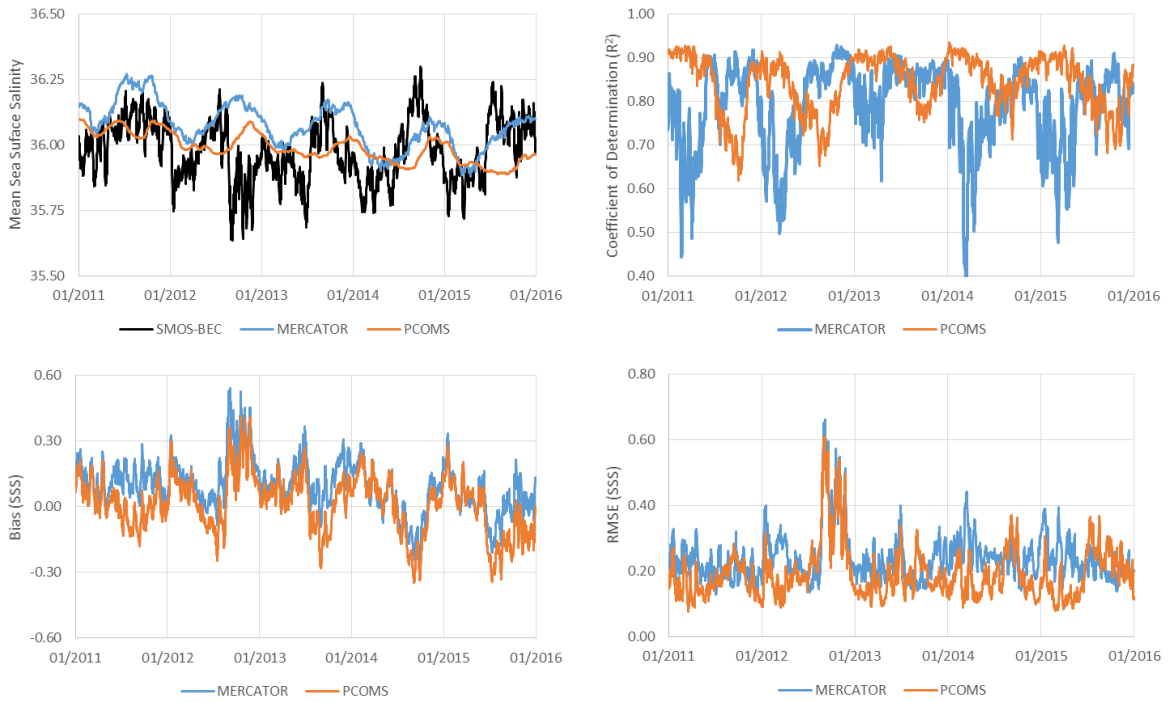


Figure 16 Daily mean sea surface salinity for PCOMS, MERCATOR and SMOS-BEC spatially averaged over the study-domain for the period 2011-2015 (top left). Temporal evolution of the daily metrics for the PCOMS and MERCATOR compared with the SMOS-BEC SSS spatially averaged over the study-domain: correlation coefficient (top right), bias (bottom left) and RMSE (bottom right).

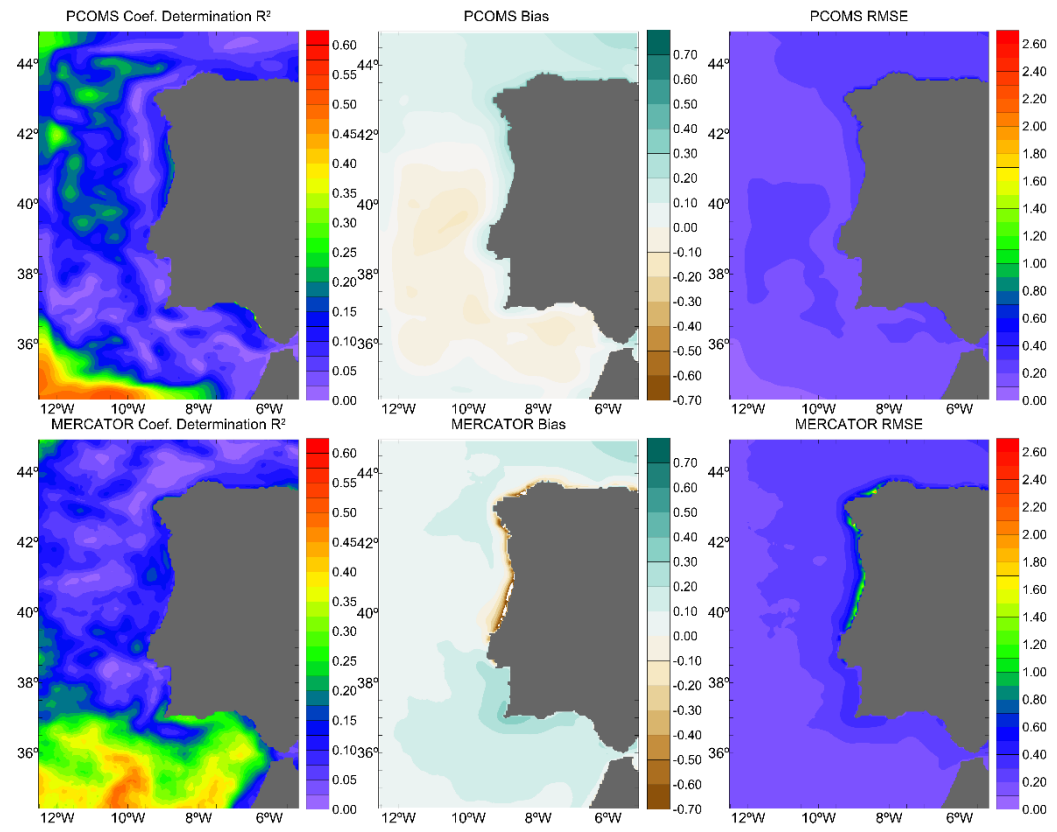


Figure 17 Coefficient of determination (left), bias (centre) and RMSE (right) maps obtained by comparing sea surface salinity from PCOMS (top) and MERCATOR (bottom) with SMOS-BEC for the period 2011-2015.

**Table IX. Mean sea surface salinity spatially averaged over the study-domain of PCOMS and MERCATOR and the main statistics when compared with the SMOS- BEC SSS during the period 2011-2015.**

	PCOMS	MERCATOR
<b>Mean SSS</b>	35.99	36.07
<b>Coefficient of correlation (R<sup>2</sup>)</b>	0.84	0.79
<b>Bias SSS</b>	0.01	0.10
<b>Root Mean Square Error SSS</b>	0.19	0.24

The MERCATOR solution assimilates T-S profiles from ARGO floats to elaborate the salinity fields. During the study period (2010-2015), Portugal was not a member of the ARGO consortium (<http://www.euro-argo.eu>) and for this reason only a limited number of floats covered the Portuguese waters. The scarcity of operational measurements can be regarded as a source of error for the MERCATOR system and thus for the PCOMS downscaling. In addition, it should be remarked that the SMOS-BEC product is still under ongoing development and its accuracy will have to be further evaluated.

### 4.3. Western Iberia surface circulation climatology maps

Once that the PCOMS model application results were compared and errors typified with monitoring stations and remote sensing data, modelling results were used to draw the synoptic view of ocean surface thermohaline circulation by providing monthly, seasonal, annual and full period maps of surface circulation, temperature and salinity. Seasons were defined considering full months with the following criteria: winter (December, January and February), spring (March, April and May), summer (June, July and August) and autumn (September, October and November).

#### 4.3.1. Surface currents

Mean surface currents in the western Iberia ocean region for the entire analysed period showed some typical features such as the Strait of Gibraltar strong circulation, the signal of submarine mountains and the currents occurring in the Tagus Plateau in the centre of Portugal and limited in the north by the Peniche Peninsula and the Berlengas Islands, in the south by the Lisbon/Setubal Canyon and in the West by the Estremadura Promontory (Figure 18).

The latter feature has been identified as a diurnal continental shelf wave (CSW) trapped in Tagus Plateau which generation is linked to the coastal bathymetry being the shelf width and slope strength relevant for the growing amplitude of the trapped wave mode (Fortunato *et al.*, 2002; Quaresma and Pichon, 2013). The Tagus Plateau CSW would increase the currents intensities on that region influencing the mean averaged surface velocities which are around 0.20 ms<sup>-1</sup> in their limits. Currents with that intensity are also observed, on average, near the Galician coast, the Ria Formosa and in some areas near the continental shelf break around 42°N. Mean values for surface currents decrease landwards and in sheltered waters such as the Tagus-Sado estuarine region the mean values are low. It's important to recall here that this version of hydrodynamic results were disregarding the estuarine influence.

The general circulation in the Western Iberia region has several directions depending on the section, northern that Finisterre Cape (43°N) currents flow eastwards from the open ocean in all the sector. Around 41°N, surface waters approach the coast they bifurcate in two branches: the northern branch flows towards the coast and then heads to Cape Finisterre while the southern branch flows southwards off the continental shelf and approaches the coast near the Estremadura Promontory and continues along the coast until reaching the São Vicente Cape (37°N). Southern than Cape São Vicente, surface circulation, drawn by the residual currents, can be divided between coastal and offshore currents: a coastal circulation branch and a more intense offshore branch flow towards the Strait of Gibraltar separated by a counter current towards the Atlantic Ocean.

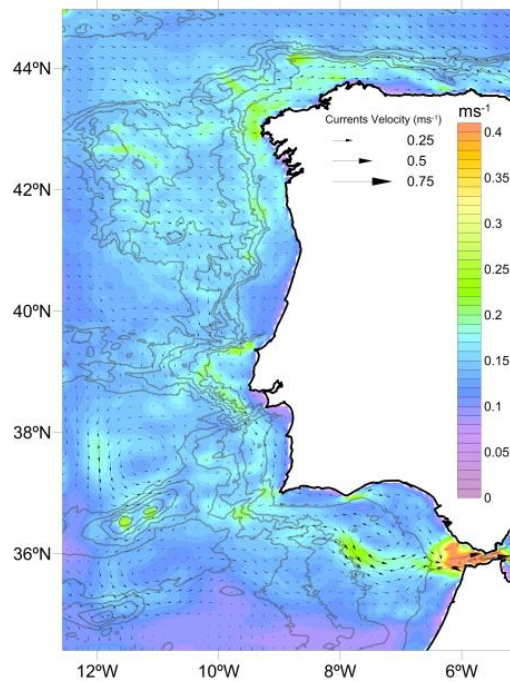


**Figure 18 Mean surface current velocity for the entire studied period. Vectors represent the mean direction and only every fifth vector is plotted.**

The described pattern is not permanent and some interannual variability was observed in the modelling results. As described in Chapter II, the years 2011 and 2012 were weaker in terms of wind intensity and this is reflected in less intense currents with special weight in the northern half of western Iberia (Figure 19). In 2012 and following years, the equatorward currents in southern half, from around 39°N, were more intense. The year 2015 appears as the year with the strongest residual currents in all the system. Also the year 2013, the currents in the northern sector were stronger than average. In this sector, currents run along the coast from Cape Estaca de Bares region, reaching its regional maximum around the Cape Finisterre and continues southwards along the continental shelf break area. In this sector, in the years with most intense currents, such as 2013 and 2015, the current covers a band that extends from the continental platform to the coast that leaves a sheltered area in the Galician coast and detaches from the coast below the latitude of 42°N,

Seasonally, spring and summer periods show similar circulation patterns but with stronger intensities during the latter period. During those periods, water flows from the northern Iberia into the Atlantic and contours all the Iberian Peninsula western coast towards the south without major interruptions. During summer, this equatorward current reaches a maximum of  $0.4 \text{ ms}^{-1}$  around Cape Carvoeiro and local maximums around  $0.3 \text{ ms}^{-1}$  in Finisterre, Espichel and São Vicente capes. Southwards, surface waters flow into the Gulf of Cádiz and follow different paths towards the Strait of Gibraltar (Figure 20). Also during summer, some paths towards the open ocean can be clearly distinguished along the western coast, these paths will favour the transport of water with dissolved substances along with floating matter from coastal areas such as nutrients and fish larvae (Nogueira *et al.*, 2013). During autumn and winter periods, circulation patterns southern than Cape Carvoeiro are similar. Between that Carvoeiro and Finisterre capes, the equatorward current weakens and it's located offshore while a poleward coastal counter current can be observed. The latter counter current is observed with more definition during the autumn period. In the northern sector of the IP, water circulates eastward with a more defined pattern during winter time.

Within the summer period, July and August are the months with stronger net transport towards the south (Figure 21). With the northern winds relaxation, the Iberian Poleward Current (IPC) from the Gulf of Cádiz to the Northern coasts of the IP can be observed clearly in October and December.

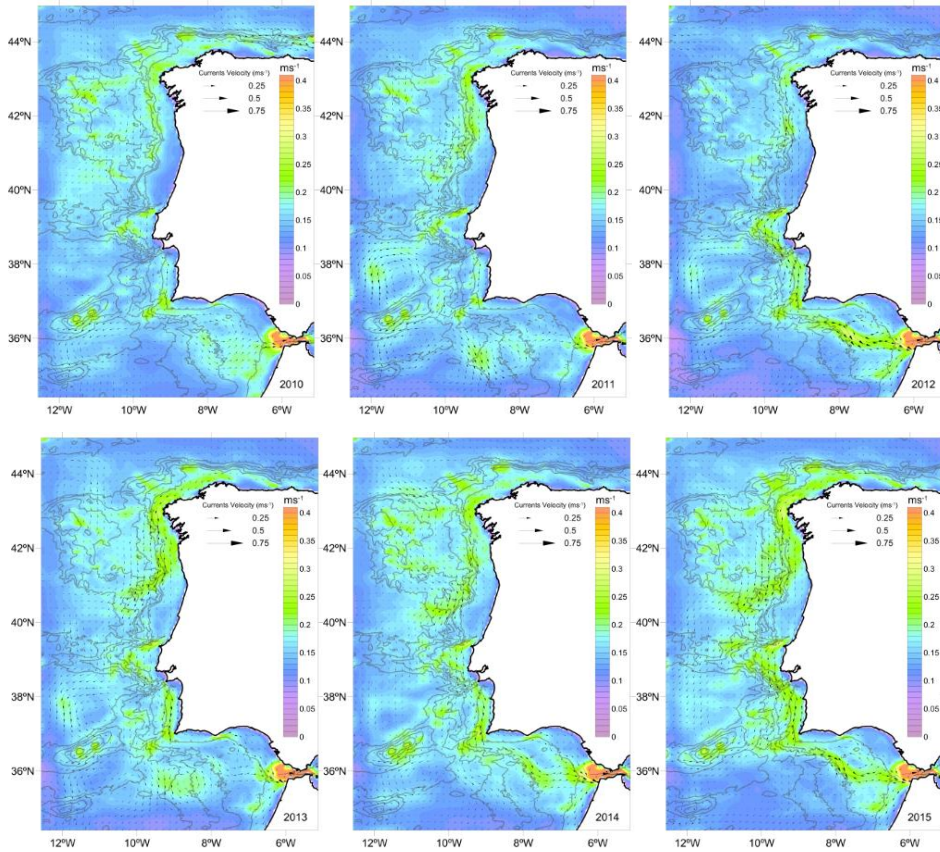


Figure 19 Mean surface current velocity for each year of the studied period. Isobaths are represented every 1000 m starting at 500 m. Vectors represent mean direction every fifth cell.

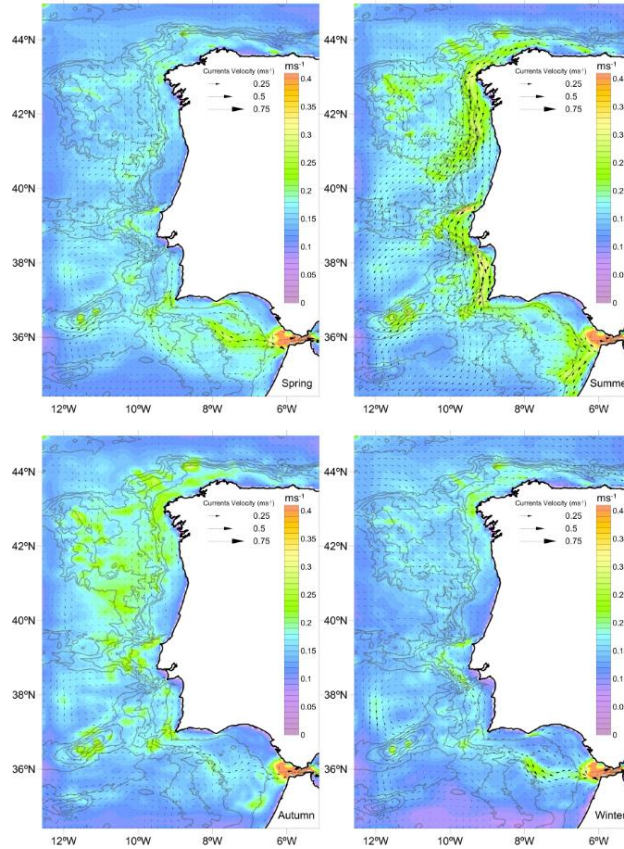


Figure 20 Seasonal surface current velocity for the entire analysed period. Isobaths are represented every 1000 m starting at 500 m. Vectors represent mean direction every fifth cell.

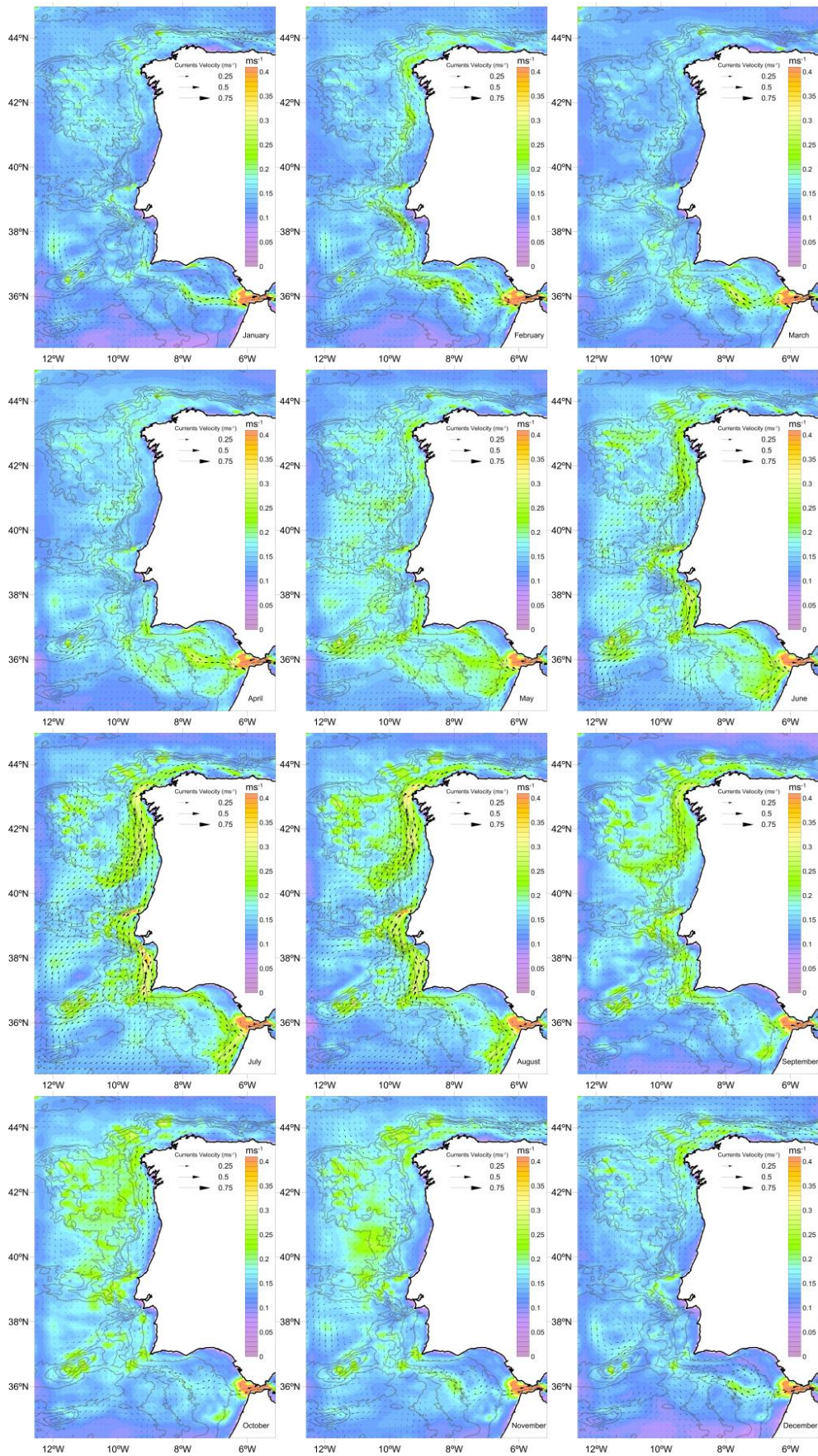
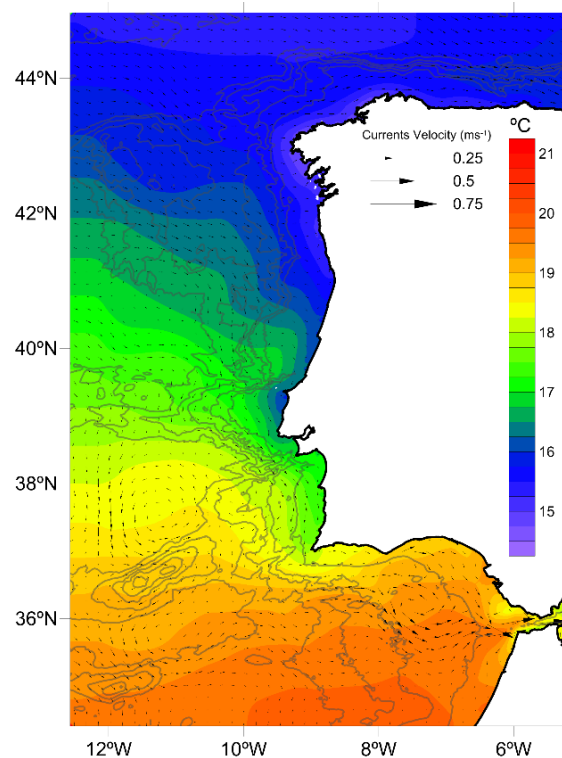


Figure 21 Monthly surface current velocity for the entire analysed period. Isobaths are represented every 1000 m starting at 500 m. Vectors represent mean direction every fifth cell.

### 4.3.2. Sea Surface Temperature

As described in the EO SST validation, the SST from the PCOMS model present a meridional and a coastal-offshore gradients. The former is clearly recognisable in all the offshore waters while the later is present in all the coastal area though more intense in some specific areas where upwelling filaments develop. Another feature that can be visible in the entire period graph is the presence of the poleward current that runs along the continental shelf break and bring a tongue of warmer waters between the coastal and offshore waters (Figure 22). This tongue of warm water suffers interannual variation and can be masked by the upwelling currents that flows offshore. In years with intense upwelling events, such as 2013 and 2015, the displacement of the tongue by upwelling filaments can be clearly observed in latitudes between 40°N and 42°N (Figure 23).

Meridional gradient range for western Iberian waters remains relatively constant between seasons with differences around 4°C (Figure 24). However, coastal gradients intensify during the summer season due to the upwelling processes in western Iberia and warming of shallow waters in the Cádiz area. The latter region is also colder during the winter season for the same reason. Figure 25 shows the complete evolution of surface water temperatures in monthly maps.



**Figure 22** Mean surface water temperature for the entire studied period. Vectors represent mean direction every fifth cell.

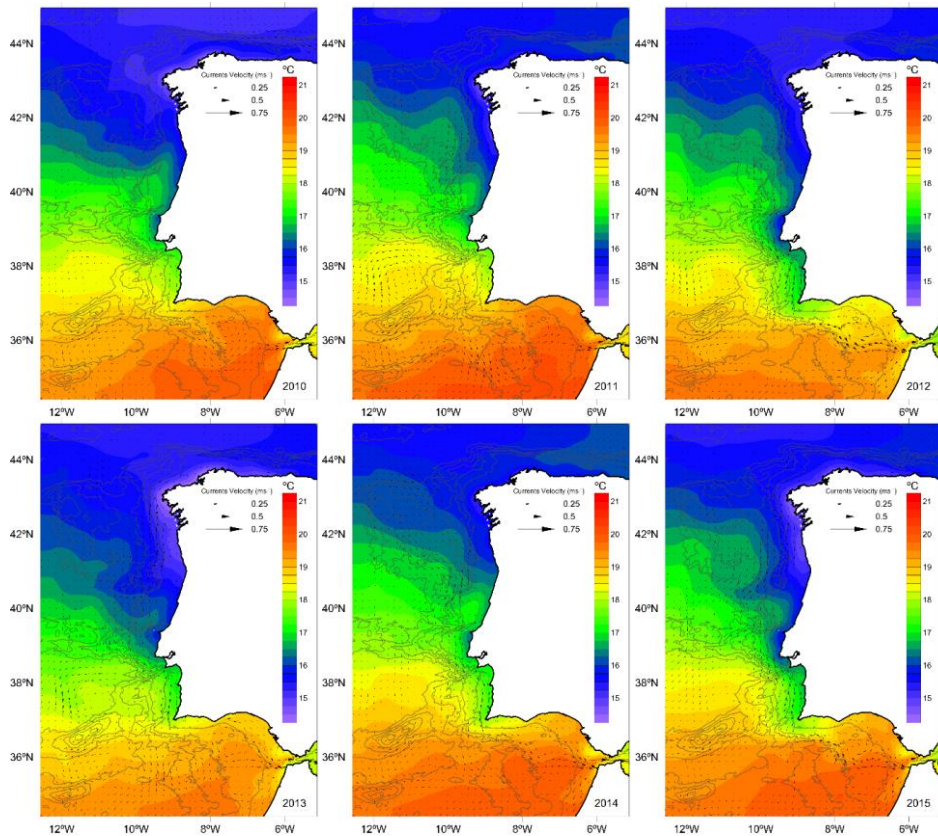


Figure 23 Mean surface temperature for each year of the studied period. Isobaths are represented every 1000 m starting at 500 m. Vectors represent mean direction every fifth cell.

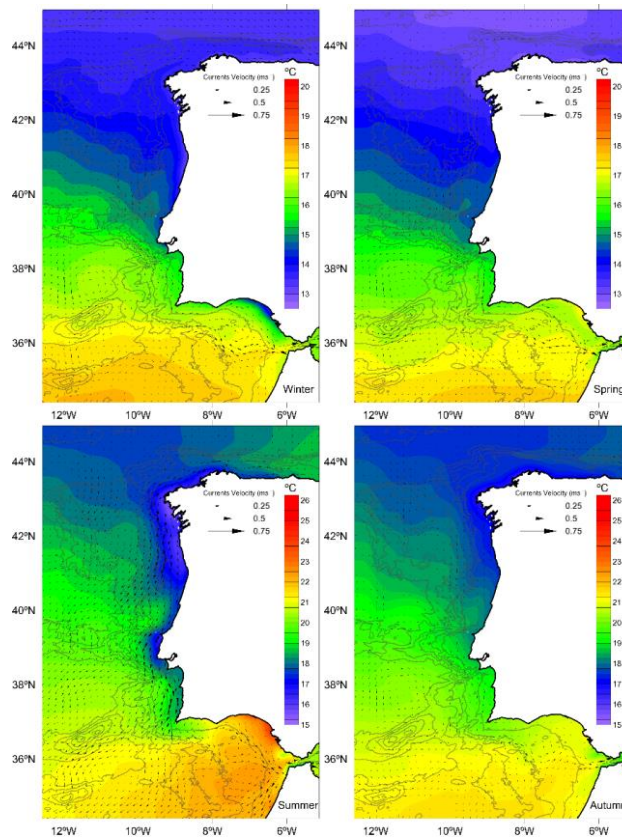


Figure 24 Seasonal surface temperature for the entire analysed period. Notice that two colour scales were used for winter-spring and for summer-autumn seasons. Isobaths are represented every 1000 m starting at 500 m. Vectors represent mean direction every fifth cell.

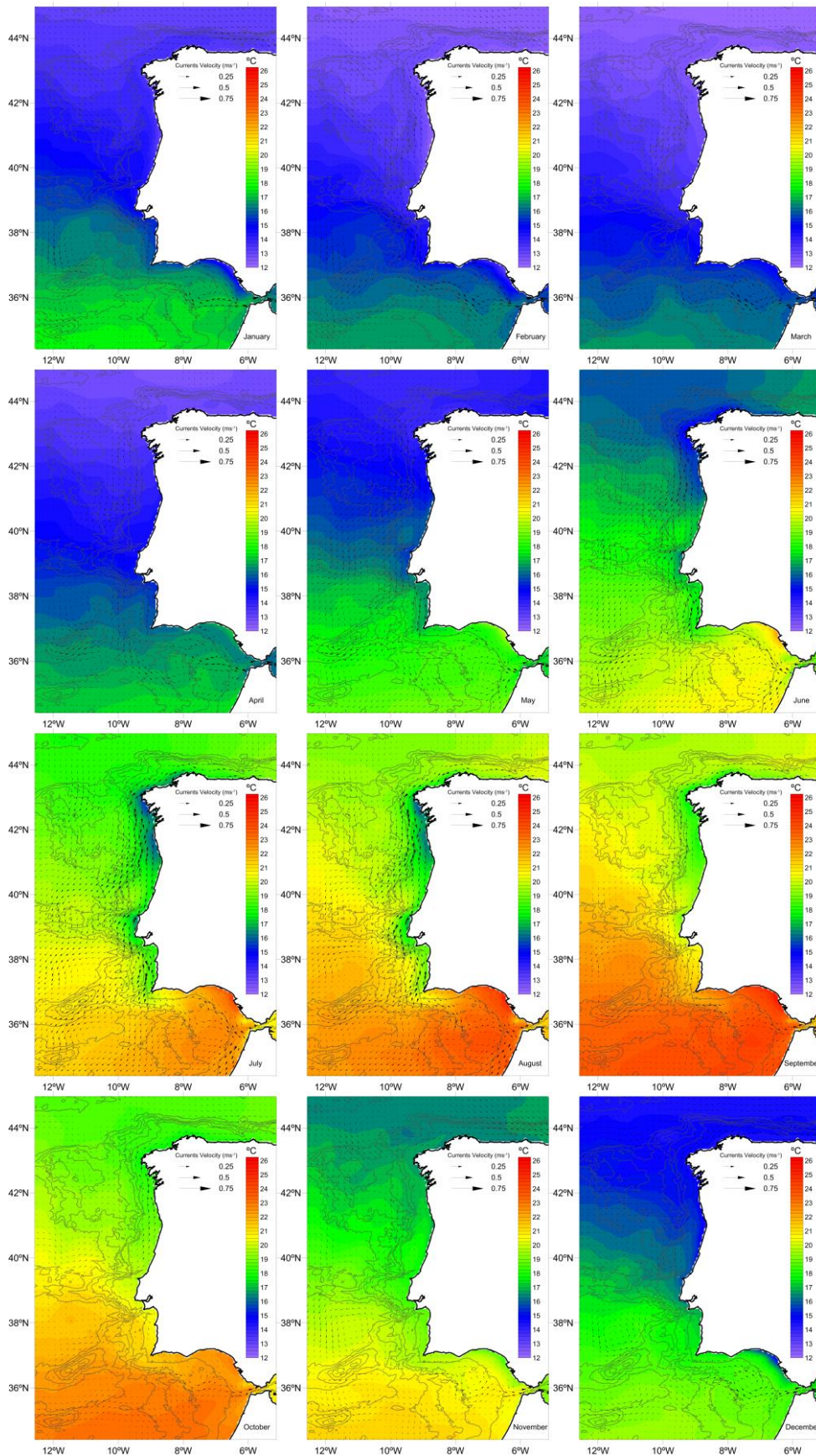


Figure 25 Monthly surface temperature for the entire analysed period. Isobaths are represented every 1000 m starting at 500 m. Vectors represent mean direction every fifth cell.

### 4.3.3. Sea Surface Salinity

Due to the impact of inaccurate boundary conditions in the PCOMS domain, in this subsection the mean value for the entire period (Figure 26), annual (Figure 27), seasonal (Figure 28) and monthly (Figure 29) values are represented so they can be compared with the results with estuarine inputs in Chapter VII. Figure 27 serves also to observe the progressive propagation of the salinity boundary conditions within the PCOMS domain.

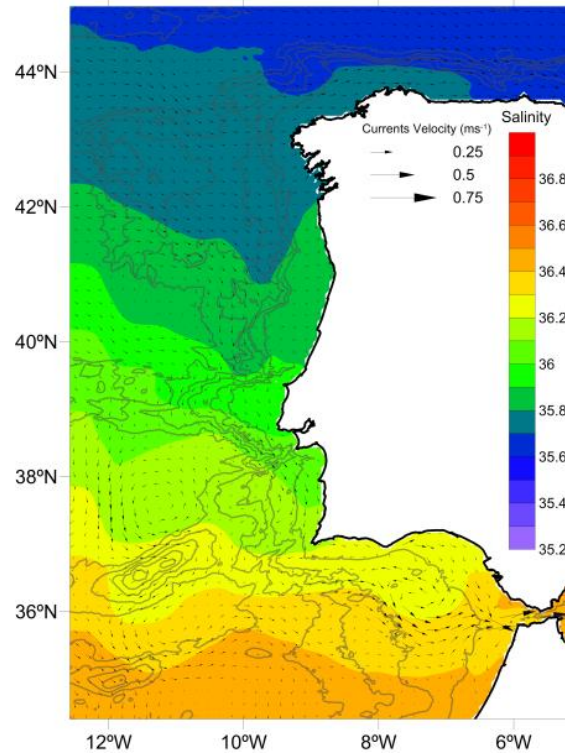


Figure 26 Mean sea surface salinity for the entire studied period. Vectors represent mean direction every fifth cell.

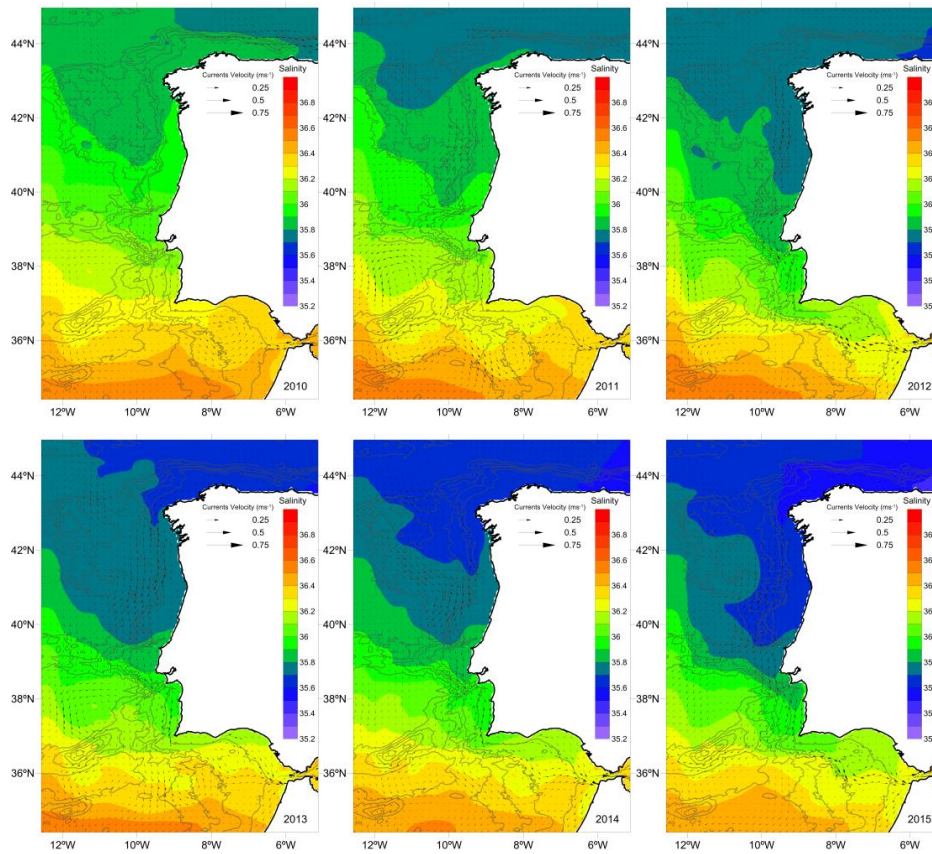


Figure 27 Mean salinity for each year of the studied period. Isobaths are represented every 1000 m starting at 500 m. Vectors represent mean direction every fifth cell.

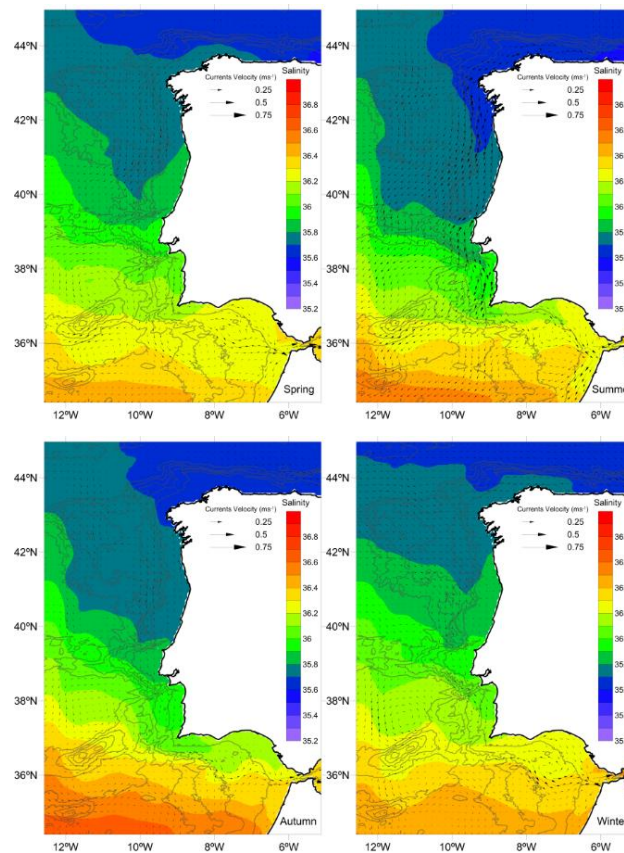


Figure 28 Seasonal salinity for the entire analysed period. Isobaths are represented every 1000 m starting at 500 m. Vectors represent mean direction every fifth cell.

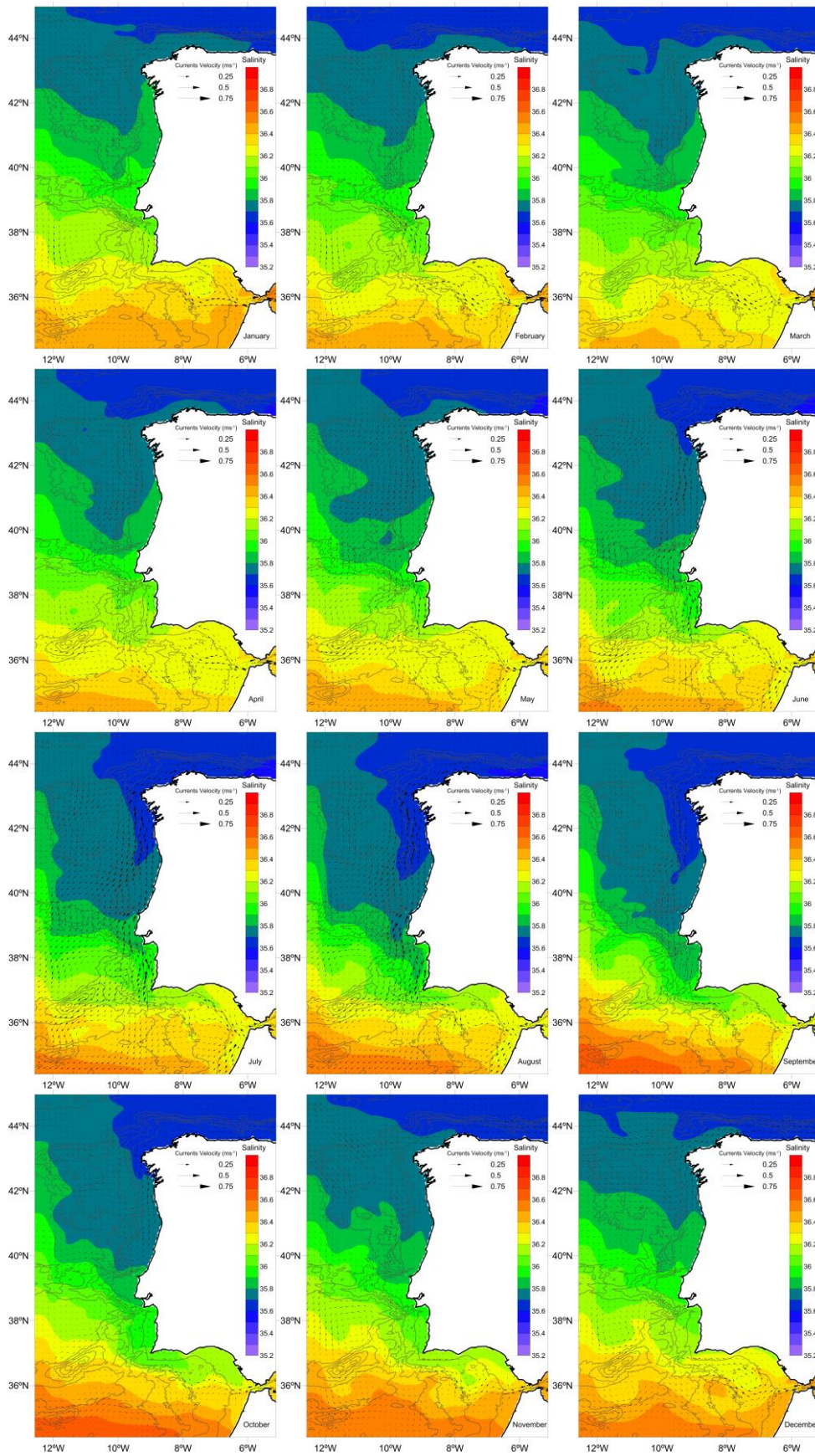
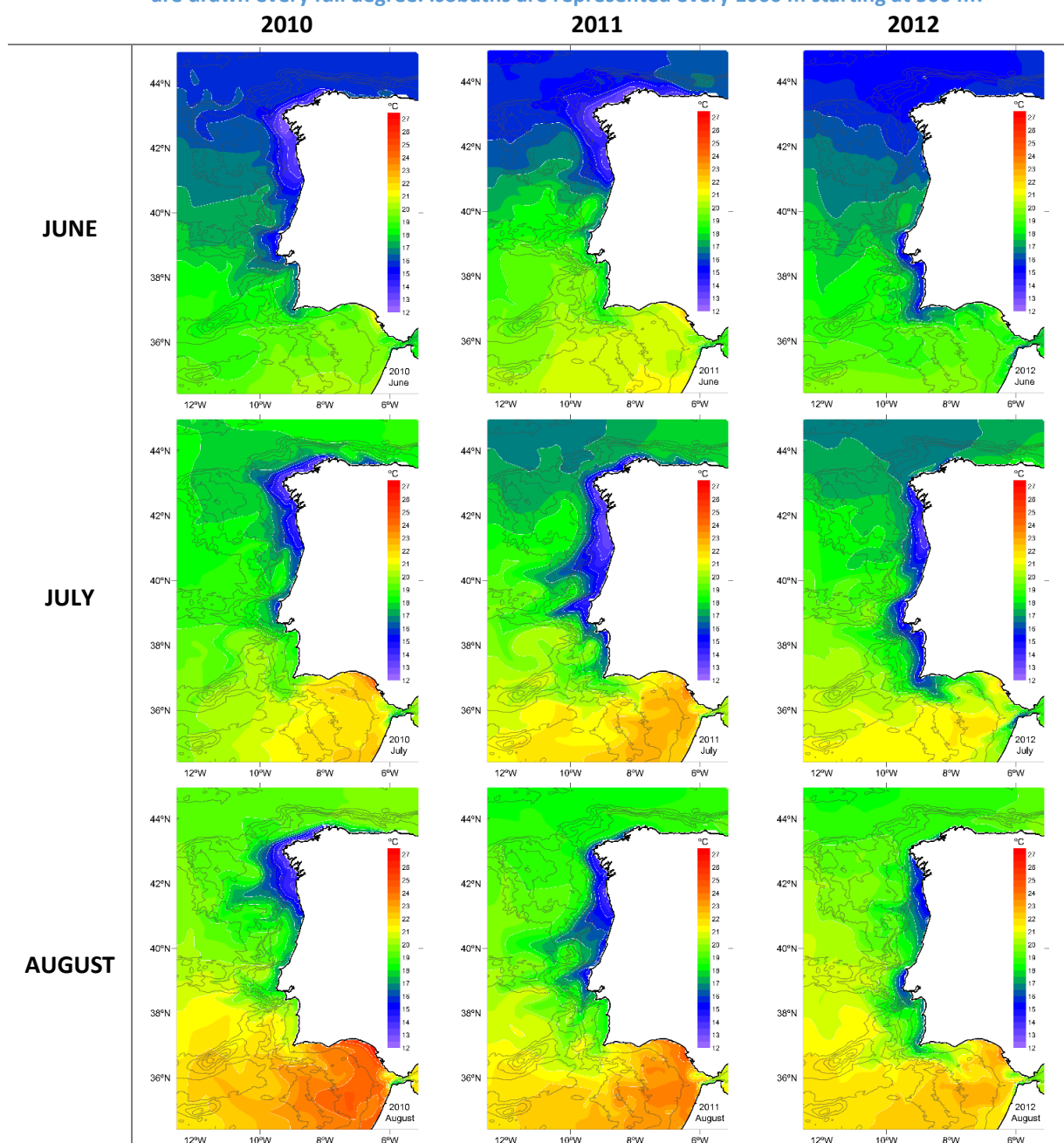


Figure 29 Monthly salinity for the entire analysed period. Isobaths are represented every 1000 m starting at 500 m. Vectors represent mean direction every fifth cell.

#### 4.4. Discussion and Conclusion

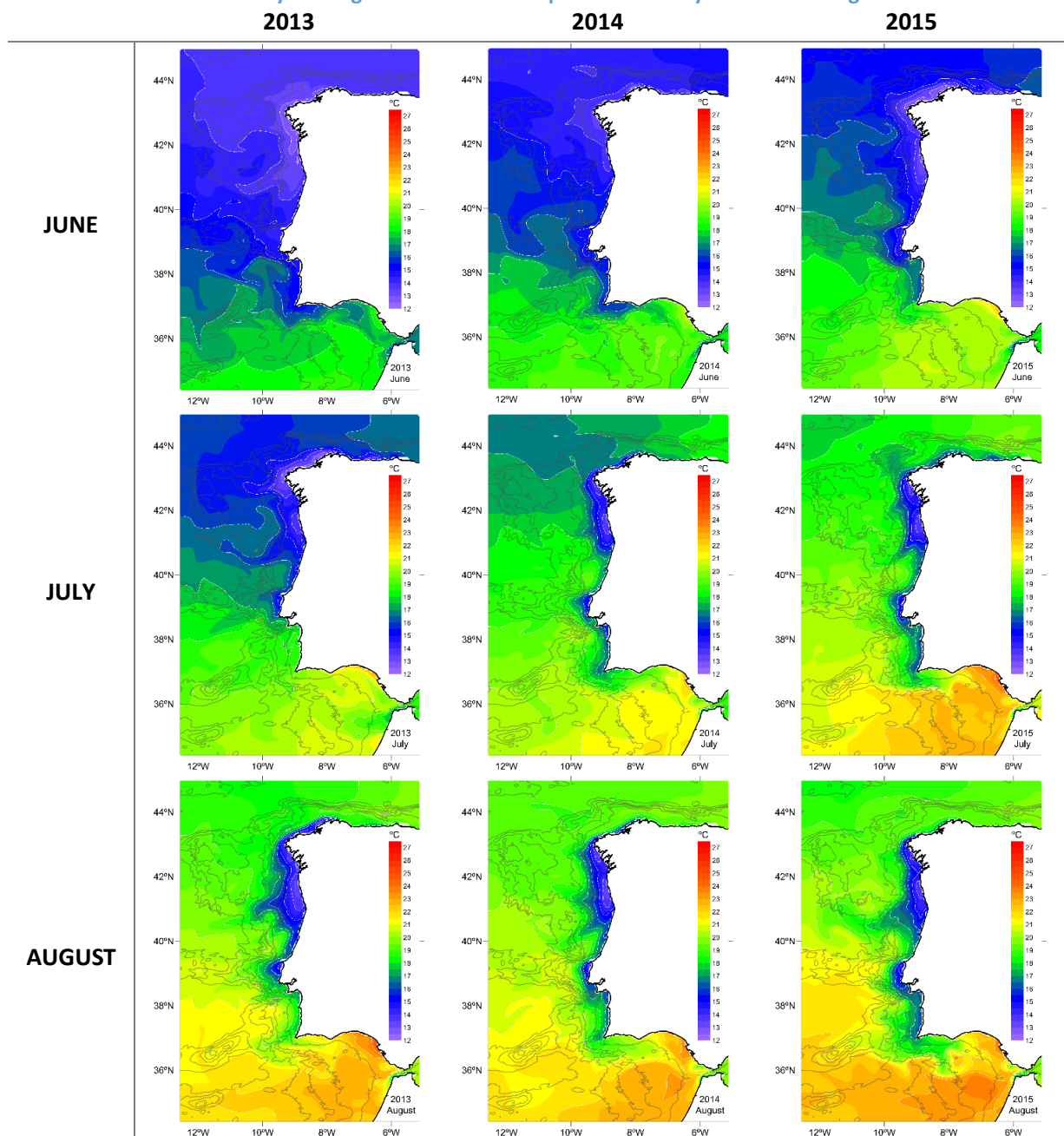
Sea surface temperature is commonly used as an indicator of upwelled water that reach the surface with lower temperatures than the surrounding waters. Generally, this type of analysis uses remote sensing SST and compare coastal temperature with the temperature observed at the same latitude and separated by a defined distance from the coastal observation. A drawback of this methodology is that offshore surface water temperature is not a conservative property and evolves along the year cycle. In order to identify the main areas where upwelling events took place, the 5<sup>th</sup> percentile was identified as a metric able to represent statistically the presence of lower temperature observed for each cell. Table X shows the fifth percentile for western Iberia waters during each summer month of the analysis period. These maps allow to observe the main upwelling areas, the path of the upwelling filaments and the interannual variability. This indicator provides more information than the mean monthly value that tend to hide the presence of less intense filaments.

**Table X. 5<sup>th</sup> percentile of the SST for each summer month (JJA) of the period 2010-2015. White isolines are drawn every full degree. Isobaths are represented every 1000 m starting at 500 m.**



In Table X, it can be observed that the complete western area of the IP is subjected to upwelling events and that the upwelling filaments can be located in several areas such as the North-western coast of Galicia, the Douro region, the Estremadura promontory from Peniche to the Sado estuary and the entire southern coast turning the Cape São Vicente into the southern coasts. The extension of upwelling filaments into the open ocean can be clearly observed by using the 5<sup>th</sup> percentile. An outstanding example of this method is the year 2011 analysis where two massive filaments were observed continuously during the months of July and August. The filaments were centred in the Douro region and the Estremadura promontory and extended further that 10 °W with temperatures around 16.5 °C. According to these results most of the upwelling areas are active every year and leave their signature in the SST. For instance the south-western filament that extent further than Cape São Vicente is more visible in years 2012, 2013, 2014 and 2015 than in previous years.

Table X. Cont. 5<sup>th</sup> percentile of the SST for each summer month (JJA) of the period 2010-2015. White isolines are drawn every full degree. Isobaths are represented every 1000 m starting at 500 m.



The PCOMS surface circulation represented satisfactory most of the described features including seasonal features such as the Iberian Poleward Current (IPC) during winter periods and the upwelling/downwelling conditions during summer and winter periods. The main thermal gradients and salinity gradients are represented with the exception of the fresh water fronts that will be discussed in a later stage of this research. A comprehensive list of *in situ* stations were gathered to validate temperature, salinity and currents. In addition, EO SST and, to the author knowledge for the first time in an application of this kind, EO SSS.

#### 4.5. References

Bell C, Vassie JM, Woodworth PL. POL/PSMSL Tidal Analysis Software Kit 2000 (TASK-2000). Technical Report, Permanent Service for Mean Sea Level, CCMS Proudman Oceanographic Laboratory. 1999; 20pp

Campuzano FJ, Juliano M, Fernandes R, Pinto L, Neves R. Downscaling from the deep ocean to the estuarine intertidal areas: an operational framework for the Portuguese exclusive economic zone. 6th SCACR – International Short Course/Conference on Applied Coastal Research, 4-7 June 2013, Lisbon, Portugal.

Chin TM, Vazquez-Cuervo J, Armstrong EM. A multi-scale high-resolution analysis of global sea surface temperature. *Remote Sensing of Environment*. 2017; 200: 154-169. DOI: [10.1016/j.rse.2017.07.029](https://doi.org/10.1016/j.rse.2017.07.029).

Crespo BG, Figueiras FG. A spring poleward current and its influence on microplankton assemblages and harmful dinoflagellates on the western Iberian coast. *Harmful Algae*. 2007; 6(5): 686-699. DOI: [10.1016/j.hal.2007.02.007](https://doi.org/10.1016/j.hal.2007.02.007).

Drillet Y, Bourdalle-Badi R, Siefried L, Le Provost C. Meddies in the Mercator North Atlantic and Mediterranean Sea eddy-resolving model. *Journal of Geophysical Research*. 2005; 110(C3): C03016.

Fortunato AB, Pinto L, Oliveira A, Ferreira JS. Tidally generated shelf waves off the western Iberian coast. *Continental Shelf Research*. 2002; 22, 1935-1950.

Fréon P, Alheit J, Barton ED, Kifani S, Marchesiello P. 9 Modelling, forecasting and scenarios in comparable upwelling ecosystems: California, Canary and Humboldt, In: Vere Shannon, Gotthilf Hempel, Paola Malanotte-Rizzoli, Coleen Moloney and John Woods, Editor(s), *Large Marine Ecosystems*, Elsevier. 2006; 14: 185-220. DOI: [10.1016/S1570-0461\(06\)80014-5](https://doi.org/10.1016/S1570-0461(06)80014-5).

Isern-Fontanet J, Olmedo E, Turiel A, Ballabrera-Poy J, García-Ladona E. Retrieval of eddy dynamics from SMOS sea surface salinity measurements in the Algerian Basin (Mediterranean Sea), *Geophysical Research Letters*. 2016; 43(12): 6427-6434.

Lellouche J-M, Le Galloudec O, Drévilion M, Régnier C, Greiner E, Garric G, Ferry N, Desportes C, Testut C-E, Bricaud C, Bourdallé-Badie R, Tranchant B, Benkiran M, Drillet Y, Daudin A, De Nicola C. Evaluation of global monitoring and forecasting systems at Mercator Océan. *Ocean Science*. 2013; 9(1): 57-81. DOI: [10.5194/os-9-57-2013](https://doi.org/10.5194/os-9-57-2013)

Lorente P, Piedracoba S, García Sotillo M, Aznar R, Amo-Baladrón A, Pascual Á, Soto-Navarro J, Álvarez-Fanjul E. Ocean model skill assessment in the NW Mediterranean using multi-sensor data. *Journal of Operational Oceanography*. 2016; 9(2): 75-92. DOI: [10.1080/1755876X.2016.1215224](https://doi.org/10.1080/1755876X.2016.1215224).

Mason E, Coombs S, Oliveira PB. An overview of the literature concerning the oceanography of the Eastern North Atlantic Region. *Relatórios Científicos e Técnicos IPIMAR*. 2006; 33, 57pp.

Murray MT. A general method for the analysis of hourly heights of the tide. *International Hydrographic Review*. 1964; 41(2): 91-101.

Nogueira J, Campuzano FJ, Neves R (2013). Sardine larvae vertical migration and horizontal dispersion patterns related to light intensity in the dynamic western Portuguese coast: a numerical study. In: Ocean modelling for coastal management. Case studies with MOHID, M. Mateus & R. Neves (eds.), IST Press. pp 161-173.

NOAA Technical Memorandum NOS CO-OPS 021 - Tidal Current Analysis Procedures and Associated Computer Programs. Silver Spring, Maryland. March 1999

Olmedo, E, Martínez J, Umbert M, Hoareau N, Portabella M, Ballabrera-Poy J, Turiel A. Improving time and space resolution of SMOS salinity maps using multifractal fusion. Remote Sensing of Environment. 2016; 180: 246-263.

Olmedo E, Martínez J, Turiel A, Ballabrera-Poy J, Portabella M. Debiased non-Bayesian retrieval: A novel approach to SMOS Sea Surface Salinity. Remote Sensing of Environment. 2017; 193: 103-126.

Peliz Á, Dubert J, Santos AMP, Oliveira PB, Le Cann B. Winter upper ocean circulation in the Western Iberian Basin—Fronts, Eddies and Poleward Flows: an overview. Deep Sea Research Part I: Oceanographic Research Papers. 2005; 52(4): 621-646. DOI: [10.1016/j.dsr.2004.11.005](https://doi.org/10.1016/j.dsr.2004.11.005).

Peliz Á, Rosa TL, Santos AMP, Pissarra JL. Fronts, jets, and counter-flows in the Western Iberian upwelling system. Journal of Marine Systems. 2002; 35(1–2): 61-77. DOI: [10.1016/S0924-7963\(02\)00076-3](https://doi.org/10.1016/S0924-7963(02)00076-3).

Quaresma LS, Pichon A. Modelling the barotropic tide along the West-Iberian margin. Journal of Marine Systems. 2013; 109-110, S3-S25.

# Chapter V - Coupling watersheds, estuaries and regional ocean through numerical modelling for Western Iberia: a novel methodology.

---

## Publication information

This chapter was published with the following details:

Campuzano F, Brito D, Juliano M, Fernandes R, de Pablo H, Neves R. Coupling watersheds, estuaries and regional ocean through numerical modelling for Western Iberia: a novel methodology. *Ocean Dynamics*. 2016; 66(12): 1745–1756. DOI: [10.1007/s10236-016-1005-4](https://doi.org/10.1007/s10236-016-1005-4).

## Abstract

An original methodology for integrating the water cycle from the rain water to the open ocean by numerical models was set up using an offline coupling technique. The different components of the water continuum, including watersheds, estuaries and ocean, for Western Iberia were reproduced using numerical components of the MOHID Water Modelling System (<http://www.mohid.com>). This set of models, when combined through this novel methodology, is able to fill information gaps, and to include, in a realistic mode, the fresh water inputs in terms of volume and composition, into a regional ocean model. The designed methodology is illustrated using the Tagus River, estuary and its region of fresh water influence as case study and its performance is evaluated by means of river flow and salinity observations.

## 5.1 Introduction

River discharges exert a strong influence in their neighbouring coastal areas in many ways including the modification of water stratification (Garvine and Witney, 2006), the introduction of significant fluctuations in circulation patterns and the modulation of upwelling events impact (Santos *et al.*, 2007; Banas *et al.*, 2009). They induce convergent areas near their discharge area, regulate the alongshore transport and exchange properties with the outer shelf while generating nutrient rich areas that provide food for fish larvae (Santos *et al.*, 2007; Ribeiro *et al.*, 2005).

Despite their importance, the incorporation of river and estuarine fluxes into regional ocean numerical models has been generally disregarded. One of the main reasons for this omission is the inherent difficulty of including the temporal variability associated to the estuarine inputs. This variability is related to several factors including, among others, the seasonal and interannual change in fresh water volume and its associated properties reaching the estuaries, the occurrence of drastic episodic events (i.e. droughts and floods), the fresh water mixing and the water properties evolution along the estuary subjected to the tidal cycle with residence times and tidal prisms specific for each estuary.

In recent times, due to an increase in the numerical modelling capacities and the need of operational forecast models with high accuracy in coastal areas, efforts have been made to include river discharges into the regional and coastal models. This subject is still an open subject of research, due to the number of existing uncertainties.

Starting at the watershed level, the river runoff reaching the coastal area is unavailable or unmonitored for many rivers. This is an increasing problem due to the current context of a global decline of the hydrometric networks (Mishra and Coulibaly, 2009). For this reason, river climatologies are generally imposed as land boundary conditions in coastal or regional ocean models - thus ignoring the river variability in flow and properties. Moreover, for small rivers or poorly studied rivers, building a river climatology could also be regarded as a challenge.

Downstream, the method of including riverine inputs, regarding the complex and singularity of estuarine dynamics, into coarse regional ocean models, generally with horizontal grid resolution of km's, has been issued in several ways. For areas with a low tidal signal, i.e. the Mediterranean Sea, direct river discharge of volume and water properties could be regarded as a reasonable approximation (Estournel *et al.*, 1997). However, for areas with a significant tidal signal, this approach is not realistic enough to represent the coastal processes and more complex solutions are needed. Herzfeld (2015) summarised some of the most typical methods to include river inputs into regional ocean models. In the horizontal plane, the most common methods are: the simple inlet method, consisting in making a "rectangular breach in the coastal wall with uniform inflow water properties, including density and discharge velocity" (Garvine and Witney, 2006) and the point source method consisting in the addition of a volume flux of zero salinity water directly into one or more layers (Schiller and Kourafalou, 2010). Another common practice consists in adding fresh water discharges into non-realistic channels to induce an initial mixing (Lacroix *et al.*, 2004). A more sophisticated method consists in including the desired estuary in the regional model domain. The latter approach try to reproduce the estuary volume, bathymetry and dynamics by using refined grids on the estuarine and adjacent coast area. This approach seems to be adequate to study the Region of Freshwater Influence (ROFI) of isolated rivers (i.e. Banas *et al.* (2009) and Liu *et al.* (2009) for the Columbia River). Another subject of research is the vertical distribution of the river discharge - Herzfeld (2015) proposed a dynamic adjustment in order to obtain more realistic inputs in the coastal area.

In this paper, we present a novel numerical modelling methodology to include, in a realistic mode, the fresh water inputs, in terms of volume and water properties, from the rain water to its incorporation into a regional ocean model. The different interfaces encountered by the runoff water from the watersheds to the open ocean were reproduced using the different components of the MOHID Water Modelling System (<http://www.mohid.com>; Neves, 2013). The employed methodology is illustrated using the Tagus River, estuary and ROFI as a case study. The obtained modelling results were compared with *in situ* observations and with a state-of-the-art regional ocean model for the same study area.

## 5.2 Study Area

The largest rivers of the Iberian Peninsula, with the exception of the Ebro River, discharge on the Atlantic coast draining on its way almost two thirds of the territory. In Portugal, river mouths concentrate in the northern part of the territory (Figure 1) while the Tagus River, the largest river of Iberia, reaches the coast almost isolated. Additionally, northern rivers present higher flows related to a latitudinal rain gradient, with mean annual precipitation values around 3000 mm in the Northwest of Portugal and below 1000 mm on the southern half of the territory (Portuguese Water Atlas, <http://geo.snirh.pt/AtlasAgua/>). Due to the scope of the present work, the methodology is applied focusing in the Tagus River, estuary and its adjacent area.

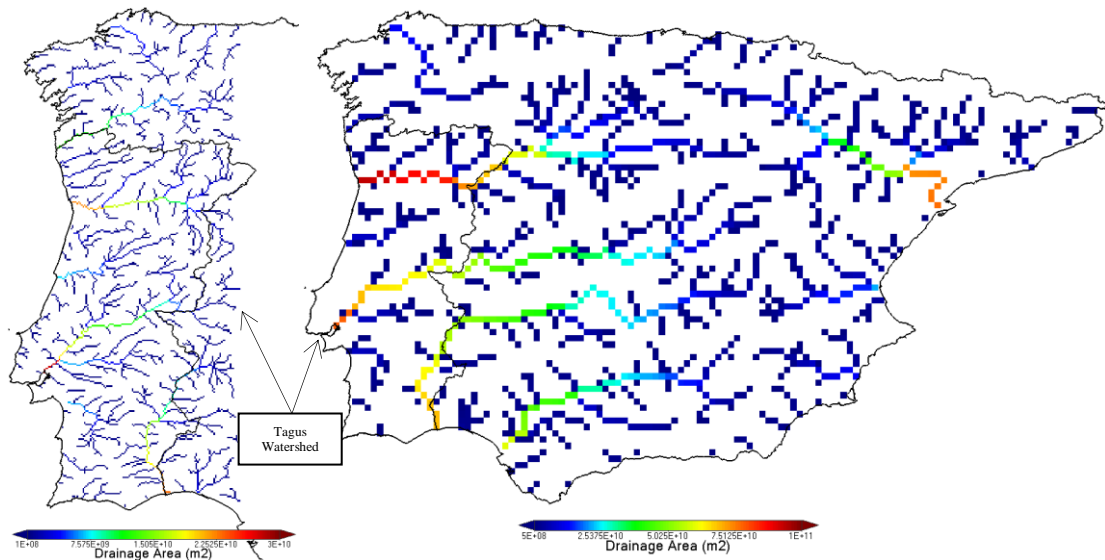


**Figure 1. Accumulated drainage area for the main water lines in the Western Iberian Peninsula (WI model domain, left) and in the Iberian Peninsula (IP model domain, right). Drainage networks were obtained with the MOHID Land model using 2 and 10 km horizontal resolution respectively.**

The Tagus River, 1 000 km long, is the longest river of the Iberian Peninsula draining an area around 80 000 km<sup>2</sup>, with 55 000 and 25 000 km<sup>2</sup> located in Spain and Portugal territory respectively. Its estuary, 320 km<sup>2</sup> wide, is the largest in Portugal and one of the largest in Europe (Figure 2). The estuary area is inhabited by a population around 2.5 million, almost a quarter the overall Portugal population. Morphologically, the estuary can be divided in three main areas, a straight, narrow channel of 16 km long and 2 km wide with W-E orientation and maximum depths around 45 m; an inner bay 25 km long and 15 km wide oriented SW-NE with depths comprised between 5 and 10 meters and the upper shallow estuary about 100 km<sup>2</sup> wide encompassing large mudflats and salt marshes separated by shallow channels. The Tagus River is the main source of fresh water in the estuary with flows typically varies between 50 and 2 000 m<sup>3</sup>s<sup>-1</sup>, although is affected by human activities and management (i.e. dams, agriculture, etc). The Sorraia and Trancão rivers, with mean river flow of 39 and 6 m<sup>3</sup>s<sup>-1</sup> respectively, are other minor fresh water contributors to the estuary.

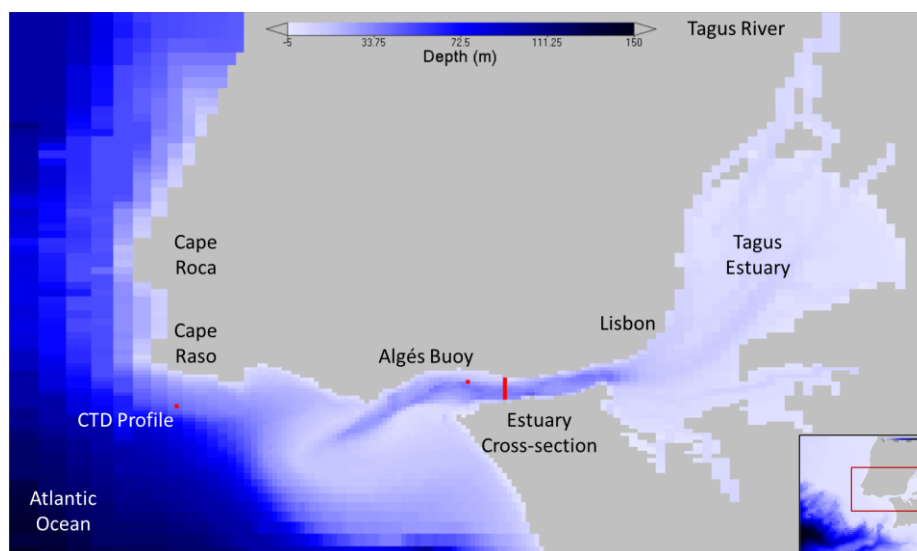


**Figure 2. Detail of the TagusMouth model bathymetry where it can be identified the Tagus River and estuary and the connection channel to the adjacent coastal area; the full modelling domain in the box. The map also indicates the locations of the Algés buoy, the CTD campaign and the latitudinal cross-section where the estuarine fluxes are calculated.**

From the hydrodynamic point of view, the Tagus estuary is a semi-diurnal mesotidal estuary with tidal ranges varying from 1 m during neap tides up to almost 4 m during spring tides. The tide propagates up to almost 80 km landward from Lisbon and the mean residence time of the estuary is around 25 days (Braunschweig *et al.*, 2003). The combined effects of low average depth, strong tidal currents, and low input of river water classify the Tagus estuary as a globally well-mixed estuary, with significant stratification only occurring during high river discharge periods.

## 5.3 Materials and Methods

### 5.3.1. Numerical models

In order to reproduce the water continuum for the Portuguese coastal area, from the precipitation areas until its evacuation in the open ocean, a system of coupled numerical models was designed to include the different temporal and spatial scales. Each system element - river catchment, estuary and open ocean - was simulated through numerical models using the different components of the MOHID Water Modelling System (<http://www.mohid.com>; Neves, 2013).

The MOHID Water Modelling System is an open source modular finite volumes modelling system written in ANSI FORTRAN 95 using an object oriented programming philosophy integrating several numerical programs and supported by graphical user interfaces that manage all the pre- and post-processing operations. The core numerical models are MOHID Water and MOHID Land.

The MOHID Land model is a 3D distributed, continuous, physically based, variable time step model using a finite volume approach based on mass and momentum balance equations for land areas (e.g. watersheds, agriculture plots, urban areas). The simulated processes include water and property transport in porous media, river runoff, erosion, evapotranspiration and vegetation growth and water quality processes, i.e. mineralization, nitrification, denitrification in porous media and rivers. The MOHID Water model is a 3D integrated model, capable of simulating a wide range of processes (e.g. hydrodynamics, transport, water quality, oil spills) in surface water bodies (oceans, coastal areas, estuaries and reservoirs).

At the watershed level, the MOHID Land model (Brito *et al.*, 2015) estimates operationally water flow and associated properties (i.e. temperature, oxygen and nutrient concentrations) for the main river catchments discharging in the Western Iberian coast. Two domains with different horizontal resolution, 2 km for the West Iberia region (WI domain) and 10 km for the Iberian Peninsula (IP domain), were designed to represent adequately the Portuguese catchments and to include the spatial scale of the large trans-boundary rivers as the Tagus, Douro and Guadiana rivers (Figure 1). Both domains were populated with topographic data from the NASA digital terrain elevation database and land use data from the Corine Land Cover 2006 – CLC2006 (EEA, 2007). Waterproofing and Manning resistance were defined following van der Sande *et al.* (2003) and Chow (1959) suggested correspondences. Soil map distribution and hydraulic characteristics, necessary to estimate the van Genuchten model parameters, were obtained from the Joint Research Centre database (<http://eusoils.jrc.ec.europa.eu/>).

Currently, the watershed model applications disregard the effects of human consumption, water reservoirs or dam management that could modify the amount and timing of the water reaching the coastal zone. Methods to correct those effects are planned to be implemented in future versions of the model.

Downstream, several operational estuarine applications impose the watershed modelling results as land boundary conditions. In the case of the Portuguese estuaries, this type of input is used in the absence of automatic monitoring stations data and to complete the observations

with non-monitored variables i.e. temperature, nutrient and oxygen concentrations, etc. The estuarine models are able to simulate the site-specific inner estuary dynamics and their connection with the open ocean waters.

The Tagus estuary and adjacent coast model application (Figure 2, De Pablo *et al.*, 2013), hereafter referred as TagusMouth, has a variable horizontal resolution ranging from 2 km off the coast up to 250 m in the estuarine mouth region comprised by the range of latitudes (38.16 °N, 39.21 °N) and longitudes (8.90 °W, 10.02 °W) resulting in a grid of 120x145 cells. The model domain limits and horizontal resolutions allow the model application to simulate accurately the estuarine plume dynamics while covering most of the Tagus ROFI.

As the Tagus River is the main source of fresh water in the estuary, its forcing can be considered as the main source of salinity variability. The closest river flow monitoring station to the Tagus estuary is the Almourol station (39.22 °N, 8.67 °W), located 70 km off the head of the estuary and part of the Portuguese river hydrometric observation network (<http://snirh.pt>). In the present study, four Tagus River forcing scenarios will be evaluated in the TagusMouth application: daily averaged river flows from the hydrometric station (Almourou Scenario), a monthly climatology built using several years of flow observations for that same station (Climatology Scenario), river flow calculated by the MOHID Land watershed model for the Iberian Peninsula (MOHIDLand\_IP Scenario) and Western Iberia model domains (MOHIDLand\_WI Scenario). Other minor sources of fresh water discharging in the estuary, i.e. Sorraia and Trancão rivers, were included using climatological flow values for all the modelling scenarios.

The Portuguese Coast Operational Modelling System (hereafter referred as PCOMS; Mateus *et al.*, 2012) is the regional ocean model application and is composed of two nested domains: the West Iberia (2D) and the Portugal (3D) domains covering the Iberian Atlantic coast and its contiguous ocean. Both domains present a constant horizontal resolution of 0.06° ( $\approx$  5.2 km) populated with bathymetric information derived from the EMODnet Hydrography portal (<http://www.emodnet-hydrography.eu>). The West Iberia domain covers the area limited the following range of latitudes (33.48 °N, 45.90 °N) and longitudes (4.20 °W, 13.50 °W) resulting in a grid of 207 x 155 cells with maximum depths reaching 5600 m. The Portugal domain covers the area comprised by the latitudes (34.38 °N, 45.00 °N) and the longitudes (5.10 °W, 12.60 °W) resulting in a grid of 177 x 125 cells and maximum depths around 5300 m. The Portugal domain is located centred in the West Iberia domain, leaving 15 cells of difference in every direction, that downscales the Mercator-Océan PSY2V4 North Atlantic solution (Drillet *et al.*, 2005) (Figure 3). Tides are forced along the ocean boundary of the West Iberia (2D) model domain, using the global tide solution FES2004 (Lyard *et al.*, 2006). Hereafter, the 3D Portugal model domain would be referred as PCOMS.

The PCOMS and the TagusMouth model applications are fully 3D baroclinic hydrodynamic and ecological model applications operated by the MOHID Water model. They share a common vertical discretisation consisting on a mixed vertical geometry composed of a sigma domain with 7 layers from the surface until 8.68 m depth, with variable thickness decreasing up to 1 m at the surface, on top of a Cartesian domain of 43 layers with thickness increasing towards the bottom. The TagusMouth model application receives open ocean boundary conditions from a PCOMS version without river inputs as described in Campuzano *et al.* (2012).

Each component of this modelling system was forced with the higher horizontal resolution meteorological model available for its domain. Meteorological model applications provide 3D fields that include relevant model forcing variables (i.e. precipitation, solar radiation, wind modulus and direction, relative humidity, air temperature, etc.) and whose surface layer is interpolated for each modelling domain by triangulation. The MOHID Land IP domain, was forced using WRF model results (Skamarock *et al.*, 2005) with 12 km horizontal resolution

generated by Meteogalicia (<http://www.meteogalicia.es>). The MOHID Land WI and the MOHID Water PCOMS domains used, as atmospheric boundary conditions, MM5 modelling results (Grell *et al.*, 1994) with a horizontal resolution of 9 km provided by the IST meteorological group. The Tagus Mouth MOHID Water application was forced using 3 km horizontal resolution WRF model results also provided by the IST meteorological group (<http://meteo.tecnico.ulisboa.pt/>; Trancoso, 2012).

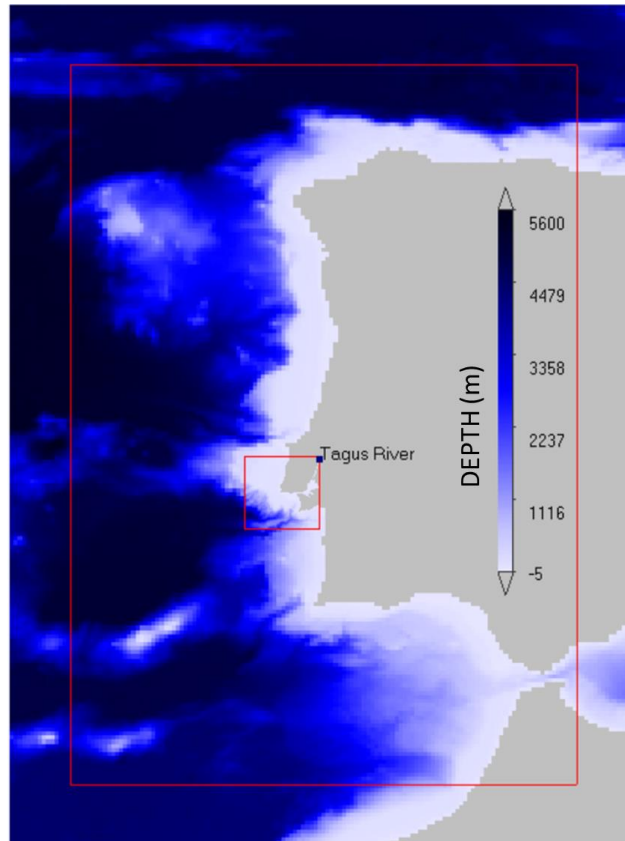


**Figure 3. Bathymetry of the PCOMS regional ocean operational system and TagusMouth domains. The full domain correspond to the 2D West Iberian domain while the outer box indicates the 3D Portugal domain limits and the inner box indicates the TagusMouth domain limits.**

To evaluate the presented methodology, the regional ocean model would be compared with results from a state-of-the-art regional model covering the study area: the operational IBI (Iberian Biscay Irish) Ocean Analysis and Forecasting system (hereafter referred as CMEMS-IBI; <http://marine.copernicus.eu/>). This is the regional ocean model of the European Commission Copernicus Programme based on a NEMO model application run at  $0.028^\circ$  ( $\approx 2.40$  km) horizontal resolution and operated by Puertos del Estado and Mercator-Océan that includes high frequency processes (i.e. tidal forcing, surges and high frequency atmospheric forcing, fresh water river discharge, etc.). The CMEMS-IBI model application includes the Tagus estuary with an inlet in their domain that simulates the estuary morphology.

### 5.3.2. Coupling the Estuary-Ocean Interface

In order to include the estuarine fluxes into a regional ocean model with coarser horizontal resolution a novel methodology was designed. Flow time series (positive during ebb conditions and negative during flood conditions) and properties concentration (i.e. temperature and salinity) are extracted for each cell of a defined 2D cross-section. For the TagusMouth case study, a meridional cross-section was defined in the estuarine channel (Figure 2). The vertical correspondence between the PCOMS and the TagusMouth model grids

allows to add directly each estuarine layer fluxes in the corresponding layer of the PCOMS domain providing the implementation of an effective off-line 2D boundary condition.

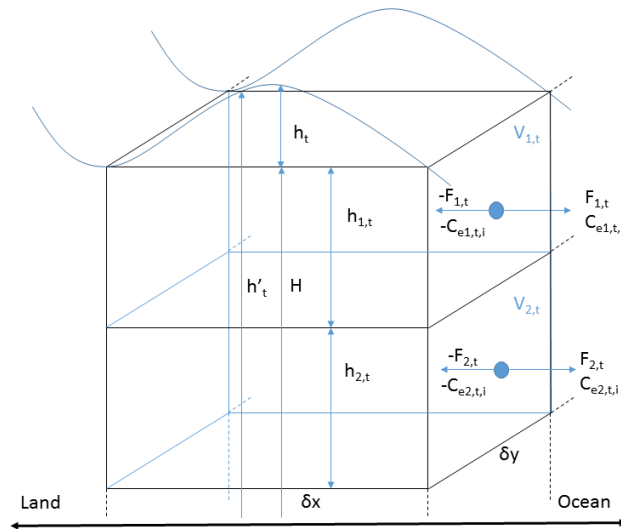


**Figure 4. Diagram representing the flow and concentration calculations performed in the estuary model cross-section cells that is imposed as land boundary conditions in the regional ocean model.  $\delta x$  and  $\delta y$  correspond to the cell horizontal dimensions while the cell horizontal dimensions while  $H$  correspond to the constant depth for each cell.  $h_t$  corresponds to the instantaneous value of the free surface that varies in time and  $h'_t$  is total depth that is decomposed in several layers  $h_{a,t}$  (a representing the number of the vertical layer from top to bottom) according to the vertical geometry of the model.  $V_{a,t}$  is the instantaneous volume that multiplied by the instantaneous velocity provides each cell instantaneous flow ( $F_{a,t}$ ).  $C_{e a,t,i}$  stands for the estuarine concentration for each water property  $i$  (i.e. temperature, salinity).**

Figure 4 represents schematically the fluxes calculation performed in the estuarine model application, that are later imposed in estuary-ocean interface.  $H$ , in the diagram, represents the constant bathymetric depth for a horizontal cell related to the hydrographic zero while  $h_t$  corresponds to the free surface that varies in time mainly due to the atmospheric and astronomic tides.  $h'_t$  is the sum of both the permanent and the variable heights that is decomposed in several layers according to the vertical geometry of the model. Thus, each cell vertical dimension  $h_{a,t}$  ( $a$  representing the number of the vertical layer) would evolve in time while the cell horizontal dimensions ( $\delta x$  and  $\delta y$ ) are constant. With these values, the instantaneous volume for each cell ( $V_{a,t}$ ) can be obtained, and by multiplying it with the cross-section velocity, the corresponding instantaneous flow ( $F_{a,t}$ ) would be obtained. The flow value has positive sign during ebb periods and negative during flood periods. The instantaneous concentration ( $C_{e a,t,i}$ ) for any water property  $i$  (i.e. temperature, salinity, nutrients, etc.) associated to the instantaneous flow corresponds to the estuarine value calculated by the model at each cell centre.

The MOHID Water model allows to input positive and negative flows, and by following this approach, the tidal intermittent fluxes coming from the estuarine models can be included into the regional ocean model. This methodology could be applied to 2D or 3D estuarine models. Currently, it is implemented in an offline delayed mode by obtaining a set of time series that are independent from the receiving model. This approach also allows to calculate the estuarine fluxes from previous modelling results and to couple several operational estuarine models with different time steps to a single regional ocean model. Additionally, this method would allow to provide land boundary conditions to other regional ocean models simulating the same study area. In future versions of the application, this methodology could be implemented in an online coupled mode by using the Open Modelling Interface framework (OpenMI) as was previously done in other MOHID model applications (i.e. Pina *et al.*, 2015).

### 5.3.3. Operational Modelling

This set of numerical models is integrated and synchronised through the ART software (Automatic Running Tool), a software for the automation of model simulations developed at IST that is currently used by many operational applications (Ascione Kenov *et al.*, 2014; Brito *et al.*, 2015). The ART tool is a standalone application, independent, compiled, and able to run in any Windows operative system. This tool can be seen as the “heart” of an operational framework, controlling the execution of other auxiliary standalone applications or even scripts (e.g. conversion of file formats, interpolation and specific downloading procedures), adapting automatically the configuration files and launching those applications (Figure 5). The ART tool pre-processes the boundary conditions from different sources needed for the model simulations; executes the MOHID Water and Land model applications using the configured files, and coordinates the sequence described in this study. After each estuarine model has finished, it executes the River Out software. A software designed specifically to extract and calculate the fluxes and concentrations (as described above) for all the cells comprised between two defined coordinates and to store them in an organised manner. Those fluxes are latter accessed by the ART software controlling the PCOMS regional model and incorporated through pre-configured files. The operational tool finally stores, graphs and distributes the model results via OPeNDAP, ftp, smartphone and Webpages during the post-processor operations. This software can either be used to automatize real time nowcast / forecast solutions, hindcast scenarios, or mixed solutions (hindcast + nowcast + forecast).

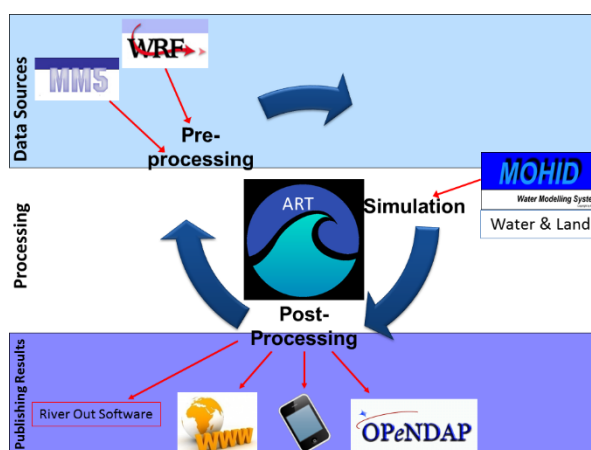


Figure 5. General scheme of the Automatic Running Tool (ART) where it can be distinguished the pre-processing, simulation and post-processing cycle of operations including only the elements used for the MOHID Land and MOHID Water applications used in this work. The River Out software is executed during the post-processing operations of the estuarine model application.

## 5.4 Results and Discussion

River flow was used as indicator to evaluate the performance of the watershed model applications while salinity concentrations was the selected indicator for the estuarine and regional ocean model applications. An additional difficulty to validate the proposed methodology is the scarcity of continuous salinity observations in the estuarine and coastal areas that currently cannot be compensated by satellite imagery for this resolutions.

### 5.4.1. Watershed Modelling

In order to provide an insight of the advantages of using watershed modelling, the Tagus River modelling results obtained with the MOHID Land IP and WI domains were compared with the streamflow measured by the Almourol hydrometric station and with the climatology derived from the same station data (Figure 6). Both model domains show a good agreement in terms of flow and peak timing, though it can be observed that following dry periods the model

overpredicted flow values. That effect could be related to watershed management through dams' retention, irrigation, human consumption, etc. On the other hand, the main weakness of river climatologies is its incapacity to include the interannual variability compared to model applications that are in agreement with the main trends. Statistically, the coefficient of determination ( $R^2$ ) between the observed data with the IP domain, the WI domain and the climatology, for the period 2011-2013, is 0.59, 0.34 and 0.06 respectively. The coefficient of determination for the model applications are of the same range of magnitude to similar studies i.e. Yang *et al.* (2014) obtained  $R^2$  around 0.6 for three watersheds with drainage area between 30 and 300 km<sup>2</sup>. That area is much smaller than the 25 000 and 80 000 km<sup>2</sup> area drained for the Tagus River by the MOHID Land WI and IP model applications respectively. Please refer to Brito *et al.* (2015) for a broader description of the watershed modelling results.

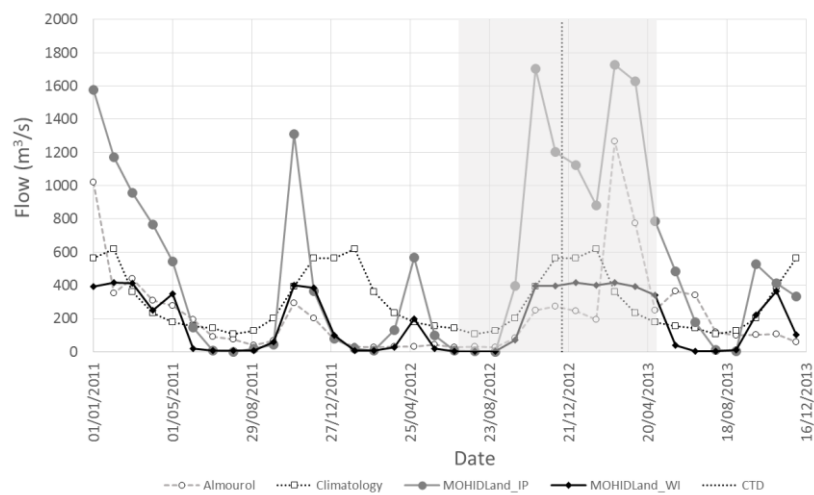


**Figure 6. Monthly averaged Tagus River flow for the period 2011-2013 observed by the Almourol hydrometric station (white circle marks and dashed line), river climatology (white square marks and dotted line) and obtained with the MOHID Land IP (grey circle marks and solid line) and WI (black diamond marks and solid line) model domains. The grey area corresponds to the period monitored by the Algés coastal buoy. The vertical dotted line indicates the date when the CTD campaign took place.**

#### 5.4.2. Estuarine Modelling

To evaluate the effect of the Tagus River forcing in the TagusMouth estuarine application, the period from 1 October 2012 to 30 April 2013 was simulated using as boundary conditions the four defined scenarios: Almourol, Climatology, MOHIDLand\_IP and MOHIDLand\_WI (Figure 6). The simulation period was selected due to the availability of a continuous salinity record measured by a monitoring buoy in Algés (38.694 °N, 9.237 °W) deployed by the SimTejo water utility (Figure 2), hereafter referred as Algés buoy. The Algés buoy due to its location, in the vicinity of the estuarine mouth, was able to record the salinity concentration in the estuary-ocean interface during the simulation period.

Figure 7 represents the mean daily salinity values observed by the Algés buoy along with the salinity values in the corresponding model domain cell for each TagusMouth modelling scenario. In April 2013, the Algés buoy was able to observe the effect of an extreme rain event in the salinity values at the estuarine mouth with salinity concentrations reaching values under 10. Modelling results obtained using the Almourol Scenario - thus the most realistic scenario - were able to adequately reproduce that event, allowing us to gain confidence in the TagusMouth model application. This scenario shows a high correspondence in time and magnitude in the whole simulated period and indicates that the TagusMouth model setup and parameterisations are able to represent adequately the Tagus estuary dynamics and

therefore, can serve to quantify the output fluxes. The coefficient of determination ( $R^2$ ) between the Algés buoy observations and the Almourol modelling scenario for the modelled period was 0.89 with a root mean square error (RMSE), expressed in salinity units, of 2.55. When the buoy observations are compared with the scenarios using the MOHID Land results, the  $R^2$  and the RMSE are 0.58 and 5.67 respectively for the IP domain and 0.40 and 4.31 respectively for the WI domain. The MOHID Land IP scenario, even if generally overestimating the river flow, follows quite well the Tagus River flow general trends and is able to reproduce the peaks associated to extreme events. The MOHID Land WI scenario presents on average a lower error than the IP scenario; however it is not able to reproduce extreme events thus its correlation is penalised. Finally, the Climatology scenario presents the lowest  $R^2$ , 0.20, and a RMSE similar to the WI domain, 4.71. Consequently, it could be concluded that the climatology scenario had the worst performance for modelling the estuarine concentrations at the ocean-estuary interface for the modelled period.

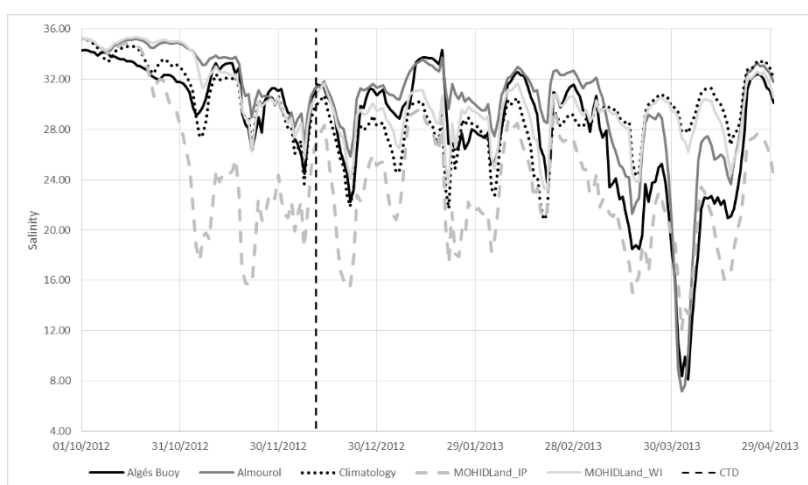


**Figure 7. Salinity values at the location of the Algés monitoring buoy for the simulation period observed by the monitoring buoy (solid black line) and modelled by the TagusMouth model application for the four forcing scenarios: Almourol station (solid dark grey line), Tagus River climatology (dotted black line), MOHIDLand\_IP (dashed light grey line) and MOHIDLand\_WI Domain (solid light grey line). The vertical dashed dark line indicates the date when the CTD campaign was performed.**

### 5.4.3. Ocean Modelling

Following the methodology described above, the fluxes and concentrations for each of the four TagusMouth modelling scenarios were obtained at the defined meridional cross-section (Figure 2). Those fluxes were imposed in the corresponding land-ocean boundary cell in an off-line coupled mode with a time step low enough to incorporate the tidal signal. In this study a fixed time step of 900 s was used. Due to the difference of horizontal resolution between the PCOMS and the TagusMouth grids, both grids at the estuary-ocean interface present different depth values at that boundary cell and the vertical implementation of the estuarine fluxes was limited to the first 10 m which is the depth of the receiving grid cell.

In order to evaluate the adequateness of this novel technique to represent the ROFI for the Tagus River, modelling results for both the PCOMS and the TagusMouth model applications were evaluated using a salinity profile obtained during a CTD campaign that took place in coastal waters near the estuarine mouth (Figure 2) during the simulated period (11 December 2012 12h). Additionally, the salinity profile was also compared with modelling results from CMEMS-IBI model for the same date, along the four modelling scenarios.

To compare the level of agreement between the observations and the modelling results, the salinity result at the closest depth of the modelling levels was selected for the top 20 m (Figure 8). The salinity profile shows a salt wedge of estuarine water in the top 12 m increasing up to

36 in deeper waters. During that monitoring campaign, a flow under  $300 \text{ m}^3\text{s}^{-1}$  was measured in the Tagus River, almost half of the climatological value for that period, while the MOHID Land WI and IP domains calculated river flows around 400 and  $1200 \text{ m}^3\text{s}^{-1}$  respectively (Figure 6). The differences in river flow do not produce a high impact in the salinity values detected at the estuarine mouth with only 1 salinity unit for the Almourol, MOHID Land WI and river climatology scenarios (Figure 7). That could be due to the volume of the Tagus estuary tidal prism compared to the magnitude of the river flow. However in the case of the MOHID Land IP scenario, the obtained surface salinity was 26, around 4 units below the other scenarios. The difference in salinity concentrations could influence the extension and vertical distribution of the estuary's plume.

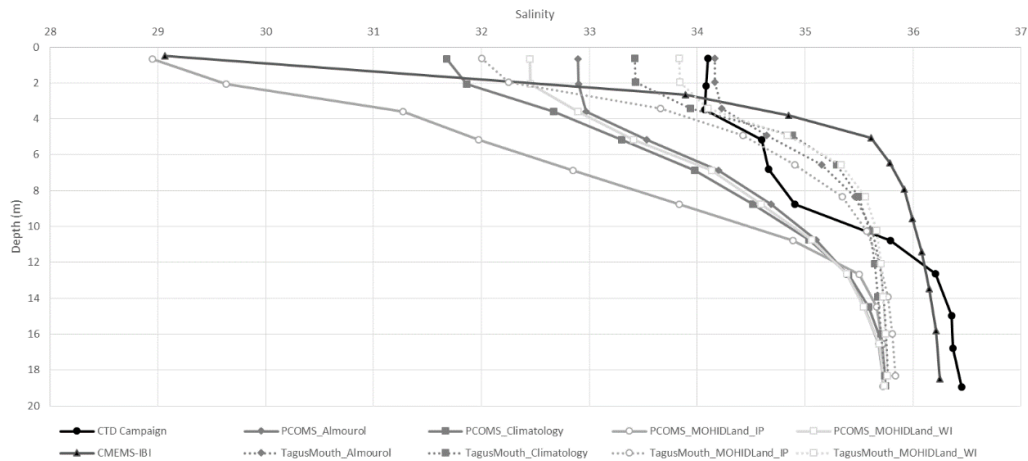


**Figure 8. CTD salinity profile above 20 m depth observed during a coastal campaign in 11 December 2012 at 12h and the salinity profiles obtained with the four modelling scenarios for the PCOMS and TagusMouth modelling domains and the salinity profile from the CMEMS-IBI model for the same date.**

Figure 8 shows the salinity profile of the TagusMouth and PCOMS modelling scenarios and the CMEMS-IBI profile for the same date and time. All the TagusMouth modelling scenarios present higher coefficient of determination than 0.8 and a root mean square error below 1 (Table I). The Almourol scenario provide the best fit and the smallest error, followed by the MOHID Land WI scenario. The application forced by the climatology obtained lower correlation though lower error than the MOHID Land IP scenario. As indicated by the validation with the Algés buoy, the MOHID Land IP scenario would be the most adequate forcing for extreme situations which was not the case during this CTD campaign.

In relation with their TagusMouth scenario counterparts, the PCOMS salinity profiles present a slightly higher correlation with the observed data though doubling their RMSE. On the other hand, the CMEMS-IBI model, an application with higher horizontal resolution, but with a different methodology to include the Tagus River, presents the lowest coefficient of determination and an error only surpassed by the MOHID Land IP scenario.

The PCOMS salinity profiles presented slightly lower salinity values than their correspondent profiles for the TagusMouth application (Figure 8). This numerical effect is due to the horizontal resolution difference between the regional ocean model  $0.06^\circ$  ( $\approx 5.2 \text{ km}$ ) and the estuarine model in the coupling area  $0.003^\circ$  ( $\approx 250 \text{ m}$ ). The TagusMouth and the PCOMS model applications presented similar surface horizontal distribution in concentration and extension during the CTD monitoring campaign as can be seen, as an example, in Figure 9 where both models were forced with the Almourol scenario. This image illustrates the Tagus plume heading to the North due to the Coriolis Effect and to the poleward general circulation, typical of the winter circulation regime in this coastal region.

Table I. Coefficient of determination ( $R^2$ ) and Root Mean Square Error (RMSE) between the CTD salinity profile and the salinity profiles obtained for the four PCOMS and TagusMouth modelling scenarios and the CMEMS-IBI model.

Model Application	Scenario	$R^2$	RMSE
CMEMS-IBI	-	0.36	1.64
PCOMS	Almourol	0.94	0.87
	Climatology	0.90	1.27
	MOHID Land IP	0.89	2.49
	MOHID Land WI	0.93	1.02
TagusMouth	Almourol	0.86	0.44
	Climatology	0.80	0.56
	MOHID Land IP	0.82	0.93
	MOHID Land WI	0.83	0.49

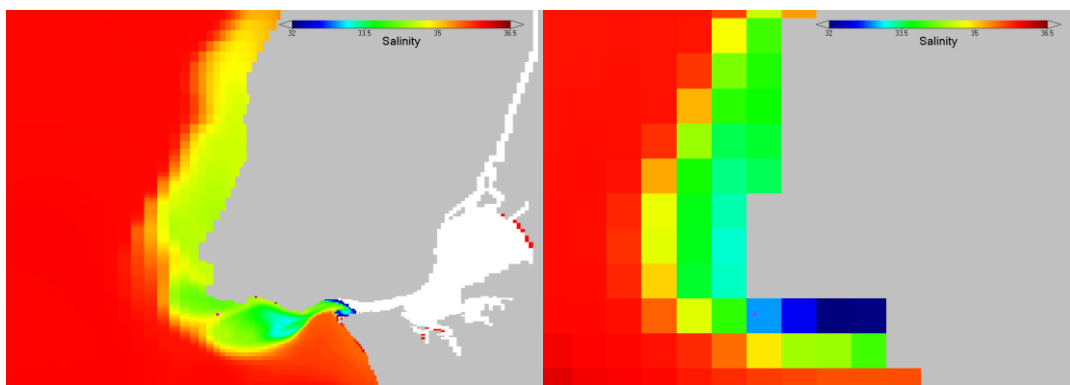


Figure 9. Surface salinity for the TagusMouth (left) and PCOMS (right) domains during the coastal campaign in 11 December 2012 at 12h for the Almourol modelling scenario. Salinity values below 32 are represented in white. The CTD location is also depicted in both images.

## 5.5 Conclusions

By improving the calculation of the fresh water quantity and quality reaching the coastal area, managers and scientists would be able to better reproduce the haline fronts that affect coastal hydrodynamics and the associated ecological processes as the all-year-round low salinity water lens in Northern Portugal, known as Western Iberia Buoyant Plume (WIPB; Peliz *et al.*, 2002). In addition, estimating correctly the land ocean exchange would allow to better understand the nutrient budgets, paths and fate and to evaluate their importance in preserving the ecosystem functions as the fish recruitment variability associated to the river plumes (Santos *et al.*, 2004).

A novel methodology for integrating the water cycle from the rain water to the open ocean by numerical models was set up using an offline coupling technique. The different components of the water continuum, including watersheds, estuaries and regional ocean, were evaluated using the Tagus River, estuary and its associated ROFI as case study. For simplicity, only flow and salinity concentrations were used as quantifiable indicators of the simulations performance for the period between October 2012 and May 2013 when a monitoring buoy was moored at the estuarine mouth and a CTD campaign was performed in the ROFI area.

The watershed applications for the Iberian Peninsula and Western Iberia, described in more detail in Brito *et al.* (2015), allowed to determine the inland waters contribution to the coastal area, in terms of volume and composition. The main advantages of watershed modelling were to complete the hydrometric monitoring networks providing gapless river flow data and non-

monitored variables and to extent their information to non-covered areas. Additionally, watershed numerical modelling allow to forecast river flow and water properties allowing a more efficient management of the modelled systems.

It could be also concluded that even in the case of large and complex watersheds, as the Tagus River, numerical modelling is a useful tool for the estimation of the river contributions to the coastal area. Modelling results have shown that during average conditions the WI modelling domain was able to provide a good estimate of the river flow while during strong events the complete catchment fits better the observations. Future work should be done in order to combine both domains to provide the most probable flow, perhaps through the use of artificial neural networks. In any case, the watershed model approach has shown to produce a more realistic land boundary condition than using river climatologies.

At the estuary level, the MOHID Land scenarios performed better than the climatological values when implemented as land boundary conditions and could be regarded as suitable river forcing for areas without hydrometric monitoring stations or to complete time gaps. From the operational point of view, estuarine applications require larger computational time due to the finer horizontal resolution that implies a shorter model time step. By using multiple regular grids and avoiding to include those high resolution areas embedded in a single ocean regional model, this methodology allows to reduce the regional ocean model computational time and to include several estuaries with adapted horizontal resolutions specific for each estuary thus not being limited by the design of an irregular and complex single grid.

The estuarine fluxes from the four modelling scenarios were inserted in the PCOMS ocean regional model using a novel offline methodology that proved to recreate adequately a salinity profile observed during the simulation period. However, due to the large differences in horizontal resolutions between the estuarine and the regional ocean model and the location of the estuarine mouth, confined in a semi-enclosed coastal bay, the salinity dispersion is slightly different in both modelling domains. Improving the regional ocean model horizontal resolution would influence positively the capacity to replicate plume dynamics and concentrations, as was also observed by Herzfeld (2015).

The approach followed in this methodology allow to continuously improve the solution by substituting direct discharges by estuarine fluxes, if an estuarine application becomes available or if a new river monitoring station is installed. However, the time step of the offline estuarine fluxes would be limited by the stored modelling results time step. That limitation should be taken into consideration when running estuarine models in order to include the tidal signal with enough detail.

The main objectives of the present study were to introduce the use of large multi-watershed model applications as land boundary conditions for estuarine models and to evaluate the use of those estuarine model applications to include the fresh water influence into regional ocean models using a novel methodology. Each component of the system - watershed, estuarine and regional ocean model applications - will be further evaluated and validated in future works as, due to the complexity of the system, it could not be covered in a single research paper.

The developed methodology is generic and has already been applied to several estuaries in the Portuguese coast favouring the achievement of more precise coastal circulation and to study their influence in the creation of salinity and temperature fronts and the nutrient coastal input. When combined through this methodology, this set of operational models are able to provide gapless data of fresh water for large regional areas and to improve the reproduction of coastal hydrodynamics. The operational version of the models described in this work is accessible at <http://forecast.maretec.org/>.

## 5.6 References

- Ascione Kenov I, Campuzano F, Franz G, Fernandes R, Viegas C, Sobrinho J, de Pablo H, Amaral A, Pinto L, Mateus M, Neves R (2014). Advances in Modeling of Water Quality in Estuaries, In: Remote Sensing and Modeling, C.W. Finkl & C. Makowski (Eds.). Springer International Publishing, pp. 237-276. DOI: [10.1007/978-3-319-06326-3\\_10](https://doi.org/10.1007/978-3-319-06326-3_10)
- Banas NS, MacCready P, Hickey BM. The Columbia River plume as cross-shelf exporter and along-coast barrier. *Continental Shelf Research*. 2009; 29: 292–301.
- Braunschweig F, Martins F, Chambel P, Neves R. A methodology to estimate renewal time scales in estuaries: the Tagus Estuary case. *Ocean Dynamics*. 2003; 53(3): 137-145.
- Brito D, Campuzano FJ, Sobrinho J, Fernandes R, Neves R. Integrating operational watershed and coastal models for the Iberian Coast: Watershed model implementation – A first approach. *Estuarine, Coastal and Shelf Science*. 2015; 167, Part A: 138-146. DOI: [10.1016/j.ecss.2015.10.022](https://doi.org/10.1016/j.ecss.2015.10.022).
- Campuzano FJ, Fernandes R, Leitão PC, Viegas C, de Pablo H, Neves R (2012). Implementing local operational models based on an offline downscaling technique: The Tagus estuary case. 2.as Jornadas de Engenharia Hidrográfica, 20-22 June 2012, Lisbon, Portugal. Extended abstracts: 105-108.
- Chow VT (1959). *Open-channel hydraulics*, 680 pages, McGraw-Hill, 1959.
- De Pablo H, Brito D, Mateus M, Trancoso AR, Campuzano FJ, Pinto L, Neves R (2013). An integration methodology to estimate water fluxes and constituents budgets in coastal areas: application to the Tagus coastal area. In: *Ocean modelling for coastal management. Case studies with MOHID*, M. Mateus & R. Neves (eds.), IST Press. pp 213-224
- Drillet Y, Bourdalle-Badi R, Siefrid L, Le Provost C. Meddies in the Mercator North Atlantic and Mediterranean Sea eddy-resolving model. *Journal of Geophysical Research*. 2005; 110(C3): C03016.
- EEA (2007). CLC2006 technical guidelines. Technical report, 17. EEA Copenhagen. [http://www.eea.europa.eu/publications/technical\\_report\\_2007\\_17](http://www.eea.europa.eu/publications/technical_report_2007_17).
- Estournel C, Kondrachoff V, Marsaleix P, Vehil R. The plume of the Rhone: numerical simulation and remote sensing. *Continental Shelf Research*. 1997; 17(8): 899-924.
- Garvine RW, Whitney MM. An estuarine box model of freshwater delivery to the coastal ocean for use in climate models. *Journal of Marine Research*. 2006; 64: 173–194.
- Grell GA, Dudhia J, Stauffer D (1994). A description of the fifth-generation Penn State/NCAR Mesoscale Model (MM5). NCAR Technical Note NCAR/TN-398+STR.
- Herzfeld M. Methods for freshwater riverine input into regional ocean models. *Ocean Modelling*. 2015; 90: 1–15.
- Lacroix G, Ruddick K, Ozer J, Lancelot C. Modelling the impact of the Scheldt and Rhine/Meuse plumes on the salinity distribution in Belgian waters (southern North Sea). *Journal of Sea Research*. 2004; 52: 149–163.
- Liu Y, MacCready P, Hickey BM, Dever EP, Kosro PM, Banas NS. Evaluation of a coastal ocean circulation model for the Columbia River plume in summer 2004. *Journal of Geophysical Research: Oceans*. 2009; 114 (C2): 2156-2202
- Lyard F, Lefevre F, Letellier T, Francis O. Modelling the global ocean tides: modern insights from FES2004. *Ocean Dynamics*. 2006; 56: 394-415.

Mateus M, Riflet G, Chambel P, Fernandes L, Fernandes R, Juliano M, Campuzano F, de Pablo H, Neves R. An operational model for the West Iberian coast: products and services. *Ocean Science*. 2012; 8: 713-732.

Mishra AK, Coulibaly P. Developments in hydrometric network design: A review. *Reviews of Geophysics*. 2009; 47(2), RG2001.

Neves R (2013). The MOHID concept. In: *Ocean modelling for coastal management - Case studies with MOHID*. M. Mateus & R. Neves (eds.), IST Press, Lisbon, Portugal, pp. 1-11.

Peliz Á, Dubert J, Santos AMP, Oliveira PB, Le Cann B. Winter upper ocean circulation in the Western Iberian Basin—Fronts, Eddies and Poleward Flows: an overview. *Deep-Sea Research I*. 2005; 52: 621–646.

Peliz Á, Rosa TL, Santos AMP, Pissarra JL. Fronts, jets, and counter-flows in the Western Iberian upwelling system, *Journal of Marine Systems*. 2002; 35(1–2): 61-77.

Pina RD, Braunschweig F, Silva A, Ochoa-Rodriguez S, Simões NE, Mijic A, Marques AS, Maksimović Č (2015). Urban stormwater modelling with MOHID. UDM 2015 - 10th International Urban Drainage Modelling Conference 20-23 September 2015 Mont-Sainte-Anne, Québec, Canada.

Ribeiro AC, Peliz Á, Santos AMP. A study of the response of chlorophyll-a biomass to a winter upwelling event off Western Iberia using SeaWiFS and in situ data. *Journal of Marine Systems*. 2005; 53: 87– 107.

Santos AMP, Chícharo A, Dos Santos A, Moita T, Oliveira PB, Peliz Á, Ré P. Physical–biological interactions in the life history of small pelagic fish in the Western Iberia Upwelling Ecosystem. *Progress in Oceanography*. 2007; 74: 192–209.

Santos AMP, Peliz Á, Dubert J, Oliveira PB, Angélico MM, Ré P. Impact of a winter upwelling event on the distribution and transport of sardine (*Sardina pilchardus*) eggs and larvae off western Iberia: a retention mechanism. *Continental Shelf Research*. 2004; 24(2): 149-165

Schiller RV, Kourafalou VH. Modeling river plume dynamics with the Hybrid Coordinate Ocean Model. *Ocean Modeling*. 2010; 33(1–2): 101–117.

Skamarock WC, Klemp JB, Dudhia J, Gill DO, Barker DM, Wang W, Powers JG (2005). A Description of the Advanced Research wrf Version 2. Tech. Rep., National Center for Atmospheric Research.

Trancoso AR (2012) *Operational Modelling as a Tool in Wind Power Forecasts and Meteorological Warnings*, PhD in Environmental Engineering, Instituto Superior Técnico, Technical University of Lisbon.

van der Sande CI, de Jong SM, de Roo APJ (2003). A segmentation and classification approach of IKONOS-2 imagery for land cover mapping to assist flood risk and flood damage assessment. *International Journal of Applied Earth Observation and Geoinformation*, 4(3): 217-229.

Yang P, Ames DP, Fonseca A, Anderson D, Shrestha R, Glenn N F, Cao Y. What is the effect of LiDAR-derived DEM resolution on large-scale watershed model results? *Environmental Modelling & Software*. 2014; 58, 48-57.



# Chapter VI - Coupling watersheds, estuaries and regional oceanography through numerical modelling in the Western Iberia: Thermohaline flux variability at the ocean-estuary interface.

---

## Publication information

This chapter has been published for publication as a book chapter with the following details: Campuzano FJ, Juliano M, Sobrinho J, de Pablo H, Brito D, Fernandes R, Neves R (2018). Coupling Watersheds, Estuaries and Regional Oceanography through Numerical Modelling in the Western Iberia: Thermohaline Flux Variability at the Ocean-Estuary Interface. In: Estuary. W. Froneman (Ed), InTech, Rijeka, Croatia. DOI: [10.5772/intechopen.72162](https://doi.org/10.5772/intechopen.72162).

## Abstract

The correct characterisation of the water and properties exchanges at the estuary-ocean interface is a key information to understand the estuarine plume influence in coastal circulation and in the generation of haline fronts. In this work, the main eight Portuguese estuaries were modelled using the MOHID Water numerical model for the period 2010-2015. Water fluxes and associated properties were computed numerically at each estuarine mouth. These results served to estimate precisely tidal prisms, tidal flows and to describe the annual evolution of water temperature and salinity at the estuarine mouths. Those fluxes could serve to improve the land boundary conditions for regional ocean models. Moreover, the numerical analysis of the estuarine fluxes allow us to characterise better each of the studied systems as two neighbouring estuaries could present very different fluxes and water properties. Where available, modelling results were compared with observed data from stations near the estuary mouth.

## 6.1. Introduction

An estuary was defined as "a semi-enclosed coastal body of water, which has a free connection with the open sea, and within which sea water is measurably diluted with freshwater derived from land drainage" (Pritchard, 1967). On its way to the open ocean, fresh water carried by rivers is mixed with the saltier ocean water aided mainly by the action of tides and atmospheric forces. The salinity of the estuarine fluxes that are incorporated in the near ocean depends of several factors such as the estuary tidal prism and the river run off. While the size of the tidal prism is controlled by the morphology of each particular area, the fresh water inputs are controlled by natural factors such as rainfall and human fresh water management upstream the river mouth i.e. water irrigation, storage for electricity and deviation to other watersheds. The natural and manmade variability of the fresh water volume and properties is a constraint to characterise the estuarine waters that flow from estuaries to the open ocean due to the lack of permanent monitoring stations. This characterisation is capital to understand their influence in coastal hydrodynamics and ecological processes.

From the European environmental legislation perspective, estuaries are typically regarded as transitional waters in the EU Water Framework Directive (WFD, Directive 2000/60/EC) and therefore may mostly fall outside the scope of EU Marine Strategy Framework Directive (MSFD, Directive 2008/56/EC). However certain estuaries may have estuarine plumes which extend beyond transitional waters limit, 1 nautical mile from baseline, into coastal waters or beyond; in these cases the estuarine habitat would fall within the scope of MSFD (European Commission, 2012). For this reason, the exclusion of estuaries and other transitional waters from the MSFD has been questioned (Borja *et al.*, 2010). In any case, though WFD requires the monitoring of several biological and chemical elements for the establishment of reference conditions in terms of water quality, long-term continuous monitoring with high temporal resolution are rarely deployed in estuaries (Garel *et al.*, 2009) and when deployed some sensors show lower adaptation for longstanding observation (Garel and Ferreira, 2015). For these reason, numerical models are able to support *in situ* monitoring by completing the datasets spatially and temporally and by contrasting the ambiguous observed values. Also numerical models can assist to describe the transitional waters including the extension and influence of the estuarine plumes in the near ocean.

In this chapter, the tidal prism and estuarine fluxes will be characterised with the aid of numerical models and the existing monitoring stations from the main Portuguese estuaries. This work also aims to describe in more detail the estuarine component of the methodology to couple watersheds, estuaries and regional oceans through numerical modelling for Western Iberia (Campuzano *et al.*, 2016).

## 6.2. Study Area

In this study, fluxes from the eight largest Portuguese estuaries were analysed, from North to South: Minho, Lima, Douro, Ria de Aveiro (hereafter referred as Aveiro estuary), Mondego, Tagus, Sado and Guadiana (Figure 1). All these estuaries receive the name from the main river discharging on it except for Aveiro where the principal fresh water source is the Vouga River. Their associated river catchments are distributed in areas with different climate characteristics, for example the annual rainfall gradient between the two most distant rivers, Minho and Guadiana is around 1700 mm (AEMET and IM, 2011). From the administrative point of view, Douro, Guadiana, Lima, Minho and Tagus are international rivers while the drainage areas of the Vouga, Mondego and Sado rivers fall entirely within the Portuguese territory.

## 6.3. Material and methods

### 6.3.1. Monitoring networks

In order to force and validate the estuarine numerical model applications, automatic data collected along the estuarine continuum from hydrometric stations and estuarine buoys were gathered in this work. Hydrometric data is relevant to provide reliable boundary conditions on the river side while the *in situ* estuarine data collected by the monitoring stations were used to validate the modelling results. Although influenced by the global decline context (Mishra and Coulibaly, 2009), the hydrometric network is a more stable and reliable source of data when comparing with long term autonomous monitoring in estuarine systems which is generally scarce. In fact, none of the estuarine stations described below are currently in operation. Moreover, to guarantee high performance, the sensors equipped in the estuarine stations require periodic calibration (Garel *et al.*, 2009). For instance, the performance of temperature sensors are more reliable than salinity ones (Garel and Ferreira, 2015).

The Portuguese river hydrometric observation network, belonging to the Portuguese Environmental Agency (APA, by its acronym in Portuguese), is responsible to monitor the fresh water flow in all the territory and data is made freely available in the SNIRH website (<http://snirh.pt>). Reliable automatic

stations for the study period were available in the Douro, Guadiana, Mondego and Tagus rivers and are Albufeira de Crestuma, 20 km upstream from Douro estuarine mouth, Açude de Pedrogão, 130 km upstream from Guadiana estuary mouth, Açude de Coimbra, 45 km upstream from Mondego estuary mouth, and Almourol, 130 km upstream from the Tagus estuary mouth. The location of those stations will exclude the contributions to the river flow due to rainfall and other minor tributaries between the station and the head of the estuary, which can be relevant in heavy rainy areas.

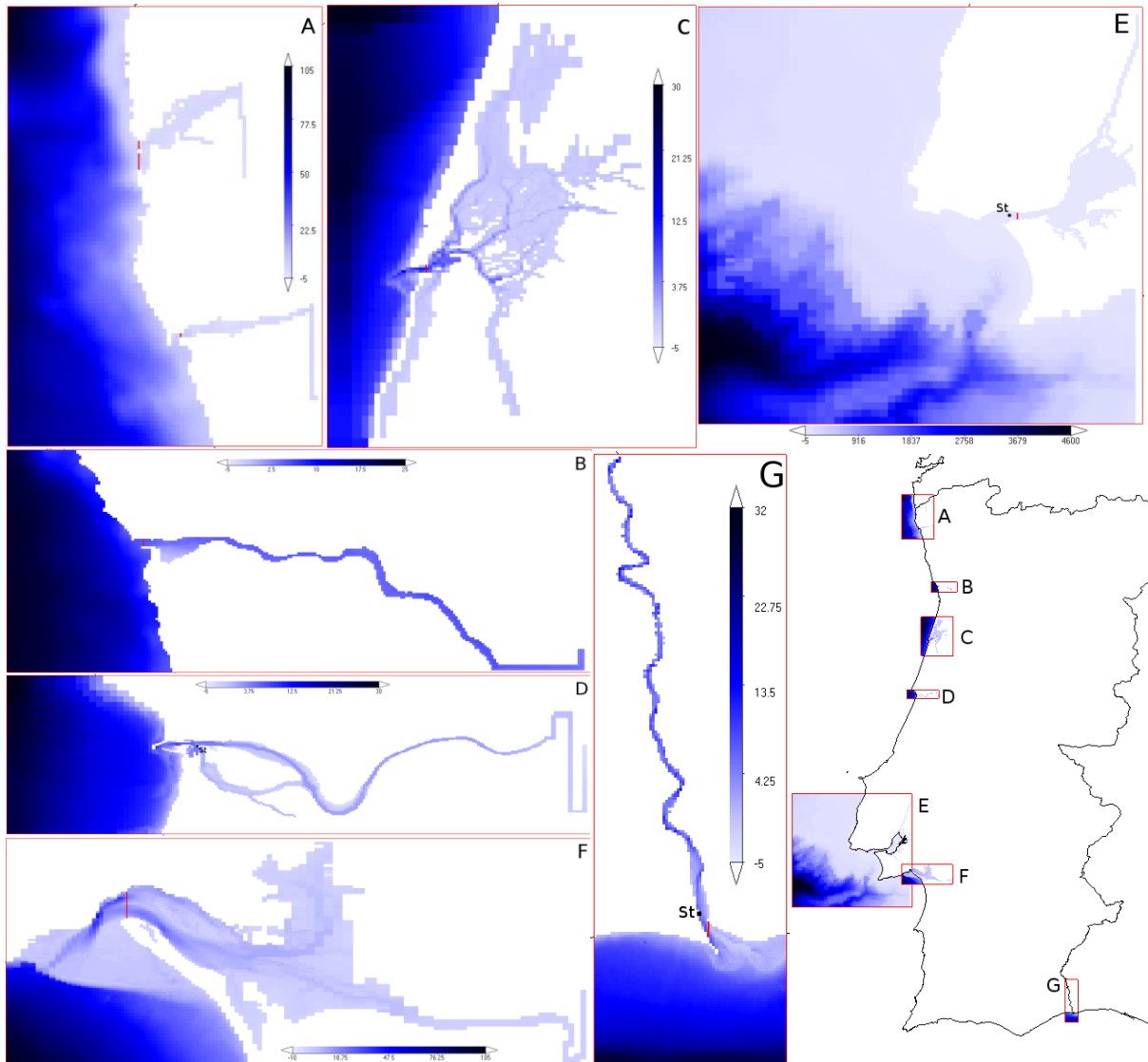


**Figure 1. Bathymetry and model domain of the estuaries analysed in this work and its location in the Portuguese context (bottom right): A) Minho (top) and Lima (bottom), B) Douro, C) Aveiro, D) Mondego, E) Tagus, F) Sado and G) Guadiana. In each estuary, a red line indicates the location of the cross-section where the estuarine fluxes were calculated. Monitoring stations in the Guadiana, Mondego and Tagus estuaries is indicated with “St”.**

In Portugal, several estuaries were monitored continuously during the simulated period, 2010-2015. The SIMPATICO network composed by three *in situ* monitoring stations in the Guadiana (37.188°N, 7.411°W), Mondego (40.144°N, 8.856°W) and Tagus (39.058°N, 8.774°W) estuaries collected continuous water-quality and currents (Garel *et al.*, 2009). For the purpose of this work, only the Guadiana and Mondego observations from the SIMPATICO network are adequate since the monitoring station in the Tagus estuary is located 40 km upstream from the Tagus mouth and thus unable to represent the estuarine mouth conditions. Instead, a monitoring buoy, hereafter referred

as Algés buoy (38.694°N, 9.237°W), deployed by the water utility SimTejo was used to represent the Tagus water conditions in the in the estuary-ocean interface (Figure 1).

### 6.3.2. Numerical models

Each studied estuary was simulated for the 2010-2015 period using the MOHID Water model. The MOHID Water model is an open source numerical model included in MOHID Water Modelling System (<http://www.mohid.com>; Neves, 2013) developed continuously since 1985 mainly at the Instituto Superior Técnico (IST) from the Universidade de Lisboa. The model adopted an object oriented philosophy model for surface water bodies that integrates different scales and processes using finite volumes. The core of the model is a fully 3D hydrodynamic model which is coupled to different modules comprising water quality, atmosphere processes, discharges, oil dispersion, mixing zone model for point source discharges, etc. The MOHID Water model has been applied to many coastal and estuarine areas worldwide and has shown its ability to simulate successfully very different spatial scales from large coastal areas to coastal structures.

For this study, most of the estuarine modelling applications were simulated using modelling grids, domains and bathymetries from previous studies (Table I). The bathymetries of the Minho, Lima and Sado estuarine model applications were updated on their ocean side using improved global bathymetric databases such as the EMODnet Hydrography portal (<http://www.emodnet-hydrography.eu>). Only the Guadiana estuary model domain was fully developed for this study, using a 100 m resolution bathymetry model for the Guadiana estuary provided by the Instituto Hidrográfico (<http://www.hidrografico.pt>).

Boundary conditions were updated for most of the applications, on the ocean side, the estuarine models were nested to the Portuguese Coast Operational Modelling System (hereafter referred as PCOMS; Mateus *et al.*, 2012) following the downscaling methodology described in Campuzano *et al.* (2012). On the land side, Douro, Guadiana, Mondego and Tagus estuaries were forced by river flow data obtained from the closest stable monitoring station from the Portuguese river hydrometric observation network (<http://snirh.pt>; Table I). Due to the limited data available for the rivers discharging in the Aveiro, Lima, Minho and Sado estuaries, flow data were obtained from a watershed model for West Iberia with 2 km horizontal resolution (WI MOHID Land) described in Brito *et al.* (2015). Climatologies or constant values were only used for minor rivers or other sources of fresh water such as urban waste water treatment plants (UWWTPs). As monitoring stations providing reliable and regular water properties were not found for any of the rivers, water temperature, in all the estuarine applications, was obtained from the WI MOHID Land model application and river salinity was considered as pure fresh water.

Each estuarine application was forced with the higher horizontal resolution meteorological model available for its domain. Meteorological model applications provide 3D fields that include relevant model forcing variables (i.e. precipitation, solar radiation, wind modulus and direction, relative humidity, air temperature, etc.) and whose surface layer is interpolated for each modelling domain by triangulation. The Minho, Lima and Douro estuaries were forced using WRF model results (Skamarock *et al.*, 2005) with 4 km horizontal resolution generated by Meteogalicia (MG, <http://www.meteogalicia.es>). The TagusMouth model application is forced using 3 km horizontal resolution WRF model results provided by the IST meteorological group (IST, <http://meteo.tecnico.ulisboa.pt>). The Aveiro, Guadiana, Mondego and Sado modelling domains used, as atmospheric boundary conditions, MM5 modelling results (Grell *et al.*, 1994) with a horizontal resolution of 9 km provided also by the IST meteorological group (Trancoso, 2012).

All the estuarine models were implemented in 2D depth integrated domains except for the Tagus application, hereafter referred as TagusMouth, which is a fully 3D baroclinic hydrodynamic and ecological application. The TagusMouth vertical discretisation consists of a mixed vertical geometry which is composed of a sigma domain with 7 layers from the surface until 8.68 m depth, with

variable thickness decreasing up to 1 m at the surface, on top of a Cartesian domain of 43 layers with thickness increasing towards the bottom.

**Table I. Estuary mouth coordinates, horizontal resolution, model domain dimension, sources of meteorological forcing and fresh water and previous model description reference. Cross-section estuarine fluxes are calculated along the defined longitude while latitude indicates the centre of the mouth section. \* indicate the zonal resolution at the mouth in irregularly sized grids. Observations were obtained from the SNIRH web portal (<http://www.snirh.pt>), model results were obtained from the West Iberia domain (WI MOHID Land model application) described in Brito *et al.* (2015).**

Estuary	Mouth Location		Horizontal Res.	Dimension (cells number)		Meteorology Model	Fresh water sources	References
	Lat.	Long.		Zonal	Meridional			
<b>Aveiro</b>	40.645 °N	8.740 °W	0.0022*	87	81	MM5 IST-9 km	<b>Model:</b> Vouga MOHID Land <b>Climatology:</b> Antuã, Boco, Caster and Mira rivers	Saraiva (2005) & Sobrinho (2012)
<b>Douro</b>	41.146 °N	8.671 °W	0.0010	244	115	WRF MG-4 km	<b>SNIRH:</b> Albufeira de Crestuma station	Kenov I. (pers. Comm.)
<b>Guadiana</b>	37.178 °N	7.405 °W	0.0018	70	221	MM5 IST-9 km	<b>SNIRH:</b> Pedrogão station	developed for this study
<b>Lima</b>	41.686 °N	8.835 °W	0.0040	70	105	WRF MG-4 km	<b>Model:</b> Lima MOHID Land	updated from Saraiva <i>et al.</i> (2007)
<b>Minho</b>	41.858 °N	8.875 °W					<b>Model:</b> Minho MOHID Land	
<b>Mondego</b>	40.145 °N	8.866 °W	0.0035	206	97	MM5 IST-9 km	<b>SNIRH:</b> Açude de Coimbra station	Kenov <i>et al.</i> (2012)
<b>Sado</b>	38.503 °N	8.905 °W	0.0060	94	90	MM5 IST-9 km	<b>Model:</b> Sado MOHID Land	updated from Martins <i>et al.</i> (2002)
<b>Tagus</b>	38.685 °N	9.222 °W	0.0027*	145	120	WRF IST-3 km	<b>SNIRH:</b> Almourol station <b>Climatology:</b> Sorraia and Trancão rivers <b>Constant:</b> UWWTPs of Alcântara, Beirolas, Chelas, S. João da Talha and Guia	Fernandes (2005) & Campuzano <i>et al.</i> (2012)

This set of numerical models is integrated and synchronised through the ART software (Automatic Running Tool; Figure 2), a software for the automation of model simulations developed at IST that is currently used by many operational applications (Ascione Kenov *et al.*, 2014; Brito *et al.*, 2015; Campuzano *et al.*, 2016). The ART tool is a standalone application, independent, compiled, and able to run in any Windows operative system. This tool can be seen as the “heart” of an operational framework, controlling the execution of other auxiliary standalone applications or even scripts (e.g. conversion of file formats, interpolation and specific downloading procedures), adapting automatically the configuration files and launching those applications. The ART tool pre-processes the boundary conditions from different sources needed to run the model; executes the MOHID Water and Land model applications using the configured files. After each estuarine model has concluded, it executes the River Out software, a software designed specifically to extract and

calculate the water fluxes and concentrations for all the cells comprised at a fixed longitude and between two defined latitudes and to store them in an organised manner.

Table I summarises the main characteristics of the estuarine model applications including the modelling domains, their location of their mouth where the fluxes were calculated, the source of fresh water forcing and the reference of the previous study. Most of the numerical models here described are currently running operationally in the MARETEC research centre (<http://forecast.maretec.org>).

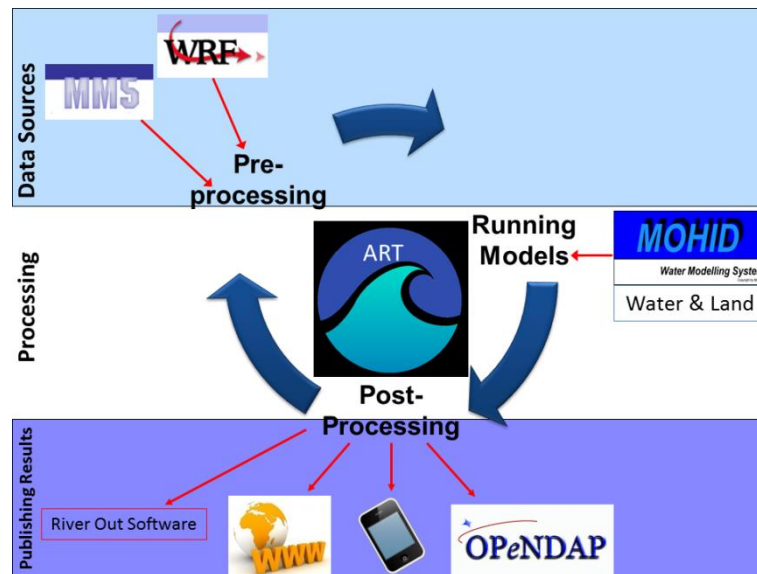


**Figure 2. General scheme of the Automatic Running Tool (ART) depicting the pre-processing, modelling and post-processing cycle of operations with the elements used for the MOHID Land and MOHID Water applications used in this work. The River Out software is executed during the post-processing operations of the estuarine model application.**

## 6.4. Results and Discussion

In Portuguese estuaries, ocean and fresh water meet controlled by the tidal regime, estuary geomorphology and river discharge. A useful parameter to characterise the estuaries and that englobe the tidal regime and the geomorphology is the tidal prism. The tidal prism, as defined by Hume (2005), is “the amount of water that flows into and out of an estuary or bay with the flood and ebb of the tide, excluding any contribution from freshwater inflows”.

The defined cross-sections serve to estimate numerically and accurately the amount of water flowing through the estuarine mouth and thus to estimate tidal prisms. Tidal prism volumes were calculated by integrating the hourly ebb and flood flows for each tidal cycle. For each estuary, mean tidal prism values were obtained considering the entire dataset and differentiating between ebb and flood conditions obtaining volumes with a similar order of magnitude than the ones found in the literature (Table II).

The amount of water discharged by the river affects the duration and intensity of the flood and ebb tides. Ebb tidal prisms are generally larger as they include the river flow in addition to the flushing tide. Furthermore, high river discharges constraint the beginning of the estuary flooding. The difference between flood and ebb tidal prisms is larger in estuaries with low tidal prism and high river discharge such in the Douro. When the Douro river flow is removed from the fluxes calculation, the obtained tidal prisms present similar volumes for both flood and ebb tides, around  $1.21 \times 10^7 \text{ m}^3$ . As can be seen in Table II, the Douro estuary could be defined as an extreme case in Portuguese estuaries as the other rivers do not influence so largely the tidal prism and differences between ebb

and flood are similar. For instance, the tidal prism of the Ria de Aveiro without the Vouga river discharge was  $6.81 \times 10^7 \text{ m}^3$  which is close to the mean tidal prism.

As the estuarine fluxes changes in direction following the ebb and flood conditions, the net flux is similar to the river flow and always towards the ocean. However, the discharge momentum is far more intense than the river flow and evolves with time following the spring and neap tidal cycles. In order to provide a statistical indicator of the exchanged flow with the ocean, the standard deviation ( $\sigma$ ) could be used as indicator of the mean volume exchanged in the estuarine mouth and  $\pm 2\sigma$  would result in the average maximum volume that circulates through the estuarine-ocean connection (Table II). This value allow to see the magnitude of the exchanged flow and the influence in the neighbouring ocean circulation where the Tagus estuary exchanges a flow larger than all the other estuaries together (around  $24000 \text{ m}^3\text{s}^{-1}$ ), followed by the Sado and Aveiro with halve and a tenth of the Tagus flow respectively. In a similar way than with tidal prism calculation and due to the importance of river discharge in the Douro estuary, the  $\sigma$  of the estuarine flow was also obtained removing the river flow and this value reduced to  $643.51 \text{ m}^3\text{s}^{-1}$ . On average, the total flow from the eight estuaries to the neighbouring ocean is around  $55000 \text{ m}^3\text{s}^{-1}$ .

**Table II. Tidal prism (TP) for the entire study period and distinguishing between flood and ebb periods for each of the estuarine systems and bibliographic reference volume. The table also included the estuarine flow standard deviation considered as an indicator of the flow at the ocean-estuary interface.**

Estuary	Mean TP ( $\times 10^7 \text{ m}^3$ )	Flood Mean TP ( $\times 10^7 \text{ m}^3$ )	Ebb Mean TP ( $\times 10^7 \text{ m}^3$ )	Flow std. deviation ( $\sigma$ ) ( $\text{m}^3\text{s}^{-1}$ )	TP Reference volume ( $\times 10^7 \text{ m}^3$ )
<b>Aveiro</b>	$6.83 \pm 1.82$	$6.61 \pm 1.86$	$7.04 \pm 1.76$	3518.92	6.00 (Picado <i>et al.</i> , 2010) 7.00 (Vicente, 1985) 11.90 (Ferreira <i>et al.</i> , 2003)
<b>Douro</b>	$2.20 \pm 12.23$	$0.83 \pm 0.49$	$3.56 \pm 23.97$	875.99	0.55 (Verhagen, 1982) 2.09 (Ferreira <i>et al.</i> , 2003)
<b>Guadiana</b>	$2.96 \pm 1.74$	$2.73 \pm 0.74$	$3.19 \pm 2.73$	1467.16	0.60 (Ferreira <i>et al.</i> , 2003)
<b>Lima</b>	$1.24 \pm 0.57$	$1.08 \pm 0.52$	$1.40 \pm 0.61$	749.74	0.90 (Ferreira <i>et al.</i> , 2003)
<b>Minho</b>	$3.10 \pm 1.53$	$2.79 \pm 1.39$	$3.41 \pm 1.66$	1612.07	0.55 (Ferreira <i>et al.</i> , 2003)
<b>Mondego</b>	$1.53 \pm 0.86$	$1.41 \pm 0.52$	$1.64 \pm 1.10$	802.58	0.99 (Duarte & Vieira, 2009)
<b>Sado</b>	$29.93 \pm 7.98$	$29.83 \pm 7.95$	$30.02 \pm 8.00$	15064.64	40.00 (Brito <i>et al.</i> , 2013)
<b>Tagus</b>	$62.47 \pm 15.96$	$62.01 \pm 16.50$	$62.93 \pm 15.42$	31753.82	75.00 (Neves, 2010)

Depending on the tidal prism and the size of the river discharges, the properties of the water exchanged with the coastal area will fluctuate between different values. Figure 3 and Figure 4 indicate the evolution of the mean modelled temperature and salinity in each of the estuaries during the study period. Temperature and salinity values shown for the Tagus estuary in these figures correspond to its surface layer and therefore can be directly compared with the observations. In the rest of model applications, since they are bidimensional, temperature and salinity represent the vertically integrated values for the entire water column.

Surface water temperatures in the Atlantic Ocean around Portugal show a clear seasonal pattern with maximum temperatures during the summer months (JJA) and lower temperatures in winter period (DJF) (Figure 3; Table IV). Estuaries dominated by the tidal component, i.e. large tidal prism,

present smaller range of temperatures as ocean surface temperatures fluctuates less along the year compared with river temperature. As example, the water fluxes temperature for the Sado and Tagus estuaries is mostly comprised between 10 and 25 °C while Douro, Lima and Mondego estuarine fluxes can reach values under 5°C. The river effect in the fluxes temperature is more recognisable during the winter period (DJF) as during this season inland temperatures are lower and the river flow is higher.

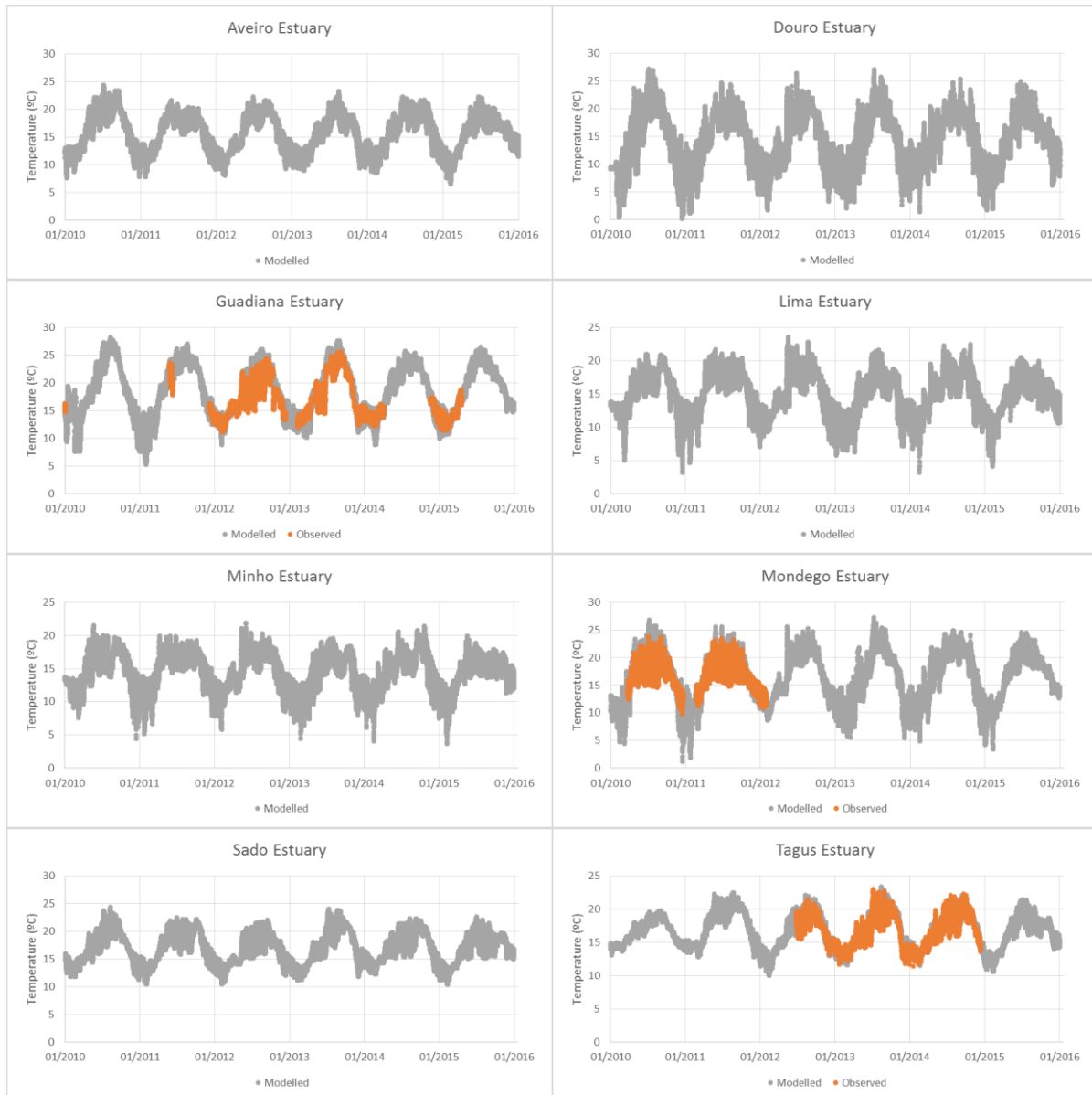


**Figure 3. Mean temperature of the water fluxes at the estuarine mouth cross-section. The graphs show the mean modelled value (in grey) for each estuary and for the entire period 2010-2015 and where available the observed data is also shown (in orange). The Tagus estuary values correspond in this graph to its surface layer. Estuaries are ordered alphabetically from top to bottom.**

The river flow influence in the estuarine fluxes is more detectable in the salinity concentration and configures different estuarine patterns (Figure 4). Estuaries with large tidal prisms, such as Sado and Tagus, present salinity concentrations higher than 0 even during high river flows such as the Tagus flooding event of April 2013. On the other hand, the Douro estuary exchanges fresh water with the near ocean in multiple occasions of every season and as a consequence its fluxes present a mean salinity around 11 (Table V). The Gadiana, Lima and Mondego estuaries eventually exchanges fresh water fluxes during the winter season except on extremely dry years such as 2012. Regarding the

observed and modelled river flows (Figure 4) it can be observed the heterogeneity in the distribution of river flow highest peaks and intensities and thus the highest river event during the study period do not coincide for all the studied estuaries.

As mentioned above, three estuaries, Guadiana, Mondego and Tagus, had monitoring devices near the mouth of the estuary during the study period. The Algés buoy was monitoring near the Tagus estuary mouth for the period 27/06/2012-12/12/2014. The SIMPATICO station for the Mondego estuary collected data between 30/10/2007 and 02/02/2012 while in the Guadiana estuary data was available for the period 19/03/2008 to 21/04/2015. The SIMPATICO dataset collected at the Guadiana estuary until April 2014 (Garel and Ferreira, 2015) is publicly available in machine-readable format at PANGAEA (DOI: [10.1594/PANGAEA.845750](https://doi.org/10.1594/PANGAEA.845750)).

As was mentioned, temperature sensors performance is far larger better than the salinity sensors during long term deploy. In that sense, the Guadiana estuary valid temperature data were 99% while salinity valid data were 67.1% (Garel and Ferreira, 2015) with 20% of invalid data and 12.9% of ambiguous data. Also in the Tagus estuary, the Algés buoy salinity values were identified as valid until 30/04/2013 after that the sensor lost its calibration. Valid temperature and salinity data for the three monitoring stations are represented in Figure 3 and Figure 4. When compared with the modelled data, the coefficient of determination for temperature is larger than for salinity in each station and the best model performance were the Guadiana and Tagus estuaries (Table III). The SIMPATICO station in the Mondego estuary does not show a high performance in the salinity and could be due to several reasons: as its location in the entrance of the southern branch (Garel *et al.*, 2009; Figure 1) that may not be then so representative of the fluxes at the Mondego mouth as most of the main entrance of fresh water takes place in the northern branch. In addition, this is a raw comparison between the observed data at the surface with depth integrated modelling results.

**Table III. Coefficient of determination ( $R^2$ ) between the modelling results and the available observed data for the Guadiana, Mondego and Tagus estuaries. The number of valid values is indicated within brackets.**

Estuary	Temperature $R^2$	Salinity $R^2$
Guadiana	0.90 (N 21435)	0.74 (N 12057)
Mondego	0.79 (N 14741)	0.32 (N 14741)
Tagus	0.92 (N 20944)	0.83 (N 7377)

From the modelling results, a preliminary climatology of water temperature and salinity in the ocean-estuary interface can be obtained that illustrate their variability along the year and provide a global picture of the thermohaline fluxes from the Portuguese estuaries. Table IV and Table V list the monthly averaged temperature and salinity, respectively, calculated by the model at the ocean-estuary interface for the period 2010-2015 (Figure 5). February is the month presenting coldest temperatures for all the estuaries while the warmest month takes place between July (i.e. Douro) and October (i.e. Minho). The estuary location influences the summer maximum temperature as western Iberia coast is subjected during summer to upwelling events that bring cold nutrient-rich waters to the ocean surface. For that reason, winter temperatures provide a clearer image of the river discharges contribution to the estuarine water as it coincides with the rainy season. As a result, it can be concluded that the salinity concentrations of the Douro and the Tagus estuaries are, on average, the most and least influenced by river discharge respectively.

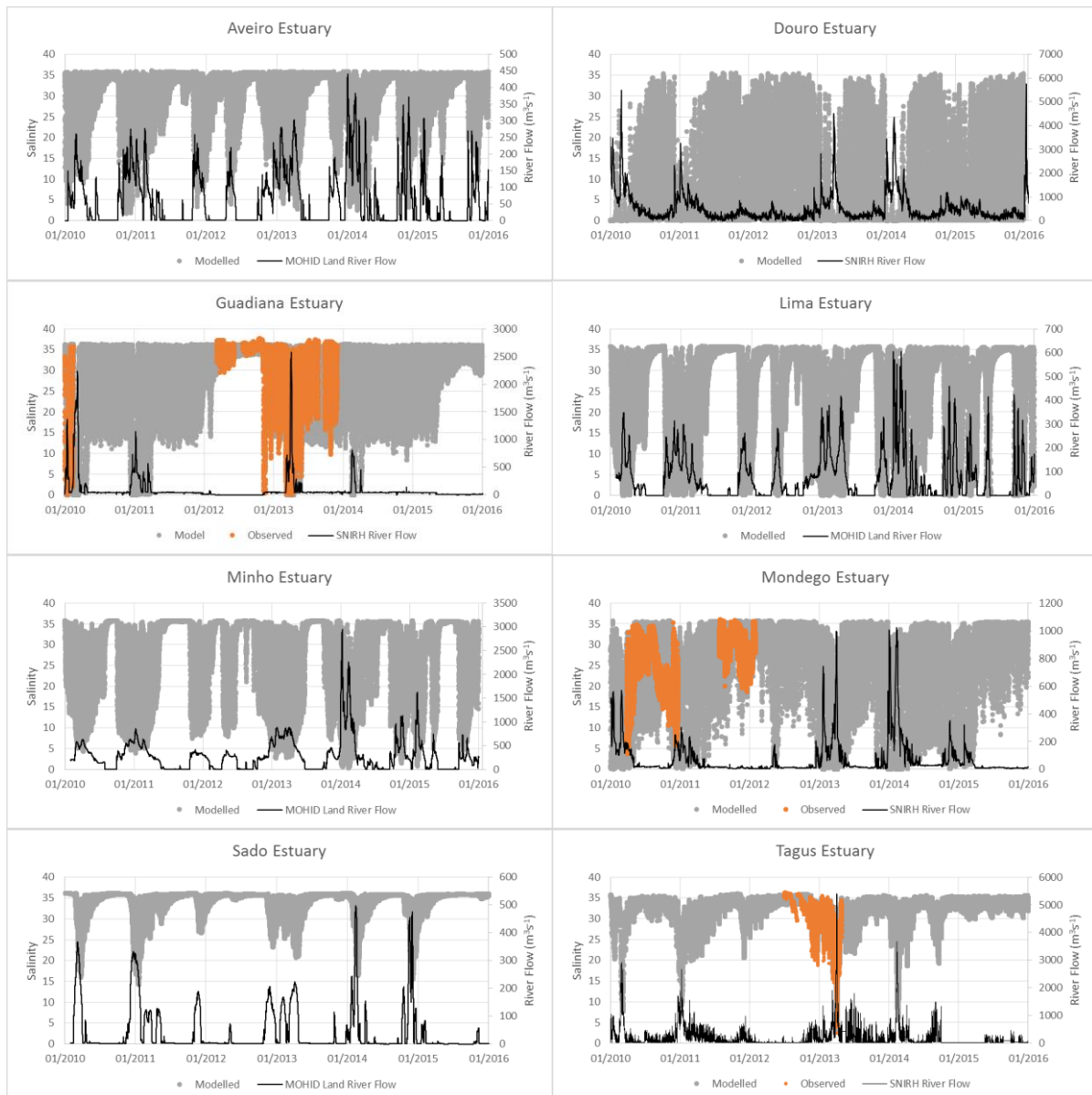


**Figure 4. Mean salinity of the water fluxes at the estuarine mouth cross-section. Graphs show the mean modelled value (in grey) for each estuary and for the entire period 2010-2015 and where available the observed data is also shown (in orange). The Tagus estuary values correspond in this graph to its surface layer. The river flow imposed in the model is displayed with a continuous black line and a secondary axis value and indicated whether the source are observations (SNIRH) or watershed model results (MOHID Land). Estuaries are ordered alphabetically from top to bottom.**

Salinity is a more conservative indicator to study the river effect as the salinity values in the near ocean neither vary largely with latitude nor are affected largely by the upwelled waters. Fluxes from Sado and Tagus estuaries could be categorised as saline because monthly averaged salinities are always above 30 during all the year round. Generally, the Aveiro estuary exchanges saline water during summer and autumn months and brackish waters, salinity between 5 and 30, during winter and spring months while Lima, Minho and Mondego estuarine mouths are dominated by brackish water during most of the year. Almost fresh water, salinity below 5, can reach the Douro estuarine mouth during the first three months of the year and, on average, maximum salinity observed during August is still far from considered as saline. Still the highest ranges of salinities at their mouths are observed in the Lima estuary followed by the Douro estuary and far from the very stable Sado and Tagus estuaries.

**Table IV. Mean monthly modelled temperature for eight analysed estuaries calculated at the ocean-estuary defined cross-sections during the 2010-2015 period. Total average value and range of values are also shown.**

Month	Aveiro	Douro	Guadiana	Lima	Minho	Mondego	Sado	Tagus
January	11.82	9.01	13.44	11.16	11.60	11.57	13.68	13.72
February	11.28	8.42	12.83	10.83	10.92	11.15	12.96	13.07
March	12.76	10.76	13.86	12.36	12.18	12.83	14.12	13.98
April	14.96	13.97	16.60	14.86	14.17	15.69	15.86	15.63
May	16.67	15.84	19.19	16.42	15.37	17.82	17.29	17.04
June	18.07	18.03	21.51	17.58	16.16	19.65	18.56	18.10
July	18.51	19.38	23.81	17.83	16.17	21.07	19.57	18.76
August	18.56	19.16	24.59	17.51	15.88	21.24	19.61	19.20
September	18.89	18.74	23.77	18.06	16.86	20.97	19.96	19.77
October	18.04	16.74	21.29	17.15	17.12	19.15	19.59	19.31
November	15.08	12.27	17.60	13.67	14.50	15.23	17.07	17.17
December	12.96	9.87	14.79	11.86	12.60	12.38	14.75	14.92
<b>Average</b>	15.66	14.38	18.64	14.96	14.48	16.66	16.94	16.81
<b>Range</b>	7.61	10.96	11.76	7.23	6.20	10.09	7.00	6.70

The difference in terms of salinity values between the estuarine fluxes and the ocean saline waters is responsible of generating fronts of different intensity that can influence the surface circulation on large coastal areas. In the Northern halve of Portugal and due to the accumulation of estuaries is responsible of modifying locally the coastal circulation and also, due to the accumulation of rivers, of creating sharp haline fronts. As a result, a low salinity water lens, upper salinity limit below 35.7–35.8, denominated as Western Iberia Buoyant Plume (WIBP), extends along the northern Portuguese coast being referred as a permanent feature of this part of the coast and with a varying intensity along the year (Peliz *et al.*, 2002, 2005).

**Table V. Mean monthly modelled salinity for eight analysed estuaries calculated at the ocean-estuary defined cross-sections. The table also show the average value and the range of values.**

Month	Aveiro	Douro	Guadiana	Lima	Minho	Mondego	Sado	Tagus
January	26.91	5.12	25.08	15.45	20.12	15.88	32.61	32.20
February	27.41	4.81	24.36	14.81	18.92	17.24	32.51	31.31
March	29.50	5.10	23.38	19.22	21.92	16.79	32.05	31.47
April	29.51	6.19	26.47	19.65	23.91	20.92	32.95	32.09
May	30.27	9.25	29.41	20.86	24.90	24.25	34.14	33.05
June	32.94	14.75	30.49	29.51	29.99	28.53	35.01	33.37
July	34.52	19.19	30.52	32.68	33.74	29.05	35.51	33.52
August	35.15	20.97	30.55	34.38	35.27	29.46	35.73	33.75
September	34.46	18.53	30.64	31.65	33.69	30.46	35.80	33.55
October	31.42	15.71	30.71	21.97	27.89	31.15	35.73	33.97
November	27.19	9.80	30.68	13.17	21.83	28.95	34.43	33.44
December	28.68	9.50	28.42	17.16	23.30	23.17	32.10	32.64
<b>Average</b>	30.66	11.58	28.39	22.54	26.29	24.65	34.05	32.86
<b>Range</b>	8.25	16.16	7.33	21.21	16.35	15.28	3.75	2.67

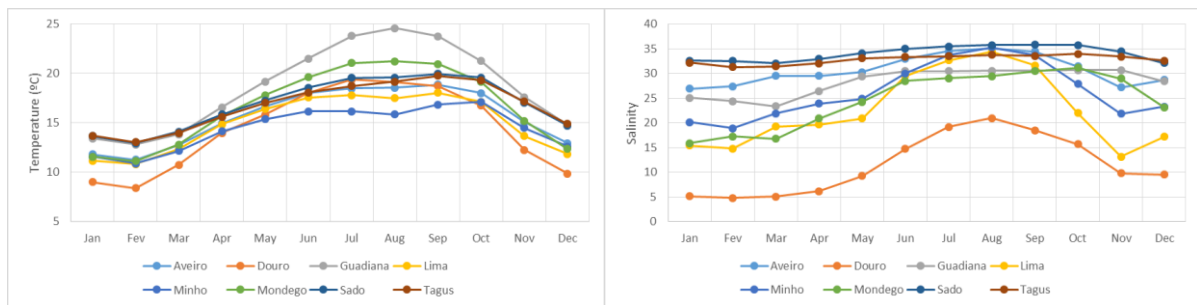


**Figure 5. Mean monthly temperature (left) and salinity (right) obtained by numerical modelling at the estuarine mouth for eight Portuguese estuaries for the period 2010-2015.**

To illustrate the influence in the near ocean by the estuarine plumes, the salinity average for the Douro and the Tagus estuary, the two most extreme estuaries of the study in terms of saline concentration, was obtained for the winter (DJF) and summer (JJA) seasons for the 2010-2015 period. Both estuaries present large plumes on both seasons and the region with salinity values below the WIBP upper limit (37.75) encloses a large portion of the near ocean (Figure 6). The baseline in the Douro region that serves to identify the interior waters is out of the study domain. On the other hand, the Tagus plume extends further than the 1 nautical mile limit from baseline, the limit the application of the MSFD and WFD, even during summer conditions. The baseline coincides with the coastline in the case of the Minho, Lima, Aveiro and Guadiana estuaries. For that reason and due to the implications that will have in the implementation of both EU directives, the research on the estuarine plumes extension and influence in the neighbouring waters is essential.

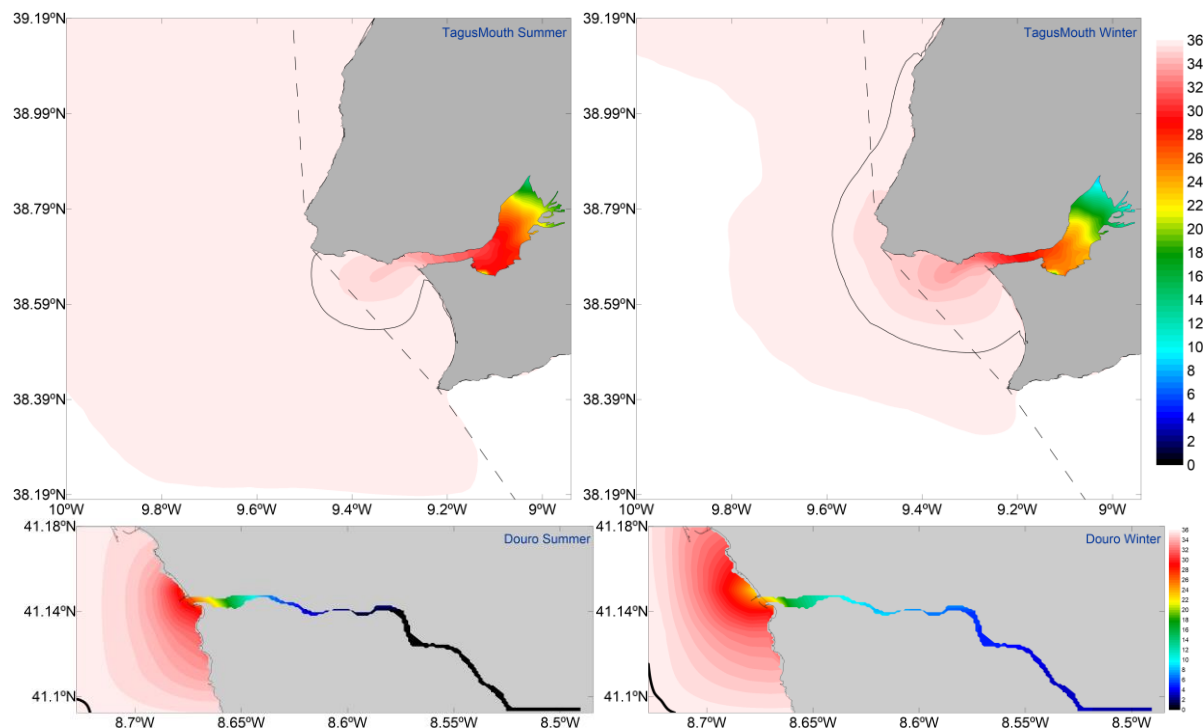


**Figure 6. Mean summer (JJA) salinity (left) and winter (DJF) salinity (right) for the Tagus (top) and Douro (bottom) estuaries for the period 2010-2015. The continuous line indicate the salinity value of 35.75. Dashed line in Tagus graphs indicates the baseline for defining internal waters.**

## 6.5. Conclusions

Monitoring networks along the estuarine continuum from the river catchment until the open ocean should be encouraged in order to evaluate the transfer of properties and momentum in the land-ocean interface. While open ocean and hydrometric monitoring networks are relatively well established, operational estuarine monitoring is far from consolidated. Numerical models are able to help in the design of the monitoring networks, validation of observed data and able to complete spatially and temporally all those networks. In addition, numerical model complete the *in situ* data by providing non-observed variables and forecasts. Modelling results allow also to calculate complex indicators such as tidal prisms, the area of influence of the estuarine waters and to estimate accurately estuarine fluxes that would serve as boundary conditions for ocean regional models such as offline coupling method applied to PCOMS (Campuzano *et al.*, 2016). This type of analysis provide valuable information to characterise the estuarine systems as this was able to show that two neighbouring estuaries can differ largely in flow and salinity fluxes.

## 6.6. References

AEMET, IM, 2011. Atlas climático ibérico/Iberian climate atlas. Agencia Estatal de Meteorología, Ministerio de Medio Ambiente y Rural y Marino, Madrid. Instituto de Meteorologia de Portugal, 80 pp. Available for download [here](#). Accessed 03 Sept 2017.

Ascione Kenov I, Campuzano F, Franz G, Fernandes R, Viegas C, Sobrinho J, de Pablo H, Amaral A, Pinto L, Mateus M, Neves R (2014). Advances in Modeling of Water Quality in Estuaries, In: Remote Sensing and Modeling, C.W. Finkl & C. Makowski (Eds.). Springer International Publishing AG, Cham, Switzerland, pp. 237-276. DOI: [10.1007/978-3-319-06326-3\\_10](https://doi.org/10.1007/978-3-319-06326-3_10)

Borja A, Elliott M, Carstensen J, Heiskanen A-S, van de Bund W. Marine management – Towards an integrated implementation of the European Marine Strategy Framework and the Water Framework Directives. *Marine Pollution Bulletin*. 2010; 60(12): 2175-2186. DOI: [10.1016/j.marpolbul.2010.09.026](https://doi.org/10.1016/j.marpolbul.2010.09.026).

Brito D, Campuzano FJ, Sobrinho J, Fernandes R, Neves R. (2015). Integrating operational watershed and coastal models for the Iberian Coast: Watershed model implementation – A first approach. *Estuarine, Coastal and Shelf Science*, 167, Part A: 138-146. DOI: [10.1016/j.ecss.2015.10.022](https://doi.org/10.1016/j.ecss.2015.10.022)

Brito P, Costas S, Rebêlo L, FitzGerald D. Record of ebb-channel shifting within an ebb-tidal delta, the Sado Estuary, Portugal [Abstract]. In: International Coastal Symposium 2013: ICS2013: Book of Abstracts; 8-12 April 2013; Plymouth, UK. p. 33

Campuzano F, Brito D, Juliano M, Fernandes R, de Pablo H, Neves R. Coupling watersheds, estuaries and regional ocean through numerical modelling for Western Iberia: a novel methodology. *Ocean Dynamics*. 2016; 66(12): 1745–1756. DOI: [10.1007/s10236-016-1005-4](https://doi.org/10.1007/s10236-016-1005-4)

Campuzano FJ, Fernandes R, Leitão PC, Viegas C, de Pablo H, Neves R. Implementing local operational models based on an offline downscaling technique: The Tagus estuary case. 2.as Jornadas de Engenharia Hidrográfica, 20-22 June 2012, Lisbon, Portugal. Extended abstracts: 105-108.

Duarte AALS, Vieira JMR. Effect of tidal regime on estuarine residence time spatial variation. Proceedings of the 5th International Conference on Energy, Environment, Ecosystems and Sustainable Development (EEESD '09). N. Mastorakis (Ed) 28-30 September Athens (Greece). pp. 240-245.

European Commission 2012. Links between the Marine Strategy Framework Directive (MSFD 2008/56/EC) and the Nature Directives (Birds Directive 2009/147/EEC (BD) and Habitats Directive 92/43/EEC (HD)). Available for download [here](#). Accessed 03 Sept 2017.

Fernandes L (2005). Modelling of arsenic dynamics in the Tagus Estuary. MSc dissertation thesis. Technical University of Lisbon, Portugal.

Ferreira JG, Simas T, Nobre A., Silva MC, Schifferegger K, Lencart-Silva J. Identification of sensitive areas and vulnerable zones in transitional and coastal Portuguese systems. Application of the United States National Estuarine Eutrophication Assessment to the Minho, Lima, Douro, Ria de Aveiro, Mondego, Tagus, Sado, Mira, Ria Formosa and Guadiana systems. Lisbon: INAG - Instituto da Água and IMAR – Institute of Marine Research; 2003. 168p.

Garel E, Ferreira Ó. Multi-year high-frequency physical and environmental observations at the Guadiana Estuary. *Earth System Science Data*. 2015; 7(2): 299-309.

Garel E, Nunes S, Neto JM, Fernandes R, Neves R, Marques JC, Ferreira Ó. The autonomous Simpatico system for real-time continuous water-quality and current velocity monitoring: Examples of application in three Portuguese estuaries. *Geo-Marine Letters*. 2009; 29: 331–341. DOI: [10.1007/s00367-009-0147-5](https://doi.org/10.1007/s00367-009-0147-5).

Grell GA, Dudhia J, Stauffer D (1994). A description of the fifth-generation Penn State/NCAR Mesoscale Model (MM5). NCAR Technical Note NCAR/TN-398+STR.

Hume TM. (2005). Tidal Prism. In: *Encyclopedia of Coastal Science*. M.L. Schwartz (ed.), Springer Netherlands, pp. 981-982. DOI: [10.1007/1-4020-3880-1\\_320](https://doi.org/10.1007/1-4020-3880-1_320).

Kenov IA, Garcia AC, Neves R. Residence time of water in the Mondego Estuary (Portugal). *Estuarine, Coastal and Shelf Science*. 2012; 106: 13–22.

Martins F, Leitão P, Neves R. Simulating vertical water mixing in homogeneous estuaries: the SADO Estuary case. *Hydrobiologia*. 2002; 475/476: 221-227.

Mateus M, Riflet G, Chambel P, Fernandes L, Fernandes R, Juliano M, Campuzano F, de Pablo H, Neves R. An operational model for the West Iberian coast: products and services, *Ocean Science*. 2012; 8: 713-732.

Mishra AK, Coulibaly P. Developments in hydrometric network design: A review. *Reviews of Geophysics*. 2009; 47(2), RG2001.

Neves FJ (2010). Dynamics and hydrology of the Tagus estuary: results from in situ observations. PhD dissertation thesis, Universidade de Lisboa, Portugal.

Neves R (2013). The MOHID concept. In: *Ocean modelling for coastal management - Case studies with MOHID*. M. Mateus & R. Neves (eds.), IST Press, Lisbon, Portugal, pp. 1-11.

Peliz Á, Dubert J, Santos AMP, Oliveira PB, Le Cann B. Winter upper ocean circulation in the Western Iberian Basin—Fronts, Eddies and Poleward Flows: an overview. *Deep-Sea Research I*. 2005; 52: 621–646.

Peliz Á, Rosa TL, Santos AMP, Pissarra JL. Fronts, jets, and counter-flows in the Western Iberian upwelling system, *Journal of Marine Systems*. 2002; 35(1–2): 61-77.

- Picado A, Dias JM, Fortunato A. Tidal changes in estuarine systems induced by local geomorphologic modifications. *Continental Shelf Research*. 2010; 30: 1854-1864. DOI: [10.1016/j.csr.2010.08.012](https://doi.org/10.1016/j.csr.2010.08.012).
- Pritchard DW (1967). What is an estuary: physical viewpoint. In: Estuaries Lauf, G. H. (ed.), American Association for the Advancement of Science Publication No. 83. Washington, DC. pp. 3–5
- Saraiva S (2005). Modelação ecológica da Ria de Aveiro: o papel das macroalgas. MSc dissertation thesis. Technical University of Lisbon, Portugal.
- Saraiva S, Pina P, Martins F, Santos M, Braunschweig F, Neves R. Modelling the influence of nutrient loads on Portuguese estuaries. *Hydrobiologia*. 2007; 587(1): 5-18.
- Skamarock WC, Klemp JB, Dudhia J, Gill DO, Barker DM, Wang W, Powers JG (2005). A Description of the Advanced Research WRF Version 2. Tech. Rep., National Center for Atmospheric Research.
- Sobrinho JL (2012). Balanço de nutrientes na plataforma continental ao largo da Região de Aveiro. MSc dissertation thesis. Instituto Superior Técnico, Universidade de Lisboa, Portugal.
- Trancoso AR (2012). Operational Modelling as a Tool in Wind Power Forecasts and Meteorological Warnings. PhD dissertation thesis. Instituto Superior Técnico, Technical University of Lisbon, Portugal.
- Verhagen HJ. Hydro-morphological study Douro Estuary: Part 3 – Tidal current calculations. Report P613 for Administração dos Portos do Douro e Leixões (ADPL). Delft: Hydrodynamic; 1982. 25p. uuid: [727b9547-6440-4907-89f1-842467c0d464](https://nbn-resolving.org/urn:nbn:nl:ui:25-727b9547-6440-4907-89f1-842467c0d464)
- Vicente CM. Caracterização hidráulica e aluvionar da Ria de Aveiro, Utilização de modelos hidráulicos no estudo de problemas da Ria, in: Jornadas da Ria de Aveiro, III, Edição da Chara Municipal de Aveiro, Aveiro, Portugal, 41-58, 1985.



# Chapter VII - Coupling of watersheds, estuaries and regional seas through numerical modelling for Western Iberia: Regional ocean sea surface salinity and temperature patterns.

---

## Abstract

An original methodology for integrating the water cycle from the rain water to the open ocean by numerical models was set up using an offline technique. The different components of the system, including watersheds, estuaries and regional ocean, for Western Iberia were reproduced using numerical models of the MOHID Water Modelling System (<http://www.mohid.com>). This set of operational models, when combined, is able through this novel methodology to fill information gaps. In this chapter the impact of the estuarine and river fluxes, described in previous chapters, were implemented as land-ocean boundary conditions in a regional ocean model covering the Western Iberia region. The performance of the methodology was evaluated aided by *in situ* cruises and observations. The modelling results served to study seasonal and interannual evolution of the sea surface salinity including the Western Iberia Buoyant Plume (WIBP) patterns and its interaction with the feature described in this document as the Western Iberia Central Plume (WICP) resulting from the Tagus-Sado estuaries contribution. Modelling results were used, in combination with observed data, to analyse an extreme runoff event during April 2013. The extension of the plume influence on the salinity fields were evaluated for wet (downwelling dominated) and dry (upwelling dominated) seasons.

## 7.1. Introduction

Rivers discharges exert a strong influence in their neighbouring coastal area in several ways, modifying the water stratification (Garvine and Witney, 2006), introducing significant fluctuations in circulation patterns and modulating the impact of upwelling events (Santos *et al.*, 2007; Banas *et al.*, 2009). They induce convergent areas near their discharge area, regulate the alongshore transport and exchange properties with the outer shelf while creating nutrient rich areas and food for fish larvae (Santos *et al.*, 2007; Ribeiro *et al.*, 2005).

Traditionally, operational regional ocean models have, in general, disregarded the land-ocean boundary conditions or have included river flow or runoff climatologies using simple approximations such as adding them directly or, to simulate the estuarine mixing, through excavated channels in the modelling grid. Several limitations for achieving realistic land-ocean boundary conditions contribute to the current state-of-the-art including the absence or difficult access to operational river runoff data, the local-specific estuary features (tidal prisms, residence time, etc.) that modify the fresh water properties, the need to take into consideration processes with different time scales, such as spring-neap and flood-ebb tides and river runoff variability. In addition, estuary plumes have been generally regarded more as a local coastal feature influencing only the estuary surrounding waters than a regional ocean scale feature.

In recent times, watershed modelling results have emerged as a possibility to provide accurate land-boundary conditions and to substitute traditionally used river climatologies. However, both products,

river climatologies and watershed models, have their own limitations. River climatologies main weakness is the incapacity to include the interannual variability compared to watershed model applications which, in general, follow the main river flow trends (Campuzano *et al.*, 2016). On the other hand, watershed models tend to overestimate river flows, especially during dry seasons when due to reduced availability of fresh water, human management activities such as dams' retention, irrigation, human consumption, etc., alter more intensively the natural river flow (Campuzano *et al.*, 2016).

Accurate land-ocean boundary conditions that represent satisfactorily the regional ocean salinity fields is a common challenge for the modelling community. Two recent analysis of regional operational model applications from the EU Copernicus Marine Environment Monitoring Services (CMEMS MFC) for the Atlantic-Iberian Biscay Irish waters (IBI) and the European North West Shelf (NWS) can aid to illustrate the current land-boundary conditions in state-of-the-art operational applications. For instance, Aznar *et al.* (2016) when evaluating the IBI system detected that salinity was the least accurate property of the twelve modelled variables due to the large uncertainties regarding the runoff and river discharge forcing. The NWS system will revert back to climatological river flow (Graham *et al.*, in review) since it was detected a significant excess of fresh water in the German Bight region (O'Dea *et al.*; 2016).

From the monitoring point of view, operational salinity sensors in coastal areas are scarce and Earth Observation products (EO) can only provide some indirect information related to fresh water inputs in coastal areas. EO Sea Surface Temperature (SST) is able to identify the thermal signature associated to the rivers discharge only during periods when contrasting temperatures between the fresh water and the surrounding waters, i.e. colder/warmer river discharges during winter/summer than the receiving environment. This signature rapidly disappear as the shallow and stable water lens adopts the surrounding waters temperature (Ribeiro *et al.*, 2005). EO Sea Surface Salinity products (SSS) such as Aquarius (Lagerloef *et al.*, 2012) and SMOS (Soil Moisture and Ocean Salinity; Boutin *et al.*, 2013) are nowadays giving their first steps in providing near ocean salinity fields however it is currently unable to provide river plume gradients except for large dimension rivers such as the Amazon (Grodky *et al.*, 2014), Congo (Hopkins *et al.*, 2013) or Mississippi (Gierach *et al.*, 2013) rivers. For that reason, monitoring SSS using SMOS data in western Iberia is challenging due to the initial resolution, typically 30-100 km, and because of the contamination by the nearby land, especially in the first 36 km from the coast (Zine *et al.*, 2007). However, future for EO SSS products is promising as was shown in this thesis.

In western Iberia, the relatively recent detection and description of a significant regional feature associated to fresh water inputs increased the attention to this subject from the oceanographic point of view. The Western Iberia Buoyant Plume (WIBP; Péliz *et al.*, 2002) is an all-year-round low salinity water lens that extends along the Northwest Iberia coastal area due to the accumulation of several fresh water sources, such as the Douro, Minho and Mondego rivers along with other smaller rivers and the Galician Rias. According to Brito *et al.* (2015), the area comprised between the Mondego and the Minho River (Figure 1) receives around  $45000 \text{ Hm}^3\text{year}^{-1}$  corresponding to 55% of the total volume of water discharged in the Portuguese coast. Since its first description, the WIBP has been subject of the several research studies related to ocean productivity (i.e. Ribeiro *et al.*, 2005; Picado *et al.*, 2014) and larvae and eggs dispersal (i.e. Santos *et al.*, 2004, 2006 and 2007; Peliz *et al.*, 2007; Queiroga *et al.*, 2007).

Some previous modelling studies have investigated the WIBP behaviour under seasonal conditions. Peliz *et al.* (2007), implementing the Tagus, Minho and Mondego rivers with fixed values for flow, salinity and temperature to simulate spring conditions. Otero *et al.* (i.e. 2008, 2009 and 2013) have studied the WIBP plumes evolution focusing in the north-western Iberia region with its southern limit at the Douro River during autumn-winter conditions. In these studies, fourteen rivers were incorporated through eleven 10 m depth channels excavated in the coastal model. Mendes *et al.* (2016) and Souza *et al.* (2014a and 2014b) investigated the link between the Douro and Minho rivers

with the Galician rias. However, most of these studies focused on data at isolated locations along the coast and during short periods of time, providing a localized knowledge (Picado *et al.*, 2014).

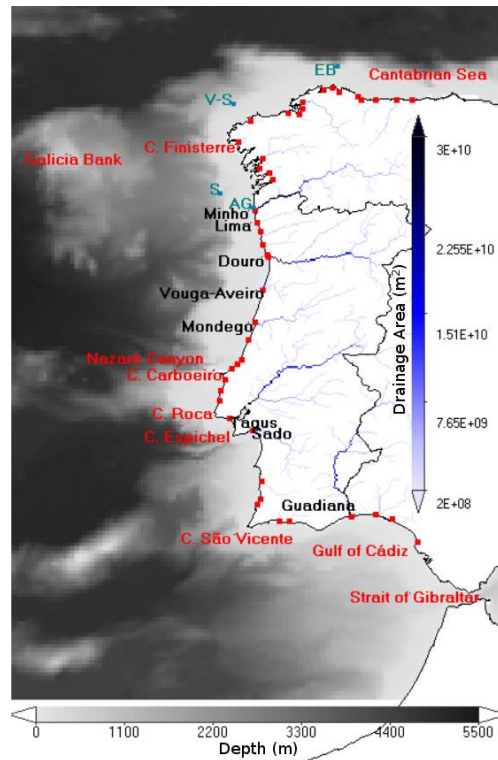


**Figure 1.** Portugal domain bathymetry from the PCOMS application and drainage area from the MOHID Land WI domain. The location of the 44 river discharges implemented in the PCOMS are marked with red squares (Table I) and the rivers implemented with estuarine applications include their name next to its discharge location. Some ocean and coastal features from the Western Iberia region are displayed in red. The monitoring buoys used for model validation are displayed in light blue using an acronym: EB - Estaca de Bares, V-S – Villano-Sisargas, S - Silleiro Buoy and AG - A Guarda.

In this chapter, the impact of the numerical implementation of 44 rivers, eight of them using estuarine model applications, in a regional model for western Iberia will be analysed for the period 2011-2015. To the author knowledge, this is the first study of its kind covering the entire western Iberia regional ocean and using realistic estuarine boundary conditions able to analyse the annual and interannual seasonality.

The main objective of the present research and of the methodology described in Campuzano *et al.* (2016) was to explore the capacity to improve the thermohaline circulation in coastal areas by a better characterisation of the land-ocean boundary conditions, with special regard to the salinity fields. This is the final chapter of a set of research publications where the different components of the methodology (Campuzano *et al.*, 2016) were analysed including the adaptation and implementation of state-of-the-art hydrological models to multicatchment modelling domains (Brito *et al.*, 2015) and the off-line extraction and analysis of estuarine fluxes properties in order to be integrated, including their temporal evolution, into regional mesoscale grids (Campuzano *et al.*, 2018).

## 7.2. Material and Methods

### 7.2.1. Numerical modelling

In this chapter the regional ocean model for western Iberia PCOMS (Portuguese Coast Operational Modelling System; Mateus *et al.*, 2012) was coupled in an offline mode with estuarine and watershed modelling applications in order to evaluate their impact in the thermohaline circulation fields. The PCOMS is a 3D full baroclinic hydrodynamic and ecological regional ocean model application that

downscales the Mercator-Océan PSY2V4 North Atlantic solution (Drillet *et al.*, 2005) using the MOHID Water model (<http://www.mohid.com>; Neves, 2013).

The PCOMS system is composed of two nested domains: WestIberia (2D) and Portugal (3D) covering the Iberian Atlantic coast and its contiguous ocean with a horizontal resolution of 0.06° populated with bathymetric information derived from the EMODnet Hydrography portal (<http://www.emodnet-hydrography.eu>). The WestIberia domain covers the area limited the following range of latitudes (33.48 °N, 45.90 °N) and longitudes (4.20 °W, 13.50 °W) resulting in a grid of 207 x 155 cells. The Portugal domain, hereafter referred as PCOMS (Figure 1), covers the area comprised by the latitudes (34.38 °N, 45.00 °N) and the longitudes (5.10 °W, 12.60 °W) resulting in a grid of 177 x 125 cells. The vertical discretisation consists on a mixed vertical geometry composed of a sigma domain with 7 layers from the surface until 8.68 m depth, with variable thickness decreasing up to 1 m at the surface, on top of a Cartesian domain with 43 layers with thickness increasing towards the bottom. Tides are forced using the global tide solution FES2012 along the open ocean boundary (Carrère *et al.*, 2013). The PCOMS 3D domain used, as atmospheric boundary conditions, MM5 model results (Grell *et al.*, 1994) with a horizontal resolution of 9 km provided by the IST meteorological group (<http://meteo.tecnico.ulisboa.pt>; Trancoso, 2012).

At the watershed level, the MOHID Land model (Brito *et al.*, 2015) estimates operationally water flow and associated properties (i.e. temperature, oxygen and nutrient concentrations) for the main river catchments discharging in the Western Iberia coast. Two domains with different horizontal spatial resolution and covered area were designed to represent adequately the Portuguese catchments, 2 km resolution domain covering Western Iberia (MOHID Land WI domain), and to cover the spatial scale of the large trans-boundary rivers as the Tagus, Douro and Guadiana rivers that discharge in Western Iberia, 10 km resolution domain covering the Iberian Peninsula (MOHID Land IP domain).

The main objective of this chapter, and one of this thesis, was to implement the land-ocean boundary conditions following the methodology described in Campuzano *et al.* (2016) in the Western Iberia regional ocean model. A total of 44 rivers were implemented in the PCOMS regional ocean model (Figure 1, Table I). Eight of them, ordered from North to South: Minho, Lima, Douro, Vouga (Ria de Aveiro), Mondego, Tagus, Sado and Guadiana, were included as estuarine fluxes in the regional ocean application. Detailed information related to the estuarine models, their forcing and the cross-section location where fluxes were obtained can be found in Campuzano *et al.* (2018). The other 36 rivers were imposed directly in the regional model as continuous discharges using flow and temperature from the MOHID Land watershed model application (Brito *et al.*, 2015). The salinity of these rivers was defined as constant with a value of 32. This value can be regarded as conservative since it corresponds to the average salinity for well-mixed rivers in large estuaries, such as Aveiro, Tagus or Sado estuaries (Campuzano *et al.*, 2018). This approach was adopted to take into consideration the tendency of watershed models to overestimate flows and avoid the excess of fresh water. For this reason, the salinity signature from some large rivers in the regional model, such as the Guadalquivir River, could be underrepresented.

In the case of estuarine discharges, once the fluxes were calculated in Campuzano *et al.* (2018), water flow and properties from each cell were coupled in an off-line mode to the corresponding land-ocean boundary cell in the PCOMS domain. In the case of a 3D estuarine model application, i.e. the Tagus estuary application (Campuzano *et al.*, 2012; hereafter referred as Tagus Mouth), the fluxes were obtained for each vertical layer and injected in the PCOMS corresponding vertical layer. Each time series from each layer was inputted as a discharge input file in the corresponding vertical layer until reaching the bottom of the receiving model, 10 m in this particular case. The vertical correspondence between the PCOMS and the Tagus Mouth model grids allow to add the fluxes from each estuarine layer in the corresponding layer of the PCOMS domain and thus providing the implementation of an effective off-line 3D boundary condition. For the 2D estuarine model applications, hourly fluxes were imposed in the surface layer. This methodology could be applied to 2D or 3D estuarine models,

obtaining a set of time series files independent from the receiving model and allowing to extract the information from previous modelling results in a delayed mode.

**Table I. River name, coordinates, sources of land-ocean boundary conditions including 2D or 3D estuarine fluxes and model results from the West Iberia domain (MOHID Land WI domain) and Iberian Peninsula domain (MOHID Land IP domain) described in Brito *et al.* (2015).**

River	Latitude	Longitude	Source
Landro	43.77 °N	7.59 °W	MOHID Land WI domain
Mera	43.77 °N	7.83 °W	MOHID Land WI domain
Sor	43.77 °N	7.65 °W	MOHID Land WI domain
Ouro	43.65 °N	7.29 °W	MOHID Land WI domain
Eo	43.59 °N	7.05 °W	MOHID Land WI domain
Esva	43.59 °N	6.45 °W	MOHID Land WI domain
Xuvia	43.59 °N	8.25 °W	MOHID Land WI domain
Masma	43.59 °N	7.23 °W	MOHID Land WI domain
Navia	43.59 °N	6.75 °W	MOHID Land WI domain
Eume	43.41 °N	8.37 °W	MOHID Land WI domain
Mandeo	43.41 °N	8.37 °W	MOHID Land WI domain
Mero	43.41 °N	8.37 °W	MOHID Land WI domain
Anllóns	43.23 °N	9.03 °W	MOHID Land WI domain
Xallas	42.93 °N	9.33 °W	MOHID Land WI domain
Ulla	42.51 °N	8.97 °W	MOHID Land WI domain
Umia	42.51 °N	8.97 °W	MOHID Land WI domain
Lérez	42.33 °N	8.85 °W	MOHID Land WI domain
Verdugo	42.21 °N	8.85 °W	MOHID Land WI domain
Minho	41.85 °N	8.91 °W	2D Estuarine fluxes
Lima	41.67 °N	8.85 °W	2D Estuarine fluxes
Ave	41.31 °N	8.79 °W	MOHID Land WI domain
Leça	41.19 °N	8.73 °W	MOHID Land WI domain
Douro	41.13 °N	8.67 °W	2D Estuarine fluxes
Vouga (Aveiro)	40.65 °N	8.79 °W	2D Estuarine fluxes
Mondego	40.17 °N	8.91 °W	2D Estuarine fluxes
Lis	39.87 °N	9.03 °W	MOHID Land WI domain
Alcobaça	39.61 °N	9.08 °W	MOHID Land WI domain
Tornada	39.51 °N	9.21 °W	MOHID Land WI domain
Arnoia	39.45 °N	9.27 °W	MOHID Land WI domain
Grande	39.27 °N	9.39 °W	MOHID Land WI domain
Sizandro	39.09 °N	9.45 °W	MOHID Land WI domain
Lizandro	38.97 °N	9.45 °W	MOHID Land WI domain
Tagus	38.67 °N	9.27 °W	3D Estuarine fluxes
Sado	38.43 °N	8.85 °W	2D Estuarine fluxes
Mira	37.71 °N	8.85 °W	MOHID Land WI domain
Seixe	37.47 °N	8.85 °W	MOHID Land WI domain
Aljezur	37.35 °N	8.91 °W	MOHID Land WI domain
Guadiana	37.17 °N	7.41 °W	2D Estuarine fluxes
Piedras	37.17 °N	7.05 °W	MOHID Land WI domain
Odiel	37.11 °N	6.87 °W	MOHID Land WI domain
Tinto	37.11 °N	6.87 °W	MOHID Land WI domain
Alcantarilha	37.05 °N	8.37 °W	MOHID Land WI domain
Arade	37.05 °N	8.49 °W	MOHID Land WI domain
Guadalquivir	36.81 °N	6.45 °W	MOHID Land IP domain

The MOHID Water model allows the input of positive and negative flows and by following this approach the intermittent fluxes, due to the tidal signal, from the estuarine model were imposed in the boundary cells of the PCOMS regional ocean model. Figure 2 represents schematically the fluxes calculation performed in the estuarine model application, that are later imposed in estuary-ocean interface.  $H$ , in the diagram, represents the constant bathymetric depth for a horizontal cell related to the hydrographic zero while  $h_t$  corresponds to the free surface that varies in time mainly due to the atmospheric and astronomic tides.  $h'_t$  is the sum of both the permanent and the variable heights that is decomposed in several layers according to the vertical geometry of the model. Thus, each cell

vertical dimension  $h_{a,t}$  ( $a$  representing the number of the vertical layer) would evolve in time while the cell horizontal dimensions ( $\delta x$  and  $\delta y$ ) are constant. With these values, the instantaneous volume for each cell ( $V_{a,t}$ ) can be obtained, and by multiplying it with the cross-section velocity, the corresponding instantaneous flow ( $F_{a,t}$ ) would be obtained. The flow value has positive sign during ebb periods and negative during flood periods. The instantaneous concentration ( $C_{e_{a,t,i}}$ ) for any water property  $i$  (i.e. temperature, salinity, nutrients, etc.) associated to the instantaneous flow corresponds to the estuarine value calculated by the model at each cell centre. During flood conditions the water volume and properties are subtracted from the PCOMS discharging cell using the concentrations obtained from the estuary fluxes ( $C_{e_{a,t,i}}$ ). Originally in the MOHID model code, when the discharged flow was negative the value of the subtracted property was obtained from the receiving environment. This condition generated an inconsistency in the model results increasing numerically the salinity around the discharge area.

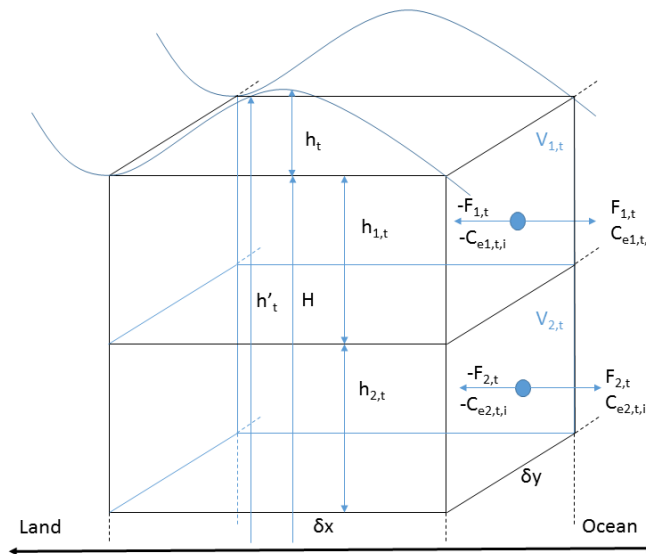


**Figure 2.** Diagram representing the flow and concentration calculations performed in the estuary model cross-section cells that is imposed as land boundary conditions in the regional ocean model.  $\delta x$  and  $\delta y$  correspond to the cell horizontal dimensions while the cell horizontal dimensions while  $H$  correspond to the constant depth for each cell.  $h_t$  corresponds to the instantaneous value of the free surface that varies in time and  $h'_t$  is total depth that is decomposed in several layers  $h_{a,t}$  ( $a$  representing the number of the vertical layer from top to bottom) according to the vertical geometry of the model.  $V_{a,t}$  is the instantaneous volume that multiplied by the instantaneous velocity provides each cell instantaneous flow ( $F_{a,t}$ ).  $C_{e_{a,t,i}}$  stands for the estuarine concentration for each water property  $i$  (i.e. temperature, salinity).

During this work, the wind drag coefficient  $C_d$  implemented in the MOHID water model was updated by including the modifications for low wind speeds considered in Trenberth *et al.* (1990) to the general parameterisation proposed by Large and Pond (1981) (Equation 1):

$$\begin{cases} 2.18 \cdot 10^{-3} & \text{if } |U| \leq 1 \text{ ms}^{-1} \\ \left(0.62 + \frac{1.56}{|U|}\right) \cdot 10^{-3} & \text{if } 1 \text{ ms}^{-1} < |U| < 3 \text{ ms}^{-1} \\ 1.14 \cdot 10^{-3} & \text{if } 3 \text{ ms}^{-1} \leq |U| < 10 \text{ ms}^{-1} \\ (0.49 + 0.065|U|) \cdot 10^{-3} & \text{if } 10 \text{ ms}^{-1} \leq |U| < 26 \text{ ms}^{-1} \\ 2.18 \cdot 10^{-3} & \text{if } |U| > 26 \text{ ms}^{-1} \end{cases} \quad \text{Equation 1}$$

This new parameterisation has an impact in the upwelling/downwelling extension since it provide less weight to winds between 3 and 10  $\text{ms}^{-1}$  (Figure 3) compared to the previous parameterisation programmed in MOHID (Equation 2):

$$\begin{cases} 1.20 \cdot 10^{-3} & \text{if } |U| \leq 4 \text{ ms}^{-1} \\ 1.20 \cdot 10^{-3} & \text{if } 4 \text{ ms}^{-1} < |U| < 11 \text{ ms}^{-1} \\ (0.49 + 0.065|U|) \cdot 10^{-3} & \text{if } 10 \text{ ms}^{-1} \leq |U| < 26 \text{ ms}^{-1} \\ 2.18 \cdot 10^{-3} & \text{if } |U| > 26 \text{ ms}^{-1} \end{cases} \quad \text{Equation 2}$$

Since Large and Pond (1981) is not applicable for winds under  $4 \text{ ms}^{-1}$  or above  $26 \text{ ms}^{-1}$ , constant values were assumed in the previous version (Equation 2). The upper limit were maintained in the new formulation (Equation 1). This newly implemented parameterisation has been adopted in other research studies such as Friedland *et al.* (2007) and Relvas and Barton (2005).

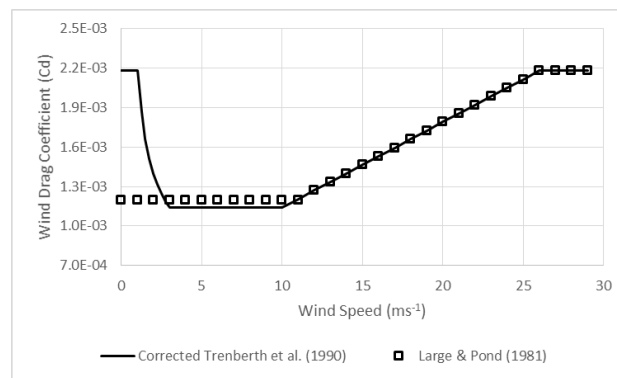


**Figure 3. Drag coefficient evolution with wind speed according to the pure Large and Pond (1981) parameterisation and the version corrected for low velocities by Trenberth *et al.* (1990).**

This integrated water cycle modelling approach, including catchment, estuary and ocean, was simulated from February 2010 until the end of 2015. In order to leave a period for reaching equilibrium, only the complete years will be taken into consideration for the evaluation period i.e. 2011-2015 period. The MOHID version for the PCOMS simulations was a release double precision 64 bits with no code parallelisation (i.e. OpenMP or MPI multiprocessor interfaces).

## 7.2.2. *In situ* observations

The validation of the modelling results in Western Iberia open ocean waters will be restricted to punctual cruises and to multiparametric buoys located in Spanish waters, near the northern Portuguese boundary, and equipped with salinity sensors since permanent monitoring stations observing salinity are absent/unavailable in the Region of Fresh Water Influence (ROFI) in Portugal.

### 7.2.2.1. IPMA Cruises

Salinity and temperature collected during two cruises performed during the spring season of 2011 and 2015, hereafter referred as PELAGOS11 and PELAGOS15 cruises respectively, by the Portuguese Institute for Sea and Atmosphere, I. P. (IPMA, on its Portuguese acronym) provided to the author by M.M. Angélico and P. Oliveira will aid to evaluate the modelling results.

Both cruises correspond to the spring acoustic surveys performed onboard of IPMA R/V “Noruega” to evaluate the small pelagic fish abundance in the continental shelf waters of the ICES Division IXa which covers mainland Portugal and the Gulf of Cádiz. The PELAGOS surveys focus on the continental platform area limited offshore approximately by the 200 m isobath. Cruises started near the northern limit of Portuguese waters and moved southwards describing a zigzag track until reaching the vicinity of the Strait of Gibraltar. The PELAGOS11 cruise took place from 19<sup>th</sup> April to 16<sup>th</sup> May 2011 (Figure 4) and the PELAGOS15 took place from 13<sup>th</sup> April to 18<sup>th</sup> May 2015 (Figure 5). During the PELAGOS15 survey, along with the CTD profiles, SSS and SST continuous records, four minutes interval, were collected using an onboard thermosalinograph (TSG) in the northern sector of the cruise until around 38.2°N (Figure 6, Table V).

### 7.2.2.2. Multiparametric buoys

As mentioned in the Chapter IV, some multiparametric buoys located in Spanish waters are equipped with salinity sensors. From those stations, three open water buoys and one coastal buoy were selected for comparing with the integrated modelling method results. The coastal buoy of A Guarda is the southernmost station and is located in the vicinity of the Minho estuary mouth while the other three buoys are moored in open ocean conditions (Table II). Hourly observations for these stations covering the 2011-2015 period were obtained through the In Situ Thematic Assemble Centre (INS-TAC) of the Copernicus Marine Environment Monitoring Service (CMEMS; <http://marine.copernicus.eu/>).

**Table II. List of multiparametric buoys used in this study indicating their location and the available data period. The superscript next to the station name indicates the institution responsible for the multiparametric buoy: <sup>1</sup> stations maintained by Puertos del Estado (Spain) and <sup>2</sup> stations maintained by Xunta Galicia/MeteoGalicia/IM (Spain). Coastal stations are indicated with \*.**

Buoy	Latitude	Longitude	Depth (m)	Period Available
Estaca de Bares <sup>1</sup>	44.06 °N	7.62 °W	1800	01/01/2010 - 31/12/2015
Villano-Sisargas <sup>1</sup>	43.49 °N	9.21 °W	386	01/01/2010 - 31/12/2015
Silleiro <sup>1</sup>	42.12 °N	9.40 °W	600	01/01/2010 - 31/12/2015
A Guarda <sup>2,*</sup>	41.90 °N	8.90 °W	40	14/06/2011 - 31/12/2015

## 7.3. Results

### 7.3.1. Model validation

#### 7.3.1.1. IPMA Cruises

In order to evaluate the accuracy of the modelling results obtained by the proposed methodology, temperature and salinity values were obtained at the surface layer for the closest time and location to the PELAGOS monitored positions from the PCOMS and MERCATOR modelling results. The MERCATOR application produce daily outputs, while PCOMS results are hourly, and was used as the reference solution. Due to the horizontal spatial resolution of the modelling domains, some monitoring positions were excluded from the analysis as they fell in modelling land cells.

Although both monitoring cruises took place during similar dates, the 2011 campaign registered, in general, warmer SST and lower SSS in the proximity of the river mouths when compared with the 2015 campaign. Both cruises took place during months out of upwelling-dominated season and for this reason the across-shore temperature is relatively constant and the main source of SST variability is related to the meridional SST gradient.

Figure 4 shows the PCOMS and MERCATOR temperature and salinity values corresponding to the PELAGOS11 cruise. Slight salinity differences can be found between the two modelling results in the WIBP area and near the Tagus estuary ROFI where PCOMS results are fresher than MERCATOR values. Some minor SST differences can also be identified in the WIBP region and in the Gulf of Cádiz. In this case MERCATOR temperature is warmer when compared with the PCOMS results on those regions.

When compared with the PELAGOS11 observed values, the PCOMS salinity results present the same salinity patterns with a meridional SSS gradient and the presence of two low salinity areas corresponding to the Tagus estuary plume, including its transport towards the north, and the WIBP in the northern sector. The MERCATOR solution presents a continuous land-ocean salinity gradient in the northern sector with no particular spatial structure and the Tagus estuary plume is non-detectable. Regarding the SST, field observations describe a meridional gradient between 15 and 21°C approximately (Table III). Two other features can be distinguished from this gradient: the presence of slightly colder water in the northern sector coastal areas and the warmer temperatures in the inner

area of the Gulf of Cádiz. Both regional ocean models present a similar meridional gradient with slightly lower SST in the PCOMS application. They also reproduce the presence of the warmer waters in the Gulf of Cádiz and in the PCOMS case the signature of the river colder water can be also distinguished.

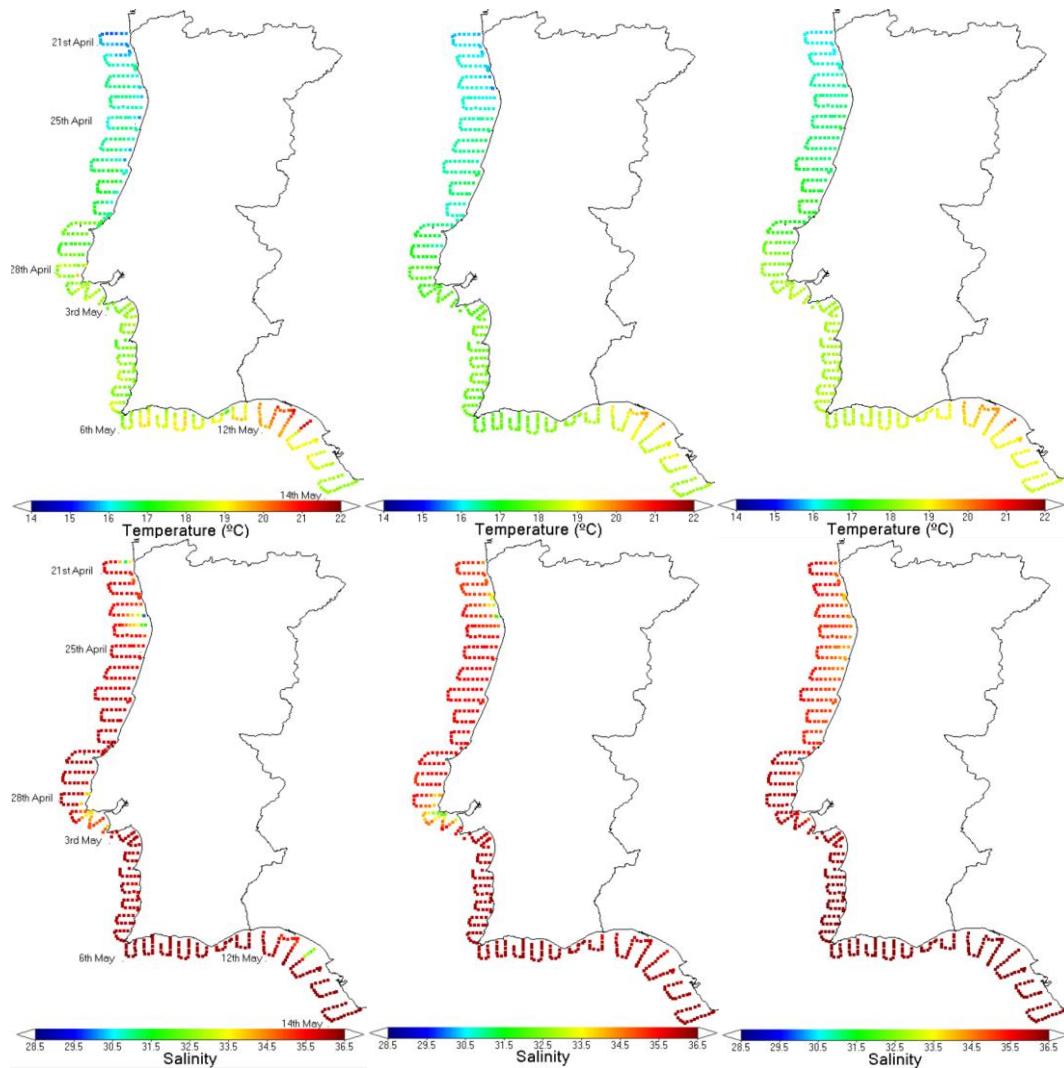


Figure 4 PELAGOS11 surface temperature (top row) and salinity (bottom row) observed with CTD during the cruise (left) and obtained from the PCOMS (centre) and MERCATOR (right) modelling results.

Table III. SST and SSS mean, minimum and maximum values observed during the PELAGOS11 cruise and calculated by the PCOMS and MERCATOR numerical model applications. Statistic indexes, including coefficient of determination ( $R^2$ ), bias and Root Mean Square Error (RMSE), comparing each modelling results set and the observed values are also listed. The number of valid values is indicated within brackets.

	Temperature (°C) (N=466)				Salinity (N= 466)			
	Mean (Min.-Max.)	$R^2$	Bias	RMSE	Mean (Min.-Max.)	$R^2$	Bias	RMSE
PCOMS	17.34 (15.49-19.90)	0.87	-0.44	0.66	35.66 (31.86-36.36)	0.38	-0.14	0.67
MERCATOR	17.83 (15.87-20.38)	0.89	0.05	0.42	35.87 (33.88-36.43)	0.17	0.08	0.77
PELAGOS11	17.78 (15.25-21.40)	-	-	-	35.80 (29.90-36.43)	-	-	-

SST MERCATOR and PCOMS obtained similar metrics (Table III) when compared with the PELAGOS11 cruise. MERCATOR presented slightly better coefficients of determination ( $R^2$ ), bias and root mean square error (RMSE). On the other hand, SSS metrics from the PCOMS version with implemented river inputs are quantitatively better than MERCATOR values, with  $R^2$  values more than double than

MERCATOR and lower RMSE. In addition, the PCOMS SSS minimum value was closer to the observed SSS minimum.

In the PELAGOS15 campaign, observations were performed using two methods, CTD and an onboard thermosalinograph (TSG) in the northern sector of the cruise until approximately 38.2°N. This cruise monitored the western Iberia waters southwards during most of the monitoring period except for the Spanish part of the Gulf of Cádiz that was performed northwards. The CTD and TSG datasets show good SST and SSS data consistency and the clear advantage of the latter is to provide higher data density (Figure 5 and Figure 6). SST and SSS for the locations of both datasets were obtained for PCOMS and MERCATOR (Figure 5 and Figure 6). SST during the cruise display a meridional gradient that in their northern sector (Tagus estuary northwards) include some mesoscale structures that were not captured by the model applications. As in the previous campaign, the inner part of the Gulf of Cádiz present warmest waters. It should also be taken into consideration that this region was the last monitored region with one month of difference respect the northernmost monitored waters.

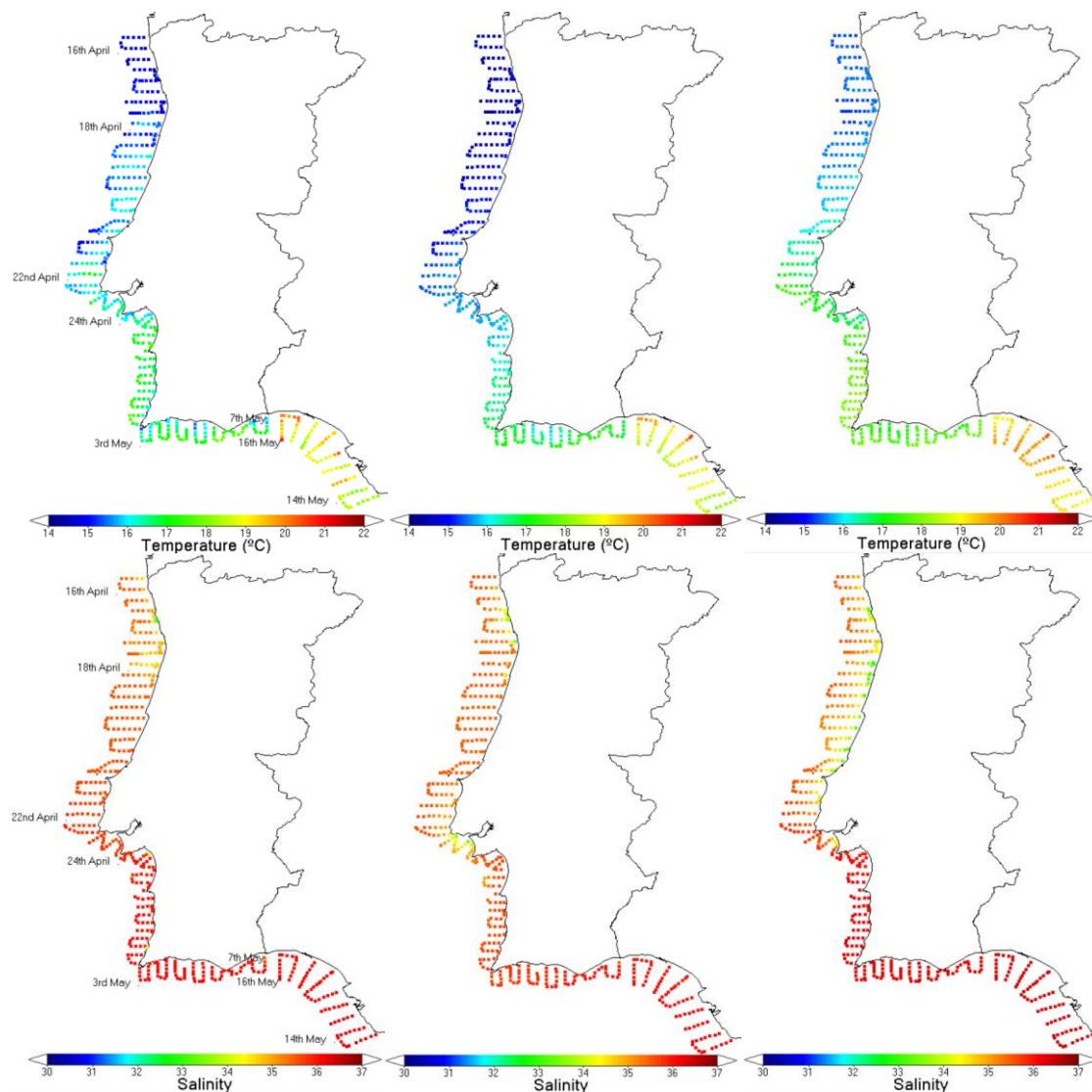


**Figure 5** PELAGOS15 surface temperature (top row) and salinity (bottom row) observed with CTD during the cruise (left) and obtained from the PCOMS (centre) and MERCATOR (right) modelling results.

In this cruise, the SST metrics of the PCOMS application obtains better values than MERCATOR (Table IV). However, the SSS performance is lower than MERCATOR modelling results. Surface salinity data collected during the monitoring campaign showed the typical WIBP signature on its northern sector, however the Tagus estuary signature was not detected. In the PCOMS modelling results both signals

the WIBP, with a similar pattern than in the campaign, and a well-defined Tagus plume can be observed. The Tagus plume appears in the PCOMS model due to a failure in the hydrometric monitoring station, the Almourol station, upstream the Tagus River and used as source data to force the river flow in TagusMouth 3D estuarine model application as described in Campuzano *et al.* (2018). The hydrometric station was out of service from 17<sup>th</sup> of December 2014 until 15<sup>th</sup> of May 2015 and under these circumstances the estuarine operational modelling service uses the last river flow data available to force the model. Apparently, river discharges during the PELAGOS15 campaign were lower than the imposed value and this incident with the forcing data can explain the difference between the observed and modelled PCOMS results. Except for this area, the salinity pattern is very similar to the PELAGOS15 cruise observed data when compared with the MERCATOR salinity pattern that shows a zonal salinity gradient between the WIBP and the Tagus estuary not found in the monitoring campaign. The RMSE values indicate that the difference between PCOMS and the cruise data is lower than when compared with the MERCATOR modelling results.

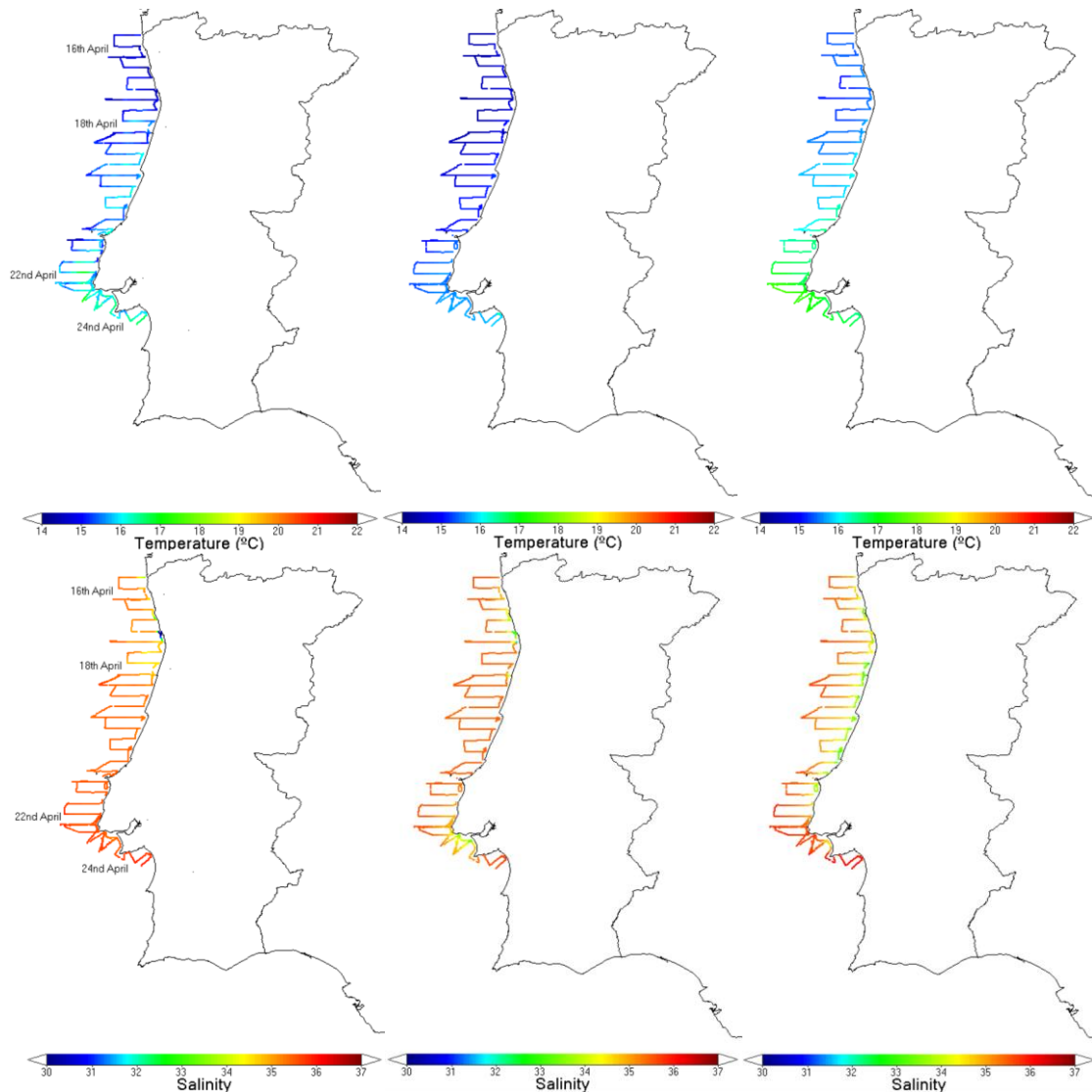


**Figure 6** PELAGOS15 sea surface temperature (top row) and salinity (bottom row) observed with TSG during the cruise (left) and obtained from the PCOMS (centre) and MERCATOR (right) modelling results.

When the PCOMS and MERCATOR modelling results are compared with the TSG data from the same survey, the coefficient of determination decrease for both numerical products since the spatial resolution of the modelling products are not able to represent some of the SST mesoscale structures and the river plumes with the same detail than the observed values (Figure 6). However, in this case

the PCOMS show a slightly better coefficient of determination, bias and RMSE than MERCATOR for SST and SSS (Table V).

**Table IV. SST and SSS mean, minimum and maximum values observed during the PELAGOS15 cruise and calculated by the PCOMS and MERCATOR numerical model applications. Statistic indexes, including coefficient of determination ( $R^2$ ), bias and Root Mean Square Error (RMSE), comparing each modelling results set and the observed values are also listed. The number of valid values is indicated within brackets.**

	Temperature (°C) (N=449)				Salinity (N= 449)			
	Mean (Min.-Max.)	$R^2$	Bias	RMSE	Mean (Min.-Max.)	$R^2$	Bias	RMSE
<b>PCOMS</b>	16.09 (14.15-20.49)	0.89	-0.38	0.62	35.53 (31.73-36.23)	0.40	-0.20	0.45
<b>MERCATOR</b>	17.07 (15.21-20.43)	0.84	0.61	0.83	35.61 (32.88-36.43)	0.55	-0.12	0.57
<b>PELAGOS15</b>	16.46 (14.07-20.98)	-	-	-	35.73 (32.46-36.33)	-	-	-

**Table V. SST and SSS mean, minimum and maximum values observed using a thermosalinograph (TSG) during the PELAGOS15 cruise and calculated by the PCOMS and MERCATOR numerical model applications. Statistic indexes, including coefficient of determination ( $R^2$ ), bias and Root Mean Square Error (RMSE), comparing each modelling results set and the observed values are also listed. The number of valid values is indicated within brackets.**

	Temperature (°C) (N=2669)				Salinity (N= 2669)			
	Mean (Min.-Max.)	$R^2$	Bias	RMSE	Mean (Min.-Max.)	$R^2$	Bias	RMSE
<b>PCOMS</b>	14.96 (14.14-16.34)	0.67	-0.45	0.57	35.16 (29.64-35.68)	0.15	-0.16	0.65
<b>MERCATOR</b>	16.05 (14.98-17.56)	0.58	0.66	0.97	34.93 (32.70-36.17)	0.09	-0.35	1.52
<b>PELAGOS15</b>	15.41 (13.99-17.21)	-	-	-	35.32 (30.01-35.92)	-	-	-

### 7.3.1.2. Multiparametric buoys

In this section, only the PCOMS results were compared with hourly records of temperature, Figure 7 and Table VI, and salinity, Figure 8 and Table VII, collected continuously by the moored stations. Due to the high temporal frequency and the possibility of sensor outliers, the 5<sup>th</sup> and 95<sup>th</sup> percentile values were used instead of minimum and maximum respectively.

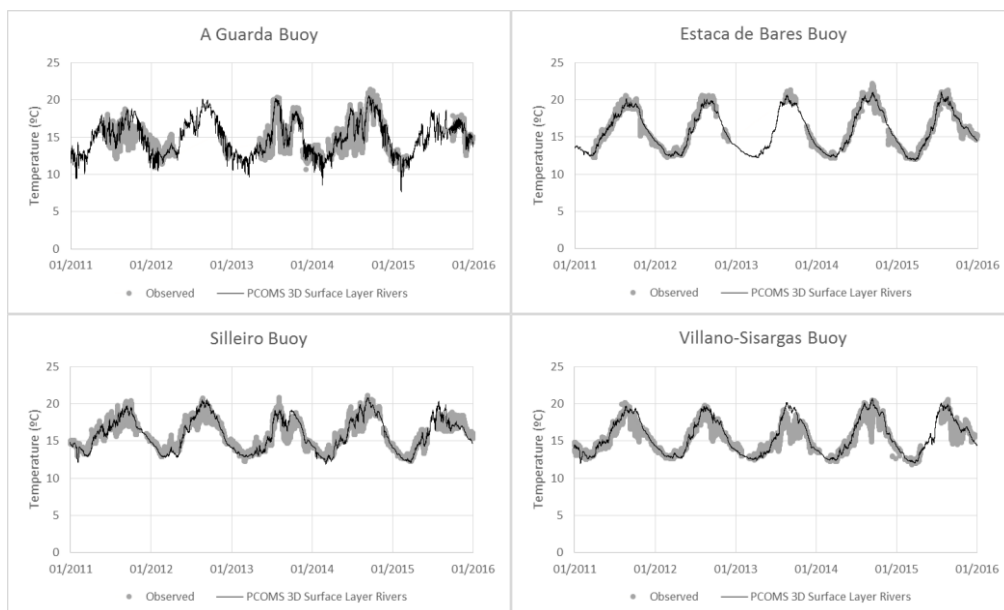


**Figure 7 Sea surface temperature observed (grey dots) and modelled (solid black line) by A Guarda (top row left), Estaca de Bares (top row right), Silleiro (bottom row left) and Villano-Sisargas (bottom row right) multiparametric buoys in for the 2011-2016 period.**

In Figure 7 it can be observed how the most influenced stations by the WIBP and upwelling events are the A Guarda and Silleiro buoys. The coastal station shows how the increase in summer temperature is interrupted by upwelling events with different intensities depending on the year. PCOMS model results simulate the temperature curve successfully though it seems to present colder temperatures than observed during some winter periods. This difference could be due to low river temperature modelled during this season in this area, and should be further investigated. Regarding the off-shore buoys, upwelling conditions effect on observed temperature decreases northwards. Estaca de Bares buoy, located in the North of the IP, and Villano-Sisargas buoy, located well-offshore from the western Iberian coast, present a relatively regular temperature cycle. The Silleiro buoy present a less smooth curve when compared with the other offshore buoys. During strong upwelling conditions, such as in summer 2013, Silleiro recorded temperature present the same seasonal disruption as A Guarda buoy. Table VI lists some statistics for the observed and modelled water temperature where it can be seen the good fit between the mean, range,  $R^2$ , Bias and RMSE.  $R^2$  is higher than 0.70 for all the stations and higher than 0.88 when only considering the offshore buoys.

**Table VI. Mean, minimum ( $P_{05}$ ) and maximum ( $P_{95}$ ) sea temperature observed by the multiparametric buoys and obtained by the PCOMS model for the period 2001-2015. Statistic indexes, including coefficient of determination ( $R^2$ ), bias, Root Mean Square Error (RMSE) were obtained comparing the PCOMS dataset with the observed values are also listed. The number of valid values (N) is also indicated.**

Buoy Name	Mean Observed Temperature (°C) ( $P_{05}$ - $P_{95}$ )	Mean Modelled Temperature (°C) ( $P_{05}$ - $P_{95}$ )	$R^2$	Bias (°C)	RMSE (°C)	N
A Guarda	14.90 (12.10-19.21)	15.19 (11.85-19.10)	0.73	0.29	1.55	24796
Estaca de Bares	16.27 (12.40-20.40)	16.21 (12.42-20.06)	0.99	-0.06	0.18	31170
Villano-Sisargas	15.47 (12.60-19.10)	15.81 (12.54-19.52)	0.88	0.33	0.89	38161
Silleiro	15.84 (13.00-19.20)	15.80 (12.67-19.60)	0.89	-0.04	0.61	40377

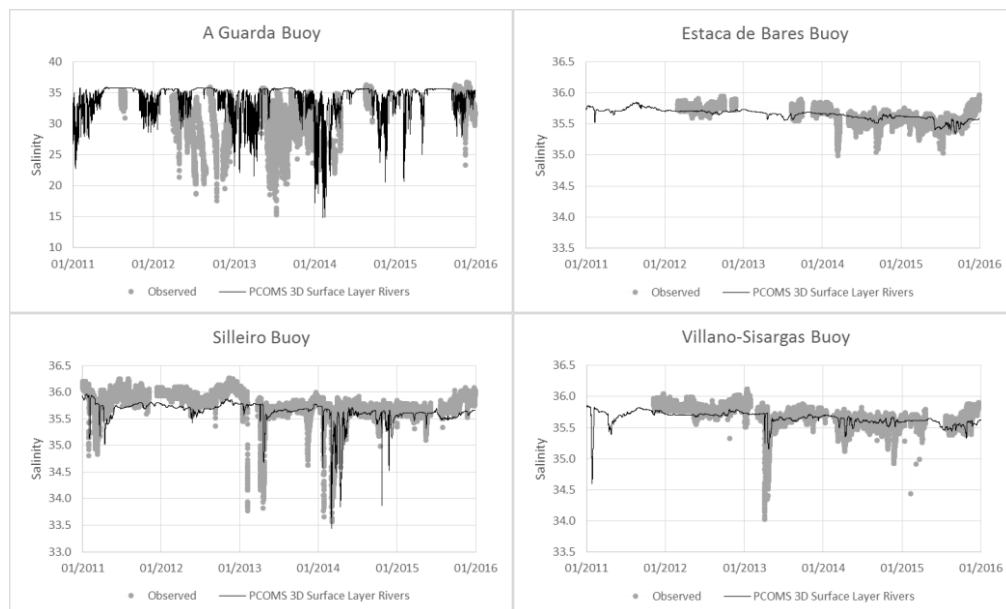


**Figure 8 Sea surface salinity observed (grey dots) and modelled (solid black line) by A Guarda (top row left), Estaca de Bares (top row right), Silleiro (bottom row left) and Villano-Sisargas (bottom row right) multiparametric buoys in for the 2011-2016 period.**

Observing the salinity evolution in the multiparametric monitoring stations (Figure 8) allow to evaluate the model performance and also to understand a little more about the WIBP temporal and spatial influence. A Guarda buoy, the coastal station, is obviously the most affected by fresh water inputs with salinity values failing down to 15 salinity units. Several large rain events are identified by the buoy

and model, such as those taking place in early 2013 and 2014. However the salinity data collected by A Guarda buoy appear to be very fragmented and low values are detected during summer periods where no significant input is detected, see Campuzano *et al.* (2018), such as during summer 2013. The absence of a similar drop in the salinity values observed by the offshore buoys during the same periods confirm that some salinity records in this buoy may be unreliable. The three offshore buoys show a descending salinity trend during most of the analysed period. These stations also show how the WIBP influence oceanic waters decreasing in some cases to salinity values below 34. The modelling results represent the main salinity trend and capture the main river discharge events. The timing and salinity values are better characterised in the Silleiro buoy than in the other offshore buoys. In Villano-Sisargas and Estaca de Bares buoys modelling results, the WIBP signature is present in the model though its influence is underestimated probably due to the constant salinity value of 32 used for characterising the river discharges and by numerical diffusion. Silleiro and Villano-Sisargas salinity sensors appear to have been recalibrated simultaneously in early 2013 and after that date observations from those stations moved closer to the modelling results. Table VII synthetises the modelling and observed salinity values aided by commonly used metrics. Even if low salinity peak coincide in several periods such as early 2011 and 2014, the metrics resulting from the salinity values comparison in the A Guarda buoy are very low due to the reasons mentioned above including the model resolution and the reliability of the observations. The salinity observations and modelling results for the offshore buoys show a better level of agreement with similar salinity mean and range values obtaining  $R^2$  between 0.35 and 0.52. Despite these results, better fits could be expected by refining grids and by improving the characterisation of the non-estuarine river inputs. In addition, salinity observations should be contrasted in order to identify ambiguous values.

**Table VII. Mean, minimum ( $P_{05}$ ) and maximum ( $P_{95}$ ) sea salinity observed by the multiparametric buoys and obtained by the PCOMS model for the period 2001-2015. Statistic indexes, including coefficient of determination ( $R^2$ ), bias, Root Mean Square Error (RMSE) were obtained comparing the PCOMS dataset with the observed values are also listed. The number of valid values (N) is also indicated.**

Buoy Name	Mean Observed	Mean Modelled	$R^2$	Bias	RMSE	N
	Salinity ( $P_{05}$ - $P_{95}$ )	Salinity ( $P_{05}$ - $P_{95}$ )				
<b>A Guarda</b>	30.95 (23.81-35.52)	34.18 (30.13-35.69)	0.01	3.23	28.45	15464
<b>Estaca de Bares</b>	35.63 (35.42-35.82)	35.61 (35.44-35.71)	0.41	-0.02	0.01	23097
<b>Villano-Sisargas</b>	35.69 (35.45-35.93)	35.64 (35.49-35.76)	0.50	-0.04	0.02	30751
<b>Silleiro</b>	35.76 (35.36-36.06)	35.63 (35.29-35.83)	0.35	-0.14	0.07	39380

### 7.3.2. Sea Surface Salinity climatology

Currently, numerical modelling is the only method able to cover the temporal and spatial gaps between monitoring cruises and stations. While remote sensing applications for coastal salinity are under development, field surveys are only capable of providing snapshots of the salinity fields and reliable continuous records by multiparametric buoys are scarce, numerical models provide spatial and temporal continuous salinity fields. In order to evaluate the annual and interannual variability of Western Iberia SSS, the mean value for the entire period (Figure 9) was completed with mean annual (Figure 10), seasonal (Figure 11) and monthly (Figure 12) fields for the period 2011-2015. On the light of the data collected by the multiparametric buoys, the upper limit of the WIBP front was restricted to 35.5 instead of the value of 35.6 (Otero *et al.*, 2008; Mendes *et al.*, 2016) or 35.7 (Peliz *et al.*, 2002; Santos *et al.*, 2004) as in northern waters the range of values 35.6-35.7 can still be regarded as an open ocean value not influenced by terrestrial inputs (Figure 8).

The mean annual salinity distribution in the Western Iberian regional ocean for the period 2011-2015 is illustrated in Figure 9. On this figure, two areas influenced by fresh water inputs can be clearly distinguished: the WIBP that includes the coastal area from the Mondego estuary mouth up to the Galician rias and the Tagus-Sado estuarine plumes area, hereafter referred as West Iberia Central

Plume (WICP), that extends from Cape Espichel until Cape Carvoeiro. Between these two areas, in the neighbouring waters of the Nazaré canyon, mean salinity values slightly saltier than open ocean waters, though this area present a high seasonal variability. The isolated salinity signature of the Guadiana and Guadalquivir river plumes are also easily spotted in the Gulf of Cádiz. The salinity field suffers large interannual variability according to the wet and dry years depending on the weather regimes (Figure 10). 2012 was on average the driest year of the analysed set followed closely by 2015. On the other hand, 2014 was the rainiest year of the series followed narrowly by 2013 while 2011 could be regarded as an intermediate year. In 2012, rivers influence appears to be concentrated, on average, near their estuary mouth with some rivers' signals missing, such as the Guadiana and Sado rivers. On the other hand, in 2013 and more clearly in 2014, the WIBP extends offshore and entire WIBP coastal area present values below 35. Interannual salinity minima is located around the estuarine mouth and changes accordingly to the estuarine interannual variability as seen in Campuzano *et al.* (2018). During 2014, the surface area covered by the WIBP extend westwards and clearly turns the Cape Finisterre reaching the Cantabrian Sea. In 2015, the WIBP covered area reduced and moved landwards. In the same year, salinity values below 35 are found around the estuarine mouths and disconnected from each other within the WIBP region.

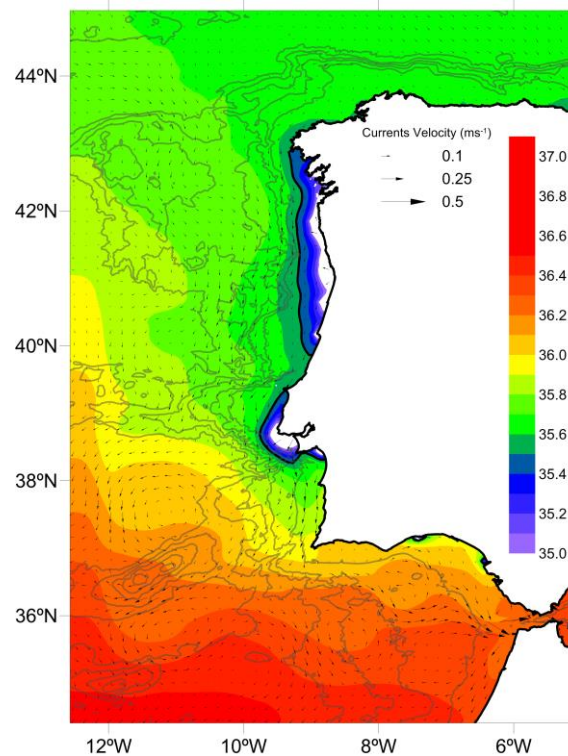


**Figure 9 Mean sea surface salinity for the study period 2011-2015. The thick black line indicates the WIBP salinity upper limit (35.5) and the white are is below salinity 35. Vectors represent mean current intensity and direction every third cell.**

The mean salinity value for each season of the studied period can be observed in Figure 11. Seasons were defined considering full months with the following criteria: winter (December, January and February), spring (March, April and May), summer (June, July and August) and autumn (September, October and November). The modelling results solution agrees with the definition of the WIBP given by Peliz *et al.* (2002) that states that this plume is present all year round even with the significant decrease of runoff in summer. The WIBP persist through the spring transition to summer upwelling conditions and stretches offshore (Relvas *et al.*, 2007; Picado *et al.*, 2014). In addition to the runoff variation, the prevailing wind regime in each season influences the WIBP distribution since it is advected offshore with northerly winds and converges to the coast with southerlies (Peliz *et al.*, 2002; Santos *et al.*, 2004, Ribeiro *et al.*, 2005). Southerly wind regimes are generally associated with rainfall episodes which barely occurs during the summer months (Trigo and DaCamara, 2000).

During typical winter conditions, the prevailing downwelling favourable winds from the south-west generate convergent transport towards the coast and the WIBP remain in the inner shelf and rivers feed the a coastally trapped branch of the poleward current advecting low salinity waters (Relvas *et al.*, 2007; Picado *et al.*, 2014). During the upwelling conditions, the Ekman surface plume is transported offshore and advected along the shelf (Santos *et al.*, 2004; Relvas *et al.*, 2007). During autumn several surface salinity minima are located around the estuarine mouth and poleward circulation dominates in the inner shelf reaching the Galician rias. The winter season increases the volumes discharged in the coastal areas and the salinity values below 35 occupy the inner shelf from the Mondego River up to the Galician Rias and the WIBP influence extends further than Cape Finisterre. During spring, the relaxation of northern winds, the abundance of less salty water in the coastal area and the beginning of upwelling-dominated wind conditions spread the WIBP off the continental shelf in south west direction and equatorward, as part of the upwelling induced current, occupying a large area of the Portuguese continental platform near the Nazaré Canyon area.

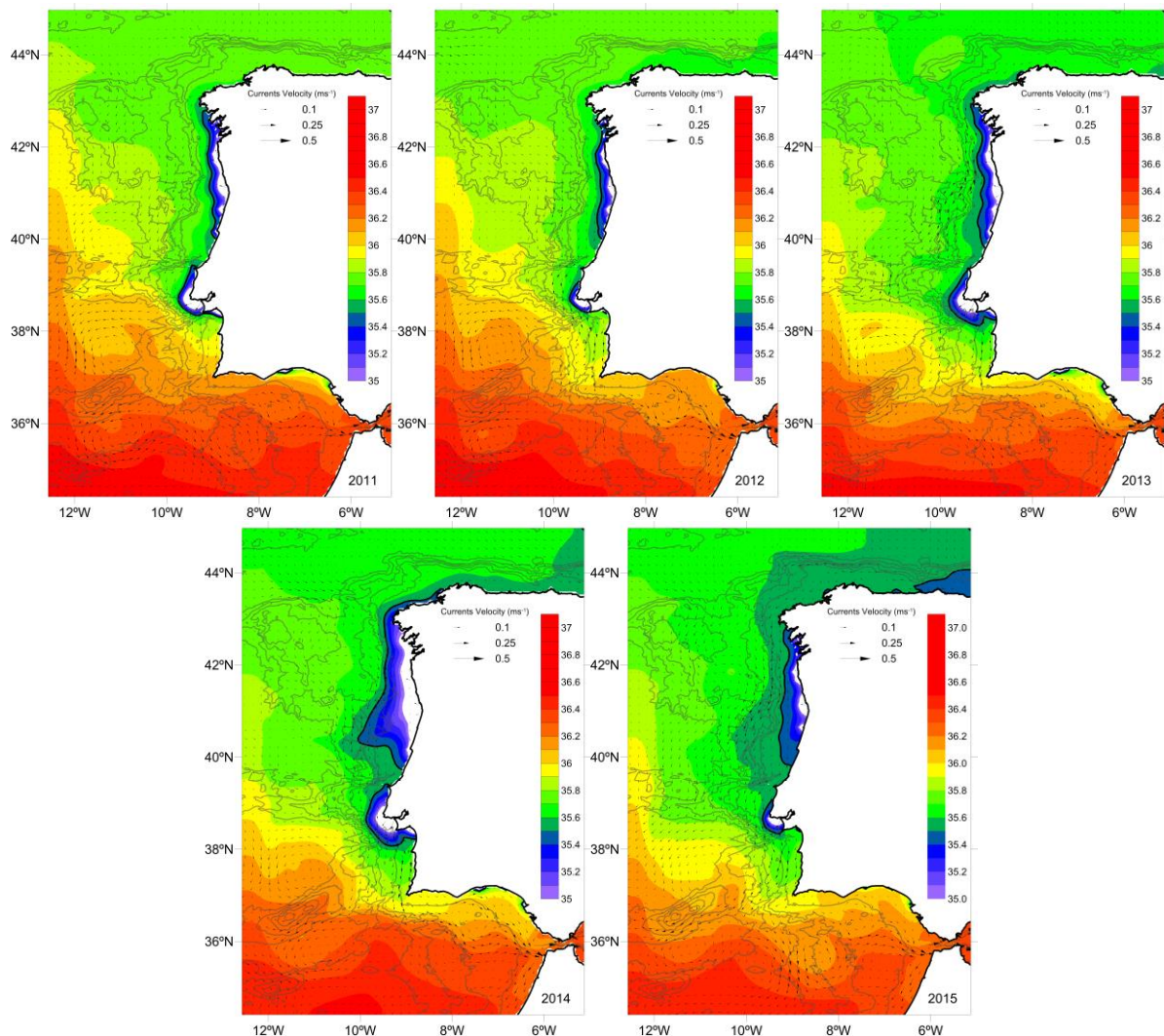


**Figure 10** Mean sea surface salinity for each year of the studied period. The thick black line corresponds to the 35.5 salinity value and white areas are below salinity 35. Isobaths are represented every 1000 m starting at 500 m. Vectors represent mean direction every third cell.

During this period, offshore equatorward current dominate in the surface while in some coastal areas northern from Douro River coastal poleward currents are observed. Finally, during summer the salinity zonal gradients decrease due to lower fresh water inputs and only in some estuarine areas SSS below 35 are observed. However, low salinity waters are transported southwards due to the predominant surface circulation and connecting with the Tagus estuary plume. The latter plume appear isolated

during this period of the year. Nevertheless, during winter and spring conditions, the Tagus and Sado estuary plumes were connected with salinity values below 35.5 in what it was defined in this chapter as the WICP. The WICP influence during this period extends further than Cape Carvoeiro and enters the Nazaré Canyon area.

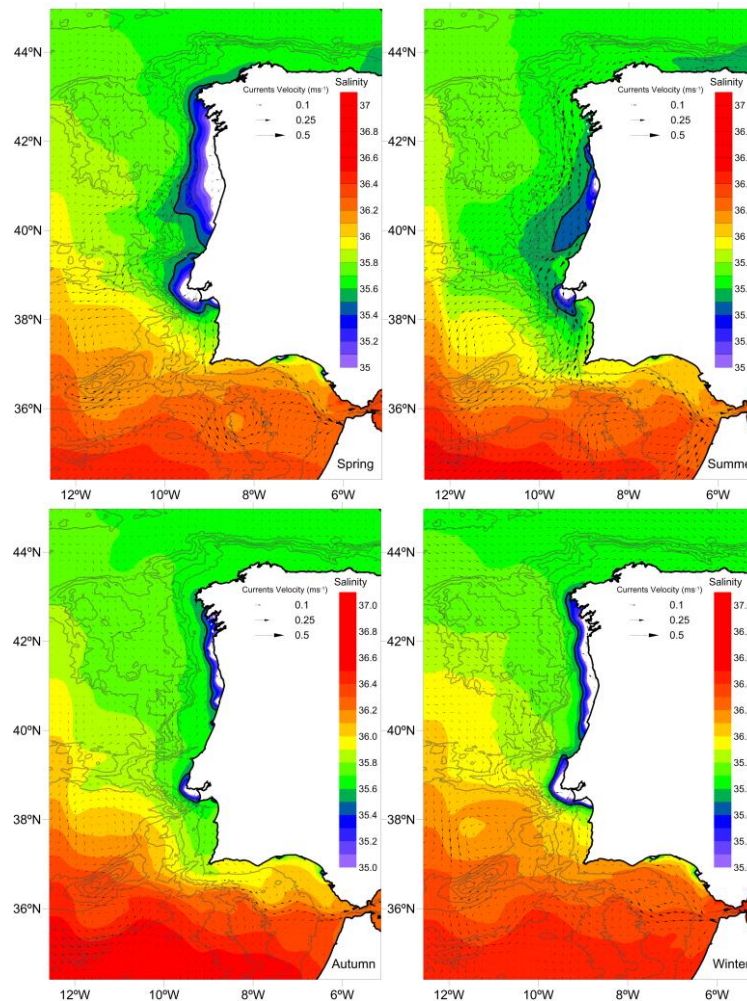


**Figure 11** Seasonal sea surface salinity for the 2011-2015 period. The thick black line corresponds to the 35.5 salinity value and white areas are below salinity 35. Isobaths are represented every 1000 m starting at 500 m. Vectors represent mean direction every third cell.

The WIBP evolution from a narrow water mass constrained against the coast to a spread lens that covers wide areas of the continental platform and offshore waters can be observed in the monthly climatology salinity fields (Figure 12). The maximum expression of the coastal WIBP can be found in January where the WIBP salinity offshore limit, 35.5, is found approximately 30 km offshore. During this month the WIBP and WICP appear as one single ROFI that extends from the Sado plume area to northern areas of Cape Finisterre. This salinity distribution contrast abruptly with the mean August salinity distribution where the Tagus and Douro plumes appear as the only areas with values below 35 though the signature of the WIBP can still be noticed. This reduction is the result of the combination of reduced river inputs and the effect of the upwelling conditions during July that extend and mix the WIBP with offshore waters. Minimum mean salinity concentration for January and August were respectively around 20 and 30.

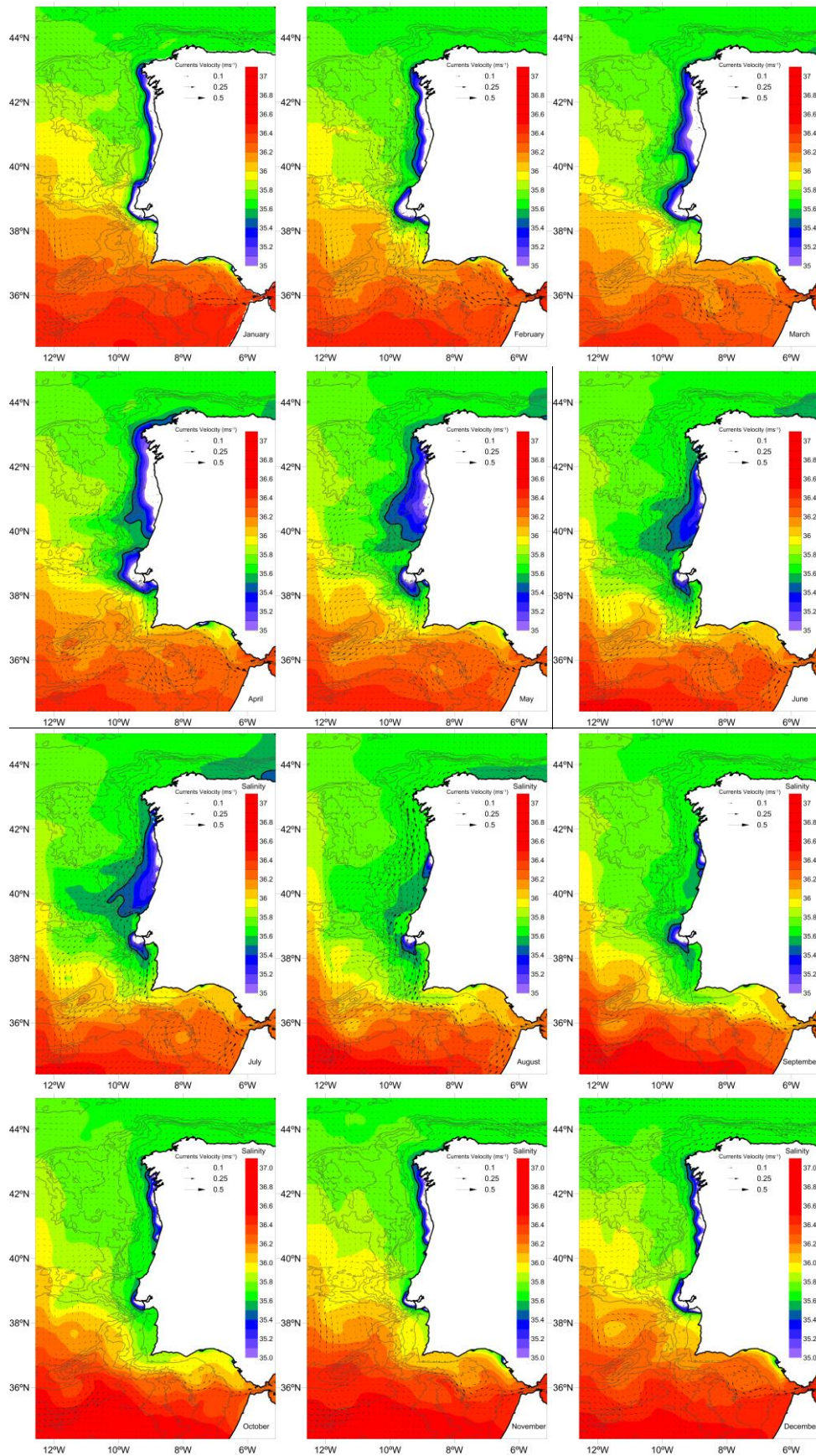


Figure 12 Monthly mean surface salinity for the 2011-2015 period. The thick black line corresponds to the 35.5 salinity value and white areas are below salinity 35. Isobaths are represented every 1000 m starting at 500 m. Vectors represent mean direction every third cell.

### 7.3.3. Case study: April 2013 extreme event

On early spring of 2013, a severe rain event affected the Western Iberia territory reaching maximum peak flows around  $4500 \text{ m}^3\text{s}^{-1}$  in the Douro River on the 30<sup>th</sup> of March and around  $5400 \text{ m}^3\text{s}^{-1}$  in the Tagus River on the 2<sup>nd</sup> of April (Campuzano *et al.*, 2018). In order to evaluate the performance of the model and to describe a complex scenario, the area affected by the WIBP will be described in detail for the month of April. Figure 13 shows the surface salinity between the 2<sup>nd</sup> of April and the 4<sup>th</sup> of May with a three days interval. In order to identify, the source of temperature, salinity and current intensity variation, a PCOMS version with the same exact configuration but removing the river forcing (PCOMS without Rivers) simulated the same period starting the 15 of March 2013 (Figure 14).

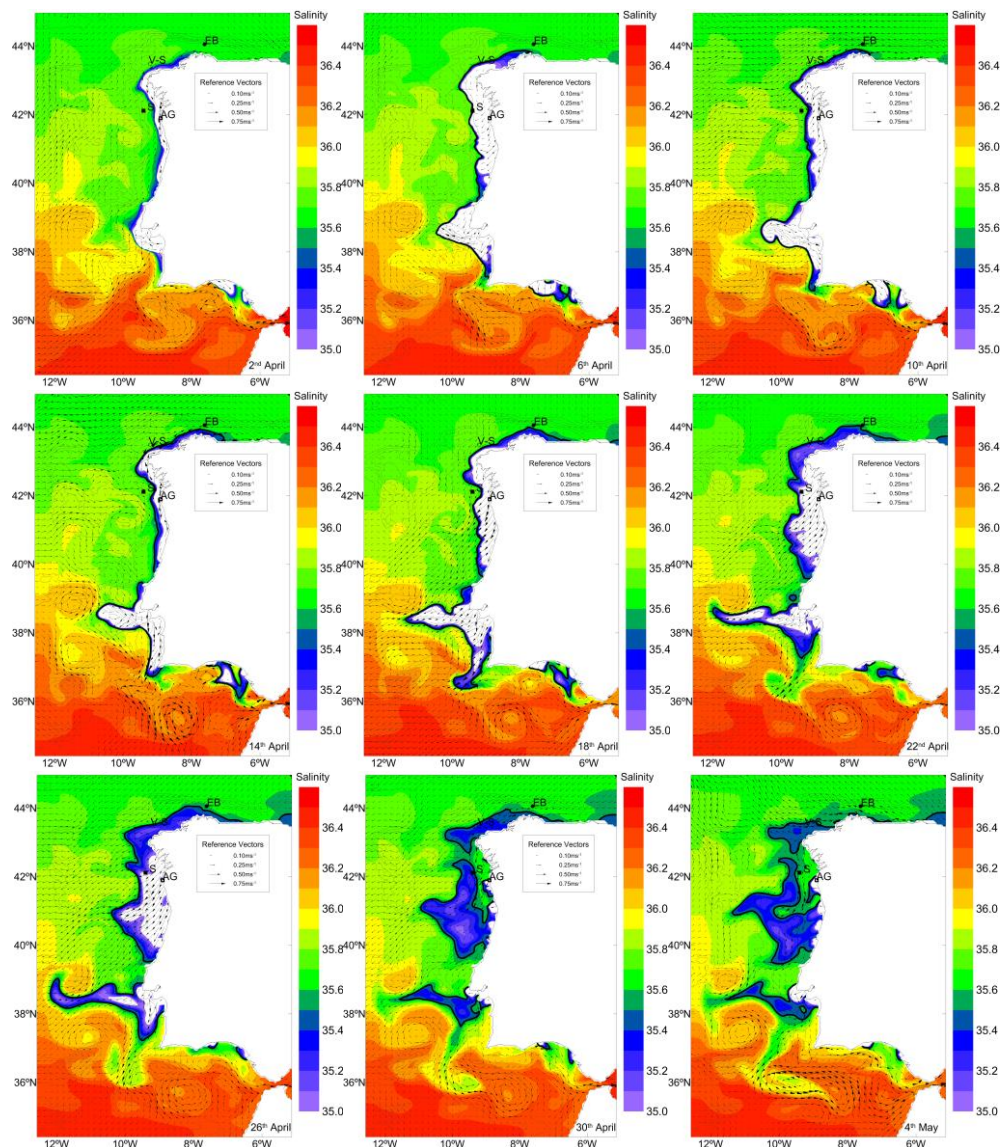
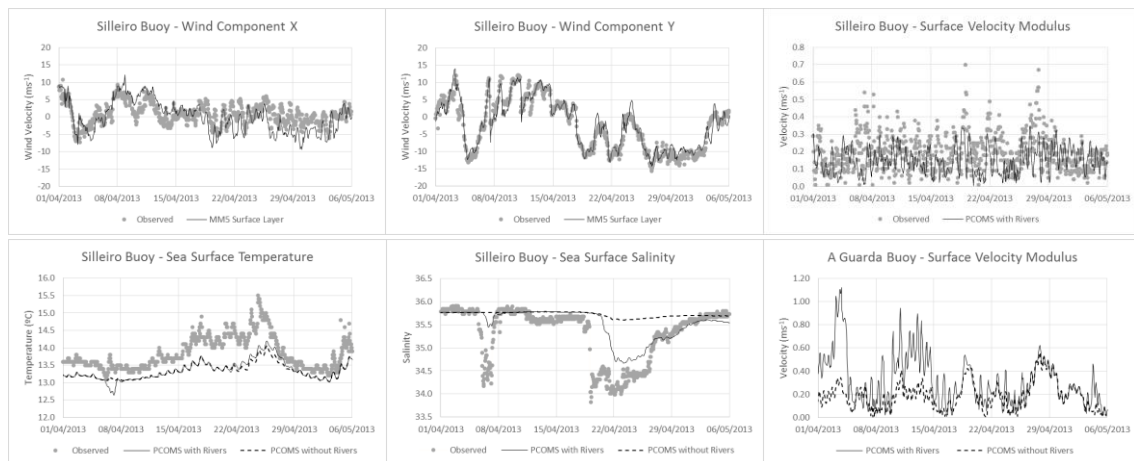


Figure 13 Mean daily surface salinity field for western Iberia between the 2<sup>nd</sup> of April and the 4<sup>th</sup> of May. Salinity maps are represented with four day interval and are read from left to right and from top to bottom. The map show the location of relevant observation buoys (EB-filled circle, V-S with an empty circle, S-filled square Buoy and AG-empty square). The thick black line corresponds to the 35.5 salinity value and white areas are below salinity 35. Isobaths are represented every 1000 m starting at 500 m. Vectors represent mean direction every third cell.

Within this month, atmospheric conditions and surface circulation in the northwest of the Iberian Peninsula changes abruptly and for that reason the WIBP describe an unusual pattern evolution. At the beginning of this period, the WIBP was a narrow band attached to the coastline and flows polewards under typical winter conditions. This circulation pattern is reinforced by the large amount

of river inputs that tends to circulate to the North deviated by the Coriolis force (Otero *et al.*, 2008) and by the increasing intensity of southern winds with a meridional component that reaches values over  $13 \text{ ms}^{-1}$  in the early hours of the 3<sup>rd</sup> of April (Figure 14). As a result, velocity peaks larger than  $1.1 \text{ ms}^{-1}$  were obtained in the A Guarda buoy location from the modelling version with rivers (Figure 14). Velocities up to  $1 \text{ ms}^{-1}$  or slightly higher have been previously described for this area with numerical model simulations under high river discharge conditions and strong wind-favourable conditions (Marta-Almeida *et al.*, 2002; Ruiz Villarreal *et al.*, 2005; Otero *et al.*, 2013; Mendes *et al.*, 2016). Although during some periods modelled velocities from both versions, with and without rivers, are similar, it can be seen the influence of river discharges in the coastal velocities. When moving offshore, the differences between the versions with and without rivers reduces, i.e. velocities in Silleiro buoy are almost identical (not shown).



**Figure 14** Observed and modelled 10 m height zonal (top row, left) and meridional (top row, centre) wind intensity, sea surface current velocity (Top row, right), sea surface temperature (bottom row left) and sea surface salinity (bottom row centre) at the Silleiro buoy location for the period 1<sup>st</sup> of April-6<sup>th</sup> of May of 2013. The modelled velocity in A Guarda buoy location is also shown (bottom row right). In Silleiro Buoy temperature and velocity graphs and in A Guarda surface velocity graph modelling results are displayed with (PCOMS with Rivers) and without rivers (PCOMS without Rivers) forcing.

The downwelling conditions change abruptly when winds suddenly rotate and turn into northern winds of up to  $13 \text{ ms}^{-1}$  in less than 36 hours generating strong upwelling conditions and spreading the WIBP offshore - and southwards. These wind conditions maintained for the following two days and allowed the sensors of Silleiro buoy to register the salinity and temperature signal of the WIBP (Figure 13 and Figure 14). From the 7<sup>th</sup> of April and for the following ten days southern wind conditions returned and confined again the WIBP against the coast. During this period, ocean salinity values were restored in the Silleiro buoy area. After this period, the northern wind returned and stayed, without almost any interruption, until practically the end of the study period. These upwelling conditions transported the WIBP and the WICP towards the open ocean with its signature being observed further than the  $10^{\circ}\text{W}$  and interacting with mesoscale structures. The plume is displaced offshore crossing the slope-current, undergoing seaward stretching and meridional elongation as part of the upwelling process as described in Ribeiro *et al.* (2005) for a winter upwelling event. In the southern limit of the WICP, the plume is seen interacting with the mesostructures of the Gulf of Cádiz. As the freshwater input diminished, the plume intensity decreased due to wind mixing and surface spreading. This is frequent situation during spring and summer when northerly winds are predominant (Otero *et al.*, 2013). In some areas the WIBP detached from land and a secondary minimum of salinity was observed more than 100 km offshore. Examples of this behaviour were described by Santos *et al.* (2004) and Ribeiro *et al.* (2005) for winter upwelling conditions. By the end of the analysed period, the sea surface salinity field becomes patchy and waters with typical ocean salinity were found surrounded by WIBP waters. The separation of the WIBP from the coast was observed by Santos *et al.* (2004) finding typical

ocean salinity values near the coast such as in the latter dates of the detailed analysed period. Also during these period, the river plumes extends as bulges in the coastal area.

During this period, the Silleiro buoy recorded salinity values below 34 which are more similar to estuarine values than typical open ocean conditions. On the 6<sup>th</sup> of April the observed salinity and temperature decreased by the arrival of WIBP waters. Only the PCOMS version with rivers is able to reproduce this effect. On the 19<sup>th</sup> of April a second decrease in salinity was observed by the monitoring platform, this time the decrease in salinity appears to come with an increase in surface water temperature. However, it can be observed that both model applications reproduce this temperature increase while the salinity decrease was only reproduced by the PCOMS version including the river discharges. This is one of the reasons why EO SST is not an adequate tool to monitor the WIBP since the shallow and stable plume acquires rapidly the thermal signature of the surrounding waters (Ribeiro *et al.*, 2005). On the other hand, it can be observed a great correspondence between observed and the modelling results with rivers though the timing and intensity of the WIBP could be still improved (Figure 14). The numerical model with the described land-boundary conditions is able to simulate with high accuracy and a minor bias the temporal evolution of the salinity and temperature of the WIBP as observed at the Silleiro buoy in terms of time and value.

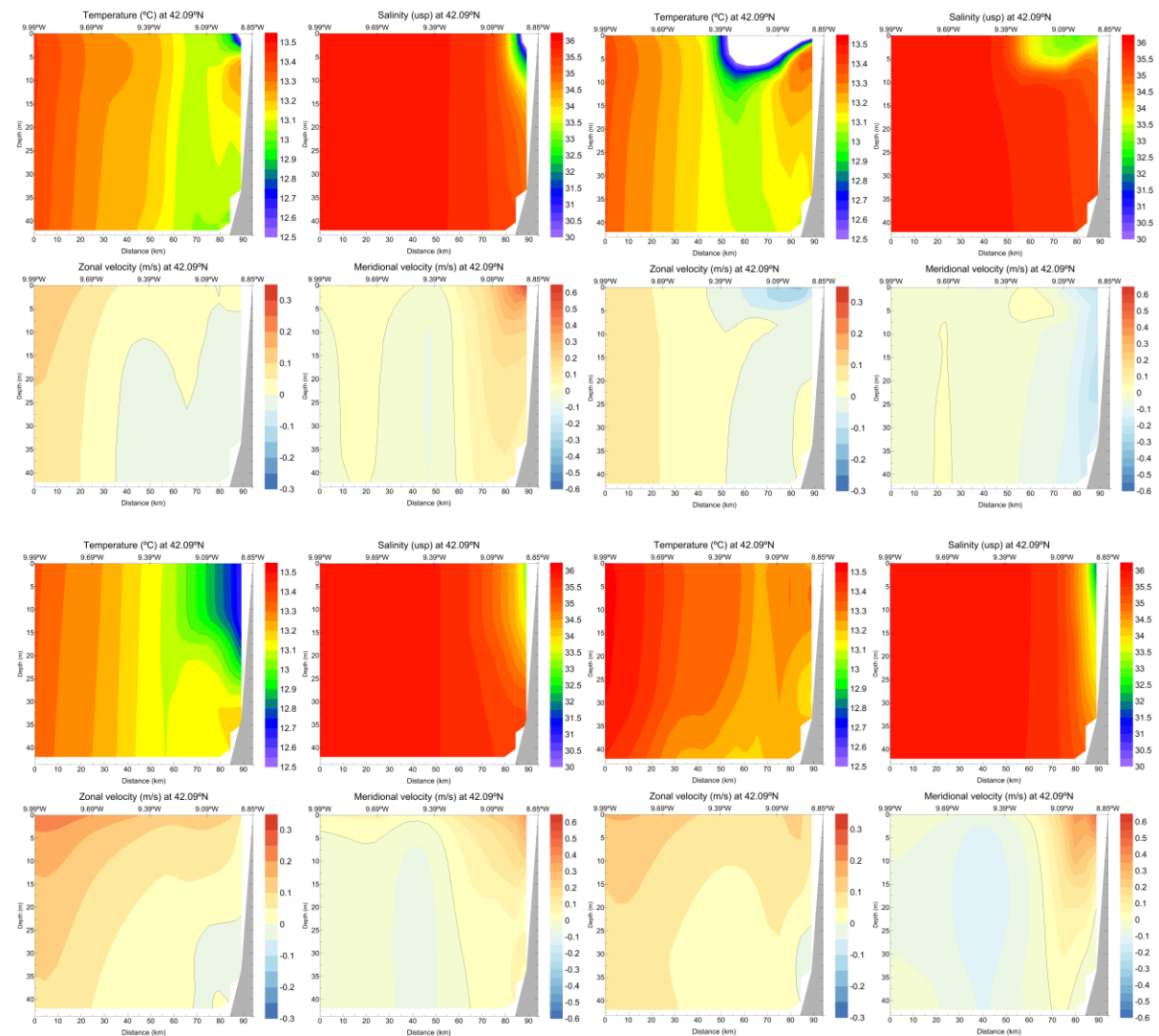


Figure 15 Daily average cross-section representing the top 50 m of water temperature, salinity and zonal and meridional velocity for the 2<sup>nd</sup>, 6<sup>th</sup>, 10<sup>th</sup> and 14<sup>th</sup> of April 2013, from left to right and from top to bottom, at the latitude of Silleiro buoy (coordinates 42.09°N, 9.40°W). These dates correspond to the first four instants of Figure 13.

Figure 15 show the vertical section for the top 50 m at the latitude corresponding to the Silleiro buoy location for the 2<sup>nd</sup>, 6<sup>th</sup>, 10<sup>th</sup> and 14<sup>th</sup> of April 2013. For each date, sea water temperature, sea temperature and zonal and meridional velocity were represented. These dates correspond to the first four instants of Figure 13. On those dates it can be seen how originally, 2<sup>nd</sup> of April, a cold plume flowing north was attached to the coastal area on top of a warmer water mass until the large plume generated by the severe rainfalls arrived to the vicinity of the monitoring buoy on the 6<sup>th</sup> of April. During this period, and agreeing with the observations performed during a winter upwelling (Santos *et al.*, 2004), the plume was thicker on the coastward side and the core of the plume continue flowing to the north with lower intensity than previously while the coastal area was flowing equatorward. As the meteorological conditions change towards downwelling favourable conditions, the stratified flume starts to retreat to the coast on the 10<sup>th</sup> of April. On the 14<sup>th</sup> of April the plume was again attached to the coastal area flowing northwards and vertically mixed. These results are in agreement with the salinity distributions found theoretically for a plume response to upwelling and downwelling conditions (Fong and Geyer, 2011).

Another striking result from the modelling simulations is the WICP large influence of vast areas according to the dominant winds (Figure 13). During this month, fresher waters from both estuaries were able to turn the Cape São Vicente and accessing the western part of the Gulf of Cadiz (14<sup>th</sup> of April) and to reach the westernmost area of the PCOMS domain, 12°W, in less than two weeks (26<sup>th</sup> of April).

## 7.4. Discussion

During the rainy season, the general circulation of Western Iberia is dominated by the Iberian poleward current (IPC; Frouin *et al.*, 1990) a current located along the continental slope and well defined from Cape Carvoeiro northwards that is observed from the beginning of the winter season until the spring transition in April-May (Revas *et al.*, 2007). Santos *et al.* (2004) described a retention mechanism based in the interaction between the IPC and the WIBP where convergence areas of great importance for the retention of fish eggs and larvae were generated in the shelf break (Santos *et al.*, 2006). However, if the Ekman transport is intense and persistent the WIBP can spread over the IPC, as Ribeiro *et al.* (2005) observed in upwelling events occurring during the winter season. River discharges in the WIBP area will eventually fed the IPC and thus advected northwards.

Although the WIBP intensity depends on the river runoff which has a marked seasonality, this buoyant plume is present all year round (Peliz *et al.*, 2002). In order to evaluate the interannual and seasonal surface salinity variability in Western Iberia, the mean value for the three rainiest months (JFM; Figure 16), according to the mean salinity estuarine outflow (Campuzano *et al.*, 2018), and for the summer period (JJA; Figure 17) were obtained. The plume time scale response is of the order of hours (Otero *et al.*, 2008) and it may be only occasionally present at many locations (Hetland, 2005) and due to this fact the mean value can hide some areas under the river plume influence. For this reason, to evaluate the region of fresh water influence (ROFI), the annual 5<sup>th</sup> percentile was estimated for the wet season (Figure 18) and dry seasons (Figure 19).

During the wet season, the WIBP is confined to the inner-shelf from the Mondego River northwards and attached to the coast with salinity values lower than 35.5. During wet years such as 2011 and 2013 the WIBP and the WICP were joined forming a continuous plume. Even if less frequent, upwelling wind conditions has been regularly observed during these months (i.e. Santos *et al.*, 2004; Ribeiro *et al.*, 2005; Otero *et al.*, 2013). Wind relaxation periods and upwelling conditions combined with high rivers discharges expand the WIBP westwards covering large areas off the continental shelf such as in 2014. In the same year, the WIBP area, identified by the solid black line 35.5 in the graph, was able to turn the Cape Finisterre. When analysing the corresponding salinity 5<sup>th</sup> percentile (Figure 18), it can be seen how in particular years with intense IPC the region of influence can reach offshore waters northern than 40°N. The area affected by the fresh water during at least 5% of the time differs significantly in size when compared to the mean value except during dry years such as 2012. In the years 2013-2015,

upwelling conditions took place within this period and the 5<sup>th</sup> percentile show the influence of the WIBP well off the shelf break. In the year 2014, salinities below the 35 reached areas located western than 10°W. In almost every analysed year, the Nazaré canyon surrounding waters, an area poor in river discharges, were influenced by river inputs from the WIBP and the WICP.

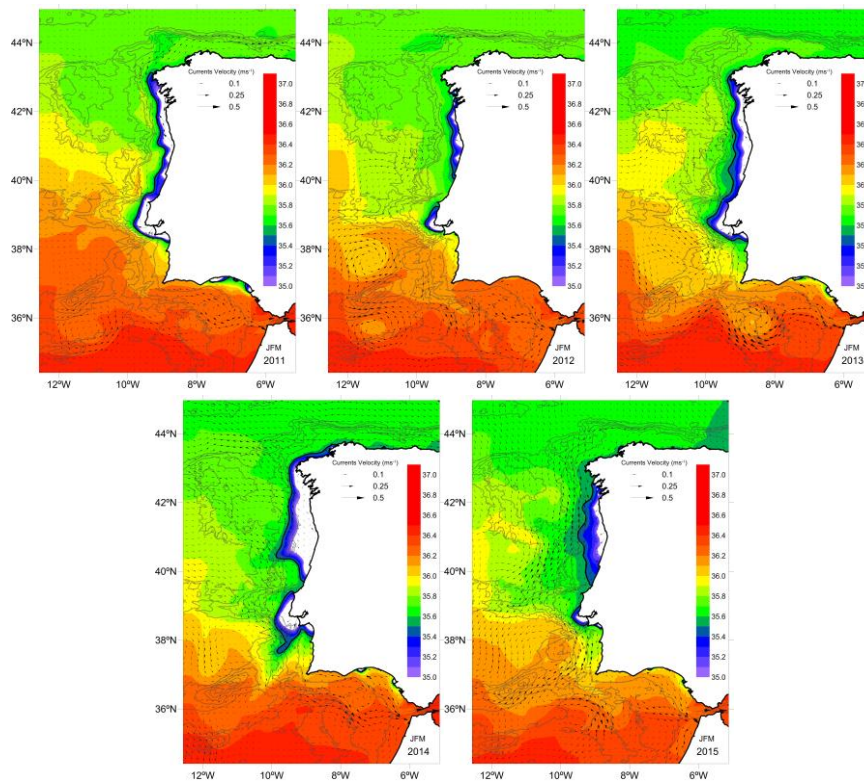


**Figure 16 Mean sea surface salinity for the three rainiest months (JFM) of the period 2011-2015. The 35.5 isohaline (thick black line) is marked as buoyant plume limit. White areas correspond to salinity values below 35. Isobaths are represented every 1000 m starting at 500 m. Vectors represent mean current intensity and direction every third cell.**

Summer mean values (Figure 17) present a salinity field pattern quite different from the wet period with elongated plumes with southwest orientation. During this period, river plumes reduce significantly and sometimes are limited to the neighbouring areas of the estuarine mouths, i.e. 2011. In the year 2012, even if this year was on average the driest year of the analysed series, the salinity fields were strongly influenced with a large WIBP. In 2013, the WIBP area was reduced and the Tagus ROFI presented an extension larger than usual. In summer 2014, the WIBP signal was large and occupy an extended area offshore and connected with the Tagus estuary plume. In 2015, the plumes with low salinity values were the Douro and Tagus plumes with a reduced ROFI in comparison with the previous year. In this year, can be distinguished a mass of low salinity entering the northern part of the domain that could be due to wrong boundary conditions as referred in previous chapters. When the 5<sup>th</sup> percentile distribution is analysed (Figure 19) it can be observed that despite the low river inputs during the summer season the ocean area influenced is large due to the upwelling winds spreading, i.e. 2013, 2014 and 2015. The water from these plumes was generally transported offshore and southwards and interacted with mesoscale structures. Though the advections patterns are relatively constant during these season, the interannual variation in river runoff and wind conditions results in a wide variety of salinity patterns.

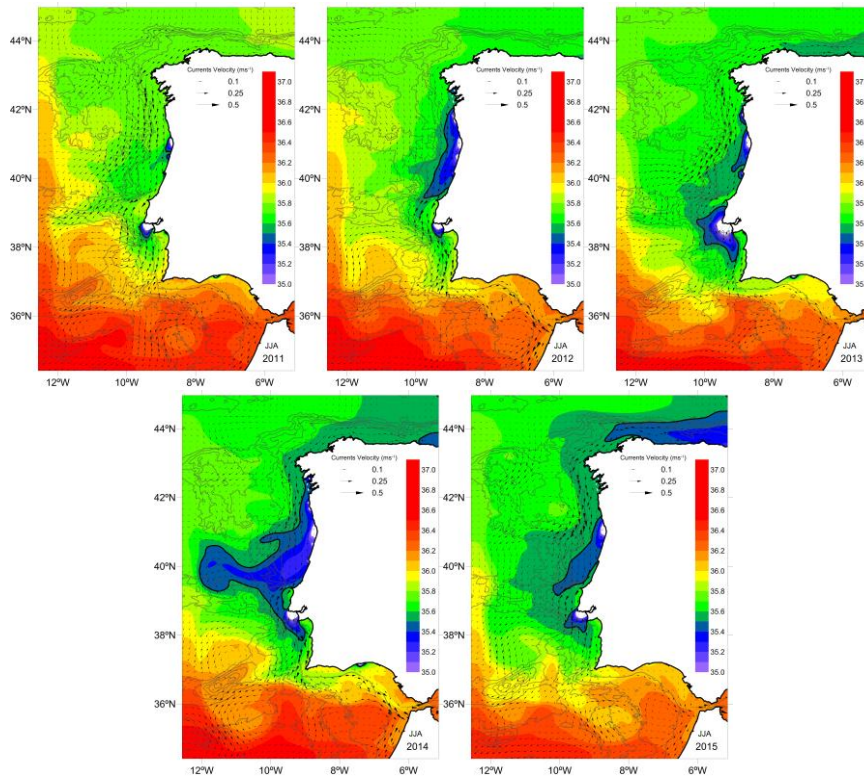


Figure 17 Mean sea surface salinity for each summer (JJA) of the period 2011-2015. The 35.5 isohaline (thick black line) is marked as buoyant plume limit. White areas correspond to salinity values below 35. Isobaths are represented every 1000 m starting at 500 m. Vectors represent mean current intensity and direction every third cell.

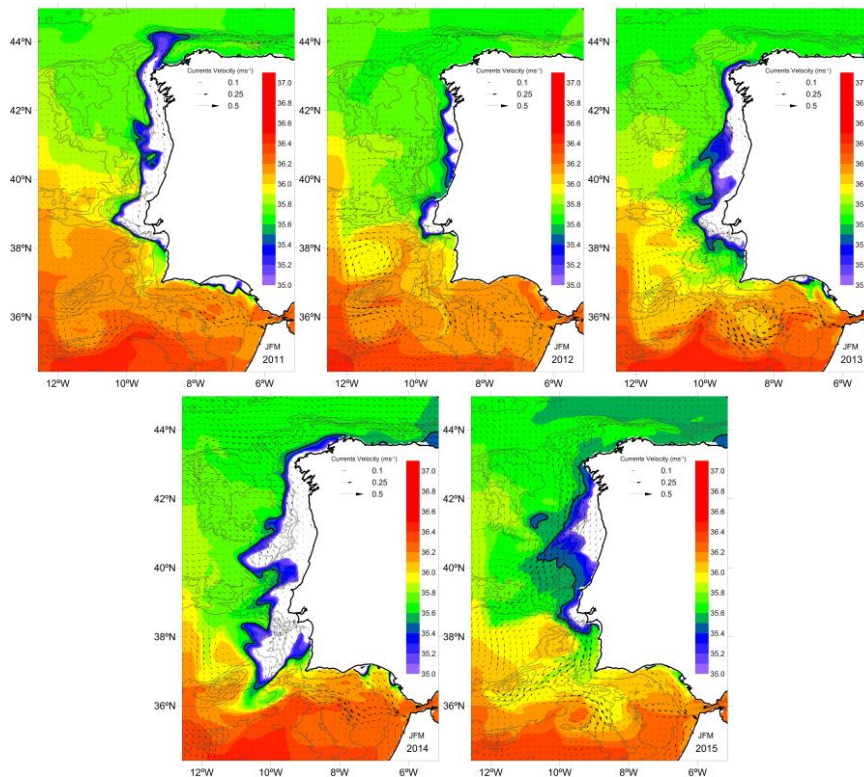
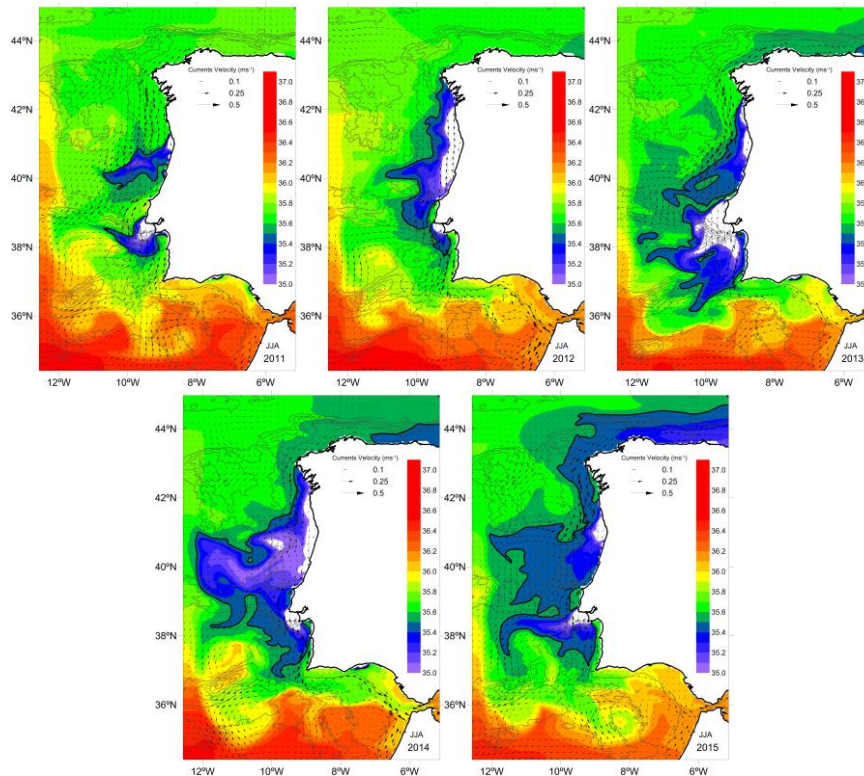


Figure 18 Sea surface salinity 5<sup>th</sup> percentile for the three rainiest months (JFM) of the period 2011-2016. The 35.5 isohaline (thick black line) is marked as buoyant plume limit. White areas correspond to salinity values below 35. Isobaths are represented every 1000 m starting at 500 m. Vectors represent mean current intensity and direction every third cell.



**Figure 19** Sea surface salinity 5<sup>th</sup> percentile for each summer season (JJA) of the period 2010-2015. The 35.5 isohaline (thick black line) is marked as buoyant plume limit. White areas correspond to salinity values below 35. Isobaths are represented every 1000 m starting at 500 m. Vectors represent mean current intensity and direction every third cell.

A Hovmöller diagram of the monthly averaged salinity values found in the land-ocean interface was represented to try to summarize the spatial and temporal salinity heterogeneity (Figure 20). In this graph, salinity variation can be easily observed indicating dry years such as 2012 and wet years such as 2013 and 2014. Some years presented an almost continuous river input period, such as 2011 and 2014, while other years, such as 2012 and 2015, presented two clearly separated rain seasons: one in winter and other in spring. This graph allows us also to assess the spatial heterogeneity of the discharges. Two main areas can be distinguished coinciding with the WICP area (around 39°N), including the Tagus River as the main driver, and the WIBP area (around 41.5°N), centred in the Douro River. The peak time of river discharges, in these two areas, may not coincide and though generally the WIBP is more intense the WICP led the discharges in winter 2011 and April 2013. These two areas appear generally connected with salinities under 35.5 and during large rainy events such in early spring of 2014 they can generate a front along all the coast with low salinity values. Salinities under 35.5 are observable in the coastal areas of the WIBP during most of the year with the exception of some summer periods. In the case of the WICP, it is absent during most of the summer periods and in some years it can extend southwards to the vicinity of Cape São Vicente as in years 2012, 2013 and 2014. It should be borne in mind that due to technical problems in the Tagus hydrometric station during November 2014-May 2015 the Tagus fluxes might be miscalculated.

## 7.5. Conclusions

Since salinity remote sensing is starting to give its first steps in coastal areas and *in situ* monitoring has low frequency, numerical modelling is currently the only tool able to represent and estimate the temporal and spatial scale of the WIBP and other estuarine plumes. Taking into consideration the numerical modelling limitations and assumptions, the salinity modelling results provided by the methodology described in Campuzano *et al.* (2016) improve significantly salinity fields and aid to the delimitation of region of fresh water influence and salinity fronts.

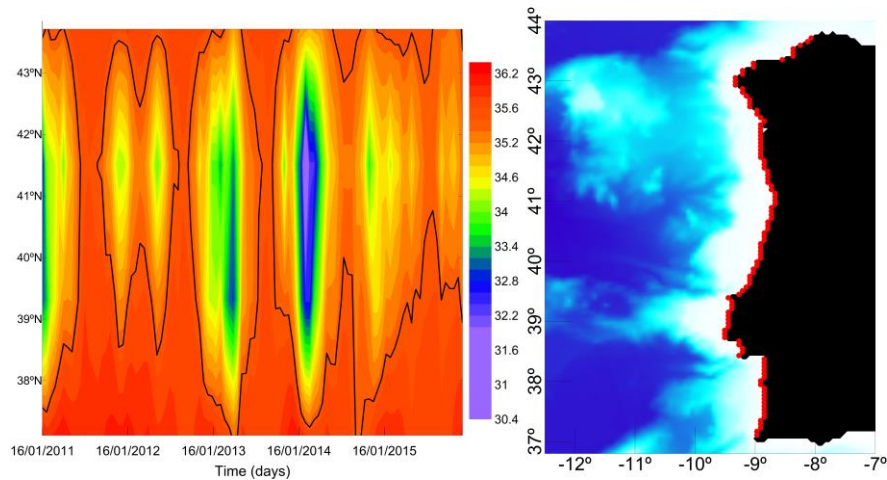


**Figure 20 Monthly averaged salinity along the western Iberia coast area for the June 2010-December 2015 period. The 35.5 isohaline (thick black line) is marked as buoyant plume limit.**

The modelling results were compared with cruise surveys covering the Portuguese waters and with operational multiparametric buoys equipped with sensors. The cruise comparisons allowed to evaluate the values and patterns obtained by the modelling methodology and the improvement with a reference solution. In addition, a case study of high river discharges in April 2013 was evaluated with focus in the north-western shelf due to the availability of observed data. The model was capable of reproducing the main patterns of the WIBP plume and to complete the available information. Overall results were in agreement with the observed values and were able to represent WIBP features described in the bibliography. In addition, comparisons of the numerical system including and excluding the river discharges allowed to evaluate the impact of high river runoff in the coastal current intensities.

A description of the temporal and spatial variability of the seas surface salinity was provided by generating an annual, monthly and seasonal climatology. The climatological analysis served to describe the WIBP evolution along all the year and its interannual variability since most of previous studies focused on particular seasons or field surveys. The salinity spatial distribution was also obtained considering the wet and dry periods which implicitly are considering the IPC controlled and upwelling dominated periods respectively. The results showed two distinct patterns, during wet periods the WIBP is a low salinity narrow plume attached to the coast flowing polewards and subjected to dominating downwelling process. On the other hand, during the dry season and due to the northern winds the WIBP is subjected to upwelling conditions that spread the plume offshore and equatorward occupying large areas of the near ocean and the continental shelf. On this work, the author noticed the presence of a secondary plume resulting from the contributions of the Tagus and Sado estuaries, named West Iberian Central Plume (WICP) and that during some periods of the year is connected with low salinities with the WIBP and generated a common salinity front that covers most of the Western Iberian coast.

An original form to evaluate the area influenced by the fresh water discharged in the coastal area was to compute the 5<sup>th</sup> percentile of the modelled salinity. This approach allowed to estimate the outer reaches of the plume which are highly dynamic and can be masked in climatological mean values. From this results, it could be identified the paths followed by the buoyant plumes and to identify the areas influenced by the salinity plumes. An interesting outcome of this analysis was to see that the summer dominance of near Atlantic Ocean by the WIBP and WICP can switch between years. The salinity 5<sup>th</sup> percentile allowed to identify the winter years with some upwelling activity as the salinity signal widens offshore.

The described methodology will allow to obtain a more precise coastal circulation and to simulate the generation of salinity and temperature fronts. By coupling the land boundary conditions into the

regional ocean models in a delayed mode any improvement in the watershed and estuarine model applications will directly benefit the receiving regional ocean model.

## 7.6. References

Aznar R, Sotillo MG, Cailleau S, Lorente P, Levier B, Amo-Baladrón A, Reffray G, Álvarez-Fanjul E. Strengths and weaknesses of the CMEMS forecasted and reanalyzed solutions for the Iberia–Biscay–Ireland (IBI) waters. *Journal of Marine Systems*. 2016; 159: 1-14.

Banas NS, MacCready P, Hickey BM. The Columbia River plume as cross-shelf exporter and along-coast barrier. *Continental Shelf Research*. 2009; 29: 292–301.

Boutin J, Martin N, Reverdin G, Yin X, Gaillard F. Sea surface freshening inferred from SMOS and ARGO salinity: Impact of rain. *Ocean Science*. 2013; 9: 183-192. DOI: [10.5194/os-9-183-2013](https://doi.org/10.5194/os-9-183-2013).

Brito D, Campuzano FJ, Sobrinho J, Fernandes R, Neves R. Integrating operational watershed and coastal models for the Iberian Coast: Watershed model implementation – A first approach. *Estuarine, Coastal and Shelf Science*. 2015; 167, Part A: 138-146. DOI: [10.1016/j.ecss.2015.10.022](https://doi.org/10.1016/j.ecss.2015.10.022).

Campuzano F, Brito D, Juliano M, Fernandes R, de Pablo H, Neves R. Coupling watersheds, estuaries and regional ocean through numerical modelling for Western Iberia: a novel methodology. *Ocean Dynamics*. 2016; 66(12): 1745–1756. DOI: [10.1007/s10236-016-1005-4](https://doi.org/10.1007/s10236-016-1005-4).

Campuzano FJ, Juliano M, Sobrinho J, de Pablo H, Brito D, Fernandes R, Neves R (2018). Coupling Watersheds, Estuaries and Regional Oceanography through Numerical Modelling in the Western Iberia: Thermohaline Flux Variability at the Ocean-Estuary Interface. In: Estuary. W. Froneman (Ed), InTech, Rijeka, Croatia. DOI: [10.5772/intechopen.72162](https://doi.org/10.5772/intechopen.72162).

Carrère L, Lyard F, Cancet M, Guillot A, Roblou L. FES2012: A new global tidal model taking advantage of nearly 20 years of altimetry. *Proceedings of 20 Years of Altimetry meeting*. Venice, Italy, 24-29 September 2013.

Drillet Y, Bourdalle-Badi R, Siefrid L, Le Provost C. Meddies in the Mercator North Atlantic and Mediterranean Sea eddy-resolving model. *Journal of Geophysical Research*. 2005; 110(C3): C03016. DOI: [10.1029/2003JC002170](https://doi.org/10.1029/2003JC002170).

Fong DA, Geyer WR. Response of a river plume during an upwelling favorable wind event. *Journal of Geophysical Research: Oceans*. 2001; 106 (C1): 1067-1084. DOI: [10.1029/2000JC900134](https://doi.org/10.1029/2000JC900134).

Friedland KD, Miller MJ, Knights B. Oceanic changes in the Sargasso Sea and declines in recruitment of the European eel. *ICES Journal of Marine Science* 2007; 64 (3): 519-530. DOI: [10.1093/icesjms/fsm022](https://doi.org/10.1093/icesjms/fsm022).

Frouin R, Fiúza AF, Ambar I, Boyd TJ. Observations of a poleward surface current off the coasts of Portugal and Spain during winter. *Journal of Geophysical Research*. 1990; 95: 679-691.

Garvine RW, Whitney MM. An estuarine box model of freshwater delivery to the coastal ocean for use in climate models. *Journal of Marine Research*. 2006; 64: 173-194.

Graham JA, O’Dea E, Holt J, Polton J, Hewitt HT, Furner R, Guihou K, Brereton A, Arnold A, Wakelin S, Castillo Sanchez JM, Mayorga Adame, CG. AMM15: A new high resolution NEMO configuration for operational simulation of the European North West Shelf. *Geoscientific Model Development Discussions*. 2017; in review. DOI: [10.5194/gmd-2017-127](https://doi.org/10.5194/gmd-2017-127).

Gierach MM, Vazquez-Cuervo J, Lee T, Tsonos VM. Aquarius and SMOS detect effects of an extreme Mississippi River flooding event in the Gulf of Mexico. *Geophysical Research Letters*. 2013; 40: 5188–5193. DOI: [10.1002/grl.50995](https://doi.org/10.1002/grl.50995).

Graham JA, O’Dea E, Holt J, Polton J, Hewitt HT, Furner R, Guihou K, Brereton A, Arnold A, Wakelin S, Castillo Sanchez JM, Mayorga Adame, CG. AMM15: A new high resolution NEMO configuration for

operational simulation of the European North West Shelf. Geoscientific Model Development Discussions. 2017; in review <https://doi.org/10.5194/gmd-2017-127>

Grodsky SA, Reverdin G, Carton JA, Coles VJ. Year-to-year salinity changes in the Amazon plume: Contrasting 2011 and 2012 Aquarius/SACD and SMOS satellite data. Remote Sensing of Environment. 2014; 140: 14-22. DOI: [10.1016/j.rse.2013.08.033](https://doi.org/10.1016/j.rse.2013.08.033).

Hetland RD. Relating river plume structure to vertical mixing. Journal of Physical Oceanography. 2005; 35: 1667-1688. DOI: [10.1175/JPO2774.1](https://doi.org/10.1175/JPO2774.1).

Hopkins J, Lucas M, Dufau C, Sutton M, Stum J, Lauret O, Channelliere C. Detection and variability of the Congo River plume from satellite derived sea surface temperature, salinity, ocean colour and sea level. Remote Sensing of Environment. 2013; 139: 365-385. DOI: [10.1016/j.rse.2013.08.015](https://doi.org/10.1016/j.rse.2013.08.015).

Lagerloef G, Wentz F, Yueh S, Kao H-Y, Johnson GC, Lyman JM. Aquarius satellite mission provides new, detailed view of sea surface salinity. State of the Climate 2011. Bulletin of the American Meteorological Society. 2012; 93(7): S70–S71.

Large W, Pond S. Open Ocean momentum flux measurements in moderate to strong winds. 1981: Journal of Physical Oceanography. 1981; 11: 324-336. DOI: [10.1175/1520-0485\(1981\)011<0324:OOMFMI>2.0.CO;2](https://doi.org/10.1175/1520-0485(1981)011<0324:OOMFMI>2.0.CO;2)

Marta-Almeida M, Dubert JP, Peliz A. Simulations of extreme shelf current along the North-Western Iberian Shelf forced by wind and river runoff. Proceedings of 3<sup>rd</sup> Iberian meeting on Geophysics and Geodesy. Valencia, Spain, 4–8 February 2002. pp 1555–1559.

Mateus M, Riflet G, Chambel P, Fernandes L, Fernandes R, Juliano M, Campuzano F, de Pablo H, Neves R. An operational model for the West Iberian coast: products and services. Ocean Science. 2012; 8: 713-732.

Mendes R, Sousa MC, deCastro M, Gómez-Gesteira M, Dias JM. New insights into the Western Iberian Buoyant Plume: Interaction between the Douro and Minho River plumes under winter conditions. Progress in Oceanography. 2016; 141: 30-43. DOI: [10.1016/j.pocean.2015.11.006](https://doi.org/10.1016/j.pocean.2015.11.006).

Neves R (2013). The MOHID concept. In: *Ocean modelling for coastal management - Case studies with MOHID*. M. Mateus & R. Neves (eds.), IST Press, Lisbon, Portugal, pp. 1-11.

O'Dea E, Furner R, Wakelin S, Siddorn J, While J, Sykes P, King R, Holt J, Hewitt H. The CO5 configuration of the 7 km Atlantic Margin Model: large-scale biases and sensitivity to forcing, physics options and vertical resolution. Geoscientific Model Development. 2017; 10: 2947-2969. DOI: [10.5194/gmd-10-2947-2017](https://doi.org/10.5194/gmd-10-2947-2017).

Otero P, Ruiz-Villarreal M, García-García L, González-Nuevo G, Cabanas JM. Coastal dynamics off Northwest Iberia during a stormy winter period. Ocean Dynamics. 2013; 63: 115. DOI: [10.1007/s10236-012-0585-x](https://doi.org/10.1007/s10236-012-0585-x).

Otero P, Ruiz-Villarreal M, Peliz Á. River plume fronts off NW Iberia from satellite observations and model data. ICES Journal of Marine Science. 2009; 66: 1853–1864. DOI: [10.1093/icesjms/fsp156](https://doi.org/10.1093/icesjms/fsp156).

Otero P, Ruiz-Villarreal M, Peliz A. Variability of river plumes off Northwest Iberia in response to wind events. Journal of Marine Systems. 2008; 72(1–4): 238-255. DOI: [10.1016/j.jmarsys.2007.05.016](https://doi.org/10.1016/j.jmarsys.2007.05.016).

Peliz Á, Dubert J, Santos AMP, Oliveira PB, Le Cann B. Winter upper ocean circulation in the Western Iberian Basin—Fronts, Eddies and Poleward Flows: an overview. Deep-Sea Research I. 2005; 52: 621–646.

Peliz A, Marchesiello P, Dubert J, Marta-Almeida M, Roy C, Queiroga H, A study of crab larvae dispersal on the Western Iberian Shelf: Physical processes. Journal of Marine Systems. 2007; 68(1–2): 215-236. DOI: [10.1016/j.jmarsys.2006.11.007](https://doi.org/10.1016/j.jmarsys.2006.11.007).

Peliz Á, Rosa TL, Santos AMP, Pissarra JL. Fronts, jets, and counter-flows in the Western Iberian upwelling system, *Journal of Marine Systems*. 2002; 35(1–2): 61-77.

Picado A, Alvarez I, Vaz N, Varela R, Gomez-Gesteira M, Dias JM. Assessment of chlorophyll variability along the northwestern coast of Iberian Peninsula. *Journal of Sea Research*. 2014; 93: 2-11. DOI: [10.1016/j.seares.2014.01.008](https://doi.org/10.1016/j.seares.2014.01.008).

Queiroga H, Cruz T, dos Santos A, Dubert J, González-Gordillo JI, Paula J, Peliz Á, Santos AMP. Oceanographic and behavioural processes affecting invertebrate larval dispersal and supply in the western Iberia upwelling ecosystem. *Progress in Oceanography*. 2007; 74(2–3): 174-191. DOI: [10.1016/j.pocean.2007.04.007](https://doi.org/10.1016/j.pocean.2007.04.007).

Relvas P, Barton E. A separated jet and coastal counterflow during upwelling relaxation off Cape São Vicente (Iberian Peninsula). *Continental Shelf Research*. 2005; 25(1): 29-49. DOI: [10.1016/j.csr.2004.09.006](https://doi.org/10.1016/j.csr.2004.09.006).

Relvas P, Barton ED, Dubert J, Oliveira PB, Peliz Á, da Silva JCB, Santos AMP. Physical oceanography of the western Iberia ecosystem: Latest views and challenges. *Progress in Oceanography*. 2007; 74(2–3): 149-173. DOI: [10.1016/j.pocean.2007.04.021](https://doi.org/10.1016/j.pocean.2007.04.021).

Ribeiro AC, Peliz Á, Santos AMP. A study of the response of chlorophyll-a biomass to a winter upwelling event off Western Iberia using SeaWiFS and in situ data. *Journal of Marine Systems*. 2005; 53(1–4): 87-107. DOI: [10.1016/j.jmarsys.2004.05.031](https://doi.org/10.1016/j.jmarsys.2004.05.031).

Ruiz-Villarreal M, Bolding K, Burchard H, Demirov E (2005). Coupling of the GOTM turbulence model to some three-dimensional ocean models. In: *Marine turbulence: theories. Observations and Models. Results of the CARTUM Project*. HZ Baumert, J Simpson, J Sündermann (eds), Cambridge University Press, Cambridge, pp. 225–237.

Santos AMP, Chícharo A, Dos Santos A, Moita T, Oliveira PB, Peliz Á, Ré P. Physical–biological interactions in the life history of small pelagic fish in the Western Iberia Upwelling Ecosystem. *Progress in Oceanography*. 2007; 74: 192–209.

Santos AMP, Peliz Á, Dubert J, Oliveira PB, Angélico MM, Ré P. Impact of a winter upwelling event on the distribution and transport of sardine (*Sardina pilchardus*) eggs and larvae off western Iberia: a retention mechanism. *Continental Shelf Research*. 2004; 24(2): 149-165.

Santos AMP, Ré P, dos Santos A, Peliz Á. Vertical distribution of the European sardine (*Sardina pilchardus*) larvae and its implications for their survival. *Journal of Plankton Research*. 2006; 28(5): 523–532. DOI: [10.1093/plankt/fbi137](https://doi.org/10.1093/plankt/fbi137).

Sousa MC, Vaz N, Alvarez I, Gomez-Gesteira M, Dias JM. Modeling the Minho River plume intrusion into the Rias Baixas (NW Iberian Peninsula). *Continental Shelf Research*. 2014a; 85: 30-41. DOI: [10.1016/j.csr.2014.06.004](https://doi.org/10.1016/j.csr.2014.06.004).

Sousa MC, Vaz N, Alvarez I, Gomez-Gesteira M, Dias JM. Influence of the Minho River plume on the Rias Baixas (NW of the Iberian Peninsula). *Journal of Marine Systems*. 2014b; 139: 248–260. DOI: [10.1016/j.jmarsys.2014.06.012](https://doi.org/10.1016/j.jmarsys.2014.06.012).

Trancoso AR (2012). Operational Modelling as a Tool in Wind Power Forecasts and Meteorological Warnings. PhD dissertation thesis. Instituto Superior Técnico, Technical University of Lisbon, Portugal.

Trenberth KE, Large WG, Olson JG. The mean annual cycle in global ocean wind stress. *Journal of Physical Oceanography*. 1990; 20, 1742-1760. DOI: [10.1175/1520-0485\(1990\)020<1742:TMACIG>2.0.CO;2](https://doi.org/10.1175/1520-0485(1990)020<1742:TMACIG>2.0.CO;2).

Trigo RM, DaCamara CC. Circulation weather types and their influence on the precipitation regime in Portugal. *International Journal of Climatology*. 2000; 20: 1559–1581. DOI: [10.1002/1097-0088\(20001115\)20:13<1559::AID-JOC555>3.0.CO;2-5](https://doi.org/10.1002/1097-0088(20001115)20:13<1559::AID-JOC555>3.0.CO;2-5).

Zine S, Boutin J, Waldteufel P, Vergely JL, Pellarin T, Pascal L. Issues About Retrieving Sea Surface Salinity in Coastal Areas From SMOS Data. Transactions on geoscience and remote sensing. 2007; 45(7): 2061-2072. DOI: [10.1109/TGRS.2007.894934](https://doi.org/10.1109/TGRS.2007.894934).

# Chapter VIII - Evaluation of Upwelling transport in Western Iberia through ocean circulation and meteorological numerical models.

---

## Abstract

In this chapter, upwelling conditions for the Western Iberia region were evaluated using as indexes the offshore and coastal Ekman transport, Ekman pumping, offshore and coastal sea surface temperature difference and vertical velocity from 3D ocean circulation model. The methods, limitations and results for upwelling estimation methods were described and intercompared taking into consideration the spatial and temporal distribution of this phenomenon.

## 8.1. Introduction

Coastal upwelling is the process responsible for transporting deep nutrient-rich waters to the euphotic area where the nutrients made available are consumed by primary producers such as phytoplankton and thus entering into the trophic web. Given the strong influence with primary production and thus fisheries (Santos *et al.*, 2004 and 2007; Nogueira *et al.*, 2013) and offshore aquaculture activities (Fragoso and Icely, 2009) and its relation to harmful algae blooms (HABs) and marine ecosystems (Pitcher *et al.*, 2010; Moita *et al.*, 2003; Loureiro *et al.*, 2005), the upwelling events intensity, timing, seasonality, interannual evolution, spatial structure and future evolution due to climate change have been intensively studied intensively around the world (i.e. Wang *et al.*, 2015).

The Western Iberian ocean region falls at the northern extreme of the Canary Upwelling Ecosystem (CUE), one of the four main Eastern Boundary Upwelling Systems (EBUSs), along with the Benguela ecosystem, the California current and the Humboldt Current (Fréon *et al.*, 2006; Mason *et al.*, 2006). Recently, evidences of a progressive weakening of the upwelling regime in the last decades off the West Portuguese coast has been found especially in the warm season (April-September) (Lemos and Pires, 2004), contradicting previous analysis performed by Bakun (1990). Long-term changes in upwelling patterns off Portugal in recent decades have modified the sardine fishery (Borges *et al.*, 2003). Coastal upwelling along the western coast of the Iberian Peninsula (IP) (36-44°N) is a frequent phenomenon during the spring-summer months

Indirect indexes were derived as measuring directly the temporal and spatial extension of upwelling waters is unfeasible due to the technical difficulties to observe continuously below the euphotic area. Generally, coastal upwelling was calculated by deriving indexes associated to main wind component responsible of Ekman transport ( $UI_{ET}$ ) and/or by temperature differences between coastal areas and open ocean waters ( $UI_{SST}$ ) (i.e. Alvarez *et al.*, 2008a, 2008b, 2010 and 2011; Fiúza *et al.*, 1982; Gonzalez-Nuevo *et al.*, 2014; Pitcher *et al.*, 2010).

Other upwelling processes such as the Ekman pumping ( $UI_{EP}$ ) are commonly disregarded due to the general use of remote sensing wind data that has low accuracy near the coastal areas (Bravo *et al.*, 2016). In Western Iberia, previous upwelling studies were based in QuikSCAT satellite wind data (Alvarez *et al.*, 2008a, 2008b, 2010 and 2011) that limit the calculation of the Ekman pumping component due to the land masks of those products that are unable to resolve properly the wind drop-off.

In this study, meteorological and ocean numerical model results were analysed to characterise and quantify the upwelled waters in Western Iberia oceanic region. Upwelling indicators based on sea surface temperature and Ekman transport and pumping contributions were calculated for the period (2011-2015) and compared with vertical transport estimation based in 3D regional ocean model results.

## 8.2. Study area and numerical model

The Portuguese Coast Operational Modelling System (hereafter referred as PCOMS; Mateus *et al.*, 2012) is the regional ocean model application and is composed of two modelling domains with constant horizontal resolution of 0.06° (≈6 km): the West Iberia (2D) and the Portugal (3D) domains covering the Iberian Atlantic coast and its contiguous ocean operated by the MOHID Water model (<http://www.mohid.com>; Neves, 2013).

The MOHID Water, part of the MOHID Modelling System, is an open source numerical model programmed in ANSI FORTRAN 95 using an object orientated philosophy. This system is being developed since 1985 mainly by the MARETEC group at the Instituto Superior Técnico (IST) of the Universidade de Lisboa. The model adopted an object oriented philosophy integrating different scales and processes. The core of the model is a fully 3D hydrodynamic model which is coupled to different modules comprising water quality, atmosphere processes, discharges, oil dispersion, jet mixing zone model for point source discharges. The WaterQuality module coupled in the PCOMS is basically a nutrient- phytoplankton-zooplankton (NPZ) model adapted from a model developed at USEPA (U.S. Environmental Protection Agency) (Bowie *et al.*, 1985).

The West Iberia domain covers the area limited the following range of latitudes (33.48°N, 45.90°N) and longitudes (4.20°W, 13.50°W) resulting in a grid of 207 x 155 cells with maximum depths reaching 5600 m. The Portugal domain is nested in the West Iberia domain in a central position, leaving 15 cells of difference in every direction, and covers the area comprised by the latitudes (34.38°N, 45.00°N) and the longitudes (5.10°W, 12.60°W) resulting in a grid of 177 x 125 cells and maximum depths around 5300 m. The latter domain is a fully 3D baroclinic hydrodynamic and ecological model applications that downscales the Mercator-Océan PSY2V4 North Atlantic solution (Drillet *et al.*, 2005). Both domains were populated with bathymetric information derived from the EMODnet Hydrography portal (<http://www.emodnet-hydrography.eu>) as available in January 2012. Tides are forced along the ocean boundary of the West Iberia (2D) model domain, using the global tide solution FES2012 (Carrère *et al.*, 2013). The vertical discretisation consists on a mixed vertical geometry composed of a sigma domain with 7 layers from the surface until 8.68 m depth, with variable thickness decreasing up to 1 m at the surface, on top of a Cartesian domain of 43 layers with thickness increasing towards the bottom. For simplicity, hereafter, the 3D Portugal model domain would be referred as PCOMS as all the analysed model results in this work correspond to this domain.

In the atmosphere boundary, the PCOMS system was forced by three-hour model results obtained from a MM5 model application (Meteorological Model 5; Grell *et al.*, 1994) consisting in two nested grids with a horizontal resolution of 27 km and 9 km respectively and operated by the IST meteorological group (<http://meteo.tecnico.ulisboa.pt/>; Trancoso, 2012). From the nutrients point of view, the PCOMS domain was initialised and is forced at its boundaries by 3D monthly climatological fields of oxygen, nitrate and phosphate from the World Ocean Atlas 2009 (WOA09; Garcia *et al.*, 2010a and 2010b).

## 8.3. Data and Methods

### 8.3.1. Ekman Transport Calculation

The Upwelling Index related to the Ekman Transport,  $UI_{ET}$ , can be calculated as the transport component in the direction perpendicular to the coast as defined by Bakun (1973): “The magnitude of the offshore component is considered an indication of the amount of water upwelled through the

bottom of the Ekman layer to replace that driven offshore". The formulas used to calculate the Ekman transport in each direction are based in the surface wind stress (Equation 1):

$$Q_x = \frac{\tau_y}{\rho_w f} \cdot 1000 \quad Q_y = -\frac{\tau_x}{\rho_w f} 1000 \quad \text{Equation 1}$$

where  $\rho_w$  is the seawater density ( $1025 \text{ kg m}^{-3}$ ) and  $f$  is the Coriolis parameter calculated as  $2\Omega\sin(\phi)$  where  $\Omega$  is the Earth's angular velocity and  $\phi$  is the latitude. The wind stress components  $\tau_x$  and  $\tau_y$  were calculated using the bulk formula (Equation 2):

$$\tau_{(x,y)} = \rho_a C_d |U|(u, v) \quad \text{Equation 2}$$

where  $u$  and  $v$  represent the meridional and zonal wind component respectively at 10 m height,  $|U|$  is the velocity intensity modulus and  $\rho_a$  is the air density ( $1.22 \text{ kg m}^{-3}$ ).

The drag coefficient  $C_d$  have been commonly used in similar studies as constant value of  $1.3\text{-}1.4 \cdot 10^{-3}$  (i.e. Alvarez *et al.*, 2008a, 2008b, 2010 and 2011; Castro *et al.*, 1994; deCastro *et al.*, 2008; Cropper *et al.*, 2014; Gomez-Gesteira *et al.*, 2006; Loureiro *et al.*, 2005; Santos *et al.*, 2011a and 2011b). In the present study, the  $C_d$  values were calculated using the parameterisation proposed by Large and Pond (1981) including the modifications for low wind speeds considered in Trenberth *et al.* (1990) and expressed in Equation 3:

$$C_d = \begin{cases} 2.18 \cdot 10^{-3} & \text{if } |U| \leq 1 \text{ ms}^{-1} \\ \left(0.62 + \frac{1.56}{|U|}\right) \cdot 10^{-3} & \text{if } 1 \text{ ms}^{-1} < |U| < 3 \text{ ms}^{-1} \\ 1.14 \cdot 10^{-3} & \text{if } 3 \text{ ms}^{-1} \leq |U| < 10 \text{ ms}^{-1} \\ (0.49 + 0.065|U|) \cdot 10^{-3} & \text{if } 10 \text{ ms}^{-1} \leq |U| \end{cases} \quad \text{Equation 3}$$

A  $C_d$  constant value tends estimate larger upwelling/downwelling transport than the previous parameterisation (Equation 3) since the commonly used values for  $C_d$  are higher than the calculated for the wind ranges between 3 and  $12 \text{ ms}^{-1}$ .

The Western Iberia coastal orientation can be considered approximately  $90^\circ$  in the Western coast and  $0^\circ$  in the Northern and Southern coasts, calculations will be made for  $Q_x$  and  $Q_y$  respectively.  $Q_x$  negative values would be associated to upwelling favourable conditions and vice versa.  $Q_y$  positive values would be related to upwelling events in the Northern coast and downwelling events in the Southern coast and vice versa.  $Q_x$  and  $Q_y$  have been calculated for each cell and instant of the MM5 modelling results for a six-year period (2010-2015). For simplicity and to favour comparisons, the Upwelling Index related to the Ekman transport ( $UI_{ET}$ ) values were converted following the next criteria: positive values correspond to upwelling conditions and negative values to downwelling conditions ( $Q_x$  and  $Q_y$  in the South coast were multiplied by minus one).

### 8.3.2. Ekman Pumping

The vertical velocity from Ekman pumping ( $W_{EP}$ ) was estimated using Equation 4 (Stommel, 1958) which is commonly used in these kind of studies (i.e. Halpern, 2002; Renault *et al.*, 2012):

$$W_{EP} = \frac{\text{Curl}(\tau)}{\rho_w f} + \frac{\beta \tau_x}{\rho_w f^2} \quad \text{Equation 4}$$

where  $\tau$  is the wind stress,  $\beta$  is the Coriolis parameter gradient and  $\tau_x$  is the cross-shore wind stress. Since latitude variations are not significant the last term in Equation 4 was neglected. Wind stress curl was calculated for each cell of the model domain using the centred differences method, considered to produce satisfactory results (Pickett and Paduan, 2003).

### 8.3.3. Hydrodynamic model vertical transport

In parallel the amount of upwelled water and properties will be quantified by using the modelling results of PCOMS 3D model. This alternative method consists in quantifying numerically the vertical water and nutrient fluxes through a given area by using the vertical velocity ( $w$ ), the cell horizontal dimensions ( $\delta x$  and  $\delta y$  have a constant value of  $0.06^\circ$ ) and the model nutrient concentrations. Due to its complexity, only a few upwelling transport studies have been evaluated using numerical models (Myrberg and Andrejev, 2003; Jacox *et al.*, 2014).

## 8.4. Results

In this section, upwelling transport indexes obtained from meteorological numerical model, ocean circulation model and SST remote sensing are presented.

### 8.4.1. Upwelling Index from meteorological numerical model

The  $UI_{ET}$  was calculated for each instant of the MM5 model results, every three hours, and monthly averaged for the period 2010-2015 (Figure 1).

Upwelling conditions dominate clearly the western coast of the Iberian Peninsula from April to September and reach maximum values during July with a local maximum of about  $880 \text{ m}^3\text{s}^{-1}\text{km}^{-1}$  off Cape São Vicente ( $37^\circ\text{N}$ ). Downwelling conditions only predominate along the entire west coast in the months of October and December with a maximum downwelling around  $-600 \text{ m}^3\text{s}^{-1}\text{km}^{-1}$  off Cape Finisterre ( $43^\circ\text{N}$ ). In the remaining months, two different areas can be distinguished where upwelling conditions dominate southern than  $41^\circ\text{N}$  and northern areas weak downwelling conditions are present with minima between  $-70$  and  $-150 \text{ m}^3\text{s}^{-1}\text{km}^{-1}$ .

In the Western Iberian coast, zonal and meridional gradients in the Ekman transport distribution can be clearly identified (Figure 1). The Ekman transport zonal gradient is generated by a zonal wind weakening from the open ocean areas to the coastal areas and as a consequence coastal Ekman transport can halve compared with the offshore values. Although this gradient will reduce the upwelling capacity of the Ekman transport, it will contribute positively to the Ekman pumping process. Also a clear meridional gradient is observed where Ekman transport increases towards the south, indicating increased upwelling conditions, and decreases towards the North, indicating increased downwelling conditions in October and December months.

Alvarez *et al.* (2008a) found a similar distribution of upwelling conditions in this same area by using QuikSCAT satellite data for the period 2000-2006. However the intensity of the events were overestimated due to the use of a constant  $C_d$ . In example, maximum upwelling values for the month of July were  $1100\text{--}1200 \text{ m}^3\text{s}^{-1}\text{km}^{-1}$  at  $36^\circ\text{N}$ , those same values are found in our results for the same month and locations when using the same constant valued for  $C_d$  of  $1.4 \cdot 10^{-3}$  (Figure 2).

Due to the nature of the used data by Alvarez *et al.* (2008a), their results were not able to capture the complete decline of wind intensities near the coastal area as QuikSCAT satellite data minimum distance to the coast with reliable data is around 75 km and wind data close to coast ( $\sim 25$  km) are not available due to the existence of a coast mask (Alvarez *et al.*, 2008a and 2008b).

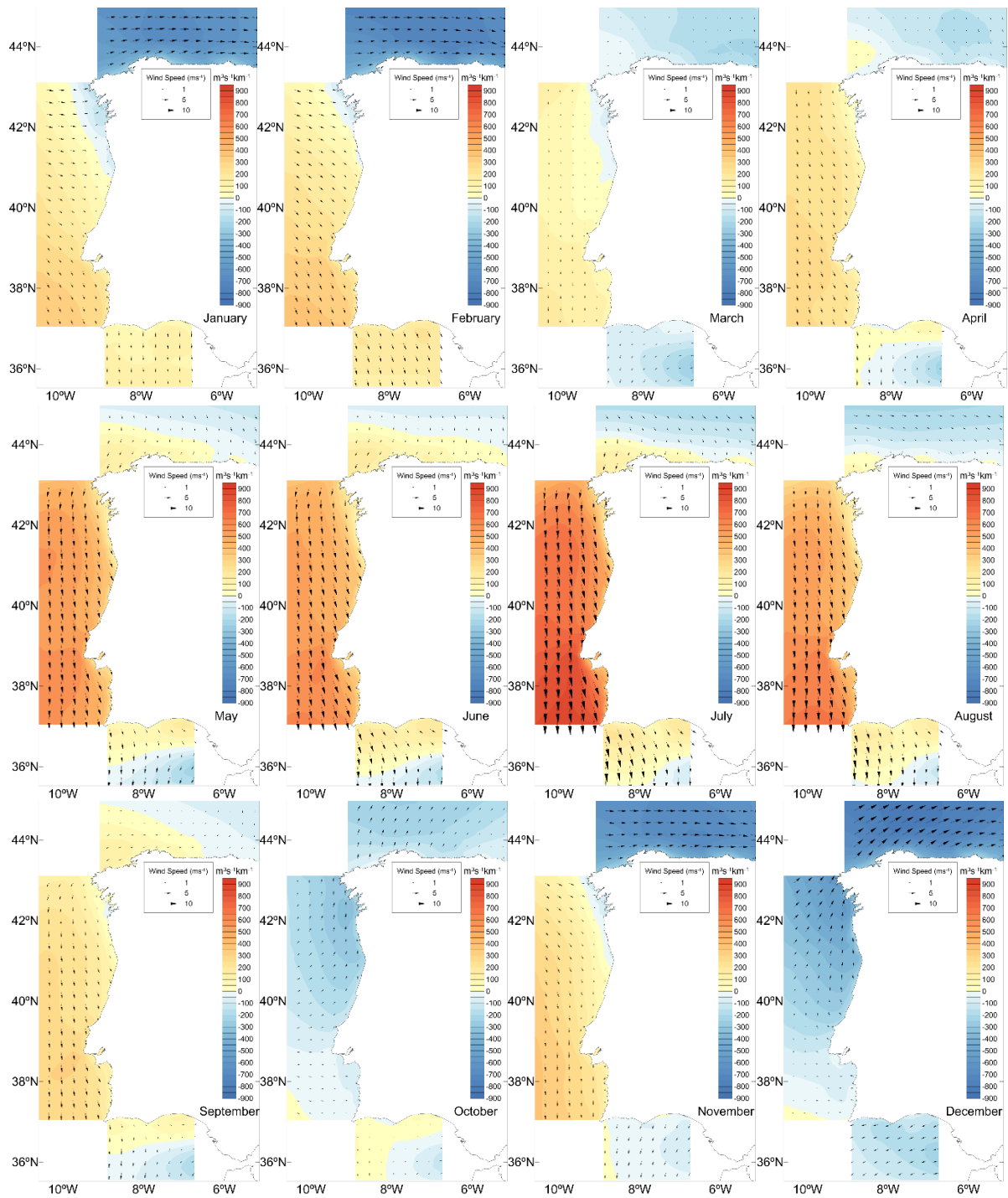
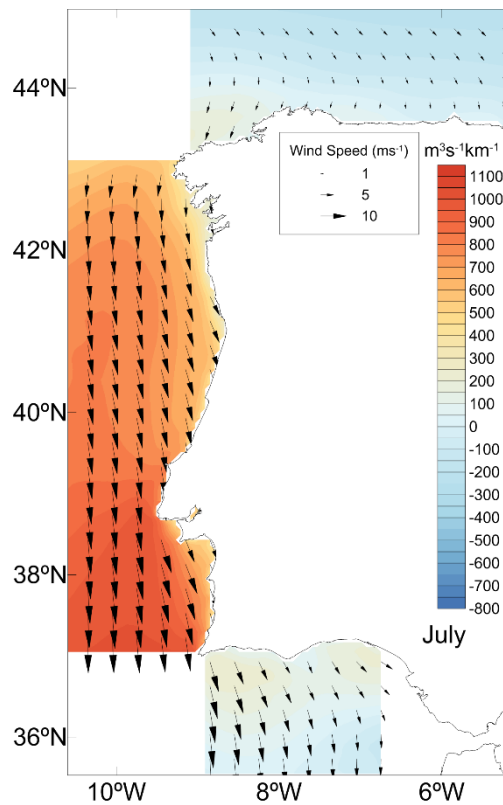


Figure 1 Monthly averaged upwelling transport for the West, North and South coasts for the period 2010-2015. Positive values indicate upwelling conditions and negative values are associated to downwelling conditions. Vectors represent the average wind direction and intensity (every fifth vector is shown).



**Figure 2** Averaged upwelling transport for the West, North and South coasts for the month of July during the period 2010-2015 using a constant drag coefficient ( $C_d$ ) of  $1.4 \cdot 10^{-3}$ . Positive values indicate upwelling conditions and negative values are associated to downwelling conditions. Vectors represent the average wind direction and intensity (every fifth vector is shown).

In the northern sector, downwelling conditions dominated during the October-March period. Maximum downwelling transport was observed during December with values lower than  $-800 \text{ m}^3\text{s}^{-1}\text{km}^{-1}$ . Those maxima reduced to values around  $-200 \text{ m}^3\text{s}^{-1}\text{km}^{-1}$  during the October and March months. In a similar way to the western coast, maximum downwelling values were found offshore and reduced towards the coast due to the wind drop-off. During the spring-summer period, April-September, the upwelling favourable conditions increased westwards. Uninterrupted upwelling conditions along the coast only took place in June, where maximum upwelling transport were observed (around  $200 \text{ m}^3\text{s}^{-1}\text{km}^{-1}$ ). During this season, two gradients were observed a meridional gradient with an offshore area with almost permanent downwelling conditions and a zonal gradient where upwelling areas are located in the western part of the analysed area and downwelling conditions prevail in the eastern area unless for some coastal areas.

In the southern sector, favourable upwelling conditions prevail except for March, November and December. Similar maximum of upwelling transport, around  $200 \text{ m}^3\text{s}^{-1}\text{km}^{-1}$ , was observed during two periods February and June-July while those values reduced to  $150 \text{ m}^3\text{s}^{-1}\text{km}^{-1}$  in January, May and August. Only during January and February the entire area presented upwelling conditions, while during the April-October period upwelling conditions dominated mainly in the coastal area and in the western coast than in offshore waters. Downwelling transport presented similar maximum around  $-250 \text{ m}^3\text{s}^{-1}\text{km}^{-1}$  in March and December.

In summary, it was observed a monthly variability of the upwelling index in the three coastal WI areas (West, North and South). In the west coast, upwelling favourable conditions prevailed during most of the year. The upwelling intensity reached its maximum during the summer period, May-August, coinciding with upwelling favourable conditions in both northern and southern coasts thus resulting in general upwelling conditions for most of western Iberia coasts. The northern and southern regions presented similar upwelling and downwelling patterns during the summer months

and in December respectively. However, during the January-February period these regions presented opposite vertical transport patterns being dominated by upwelling and downwelling conditions in the south and in the north respectively. During upwelling favourable conditions, northern and southern coasts presented vertical transports of the same magnitude. However, northern coast downwelling conditions are the more intense of the entire Western Iberia.

Despite being aware of the existing alongshore gradients in the western Iberia region and in order to compare our results with similar studies (i.e. Alvarez *et al.*, 2001 and 2008a; Picado *et al.*, 2014) the temporal evolution of the Ekman transport along the studied period was evaluated using defined transects. Monthly averaged Ekman transport was calculated for each instant and each modelling cell along three defined transects, two zonal and one meridional. The transects were defined along the northern (from 8.70°W to 5.50°W along the latitude 44.00°N), southern (from 8.70°W to 6.50°W along the latitude 36.50°N) and western (from 37.03°N to 43.05°N along the longitude 9.80°W) coasts (Figure 3).

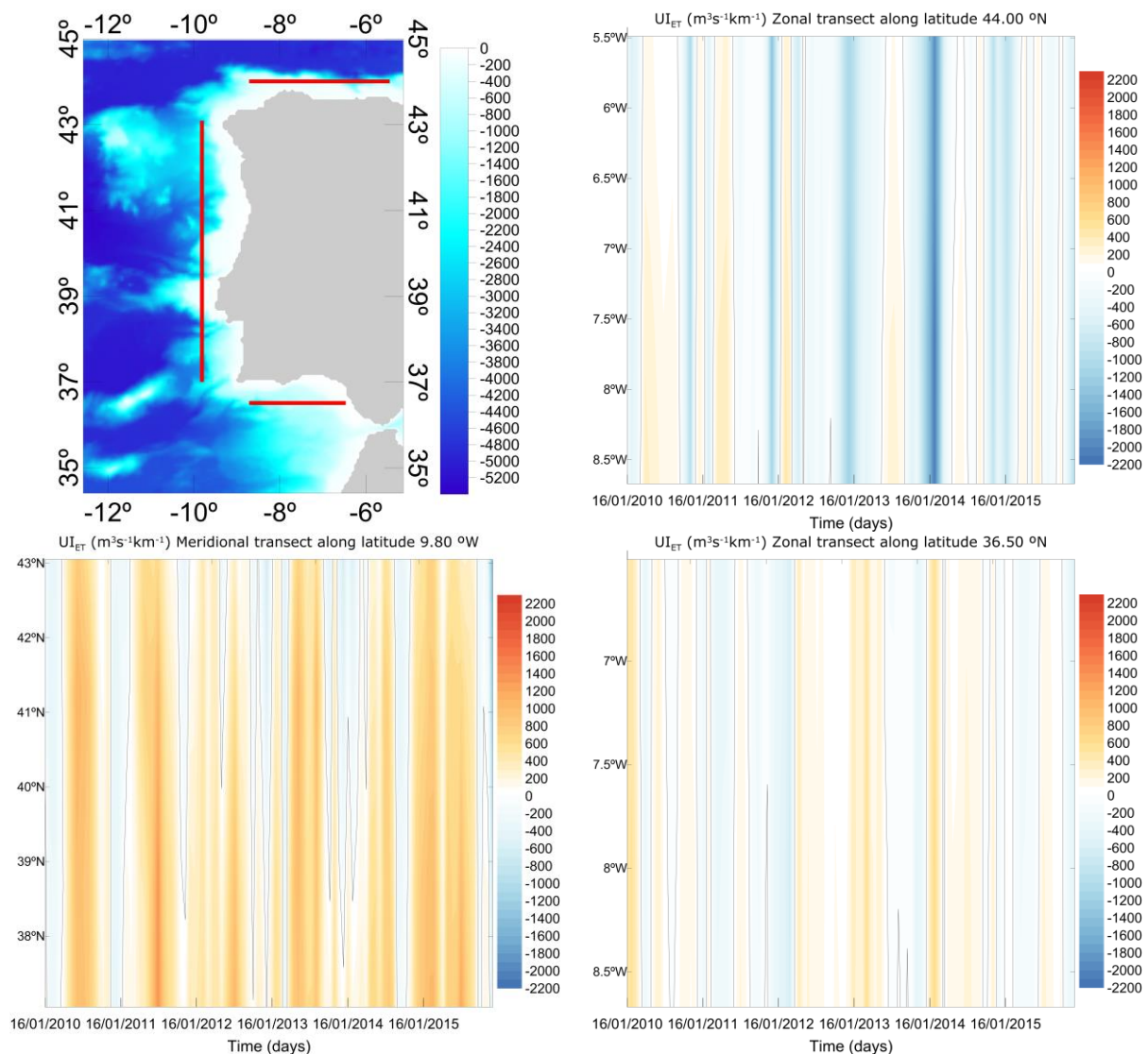


**Figure 3** Monthly upwelling transport for the northern (top right), western (bottom left) and southern (bottom right) coasts along the zonal and meridional transects (top left) for the period 2010-2015. Positive values indicate upwelling conditions and negative values are associated to downwelling conditions. The continuous line indicate the 0 value.

In the western transect, upwelling conditions prevailed during the entire analysed period with maximum values observed in the summer period. Downwelling favourable conditions were limited to the winter period and in some of the analysed years those conditions only were applied in the northern areas. The maximum upwelling event was registered in July 2011 at the southern limit of the transect when Ekman transport obtained values around  $1200 \text{ m}^3\text{s}^{-1}\text{km}^{-1}$ . The maximum downwelling event was identified in the northern margin in December 2015 with the same order of magnitude. Downwelling transport in the southern limit was lower than  $-400 \text{ m}^3\text{s}^{-1}\text{km}^{-1}$  for the entire period while upwelling transport values over  $800 \text{ m}^3\text{s}^{-1}\text{km}^{-1}$  are common in the northern reach during the studied period.

A similar seasonal pattern is observed in the northern transect, upwelling favourable conditions were related to the summer period though with a high interannual variability with summers where upwelling conditions were absent (i.e. 2012). Downwelling conditions appeared uniformly distributed along the northern section while upwelling events were mainly located in the western reach. During the analysed period, the downwelling maximum event was observed during February 2014 with lower values than  $-2200 \text{ m}^3\text{s}^{-1}\text{km}^{-1}$  while the maximum upwelling event was below  $500 \text{ m}^3\text{s}^{-1}\text{km}^{-1}$ .

The southern coast presented a balanced pattern of upwelling and downwelling events with a tendency for stronger upwelling than downwelling events. Upwelling favourable conditions were present during most of the summer periods and these conditions could take place, as in the west coast, during the early months of the year. Maximum monthly upwelling/downwelling conditions were around  $\pm 600 \text{ m}^3\text{s}^{-1}\text{km}^{-1}$  and took place during February 2014 and March 2013 respectively

Spatially averaged upwelling indexes were obtained for each transects in order to ease the results interpretation and to allow compare between areas (Figure 4). The West Iberian coast was clearly dominated by upwelling favourable conditions since downwelling favourable conditions were present only during 16 out of 72 months (22.22%). Despite the more intense upwelling conditions were concentrated in the May-August period; upwelling favourable conditions were observed in every month of the year. Examples of large winter upwelling conditions were observed in the month of February of 2012, 2013 and 2015.

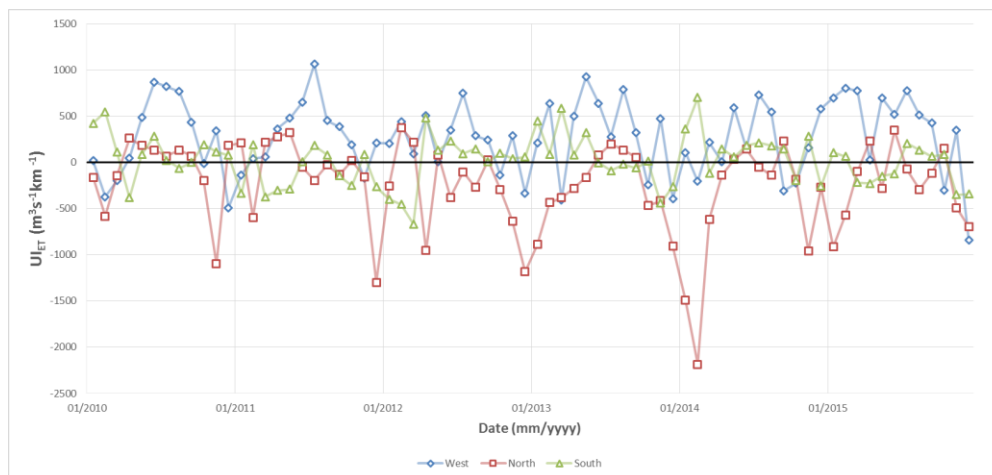


**Figure 4 Monthly spatially averaged upwelling indexes for the West (blue diamonds), North (red squares) and South (green triangles) transects for the period 2010-2015. Positive/negative values indicate upwelling/downwelling conditions.**

In the southern coast, upwelling favourable conditions prevailed during over 60% of the analysed months though their intensity was lower than in the west coast. However, at the beginning of some years, the upwelling transport in the south coast was larger than in the west coast such as in 2010 and 2014. In the northern coast, downwelling conditions dominate during 60% of the time with periods with lower transport than  $-1000 \text{ m}^3\text{s}^{-1}\text{km}^{-1}$  while the maximum upwelling was below  $500 \text{ m}^3\text{s}^{-1}$

$^1\text{km}^{-1}$ . Figure 4 also shows the remarkable differences in intensity and timing of the maximum upwelling and downwelling events among the analysed period.

On average the western and the northern Iberian coasts were characterised by net upwelling and downwelling conditions respectively for each year of the analysed period while the southern coast present an annual net upwelling/downwelling character according to the analysed year (Table 1).

**Table 1 Upwelling Index annual average for the three analysed transects in  $\text{m}^3\text{s}^{-1}\text{km}^{-1}$ .**

Year	Western Coast	Northern Coast	Southern Coast
2010	259.18	-96.56	118.26
2011	345.30	-117.15	-118.14
2012	249.08	-281.01	-19.97
2013	348.91	-289.27	54.41
2014	219.33	-469.25	142.00
2015	397.25	-234.43	-63.05
<b>Total</b>	<b>303.17</b>	<b>-247.95</b>	<b>18.92</b>

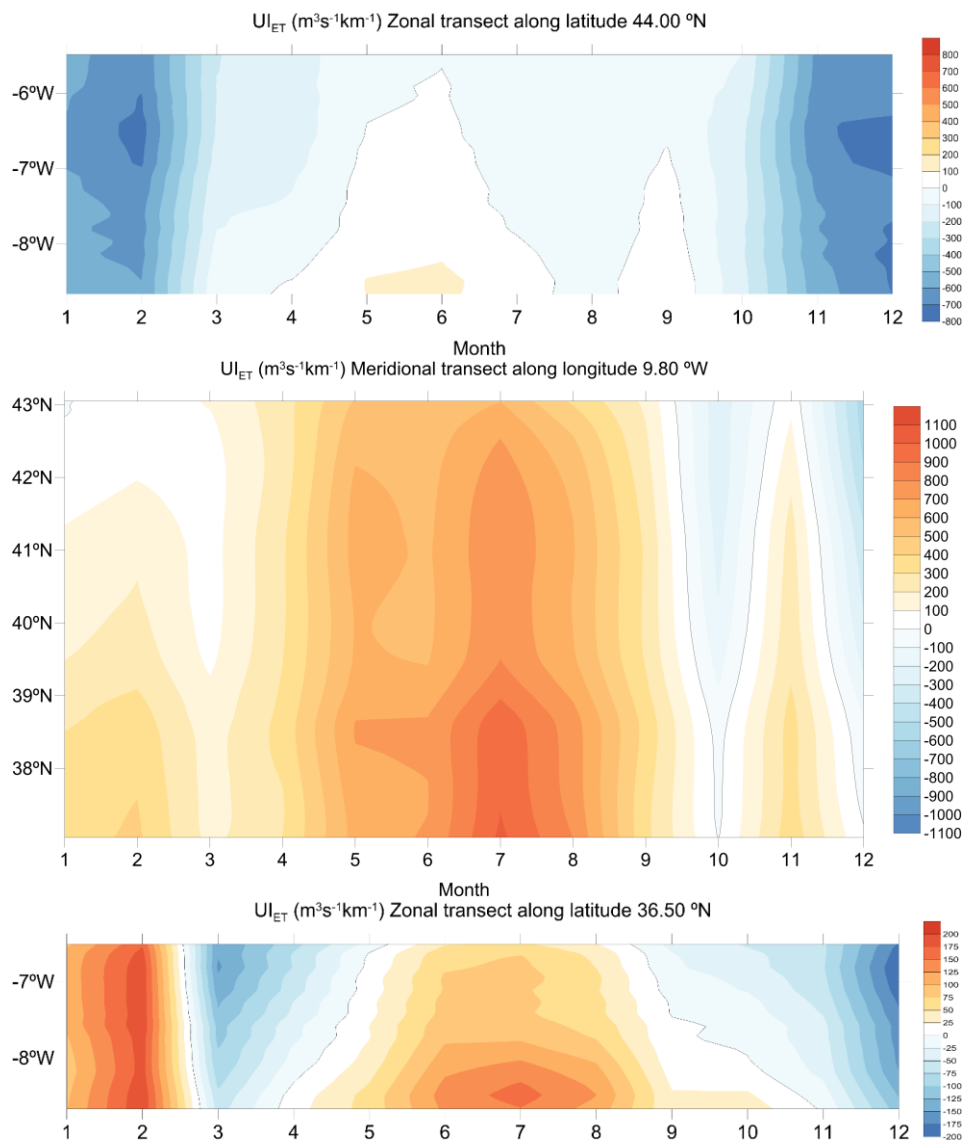


**Figure 5 Mean upwelling indexes for each month in the North (top), west (centre) and south (bottom) transects during the 2010-2016 period. Positive values indicate upwelling conditions and negative values are associated to downwelling conditions. The continuous line indicate the 0 value.**

Figure 5 shows the  $UI_{ET}$  annual cycle for each transect. In the three areas, although with different intensities, it was observed that upwelling conditions take place during the May-September period while downwelling conditions take place during the October-December period. In the west coast a clear latitudinal gradient in Ekman transport was observed with intensities decreasing northwards. In the western and southern section, the summer upwelling maximum coincide in July with values around 1020 and 150  $m^3s^{-1}km^{-1}$  respectively while in the northern section the maximum was observed in June with maximum values around 120  $m^3s^{-1}km^{-1}$ . A secondary upwelling season take place at the beginning of the year in the western and southern coast with a maximum located in February and values around 300 and 200  $m^3s^{-1}km^{-1}$  respectively. This pattern contrasts with the clear downwelling conditions prevailing simultaneously in the northern section. Finally, in the west coast upwelling conditions crosses the entire western region in November with similar intensity than the early year upwelling event though shorter in time.

In order to ease the pattern interpretation and assuming a relative homogeneity along the sections, the  $UI_{ET}$  climatological values were spatially averaged (Figure 6). The annual evolution of the Ekman transport in the three coastal areas showed a similar pattern during the May-September period. In the western and southern coasts, Ekman transport values were positive reaching their maximum in July with values above 800 and 100  $m^3s^{-1}km^{-1}$  respectively. During this period, the north coast transport are on average around the neutrality though during May, June and September they are slightly positive indicating the upwelling events can take place during this season although with low intensities (i.e. maximum reached in June with net transport below 100  $m^3s^{-1}km^{-1}$ ). Western and southern coasts showed also a tendency of similar intensity for upwelling conditions during the early months of the year. In the West coast upwelling conditions were also registered in November. Downwelling conditions were registered in the northern coast from October to April uninterruptedly.

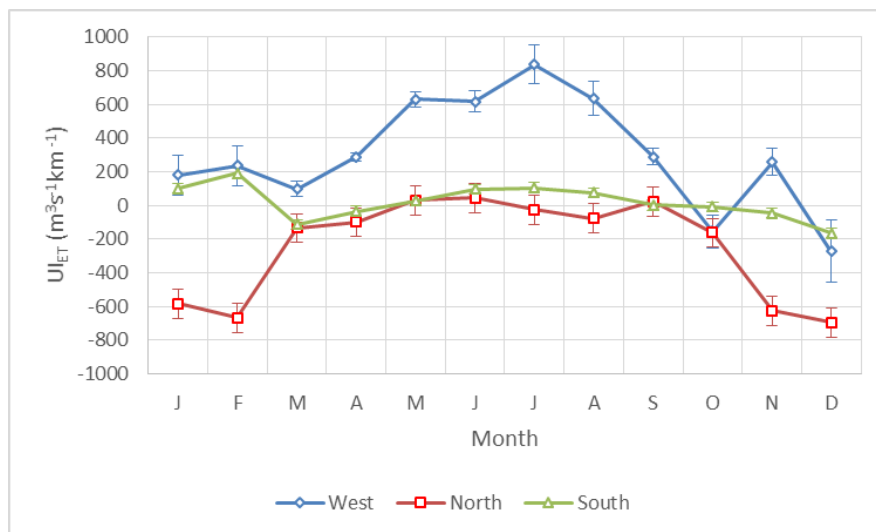


**Figure 6 Monthly spatially averaged upwelling indexes for the west (blue diamonds), North (red squares) and south (green triangles) transects for the period 2010-2015. Positive values indicate upwelling conditions and negative values are associated to downwelling conditions. The error bars were calculated using the standard deviation of the monthly data.**

The estimated Ekman transports values for the west coast are in agreement with previous studies where upwelling favourable conditions dominated from early spring until September with the maximum value in July with 800 and 1000  $m^3s^{-1}km^{-1}$  in Picado *et al.* (2014) and Alvarez *et al.* (2011) respectively. These previous studies also identified upwelling events during autumn-winter seasons with peaks between 150-600  $m^3s^{-1}km^{-1}$  in February and November.

In general, the Ekman transport observed offshore the Iberian Peninsula western coast decreases steadily northwards. Figure 7 shows the mean Ekman transport at each latitude along the longitude

9.80 °W. The decline occurs in two phases, from Cape São Vicente (37 °N) to Cape Raso (38.75 °N) the decline is soft and in some years the transport can increase locally around this area. From Cape Raso northwards the Ekman transport decreased at a higher rate. It should be noted that the Cape Raso distance is the closest land area to the longitude 9.80 °W and the calculus are performed over the continental platform. Despite this general trend, the year 2010 showed an almost uniform transport between the analysed latitudes. In the same figure, it can be observed the interannual variability of the Ekman transport in consecutive years, i.e. 2014 and 2015, can present a difference of nearly 100% (Table 1).

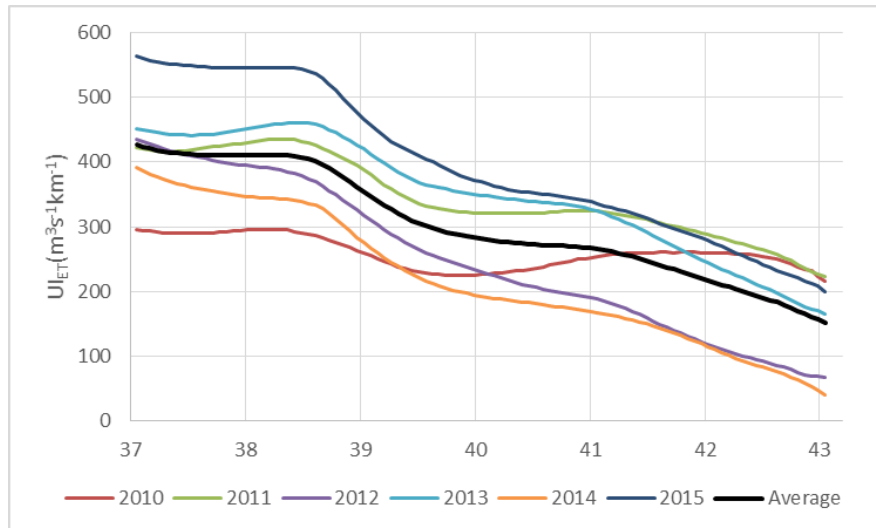


Figure 7 Annually averaged upwelling index for the Western Iberian coast. The dark thick line indicates the entire period average value.

#### 8.4.2. Upwelling pumping from meteorological numerical model

When approaching the coastal area, the wind velocity reduces and thus the Ekman transport. The wind gradient creates conditions for the generation of Ekman pumping/sucking that transport vertically waters in the coastal area. This upwelling mechanism has been less analysed since the QuikSCAT, commonly used in previous upwelling studies in the west IP, is blind near the coastal zone (Renault *et al.*, 2016) and that avoided the accurate calculation of the wind drop-off length ( $L_d$ ) associated to the coastal wind weakening.

Following the methodology suggested in Renault *et al.* (2016), the Ekman pumping velocity were obtained by using monthly mean values of MM5 model results and  $L_d$  was computed using a wind curl threshold value. According to the same authors, this approach allow to obtain a more accurate and stable  $L_d$  estimation than using along-shore wind gradient. The rationale behind this method is that in case that the wind curl values are weak their contributions for the upwelling can be neglected. Renault *et al.* (2016) defined a reference limit for the wind drop-off length based in the cross-shore wind curl ( $>3 \times 10^{-5} \text{ s}^{-1}$ ) for the US West coast. The same methodology was applied by for the Chilean coast Bravo *et al.* (2016) in this case ( $<-3 \times 10^{-5} \text{ s}^{-1}$ ).

In the current work, that limit ( $3 \times 10^{-5} \text{ s}^{-1}$ ) was applied to our study area and analysed period in both senses to quantify Ekman pumping and sucking. Figure 8-left show the mean wind curl for the entire period in western Iberia, the black continuous line marks the limit for wind drop-off ( $>3 \times 10^{-5} \text{ s}^{-1}$ ); permanent areas below the limit of ( $<-3 \times 10^{-5} \text{ s}^{-1}$ ) were not identified. On average, the west coast of the Iberian Peninsula presents wind sucking conditions, with different width and intensities, all along the coast. Three major areas can be distinguished in Western Iberia: the Galician Rias region, where Blanton *et al.* (1984) and Castro *et al.* (1994) observed stationary upwelling maximum and a recurrent upwelling filament, the northern Portugal region between the Minho and Douro rivers and the Raso-Espichel region centred around the Lisbon bay where the Tagus estuary mouth is located.

Between the last two regions and from Cape Espichel to Cape São Vicente two coastal narrow stripes with Ekman sucking conditions were identified. In Figure 8 the mean wind stress curl and Ekman pumping for the entire period are also represented including the wind curl limit value. In the northern and southern coast the wind curl is below the defined limit. However, it can be pointed out the downwelling trend observed in the northern coast and the upwelling tendency in the western part of the south coast.

Figure 8 right show the mean distribution of the Ekman pumping velocity after applying Equation 4 for the entire period. Maximum positive mean values ( $\approx 1.35 \text{ md}^{-1}$ ) were found around Capes Raso and Roca ( $38.77^\circ \text{N}$ ), the westernmost extent of mainland Portugal, while maximum negative values ( $\approx -0.62 \text{ md}^{-1}$ ) were observed in the northernmost part of the studied area.

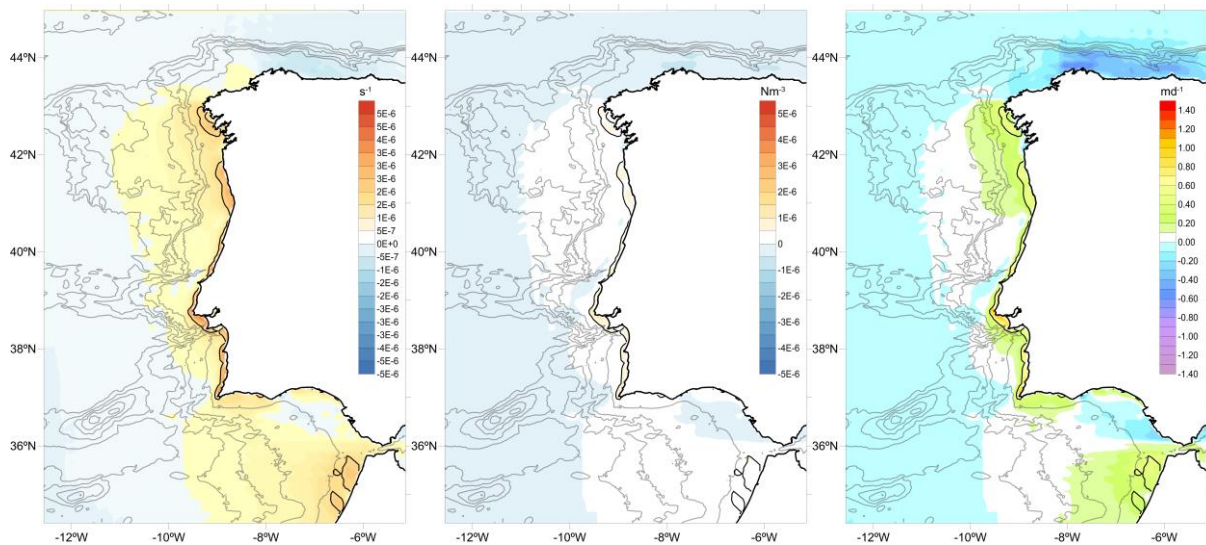


**Figure 8 Mean wind curl (left), wind stress curl (centre) and pumping velocity (right) for the period 2010-2015. Contour line indicate wind curl limit of  $3 \cdot 10^{-5} \text{ s}^{-1}$ . Isobaths are represented every 1000 m starting at 500 m.**

Figure 9, Figure 10 and Figure 11 map the mean wind curl, mean wind stress curl and mean Ekman pumping for each month of the year during the analysed period 2010-2015. In each map is included the isoline of  $\pm 3 \cdot 10^{-5} \text{ s}^{-1}$  corresponding to the mean wind curl for that particular month. In these figures it can be observed how, from April to September, upwelling conditions due to Ekman sucking dominate in almost the entire western coast, from Cape Finisterre to Cape São Vicente, and in the western side of the southern coast. Downwelling conditions according to the defined wind curl limit only appeared in the northern coast during the November-February period and in some parts of the western coast during the months of October and December. In the southern half of the western coast upwelling conditions were observed during January, February and November. In the southern coast, a distinction between the coastal stretches located western and eastern to the Ria Formosa can be done regarding Ekman pumping trends. Downwelling conditions due to Ekman pumping dominated both areas during the month of December, however, this character extended in the eastern stretch from November to February. In February Ekman pumping senses were different on both sides of the Ria Formosa. Northern than Cape Finisterre, there a local area on its western side with tendency for upwelling transport during May-June period. During the month of March, there is practically not significant transport related to Ekman pumping in the entire studied area.

The peak value for Ekman pumping ( $\approx -3.5 \text{ md}^{-1}$ ) was observed in December in the vicinity of Cape Finisterre while the maximum Ekman sucking ( $\approx 2.9 \text{ md}^{-1}$ ) took place during July near Cape Raso (Figure 11).

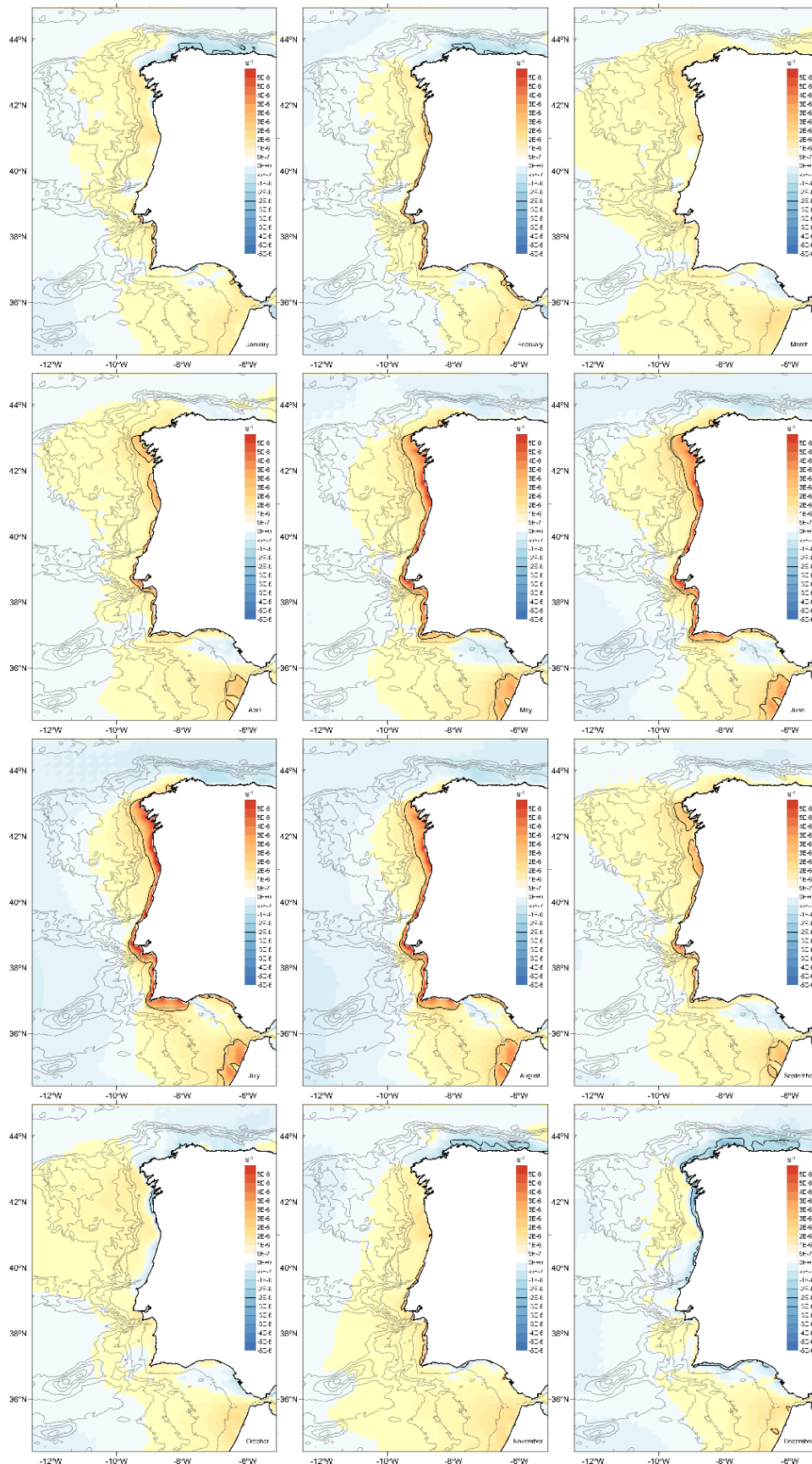


Figure 9 Monthly averaged wind curl for the period 2010-2016. Positive values indicate upwelling conditions and negative values are associated to downwelling conditions. Contour lines indicate wind curl limit value of  $\pm 3 \cdot 10^{-5} \text{ s}^{-1}$ . Isobaths are represented every 1000 m starting at 500 m.

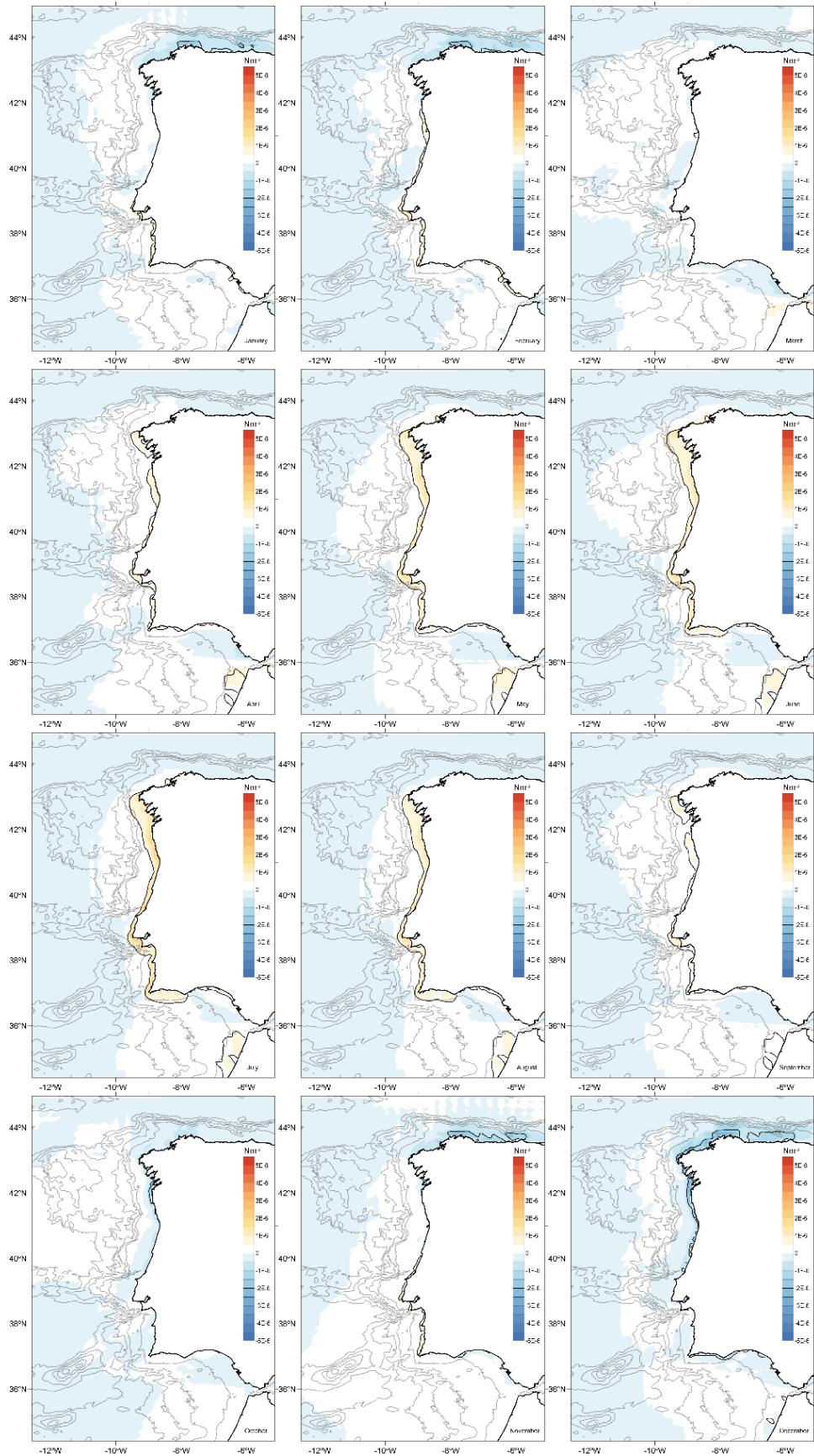


Figure 10 Monthly averaged wind stress curl for the period 2010-2016. Positive values indicate upwelling conditions and negative values are associated to downwelling conditions. Contour lines indicate wind curl limit value of  $\pm 3 \cdot 10^{-5} \text{ s}^{-1}$ . Isobaths are represented every 1000 m starting at 500 m.

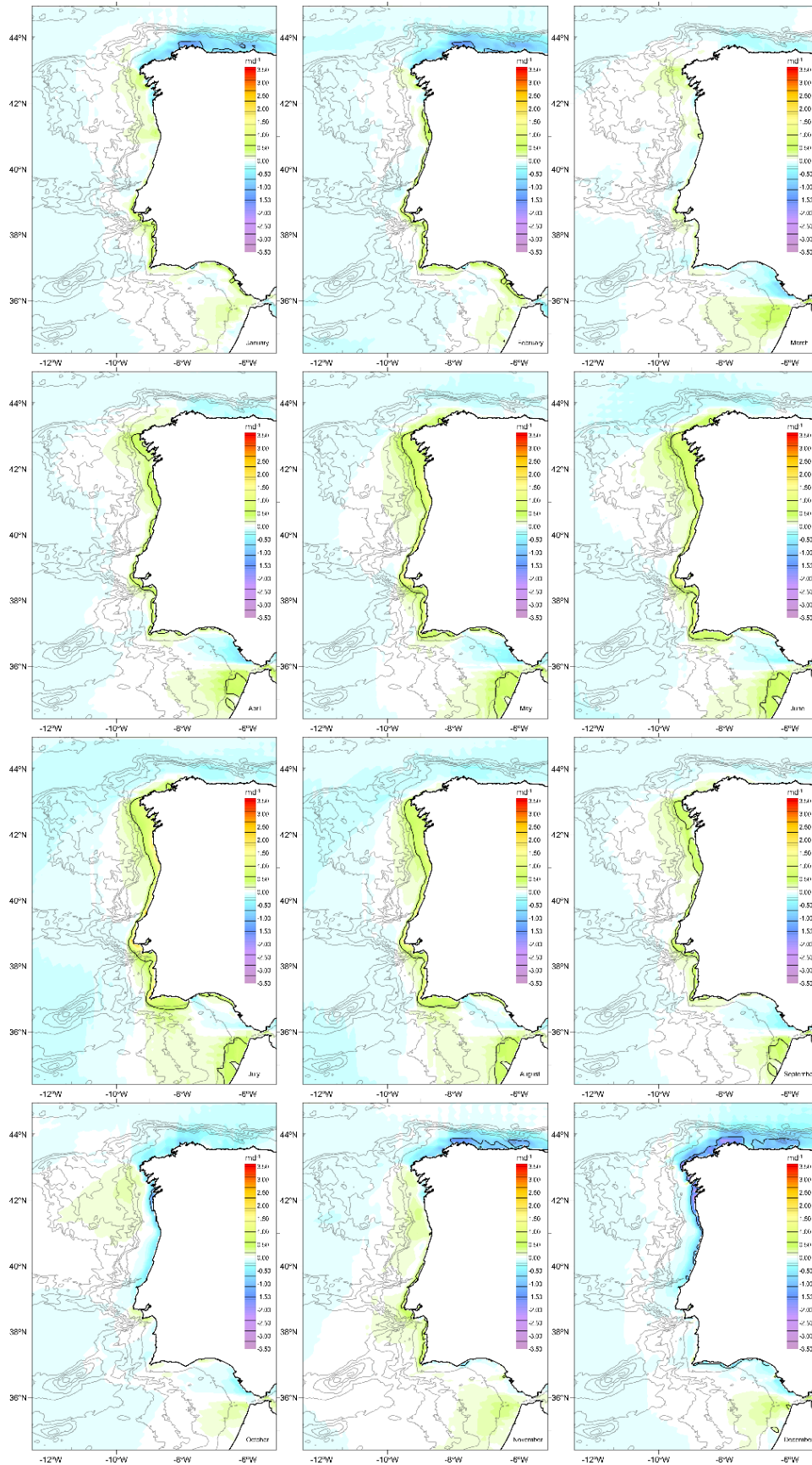
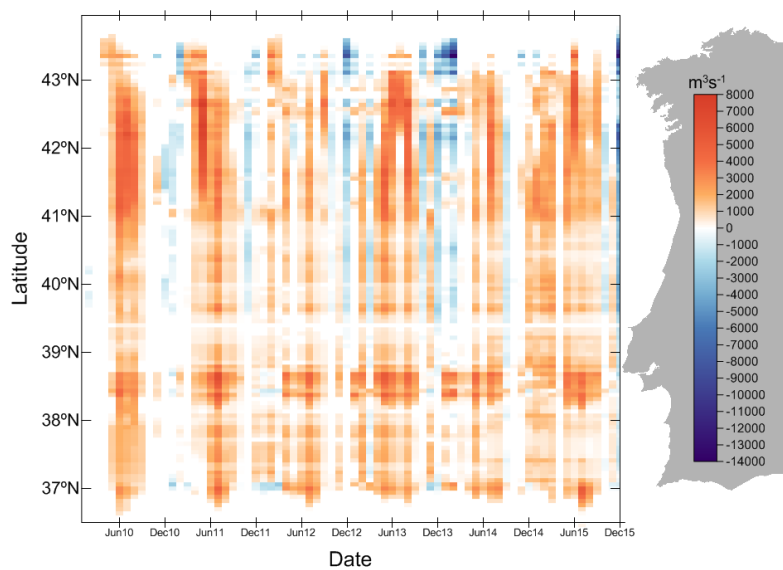
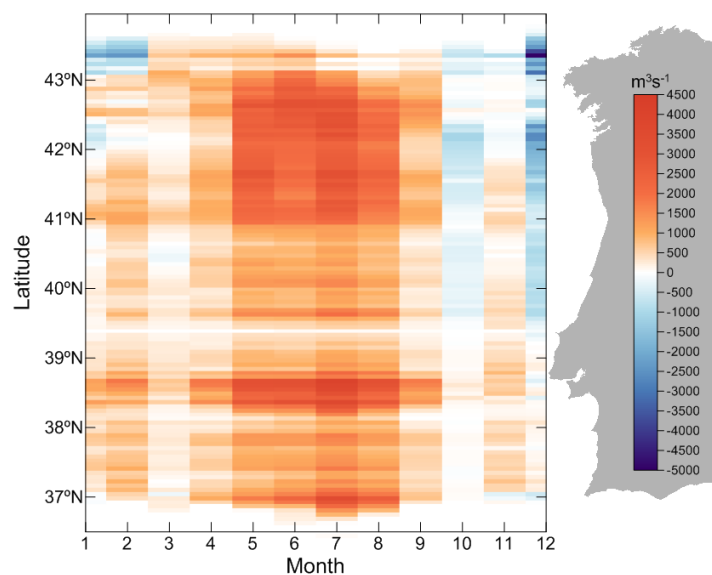


Figure 11 Monthly averaged Ekman pumping velocity for the period 2010-2016. Positive values indicate upwelling conditions and negative values are associated to downwelling conditions. Contour lines indicate wind curl limit value of  $\pm 3 \cdot 10^{-5} \text{ s}^{-1}$ . Isobaths are represented every 1000 m starting at 500 m.

Figure 12 shows the monthly integrated Ekman pumping for the analysed period where it can be observed large positive transport located mainly in the vicinity of three capes: Finisterre, Raso and São Vicente while negative transport is mainly located in the northern half of the west coast with maximum values associated to Cape Finisterre. In this figure, a clear interannual variability can be distinguished, for instance downwelling events did not happen every year. Maximum upwelling and downwelling conditions associated to Ekman pumping were observed in the Galician coast with values around  $800 \text{ m}^3\text{s}^{-1}$  (May 2011) and  $-14000 \text{ m}^3\text{s}^{-1}$  (February 2014) respectively. Using these data, an Ekman pumping climatology for the western coast of the IP was built (Figure 13). Peak Ekman sucking conditions were observed during July in the coast around Cape Raso with values around  $4000 \text{ m}^3\text{s}^{-1}$  followed by the area around Cape São Vicente ( $\approx 3500 \text{ m}^3\text{s}^{-1}$ ). Minimum values were observed in December around the Cape Finisterre with values around  $-5000 \text{ m}^3\text{s}^{-1}$ . The area comprised between latitudes of  $41.2\text{-}42.9^\circ\text{N}$  showed during the year high values of upwelling ( $2500\text{-}3000 \text{ m}^3\text{s}^{-1}$ ) though combined with maximum negative values higher than ( $-2500 \text{ m}^3\text{s}^{-1}$ ). Below the  $39^\circ\text{N}$  latitude, negative values were rare along the year.



**Figure 12 Monthly upwelling transport due to Ekman pumping in the western coast for the 2010-2016 period. Positive values indicate upwelling transport conditions and negative values are associated to downwelling transport conditions.**



**Figure 13 Mean upwelling transport due to Ekman pumping for each month in the west coast during the 2010-2016 period. Positive values indicate upwelling transport conditions and negative values are associated to downwelling transport conditions.**

### 8.4.3. Vertical transport from ocean numerical model

The above methods for quantifying the vertical transport of water assume a uniform distribution of density and disregard the effect of submarine topography and the interaction with the general ocean circulation. Generally, wind forcing is reduced to only one component considering the relation between the winds parallel to the general disposition of the coast and disregarding the coastal morphology.

In this section, the vertical velocity ( $W$ ) from the PCOMS 3D regional ocean model application were integrated and converted into transport to ease the comparison with above described methods. Monthly averaged values for vertical velocity ( $W$ ) were integrated zonally for one degree offshore the coastal area as in Figure 14. In order to evaluate the sensitivity of this method to the integration depth,  $W$  were integrated at two depths: 40 m and 100 m, hereafter referred as PCOMS\_40 and PCOMS\_100 respectively. The 40 m depth was selected for being the maximum chlorophyll in this waters and 100 m for being below the photic area.

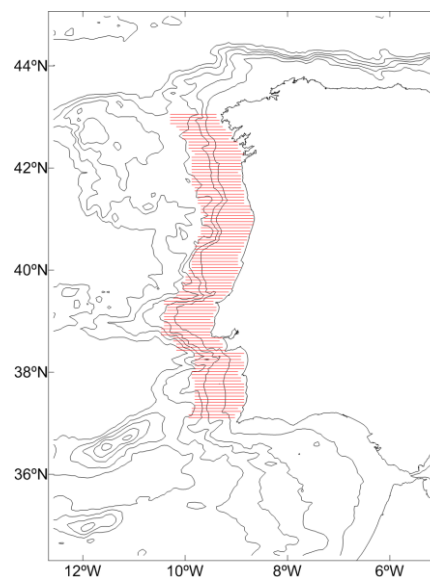


**Figure 14** One degree zonal cross-shore sections used in vertical velocity ( $W$ ) integration. Sections are separated by  $0.06^\circ$  which is the model domain spatial resolution. Isobaths are represented every 1000 m starting at 500 m.

Vertical transport in the near ocean is the resultant of several mechanisms as Ekman vertical transport and pumping and also due to the interaction of the currents with bathymetric features. Figure 15 shows the latitudinal distribution PCOMS\_40 and PCOMS\_100. In this figure it can be seen how the distribution of vertical velocity at both depths presents similar latitudinal distributions,  $R^2$  of 0.60. The presence of large bathymetric features influencing the vertical velocity can also be distinguished. For example, the area between  $39^\circ$  and  $40^\circ$  N corresponds to the area comprised by the Nazaré and Lisboa canyons, among which the Estremadura promontory is located, forcing parcels of water to climb the obstacle and once the bathymetry increases, part of the water goes down to the density equilibrium. In general, PCOMS\_100 presents greater vertical transport than PCOMS\_40. Overall values for PCOMS\_40 and PCOMS\_100 were positive (upwelling) with mean values around  $1500$  and  $2000 \text{ m}^3\text{s}^{-1}$  respectively.

When the vertical fluxes are analysed temporally, it can be observed that during upwelling periods the fluxes obtained at both depths are similar, however during downwelling-dominated months the downwelling flux is less intense at 100 m, i.e. winter 2012-2013, or even have opposite directions with upwelling conditions at 100 m and downwelling-dominated conditions at 40 m, i.e. Jan-Feb months of 2014 and 2015. From these results, it can be concluded that PCOMS\_40 was subjected to atmospheric conditions with greater intensity than PCOMS\_100.

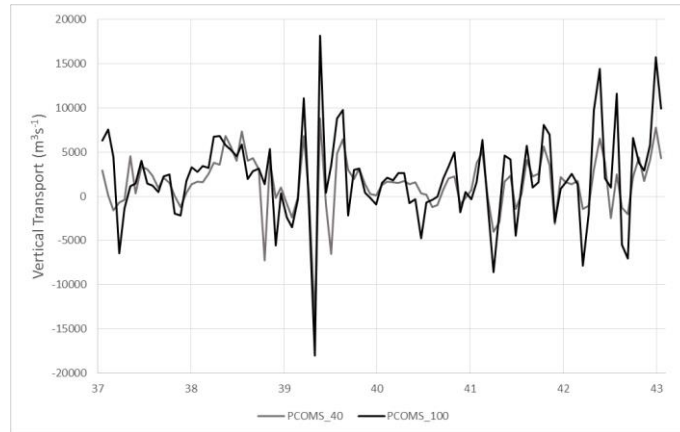


Figure 15 PCOMS one degree zonal integrated vertical velocity at 40 m (PCOMS\_40, grey line) and 100 m (PCOMS\_100, black line) latitudinal distribution for the period 2011-2015.

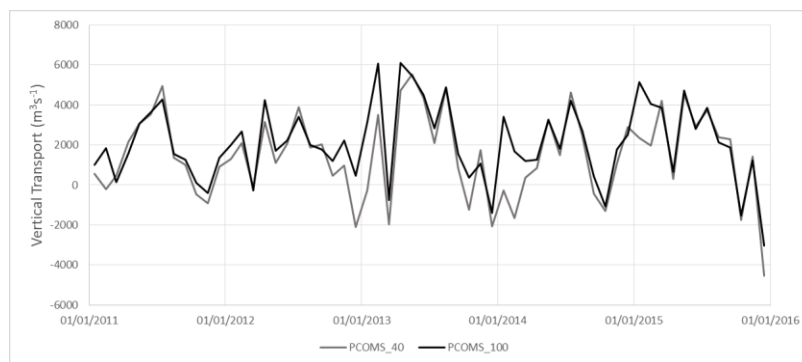


Figure 16 Monthly averaged PCOMS one degree zonal integrated vertical velocity at 40 m (PCOMS\_40, grey line) and 100 m (PCOMS\_100, black line) distribution for the latitudinal range 37.05-43.05°N.

#### 8.4.4. Upwelling from remote sensing and modelled SST

Sea surface temperature is commonly used as an indicator of upwelled water that reach the surface with lower temperatures than the surrounding waters. Generally, this type of analysis uses Earth Observation (EO) SST and compare with coastal temperature observed at the same latitude and separated by a defined distance from the coastal observation (i.e. Alvarez *et al.*, 2011). Though this method for evaluating the upwelling intensity does not quantify the vertical transport, and thus is not comparable with the previous methods, it is a commonly used method and served to evaluate the performance of the PCOMS numerical model when producing this kind of information.

To analyse the impact in temperature associated to the upwelling events, modelling results (Figure 17) and remote sensing SST (EO SST, Figure 18) were compared between the coastal area and offshore waters obtaining as a result the SST Upwelling Index ( $UI_{SST}$ ). The Multi-scale Ultra-high Resolution (MUR) was the remote sensing product used for this analysis. It provides daily SST estimates on a global  $0.01^\circ \times 0.01^\circ$  grid (Chin *et al.*, 2017; Version 4.1, <http://dx.doi.org/10.5067/GHGMR-4FJ04>, accessed in Sept. 2017). The  $UI_{SST}$  at each latitudinal point was defined as the difference in SST between the coast and the ocean (Equation 5):

$$UI_{SST} = SST_{coast} - SST_{ocean} \quad \text{Equation 5}$$

where  $SST_{coast}$  is the SST of the closest grid cell to the coast and  $SST_{ocean}$  is the SST along the same latitude that is  $3^\circ$  further west. Therefore, an increase/decrease in the  $UI_{SST}$  is equivalent to a decrease/increase in upwelling intensity. The  $3^\circ$  offset between the coastal and offshore locations was chosen in order to separate the stations as much as possible within the PCOMS model domain.

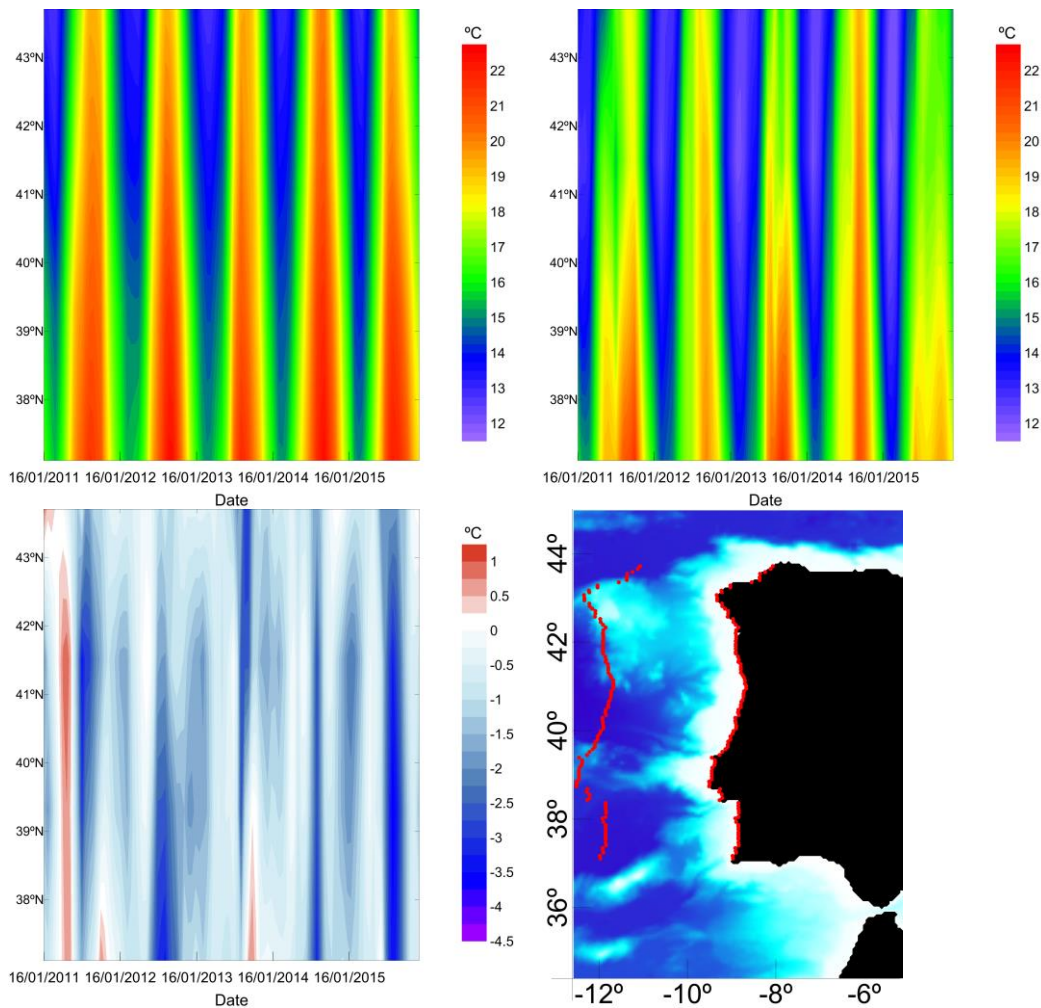
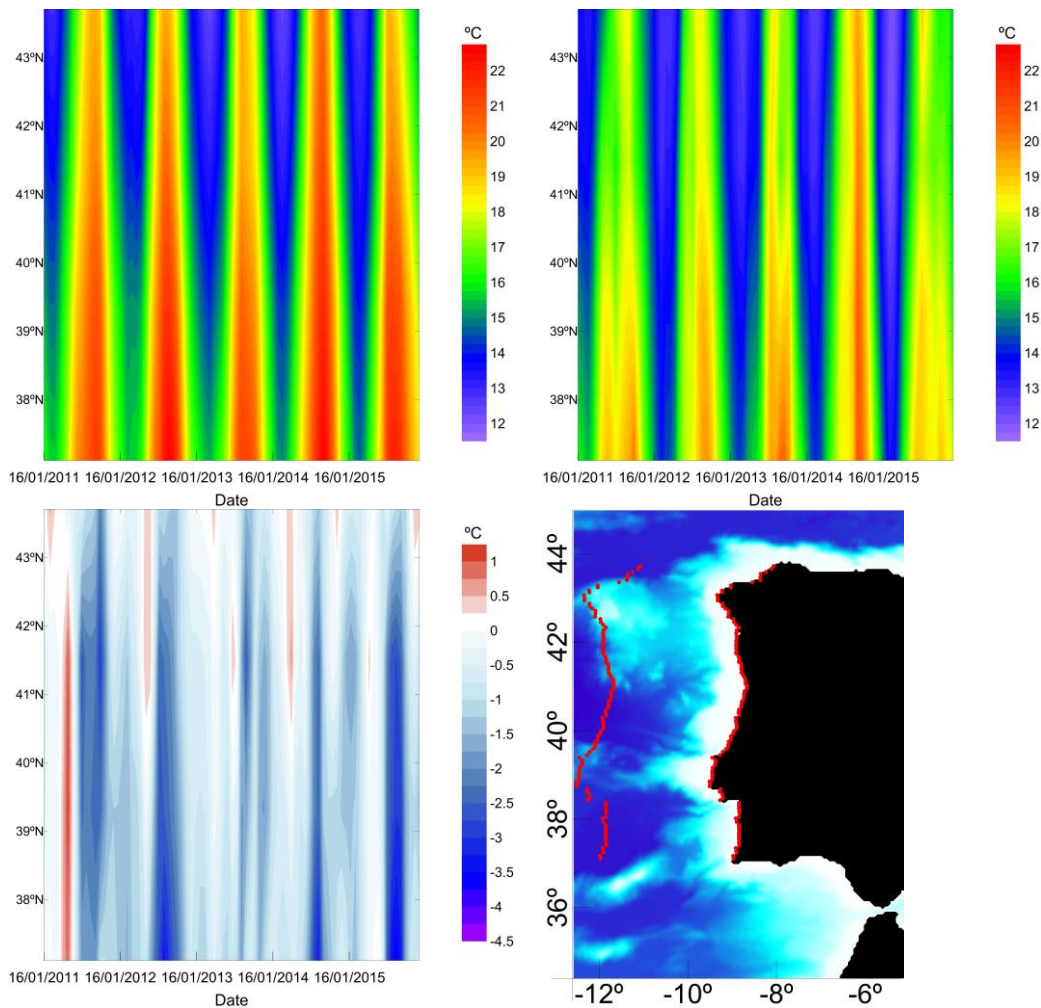


Figure 17 Spatial and temporal evolution of the PCOMS SST in offshore waters (top left), in the coastal area (top right) and its difference (bottom right) for the period 2011-2015. The analysed area is restricted to the western Iberia coast according to the locations depicted in the map (bottom left).

Offshore waters presented a regular SST cycle with some minor interannual variability in terms of maximum temperature and duration of the warm and cold periods. For the same range of latitudes, 37.04-43.71°N, the SST observed in the coastal area resembles the offshore cycle though minimum values during winter were lower and during the warm season the veins of cold water modified the extension and duration of the period in a large extent. In the same figure, the  $UI_{SST}$  calculated using Equation 5 is represented. The meridional distribution of the upwelling areas in the western coast changed significantly from one year to another. Negative values, thus colder coastal water, prevailed during the entire period with peak negative SST difference down to 3.8°C. These summer minima SST were periodic in the southern reaches of the western coast such in 2012, 2014 and 2015. However, peak minima difference in 2011 and 2013, below 2°C, were located in the region around the 41-42°N latitudinal range. In the modelling results the latter extended from that latitudinal range to the northern limit of the analysed results. The years with longer and more intense upwelling conditions were 2012 and 2015 with continuous upwelling conditions around 100 days influencing vast areas of the western Iberia. Significant positive differences were rare in the modelling results except for exceptional events such in mid-May 2011 where unusual cold waters were present offshore due to the displacement of the 40°N temperature front towards the south. A drawback of this method is that offshore SST is not a conservative property and evolves along the annual cycle and interannually.



**Figure 18** Spatial and temporal evolution of the MUR SST in offshore waters (top left), in the coastal area (top right) and its difference (bottom right) for the period 2011-2015. The analysed area is restricted to the western Iberia coast according to the locations depicted in the map (bottom left).

Monthly averaged temporal evolution of EO and modelled  $UI_{SST}$  present some periods with significant differences, such as early 2013, however in general both results present a similar pattern and the coefficient of determination ( $R^2$ ) between the two series is 0.77 (Figure 19). The obtained  $UI_{SST}$  climatology (Figure 20) shown a minimum difference between open ocean waters SST and the correspondent coastal ones occurred in the April-May period (-0.1 to -0.3°C) while the maximum difference took time during August (around -2.5°C). The latter result indicates one month lag between the  $UI_{SST}$  and upwelling indexes calculated based in wind induced vertical transport (Figure 23). This lag is in agreement with previous studies in this region (i.e. Alvarez *et al.*, 2011). On average, SST differences between offshore and coastal waters is around 1°C with coastal waters being colder than offshore waters along the entire year. Modelling and EO annual cycle of  $UI_{SST}$  shown a very similar pattern and as a consequence the  $R^2$  raised to 0.83.

EO and modelled SST obtained presented in general similar results and patterns though differences  $UISST$  tended to be larger in the modelling results, thus  $UI_{SST}$  with more negative values. Differences between both methods were expected since EO SST measures the temperature the “skin” of the ocean, approximately the top 0.01 mm or less, while the modelling SST is the average temperature in the top cell of the model domain, 0.95 m plus tidal range. Another possible issue is related to the accuracy of EO SST near the coastal area. *In situ* observations performed by Ferreira and Miranda (2005) in the upwelling region around Cape Carvoeiro and the Berlengas Islands (39.40°N) were lower than detected via remote sensing. Moreover, EO SST values showed bias of the order of 0.45-0.51°C with *in situ* SST collected from autonomous buoys (i.e. Brewin *et al.*, 2017).

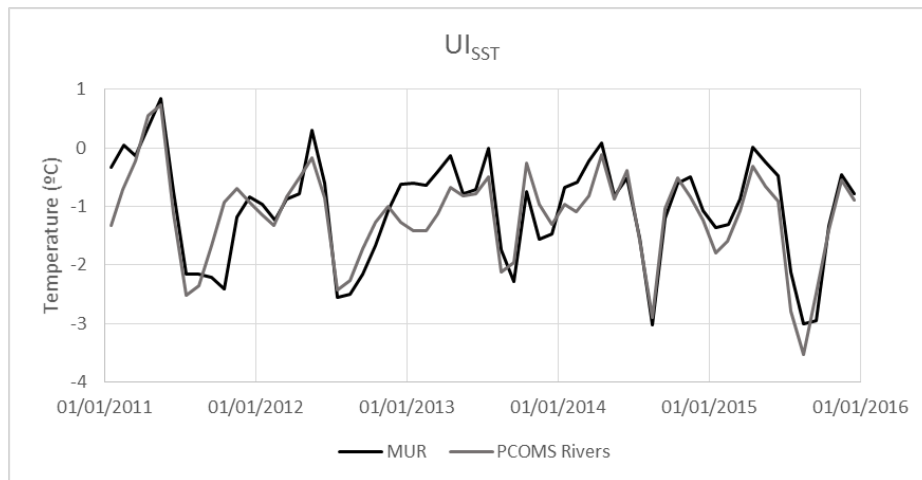


Figure 19 Monthly averaged temporal evolution of the  $UI_{SST}$  for the EO SST (MUR, black line) and the modelling results (PCOMS Rivers, grey line) for the period 2011-2015. Negative values correspond to colder coastal waters compared with offshore waters.

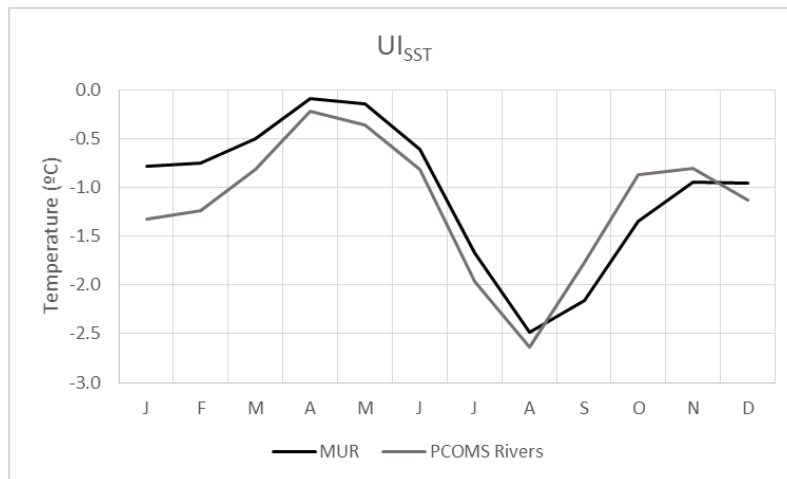


Figure 20 Monthly climatology of the  $UI_{SST}$  for the EO SST (MUR, black line) and the modelling results (PCOMS Rivers, grey line) for the period 2011-2015. Negative values correspond to colder coastal waters compared with offshore waters.

## 8.5. Discussion

In this section the presented upwelling mechanisms and methods for quantification were compared in the West coast of Western Iberia for the 2011-2015 period. In order to compare the upwelling mechanisms and methods, monthly averaged outputs from the previous analysis were converted into transport units ( $m^3s^{-1}$ ). Ekman pumping velocity and Ekman transport were converted into transport units and integrated meridionally following the methodology suggested by Bravo *et al.* (2016). Monthly Ekman transport values were multiplied by the latitudinal cell size ( $\approx 6670$  m) and Ekman pumping velocities were multiplied by the cell area and aggregated from the coast until reaching the limit of the wind drop-off length ( $L_d$ ). As in Bravo *et al.* (2016), the most coastal cell from the modelling domain was used to calculate the Ekman transport with a twofold intention: first to follow the proposed methodology and second to compare coastal and offshore Ekman transport values thus allowing to analyse the Ekman transport spatial variability. Vertical velocity ( $W$ ) was multiplied by each cell size and integrated towards the first longitudinal degree of the coast so it can be compared with the results obtained from wind intensity derived methods.

Regardless of the latitudinal changes in Ekman coastal and offshore ( $9.8^\circ W$ ) transport, Ekman pumping and oceanic vertical velocity, integrated values were monthly averaged between the latitude range of  $37.05$  and  $43.05^\circ N$ . In Figure 21, it can be seen how the Ekman pumping and

coastal Ekman transport present the same vertical transport direction during most of the time and how their relative importance changes along time. The coastal Ekman transport is the mechanism that dominates the vertical transport in coastal areas. On average Ekman pumping represents around 33% of the coastal vertical transport though it can represent more than 50 % such as during April-May 2011. Another interesting outcome is that the sum of the coastal Ekman transport and the Ekman pumping is close to the offshore Ekman transport and thus the amount of vertically transported water is conserved. In other words, the Ekman pumping mechanism compensates the wind drop-off towards the coast. In fact, the sum of the coastal Ekman transport and Ekman pumping present a coefficient of determination of 0.99 with the offshore Ekman transport. To ease, result interpretation, the integrated PCOMS vertical velocities are plotted along with the combined coastal Ekman transport and pumping (Figure 22). In this figure it can be seen how temporally the pattern and magnitude produced by the vertical velocity integration is quite close to the wind derived index. The Ekman based is closer to the PCOMS\_40 curve ( $R^2$  of 0.89) than to the PCOMS\_100 ( $R^2$  of 0.71); major differences with PCOMS\_100 were found especially during downwelling periods.

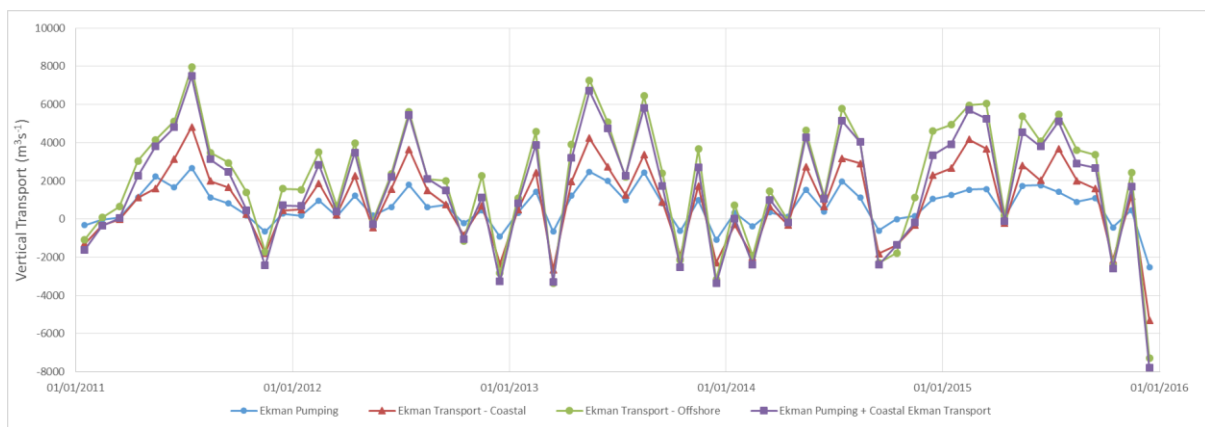


**Figure 21** Monthly averaged upwelling transport due to Ekman pumping (blue line with diamond marks), Ekman transport in offshore waters, longitude 9.8°W, (green line with circle marks) and coastal waters (red line with triangle marks) in the west coast during the 2010-2015 period. The graph also display the sum of coastal Ekman transport and Ekman pumping (purple line with square marks). Positive values indicate upwelling transport conditions and negative values are associated to downwelling transport conditions.

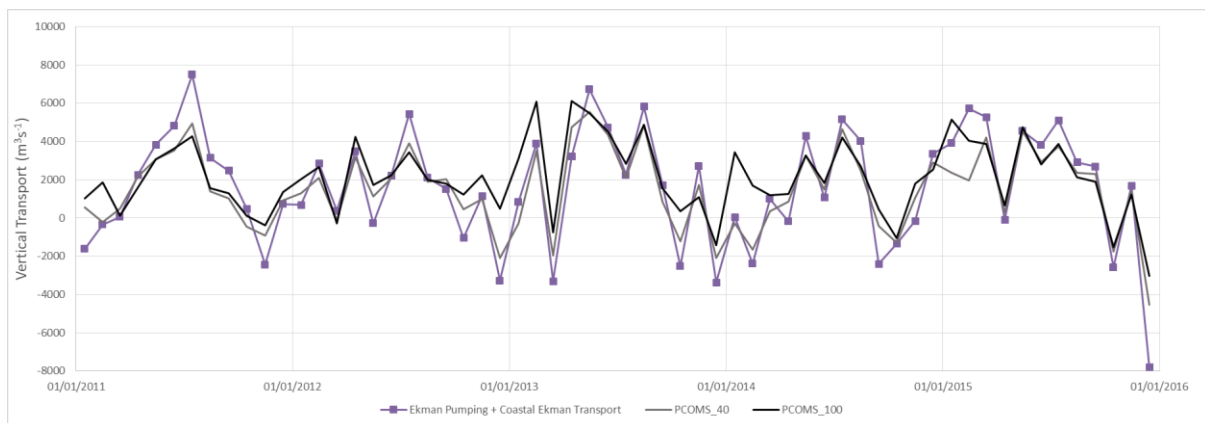


**Figure 22** Monthly averaged upwelling transport due to the combination of coastal Ekman transport and Ekman pumping (purple line with square marks) and obtained by integrating zonally the PCOMS vertical velocity at 40 m (PCOMS\_40, grey line) and 100 m depth (PCOMS\_100, black line) for one degree of longitude. Positive values indicate upwelling transport conditions and negative values are associated to downwelling transport conditions.

A monthly climatology was built the results from each upwelling index for the period 2011-2015 (Figure 23). All the metrics show a similar annual cycle with upwelling favourable conditions from

March to September with two peaks in May and July. In most of the indexes July peak is larger than May peak however the vertical velocity based indexes show that the existing difference is narrower than the obtained by wind based indexes. Upwelling favourable conditions were also found in January, February and November. Clear downwelling conditions were restricted to the months of October and December except for the PCOMS\_100 indicator that stayed almost neutral. Regarding the Ekman vertical transport mechanism, the sum of the Ekman pumping and the coastal Ekman transport corresponded to 77% of the offshore Ekman transport. When analysed temporally for the entire west coast, coastal divergence was the most important vertical transport mechanism. However, these percentages may change if the analysis is done spatially.

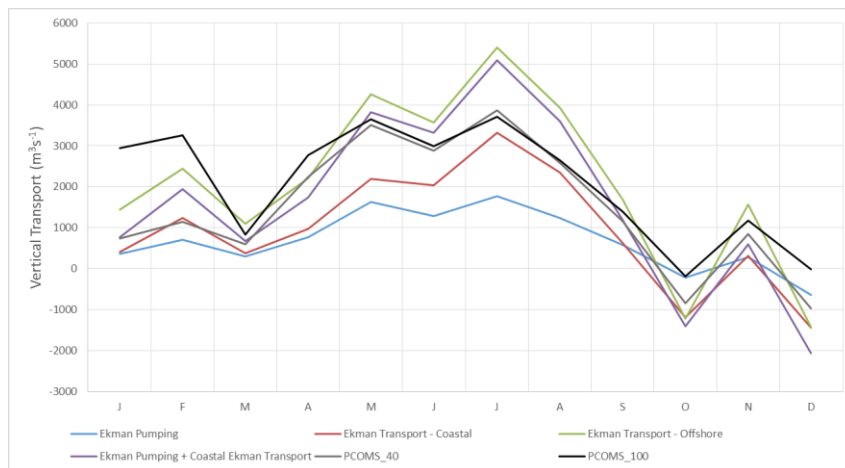


**Figure 23 Monthly spatially averaged upwelling transport due to Ekman pumping (blue line with diamond marks), Ekman transport in offshore waters, longitude 9.8 °W, (green line with circle marks) and coastal waters (red line with triangle marks) in the west coast for the 2011-2015 period. The graph also displays the sum of coastal Ekman transport and Ekman pumping (purple line with square marks) obtained by integrating zonally the PCOMS vertical velocity at 40 m (PCOMS\_40, grey line) and 100 m depth (PCOMS\_100, black line) for one degree of longitude. Positive values indicate upwelling transport conditions and negative values are associated to downwelling transport conditions.**

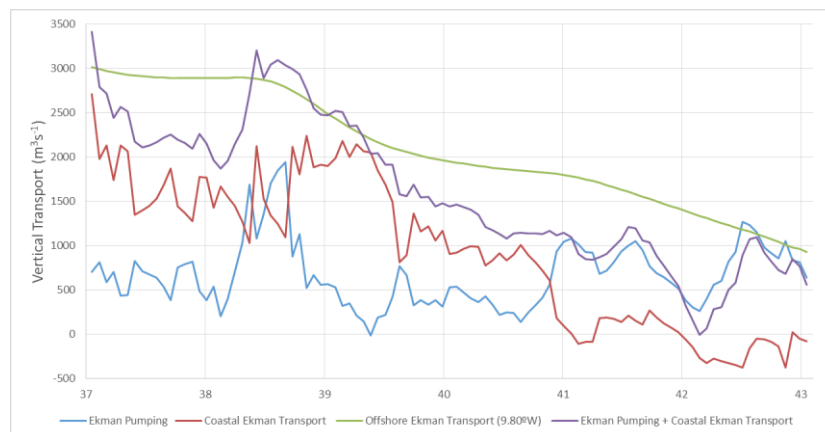


**Figure 24 Spatially averaged upwelling transport due to Ekman pumping (blue line with diamond marks), Ekman transport in offshore waters at longitude 9.8 °W (green line with circle marks) and coastal waters (red line with triangle marks) in the west coast during the 2011-2015 period. The graph also display the sum of coastal Ekman transport and Ekman pumping (purple line with square marks). Positive values indicate upwelling transport conditions and negative values are associated to downwelling transport conditions.**

Figure 24 shows that the offshore Ekman transport was not distributed according to the offshore distribution when calculated in the coastal area as the coastal accidents modify the intensity and the distribution of upwelling mechanisms. In contrast with the monthly average, the Ekman pumping and the coastal Ekman transport present different patterns along the coast and also different from

the offshore pattern. Influenced by the coastal disposition, the Ekman pumping contribution is leading the coastal Ekman transport in two areas: the Lisbon Bay and northern than 41°N. In the northernmost part of the study area, Ekman pumping surpasses the total coastal transport since coastal Ekman transport has negative values in this part of the coast.

Spatially, the mean aggregated coastal Ekman transport, including the Ekman pumping and the coastal Ekman transport present a meridional gradient from Cape São Vicente ( $\approx 3400 \text{ m}^3\text{s}^{-1}$ ) and decreasing northwards. This trend is interrupted by an increase of transport associated to the range of latitudes of 38.43-39.39 °N that correspond from Cape Espichel (38.43 °N) to Cape Carvoeiro (39.36°N). In this area and in the southernmost area, Cape São Vicente, the mean aggregated coastal transport clearly exceeded, by  $400 \text{ m}^3\text{s}^{-1}$ , the offshore Ekman transport. On the other hand, other regions presented lower upwelling transport than those obtained according to their corresponding offshore wind conditions. This is the case of the region located between the two areas described above with differences up to  $\approx 1000 \text{ m}^3\text{s}^{-1}$  and also in latitudes northern than 39.63 °N reaching the maximum difference of  $\approx 1300 \text{ m}^3\text{s}^{-1}$  at latitude 42.15 °N.

When studied spatially, the coastal Ekman transport has a lower relationship with the offshore calculated transport ( $R^2 \approx 0.75$ ) than when it was analysed temporarily, though this relation increases when aggregated with the Ekman pumping ( $R^2 \approx 0.80$ ). For this reason, it seems significant to study the Ekman transport mechanisms locally in order to estimate correctly the upwelling transport.

When the importance of the upwelling mechanisms were analysed annually, it can be observed that most of the features described above are almost permanent. In the northern sector, differences between offshore and coastal transport can reduce depending on the Ekman transport downwelling processes. However, in this area, Ekman pumping contributes, on average, to the upwelling transport more than the Ekman transport. Large inter-annual differences were observed during the study period, total coastal Ekman transport can double in consecutive years such in 2014 and 2015.

In 2011 the maximum peak for the entire coast was located in the Cape Espichel-Cape Carvoeiro area (Figure 25). The Ekman pumping contribution in this area exceeded the coastal Ekman transport during most of the analysed years. This area was identified as an area for filament development in previous literature (Oliveira *et al.*, 2008).

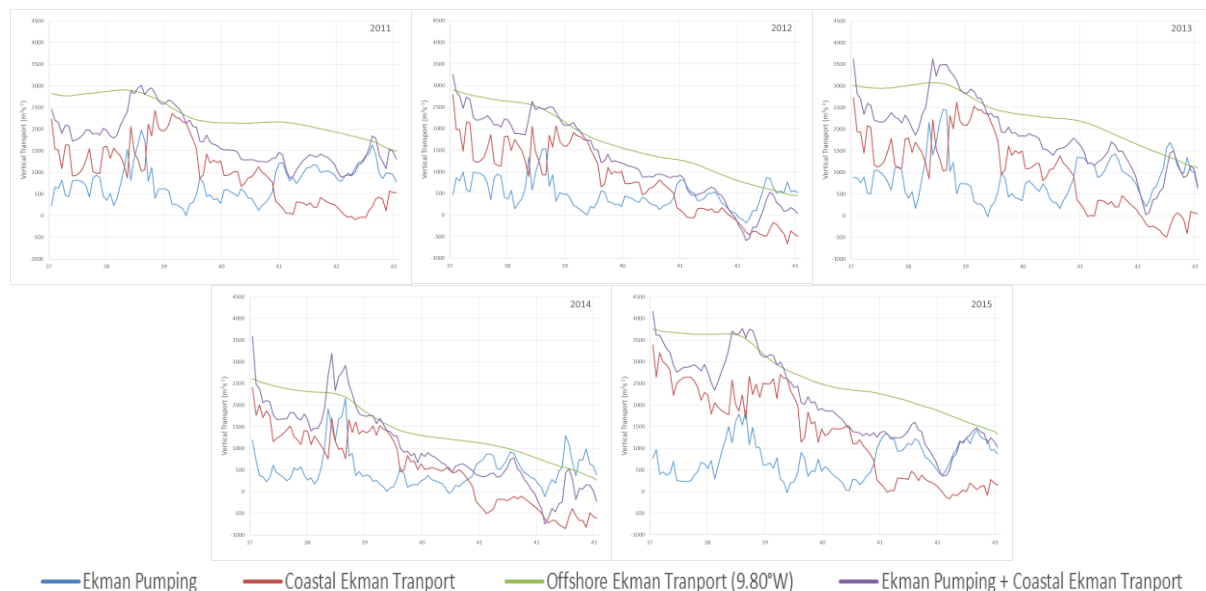


**Figure 25** Spatially averaged upwelling transport due to Ekman pumping (blue line), Ekman transport in offshore waters at longitude 9.8 °W (green line) and coastal waters (red line) in the west coast for each year of the 2011-2016 period. The graph also display the sum of coastal Ekman transport and Ekman pumping (purple line). Positive values indicate upwelling transport conditions and negative values are associated to downwelling transport conditions.

In 2011, the latitudinal gradient of upwelling transport was moderate and the difference in the aggregated coastal transport between Cape São Vicente (37.05°N) and Cape Finisterre (42.92°N) were reduced to  $500 \text{ m}^3\text{s}^{-1}$  while in general the transport in the southern cape was more than double with respect to the northern one. This result is in agreement with previous literature that described in Cape São Vicente region intense upwelling filaments with registered nutrient and chlorophyll levels even higher than in NW Iberia (Loureiro *et al.*, 2005; Fragoso and Icelly, 2009).

While the interannual profiles pattern were relatively similar for each of the mechanism, when this analysis is done analysing the most intense upwelling and downwelling month according to Figure 23 can change substantially from the upwelling to downwelling period. Figure 26 shows the mean spatial distribution of upwelling estimations during the month of July and December. In this figure maximum aggregated coastal upwelling exceeds the offshore Ekman transport in three areas: Cape São Vicente, maximum value for western Iberia around  $9000 \text{ m}^3\text{s}^{-1}$ , Cape Espichel-Carvoeiro and Cape Finisterre. On the opposite side, during downwelling conditions, the sector until Cape Roca (38.8°N) remains near equilibrium and northwards downwelling transport increases with a local maximum at 42.2°N in the Galician Rias area.

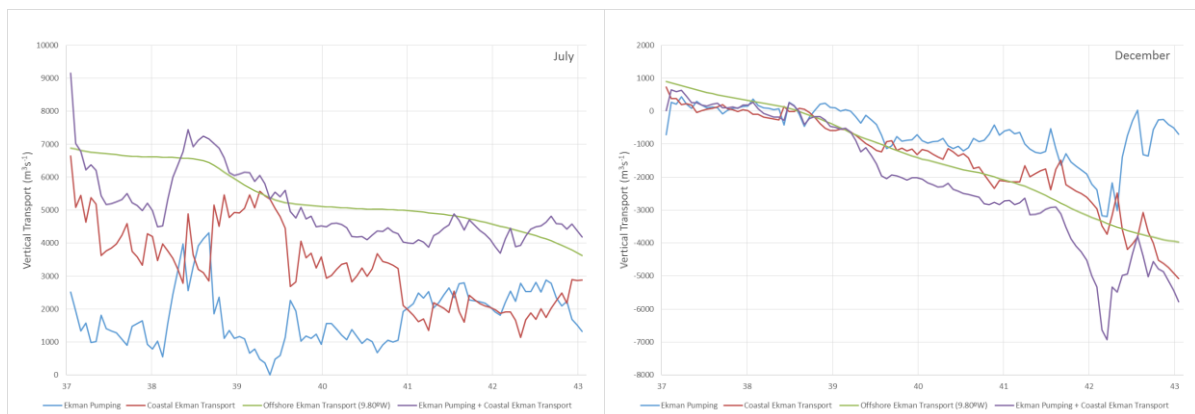


**Figure 26** Spatially averaged upwelling transport due to Ekman pumping (blue line), Ekman transport in offshore waters at longitude 9.8 °W (green line) and coastal waters (red line) in the west coast for July (left) and December (right) of the 2011-2016 period. The graph also display the sum of coastal Ekman transport and Ekman pumping (purple line). Positive values indicate upwelling transport conditions and negative values are associated to downwelling transport conditions.

To compare spatially the transport obtained by the integrated vertical velocity at 40 m and 100 m, PCOMS\_40 and PCOMS\_100 respectively, is a complicated task due to the vertical transport peaks generated by the bottom topography. In order to illustrate the origin from those vertical velocities, Figure 27 shows a vertical section along the western Iberian coast representing the mean vertical velocity during upwelling conditions, July 2013. The area between the Nazaré and Lisboa canyons is origin of vertical velocities that extend towards de surface and interfere with the area of vertical fluxes calculation.

For the reason exposed above direct comparison with integrated vertical velocity cannot be performed and values were averaged by sections of 1 latitudinal degree (Figure 28). This average is able to remove part of the noise due to vertical transport by obstacles and allow to show that transport magnitudes are similar for all the methods. Correlations between the vertical velocities based indexes and the other estimations were poor except for Ekman pumping were PCOMS\_40 and PCOMS\_100 got  $R^2$  of 0.76 and 0.46 respectively. This result may indicate the influence of Ekman pumping in the distribution of the offshore Ekman transport in the coastal area and confirms the greater impact that vertical velocity at 40 m depth are conditioned by atmospheric conditions.

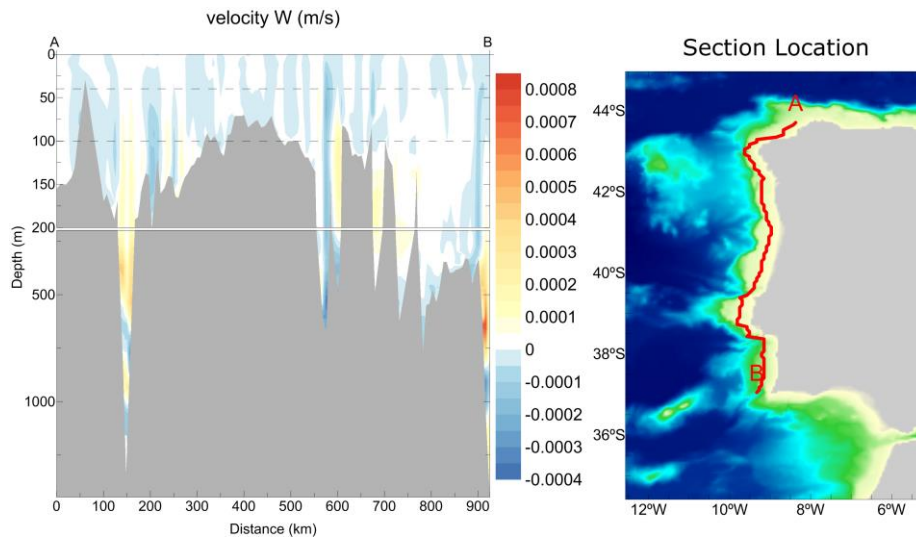


**Figure 27** Vertical section parallel to the coastline, see map on the right, representing the mean vertical velocity for July 2013. Dashed lines indicate the depths where W fluxes were calculated. Distance is measured from point A to B. Nazaré Canyon is around km 570.

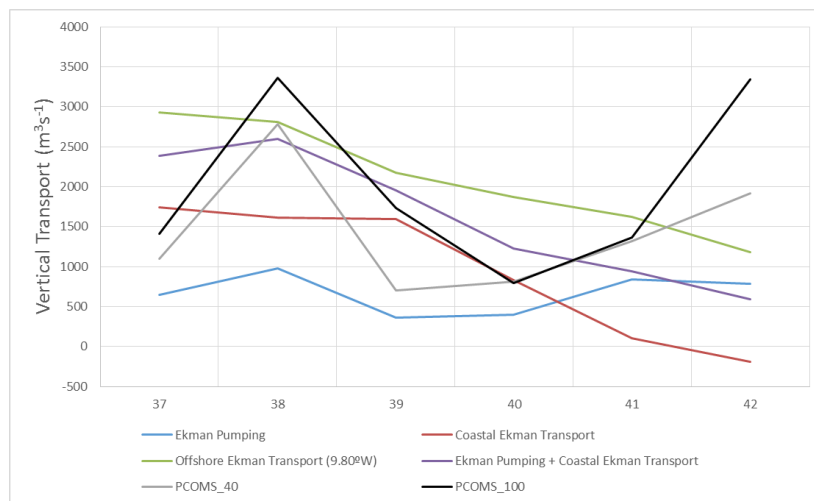


**Figure 28** Spatially averaged upwelling transport due to Ekman pumping (blue line), Ekman transport in offshore waters at longitude 9.8 °W (green line) and coastal waters (red line) in the west coast for the 2011-2016 period. The graph also displays the sum of coastal Ekman transport and Ekman pumping (purple line with square marks) obtained by integrating zonally the PCOMS vertical velocity at 40 m (PCOMS\_40, grey line) and 100 m depth (PCOMS\_100, black line) for one degree of longitude. Positive values indicate upwelling transport conditions and negative values are associated to downwelling transport conditions.

As a final result, the global and monthly integrated vertical transport for the west coast of Iberia, latitude range from 37.05 to 43.05°N, was calculated by each method described in this chapter (Table II). This result quantifies the average amount of water exchanged in the regional ocean of western Iberia between surface waters, and generally nutrient-depleted, with the deep nutrient-rich waters. During upwelling conditions this flux transports nutrient-rich waters to the photic zone which results in many implications on the ecological processes and the maintenance of trophic system and the services that are derived from them. From Table II some conclusions can be drawn. First, aggregated coastal Ekman transport, including Ekman pumping and coastal Ekman transport, present similar figure than the PCOMS\_40 and as seen above the spatial distribution of the fluxes may be conditioned by the Ekman pumping latitudinal distribution. Second, upwelling due to wind forcing is the main contributor to vertical transport to the photic area, around 70%, however other mechanisms due to the interaction of the water circulation with the local bathymetry counts for the

other 30%. The latter mechanism is general more intense during the winter period thus compensating the downwelling circulation.

**Table II. Monthly total transport in  $m^3 s^{-1}$  for the west coast of Iberia (latitude range of 37.05 to 43.05°N) obtained by estimation of offshore and coastal Ekman transport, coastal Ekman pumping and ocean vertical velocity integration at 40 and 100 m depth.**

Month	Ekman Pumping	Coastal Ekman Transport	Offshore Ekman Transport	Aggregated Coastal Ekman Transport	Integrated W at 40 m (PCOMS_40)	Integrated W at 100 m (PCOMS_100)
<b>January</b>	1786.33	2056.45	7238.81	3842.78	3645.77	14708.57
<b>February</b>	3529.66	6167.46	12192.84	9697.12	5699.65	16297.26
<b>March</b>	1494.94	1892.67	5484.00	3387.61	2950.15	4140.53
<b>April</b>	3829.08	4830.09	11054.97	8659.17	11196.70	13838.89
<b>May</b>	8155.50	10937.31	21305.61	19092.81	17528.98	18257.02
<b>June</b>	6444.62	10152.46	17821.80	16597.08	14383.68	14968.32
<b>July</b>	8838.27	16583.81	27019.24	25422.08	19340.11	18580.05
<b>August</b>	6216.70	11767.33	19663.50	17984.03	12943.82	13274.29
<b>September</b>	2866.51	3111.10	8431.74	5977.61	5761.33	6941.00
<b>October</b>	-1065.73	-5980.47	-6078.99	-7046.21	-4262.83	-925.69
<b>November</b>	1413.97	1530.50	7811.56	2944.47	4265.31	5909.27
<b>December</b>	-3173.16	-7180.63	-7093.25	-10353.79	-4874.35	-83.66
<b>Grand Total</b>	<b>40336.69</b>	<b>55868.08</b>	<b>124851.84</b>	<b>96204.77</b>	<b>88578.31</b>	<b>125905.86</b>

## 8.6. Conclusions

During the last decades, the onset of the upwelling season has been observed to occur earlier with increasing alongshore equatorward winds during the months of February and March while it has decreased during the warm season (April-September) and the loss of a secondary upwelling peak in December (Lemos and Pires, 2004). Though our study period is short for this type of analysis, our results agrees with those patterns and it has also been observed an increase in upwelling in the month of November.

Whether the used upwelling index is derived from the Ekman Transport,  $UI_{ET}$ , or from satellite temperature,  $UI_{SST}$ , both presents important limitations. The former assumes a simplified coastline consisting in a straight line where the wind component is perfectly parallel to that coast disposition, thus disregarding the coastal accidents and coastline orientations in large areas and the influence of the bathymetry. In the case of  $UI_{SST}$ , the index is limited to summer periods when the difference between ocean surface waters and upwelled waters is more intense and also limited to strong upwelling events able to generate a sea surface outcrop of colder waters thus disregarding weaker events.

The traditional method to calculate the Ekman transport includes another source of variability related to the geographical location of the calculus and its distance to the coastal area. Evaluation of  $UI_{ET}$  at different distance from the coast present different  $UI_{ET}$  index values due to the wind patterns influenced by the coastal topography.

An advantage of the numerical method proposed in this study is that a more accurate estimation of the upwelled water can be obtained as the model is considering the local values for density, bathymetry and coastal orientation. Additionally and moreover, the entry of nutrient-rich waters in productive depths could also be evaluated and the magnitude of nutrients can be quantified.

This method is also able to calculate the upwelled waters due to bathymetric constraints and to provide a continuous value when the coastline has abrupt changes its main orientation. Also could evaluate the upwelling waters not associated to coastal processes such as cyclonic eddies and the equatorial upwelling.

## 8.7. References

- Alvarez I, Gomez-Gesteira M, deCastro M, Dias JM. Spatiotemporal evolution of upwelling regime along the western coast of the Iberian Peninsula. *Journal of Geophysical Research*. 2008a; 113: C07020. DOI: [10.1029/2008JC004744](https://doi.org/10.1029/2008JC004744).
- Alvarez I, Gomez-Gesteira M, deCastro M, Gomez-Gesteira JM, Dias JM. Summer upwelling frequency along the western Cantabrian coast from 1967 to 2007. *Journal of Marine Systems*. 2010; 79(1-2): 218-226. DOI: [10.1016/j.jmarsys.2009.09.004](https://doi.org/10.1016/j.jmarsys.2009.09.004).
- Alvarez I, Gomez-Gesteira M, deCastro M, Lorenzo MN, Crespo AJC, Dias JM. Comparative analysis of upwelling influence between the western and northern coast of the Iberian Peninsula. *Continental Shelf Research*. 2011; 31(5): 388-399. DOI: [10.1016/j.csr.2010.07.009](https://doi.org/10.1016/j.csr.2010.07.009).
- Alvarez I, Gomez-Gesteira M, deCastro M, Novoa EM. Ekman transport along the Galician Coast (NW, Spain) calculated from QuikSCAT winds. *Journal of Marine Systems*. 2008b; 72(1-4): 101- 115 DOI: [10.1016/j.jmarsys.2007.01.013](https://doi.org/10.1016/j.jmarsys.2007.01.013)
- Bakun A. Coastal upwelling indices, west coast of North America, 1946–71. U.S. Department of Commerce, NOAA Technical Report NMFS–SSRF–671. 1973.
- Bakun A. Global Climate Change and Intensification of Coastal Ocean Upwelling. *Science*. 1990; 247, 198-201. DOI: [10.1126/science.247.4939.198](https://doi.org/10.1126/science.247.4939.198)
- Blanton JO, Atkinson LP, Fernández de Castillejo F, Lavin Montero A. Coastal upwelling off the Rias Bajas, Galicia, Northwest Spain, I: Hydrography studies. *Rapports et Proces-verbaux des Réunions. Conseil International pour l'Exploration de la Mer*. 1984; 183: 79-90.
- Bravo L, Ramos M, Astudillo O, Dewitte B, Goubanova K. Seasonal variability of the Ekman transport and pumping in the upwelling system off central-northern Chile (~30°S) based on a high-resolution atmospheric regional model (WRF). *Ocean Science*. 2016; 12(5): 1049-1065. DOI: [10.5194/os-12-1049-2016](https://doi.org/10.5194/os-12-1049-2016).
- Brewin RJW, de Mora L, Billson O, Jackson T, Russell P, Brewin TG, Shutler JD, Miller PI, Taylor BH, Smyth TJ, Fishwick JR. Evaluating operational AVHRR sea surface temperature data at the coastline using surfers. *Estuarine, Coastal and Shelf Science*. 2017; 196: 276-289. DOI: [10.1016/j.ecss.2017.07.011](https://doi.org/10.1016/j.ecss.2017.07.011).
- Borges MF, Santos AMP, Crato N, Mendes H, Mota B. Sardine regime shifts off Portugal: a time series analysis of catches and wind conditions. *Scientia Marina*. 2003; 67(1): 235-244.
- Bowie GL, Mills WB, Porcella DB, Campbell CL, Pagenkopf JR, Rupp GL, Johnson KM, Chan PWH, Gherini SA, Chamberlin CE (1985). Rates, constants, and kinetic formulations in surface water quality modeling. U.S. Environmental Protection Agency.
- Carrère L, Lyard F, Cancet M, Guillot A, Roblou L. FES2012: A new global tidal model taking advantage of nearly 20 years of altimetry. *Proceedings of 20 Years of Altimetry meeting*. Venice, Italy, 24-29 September 2013.
- Castro CG, Pérez FF, Alvarez-Salgado XA, Rosón G, Ríos AF. Hydrographic conditions associated with the relaxation of an upwelling event off the Galician Coast (NW Spain). *Journal of Geophysical Research: Oceans*. 1994; 99(C3): 5135–5147, DOI: [10.1029/93JC02735](https://doi.org/10.1029/93JC02735).
- Chin TM, Vazquez-Cuervo J, Armstrong EM. A multi-scale high-resolution analysis of global sea surface temperature. *Remote Sensing of Environment*. 2017; 200: 154-169. DOI: [10.1016/j.rse.2017.07.029](https://doi.org/10.1016/j.rse.2017.07.029).

Cropper TE, Hanna E, Bigg GR. Spatial and temporal seasonal trends in coastal upwelling off Northwest Africa, 1981–2012. *Deep Sea Research Part I: Oceanographic Research Papers*. 2014; 86: 94-111.

deCastro M, Gomez-Gesteira M, Alvarez I, Lorenzo M, Cabanas JM, Prego R, Crespo AJC. Characterization of fall-winter upwelling recurrence along the Galician western coast (NW Spain) from 2000 to 2005: Dependence on atmospheric forcing. *Journal of Marine Systems*. 2008; 72: 145-158. DOI: [10.1016/j.jmarsys.2007.04.005](https://doi.org/10.1016/j.jmarsys.2007.04.005).

Drillet Y, Bourdalle-Badi R, Siefrid L, Le Provost C. Meddies in the Mercator North Atlantic and Mediterranean Sea eddy-resolving model. *Journal of Geophysical Research*. 2015; 110(C3): C03016.

Ferreira JP, Miranda PMA. Modeling upwelling with a coupled atmospheric–ocean mesoscale model. 85th AMS Annual Meeting. Sixth Conference on Coastal Atmospheric and Oceanic Prediction and Processes, 2005. <https://ams.confex.com/ams/pdfpapers/84747.pdf>

Fiúza AFdG, de Macedo ME, Guerreiro MR. Climatological space and time-variation of the portuguese coastal upwelling. *Oceanologica Acta*. 1982; 5(1): 31-40. Open Access version: <http://archimer.ifremer.fr/doc/00120/23169/>

Fréon P, Alheit J, Barton ED, Kifani S, Marchesiello P. 9 Modelling, forecasting and scenarios in comparable upwelling ecosystems: California, Canary and Humboldt, In: Vere Shannon, Gotthilf Hempel, Paola Malanotte-Rizzoli, Coleen Moloney and John Woods, Editor(s), *Large Marine Ecosystems*, Elsevier. 2006; 14: 185-220. DOI: [10.1016/S1570-0461\(06\)80014-5](https://doi.org/10.1016/S1570-0461(06)80014-5).

Fragoso B, Icely JD. Upwelling events and recruitment patterns of the major fouling species on coastal aquaculture (Sagres, Portugal). *Journal of Coastal Research*. 2009; 1: 419-423.

Garcia HE, Locarnini RA, Boyer TP, Antonov JI, Baranova OK, Zweng MM, Johnson DR (2010a). *World Ocean Atlas 2009, Volume 3: Dissolved Oxygen, Apparent Oxygen Utilization, and Oxygen Saturation*. S. Levitus, Ed. NOAA Atlas NESDIS 70, U.S. Government Printing Office, Washington, D.C., 344 pp.

Garcia HE, Locarnini RA, Boyer TP, Antonov JI, Zweng MM, Baranova OK, Johnson DR (2010b). *World Ocean Atlas 2009, Volume 4: Nutrients (phosphate, nitrate, silicate)*. S. Levitus, Ed. NOAA Atlas NESDIS 71, U.S. Government Printing Office, Washington, D.C., 398 pp.

Gomez-Gesteira M, Moreira C, Alvarez I, deCastro M. Ekman transport along the Galician coast (northwest Spain) calculated from forecasted winds. *Journal of Geophysical Research: Oceans*. 2006; 111, C10005. DOI: [10.1029/2005JC003331](https://doi.org/10.1029/2005JC003331).

Gonzalez-Nuevo G, Gago J, Cabanas JM (2014) Upwelling index: a powerful tool for marine research in the NW Iberian upwelling system, *Journal of Operational Oceanography*. 2014; 7(1): 47-57. DOI: [10.1080/1755876X.2014.11020152](https://doi.org/10.1080/1755876X.2014.11020152).

Grell GA, Dudhia J, Stauffer D. A description of the fifth-generation Penn State/NCAR Mesoscale Model (MM5). NCAR Technical Note NCAR/TN-398+STR. 1994.

Halpern D. Offshore Ekman Transport and Ekman Pumping Off Peru During the 1997–1998 El Niño, *Geophysical Research Letters*. 2002; 29(5). DOI: [10.1029/2001GL014097](https://doi.org/10.1029/2001GL014097).

Jacox MG, Moore AM, Edwards CA, Fiechter J. Spatially resolved upwelling in the California Current System and its connections to climate variability. *Geophysical Research Letters*. 2014; 41. DOI: [10.1002/2014GL059589](https://doi.org/10.1002/2014GL059589).

Large W, Pond S. Open Ocean momentum flux measurements in moderate to strong winds. 1981: *Journal of Physical Oceanography*. 1981; 11: 324-336. DOI: [10.1175/1520-0485\(1981\)011<0324:OOMFMI>2.0.CO;2](https://doi.org/10.1175/1520-0485(1981)011<0324:OOMFMI>2.0.CO;2)

Lemos RT, Pires HO. The upwelling regime off the West Portuguese Coast, 1941–2000. *International Journal of Climatology*. 2004; 24: 511–524. DOI: [10.1002/joc.1009](https://doi.org/10.1002/joc.1009)

- Loureiro S, Newton A, Icelly J. Microplankton composition, production and upwelling dynamics in Sagres (SW Portugal) during the summer of 2001. *Scientia Marina*. 2005; 69: 323–341.
- Mason E, Coombs S, Oliveira PB. An overview of the literature concerning the oceanography of the Eastern North Atlantic Region. *Relatórios Científicos e Técnicos IPIMAR*. 2006; 33, 57pp.
- Mateus M, Riflet G, Chambel P, Fernandes L, Fernandes R, Juliano M, Campuzano F, de Pablo H, Neves R. An operational model for the West Iberian coast: products and services. *Ocean Science*. 2012; 8: 713-732.
- Moita MT, Oliveira PB, Mendes JC, Palma AS. Distribution of chlorophyll *a* and *Gymnodinium catenatum* associated with coastal upwelling plumes off central Portugal. *Acta Oecologica*. 2003; 24, S125–S132. DOI: [10.1016/S1146-609X\(03\)00011-0](https://doi.org/10.1016/S1146-609X(03)00011-0).
- Myrberg K, Andrejev O. Main upwelling regions in the Baltic Sea – a statistical analysis based on three-dimensional modelling. *Boreal Environmental Research*. 2003; 8: 97-112.
- Neves R. The MOHID concept. In: *Ocean modelling for coastal management - Case studies with MOHID*. M. Mateus & R. Neves (eds.), IST Press, Lisbon, Portugal. 2013; pp. 1-11.
- Nogueira J, Campuzano FJ, Neves R. Sardine larvae vertical migration and horizontal dispersion patterns related to light intensity in the dynamic western Portuguese coast: a numerical study. In: *Ocean modelling for coastal management - Case studies with MOHID*. M. Mateus & R. Neves (eds.), IST Press, Lisbon, Portugal. 2013; pp. 161-173.
- Oliveira PB, Nolasco R, Dubert J, Moita T, Peliz A. Surface temperature, chlorophyll and advection patterns during a summer upwelling event off central Portugal. *Continental Shelf Research*. 2008; 29: 759–774. DOI: [10.1016/j.csr.2008.08.004](https://doi.org/10.1016/j.csr.2008.08.004).
- Picado A, Alvarez I, Vaz N, Varela R, Gomez-Gesteira M, Dias JM. Assessment of chlorophyll variability along the northwestern coast of Iberian Peninsula. *Journal of Sea Research*. 2014; 93: 2-11. DOI: [10.1016/j.seares.2014.01.008](https://doi.org/10.1016/j.seares.2014.01.008).
- Pickett MH, Paduan JD. Ekman transport and pumping in the California Current based on the U.S. Navy's high-resolution atmospheric model (COAMPS). *Journal of Geophysical Research*. 2003; 108(C10): 3327. DOI: [10.1029/2003JC001902](https://doi.org/10.1029/2003JC001902).
- Pitcher GC, Figueiras FG, Hickey BM, Moita MT. The physical oceanography of upwelling systems and the development of harmful algal blooms. *Progress in Oceanography*. 2010; 85(1-2): 5-32. DOI: [10.1016/j.pocean.2010.02.002](https://doi.org/10.1016/j.pocean.2010.02.002).
- Renault L, Dewitte B, Marchesiello P, Illig S, Echevin V, Cambon G, Ramos M, Astudillo O, Minnis P, Ayers JK. Upwelling response to atmospheric coastal jets off central Chile: A modeling study of the October 2000 event. *Journal of Geophysical Research: Oceans*. 2012; 117, C02030. DOI: [10.1029/2011JC007446](https://doi.org/10.1029/2011JC007446).
- Renault L, Hall A, McWilliams JC. Orographic shaping of US West Coast wind profiles during the upwelling season. *Climate Dynamics*. 2016; 46(1): 273-289. DOI: [10.1007/s00382-015-2583-4](https://doi.org/10.1007/s00382-015-2583-4).
- Santos AMP, Chícharo A, Dos Santos A, Moita T, Oliveira PB, Peliz Á, Ré P. Physical–biological interactions in the life history of small pelagic fish in the Western Iberia Upwelling Ecosystem. *Progress in Oceanography*. 2007; 74(2–3): 192-209. DOI: [10.1016/j.pocean.2007.04.008](https://doi.org/10.1016/j.pocean.2007.04.008).
- Santos AMP, Peliz A, Dubert J, Oliveira PB, Angélico MM, Ré P. Impact of a winter upwelling event on the distribution and transport of sardine (*Sardina pilchardus*) eggs and larvae off western Iberia: a retention mechanism. *Continental Shelf Research*. 2004; 24(2): 149-165. DOI: [10.1016/j.csr.2003.10.004](https://doi.org/10.1016/j.csr.2003.10.004).

Santos F, Gómez-Gesteira M, deCastro M. Coastal and oceanic SST variability along the western Iberian Peninsula. *Continental Shelf Research*. 2011a; 31(19–20):2012-2017. DOI: [10.1016/j.csr.2011.10.005](https://doi.org/10.1016/j.csr.2011.10.005).

Santos F, Gómez-Gesteira M, deCastro M, Álvarez I. Upwelling along the western coast of the Iberian Peninsula: dependence of trends on fitting strategy. *Climate Research*. 2011b; 48: 213-218. DOI: [10.3354/cr00972](https://doi.org/10.3354/cr00972).

Stommel HM. *The Gulf Stream: a physical and dynamical description*. 202 pp., University of California Press, Berkeley, California, 1958.

Sousa F, Fiúza A. Recurrence of upwelling filaments off northern Portugal as revealed by satellite imagery. In: *Proceedings of the 4<sup>th</sup> AVHRR Data User's Meeting*. EUMETSAT, Darsmtadt, Germany, 1989; 219–223.

Trancoso AR. *Operational Modelling as a Tool in Wind Power Forecasts and Meteorological Warnings*, PhD in Environmental Engineering, Instituto Superior Técnico, Technical University of Lisbon. 2012.

Trenberth KE, Large WG, Olson JG. The mean annual cycle in global ocean wind stress. *Journal of Physical Oceanography*. 1990; 20, 1742-1760. DOI: [10.1175/1520-0485\(1990\)020<1742:TMACIG>2.0.CO;2](https://doi.org/10.1175/1520-0485(1990)020<1742:TMACIG>2.0.CO;2)

Wang D, Gouhier TC, Menge BA, Ganguly AR. Intensification and spatial homogenization of coastal upwelling under climate change. *Nature*. 2015; 518: 390–394. DOI: [10.1038/nature14235](https://doi.org/10.1038/nature14235).



# Chapter IX – Comparative analysis of modelled surface and vertically integrated Chl *a* in Western Iberia waters.

---

## Abstract

In this chapter, the results of the biogeochemical module coupled to a 3D circulation numerical model for the Portuguese continental coastal area were evaluated. The parameterisation of the Nutrient-Phytoplankton-Zooplankton-Detritus (NPZD) were described. Model results were evaluated by comparing surface layer Chl *a* results with remote sensing products. Vertically integrated Chl *a* were generated from the modelling results. Vertically integrated and surface patterns were compared and their monthly, seasonal and interannual evolution was described by generating a preliminary Chl *a* climatology for western Iberian waters.

## 9.1. Introduction

Several studies has used the chlorophyll *a* (Chl *a*) concentration as an indirect indicator of upwelling events in Western Iberian waters (i.e. Cravo *et al.*, 2010; Cardeira *et al.*, 2013; Oliveira *et al.*, 2008; Riveiro *et al.*, 2005). Moreover, the primary production could be regarded as one of the final outcomes of this research as is a key component of the marine ecosystem that sustains fisheries. A major constraint to evaluate biogeochemical model performance is associated to the lack of continuous and reliable observations of nutrients and plankton concentrations for that reason remote sensing Chl *a* is commonly used. The main advantage of this source of data is its ability to cover regularly large areas with a high temporal periodicity.

## 9.2. Study area

The area covered by the study correspond the western Iberian coast that is simulated by the Portuguese Coast Operational Modelling System (hereafter referred as PCOMS, Figure 2, Mateus *et al.*, 2012). The primary production on its coastal areas is limited by the nutrient supply to the photic layer where nutrients are scarce and the light needed for the phytoplankton growth is available. The two main mechanisms controlling the transport of these nutrients are the river-estuarine discharges and the upwelling processes.

The western Iberian coast with a main N-S orientation and the northern winds prevailing mainly during the summertime favours the upwelling of nutrient-rich waters to the surface areas, this process presents a signature also in the temperature as the upwelled waters are colder than the surrounding waters. During spring, phytoplankton blooms take place off the coast while during summer they take place mostly near the coast due to the coastal upwelling transport (Sutcliffe *et al.*, 2016).

## 9.3. Methods

### 9.3.1. Numerical model and configurations

The PCOMS model application consists in two nested domains WestIberia (2D) and Portugal (3D) that run the MOHID Water Modelling System (Neves, 2013; <http://www.mohid.com>) covering the Iberian Atlantic coast and its contiguous ocean. The PCOMS is 3D full baroclinic hydrodynamic and ecological regional application with a horizontal resolution of 5.6 km and with 50 vertical levels with

a resolution of down to 1 m near the surface. The application downscales the Mercator-Océan PSY2V4 North Atlantic solution (Drillet *et al.*, 2005) that provides daily values for water levels and 3D values for horizontal currents, temperature and salinity. Tides are included in the PCOMS application by forcing the WestIberia domain open ocean boundary with tidal components obtained from the FES2012 global tide solution (Carrère *et al.*, 2013). Atmospheric conditions, including wind forcing, are imposed using 9 km resolution MM5 model results operated at the Instituto Superior Técnico (<http://meteo.ist.utl.pt>). Regarding the water quality variables, the Portugal 3D domain (Longitude range: 12.6-5.1°W; Latitude range: 34.38-45°N) was initialised and forced at their open ocean boundaries by monthly climatological 3D fields for oxygen, nitrate and phosphate obtained from the World Ocean Atlas 2009 (WOA09; Garcia *et al.*, 2010a and 2010b). The phytoplankton and zooplankton modelling strategy consisted in initialising their properties with a low value and allow them to grow according to the environmental conditions until reaching equilibrium. For this reason, phytoplankton and zooplankton concentrations were initially set as  $1 \cdot 10^{-4}$  and  $3 \cdot 10^{-3}$   $\text{mg l}^{-1}$  respectively. In addition, a minimum concentration was set of  $1 \cdot 10^{-4}$  for phytoplankton and zooplankton in order to maintain a population able to grow after extreme starvation conditions. The PCOMS system simulated the period between September 2009 and December 2015. The analysed period in this chapter include the period 2011-2015 since earlier dates were regarded as the stabilisation period. In PCOMS version in this study exclude the river inputs and for this reason only the upwelling effect in the primary production were analysed.

The Water Quality Module included in the MOHID model is basically a biogeochemical nutrient-phytoplankton-zooplankton-detritus (NPZD) model adapted from the model initially developed at USEPA (U.S. Environmental Protection Agency) (Bowie *et al.*, 1985). The model simulates inorganic and organic forms of nitrogen and phosphorus as nutrients in its dissolved and particulate forms. It also calculates oxygen, phytoplankton and zooplankton concentrations. More information related to the equations and variables included in the module can be found on its user manual (MARETEC, 2006). The Water Quality module was coupled with minor parameter modifications to the original default values. In Appendix II a list of parameters and values used can be found. In summary, phytoplankton and zooplankton maximum growth interval was not limited by temperature considering the maximum optimum interval for phytoplankton growth between 10 and 25°C. Zooplankton is configured to feed exclusively on phytoplankton since the latter was the only primary producer included in the application, i.e. diatoms, ciliate and bacteria can also be included. The llevel grazing constant was increased from 1.6 to 13 in order to control the phytoplankton concentrations.

### 9.3.2. Satellite products

In order to evaluate the modelling results and due to the scarcity of long chlorophyll time series in the western Iberia near ocean, Chl *a* concentrations derived from earth observed (EO) (hereafter referred as EO\_Chla) were used to validate the model results. For this analysis, the Global Ocean Chlorophyll (Copernicus-GlobColour) from Satellite Observations – Reprocessed (PRODUCT-ID: OCEANCOLOUR\_GLO\_CHL\_L4\_REP\_OBSERVATIONS\_009\_082) with 4 km spatial resolution and daily temporal resolution was used. This product is Level 4 (L4) reprocessed product and for that reason a temporal averaging method or an interpolation procedure was applied to fill in missing data values. In order to avoid outliers or dubious satellite data, values with associated error higher than 70% were filtered and excluded from the analysis.

## 9.4. Validation

The validation of NPZD models by using EO\_Chla has important limitations. Since EO\_Chla values reflect the Chl *a* concentration at variable depths, it could be regarded as a depth integrated product. However, it might fail to include deep Chl *a* maxima if the observed radiation by the satellite was reflected in shallower waters. It is important also to note that the existence of a Subsurface Chlorophyll Maximum (SCM) associated to upwelling processes has been documented for this coastal area (Rossi *et al.*, 2013) being common during the periods of stratification that take

place between upwelling and downwelling events (Crespo *et al.*, 2008). For this reason, direct comparisons between EO\_Chla and modelling results at its surface layer, following an SST alike procedure, might produce different patterns.

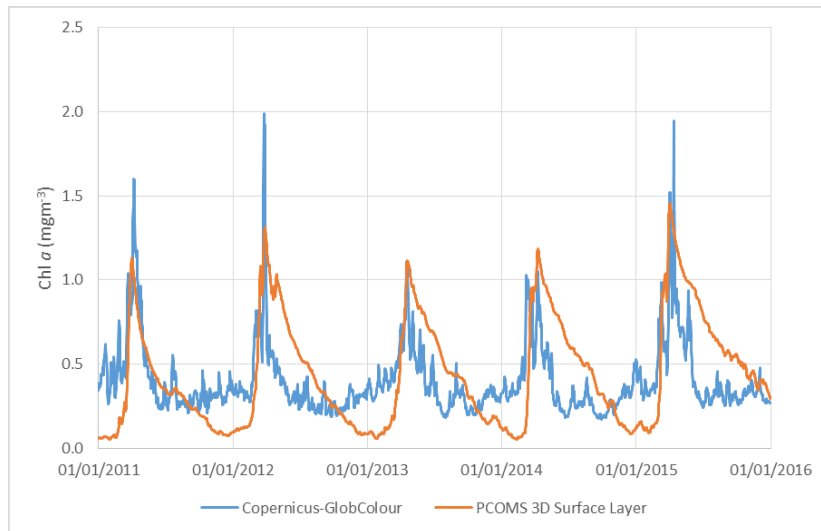


Figure 1 Mean surface Chl *a* for the Portugal 3D domain during the 2011-2015 period obtained by the surface layer of the PCOMS system (orange line) and by the remote sensing product GlobColour.

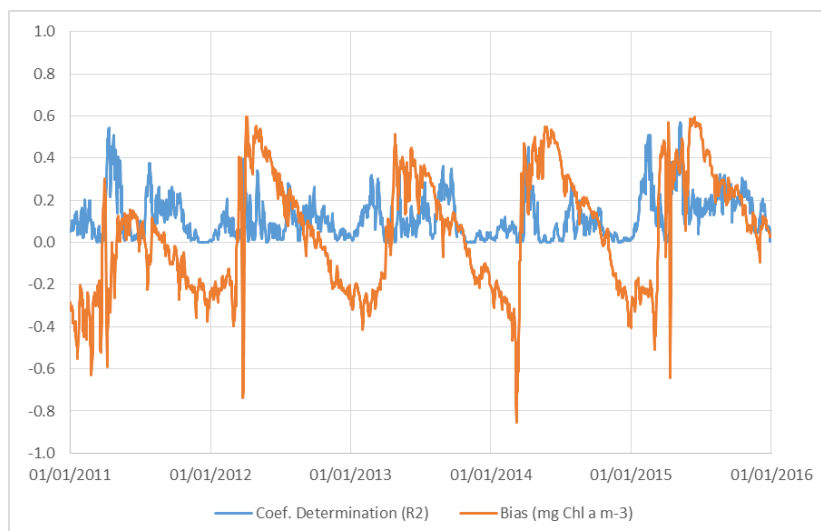
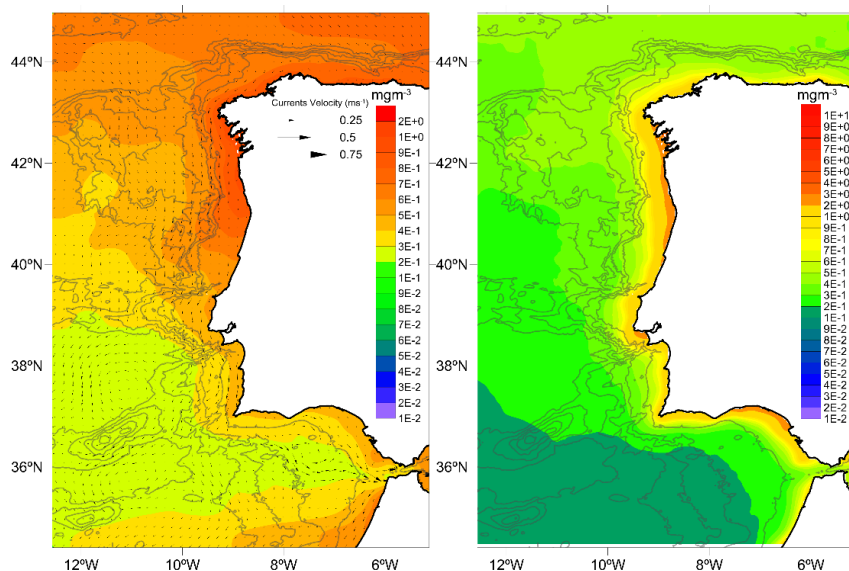


Figure 2 Evolution of the coefficient of determination (blue line) and bias (orange line) obtained by comparing the Chl *a* concentrations between the surface layer of the PCOMS system with the remote sensing product GlobColour for the western Iberia waters during the 2011-2015 period.

Bearing in mind this issue and due to the scope and time limitation of this research, the Copernicus-GlobColour was compared with the surface layer of the Portugal 3D domain. In order to evaluate the chlorophyll *a* data, phytoplankton model results were converted into chlorophyll *a* (Chl *a*) using a phytoplankton carbon to chlorophyll (C:Chl) ratio of 100. This value is comprised in the range values considered by Sathyendranath *et al.* (2009) where the ratio ranges from 10 to 150 being low in high-biomass areas and high in low-biomass areas. Figure 1 shows the temporal evolution of the mean PCOMS surface Chl *a* and the obtained from the Copernicus-GlobColour for the Western Iberia region in the period 2011-2015. In the figure it can be seen how the model reproduce quite well the spring bloom (late March-early April) while underestimates the winter period concentration. The latter effect could be due to the absence of nutrients due to river inputs. Mean values for modelled and remote sensing Chl *a* were 0.44 and 0.40 mgm<sup>-3</sup>. The coefficient of determination between both products was 0.31 which is similar to the obtained when compared *in situ* observations and remote sensing derived Chl *a* (Sutcliffe *et al.*, 2016). When analysed temporally, the coefficient of correlation

show a larger agreement with the remote sensed Chl *a* during the spring and summer bloom periods (Figure 2). However, modelling results have negative bias during the winter season and until beginning of the spring season probably for the lack of nutrients from land sources.

In Figure 3 the main Chl *a* concentrations obtained by numerical modelling and remote sensing detections for the period 2011-2015 were represented. It can be seen that both maps describe similar patterns with two clear gradients where concentrations decrease southwards and offshore. In contrast with the modelling results, the satellite mean value show the signature of some of the river plumes, i.e. Tagus. The modelling map show a trend that Chl *a* tend to follow the upwelling propagation direction towards the southwest. Despite the similarities, magnitudes in both products were different, while maximum concentration in modelling results is around 1 mg Chl *a* m<sup>-3</sup> in EO\_Chla maximum value was an order of magnitude higher, around 11.50 mg Chl *a* m<sup>-3</sup>. A validation exercise performed in the west Portuguese coast demonstrated that, in general, satellite products overestimate concentrations when compared with *in situ* observations (Sá *et al.*, 2015). Ribeiro *et al.* (2005) also found a mismatch between the high values observed near the coastal area of western Iberia by EO\_Chla and the *in situ* observations. In fact, Sá (2013) found after analysing 820 water samples from the period 2005-2012 that Chl *a* concentrations in Portuguese waters were comprised between 0.01-10.15 mgm<sup>-3</sup>.



**Figure 3 Mean Chl *a* for the period 2011-2015 obtained from the surface layer of the PCOMS 3D (left) and the Copernicus-GlobColour satellite product (right). Note the different logarithmic colour scales. Isobaths are represented every 1000 m starting at 500 m. Vectors represent mean direction every third cell.**

Nutrients are advected towards the surface entering the photic region and thus made available to the primary producers generating a deep maximum. Maximum concentration might be out of reach for remote sensors as the phytoplankton develops from surface down to 75 m, with maximum located at depths between 20-50 m (Cravo *et al.*, 2010; Cardeira *et al.*; 2013). For this reason, the phytoplankton mass could be underestimated and its spatial distribution might be incomplete. For example, Figure 4 shows the nutrients, oxygen and phytoplankton vertical distribution along a zonal cross-section from the open boundary up to the coastal area at the latitude of 41.67°N. In this figure, it can be seen the nutrients isolines uplifted near the coast due to the upwelling prevailing conditions and the phytoplankton maximum located around 50 m depth.

Taking advantage of the capacities of numerical models, Chl *a* was integrated vertically, using the trapezoidal integration method, to complete the information provided by the surface layer and the remote sensing observations. Figure 5 shows the mean integrated Chl *a* concentration for the period 2011-2015. This figure present different patterns when compared with the spatial distributions of Figure 3. In the integrated map, it should be taken into consideration the depth as shallow areas can

appear with lower values due to its shallowness thus lower concentration than deeper areas. It is important also to recall that this version is a non-river version and for that reason some areas may present lower concentrations than expected for the absence of this nutrient input, i.e. Guadalquivir, Douro and Tagus ROFIs. This map allow to observe the importance of the continental shelf region around 42°N where upwelling conditions generate a large concentration of planktonic biomass. Also near Cabo Espichel, Cabo da Roca and Cabo São Vicente appear Chl *a* concentration peaks.

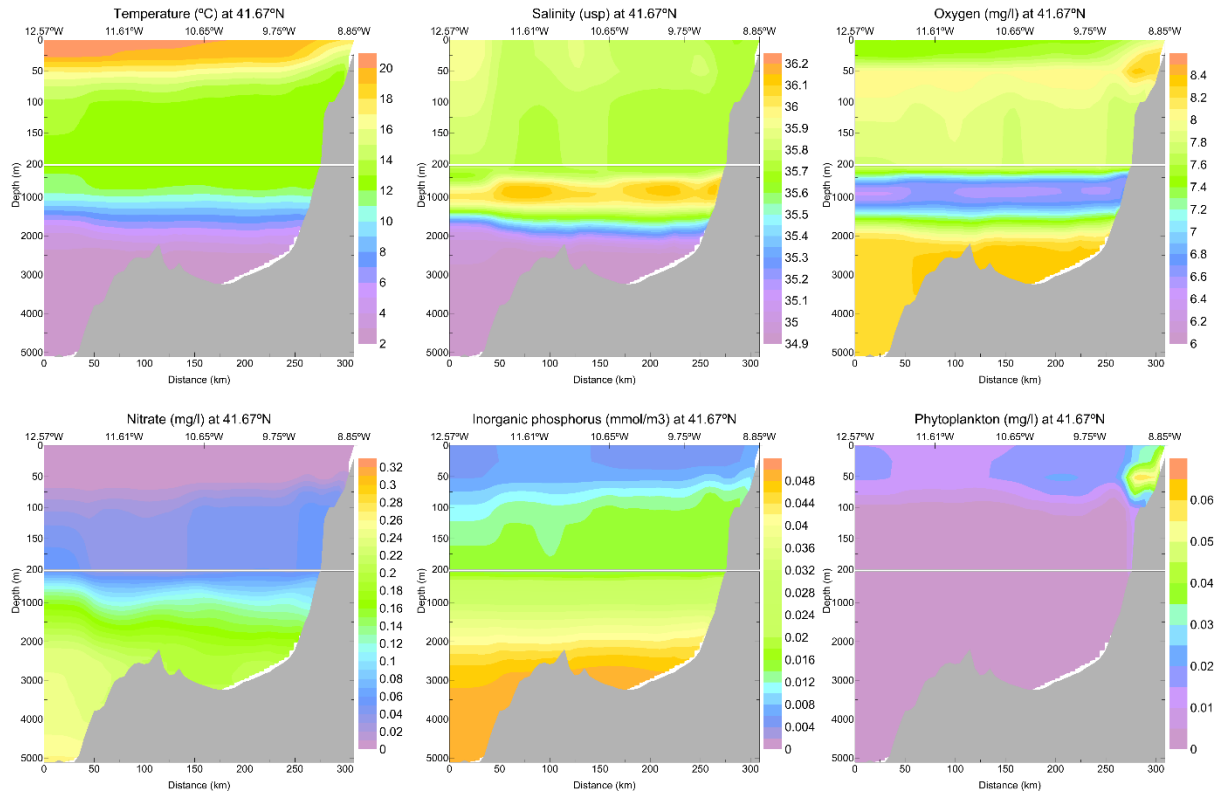


Figure 4 Zonal cross-section at 41.67°N representing mean salinity (top row, left), salinity (top row, centre), Oxygen concentration (top row, right), nitrate concentration (bottom row, left), inorganic phosphorus (bottom row, centre) and phytoplankton concentration (bottom row, right) for the month of August 2012.

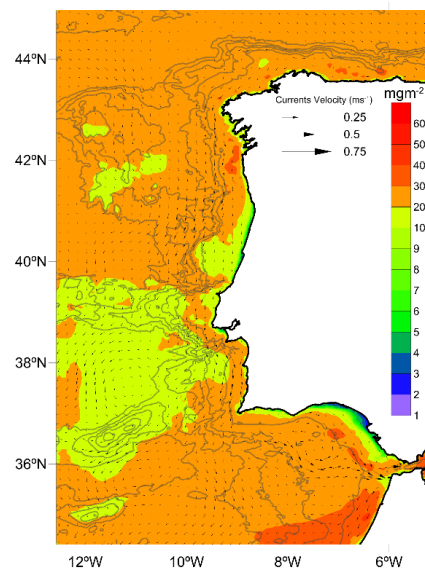


Figure 5 Mean vertically integrated Chl *a* for the study period 2011-2015. Note the logarithmic colour scale. Isobaths are represented every 1000 m starting at 500 m. Vectors represent mean current intensity and direction every third cell.

## 9.5. Chl *a* Climatology

In order to gain a deeper knowledge of the influence of upwelling conditions in the primary production generation the interannual, seasonal and monthly variability were analysed for the surface and the integrated Chl *a* concentrations. Despite the period analysed is short, the aim is to provide a preliminary climatology. Seasons were defined considering full months with the following criteria: winter (December, January and February), spring (March, April and May), summer (June, July and August) and autumn (September, October and November).

Figure 6 shows how the Chl *a* patterns are almost permanent features which intensity and extension relies in the intensity and duration of the upwelling conditions. 2015 is by far the year with higher Chl *a* concentrations, as seen in the upwelling chapter, the upwelling conditions prevail from December 2014 up to October 2015 concentrating nutrients and allowing phytoplankton to develop.

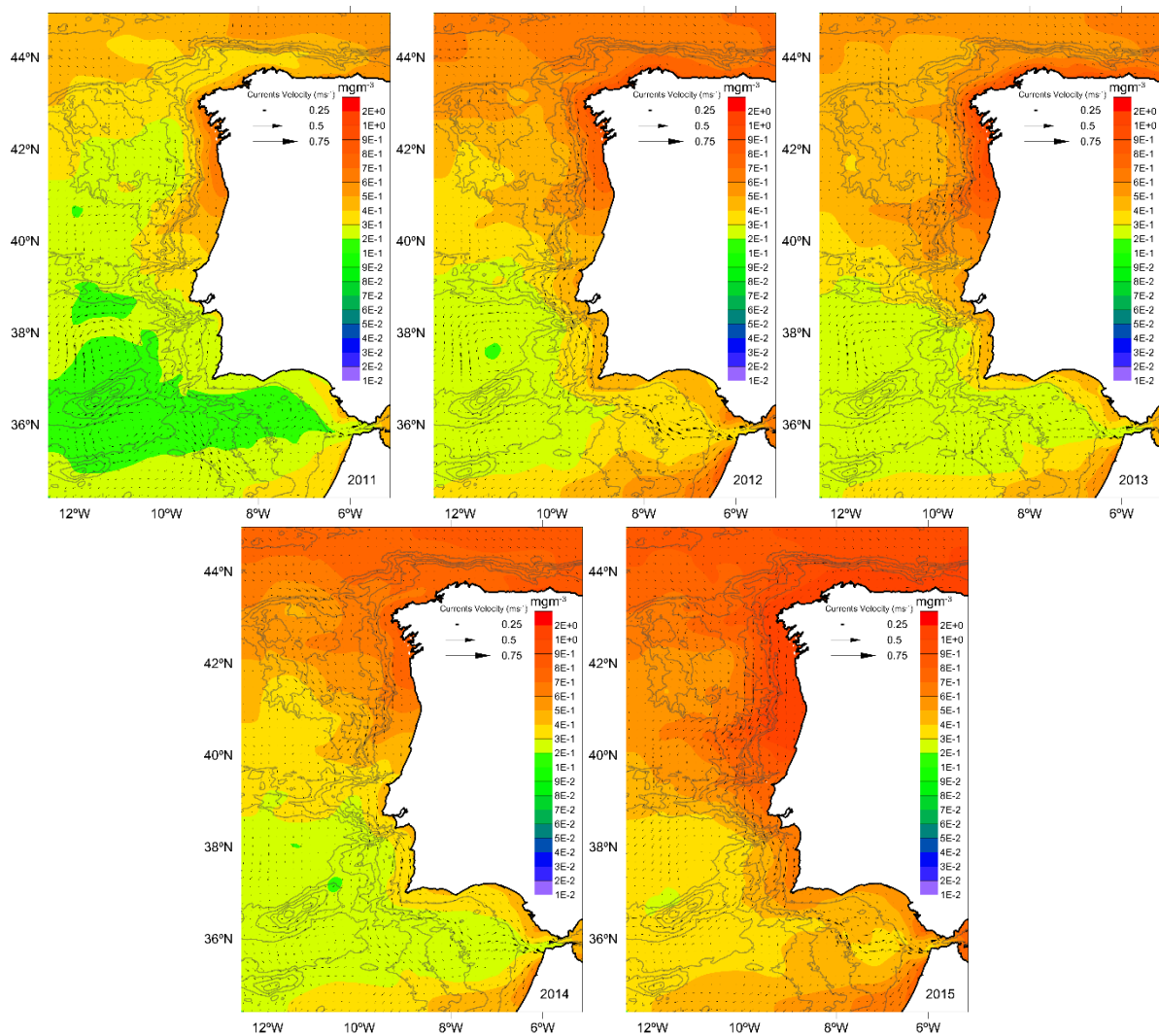
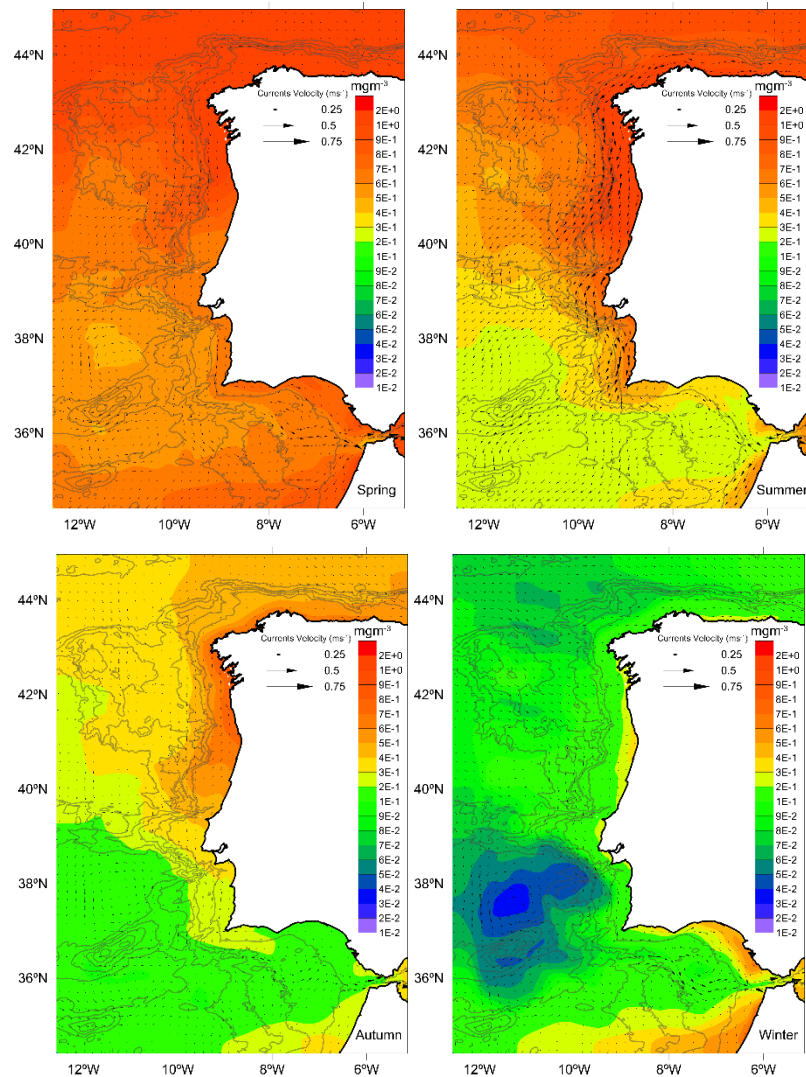


Figure 6 Mean sea surface Chl *a* for each year of the studied period. Note the logarithmic colour scale. Isobaths are represented every 1000 m starting at 500 m. Vectors represent mean direction every third cell.

Seasonally (Figure 7) it can be observed the presence of the spring bloom in the entire western Iberia near ocean, with higher intensity in the northern sector. During summer, this bloom concentrates in the coastal areas where upwelling prevailing conditions dominate. This pattern continues during autumn with a clear decline in concentrations. In winter, higher concentrations of primary producers are located in the coastal areas and in the southern open boundary.



**Figure 7** Seasonal sea surface Chl *a* for the 2011-2015 period. Note the logarithmic colour scale. Isobaths are represented every 1000 m starting at 500 m. Vectors represent mean direction every third cell.

When Chl *a* concentrations are analysed monthly (Figure 8), the previous described patterns can be observed in greater detail. Phytoplankton concentrations move from low values covering large oceanic areas in January and February to high values in the entire study area in March and April. From May up to September, upwelling favourable conditions dominate the area, from Cape São Vicente to Cape Finisterre and their surrounding areas. Also a meridional gradient can be identified in open ocean waters. During the last months of the year, the upwelling generated biomass declines and the signal of the Iberian Poleward Current can be distinguished in December. In winter months an increase of Chl *a* can be identified in waters of the Gulf of Cadiz. The starting dates and spatial distribution of the phytoplankton blooms are in agreement to those described in Friedland *et al.* (2016) for this region of the North Atlantic Ocean.

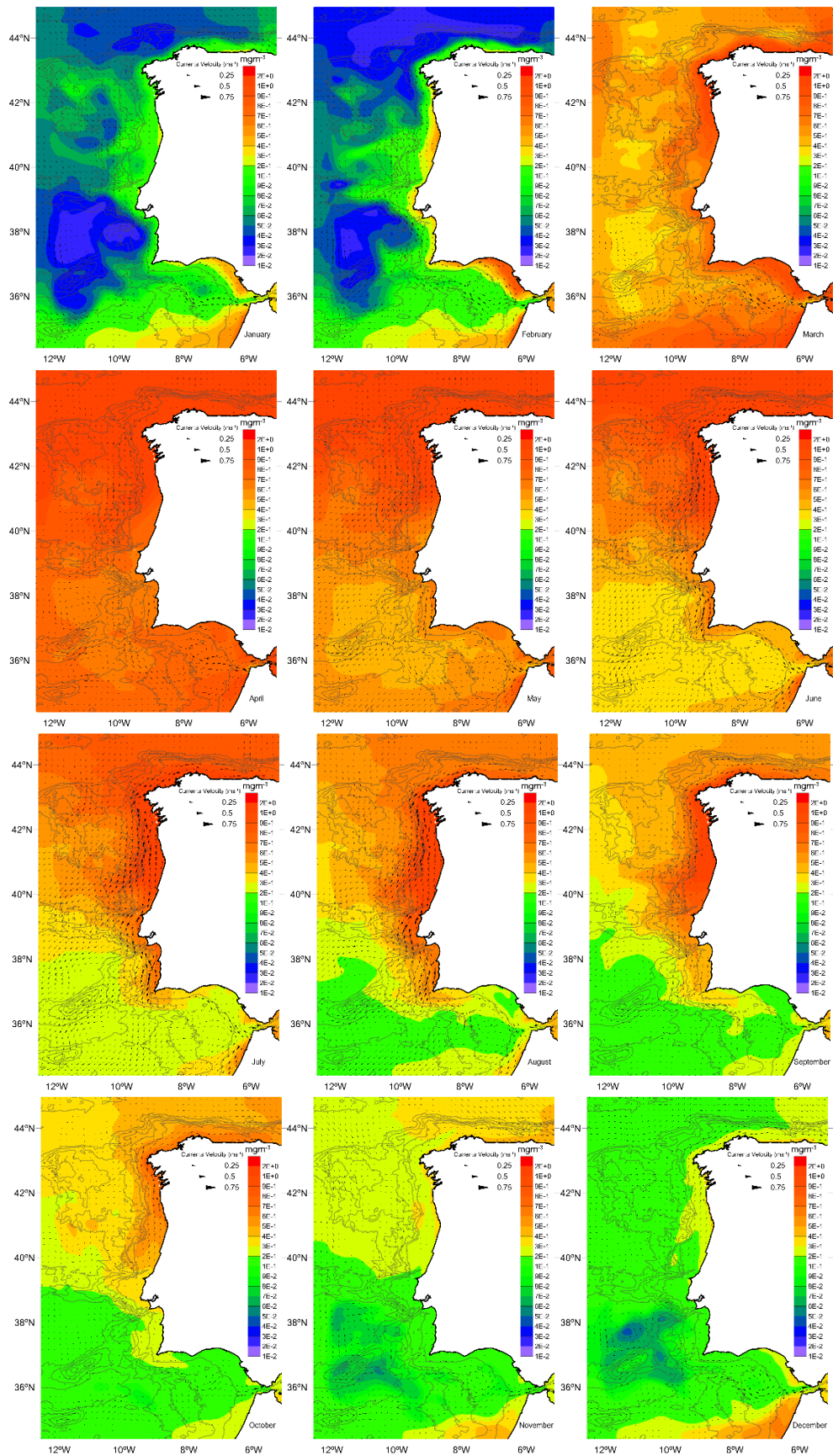
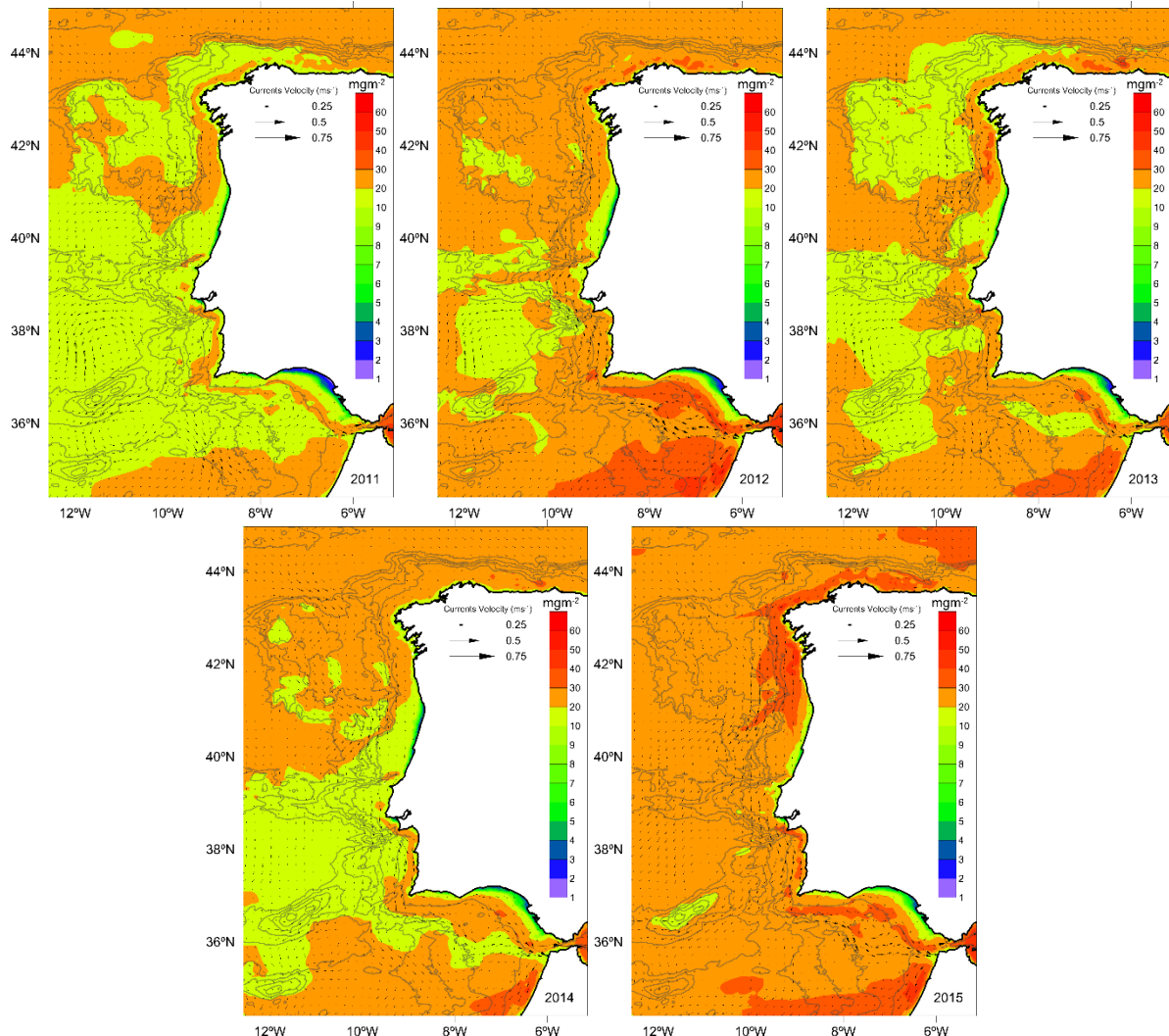


Figure 8 Monthly mean surface Chl  $\alpha$  for the 2011-2015 period. Note the logarithmic colour scale. Isobaths are represented every 1000 m starting at 500 m. Vectors represent mean direction every third cell.

When Chl *a* concentrations are integrated vertically, it can be observed how the interannual variability become clearer (Figure 9). The year 2015 stands out as the year of the analysed series with higher generated biomass around the entire western Iberia coast and in some area moving along the continental shelf break. The year 2012 and 2013 were also active in the Gulf of Cádiz and some peaks of production can be found in the coastal area around 42°N. Cape São Vicente and Cape Espichel present peaks of production in 2012 and 2013 respectively.



**Figure 9** Mean vertically integrated Chl *a* for each year of the studied period. Note the logarithmic colour scale. Isobaths are represented every 1000 m starting at 500 m. Vectors represent mean direction every third cell.

When seasonal primary production is studied integrating the water column, most of the features present in the surface layer can be identified as the dominance of the spring bloom in almost all the regional ocean and the decrease of phytoplankton during autumn/winter in almost all the area. However, some features area revealed as the summer production areas, that on the surface seemed dominated by the northern sector compared with the southern coast. Still in the figure it can be appreciated that the coastal region around 42°N present the highest values but with this parameter the region between Cape Carboeiro and Cape São Vicente appear with a similar importance to the northern sector. Another interesting feature, is the higher concentration of Chl *a* along the continental break during winter and in some areas such as the Nazaré Canyon and the Cape Espichel. The existence of this anomalies should be further investigated.

If analysed on a monthly climatology (Figure 11), it can be observed that the described features are related to the month of February. The integrated Chl *a* permit the observation of the extension of the upwelling filaments that move offshore in the subsurface. Their maximum extension take place during the month of July. During this month two main areas of upwelling appear connected through the Nazaré Canyon. During the summer months, maximum around the Cape Espichel and Cape Roca can be detected.

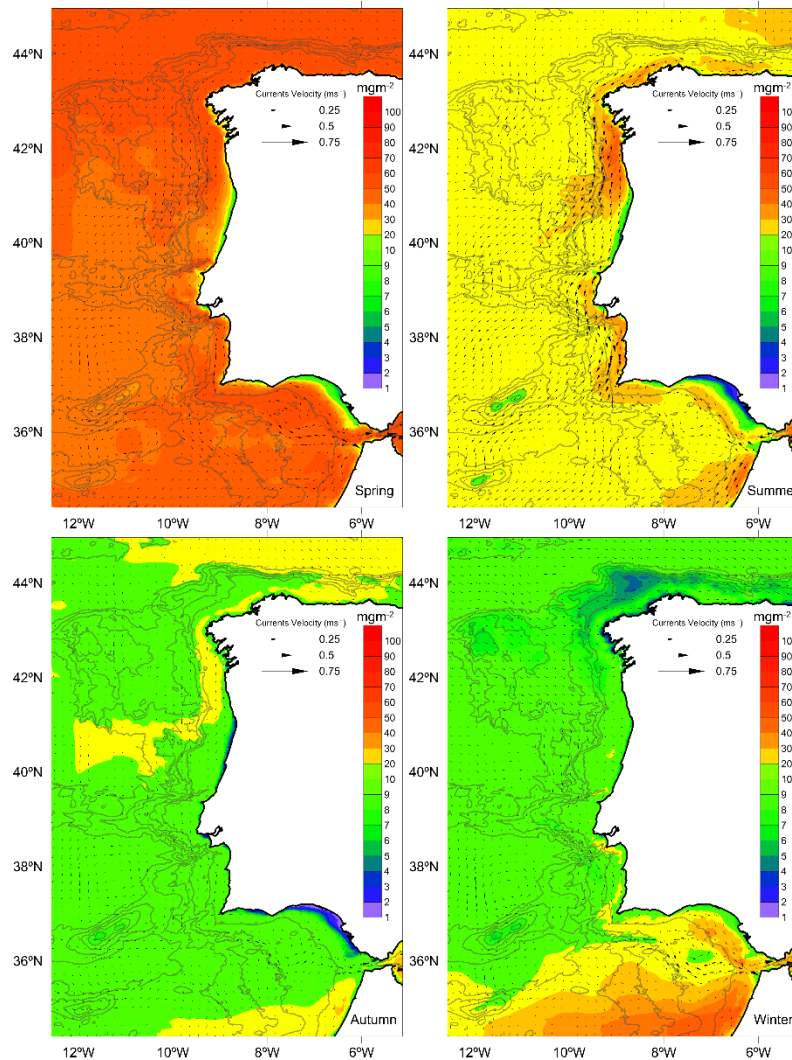


Figure 10 Seasonal vertically integrated Chl *a* for the 2011-2015 period. Isobaths are represented every 1000 m starting at 500 m. Vectors represent mean direction every third cell.

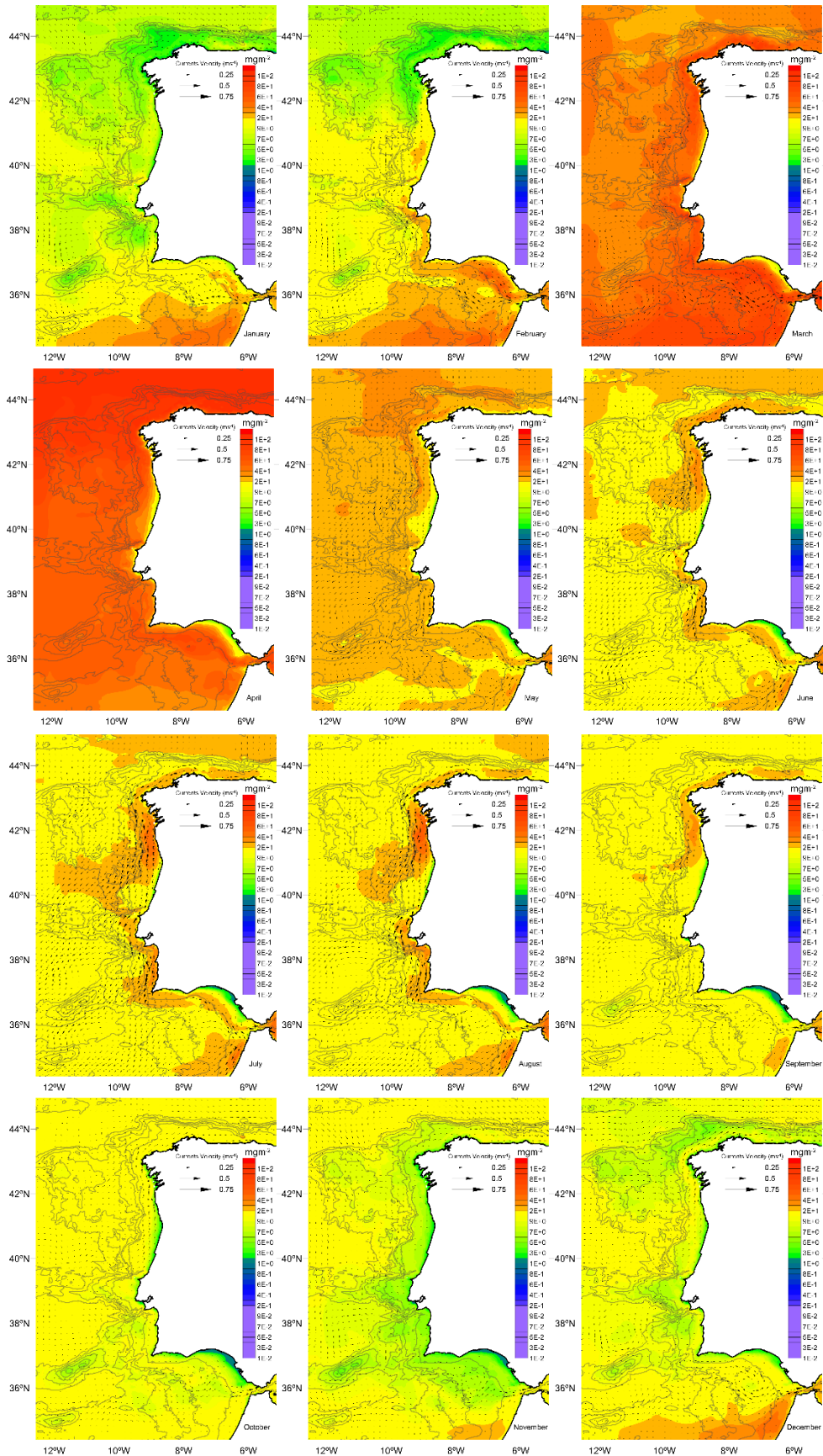
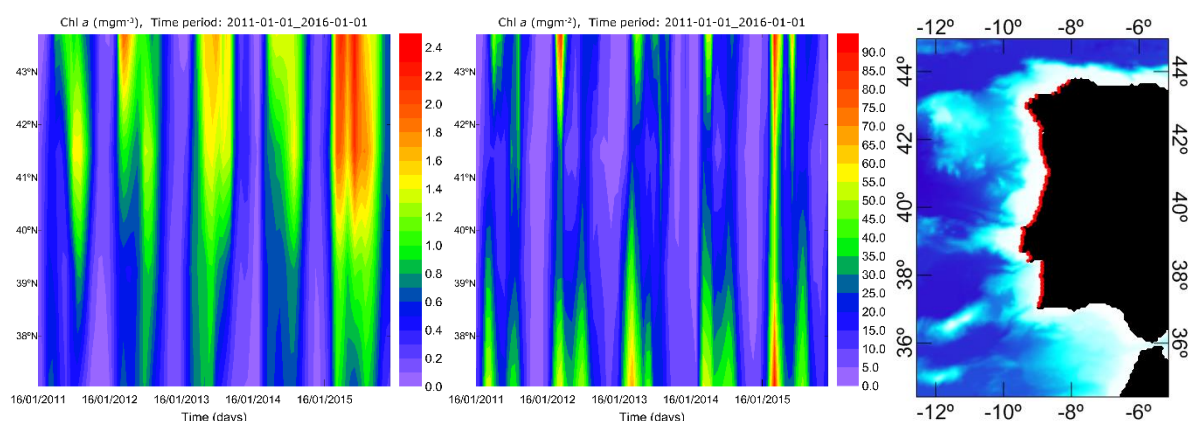


Figure 11 Monthly vertically integrated Chl *a* for the 2011-2015 period. Isobaths are represented every 1000 m starting at 500 m. Vectors represent mean direction every third cell.

## 9.6. Discussion and conclusions

In order to evaluate the in higher detail the differences in analysing Chl *a* concentrations in the surface layer or in integrated vertically. Monthly averaged Chl *a* concentrations for both parameters were obtained in the closest coastal cell of the western Iberia coast (Figure 12). In this figure, it can be observed how surface Chl *a* highlight the upwelling in the northern sector that eventually extends towards the south. This difference may be caused by the capacity of the upwelling favourable winds to generate outcrops with more facility in the northern areas. On the other hand, vertically integrated Chl *a* displays two areas of primary production located in the northern and southern reaches of the western coast that eventually join. Both indexes presented two annual peaks and they coincide in the years with maximum Chl *a* production (i.e. 2012 and 2015).



**Figure 12** Monthly mean surface Chl *a* (left) and vertical integrated Chl *a* (centre) concentration for the 2011-2015 period obtained in the western coast as indicated in the map (right).

If the temporal evolution is calculated regardless the latitudinal distribution, it can be observed the annual cycle for the surface Chl *a* and the vertically integrated Chl *a* concentrations (Figure 13). Both indexes show a similar cycle with two maxima corresponding to the spring and summer blooms. However, the intensity of these two peaks differ from one index to the other. Summer bloom, due to upwelling favourable conditions, is generally larger in the surface Chl *a* modelling results while in the vertically integrated Chl *a* is the way around. This result is even clearer when the climatology is obtained (Figure 14).

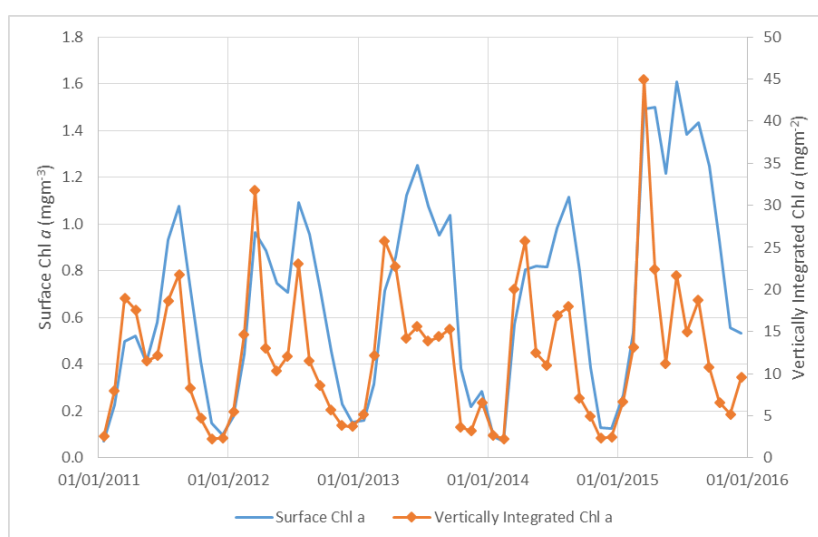


**Figure 13** Monthly mean surface Chl *a* (blue line) and vertical integrated Chl *a* (orange line with diamonds) concentration for the 2011-2015 period in the western Iberian coast.

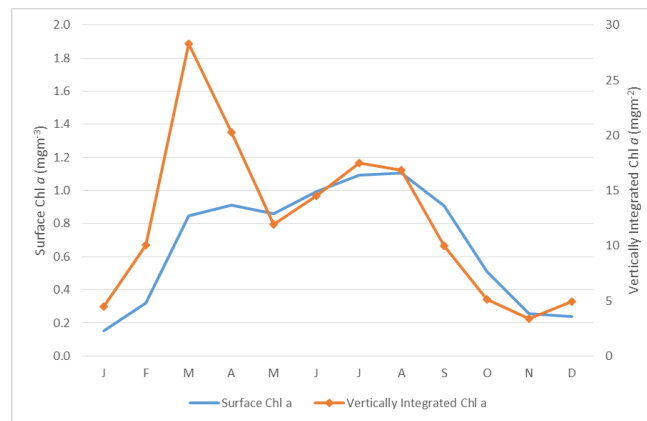


**Figure 14 Monthly climatological values for surface Chl *a* (blue line) and vertical integrated Chl *a* (orange line with diamonds) concentrations in the western Iberian coast for the 2011-2015 period.**

From these results, it can be concluded that analysing the Chl *a* production by remote sensing images or the analysis of the surface layer may lead to wrong conclusions since this results, that should be further validated, indicate the dominance of the spring phytoplankton bloom over the upwelling generated bloom.

Despite the limitations of the biogeochemical models and the challenging task to calibrate the complex interrelation of parameters. Modelling results can be regarded as a useful tool for ocean productivity evaluation. One of the main advantages of biogeochemical modelling is allowing to estimate the transfer of nutrients to the primary producers. In this study, it has been shown how integrated chlorophyll concentrations allowed to describe the spring bloom in detail and to obtain a wider picture of the upwelled nutrient rich waters in western Iberia near ocean. Some of the identified structures should be further studied through comparisons with monitoring cruises that ideally should include vertical profiles.

## 9.7. References

Bowie GL, Mills WB, Porcella DB, Campbell CL, Pagenkopf JR, Rupp GL, Johnson KM, Chan PWH, Gherini SA and Chamberlin CE (1985). Rates, constants, and kinetic formulations in surface water quality modeling. U.S. Environmental Protection Agency.

Campuzano FJ, Kenov I, Brito D, Juliano M, Fernandes R, Pinto L, Neves R. Numerical evaluation of the river nutrients influence for the Western Iberian coastal region. 3.as Jornadas de Engenharia Hidrográfica, 24-26 June 2014, Lisbon, Portugal. Extended abstracts: 263-266.

Cardeira S, Rita F, Relvas P, Cravo A. Chlorophyll a and chemical signatures during an upwelling event off the South Portuguese coast (SW Iberia). *Continental Shelf Research*. 2013; 52: 133-149. DOI: [10.1016/j.csr.2012.11.011](https://doi.org/10.1016/j.csr.2012.11.011).

Carrère L, Lyard F, Cancet M, Guillot A, Roblou L. FES2012: A new global tidal model taking advantage of nearly 20 years of altimetry. Proceedings of 20 Years of Altimetry meeting. Venice, Italy, 24-29 September 2013.

Cravo A, Relvas P, Cardeira S, Rita F, Madureira M, Sánchez R. An upwelling filament off southwest Iberia: Effect on the chlorophyll a and nutrient export. *Continental Shelf Research*. 2010; 30(15): 1601-1613. DOI: [10.1016/j.csr.2010.06.007](https://doi.org/10.1016/j.csr.2010.06.007).

- Crespo BG, Teixeira IG, Figueiras FG, Castro CG. Microplankton composition off NW Iberia at the end of the upwelling season: source areas of harmful dinoflagellate blooms. *Marine Ecology Progress Series*. 2008; 355: 31-43.
- Drillet Y, Bourdalle-Badi R, Siefrid L, Le Provost C. Meddies in the Mercator North Atlantic and Mediterranean Sea eddy-resolving model. *Journal of Geophysical Research*. 2005; 110(C3): C03016.
- Friedland KD, Record NR, Asch RG, Kristiansen T, Saba VS, Drinkwater KF, Henson S, Leaf RT, Morse RE, Johns DG, Large SI, Hjøllø SS, Nye JA, Alexander MA, Ji R. Seasonal phytoplankton blooms in the North Atlantic linked to the overwintering strategies of copepods. *Elementa: Science of the Anthropocene*. 2016; 4:99. DOI: [10.12952/journal.elementa.000099](https://doi.org/10.12952/journal.elementa.000099)
- Garcia HE, Locarnini RA, Boyer TP, Antonov JI, Baranova OK, Zweng MM, Johnson DR (2010a). World Ocean Atlas 2009, Volume 3: Dissolved Oxygen, Apparent Oxygen Utilization, and Oxygen Saturation. S. Levitus, Ed. NOAA Atlas NESDIS 70, U.S. Government Printing Office, Washington, D.C., 344 pp.
- Garcia HE, Locarnini RA, Boyer TP, Antonov JI, Zweng MM, Baranova OK, Johnson DR (2010b). World Ocean Atlas 2009, Volume 4: Nutrients (phosphate, nitrate, silicate). S. Levitus, Ed. NOAA Atlas NESDIS 71, U.S. Government Printing Office, Washington, D.C., 398 pp.
- MARETEC (2006). MOHID WaterQuality Module Manual. 42 pp. Available at: <http://www.mohid.com/PublicData/Products/Manuals/WaterQualityModuleManual.pdf>
- Mateus M, Riflet G, Chambel P, Fernandes L, Fernandes R, Juliano M, Campuzano F, de Pablo H, Neves R. An operational model for the West Iberian coast: products and services, *Ocean Science*. 2012; 8: 713-732.
- Neves R, 2013. The MOHID concept. In: M. Mateus & R. Neves (eds.). *Ocean modelling for coastal management - Case studies with MOHID*. IST Press, Lisbon, 1-11.
- Oliveira PB, Nolasco R, Dubert J, Moita T, Peliz A. Surface temperature, chlorophyll and advection patterns during a summer upwelling event off central Portugal. *Continental Shelf Research*. 2008; 29: 759-774. DOI: [10.1016/j.csr.2008.08.004](https://doi.org/10.1016/j.csr.2008.08.004).
- Ribeiro AC, Peliz Á, Santos AMP. A study of the response of chlorophyll-a biomass to a winter upwelling event off Western Iberia using SeaWiFS and in situ data. *Journal of Marine Systems*. 2005; 53(1-4): 87-107. DOI: [10.1016/j.jmarsys.2004.05.031](https://doi.org/10.1016/j.jmarsys.2004.05.031).
- Rossi V, Garçon V, Tassel J, Romagnan J-B, Stemmann L, Jourdin F, Morin P, Morel Y. Cross-shelf variability in the Iberian Peninsula Upwelling System: Impact of a mesoscale filament. *Continental Shelf Research*. 2013; 59: 97-114.
- Sá C (2013). *Ocean Colour off the Portuguese Coast: Chlorophyll a products validation and applicability*. PhD Thesis. Universidade de Lisboa
- Sá C, D'Alimonte D, Brito AC, Kajiyama T, Mendes CR, Vitorino J, Oliveira PB, da Silva JCB, Brotas V. Validation of standard and alternative satellite ocean-color chlorophyll products off Western Iberia, *Remote Sensing of Environment*. 2015; 168, 403-419. DOI: [10.1016/j.rse.2015.07.018](https://doi.org/10.1016/j.rse.2015.07.018).
- Sathyendranath S, Stuart V, Nair A, Oka K, Nakane T, Bouman H, Forget M-H, Maass H, Platt T Carbon-to-chlorophyll ratio and growth rate of phytoplankton in the sea. *Marine Ecology Progress Series*. 2009; 383: 73-84.
- Sutcliffe A, Brito AC, Sá C, Sousa F, Boutov D, Brotas V (2016). *Observação da Terra: uso de imagens de temperatura da superfície do mar e cor do oceano para a monitorização de águas costeiras e oceânicas*. DGRM, Lisboa, Portugal.

# Chapter X - Discussion, final remarks and future work.

---

## Publication information

Some contents of this chapter were submitted included in a recently submitted joint publication resulting from the EMoSEM project with the following details:

Desmit X, Thieu V, Billen G, Campuzano F, Dulière V, Garnier J, Lassaletta L, Ménesguen A, Neves R, Pinto L, Silvestre M, Sobrinho JL, Lacroix G. Reducing marine eutrophication may require a paradigmatic change. Submitted to Science of the Total Environment, VSI Eutrophication

## 10.1. Introduction

In this chapter, some issues raised during this thesis preparation and that were not included in previous chapters are briefly presented. In addition, a summary of the main conclusions from this research along with the description of the future developments and evolution of the research here presented.

## 10.2. Discussion

In this section two issues raised during this research are briefly discussed. The first is a crucial question that was on the origin of the thesis and that the author want to briefly treat as its the relative importance of nutrient inputs from river sources and from upwelled nutrient-rich waters. The second issue is related to the response of the biogeochemical model to nutrient river inputs.

### 10.2.1. Upwelling versus river nutrient discharge

One of the initial discussions at the start of this PhD was to evaluate, quantify and compare the input of nutrients in the photic area by upwelling transport and land inputs. This objective has been partly covered by studying in detail the upwelling events and the nutrients reaching the coastal area. However, this task is tough due to the difficulty to obtain continuous observations of nutrients in the near ocean and around the estuaries, in order to evaluate the nutrient concentration entering the estuary and reaching the open ocean. This question is especially interesting in the area of the WIBP where many rivers coincide. For this reason, a preliminary result will be provided waiting for in deep future research.

For this analysis on the ocean side, the mean nitrate and net fluxes were estimated at the 100 m depth interface and integrated for the first longitudinal degree. At this depth was considered that the nutrient concentrations were not influenced by the primary producers' dynamics. To evaluate the upwelling transport influence in the WIBP, the integrated fluxes and mean nitrate concentration were calculated for the region 40-42°N. On the river side, the flow of the eight main rivers in the WIBP: Lima, Minho, Douro, Vouga, Mondego, Ave, Cavado and Leça were aggregated. The Douro and Mondego river flow were obtained from the SNIRH database and the WI MOHID Land modelling results were used for the remaining six.

In terms of flow, the net volume transported at the 100 m depth interface is far greater, on average around 100 times, than the aggregated flow from the eight rivers (Figure 1). However, nitrate concentration difference in order of order of magnitude is similar on the opposite sense. Taking for instance the nitrate concentration in the River Minho obtained from the WI MOHID Land, it varies

along the year from 0.9 to 1.72 mg NO<sub>3</sub>-N l<sup>-1</sup> with an average value of 1.1 mg NO<sub>3</sub>-N l<sup>-1</sup>. This value is in agreement with the reported values to the EU (<http://www.eea.europa.eu/data-and-maps/explore-interactive-maps/nitrate-in-rivers>) where mean annual nitrate concentrations were 0.76 mg NO<sub>3</sub>-N l<sup>-1</sup> for River Minho, 1.19 mg NO<sub>3</sub>-N l<sup>-1</sup> for the River Mondego, 2.28 mg NO<sub>3</sub>-N l<sup>-1</sup> for River Ave and 2.47 mg NO<sub>3</sub>-N l<sup>-1</sup> River Vouga. In contrast, open ocean waters at 100 m depth in this area have on average concentrations around 0.03 mg NO<sub>3</sub>-N l<sup>-1</sup>. When both fluxes of nutrients are compared using for the vertical transport the nitrate concentrations calculated by the PCOMS model application and for the river discharge a conservative constant value of 1.1 mg NO<sub>3</sub>-N l<sup>-1</sup> (Figure 2), it can be seen how the river discharge dominates the nutrient input during certain periods of the year, mainly during the winter season. The general trend is that river discharge dominates during the winter period however winter upwelling events can change that pattern, i.e. winter of 2011-2012. In order to observe more clearly the patterns, a climatology was generated with the monthly results and it can be seen that river input leads the entry of nitrate during October-April while upwelling dominates from May to September (Figure 3). According to these estimations, in total river inputs would provide 3.81·10<sup>7</sup> Ton NO<sub>3</sub>-N year<sup>-1</sup> while upwelling 2.67·10<sup>7</sup> Ton NO<sub>3</sub>-N year<sup>-1</sup>.

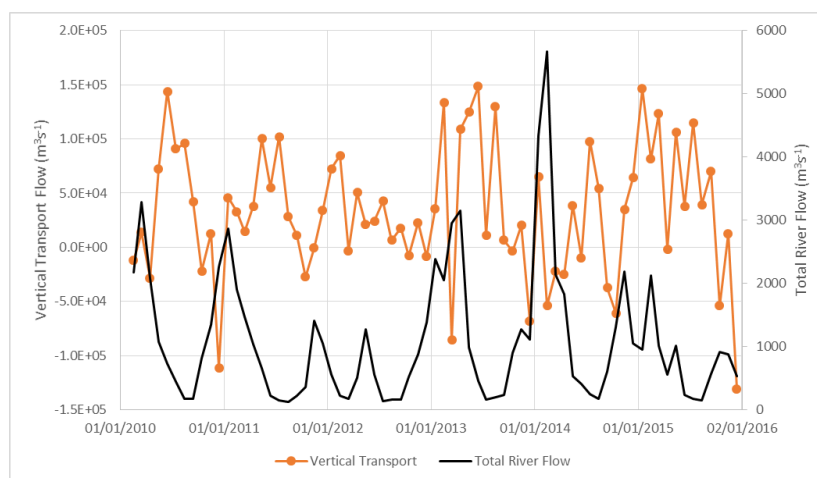


**Figure 1** Monthly net vertical transport calculated at 100 m depth and integrated for the first offshore longitudinal degree and for the range of latitudes 40-42°N (orange line with dots) and river flow for the eight main rivers discharging in the WIBP area (black line) for the period 2010-2015. Note that the river flow is represented in the secondary vertical axis.

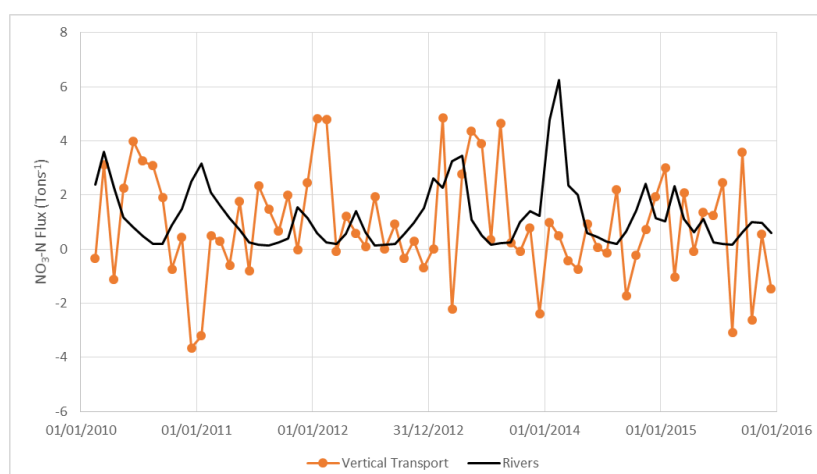


**Figure 2** Monthly averaged nitrate flux (Tons<sup>-1</sup>) due to vertical transport (orange line with dots) and due to river flow from the eight main rivers discharging in the WIBP area (black line) for the period 2010-2015.

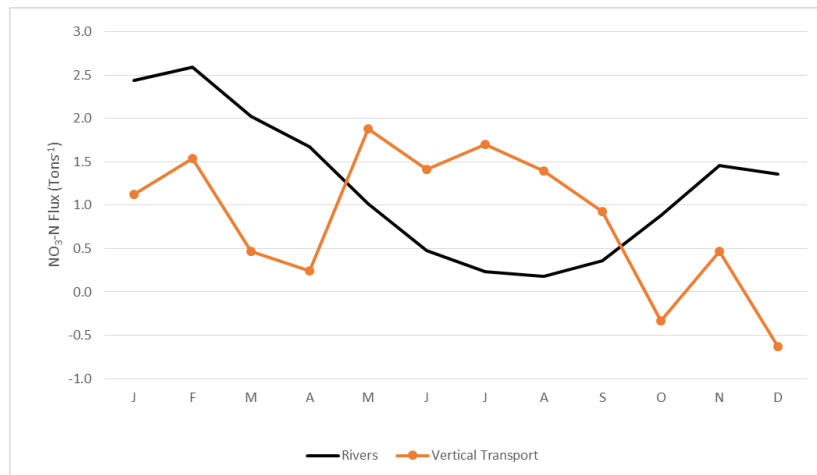


**Figure 3** Monthly climatology of nitrate flux (Tons<sup>-1</sup>) due to vertical transport (orange line with dots) and due to river flow from the eight main rivers discharging in the WIBP area (black line) for the period 2010-2015.

This result can be regarded as a preliminary result since many factors can alter or reinforce the result. In this estimation the role of estuaries as nutrient filters has been disregarded and it should be considered a certain percentage of accumulated error due to numerical models mislead, i.e. wind intensity and direction, river flow overestimation, simplified coastal line and bathymetry, etc. On the other hand, the nitrate concentration used to characterise the water was conservative and can increase due to human practices and seasons and other minor rivers and surficial waters were disregarded. The only solid conclusion from this preliminary result is that both processes present similar orders of magnitude and that further research and model validation is necessary.

#### 10.2.2. Influence of nutrients from land source in coastal waters

In the near future the biogeochemical model will be forced with the rivers discharges following the defined methodology. However, in order to provide an idea of the expected outcomes, some results obtained during the EMoSEM project are shown below. The PCOMS model simulated the input of nutrients in the Western Iberian coasts incorporating as direct discharges the outputs obtained from the pyNuts-Riverstrahler modelling framework (Desmit *et al.*, submitted). The PyNuts properties included the discharges are flow, oxygen, nitrite, nitrate, ammonia and inorganic phosphorus. Additionally, salinity concentration was included as a constant value of 32 salinity units and temperature values were obtained by the MOHID Land applications for the Iberian Peninsula and Western Iberia (Campuzano *et al.*, 2014).

The 27 rivers included as surficial direct discharges were: Alcobaça, Anllons, Arade, Arnoia, Ave, Cavado, Douro, Eo, Esva, Eume, Guadalquivir, Guadiana, Lima, Lis, Minho, Mira, Mondego, Navia, Odiel-Tinto, Piedras, Sado, Sizandro, Tagus, Ulla, Umia, Vouga and Xallas.

In Figure 4 the distribution of phytoplankton in the western coast of the Iberian Peninsula for the period of March-October can be observed for the year 2010 and 2011. These two years were contrasting in terms of precipitation, being the 2010 a wet year while 2011 was a dry year. However, the phytoplankton distribution present a similar distribution in the Atlantic front with surface maximum concentrations located in the vicinity of the discharge areas of the Douro, Tagus and Guadalquivir rivers. A continuous front of high primary production is located along the coastal area of Portugal associated to upwelling period and extending to the Northwest of the Iberian Peninsula with a larger extension in 2010 probably due to the higher river input taken place during that year. These results are in agreement with Alvarez *et al.* (2012) that identified the Chl *a* concentrations differences occurring in the Northwest of the Iberian Peninsula between the high productive west coast associated with the northerly winds along the continental shelf in contrast to the low productive north coast. It is important also to note here that the values presented correspond to chlorophyll and phytoplankton concentration at the surface.

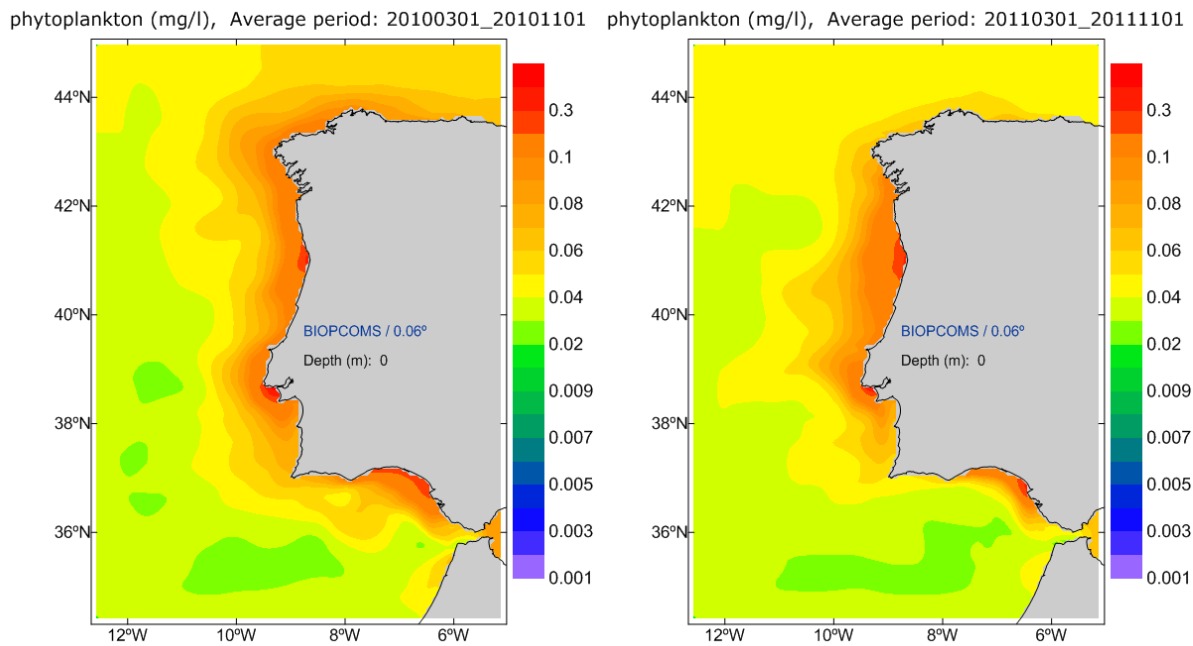


Figure 4. PCOMS surface Chlorophyll a for the period March-October 2010 (left) and March-October 2011 (right). Colour contouring corresponds to Chl a concentration on a logarithmic scale.

### 10.3. Final remarks

Some conclusions regarding numerical model applications to study regional ocean can be drawn. First, numerical modelling is an extremely useful tool for filling temporal and spatial data gaps obtained by remote sensing, moored stations and monitoring cruises as was proved along this thesis. Despite some existing constraint by a part of the ocean community that regard the different observation, monitoring and modelling components as competitors, the author thinks that the future relies in the closer integration of the *in situ* and remote monitoring with the numerical modelling results.

A second important conclusion from this research is that a numerical model application is never complete. The growing numerical capacities and the advances in computing along with the immense possibilities of model coupling (atmosphere, watershed, estuarine, ocean, waves, biogeochemical, Lagrangian, etc.) allow to obtain better integrated results and to explore from a more dynamic point of view observed data. The improvement of each numerical model will feed into each other in a synergetic way benefiting integrated models. Bearing this rationale in mind, in this research work, the integration of atmosphere-watershed-estuarine-ocean dynamics and biogeochemistry was applied to the Western Iberia regional ocean. Probably the most original contributions of this research is the demonstration that a better coupling of the land-ocean domains by improving the boundary conditions is able to explain better the observed variations in fixed monitoring stations. The author believes that the change of paradigm of incorporating the land area surrounding the studied coastal area will become more important in the near future. This division between land and ocean waters and their management will necessarily have to increase their exchanges in communication and move to a water continuum integrated approach. Examples of the complexity of separated management were discussed in this work such as the limit between the EU WFD and MSFD directives.

Another advantage of the developed methodology is that applications were simulated using open source numerical models (MM5, WRF, MOHID Water and MOHID Land) and their implementation is generic so this coupled system can be replicated elsewhere. Currently, this methodology is

employed, along with the PCOMS application, to link the watersheds and coastal waters in the Madeira Island. The offline coupled technique allow to be time efficient as refined grids, i.e. estuary model applications, that require larger computational time run simultaneously to the regional ocean and allow to produce best practical forecasts for each component of the system of models. By using regular grids and avoiding to include the high resolution areas embedded in the ocean regional models, this methodology allow to reduce the model running time and allows to include several estuaries with adapted resolutions for each case not being limited by the design of a single grid. This approach allow to continuous improvement of the forecast system components by replacing improved versions of any component without compromising the modelling system performance i.e. if an estuarine application is implemented the river flow can be easily substituted by estuarine fluxes. The implementation of watershed models to provide river flow also reduces the dependence on *in situ* monitoring stations that are subjected to reparations and failures and allow to fill the time gap and to complete the discharge with unmonitored variables. Watershed models has shown to produce a more realistic land boundary condition than river climatologies.

Despite the study period of this research corresponds to the interval of 2010-2015. The development methodology for integrating the land and ocean numerical domains, including the estuarine interface, was developed bearing in mind the improvement of regional ocean forecast and the simulations and validates were done using operational tools developed along with this thesis. Consequently, the developed system of models is able provide forecasts and the operational version of most of the described numerical model applications is accessible at <http://forecast.maretec.org/>.

Below a list of conclusions are extracted from each chapter:

Chapter I highlighted the importance of operational systems for the development of blue economy and the reliability and the long-term sustainability needed for services be developed on top of them.

Chapter II Even with the known limitations, numerical meteorological models are a key component of the ocean modelling systems and contribute significantly to reproduce adequately the ocean processes by including the atmospheric temporal and spatial variability.

Chapter III indicates the benefit for the implementation and development of regional ocean models of the continuous improvement in global tide models. As such the Portuguese Coast Operational Modelling System (PCOMS) on its current version was able to reproduce accurately the barotropic and baroclinic tides. 3D baroclinic tidal maps illustrate the modification of the tidal contours due to the density gradients and meteorological effects.

Chapter IV evaluated the suitability of the PCOMS thermohaline patterns in order to be applied for this thesis objectives. In addition, a novel method for identifying the upwelling filaments was applied for western Iberian waters. For the first time, a regional ocean model was compared with remote sensed SSS.

Chapter V concluded that improving the calculation of the fresh water quantity and quality reaching the coastal area, managers and scientists would be able to better reproduce the haline fronts that affect coastal hydrodynamics and the associated ecological processes

Chapter VI showed how modelling results can calculate complex indicators such as tidal prisms, the region of influence of the estuarine waters and to estimate accurately estuarine fluxes that would serve as boundary conditions for ocean regional models such as the offline coupling method applied to the PCOMS

Chapter VII demonstrate how numerical modelling is currently the only tool able to represent and estimate the temporal and spatial scale of the WIBP and other estuarine plumes. Taking into consideration the numerical modelling limitations and assumptions, the salinity modelling results provided by the methodology described in Campuzano *et al.* (2016) improve significantly salinity fields and aid to the delimitation of region of fresh water influence and salinity fronts.

Chapter VIII calculated the upwelling transport for western Iberian waters using alongshore wind, SST difference and by the use of numerical circulation model. The advantage of the latter method was a more accurate estimation of the upwelled water as it considers the local values for density, bathymetry and coastal orientation. Additionally and moreover, the entry of nutrient-rich waters in productive depths could also be evaluated and the magnitude of nutrients can be quantified.

Chapter IX described the modelling results of a NPZD biogeochemical model coupled to the PCOMS regional ocean model application. In this chapter, the vertical integration of Chl *a* was explored and compared with surface model results. The former index can be regarded as a useful tool for ocean productivity evaluation. However, further validation exercises should be performed to confirm some of this chapter results.

## 10.4. Future work

As stated above a numerical model application is never complete. Several improvements have been identified during the completion of this thesis. A summary of future or planned improvements for each component of the water cycle modelling system is described in this section.

The atmosphere forcing of the system of models will move from MM5 to WRF model applications for all the analysed domains. The data used in this thesis will aid to evaluate if the WRF applications perform better than its current forcing.

Regarding the watershed component, future work would include the human management along the watershed by implementing the dams' simulation in the watershed domain. Recent developments in the code of the MOHID Land allow to include dam management. This is a crucial step for controlling the flow overestimation in strongly regulated waterlines. Further validation of water parameters should be performed including temperature, sediments, oxygen and nutrient concentrations.

Currently, most of the estuary model applications are running on 2-Dimension grids with the exception of the Tagus Mouth application. In addition, all the estuary applications will be coupled with a biogeochemical module, currently only the Mondego and Douro applications are pure hydrodynamic applications. The biogeochemical results from the modelling applications need to be validated for most of this applications when using nutrients from the watershed model.

At the regional ocean model, the current PCOMS parameterisation will replace the operational version as improvement on the hydrodynamics and biogeochemical results were demonstrated. In addition, the parallelisation methods included in MOHID (openMP and MPI) will be evaluated with the PCOMS river version allowing improvements in the computational time. Currently a version of the PCOMS without rivers is providing the boundary conditions to the estuarine models, it should be studied a coupling strategy with low computing cost to enable two-way coupling between the estuarine models and the PCOMS model since it have been demonstrate exchanges of water between estuaries.

In the current PCOMS river version, 36 rivers were imposed directly in the regional model as continuous discharges using flow and temperature from the MOHID Land watershed model application (Brito *et al.*, 2015). The salinity of these rivers was defined as constant with a value of 32. In future versions, a better characterisation of the salinity should be studied since the signature of large rivers such as Guadalquivir River was underestimated. Ways to introduce tidal variability and mixing in small rivers, i.e. by using simple tidal prism models, will be studied.

The comparison of the PCOMS with the SMOS SSS and the MERCATOR reference solution, showed that the PCOMS salinity values diverges from the reference solution when the period simulated include several years. The relaxation strategy to the reference solution need to be studied in order to provide enough freedom to maintain the variability generated by the land-boundary condition.

As the main aim of this research was the influence of the upwelling/downwelling transport and the land-ocean boundary conditions mainly in the surface thermohaline properties. The PCOMS performance to represent the hydrodynamic and biogeochemical patterns in the vertical axis was partly disregarded. In the near future, these aspects will be analysed and compared by using ARGO floats and more information from monitoring cruises.

Due to the advance in computing capacities, also the PCOMS model horizontal resolution will increase to simulate with finer detail mesoscale features and to reduce the numerical diffusion that affect the river plume dynamics and concentrations, as was detected also by Herzfeld (2015).

In the near future, the fluxes will include biogeochemical properties that will allow to explore the influence of the rivers discharge in the primary production and their ecological importance in the maintenance of biological systems. The WIBP has been described as confined in the inner shelf during winter conditions due to its interaction with the Iberian Poleward Current (IPC). However, during winter upwelling conditions it was also observed spreading offshore further than 100 off the shelf-break (Ribeiro *et al.*, 2005). Chl *a* concentration has been found related to the entrance of nutrient-rich river fluxes into the coastal area (Picado *et al.*, 2014). For these reasons, the interaction between the WIBP and the upwelling/downwelling conditions should be studied in greater detail.

## 10.5. References

Alvarez I, Lorenzo MN, deCastro M. Analysis of chlorophyll *a* concentration along the Galician coast: seasonal variability and trends. *ICES Journal of Marine Science*. 2012; 69: 728–738.

Brito D, Campuzano FJ, Sobrinho J, Fernandes R, Neves R. Integrating operational watershed and coastal models for the Iberian Coast: Watershed model implementation – A first approach. *Estuarine, Coastal and Shelf Science*. 2015; 167(Part A): 138-146.

Campuzano FJ, Kenov I, Brito D, Juliano M, Fernandes R, Pinto L, Neves R. Numerical evaluation of the river nutrients influence for the Western Iberian coastal region. 3.as Jornadas de Engenharia Hidrográfica, 24-26 June 2014, Lisbon, Portugal. Extended abstracts: 263-266.

Herzfeld M. Methods for freshwater riverine input into regional ocean models. *Ocean Modelling*. 2015; 90: 1–15.

Desmit X, Thieu V, Billen G, Campuzano F, Dulière V, Garnier J, Lassaletta L, Ménesguen A, Neves R, Pinto L, Silvestre M, Sobrinho JL, Lacroix G. Reducing marine eutrophication may require a paradigmatic change. Submitted to *Science of the Total Environment*, VSI Eutrophication

Picado A, Alvarez I, Vaz N, Varela R, Gomez-Gesteira M, Dias JM. Assessment of chlorophyll variability along the northwestern coast of Iberian Peninsula. *Journal of Sea Research*. 2014; 93: 2-11. DOI: [10.1016/j.seares.2014.01.008](https://doi.org/10.1016/j.seares.2014.01.008).

Ribeiro AC, Peliz Á, Santos AMP. A study of the response of chlorophyll-a biomass to a winter upwelling event off Western Iberia using SeaWiFS and in situ data. *Journal of Marine Systems*. 2005; 53(1–4): 87-107. DOI: [10.1016/j.jmarsys.2004.05.031](https://doi.org/10.1016/j.jmarsys.2004.05.031).

# Appendix I - Additional tidal components maps



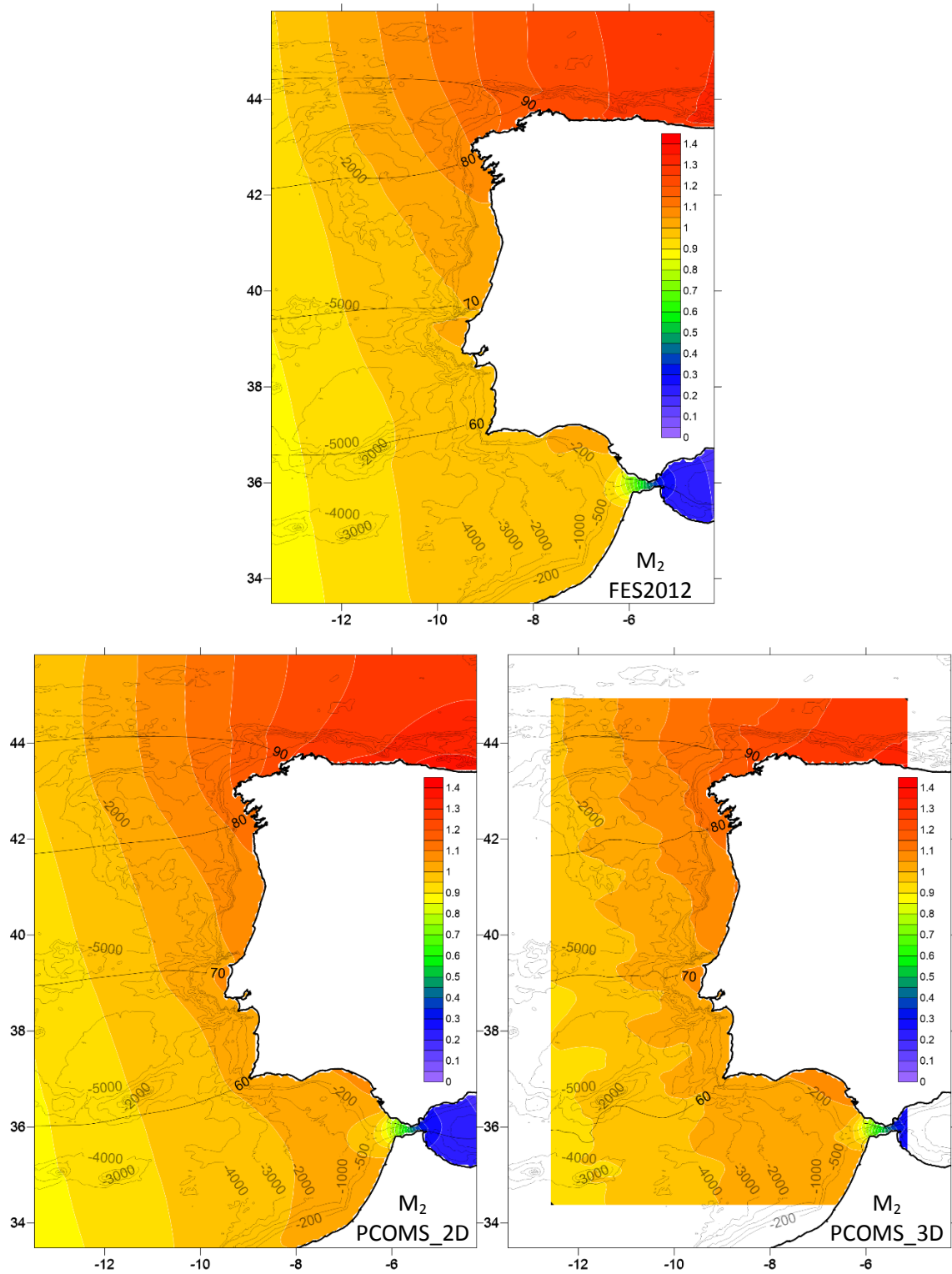


Figure Appendix I.1 M<sub>2</sub> harmonic component map from FES2012 (top) and obtained from a year simulation of the PCOMS WestIberia domain 2D (bottom left) and the PCOMS Portugal domain 3D (bottom right) forced with FES2012. Amplitude (m) is represented by the colour contour and phase by the dark isolines. Isobaths for 200 m, 500 m, 1000 m, 2000 m, 3000 m, 4000 m and 5000 m depths were added to ease interpretation.

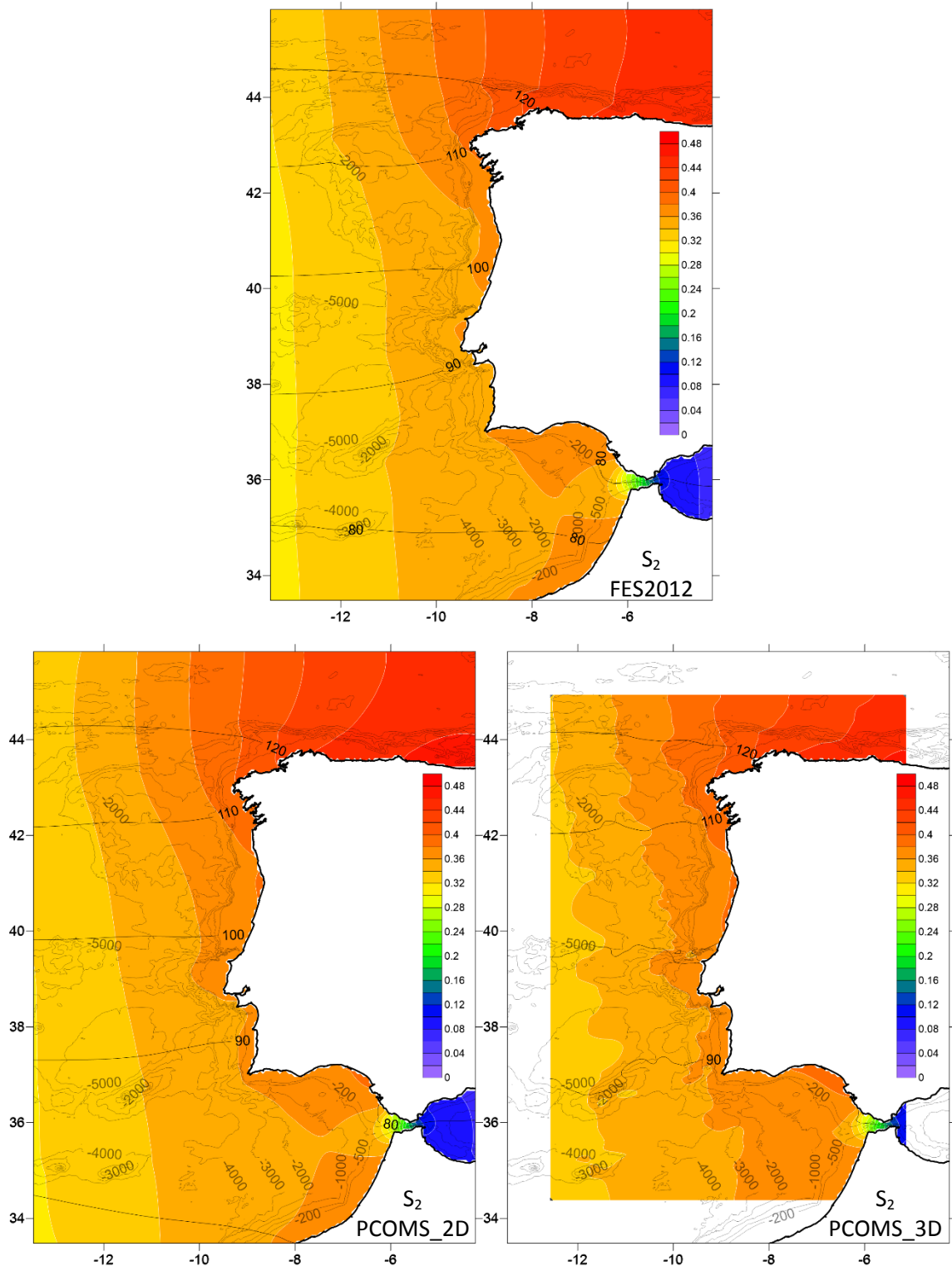


Figure Appendix I.2  $S_2$  harmonic component map from FES2012 (top) and obtained from a year simulation of the PCOMS Westberia domain 2D (bottom left) and the PCOMS Portugal domain 3D (bottom right) forced with FES2012. Amplitude (m) is represented by the colour contour and phase by the dark isolines. Isobaths for 200 m, 500 m, 1000 m, 2000 m, 3000 m, 4000 m and 5000 m depths were added to ease interpretation.

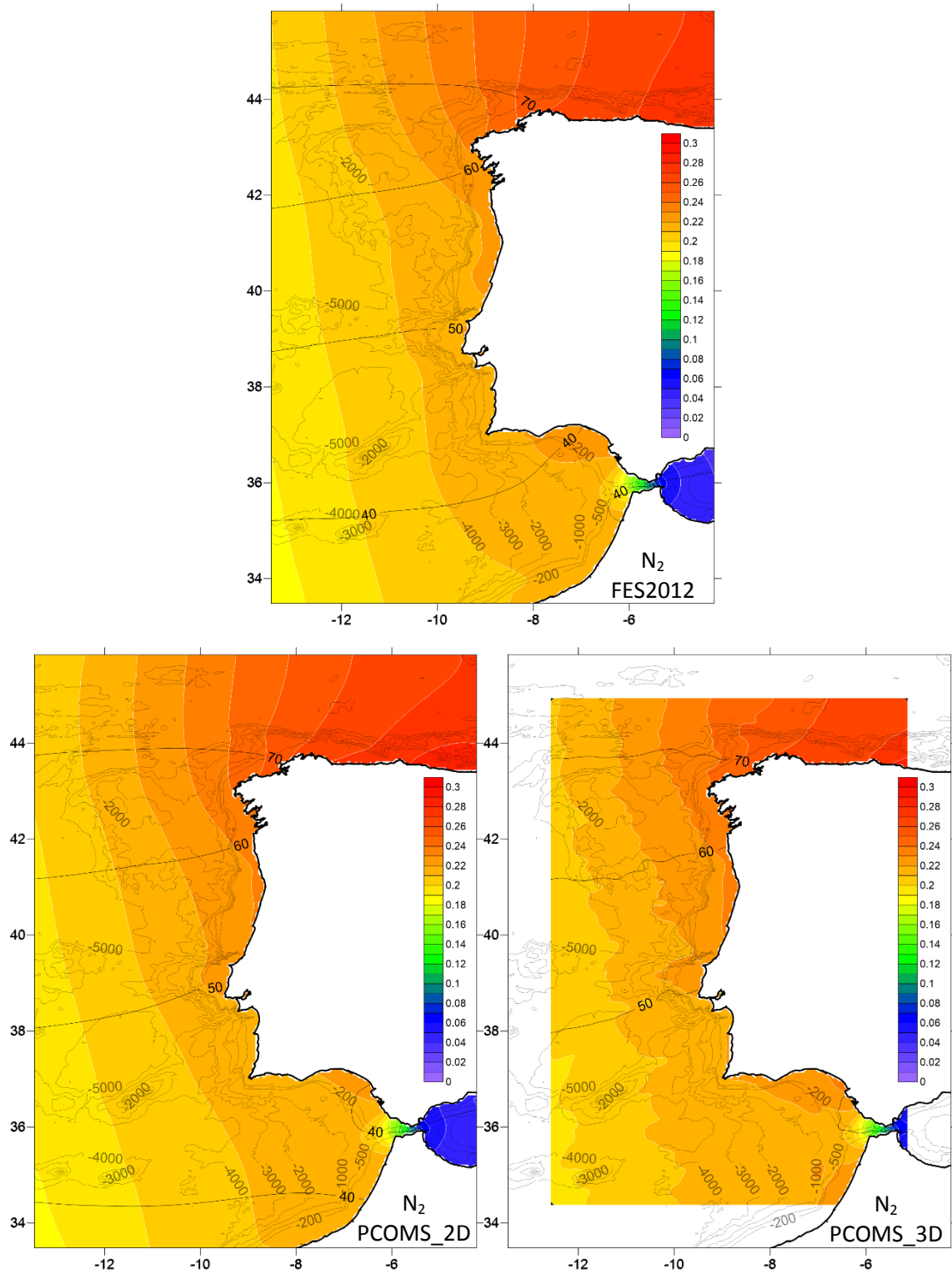


Figure Appendix I.3  $N_2$  harmonic component map from FES2012 (top) and obtained from a year simulation of the PCOMS WestIberia domain 2D (bottom left) and the PCOMS Portugal domain 3D (bottom right) forced with FES2012. Amplitude (m) is represented by the colour contour and phase by the dark isolines. Isobaths for 200 m, 500 m, 1000 m, 2000 m, 3000 m, 4000 m and 5000 m depths were added to ease interpretation.

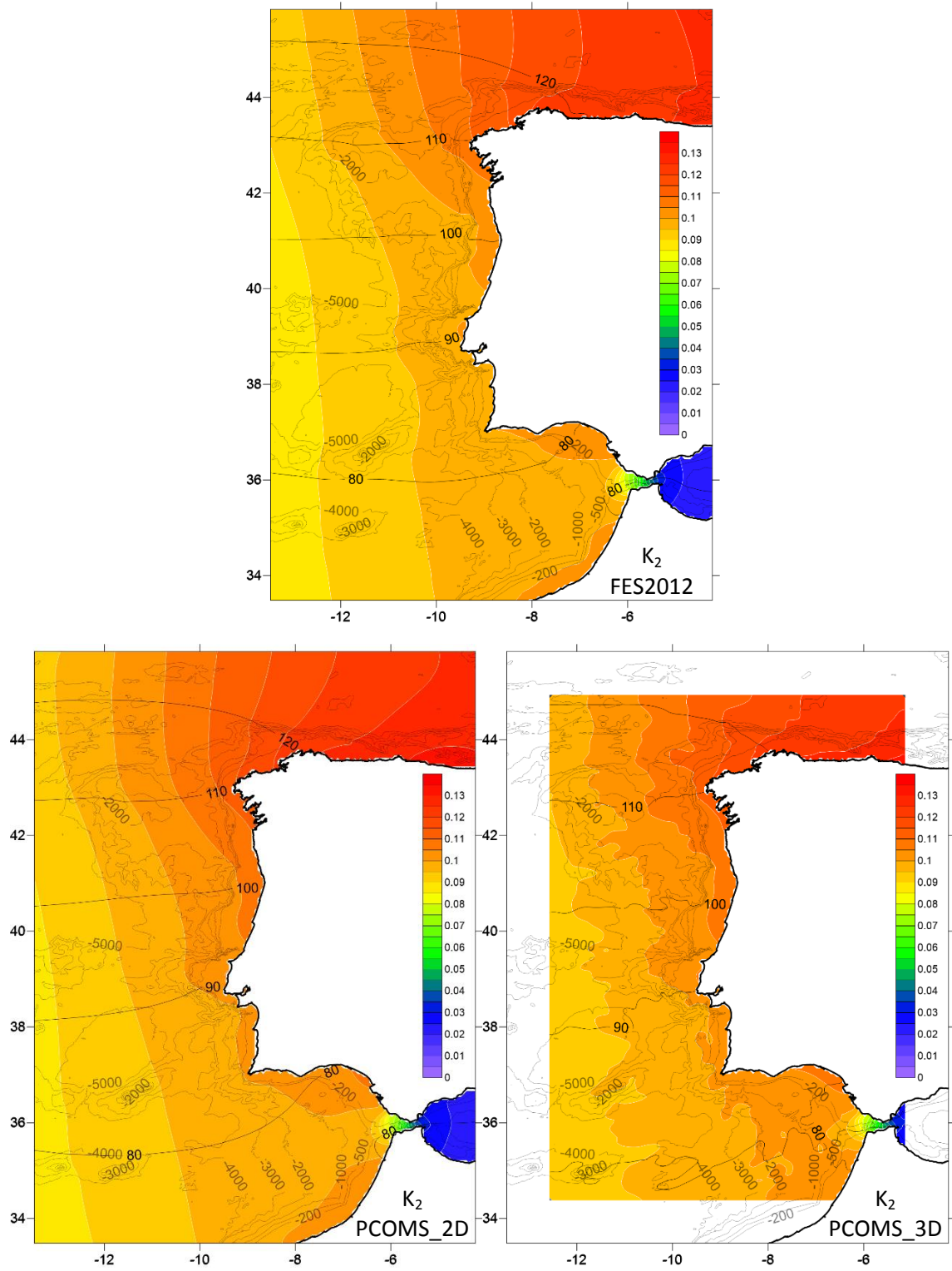


Figure Appendix I.4  $K_2$  harmonic component map from FES2012 (top) and obtained from a year simulation of the PCOMS Westberberia domain 2D (bottom left) and the PCOMS Portugal domain 3D (bottom right) forced with FES2012. Amplitude (m) is represented by the colour contour and phase by the dark isolines. Isobaths for 200 m, 500 m, 1000 m, 2000 m, 3000 m, 4000 m and 5000 m depths were added to ease interpretation.

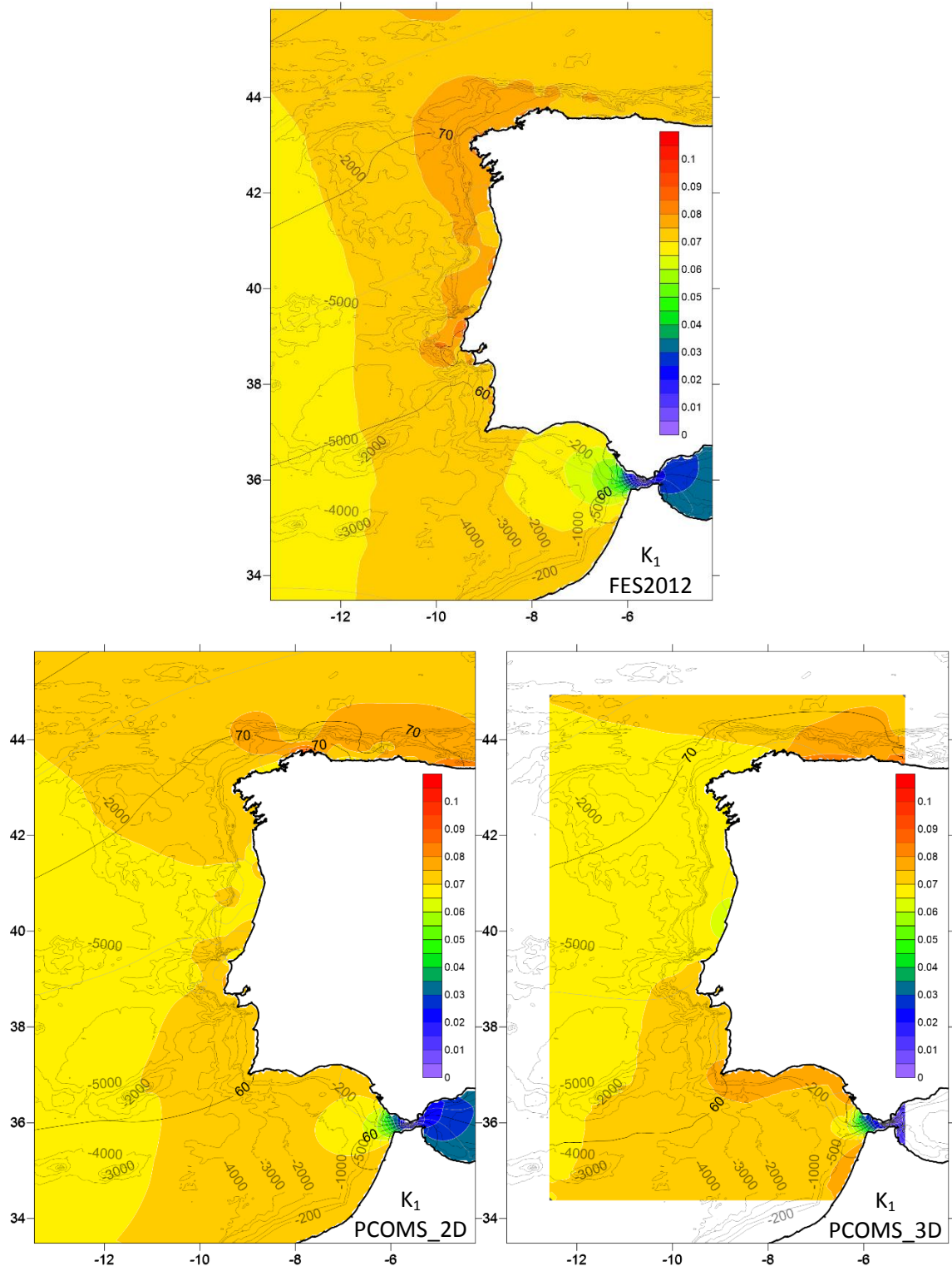


Figure Appendix I.5  $K_1$  harmonic component map from FES2012 (top) and obtained from a year simulation of the PCOMS Westberberia domain 2D (bottom left) and the PCOMS Portugal domain 3D (bottom right) forced with FES2012. Amplitude (m) is represented by the colour contour and phase by the dark isolines. Isobaths for 200 m, 500 m, 1000 m, 2000 m, 3000 m, 4000 m and 5000 m depths were added to ease interpretation.

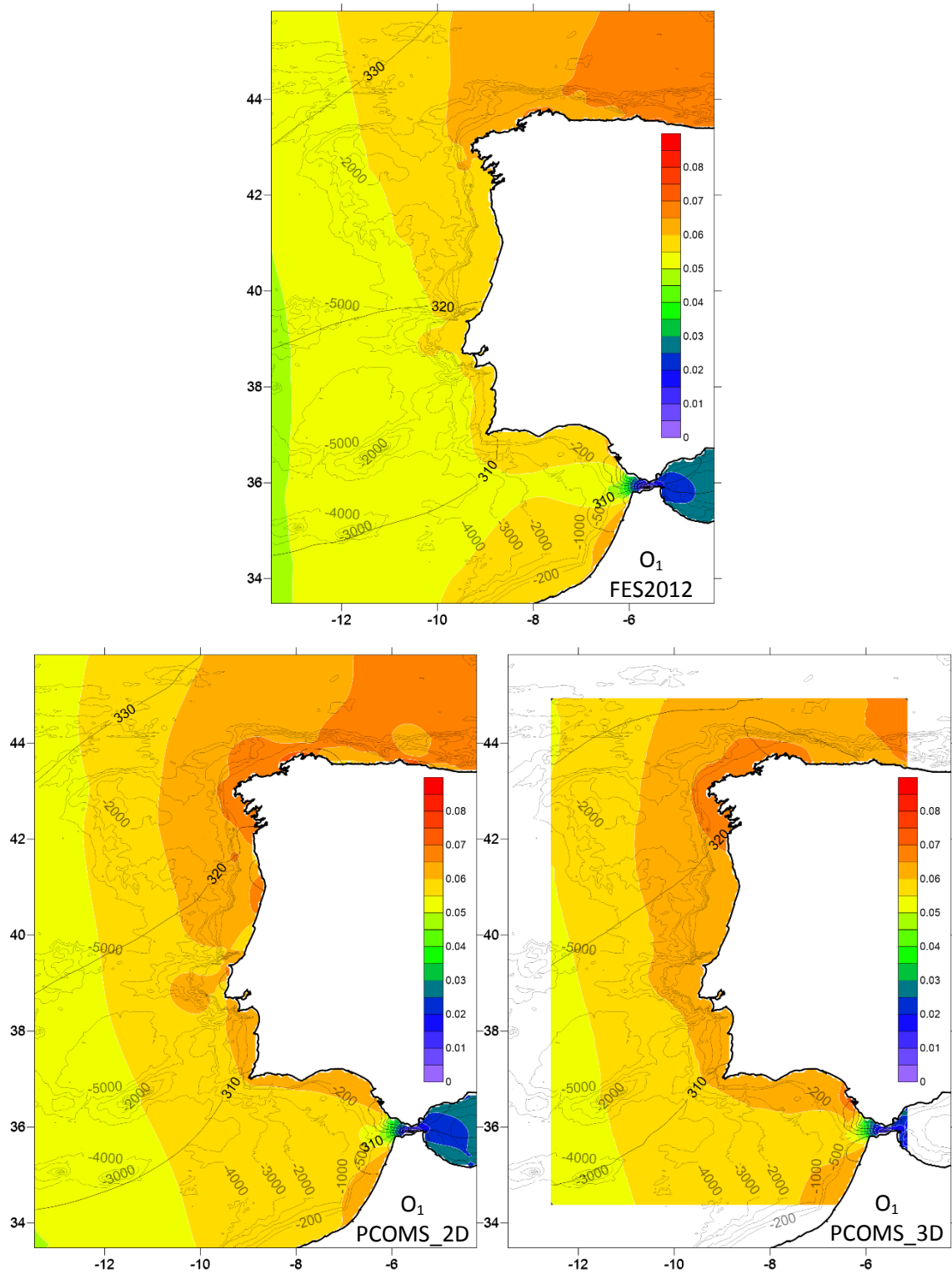


Figure Appendix I.6  $O_1$  harmonic component map from FES2012 (top) and obtained from a year simulation of the PCOMS WestIberia domain 2D (bottom left) and the PCOMS Portugal domain 3D (bottom right) forced with FES2012. Amplitude (m) is represented by the colour contour and phase by the dark isolines. Isobaths for 200 m, 500 m, 1000 m, 2000 m, 3000 m, 4000 m and 5000 m depths were added to ease interpretation.

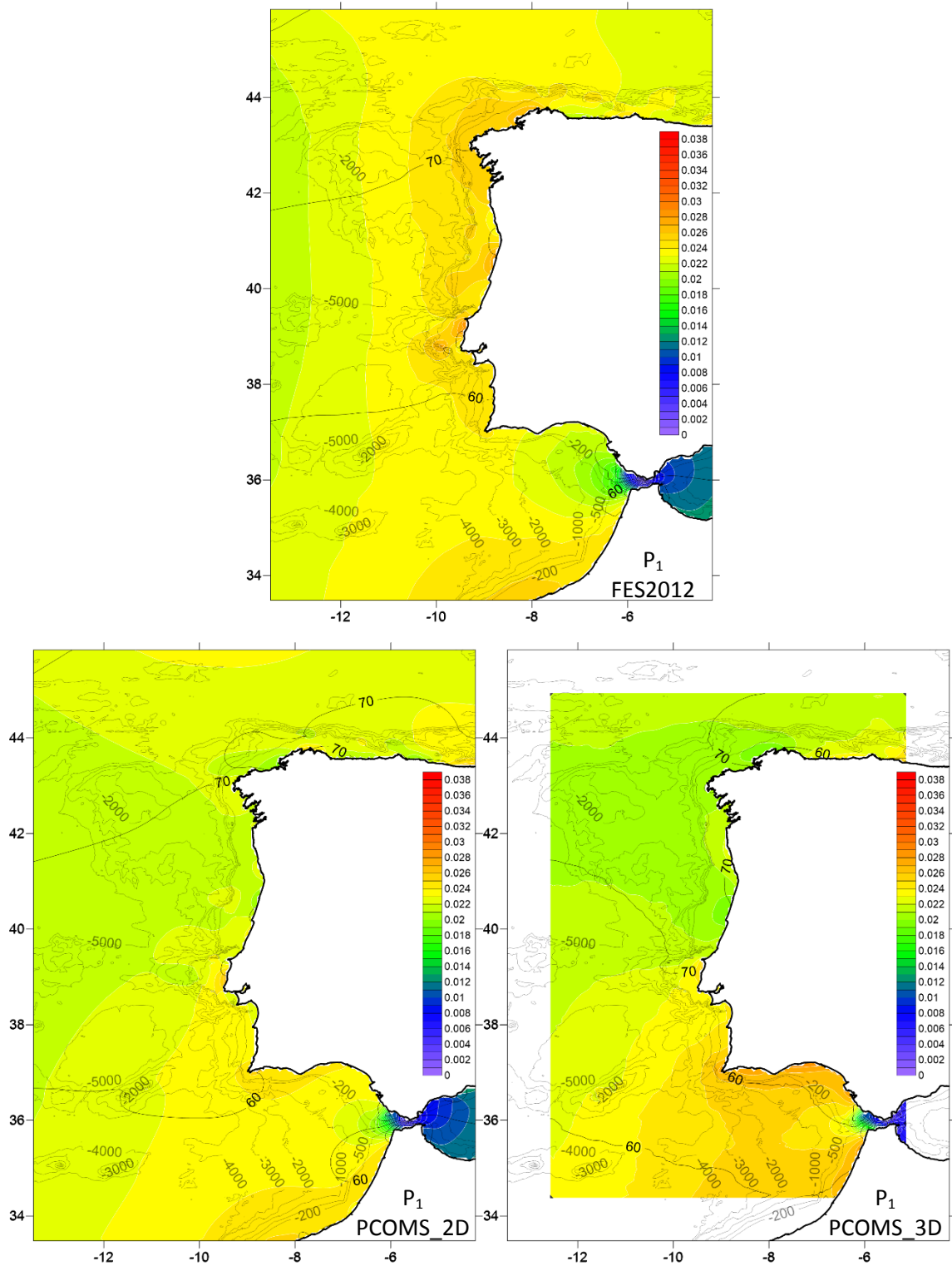


Figure Appendix I.7  $P_1$  harmonic component map from FES2012 (top) and obtained from a year simulation of the PCOMS Westberberia domain 2D (bottom left) and the PCOMS Portugal domain 3D (bottom right) forced with FES2012. Amplitude (m) is represented by the colour contour and phase by the dark isolines. Isobaths for 200 m, 500 m, 1000 m, 2000 m, 3000 m, 4000 m and 5000 m depths were added to ease interpretation.

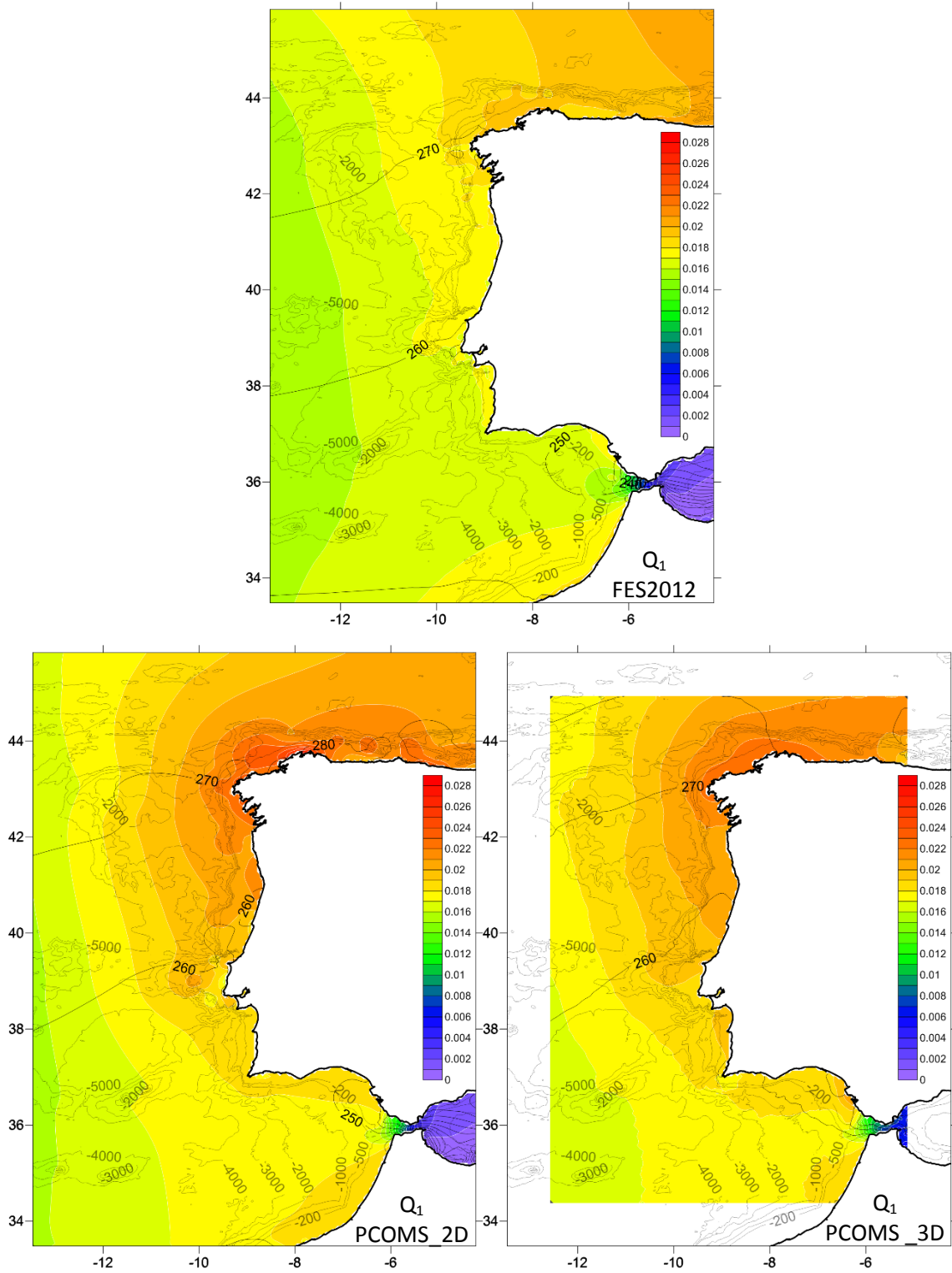


Figure Appendix I.8  $Q_1$  harmonic component map from FES2012 (top) and obtained from a year simulation of the PCOMS WestIberia domain 2D (bottom left) and the PCOMS Portugal domain 3D (bottom right) forced with FES2012. Amplitude (m) is represented by the colour contour and phase by the dark isolines. Isobaths for 200 m, 500 m, 1000 m, 2000 m, 3000 m, 4000 m and 5000 m depths were added to ease interpretation.

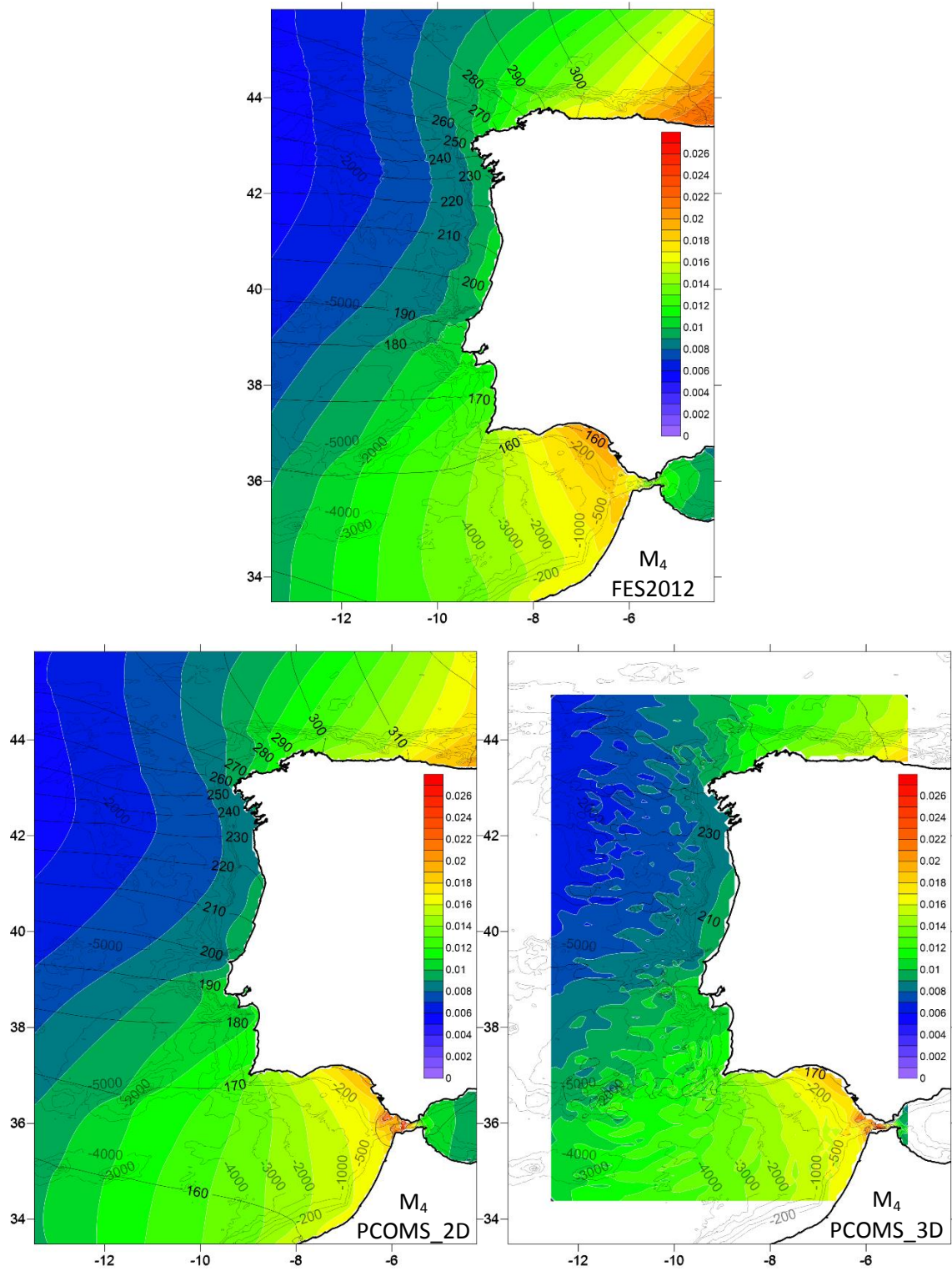


Figure Appendix I.9 M<sub>4</sub> harmonic component map from FES2012 (top) and obtained from a year simulation of the PCOMS WestIberia domain 2D (bottom left) and the PCOMS Portugal domain 3D (bottom right) forced with FES2012. Amplitude (m) is represented by the colour contour and phase by the dark isolines. Isobaths for 200 m, 500 m, 1000 m, 2000 m, 3000 m, 4000 m and 5000 m depths were added to ease interpretation.

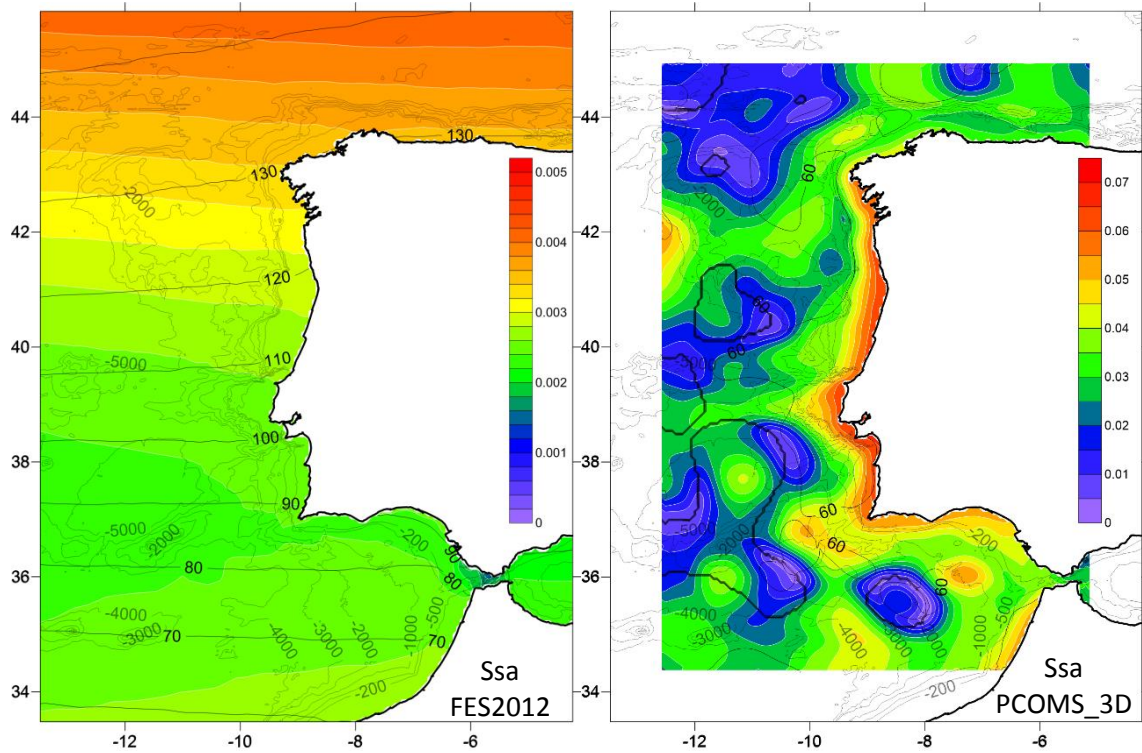


Figure Appendix I.10 Ssa harmonic component map from FES2012 (left) and obtained from a year simulation of the PCOMS Portugal domain 3D (right) forced with FES2012. Please note the difference in scale between both figures. Amplitude (m) is represented by the colour contour and phase by the dark isolines. Isobaths for 200 m, 500 m, 1000 m, 2000 m, 3000 m, 4000 m and 5000 m depths were added to ease interpretation.

# Appendix II - Water quality module parameters



Reference temperature (Ref\_Temp) = 20°C

## Nitrogen

Keyword	Variable	Description	Units	Value
<b>DENITREF</b>	$K_{dnit}^{ref}(T_{ref})$	denitrification rate at the Ref_Temp	day <sup>-1</sup>	0.125
<b>DENSATCO</b>	$K_{dnit}^{sat}$	denitrification half-saturation constant	mgO <sub>2</sub> .L <sup>-1</sup>	0.1
<b>NITRIFREF</b>	$K_{nit}^{ref}(T_{ref})$	nitrification rate at Ref_Temp	day <sup>-1</sup>	0.06
<b>NITSATCO</b>	$K_{nit}^{sat}$	nitrification half-saturation constant	mgO <sub>2</sub> .L <sup>-1</sup>	2.0
<b>NMINENR</b>	$K_{min}^{DONnr}(T_{ref})$	DONnr mineralization rate at Ref_Temp	day <sup>-1</sup>	0.1
<b>NMINR</b>	$K_{min}^{DONre}(T_{ref})$	DONre mineralization rate at Ref_Temp	day <sup>-1</sup>	0.01
<b>NOPCOEF</b>	$\theta_{dec}$	PON decomposition temperature coefficient	Adim.	1.02
<b>NOPREF</b>	$K_{dec}^{PON}(T_{ref})$	PON reference decomposition rate	day <sup>-1</sup>	0.1
<b>NSATCONS</b>	$K_N^{Phy}$	nitrogen half-saturation constant	mgN.L <sup>-1</sup>	0.014
<b>PHDECOMP</b>	$f_{orgP}$	available PON for transformation into ammonia	Adim.	0.7*
<b>TDENCOEF</b>	$\theta_{dnit}$	denitrification temperature coefficient	aim	1.046
<b>TMINNR</b>	$\theta_{min}^{DONnr}$	DONnr mineralization temperature coefficient	Adim.	1.02
<b>TMINR</b>	$\theta_{min}^{DONre}$	DONre mineralization temperature coefficient	Adim.	1.02
<b>TNITCOEF</b>	$\theta_{nit}$	nitrification temperature coefficient	Adim.	1.08

\* Modified from the default value

## Phosphorus

Keyword	Variable	Description	Units	Value
<b>PMINNR</b>	$K_{\min}^{DOPnr}(T_{ref})$	DOPnr mineralization rate at Ref_Temp	day <sup>-1</sup>	0.03
<b>PMINNRCOEF</b>	$\theta_{\min}^{DOPnr}$	DOPnr mineralization temperature coefficient	Adim.	1.064
<b>PMINR</b>	$K_{\min}^{DOPre}(T_{ref})$	DOPre mineralization rate at Ref_Temp	day <sup>-1</sup>	0.1
<b>PMINTCOEF</b>	$\theta_{\min}^{DOPre}$	DOPre mineralization temperature coefficient	Adim.	1.064
<b>PPARTMIN</b>	$K_{dec}^{POP}(T_{ref})$	POP reference decomposition rate	day <sup>-1</sup>	0.02
<b>PSATCONS</b>	$K_P^{Phy}$	phosphorus half-saturation constant	mgP.L <sup>-1</sup>	0.001
<b>TPPARTMINCOEF</b>	$\theta_{dec}$	POP decomposition temperature coefficient	Adim.	1.08

## Oxygen

Keyword	Variable	Description	Units	Value
<b>NITONRAT</b>	$\alpha_{O:N}^{NO3}$	nitrate oxygen/nitrogen ratio (oxygen production due to nitrate uptake) (3O/1N) = 48/14 g/g	Adim.	3.429
<b>ONMINRATIO</b>	$\alpha_{\min O:N}^1$	Mineralization oxygen/nitrogen ratio	Adim.	2.286
<b>OPMINRATIO</b>	$\alpha_{\min O:P}^1$	Mineralization oxygen/phosphorus ratio	Adim.	127.27
<b>PHOSOPRAT</b>	$\alpha_{O:P}^{IP}$	orthophosphate oxygen/phosphorus ratio (oxygen production due to inorganic phosphorus uptake) (4O/1P) = 64/31 g/g	Adim.	2.064
<b>PHOTOSOC</b>	$\alpha_{O:C}^{photo}$	photosynthesis oxygen/carbon ratio (2O/1C) = 32/12 g/g	Adim.	2.67
<b>PLANK_OC_RAT</b>	$\alpha_{O:C}^{plankton}$	plankton oxygen/carbon ratio (2O/1C) = 32/12 g/g	Adim.	2.67
<b>ZOCRATIO</b>	$\alpha_{O:C}^{zoo}$	zooplankton respiration oxygen/carbon ratio (2O/1C) = 32/12 g/g	Adim.	2.67

## Phytoplankton

Keyword	Variable	Description	Units	Value
<b>EXCRCONS</b>	$K_e^{Phy}$	excretion constant	Adim.	0.07
<b>FDISSDON</b>	$f_{orgD/phy}$	dissolved organic fraction of organic excretions	Adim.	0.5*
<b>FENDREPC</b>	$K_{re}^{Phy}$	endogenous respiration constant	day <sup>-1</sup>	0.0175
<b>FMORTCON</b>	$K_m^{Phy}$	phytoplankton mortality half-saturation rate	mgC.L <sup>-1</sup> .day <sup>-1</sup>	0.3
<b>FMORTMAX</b>	$m_{max}^X(T_{ref})$	maximum mortality rate at Ref_Temp	day <sup>-1</sup>	0.02
<b>FRATIONC</b>	$\alpha_{N:C}^{phy}$	phytoplankton N:C ratio (Redfield's ratio)	mgN.mgC <sup>-1</sup>	0.18
<b>FRATIOPC</b>	$\alpha_{P:C}^{phy}$	phytoplankton P:C ratio (Redfield's ratio)	mgP.mgC <sup>-1</sup>	0.024
<b>FREGSATC</b>	$K_r^{phy}$	nutrient regeneration half-saturation constant	mgC.L <sup>-1</sup>	1.0
<b>FSOLEXCR</b>	$f_{in/phy}$	soluble inorganic fraction of phytoplankton excretions	Adim.	0.4*
<b>GROWMAXF</b>	$\mu_{max}^{phy}(T_{ref})$	maximum gross growth rate at Ref_Temp	day <sup>-1</sup>	2.0
<b>PHOTOIN</b>	$I_{opt}$	optimum light intensity for photosynthesis	Wm <sup>-2</sup>	121
<b>PHOTORES</b>	$K_{rp}^{Phy}$	photosynthesis fraction oxidised by photorespiration	Adim.	0.125
<b>TFCONST1</b>	$K_1$	constant to control temperature response curve shape	Adim.	0.05
<b>TFCONST2</b>	$K_2$	constant to control temperature response curve shape	Adim.	0.98
<b>TFCONST3</b>	$K_3$	constant to control temperature response curve shape	Adim.	0.98
<b>TFCONST4</b>	$K_4$	constant to control temperature response curve shape	Adim.	0.02
<b>TFMAX</b>	$T_{max}$	maximum tolerable temperature	°C	35.0*
<b>TFMIN</b>	$T_{min}$	minimum tolerable temperature	°C	5.0*
<b>TOPTFMAX</b>	$T_{max}^{opt}$	maximum temperature for the optimal growth interval	°C	25.0*
<b>TOPTFMIN</b>	$T_{min}^{opt}$	minimum temperature for the optimal growth interval	°C	10.0*

\* Modified from the default value

## Zooplankton

Keyword	Variable	Description	Units	Value
ASS_EFIC	E	assimilation efficiency of phytoplankton by zooplankton	Adim.	0.5*
GRAZFITOMIN	$\Phi_{phy}^{\min}$	threshold standing stock of phytoplankton below which grazing cease	mgC.L <sup>-1</sup>	0.0045
GROWMAXZ	$\mu_{\max}^{zoo}(T_{ref})$	zooplankton maximum gross growth rate at Ref_Temp	day <sup>-1</sup>	0.3
IVLEVCON	$\Lambda$	Ivlev grazing constant	L.mgC <sup>-1</sup>	13*
MAXMORTZ	$m_X^{max}$	maximum rate for zooplankton natural mortality	day <sup>-1</sup>	0.04
MINMORTZ	$m_X^0$	minimum rate for zooplankton natural mortality	day <sup>-1</sup>	0.001*
PHYRATING	$\rho_p$	Proportion of phytoplankton in zooplankton ingestion	Adim.	1*
TOPTZMAX	$T_{\max}^{opt}$	maximum temperature for the optimal growth interval	°C	25.0*
TOPTZMIN	$T_{\min}^{opt}$	minimum temperature for the optimal growth interval	°C	10.0*
TZCONST1	K <sub>1</sub>	constant to control temperature response curve shape	Adim.	0.05
TZCONST2	K <sub>2</sub>	constant to control temperature response curve shape	Adim.	0.98
TZCONST3	K <sub>3</sub>	constant to control temperature response curve shape	Adim.	0.98
TZCONST4	K <sub>4</sub>	constant to control temperature response curve shape	Adim.	0.02
TZMAX	$T_{\max}$	maximum tolerable temperature	°C	35.0
TZMIN	$T_{\min}$	minimum tolerable temperature	°C	5.0
ZDISSDON	$f_{orgD/zoo}$	dissolved organic fraction of organic excretions	Adim.	0.5
ZPREDMOR	$p_{zoo}$	zooplankton predatory mortality rate	day <sup>-1</sup>	0.0077
ZRATIONC	$\alpha_{N:C}^{zoo}$	Zooplankton N:C ratio	mgN.mgC <sup>-1</sup>	0.15
ZRATIOPC	$\alpha_{P:C}^{zoo}$	zooplankton P:C ratio	mgP.mgC <sup>-1</sup>	0.024
ZREFRESP	$d_{zoo}(T_{ref})$	carbon consumption rate by respiration and non-predatory mortality at Ref_Temp	day <sup>-1</sup>	0.02
ZSOLEXCR	$f_{in/zoo}$	soluble inorganic fraction of zooplankton excretions	Adim.	0.40

\* Modified from the default value